University of Venda

SCHOOL OF ENVIRONMENTAL SCIENCES

DEPARTMENT OF MINING AND ENVIRONMENTAL GEOLOGY

PALEO-ENVIRONMENTAL CONDITIONS AND TECTONIC SETTINGS OF CRETACEOUS-TERTIARY KAOLINS IN THE EASTERN DAHOMEY AND NIGER DELTA BASINS IN NIGERIA

BY

OYEBANJO, OLAONIPEKUN MOSES
STUDENT No: 15018001

A THESIS SUBMITTED TO THE DEPARTMENT OF MINING AND ENVIRONMENTAL GEOLOGY, SCHOOL OF ENVIRONMENTAL SCIENCES, UNIVERSITY OF VENDA, IN FULFILMENT OF THE REQUIREMENTS FOR THE PHD IN ENVIRONMENTAL SCIENCES (GEOLOGY)

PROMOTER: SENIOR PROF. G.E. EKOSSE

CO-PROMOTER: PROF. J.O. ODIYO

MAY 2018

DECLARATION

I, OYEBANJO Olaonipekun Moses, Student Number 15018001, hereby declare that this thesis submitted to the Department of Mining and Environment Geology, School of Environmental Sciences, University of Venda, for the PhD in Environmental Sciences (Geology) is my own work and has not been previously submitted, in whole or in part, to any university for any degree. Information derived from the published and unpublished work of others has been acknowledged in the text and a list of those references is given.

…….. ……

Signature Date

We, the promoters, certify that this declaration is correct.

…….. ……..

Promoter's Signature Date

Senior Professor GE Ekosse

…….. ……..

Co-promoter's Signature Date

Professor JO Odiyo

DEDICATION

This thesis is dedicated to God who has been my surest and steadfast anchor through the storms of life who knows my past, present, and holds my future.

ACKNOWLEDGEMENTS

I acknowledge my indebtedness to my promoter, the Director of Research and Innovation, University of Venda, Senior Prof. G.E. Ekosse. This work is a product of his mentoring and wealth of experience on which I dwelt eclectically throughout my period of study. Also, thanks to my co-promoter, the Dean, School of Environmental Sciences, University of Venda, Prof. J.O. Odiyo whose contributions and encouragements cannot be overemphasised.

My sincere appreciation goes to the Management of University of Venda for funding this research through its Research and Publication Committee (RPC). The National Research Foundation (NRF) Competitive Programme for Rated Researchers (CPRR) grant through Senior Prof. Ekosse for the Cretaceous – Tertiary clay deposits and argillaceous sediments project is also acknowledged.

Special thanks to the Management of Obafemi Awolowo University, Ile-Ife for granting me the opportunity to pursue my doctoral degree. I express my gratitude to Dr. A. Ogunfolakan and all the academic and non-academic staff of the Natural History Museum and Geology department for their fatherly and motherly support. Kind regards to Dr. M.A. Olayiwola, Mr. Obadare, Mr. G. Akintola (my fellow brother in Christ) for their assistance during my fieldwork. Thanks to my academic mentors Profs. T.R. Ajayi, M.A. Rahaman, and Dr. I.A. Tubosun for their unwavering support and advice. I also thank Dr. M. Diko for his questions, comments and positive inputs to improve the quality of the work.

I am grateful to Prof. J. Odhiambo and Mr. P. Tshidada both in the Dept. of Soil Sciences, University of Venda for allowing me to use their laboratory for sample preparation and determination of particle size distribution, colour, pH, and electrical conductivity. Special thanks to some members of staff of the School of Environmental Sciences, University of Venda namely: Dr. F. Dacosta and Mr. C. Muzerengi for allowing me to use the Mining and Environmental Geology laboratory for the determination of Atterberg limits, Dr. E. Stam, Prof. W. Gitari, Mr G. Phindihama, and Mr. R. Mudzielwana for their permission and guidance to use the Fourier transform infrared spectroscopic instrument in the

Department of Ecology and Resource Management, and Mr. T. Nkuna for permission to use the centrifuge machine in the Hydrology and Water Resources laboratory.

The assistance of the following analytical laboratories are acknowledged: the Ithemba LABS, Cape Town and XRD Analytical and Consulting cc, Pretoria for my mineral phase identification and quantification, the Central Analytical Facility, Stellenbosch University for my geochemical, morphological, microchemical, and geochronological analyses; the Stable Isotopes Laboratory, University of Cape Town for my oxygen and hydrogen isotopic analyses, and the Department of Chemistry laboratory, University of Johannesburg for my differential thermal analysis (DTA).

I express my gratitude to all the members and leaders of Christ Tabernacle, University of Venda for making my spiritual and academic journey a memorable one.

I wish to thank all my friends and colleagues Odundun Muyiwa, Akande Waheed, Akinbola Seyi, Bankole Samson, Owoeye Damola, Badaru Segun, Nenita Bukalo, Olatunde Durowoju, Khusto Lenyanyabedi, Johanna Molepo, Avhatakali Raphalalani, Valery Phakoago, Unarine Mashao, late Edino Friday, and others.

My sincere appreciation goes to my parents and all my family members for believing in me and for the love of Christ between us. And to Prof. J.A. Fabayo, Late Prof. Imoru, the Adewales, the Fayokuns, the Alaos, the Olasunkanmis, the Fajuyigbes, the Adejuyigbes, the Bellos, the Obafemis, the Kehindes and others.

I appreciate you all. I may have missed out some wonderful names in the text, to everyone who have been with me on the journey I pass on a heartfelt thank you.

I will not forget to appreciate my loving Jewel Mrs Omosalewa Oyebanjo for her sacrifices, prayers, and encouragements which made this period of my life the best it could have ever been. Thank you so much. To my wonderful children, Joshua and Jedidiah, I love you guys beyond words can express.

Above all, to God the maker of my life, I will continue to serve you forever.

REMAIN RAPTURABLE!

ABSTRACT

The Cretaceous period marked the breaking up of Gondwana, giving rise to the separation of the African and South American continents with the subsequent emergence of the South Atlantic Ocean. Most correlation studies between the two continents with respect to paleoenvironmental conditions and tectonic settings during the Cretaceous-Tertiary periods have been concentrated more on the use of flora and fauna as indicators with less application of kaolinite as paleoenviromental proxies, hence, this study.

The research involved the evaluation of paleoenvironmental conditions and tectonic settings of four (4) selected Cretaceous-Tertiary kaolin deposits with two (2) each from the Eastern Dahomey (Eruku and Lakiri) and Niger Delta (Awo-Omama and Ubulu-Uku) Basins in Nigeria. Representative kaolin samples collected from the selected deposits were analysed for physico-chemical, mineralogical, geochemical, isotopic, and geochronological data. The geochemical data obtained by x-ray fluorescence (XRF) spectroscopy and laser ablation inductively coupled plasma mass spectrometry (LA-ICPMS) were used in unraveling the provenance and tectonic settings of the kaolins. The kaolinite stable isotopic data for oxygen and hydrogen determined using a Finnigan Delta XP Mass Spectrometer were used to assess the paleoenvironmental and paleoclimatic conditions under which the kaolins were formed. The detrital zircon geochronological data acquired by laser ablation – single collector – magnetic sectorfield – inductively coupled plasma – mass spectrometry (LA-SFICP-MS) as well as kaolinite stable isotopic data were employed in constraining the probable timing of kaolinisation. The industrial applications of the kaolins were assessed based on the physico-chemical (Colour, particle size distribution (PSD), pH, electrical conductivity, and Atterberg limits), mineralogical, and geochemical data. The mineralogical data were obtained through x-ray diffractometry (XRD), Fourier transform infrared (FTIR) spectroscopy, Thermogravimetric analysis and differential scanning calorimetry, and scanning electron microscopy (SEM). Correlative studies between selected Cretaceous African and South American kaolins were conducted.

The results showed that the dominant colour in the studied kaolins was pale red (39 %) followed by pinkish and light grey (35 %) as well as reddish yellow, light pink, light brown,

reddish brown, and pinkish white. The pH and EC values generally ranged from 4.27 to 5.29 and 0.2 to 13.1 µS/cm, respectively. The kaolins predominantly have clay to sandy clay textures with plasticity indices between 10 and 22 wt %.

Bulk mineralogical quantitative results indicated that the Cretaceous kaolins have kaolinite, quartz, and muscovite present in that decreasing order with anatase, goethite, and hematite in traces whereas Tertiary kaolins have kaolinite and quartz present in that decreasing order with anatase and goethite in traces. In the silt fractions, kaolinite and quartz were the dominant mineral constituents, whereas in the clay fractions, the dominant clay mineral was kaolinite accounting for 69 to 99 wt % with the non-clay minerals like quartz, anatase, hematite and goethite accounting for percentages between 1 to 28 wt % in the Cretaceous – Tertiary kaolins. Morphologically, the studied kaolins were characterised by pseudohexagonal stacks to books and thin platy kaolinite particles with moderate structural order.

The chemical compositions of the Cretaceous-Tertiary kaolin deposits were identical to hydrated alumino-silicates based on the dominance of SiO_2, Al_2O_3 and LOI. The chemical index of alteration (CIA) and chemical index of weathering (CIW) values varied between 96.98 to 99.39 % and 98.95 to 99.89 %, respectively. The clay fractions were enriched in Cr, Nb, Sc, Th, U, V, Zr, and LREE and depleted in Ba, Co, Rb, Sr, and HREE, respectively, relative to the average Upper Continental Crust (UCC). The Th/Sc, La/Sc, Th/Cr, and Eu/Eu* ratios were within the range of sediments derived from felsic rocks. The TiO_2 versus Al_2O_3 and La-Th-Sc plots indicated source rocks with granitic – granodioritic - gabbroic compositions. Geochemical discrimination plots showed that the Cretaceous and Tertiary kaolins were deposited in passive margin tectonic settings.

The stable isotopic results indicated that the values of the Cretaceous kaolins ranged from – 47 to – 57 ‰ and 19.1 to 19.8 ‰, respectively, with paleotemperatures between 29.0 and 32.2 ˚C, whereas the δD and $\delta^{18}O$ corresponding values for the Tertiary kaolins ranged from – 54 to – 66 ‰ and 20 to 21.5 ‰, respectively, with paleotemperatures between 17.0 and 23.9 ˚C.

The U-Pb dating of the detrital zircons showed that the Cretaceous - Tertiary kaolins have inputs from rocks of Eburnean (2500 – 2000 Ma) and Pan African (750 – 450 Ma) ages. The age of maximum deposition determined from the least to statistically robust approach corresponds to the Ediacaran Period (645 – 541 Ma) of the Neoproterozoic Era (1000 – 541 Ma).

The Cretaceous – Tertiary kaolins were formed under intense anoxic chemical paleoweathering conditions of predominantly felsic rocks in addition to contributions from intermediate and mafic rocks in passive margin tectonic settings. The Cretaceous kaolins were formed under warmer conditions relative to the Tertiary kaolins. The West African Massif rocks were the main sediment sources for the Cretaceous kaolins, whereas both the West African and Northern Nigerian Massif rocks were the major sediment sources for the Tertiary kaolins. The most probable timing of kaolinisation for the Cretaceous – Tertiary kaolins occurred between the Ediacaran (645 – 541 Ma) and Early Cretaceous Periods for the Cretaceous kaolins and between the Ediacaran Period (645 – 541 Ma) and Oligo – Miocene age for the Tertiary kaolins. The Nigerian and Brazilian Cretaceous kaolins formed under similar warm tropical paleoclimate. The study corroborated the occurrence of the Eburnean (Transamazonian) and Pan African (Brasiliano) orogenic events across the African and South American continents. Beneficiation of the Cretaceous – Tertiary kaolins will allow large scale industrial applications in paper coating, ceramics, pharmaceutical, and cosmetics industries.

The major contributions from this study have been: the better understanding of the past environmental conditions and tectonic settings, the dating of the possible timing of kaolinisation, and improvement on the potential industrial applications of the Cretaceous – Tertiary kaolins.

Keywords: Cretaceous-Tertiary, Eastern Dahomey, Niger Delta, basins, kaolins, paleoenvironmental conditions, and tectonic settings.

TABLE OF CONTENTS

LIST OF FIGURES

LIST OF TABLES

LIST OF APPENDICES

LIST OF ABBREVIATIONS

Al : Aluminium

Ar : Argon

ATR : Attenuated Total Reflectance

Au : Gold

Al_2O_3 : Aluminium oxide

CIA : Chemical index of alteration

CIW : Chemical index of weathering

Co : Cobalt

Cr : Chromium

DTA : Differential thermal analysis

Eu : Europium

FTIR : Fourier transform infrared

Ga : Giga annum (Billion years)

H_2O : Water

HREE : Heavy rare earth elements

HCl : Hydrogen chloride

HF : Hydrogen fluoride

HNO_3 : Nitric acid

LA-ICPMS : Laser ablation inductively coupled plasma mass spectrometer

K : Potassium

La : Lanthanum

LREE : Light rare earth elements

Lu : Luthetium

Ma : Mega annum (Million years)

MAT : Mean annual temperatures

MSWD : Mean square weighted deviation

NASC : North American Shale Composite

Ni : Nickel

PAAS : Post-Archean Australian Shale

Pb : Lead

ppm : parts- per- million

Pt : Platinum

REE : Rare earth elements

S : Seconds

SEM : Scanning electron microscopy

Si : Silicon

Sn : Tin

U : Uranium

UCC : Upper Continental Crust

VSMOW : Vienna Standard Mean Ocean Water

XRD : X-ray diffractometry

LIST OF UNITS AND SYMBOLS

Å	: Angstrom
°C	: Degrees Celsius
cm	: centimeter
kg	: Kilogram
km	: Kilometer
kHz	: KiloHertz
kV	: kilovolt
MHz	: MegaHertz
µl	: Microliter
µm	: Micrometer
µS	: MicroSiemens
nA	: NanoAmperes
‰	: Per mille
δ	: Per mil deviation
wt. %	: Weight percent

APPENDICES

Appendix 3.1: Analyses of Bulk Serina Standard replicate samples

	A	B	C	
Sample	Serina kao 1	Serina kao 2	Serina kao 3	Mean
dD raw	-63.2	-60.5	-60.1	
d D cor	-56.1	-53.4	-53.0	
dD corr2	-58.1	-55.4	-55.0	
dD corr3	-63.4	-60.4	-59.9	**-61.2**
dD corr4	-58.8	-55.8	-55.3	**-56.6**
Wt sample	15.47	15.24	15.62	
P	67.0	40.3	38.4	
Mass 2 V	4.156	4.454	4.287	
mg water	1.67	1.79	1.66	
wt.% water	10.80	11.75	10.62	

Appendix 4.1: Position and assignment of IR bands of the <2 µm kaolin fractions and theoretical kaolinite.

Awo-Omama

Theoretical Kaolinite	AL1 0m	AL1 1m	AL1 2m	AL2 0m	AL2 1m	AL2 2m	Assignment
3691 - 89	3690	3692	3690	3690	3690	3690	Al---O-H stretching of inner surface hydroxyl groups
3669	3669	3670	3669	3669	3670	3669	Al---O-H stretching of inner surface hydroxyl groups
3651	3651	3649	3649	3650	3650	3650	Al---O-H stretching of inner surface hydroxyl groups
3619	3620	3620	3621	3621	3621	3621	Al---O-H stretching of inner hydroxyl groups
1115 - 14	1116	1116	1118	1116	1116	1116	Si-O stretching (Longitudinal mode)
1028 - 27	1026	1026	1028	1026	1026	1026	In-plane Si-O stretching
1005 - 04	999	999	997	1002	999	997	In-plane Si-O stretching
937 - 935	938	938	938	936	936	938	OH deformation of inner surface hydroxyl groups
912	910	912	912	912	912	910	OH deformation of inner hydroxyl groups
789 - 788	794	798	798	791	795	796	OH deformation linked to Al, Mg
751 - 750	751	751	749	750	753	749	Si-O perpendicular
684 - 681	689	691	696	683	687	691	Si-O perpendicular
541	520	529	528	520	530	530	Fe-O, Fe_2O_3, Ti-O; Si-O-Al stretching

Ubulu-Uku

Theoretical Kaolinite	UL1 0m	UL1 1m	UL1 2m	UL2 0m	UL2 1m	UL2 2m	UL2 3m	Assignment
3691 - 89	3692	3692	3688	3692	3692	3688	3690	Al---O-H stretching of inner surface hydroxyl groups
3669	3669	3670	3668	3667	3668	3668	3670	Al---O-H stretching of inner surface hydroxyl groups
3651	3652	3651	3651	3651	3649	3651	3651	Al---O-H stretching of inner surface hydroxyl groups
3619	3621	3621	3619	3621	3621	3621	3619	Al---O-H stretching of inner hydroxyl groups
1115 - 14	1116	1116	1116	1116	1116	1116	1116	Si-O stretching (Longitudinal mode)
1028 - 27	1026	1028	1026	1026	1026	1024	1028	In-plane Si-O stretching
1005 - 04	1000	1000	1000	1002	1000	997	1002	In-plane Si-O stretching
937 - 935	938	938	938	936	938	936	936	OH deformation of inner surface hydroxyl groups
912	912	910	914	912	912	912	912	OH deformation of inner hydroxyl groups
789 - 788	798	800	798	798	798	798	798	OH deformation linked to Al, Mg
751 - 750	752	753	751	751	751	751	751	Si-O perpendicular
684 - 681	689	689	692	687	687	687	687	Si-O perpendicular
541	530	532	528	530	528	526	528	Fe-O, Fe_2O_3, Ti-O; Si-O-Al stretching

Lakiri

Theoretical Kaolinite	LP1 0m	LP1 2m	LP1 4m	LP2 0m	LP2 2m	LP2 4m	Assignment
3691 - 89	3688	3686	3686	3686	3688	3688	Al---O-H stretching of inner surface hydroxyl groups
3669	3669	3670	3669	3670	3669	3670	Al---O-H stretching of inner surface hydroxyl groups
3651	3651	3653	3651	3651	3651	3651	Al---O-H stretching of inner surface hydroxyl groups
3619	3619	3619	3619	3619	3619	3619	Al---O-H stretching of inner hydroxyl groups
1115 - 14	1114	1116	1114	1116	1114	1116	Si-O stretching (Longitudinal mode)
1028 - 27	1023	1026	1026	1023	1026	1026	In-plane Si-O stretching
1005 - 04	1000	1000	1000	1000	1000	998	In-plane Si-O stretching
937 - 935	938	938	938	938	938	940	OH deformation of inner surface hydroxyl groups
912	912	912	912	914	912	912	OH deformation of inner hydroxyl groups
789 - 788	794	791	796	796	793	793	OH deformation linked to Al, Mg
751 - 750	749	753	753	753	751	751	Si-O perpendicular
684 - 681	689	689	692	687	687	687	Si-O perpendicular
541	524	524	530	522	526	528	Fe-O, Fe_2O_3, Ti-O; Si-O-Al stretching

Eruku

Theoretical Kaolinite	EP1 0m	EP1 2m	EP1 4m	EP2 0m	EP2 2m	EP2 4m	EP3 0m	EP3 2m	EP3 4m	Assignment
3691 - 89	3688	3688	3688	3688	3686	3688	3688	3688	3686	Al---O-H stretching of inner surface hydroxyl groups
3669	3669	3670	3670	3670	3670	3670	3670	3670	3670	Al---O-H stretching of inner surface hydroxyl groups
3651	3651	3651	3651	3651	3651	3651	3651	3651	3651	Al---O-H stretching of inner surface hydroxyl groups
3619	3619	3619	3619	3619	3619	3619	3621	3619	3619	Al---O-H stretching of inner hydroxyl groups
1115 - 14	1116	1114	1114	1114	1114	1114	1116	1116	1114	Si-O stretching (Longitudinal mode)
1028 - 27	1026	1024	1026	1026	1026	1026	1026	1024	1024	In-plane Si-O stretching
1005 - 04	999	998	1002	1000	1000	1002	1000	1000	1000	In-plane Si-O stretching
937 - 935	938	938	940	938	936	938	936	938	936	OH deformation of inner surface hydroxyl groups
912	912	910	914	912	912	912	912	912	912	OH deformation of inner hydroxyl groups
789 - 788	796	791	794	791	791	791	791	791	793	OH deformation linked to Al, Mg
751 - 750	749	751	749	751	751	751	751	751	751	Si-O perpendicular
684 - 681	691	691	696	683	687	691	683	687	691	Si-O perpendicular
541	526	528	522	522	522	528	524	526	526	Fe-O, Fe_2O_3, Ti-O; Si-O-Al stretching

Appendix 4.2: Major Element Oxide Concentrations (wt %) of the studied kaolins.

Bulk Samples

	Al_2O_3	CaO	Cr_2O_3	Fe_2O_3	K_2O	MgO	MnO	Na_2O	P_2O_5	SiO_2	TiO_2	L.O.I.	Total
EP1 0m	28	0.03	0.02	2.61	0.45	0.04	0.01	0.02	0.1	56.53	1.96	10.03	99.8
EP1 2m	28.02	0.02	0.02	1.94	0.4	0.04	0.01	0.02	0.12	56.75	2.39	10.03	99.76
EP1 4m	36.64	0.01	0.02	1.48	0.28	bdl	0.01	0.02	0.08	47.22	1.97	12.89	100.62
EP2 0m	27.62	0.02	0.01	5.04	0.35	bdl	0.01	0.02	0.1	55.24	2.16	10.1	100.67
EP2 2m	35.68	0.02	0.01	1.73	0.4	bdl	bdl	0.02	0.13	47.59	2.55	12.48	100.61
EP2 2m*	35.42	0.02	0.02	1.7	0.4	bdl	0.01	0.02	0.14	47.56	2.52	12.48	100.29
EP2 4m	11.44	0.02	0.01	2.5	0.27	0.05	0.01	bdl	0.09	80.3	1.07	4.03	99.79
EP3 0m	26.99	0.01	0.01	3.42	0.65	bdl	0.01	0.05	0.08	58.06	1.89	9.46	100.63
EP3 2m	31.59	0.02	0.01	1.74	0.51	bdl	0.01	0.02	0.15	52.83	2.84	11.01	100.73
EP3 4m	33.67	0.02	0.02	2.38	0.32	bdl	bdl	0.03	0.17	50	2.15	11.94	100.7
LP1 0m	21.4	0.01	0.01	0.74	0.56	bdl	0.01	0.04	0.07	69.6	1.14	7.42	101
LP1 2m	38.69	0.02	0.01	0.68	0.17	bdl	bdl	bdl	0.05	45.28	2	13.92	100.82
LP1 4m	37.84	0.02	0.03	2.7	0.16	bdl	bdl	0.01	0.06	44.78	1.62	13.68	100.9
LP2 0m	39.5	0.01	0.01	1.22	0.06	bdl	0.01	0.01	0.05	44.63	1.53	13.6	100.63
LP2 2m	39.08	0.02	0.01	0.6	0.09	bdl	bdl	0.01	0.04	45.1	1.84	13.87	100.66
LP2 4m	36.81	0.01	0.01	0.59	0.13	bdl	bdl	bdl	0.1	48.44	1.49	12.94	100.52
AL1 0m	32.09	0.04	0.02	4.24	0.27	bdl	0	0.02	0.11	50.11	1.62	11.97	100.49
AL1 1m	10.86	0.04	0.01	1.39	0.08	0.06	0.01	bdl	0.06	81.44	1.99	4.26	100.2
AL1 2m	7.16	0.03	bdl	0.85	0.09	0.04	0.01	bdl	0.04	87.99	1	2.83	100.04
AL2 0m	11.99	0.02	0.01	3.7	0.1	0.04	0.01	bdl	0.06	78.54	0.83	4.71	100.01
AL2 1m	16.7	0.02	0.01	1.78	0.15	0.04	0.01	bdl	0.07	73.45	1.06	6.36	99.65
AL2 2m	29.31	0.02	0.02	2.54	0.27	0.04	0	bdl	0.11	54.73	1.58	11.11	99.73
UL1 0m	17.8	0.02	0.01	4.63	0.38	0.09	0.01	bdl	0.08	67.63	2.38	7.02	100.05
UL1 1m	25.86	0.01	0.01	7.65	0.6	0.03	0.01	0.03	0.13	54.63	1.67	10.02	100.65
UL1 2m	26.83	0.02	0.01	5.23	0.38	0.01	0.01	0.01	0.1	55.91	2.13	9.91	100.55
UL2 0m	24.28	0.02	0.01	4.98	0.49	0.02	bdl	0.02	0.09	59.5	1.87	9.37	100.65
UL2 1m	26.21	0.02	0.02	6.69	0.57	0.02	0.01	0.02	0.12	55.11	1.85	10.02	100.66

UL2 2m	18.02	0.02	0.01	6.92	0.33	0.1	0.01	bdl	0.12	65.45	2.13	6.81	99.92
UL2 3m	19.55	0.02	0.01	8.3	0.47	0.17	0.02	bdl	0.19	61.41	2.18	7.81	100.13

bdl: below detection limit; EP2 2m*: duplicate sample.

Silt Fraction

	Al_2O_3	CaO	Cr_2O_3	Fe_2O_3	K_2O	MgO	MnO	Na_2O	P_2O_5	SiO_2	TiO_2	L.O.I.	Total
EP3 2m	22.98	0.02	0.01	1.88	0.87	0.08	0.01	0.11	0.18	62.35	4.11	7.88	100.48
LP1 0m	25.39	0.02	0.01	1.09	0.62	0.06	0.01	0.07	0.12	61.68	2.14	8.83	100.04
AL1 2m	1.38	0.02	0.01	0.64	0.06	0.07	0.02	bdl	0.04	94.99	1.75	0.59	99.57
UL2 2m	6.23	0.02	0.01	7.72	0.16	0.08	0.01	0.03	0.13	80.88	2.14	2.57	99.98

bdl: below detection limit

Clay Fraction

	Al_2O_3	CaO	Cr_2O_3	Fe_2O_3	K_2O	MgO	MnO	Na_2O	P_2O_5	SiO_2	TiO_2	L.O.I.	Total	CIA	CIW
EP1 0m	37.96	0.02	0.01	2.32	0.3	bdl	bdl	0.25	0.41	44.47	1.68	13.27	100.69	98.52	99.29
EP1 2m	37.57	0.02	0.01	1.8	0.21	bdl	bdl	0.38	0.58	45.31	1.7	13.24	100.82	98.40	98.95
EP1 4m	38.56	0.01	0.1	1.33	0.19	bdl	bdl	0.2	0.25	45.14	1.48	13.54	100.8	98.97	99.46
EP2 0m	36.44	0.03	0.02	5.23	0.25	bdl	bdl	0.21	0.42	43.29	1.54	13.12	100.55	98.67	99.35
EP2 2m	35.53	0.02	0.02	1.72	0.41	bdl	0.01	0.02	0.14	47.52	2.52	13.02	100.93	98.75	99.89
EP2 4m	35.48	0.03	0.01	7.53	0.18	bdl	0.01	0.21	0.52	42.35	1.32	13.05	100.69	98.83	99.33
EP3 0m	36.67	0.02	0.01	3.96	0.25	bdl	bdl	0.23	0.36	45.03	1.28	12.9	100.71	98.65	99.32
EP3 2m	37.91	0.02	0.01	1.51	0.32	bdl	bdl	0.18	0.34	44.63	2.15	13.29	100.36	98.65	99.48
EP3 4m	38.6	0.03	0.01	1.38	0.18	bdl	bdl	0.2	0.41	44.86	1.57	13.62	100.86	98.95	99.41
LP1 0m	39.17	0.01	0.02	1.04	0.19	bdl	bdl	0.17	0.33	44.67	1.54	13.7	100.84	99.06	99.54
LP1 2m	39.21	0.02	0.01	1.12	0.05	bdl	bdl	0.17	0.3	44.25	1.32	13.91	100.36	99.39	99.52

LP1 4m	39.36	0.02	0.01	0.67	0.14	bdl	bdl	0.19	0.26	44.68	1.54	13.83	100.7	99.12	99.47
LP2 0m	38.85	0.01	0.02	2.11	0.1	bdl	bdl	0.21	0.35	44.19	1.29	13.76	100.89	99.18	99.44
LP2 2m	39.3	0.01	0.01	0.57	0.06	bdl	bdl	0.23	0.33	44.78	1.5	13.84	100.63	99.24	99.39
LP2 4m	39.26	0.02	0.01	0.63	0.11	bdl	bdl	0.22	0.37	44.75	1.24	13.81	100.42	99.12	99.39
AL1 0m	36.3	0.04	0.02	5	0.31	bdl	0.01	0.2	0.44	43.47	1.79	13.05	100.63	98.51	99.34
AL1 1m	30.11	0.02	0.02	3.41	0.21	bdl	0.02	0.29	0.49	51.01	3.95	11.2	100.73	98.30	98.98
AL1 2m	33.33	0.02	0.02	3.41	0.38	bdl	0.01	0.32	0.46	47.94	2.84	12.07	100.8	97.89	98.99
AL2 0m	36.23	0.01	0.01	5.14	0.25	bdl	bdl	0.24	0.43	43.64	1.63	13.01	100.59	98.64	99.31
AL2 1m	35.79	0.02	0.01	2.67	0.4	bdl	0.01	0.23	0.41	46.06	2.05	13.14	100.79	98.22	99.31
AL2 2m	36.73	0.01	0.02	3.16	0.33	bdl	0.01	0.23	0.42	44.64	1.8	13.47	100.82	98.47	99.35
UL1 0m	28.57	0.02	0.01	4.33	0.53	bdl	0.01	0.25	0.32	53.85	2.68	10.24	100.81	97.28	99.06
UL1 1m	28.68	0.02	0.01	6.75	0.56	bdl	0.01	0.23	0.34	51.6	1.89	10.57	100.66	97.25	99.14
UL1 2m	31.95	0.02	0.01	5.83	0.38	bdl	0.01	0.25	0.32	48.34	1.92	11.73	100.76	98.01	99.16
UL2 0m	30.27	0.02	0.01	4.32	0.55	bdl	bdl	0.26	0.36	51.56	1.99	10.95	100.29	97.33	99.08
UL2 1m	30.98	0.02	0.01	4.95	0.58	bdl	0.01	0.29	0.38	50.36	1.93	10.99	100.5	97.21	99.01
UL2 2m	33.87	0.02	0.01	4.7	0.44	bdl	0.01	0.27	0.31	47.21	2.05	11.99	100.88	97.89	99.15
UL2 3m	30.17	0.02	0.01	10.88	0.56	0.03	0.01	0.36	0.65	44.9	1.9	11.23	100.72	96.98	98.76

bdl: below detection limit

Appendix 4.3: Trace Element Concentrations (ppm) of the studied kaolins.

Bulk Samples

	Sc	V	Cr	Co	Ni	Rb	Sr	Y	Zr	Nb	Ba	Th	U
EP1 0m	16.78	117.77	124.59	7.29	43.68	16.69	72.73	35.35	850.19	45.41	202.43	31.91	4.93
EP1 2m	21.74	117.35	132.26	6.35	40.00	14.09	109.44	75.80	1517.09	59.41	250.51	35.97	7.91
EP1 4m	20.57	133.19	149.98	8.82	47.03	11.02	66.69	25.79	317.81	44.47	142.79	20.87	4.97
EP2 0m	21.89	167.96	142.28	6.03	33.21	15.08	89.78	65.26	1296.40	59.05	200.11	33.01	7.56
EP2 2m	23.57	137.03	151.67	9.06	44.39	13.39	136.10	44.45	654.89	53.28	270.29	32.43	7.83
EP2 2m*	23.97	138.28	154.75	8.70	41.98	13.57	136.33	45.10	660.76	53.43	263.78	32.59	7.57
EP2 4m	11.15	67.78	49.65	2.20	18.02	9.19	105.65	23.44	676.31	19.37	106.97	17.73	3.47
EP3 0m	19.52	130.59	128.03	6.09	31.08	22.13	59.95	60.27	1477.06	47.76	210.22	37.03	6.67
EP3 2m	24.03	130.32	144.02	7.47	41.06	19.20	151.62	59.73	835.80	63.25	310.91	34.65	7.45
EP3 4m	28.53	123.05	156.07	8.03	40.14	11.49	220.50	39.10	484.96	57.56	341.45	41.66	8.40
LP1 0m	14.83	87.16	91.66	5.69	31.14	18.24	56.21	24.47	522.27	30.07	161.41	23.99	2.58
LP1 2m	37.07	172.13	136.80	12.18	52.32	2.53	20.07	18.04	154.88	33.95	46.72	38.04	3.09
LP1 4m	31.79	114.00	138.81	8.61	50.13	6.55	32.58	26.75	327.93	45.22	87.45	40.96	4.66
LP2 0m	23.12	305.35	218.84	7.85	164.23	6.10	36.28	17.96	320.99	36.25	83.94	29.59	4.33
LP2 2m	19.14	114.86	144.15	5.91	40.39	3.69	19.91	18.91	274.06	45.20	48.29	34.35	3.61
LP2 4m	18.36	105.44	131.02	7.31	36.36	6.15	57.88	18.79	261.76	31.03	87.77	29.49	3.00
AL1 0m	18.40	136.25	166.14	3.06	24.22	16.55	104.85	20.42	317.66	52.70	165.58	26.85	3.55
AL1 1m	11.72	87.59	61.55	1.64	12.61	3.70	55.44	25.89	769.52	54.58	120.52	12.52	3.26
AL1 2m	8.40	45.82	40.13	1.17	15.96	5.30	25.78	12.39	384.57	27.58	71.55	6.92	1.70
AL2 0m	10.70	95.05	80.14	1.52	19.92	6.22	36.53	8.41	416.65	27.95	67.56	13.63	1.80
AL2 1m	12.52	102.29	78.03	2.12	19.15	9.78	59.55	13.16	358.35	32.04	95.12	16.59	2.26
AL2 2m	22.81	142.15	155.40	3.25	32.48	16.29	105.25	23.39	360.08	53.42	168.47	25.39	4.64
UL1 0m	14.98	99.94	100.86	2.47	16.14	26.75	95.74	25.97	533.83	81.41	225.99	20.27	5.35
UL1 1m	19.47	177.19	124.39	3.89	30.33	42.07	156.68	30.33	349.03	67.19	293.18	21.85	4.84
UL1 2m	18.34	136.42	93.17	2.73	16.46	27.37	128.75	47.61	992.81	185.98	224.08	30.26	6.49
UL2 0m	16.16	161.91	127.05	2.79	20.97	32.41	133.92	27.77	402.46	69.70	262.06	24.14	4.51

UL2 1m	16.97	214.78	163.06	3.12	23.52	38.52	155.03	35.50	409.26	74.37	301.37	28.73	4.54
UL2 2m	12.87	113.50	88.97	4.13	16.60	22.49	92.07	35.64	1051.85	65.59	221.24	20.61	5.82
UL2 3m	18.46	181.83	96.66	7.25	27.73	32.47	127.63	42.89	866.15	67.48	312.87	21.96	6.29

EP2 2m*: duplicate sample

Silt Fraction

	Sc	V	Cr	Co	Ni	Rb	Sr	Y	Zr	Nb	Ba	Th	U
EP3 2m	28.26	131.43	148.57	4.88	28.37	28.61	63.01	102.06	1734.89	91.49	289.30	23.38	11.20
LP1 0m	21.36	111.26	121.26	5.72	27.84	17.89	25.00	52.64	1530.40	39.17	181.02	33.17	6.47
AL1 2m	10.99	36.29	45.97	1.52	13.17	2.39	15.33	34.77	1341.90	46.41	68.35	11.75	3.86
UL2 2m	10.81	110.60	97.25	4.50	13.11	9.42	34.23	30.72	1318.35	56.86	129.03	20.18	6.01

Clay Fraction

	Sc	V	Cr	Co	Ni	Rb	Sr	Y	Zr	Nb	Ba	Th	U
EP1 0m	14.65	113.61	132.90	10.60	51.53	13.55	97.05	13.05	140.41	40.20	201.60	29.23	2.94
EP1 2m	16.66	118.15	133.90	8.68	43.16	9.41	145.03	26.66	348.65	36.99	262.55	26.09	3.87
EP1 4m	16.46	125.75	140.34	9.62	45.93	8.37	59.78	10.64	67.21	34.75	113.16	12.65	3.39
EP2 0m	15.78	163.03	149.46	7.94	45.78	12.26	122.51	16.94	202.81	38.84	221.63	26.95	3.66
EP2 2m	18.60	125.17	149.18	10.09	54.01	8.50	161.79	18.41	67.95	38.83	238.71	36.81	4.39
EP2 4m	17.84	182.52	103.46	5.93	43.67	8.50	315.37	10.16	151.48	34.21	193.60	28.02	5.12
EP3 0m	14.63	133.16	141.04	8.52	45.71	10.35	79.85	12.81	208.24	33.72	150.79	33.59	3.27
EP3 2m	17.81	120.71	139.23	9.45	42.72	13.44	205.98	19.63	106.07	48.26	334.49	34.99	4.04
EP3 4m	19.13	103.86	134.69	9.72	47.84	7.42	273.72	20.90	85.33	34.11	366.81	38.07	5.98
LP1 0m	17.44	132.87	151.90	11.52	61.53	8.40	132.75	18.21	75.68	35.02	174.48	40.55	2.46
LP1 2m	20.14	145.48	129.86	12.19	60.68	2.74	18.02	10.74	77.13	29.33	41.55	27.93	2.49
LP1 4m	19.18	98.14	127.42	8.41	45.70	6.32	28.27	9.84	77.05	42.30	68.13	29.35	3.09

LP2 0m	15.67	209.85	160.39	8.59	44.74	4.16	33.73	7.49	69.69	36.10	70.27	20.61	2.83
LP2 2m	15.98	96.69	138.98	6.71	40.76	3.26	18.71	8.93	94.26	34.23	37.92	28.23	2.23
LP2 4m	16.68	98.39	124.18	8.45	44.96	5.80	61.80	9.33	67.69	30.45	78.46	26.16	2.25
AL1 0m	18.32	150.49	177.37	3.54	28.38	19.07	118.23	17.99	263.08	62.12	185.80	27.34	3.66
AL1 1m	19.81	197.50	142.67	3.90	28.26	9.23	152.23	34.74	616.18	125.30	254.68	25.99	5.90
AL1 2m	17.96	146.52	133.08	3.36	26.41	20.73	102.82	24.00	451.71	89.15	209.72	22.27	4.35
AL2 0m	17.04	147.39	122.48	3.49	32.43	15.13	91.94	13.26	257.75	60.80	153.32	22.96	2.77
AL2 1m	18.72	140.87	148.47	3.25	34.88	23.74	157.20	21.87	287.91	67.43	251.92	28.38	4.09
AL2 2m	22.73	164.50	176.63	3.57	30.63	20.86	128.71	21.51	264.28	58.56	199.08	27.52	5.05
UL1 0m	17.08	115.05	124.51	3.32	23.96	36.56	170.22	21.81	344.79	99.96	301.63	27.79	6.07
UL1 1m	18.07	154.07	117.31	3.91	26.87	38.33	208.52	24.99	278.67	79.10	349.84	24.34	5.30
UL1 2m	16.59	123.08	93.12	2.03	18.70	28.19	189.16	37.73	773.90	202.61	285.34	31.80	6.39
UL2 0m	15.30	123.78	125.41	3.09	24.79	35.92	208.38	25.07	286.45	80.30	330.96	27.86	4.91
UL2 1m	16.50	148.19	114.17	3.12	25.42	38.98	211.40	27.55	311.05	82.59	350.78	28.08	4.42
UL2 2m	12.18	98.21	83.18	3.15	28.27	33.54	172.62	16.55	297.46	79.81	326.29	19.92	4.71
UL2 3m	18.57	190.97	110.62	6.10	36.18	39.10	206.62	26.81	323.18	73.69	428.32	25.55	5.71

Appendix 4.4: Rare Earth Element Concentrations (ppm) of the studied kaolins.

Bulk Samples

	La	Ce	Pr	Nd	Sm	Eu	Gd	Tb	Dy	Ho	Er	Tm	Yb	Lu
EP1 0m	98.53	167.89	18.46	59.84	8.61	1.80	6.32	1.01	6.13	1.32	3.76	0.53	3.87	0.63
EP1 2m	120.59	236.47	24.88	87.47	14.75	2.71	11.33	1.86	12.75	2.76	7.99	1.22	8.16	1.33
EP1 4m	83.57	143.62	16.00	56.51	9.02	1.80	7.00	0.92	5.61	1.04	2.73	0.36	2.83	0.46
EP2 0m	81.01	140.88	15.31	54.42	9.81	1.82	8.06	1.50	10.79	2.33	7.13	1.10	7.48	1.23
EP2 2m	133.54	256.24	27.74	97.50	15.86	3.35	11.51	1.66	9.63	1.84	4.63	0.67	4.56	0.66
EP2 2m*	134.71	258.01	27.80	97.77	16.13	3.34	11.64	1.76	9.69	1.81	4.86	0.68	4.23	0.69
EP2 4m	47.47	94.62	9.35	32.60	5.48	0.75	3.91	0.62	4.16	0.87	2.52	0.41	2.89	0.41
EP3 0m	93.83	179.87	18.07	58.42	8.65	1.57	7.44	1.22	9.35	2.20	6.72	1.01	7.47	1.12
EP3 2m	145.28	305.64	32.05	114.69	17.95	3.26	11.81	1.77	10.55	2.29	6.68	0.98	6.74	1.04
EP3 4m	165.79	360.51	40.09	152.33	23.18	4.47	14.92	1.90	9.26	1.65	4.23	0.53	3.83	0.59
LP1 0m	17.44	132.87	151.90	11.52	61.53	8.40	132.75	18.21	75.68	35.02	174.48	40.55	2.46	0.37
LP1 2m	20.14	145.48	129.86	12.19	60.68	2.74	18.02	10.74	77.13	29.33	41.55	27.93	2.49	0.23
LP1 4m	19.18	98.14	127.42	8.41	45.70	6.32	28.27	9.84	77.05	42.30	68.13	29.35	3.09	0.46
LP2 0m	15.67	209.85	160.39	8.59	44.74	4.16	33.73	7.49	69.69	36.10	70.27	20.61	2.83	0.28
LP2 2m	15.98	96.69	138.98	6.71	40.76	3.26	18.71	8.93	94.26	34.23	37.92	28.23	2.23	0.30
LP2 4m	16.68	98.39	124.18	8.45	44.96	5.80	61.80	9.33	67.69	30.45	78.46	26.16	2.25	0.28
AL1 0m	131.16	228.78	22.97	68.48	9.58	1.79	6.28	0.81	4.50	0.83	2.38	0.35	2.48	0.35
AL1 1m	49.25	80.48	9.09	30.25	4.90	1.03	3.95	0.67	4.58	0.97	2.95	0.44	2.97	0.47
AL1 2m	29.53	53.19	5.50	16.62	2.90	0.55	1.93	0.38	2.23	0.52	1.42	0.23	1.68	0.26
AL2 0m	41.19	69.57	7.27	23.04	3.60	0.58	2.14	0.28	1.84	0.38	1.10	0.18	1.28	0.19
AL2 1m	71.69	137.48	15.25	51.30	7.51	1.24	3.96	0.57	2.92	0.52	1.39	0.28	1.72	0.22
AL2 2m	126.11	239.55	25.33	84.71	12.80	2.21	7.53	0.95	5.31	0.95	2.82	0.42	2.79	0.36
UL1 0m	70.65	121.55	13.43	46.85	7.52	1.66	5.75	0.83	5.06	1.04	2.86	0.45	2.67	0.42
UL1 1m	102.48	174.15	19.69	71.53	11.86	2.53	8.83	1.20	6.45	1.14	3.08	0.45	2.82	0.39
UL1 2m	122.49	206.55	22.60	77.87	13.77	2.83	11.15	1.49	9.45	1.76	4.95	0.66	4.73	0.67
UL2 0m	93.30	163.20	18.05	64.27	10.15	2.08	6.87	0.98	5.38	1.01	2.97	0.42	2.77	0.40

UL2 1m	113.02	191.73	21.70	75.00	12.77	2.54	9.15	1.19	6.78	1.30	3.36	0.47	3.19	0.45
UL2 2m	73.70	131.87	14.75	52.03	9.27	1.73	7.20	1.05	6.53	1.31	3.72	0.54	3.98	0.67
UL2 3m	85.76	167.80	18.98	69.82	13.10	2.63	10.30	1.42	8.37	1.69	4.56	0.65	4.41	0.66

EP2 2m*: duplicate sample

Silt Fraction

	La	Ce	Pr	Nd	Sm	Eu	Gd	Tb	Dy	Ho	Er	Tm	Yb	Lu
EP3 2m	48.86	85.09	10.41	36.87	7.22	1.55	8.84	1.98	15.52	3.61	11.22	1.78	12.59	2.02
LP1 0m	55.28	99.93	10.84	38.44	6.16	1.05	6.31	1.07	7.94	1.89	5.98	0.96	6.75	0.99
AL1 2m	12.06	23.45	2.51	9.79	2.46	0.48	3.14	0.70	5.16	1.26	3.81	0.71	4.75	0.82
UL2 2m	27.55	52.31	5.83	20.62	3.84	0.70	3.55	0.67	4.83	1.10	3.58	0.52	4.19	0.67

Clay Fraction

	La	Ce	Pr	Nd	Sm	Eu	Gd	Tb	Dy	Ho	Er	Tm	Yb	Lu
EP1 0m	122.33	216.25	23.17	76.24	11.38	2.20	6.68	0.80	3.64	0.62	1.50	0.15	1.10	0.18
EP1 2m	133.57	272.51	27.12	94.73	14.08	2.75	10.33	1.24	5.98	1.04	2.65	0.29	2.06	0.30
EP1 4m	64.72	108.64	11.19	38.36	5.43	1.36	4.34	0.62	2.43	0.52	1.15	0.18	0.82	0.13
EP2 0m	98.57	176.62	18.63	64.61	9.81	2.04	7.23	0.89	4.17	0.68	1.76	0.23	1.36	0.19
EP2 2m	139.22	288.62	29.30	105.75	16.81	3.51	11.65	1.40	6.89	0.98	1.84	0.18	1.18	0.15
EP2 4m	97.51	188.77	18.21	59.49	8.51	1.61	4.92	0.56	2.96	0.43	1.10	0.13	1.02	0.14
EP3 0m	118.18	238.29	23.20	75.47	9.89	1.84	5.40	0.73	3.40	0.60	1.41	0.19	1.24	0.21
EP3 2m	173.34	376.78	38.09	134.55	19.54	3.65	11.33	1.34	6.03	0.95	1.96	0.23	1.29	0.15
EP3 4m	180.93	412.07	44.59	169.81	27.03	5.04	15.13	1.67	7.65	1.03	2.09	0.23	1.17	0.21
LP1 0m	348.15	727.78	65.27	209.52	28.21	5.01	17.76	1.75	6.04	0.85	1.47	0.21	0.99	0.14
LP1 2m	45.18	87.66	8.64	30.29	5.19	1.02	4.00	0.49	2.49	0.45	1.13	0.16	0.81	0.18
LP1 4m	63.05	117.94	9.60	29.22	4.18	0.94	2.98	0.36	2.31	0.44	0.91	0.17	1.20	0.13

LP2 0m	74.23	114.26	9.02	25.11	3.20	0.61	2.03	0.35	1.58	0.33	0.91	0.09	0.92	0.11
LP2 2m	42.66	82.40	6.57	21.03	3.17	0.77	1.91	0.33	1.79	0.35	1.00	0.19	0.97	0.13
LP2 4m	203.94	399.96	32.03	95.29	8.91	1.28	3.95	0.50	2.56	0.45	0.98	0.11	0.88	0.10
AL1 0m	133.73	235.19	23.42	69.90	9.99	1.84	6.29	0.81	4.64	0.80	2.06	0.30	2.06	0.29
AL1 1m	122.16	196.05	21.21	68.67	10.41	2.11	7.97	1.18	7.34	1.40	4.06	0.62	4.23	0.61
AL1 2m	107.28	185.44	18.27	55.73	8.14	1.51	5.68	0.78	4.85	0.99	2.90	0.44	2.94	0.43
AL2 0m	102.15	169.76	16.98	53.29	7.49	1.46	4.85	0.65	3.30	0.56	1.61	0.23	1.63	0.24
AL2 1m	153.63	285.92	31.77	106.06	14.34	2.79	8.55	1.07	5.83	0.97	2.52	0.37	2.58	0.34
AL2 2m	146.03	277.56	28.81	95.86	13.16	2.39	8.09	1.07	5.68	0.94	2.50	0.37	2.41	0.34
UL1 0m	113.47	196.80	20.78	67.77	10.75	2.19	7.41	0.89	4.90	0.90	2.57	0.33	2.18	0.34
UL1 1m	122.15	215.81	22.27	78.07	13.39	2.49	8.82	1.23	5.56	1.04	2.63	0.34	2.56	0.33
UL1 2m	150.92	248.62	23.96	78.53	12.89	2.60	9.30	1.30	7.83	1.51	4.17	0.56	4.04	0.53
UL2 0m	132.20	232.66	24.08	83.10	13.12	2.55	8.51	1.16	6.00	0.96	2.67	0.39	2.32	0.30
UL2 1m	134.60	232.94	24.39	84.10	13.11	2.61	9.06	1.18	6.19	1.08	2.61	0.37	2.60	0.34
UL2 2m	109.24	191.90	18.65	61.15	9.45	2.00	6.26	0.72	4.17	0.72	1.75	0.25	1.69	0.23
UL2 3m	116.07	218.87	23.61	84.12	13.75	2.97	9.76	1.22	6.72	1.13	2.86	0.46	2.54	0.38

Appendix 5.1: Normalised Absolute REE Concentrations (ppm) of the clay fractions of the studied kaolins.

	La	Ce	Pr	Nd	Sm	Eu	Gd	Tb	Dy	Ho	Er	Tm	Yb	Lu
EP1 0m	370.70	245.73	206.88	127.06	62.85	31.81	26.83	17.10	12.01	8.84	7.49	5.12	5.52	5.26
EP1 2m	404.74	309.67	242.10	157.88	77.76	39.86	41.47	26.35	19.74	14.86	13.25	9.50	10.30	8.91
EP1 4m	196.11	123.45	99.91	63.93	30.00	19.74	17.41	13.28	8.02	7.44	5.75	5.92	4.08	3.72
EP2 0m	298.68	200.70	166.34	107.68	54.17	29.57	29.02	18.88	13.75	9.69	8.80	7.63	6.78	5.63
EP2 2m	421.88	327.98	261.61	176.24	92.85	50.87	46.79	29.68	22.72	13.97	9.18	5.95	5.88	4.43
EP2 4m	295.47	214.51	162.54	99.14	47.02	23.31	19.76	11.84	9.77	6.20	5.51	4.22	5.10	3.97
EP3 0m	358.12	270.78	207.14	125.78	54.61	26.59	21.69	15.47	11.20	8.53	7.03	6.23	6.18	6.03
EP3 2m	525.26	428.16	340.04	224.24	107.93	52.90	45.48	28.53	19.88	13.50	9.80	7.57	6.45	4.43
EP3 4m	548.26	468.26	398.13	283.01	149.34	72.97	60.74	35.55	25.25	14.66	10.45	7.58	5.83	6.03
LP1 0m	1054.98	827.02	582.77	349.20	155.83	72.54	71.31	37.21	19.93	12.19	7.33	7.08	4.93	4.25
LP1 2m	136.91	99.61	77.10	50.48	28.65	14.84	16.04	10.35	8.22	6.44	5.65	5.25	4.05	5.41
LP1 4m	191.05	134.02	85.71	48.70	23.09	13.62	11.95	7.69	7.62	6.31	4.55	5.68	5.98	3.84
LP2 0m	224.92	129.84	80.49	41.84	17.65	8.78	8.15	7.38	5.20	4.77	4.54	3.15	4.60	3.28
LP2 2m	129.26	93.63	58.62	35.05	17.51	11.19	7.65	6.93	5.89	4.96	5.00	6.35	4.83	3.87
LP2 4m	617.98	454.50	285.94	158.81	49.23	18.55	15.86	10.59	8.45	6.36	4.90	3.62	4.40	2.91
AL1 0m	405.23	267.26	209.06	116.50	55.17	26.59	25.26	17.16	15.31	11.38	10.28	10.10	10.28	8.53
AL1 1m	370.18	222.78	189.38	114.44	57.49	30.51	32.01	25.17	24.21	19.99	20.30	20.60	21.13	17.96
AL1 2m	325.09	210.72	163.13	92.88	44.94	21.93	22.81	16.66	15.99	14.19	14.48	14.62	14.70	12.59
AL2 0m	309.55	192.90	151.61	88.81	41.35	21.22	19.46	13.83	10.87	7.97	8.07	7.77	8.13	7.16
AL2 1m	465.53	324.90	283.66	176.77	79.20	40.43	34.34	22.84	19.22	13.79	12.58	12.35	12.88	9.90
AL2 2m	442.52	315.40	257.23	159.77	72.68	34.64	32.47	22.80	18.73	13.39	12.48	12.32	12.03	10.09
UL1 0m	343.85	223.64	185.49	112.94	59.36	31.67	29.74	18.83	16.16	12.80	12.85	11.13	10.88	10.03
UL1 1m	370.15	245.23	198.84	130.11	73.95	36.01	35.40	26.20	18.33	14.88	13.15	11.47	12.80	9.60
UL1 2m	457.33	282.52	213.88	130.88	71.19	37.68	37.33	27.67	25.83	21.59	20.85	18.82	20.18	15.59
UL2 0m	400.61	264.38	215.00	138.50	72.46	36.88	34.16	24.69	19.80	13.72	13.33	12.90	11.58	8.94
UL2 1m	407.86	264.70	217.77	140.16	72.43	37.75	36.39	25.20	20.43	15.39	13.05	12.18	13.00	9.91
UL2 2m	331.02	218.06	166.52	101.92	52.18	28.91	25.14	15.37	13.75	10.33	8.73	8.35	8.43	6.88
UL2 3m	351.71	248.72	210.76	140.20	75.94	42.97	39.18	25.99	22.18	16.19	14.28	15.23	12.68	11.28

Appendix 5.2: Discriminant functions for major (M) and major and trace elements (MT) of the <2 µm fractions of the studied kaolins.

	Function M	Function MT
EP1 0m	-11.17	13.01
EP1 2m	-10.50	9.83
EP1 4m	-11.84	14.11
EP2 0m	-9.62	12.95
EP2 2m	-21.08	13.97
EP2 4m	-12.85	12.39
EP3 0m	-9.63	13.06
EP3 2m	-12.98	12.82
EP3 4m	-11.87	13.01
LP1 0m	-12.56	12.97
LP1 2m	-10.87	15.02
LP1 4m	-13.04	14.42
LP2 0m	-9.94	15.10
LP2 2m	-11.89	14.06
LP2 4m	-12.20	14.17
AL1 0m	-14.93	10.87
AL1 1m	-14.71	9.36
AL1 2m	-15.58	9.40
AL2 0m	-9.34	13.26
AL2 1m	-16.15	9.64
AL2 2m	-15.31	9.19
UL1 0m	-15.54	11.08
UL1 1m	-14.34	11.07
UL1 2m	-14.31	10.29
UL2 0m	-10.46	12.43
UL2 1m	-14.76	9.97
UL2 2m	-14.99	11.04
UL2 3m	-13.85	17.62

Appendix 7.1: Backscattered images of detrital zircons within the studied Lakiri kaolins.

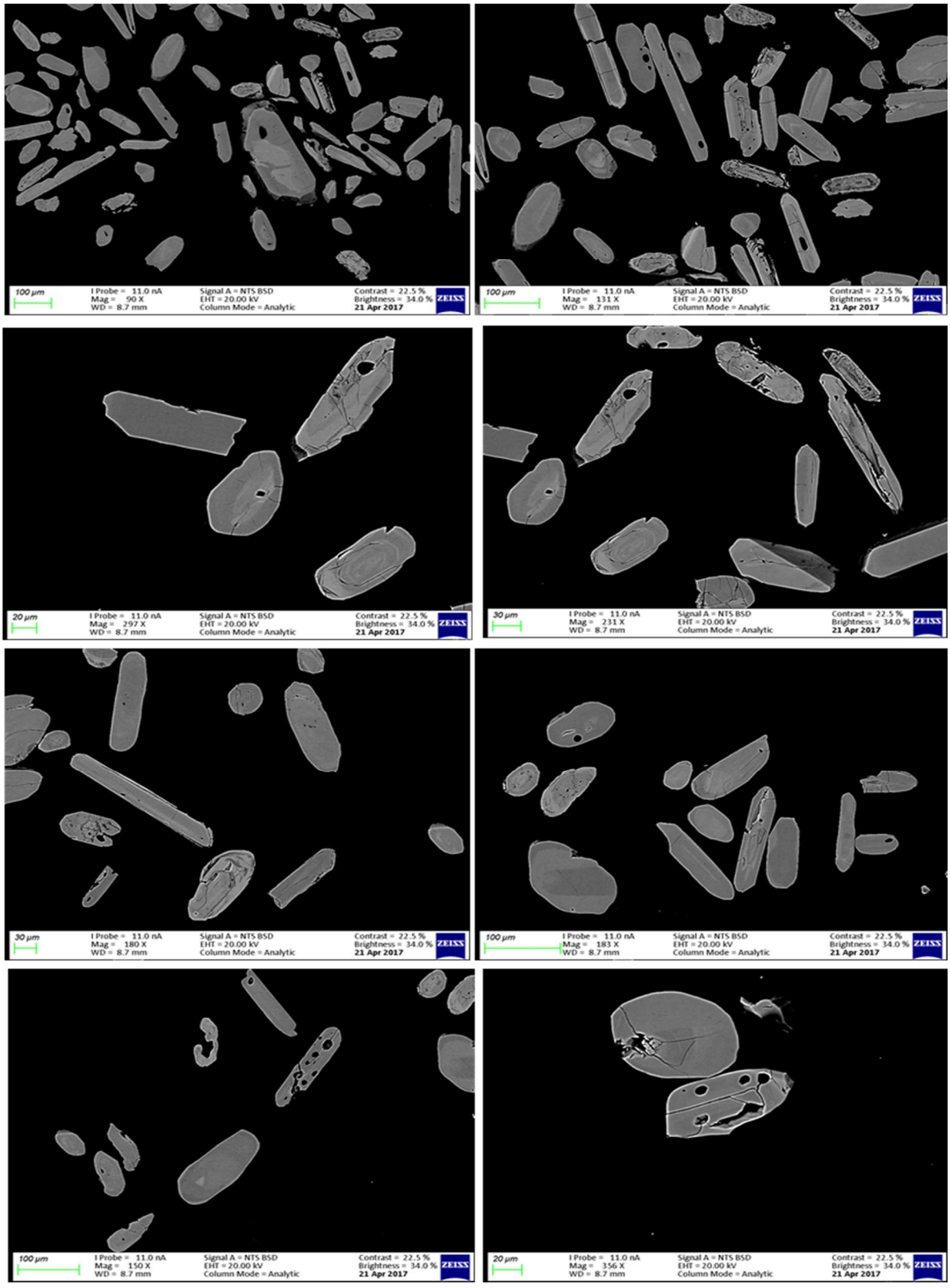

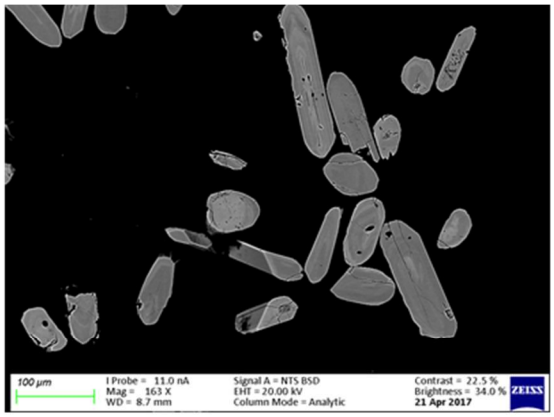

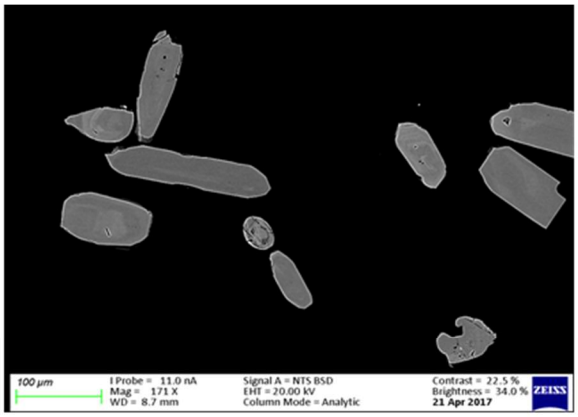

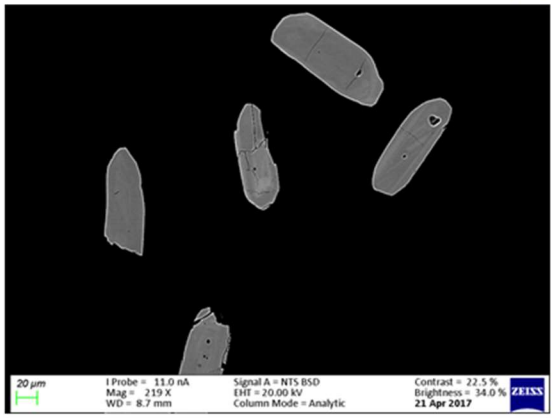

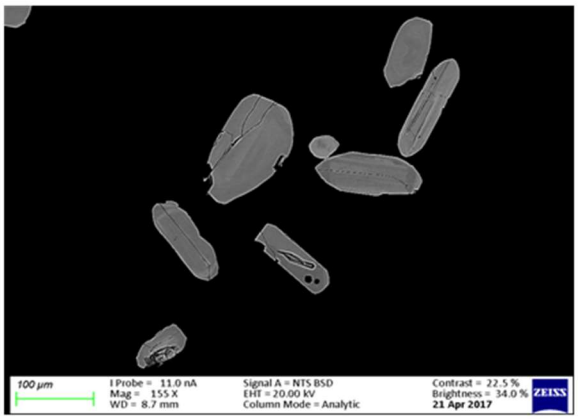

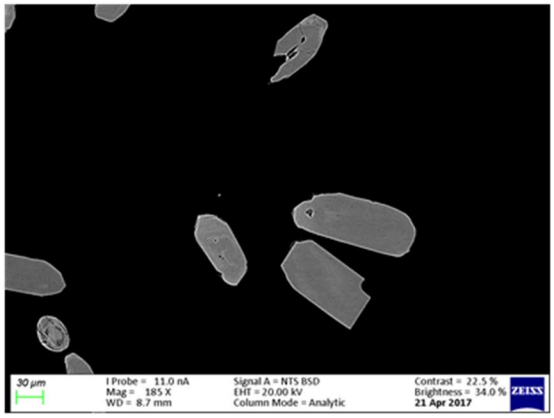

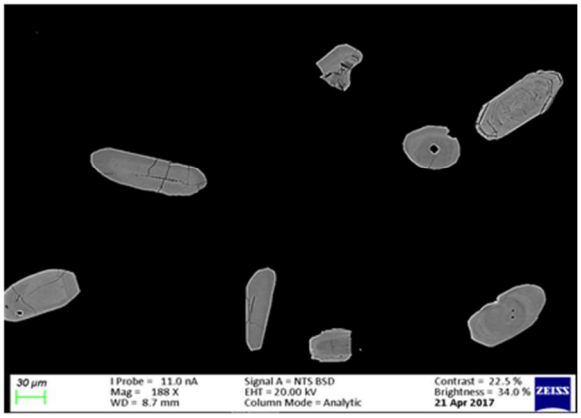

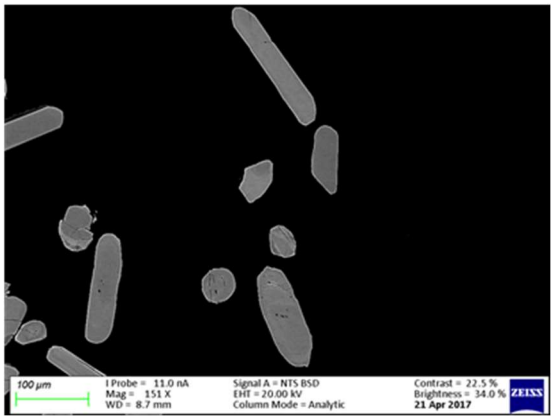

Appendix 7.2: Backscattered images of detrital zircons within the studied Eruku kaolins.

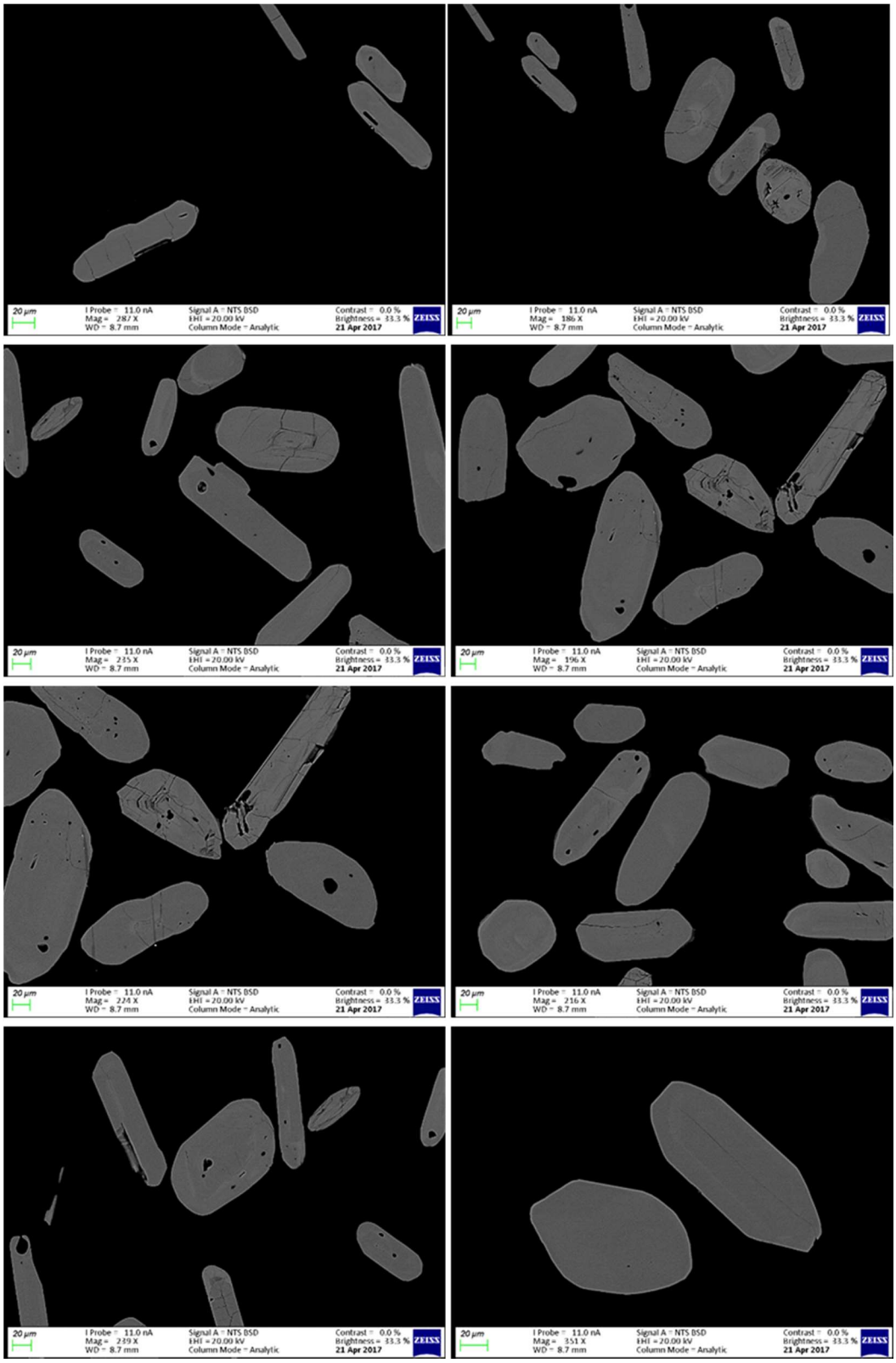

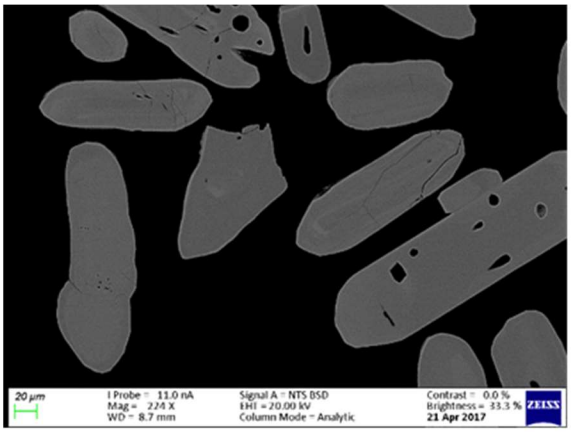

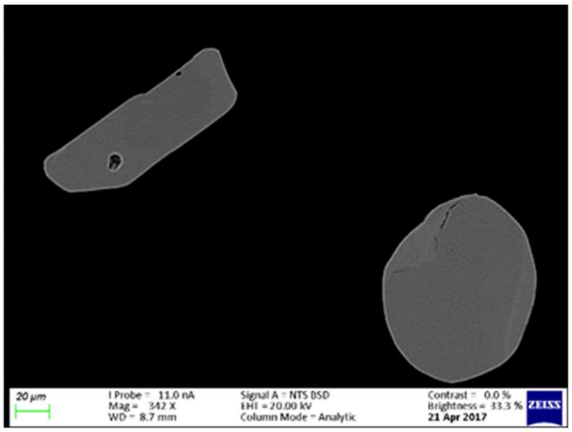

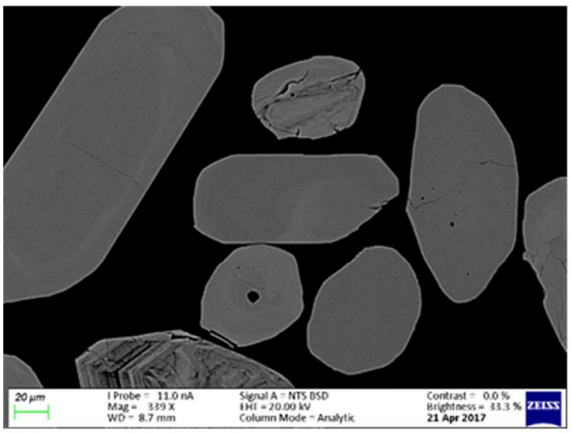

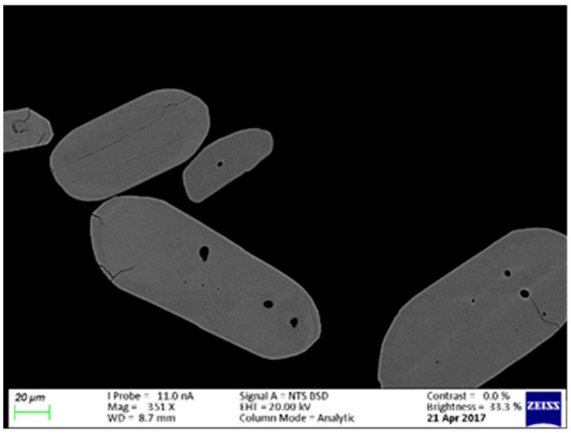

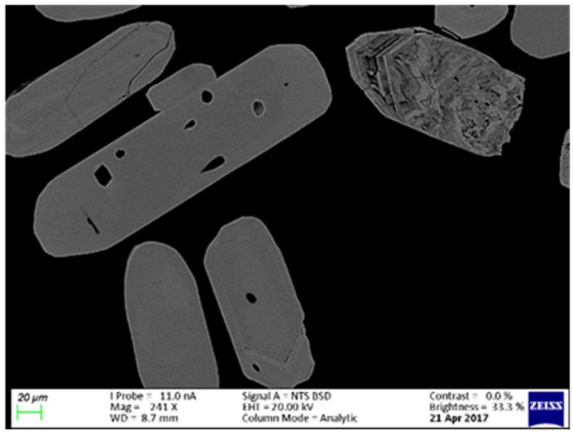

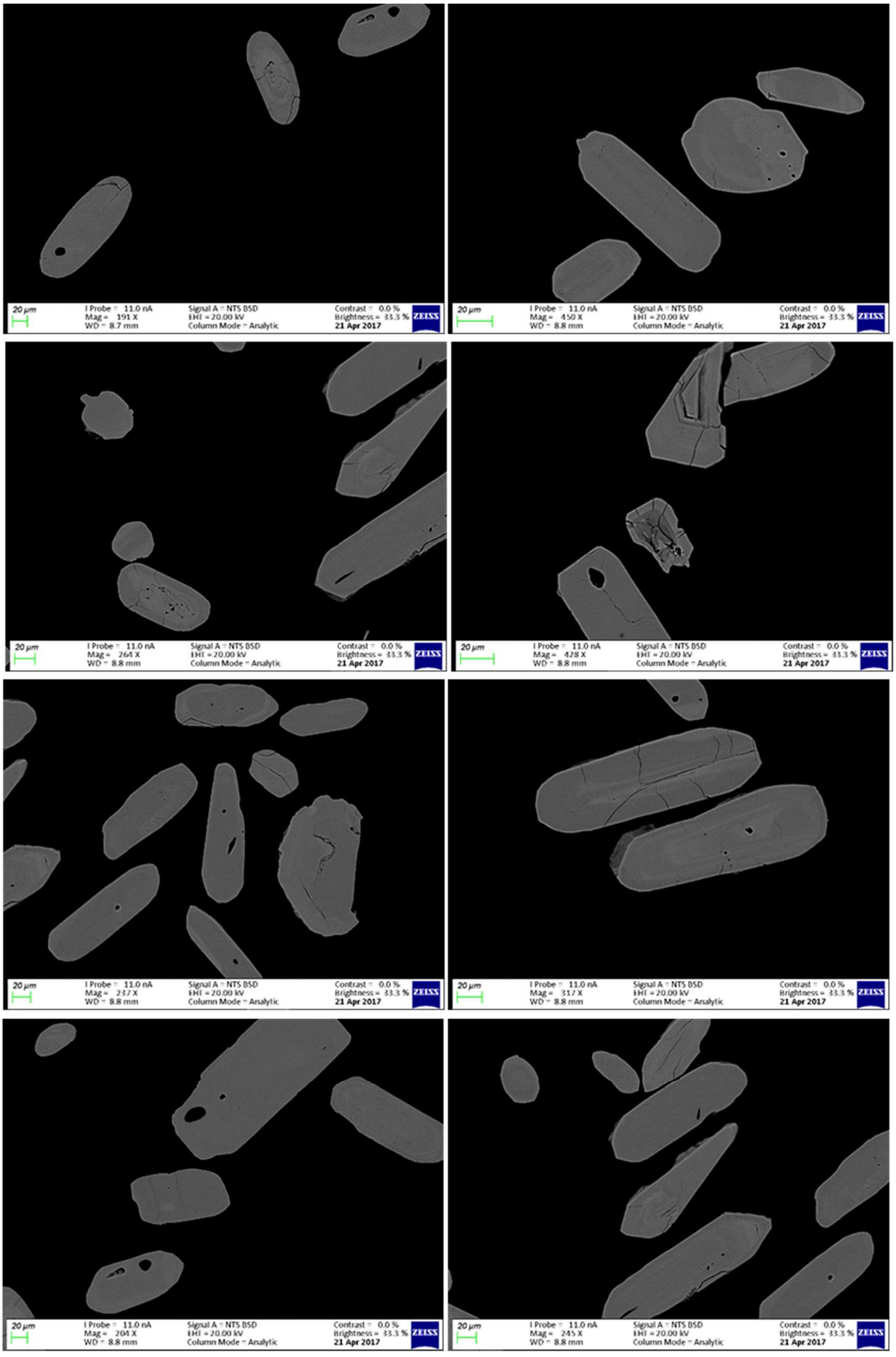

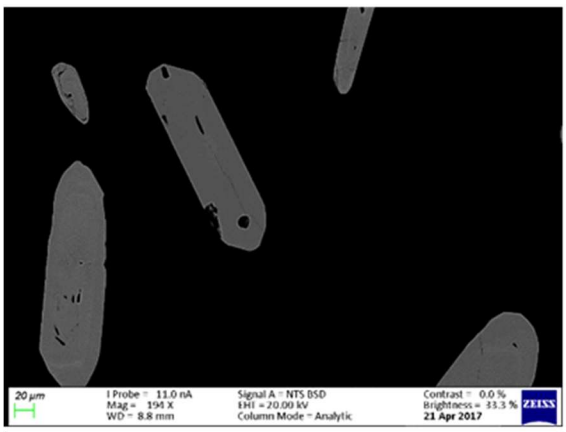

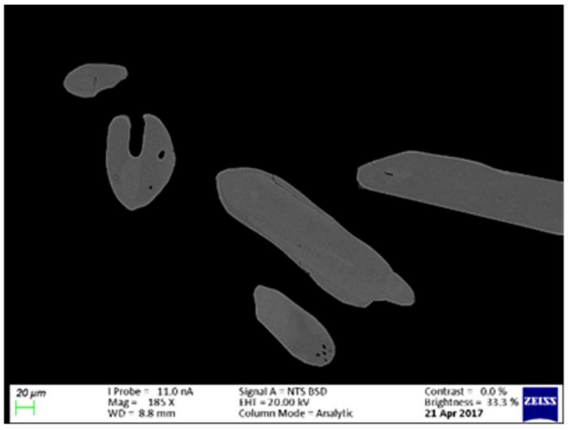

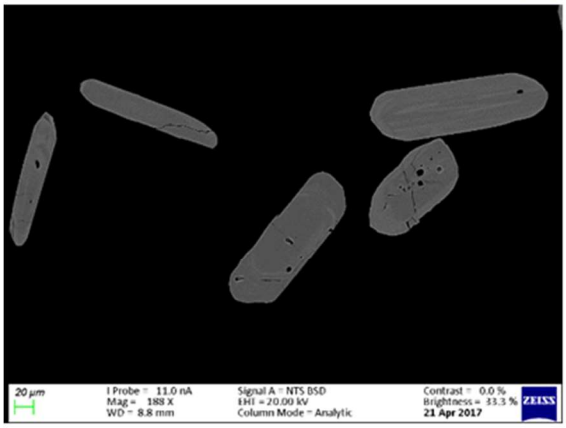

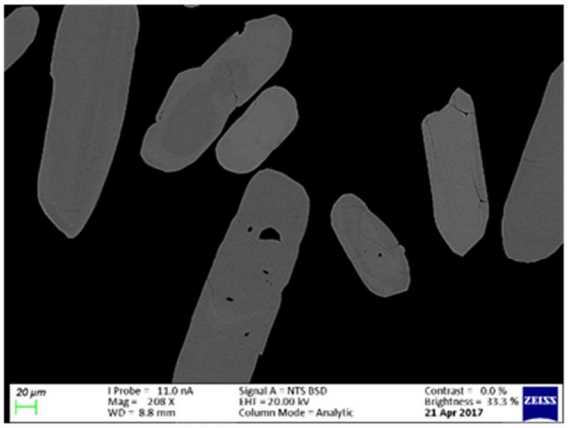

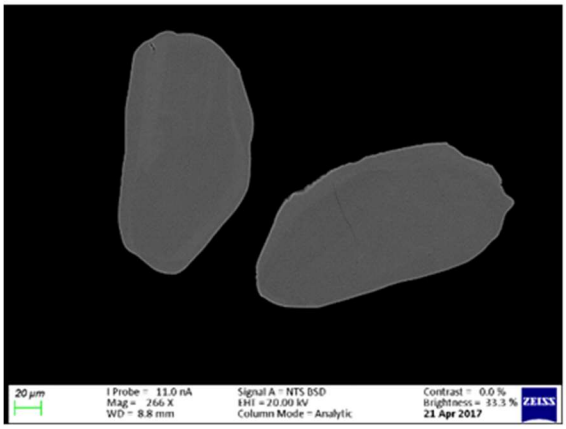

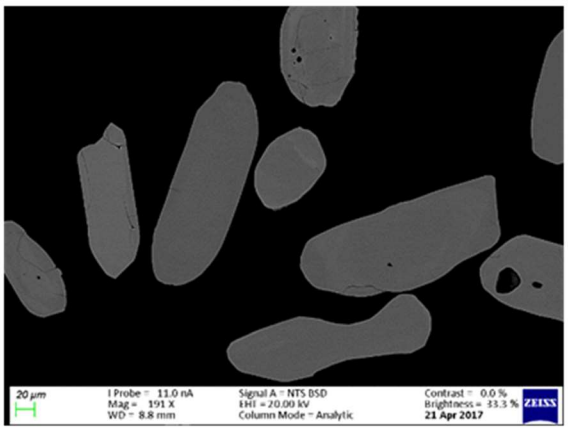

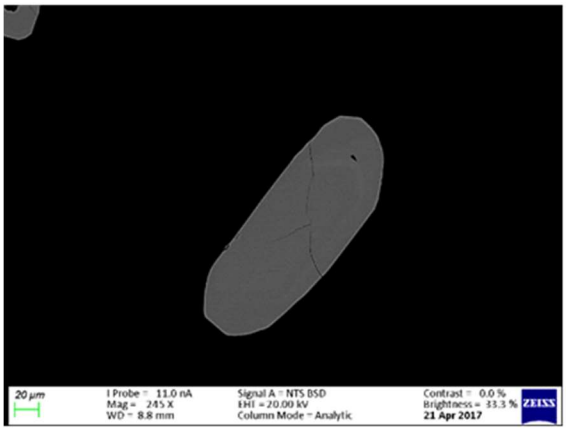

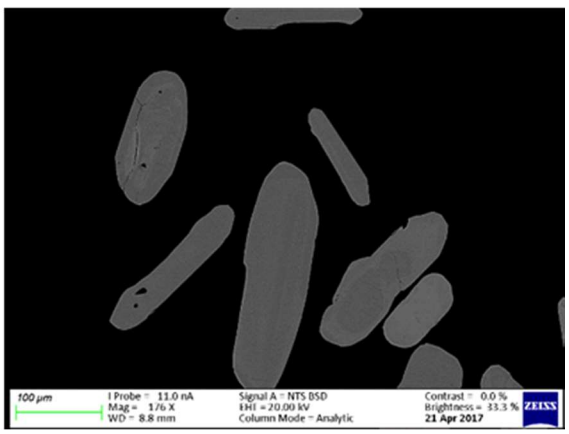

XX

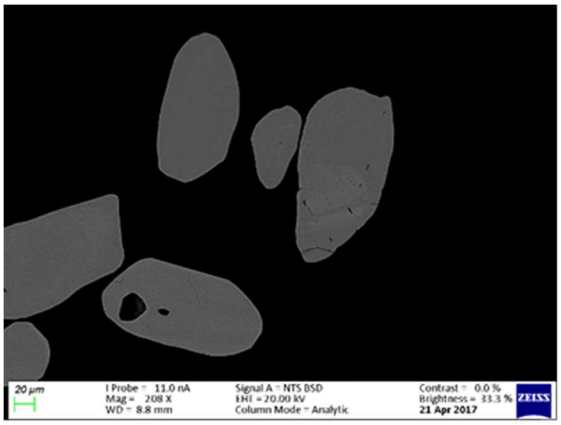

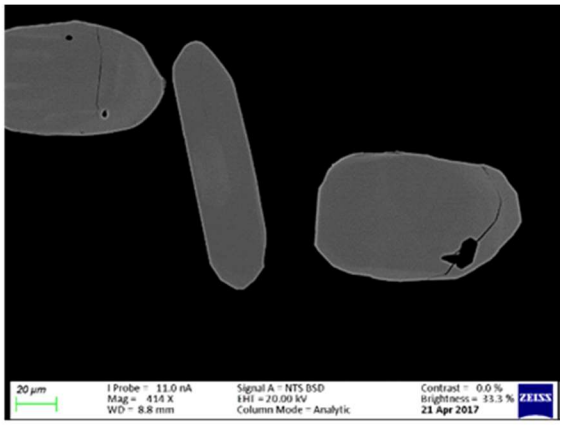

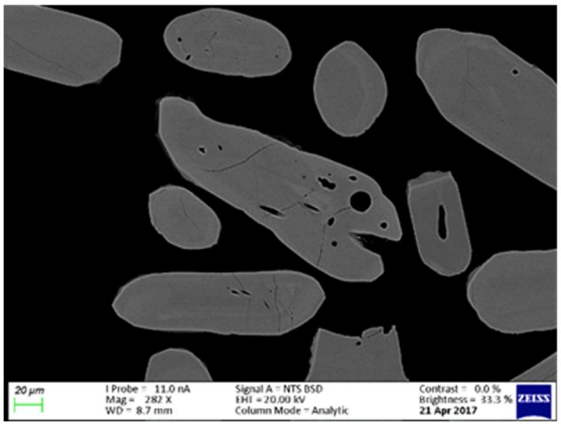

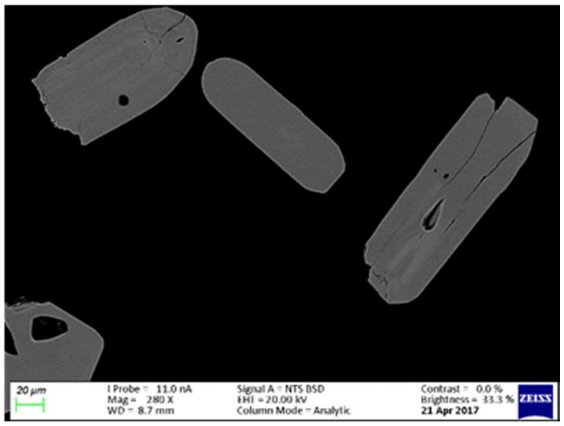

Appendix 7.3: Backscattered images of detrital zircons within the studied Awo-Omama kaolins.

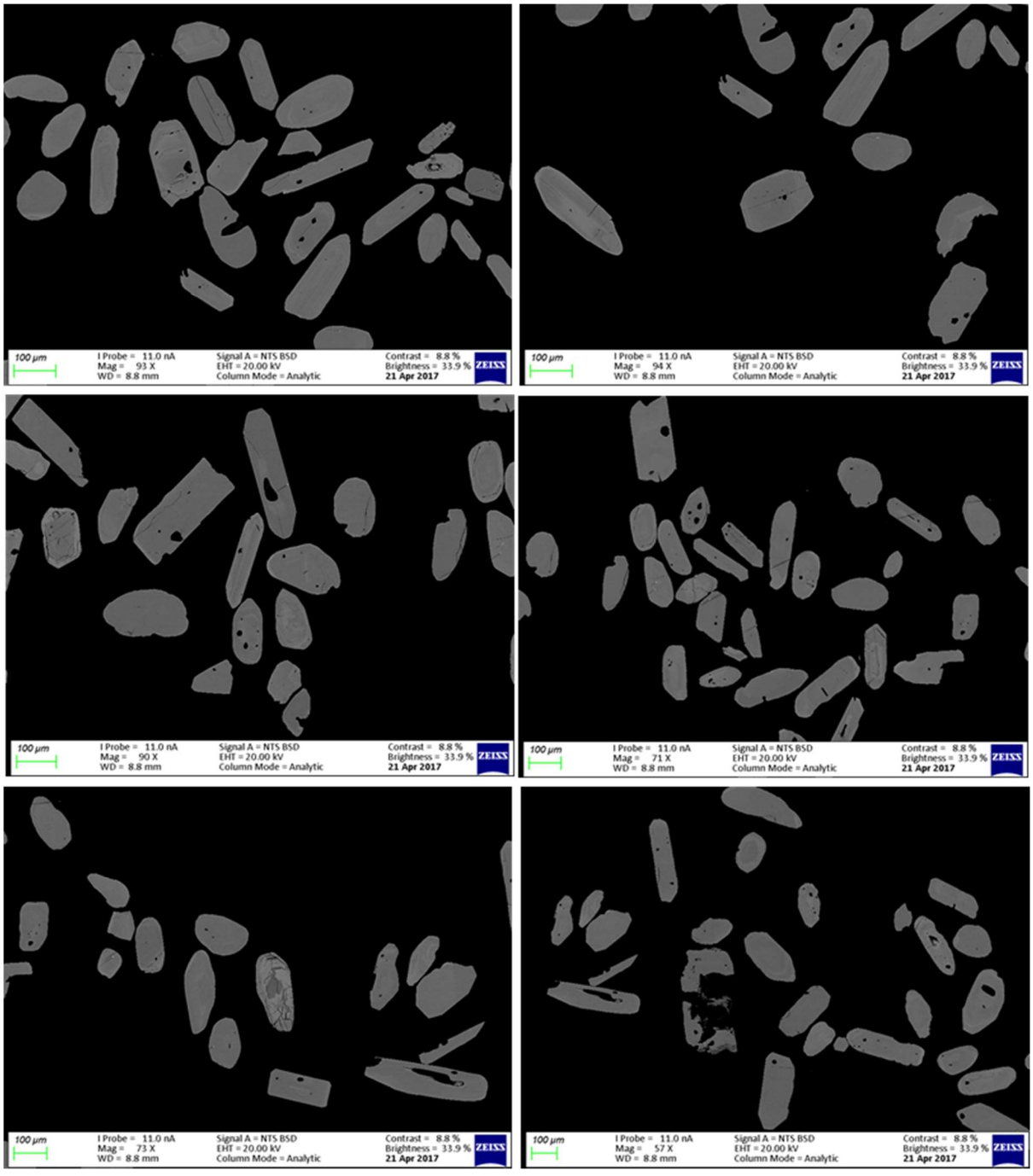

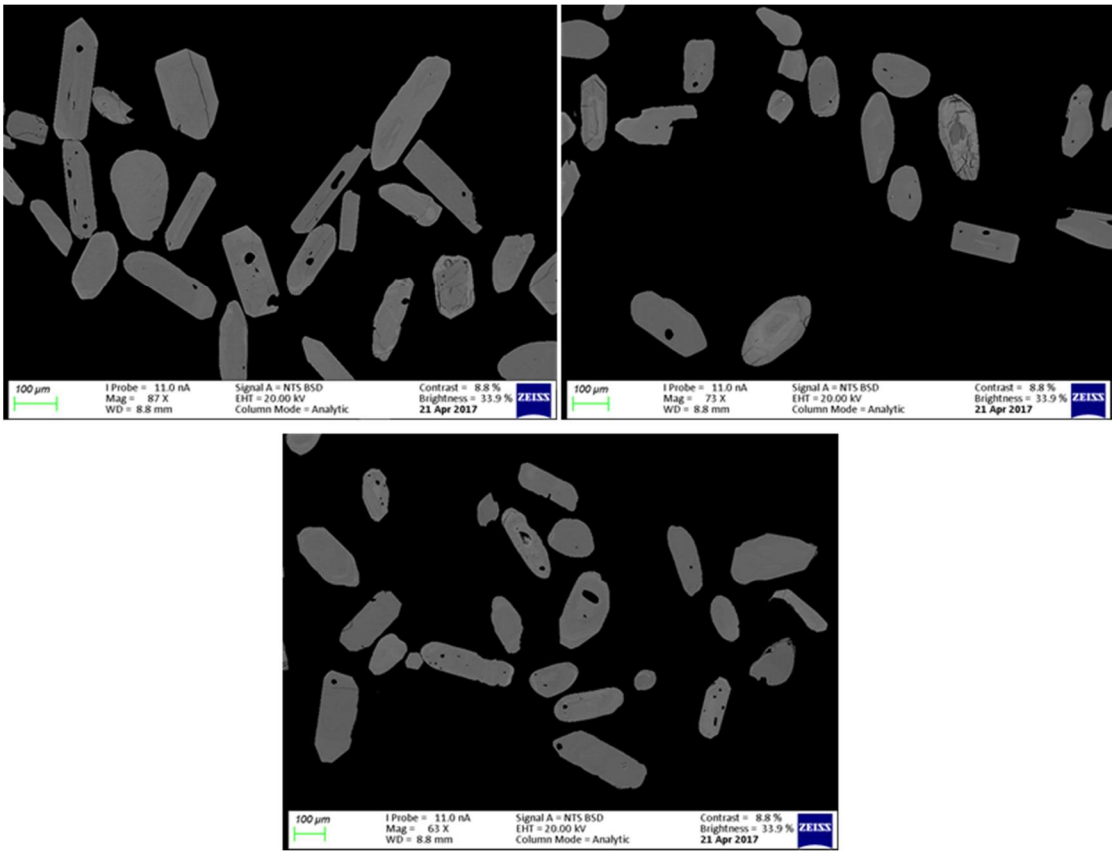

Appendix 7.4: Backscattered images of detrital zircons within the studied Ubulu-Uku kaolins.

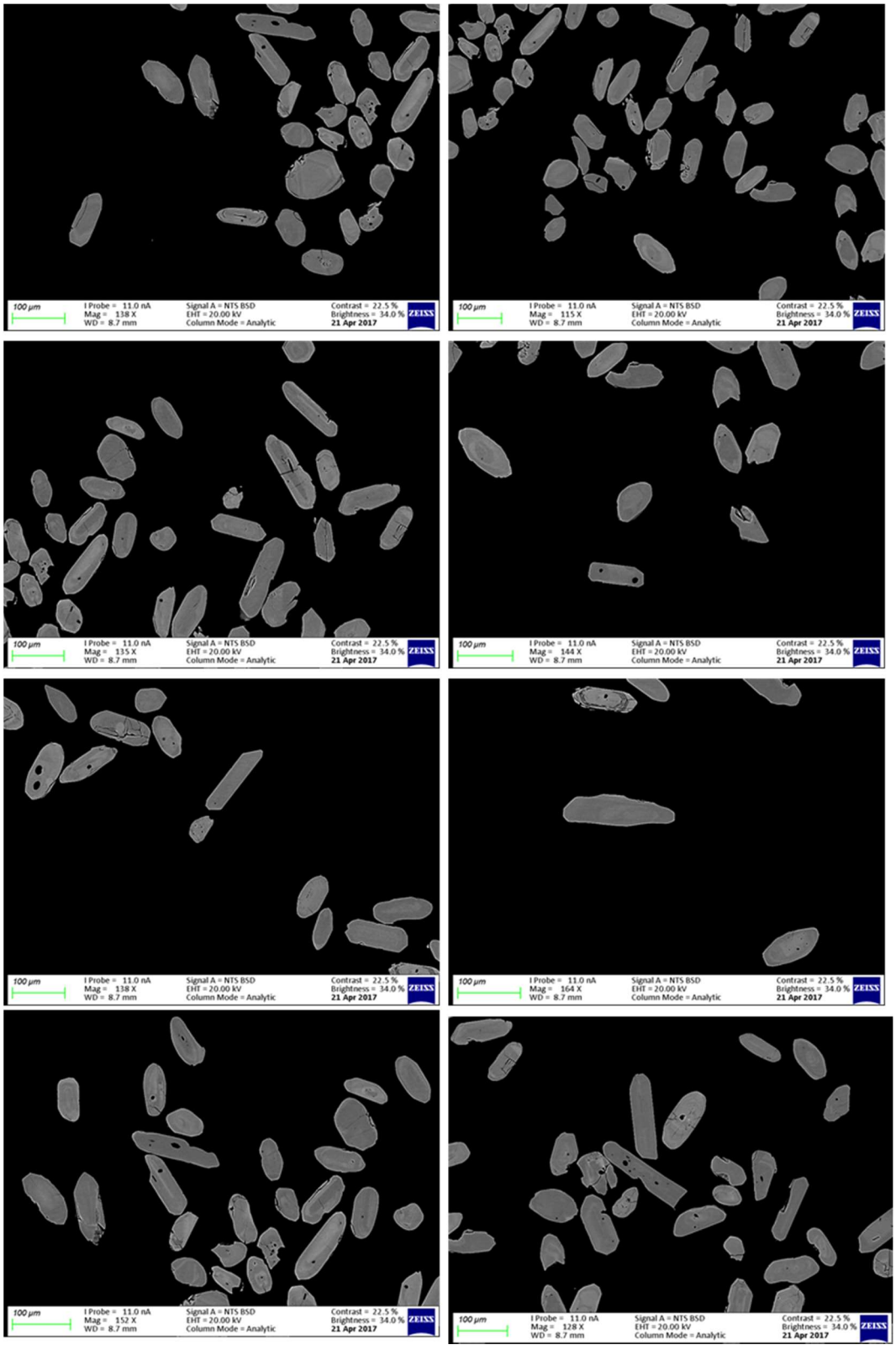

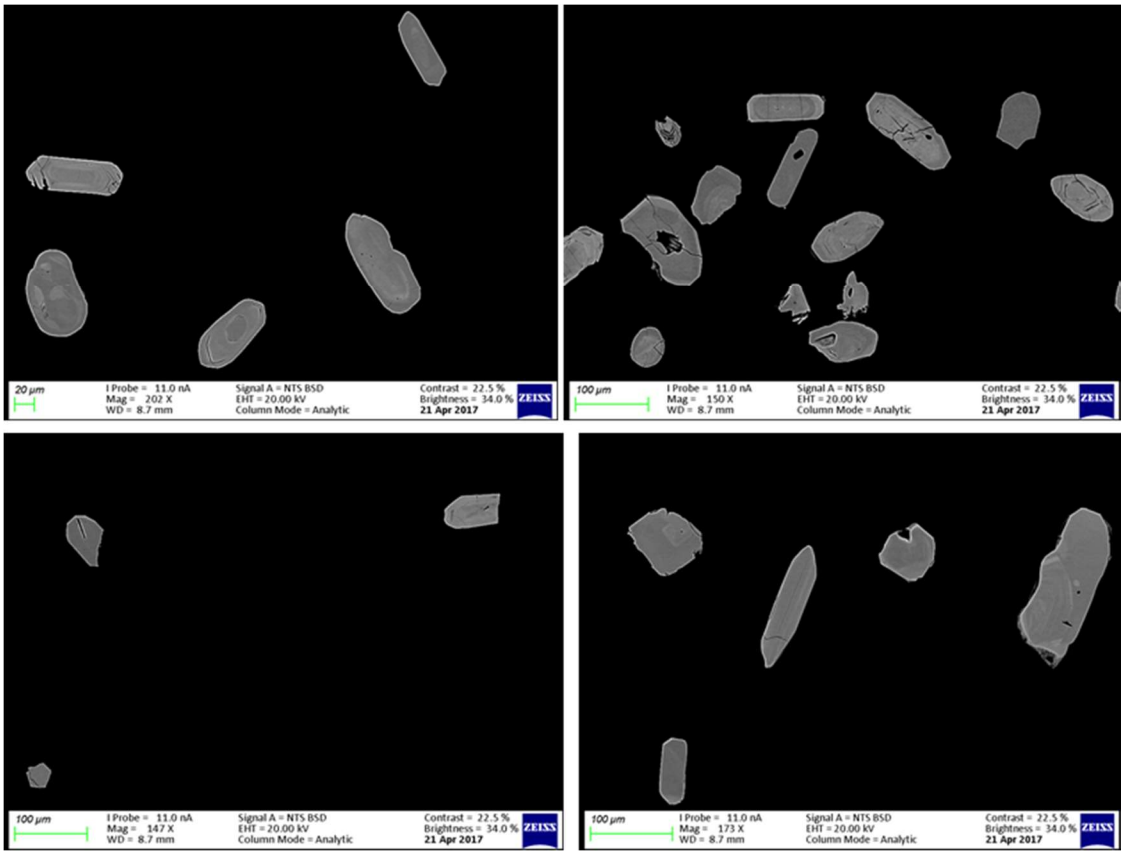

Appendix 7.5: Summary of LA-SF-ICP-MS data of GJ1, Pleosovice and M127 reference standards.

						RATIOS							AGES [Ma]						
Analysis	Sample	U [ppm][a]	Pb [ppm][a]	Th/U[a]	*206/204*	$^{207}Pb/^{235}U$[b]	2 σ[d]	$^{206}Pb/^{238}U$[b]	2 σ[d]	rho[c]	$^{207}Pb/^{206}Pb$[e]	2 σ[d]	$^{207}Pb/^{235}U$	2 σ	$^{206}Pb/^{238}U$	2 σ	$^{207}Pb/^{206}Pb$	2 σ	Conc.%
GJ1_001.FIN2	GJ1	312	28	0.03	710	0.8060	0.0140	0.0981	0.0007	0.3846	0.0597	0.0010	599	8	603	4	580	36	104
GJ1_002.FIN2	GJ1	279	25	0.03	-40	0.8130	0.0120	0.0976	0.0006	0.2040	0.0606	0.0009	604	7	600	4	609	31	99
GJ1_003.FIN2	GJ1	279	25	0.03	170	0.8130	0.0120	0.0978	0.0006	0.1296	0.0604	0.0010	604	7	601	4	601	35	100
GJ1_019.FIN2	GJ1	293	27	0.03	410	0.8320	0.0110	0.0985	0.0006	0.0612	0.0613	0.0009	614	6	606	3	637	30	95
GJ1_020.FIN2	GJ1	279	25	0.03	580	0.8170	0.0110	0.0975	0.0006	0.1505	0.0608	0.0009	605	6	600	3	621	31	97
GJ1_036.FIN2	GJ1	286	25	0.03	960	0.8140	0.0110	0.0975	0.0006	0.1709	0.0605	0.0009	604	6	600	4	606	31	99
GJ1_037.FIN2	GJ1	285	27	0.03	370	0.8150	0.0130	0.0977	0.0006	0.2421	0.0605	0.0009	604	7	601	4	606	33	99
GJ1_053.FIN2	GJ1	289	27	0.03	710	0.8080	0.0110	0.0978	0.0006	0.1360	0.0599	0.0009	601	6	602	3	585	33	103
GJ1_054.FIN2	GJ1	288	25	0.03	700	0.8150	0.0110	0.0978	0.0006	0.0825	0.0602	0.0009	604	6	602	4	602	31	100
GJ1_070.FIN2	GJ1	289	28	0.03	470	0.8090	0.0120	0.0983	0.0006	0.2070	0.0596	0.0009	601	7	604	4	572	34	106
GJ1_071.FIN2	GJ1	290	26	0.03	1000	0.8180	0.0120	0.0983	0.0006	0.1648	0.0601	0.0009	606	7	604	3	593	33	102
GJ1_087.FIN2	GJ1	288	25	0.03	620	0.8130	0.0130	0.0981	0.0006	0.2718	0.0601	0.0009	603	7	603	3	590	34	102
GJ1_088.FIN2	GJ1	283	25	0.03	880	0.8130	0.0120	0.0974	0.0006	0.1452	0.0606	0.0009	603	7	599	3	609	34	98
GJ1_104.FIN2	GJ1	283	26	0.03	570	0.8270	0.0130	0.0981	0.0006	0.1343	0.0614	0.0010	611	7	603	4	635	35	95
GJ1_105.FIN2	GJ1	283	24	0.03	430	0.8070	0.0120	0.0974	0.0006	0.2219	0.0603	0.0009	600	7	599	4	601	32	100
GJ1_121.FIN2	GJ1	282	24	0.03	1040	0.8130	0.0120	0.0979	0.0006	0.2650	0.0604	0.0009	603	7	602	3	607	31	99
GJ1_122.FIN2	GJ1	284	26	0.03	300	0.8220	0.0120	0.0976	0.0005	0.2023	0.0613	0.0009	608	7	600	3	639	31	94
GJ1_138.FIN2	GJ1	286	25	0.03	940	0.8100	0.0130	0.0983	0.0006	0.2805	0.0601	0.0009	602	7	604	4	590	33	102
GJ1_139.FIN2	GJ1	287	26	0.03	490	0.8140	0.0120	0.0981	0.0007	0.2500	0.0605	0.0008	604	6	603	4	608	30	99
GJ1_155.FIN2	GJ1	293	26	0.03	520	0.8150	0.0130	0.0975	0.0006	0.2497	0.0608	0.0010	604	8	600	4	617	35	97
GJ1_156.FIN2	GJ1	290	25	0.03	710	0.8100	0.0120	0.0980	0.0006	0.3285	0.0601	0.0009	602	7	602	4	593	32	102
GJ1_172.FIN2	GJ1	287	26	0.03	340	0.8180	0.0130	0.0976	0.0005	0.1404	0.0608	0.0010	606	7	600	3	618	35	97
GJ1_173.FIN2	GJ1	285	25	0.03	930	0.8090	0.0120	0.0980	0.0005	0.2392	0.0599	0.0009	601	7	603	3	587	31	103
GJ1_189.FIN2	GJ1	288	27	0.03	610	0.8080	0.0110	0.0980	0.0006	0.2581	0.0596	0.0008	600	6	603	4	581	30	104
GJ1_190.FIN2	GJ1	291	25	0.03	620	0.8170	0.0130	0.0979	0.0006	0.1179	0.0604	0.0009	606	7	602	4	611	33	99
GJ1_206.FIN2	GJ1	287	27	0.03	920	0.8150	0.0120	0.0972	0.0006	0.0841	0.0606	0.0009	605	7	598	4	617	34	97
GJ1_207.FIN2	GJ1	288	27	0.03	450	0.8220	0.0110	0.0981	0.0006	0.2285	0.0610	0.0008	609	6	603	4	627	29	96

GJ1_223.FIN2	GJ1	286	27	0.03	490	0.8180	0.0120	0.0982	0.0006	0.1601	0.0603	0.0009	606	7	604	4	603	33	100
GJ1_224.FIN2	GJ1	293	27	0.03	960	0.8100	0.0110	0.0979	0.0006	0.2850	0.0599	0.0008	602	6	602	3	589	30	102
GJ1_240.FIN2	GJ1	290	27	0.03	420	0.8180	0.0130	0.0977	0.0006	0.3220	0.0606	0.0009	607	7	601	3	612	33	98
GJ1_241.FIN2	GJ1	286	25	0.03	380	0.8260	0.0130	0.0978	0.0007	0.2663	0.0611	0.0009	611	7	601	4	632	34	95
GJ1_257.FIN2	GJ1	289	25	0.03	350	0.8090	0.0130	0.0980	0.0006	0.1363	0.0598	0.0010	601	7	603	4	587	35	103
GJ1_258.FIN2	GJ1	289	26	0.03	470	0.8090	0.0120	0.0979	0.0006	0.0285	0.0600	0.0010	601	7	602	4	593	34	102
GJ1_274.FIN2	GJ1	285	25	0.03	630	0.8240	0.0120	0.0982	0.0006	0.1089	0.0609	0.0009	610	7	604	4	624	35	97
GJ1_275.FIN2	GJ1	284	25	0.03	1150	0.8240	0.0120	0.0980	0.0006	0.0628	0.0611	0.0009	609	7	602	3	625	33	96
GJ1_291.FIN2	GJ1	283	25	0.03	640	0.8090	0.0120	0.0974	0.0006	0.1412	0.0602	0.0010	601	7	599	4	598	35	100
GJ1_292.FIN2	GJ1	286	29	0.03	920	0.8150	0.0110	0.0970	0.0007	0.1949	0.0610	0.0009	605	6	597	4	628	31	95
GJ1_308.FIN2	GJ1	283	24	0.03	890	0.8160	0.0100	0.0986	0.0006	0.1746	0.0601	0.0008	605	6	606	3	603	28	101
GJ1_309.FIN2	GJ1	287	26	0.03	680	0.8170	0.0120	0.0978	0.0006	0.0865	0.0608	0.0010	605	7	602	3	615	35	98
GJ1_325.FIN2	GJ1	287	25	0.03	860	0.8160	0.0120	0.0982	0.0006	0.2692	0.0605	0.0009	605	7	604	4	610	31	99
GJ1_326.FIN2	GJ1	290	27	0.03	340	0.8070	0.0120	0.0972	0.0006	0.3010	0.0602	0.0008	600	7	598	4	603	31	99
GJ1_342.FIN2	GJ1	287	26	0.03	440	0.8130	0.0120	0.0981	0.0006	0.2142	0.0602	0.0009	603	7	603	4	599	33	101
GJ1_343.FIN2	GJ1	292	26	0.03	480	0.8140	0.0120	0.0982	0.0007	0.1895	0.0602	0.0009	604	7	604	4	597	33	101
GJ1_359.FIN2	GJ1	286	27	0.03	410	0.8090	0.0120	0.0979	0.0006	0.1949	0.0600	0.0009	601	7	602	4	588	34	102
GJ1_360.FIN2	GJ1	285	24	0.03	370	0.7970	0.0130	0.0971	0.0007	0.2911	0.0595	0.0009	594	7	597	4	573	34	104
GJ1_376.FIN2	GJ1	291	26	0.03	1250	0.8080	0.0110	0.0986	0.0006	0.2563	0.0596	0.0008	601	6	606	4	574	31	106
GJ1_377.FIN2	GJ1	286	25	0.03	340	0.8260	0.0130	0.0976	0.0006	0.1302	0.0614	0.0010	610	7	600	3	635	34	95
GJ1_393.FIN2	GJ1	284	25	0.03	830	0.8100	0.0120	0.0971	0.0006	0.1706	0.0604	0.0009	602	7	598	4	602	33	99
GJ1_394.FIN2	GJ1	285	24	0.03	740	0.8190	0.0130	0.0982	0.0006	0.1760	0.0604	0.0010	606	7	604	4	600	36	101
GJ1_410.FIN2	GJ1	285	26	0.03	870	0.8250	0.0110	0.0982	0.0006	0.1951	0.0606	0.0008	610	6	604	4	613	29	99
GJ1_411.FIN2	GJ1	290	26	0.03	670	0.8360	0.0100	0.0980	0.0006	0.2064	0.0615	0.0007	616	6	603	3	649	26	93
GJ1_427.FIN2	GJ1	285	26	0.03	790	0.8190	0.0120	0.0983	0.0006	0.1450	0.0604	0.0009	607	7	604	3	611	31	99
GJ1_428.FIN2	GJ1	284	27	0.03	1030	0.8130	0.0120	0.0976	0.0006	0.3139	0.0603	0.0009	603	7	600	4	600	32	100
GJ1_444.FIN2	GJ1	295	27	0.03	940	0.8130	0.0130	0.0978	0.0006	0.2609	0.0604	0.0010	603	7	602	4	600	34	100
GJ1_445.FIN2	GJ1	292	26	0.03	650	0.8040	0.0130	0.0975	0.0006	0.1520	0.0600	0.0010	599	7	600	4	589	36	102
GJ1_461.FIN2	GJ1	289	27	0.03	470	0.8120	0.0130	0.0975	0.0006	0.1571	0.0604	0.0010	603	7	600	4	609	36	98
GJ1_462.FIN2	GJ1	289	26	0.03	740	0.8200	0.0130	0.0978	0.0006	0.2750	0.0610	0.0010	608	7	602	4	627	34	96
GJ1_478.FIN2	GJ1	288	26	0.03	-70	0.8110	0.0120	0.0983	0.0006	0.0768	0.0600	0.0009	603	7	605	4	596	34	101
GJ1_479.FIN2	GJ1	289	26	0.03	500	0.8140	0.0120	0.0977	0.0006	0.2482	0.0607	0.0009	604	7	601	4	612	33	98
GJ1_495.FIN2	GJ1	287	25	0.03	580	0.8190	0.0120	0.0981	0.0006	0.2632	0.0607	0.0009	606	7	603	4	617	31	98
GJ1_496.FIN2	GJ1	281	26	0.03	780	0.8030	0.0120	0.0976	0.0007	0.1789	0.0597	0.0009	597	7	601	4	577	34	104

GJ1_512.FIN2	GJ1	292	26	0.03	570	0.8200	0.0150	0.0978	0.0007	0.0010	0.0610	0.0012	608	9	602	4	624	43	96
GJ1_513.FIN2	GJ1	282	25	0.03	630	0.8130	0.0140	0.0980	0.0006	0.1143	0.0603	0.0011	603	8	602	4	603	39	100
GJ1_529.FIN2	GJ1	288	26	0.03	770	0.8040	0.0140	0.0978	0.0007	0.2567	0.0599	0.0010	598	8	601	4	583	37	103
GJ1_530.FIN2	GJ1	284	25	0.03	560	0.8250	0.0130	0.0976	0.0007	0.0988	0.0616	0.0010	610	7	600	4	648	35	93
GJ1_546.FIN2	GJ1	295	26	0.03	490	0.8170	0.0160	0.0978	0.0009	0.0901	0.0607	0.0012	606	9	602	5	612	45	98
GJ1_547.FIN2	GJ1	277	26	0.03	520	0.8120	0.0160	0.0982	0.0008	0.2949	0.0597	0.0011	603	9	604	5	584	41	103
A_004.FIN2	Plesovice	639	93	0.10	485	0.3911	0.0070	0.0538	0.0004	0.2213	0.0528	0.0009	336	5	338	3	307	39	110
A_021.FIN2	Plesovice	628	91	0.10	760	0.3979	0.0076	0.0537	0.0004	0.0281	0.0538	0.0011	340	6	337	2	349	45	97
A_038.FIN2	Plesovice	711	102	0.11	760	0.3962	0.0069	0.0538	0.0004	0.1510	0.0534	0.0010	339	5	338	3	334	41	101
A_055.FIN2	Plesovice	792	125	0.11	760	0.3955	0.0061	0.0538	0.0004	0.2522	0.0532	0.0008	338	4	338	2	330	34	102
A_072.FIN2	Plesovice	736	103	0.10	660	0.3991	0.0077	0.0542	0.0005	0.1995	0.0536	0.0011	341	6	340	3	344	47	99
A_089.FIN2	Plesovice	652	91	0.10	600	0.4020	0.0110	0.0543	0.0005	0.2565	0.0538	0.0014	343	8	341	3	349	57	98
A_106.FIN2	Plesovice	704	97	0.11	630	0.4024	0.0077	0.0537	0.0005	0.0385	0.0546	0.0012	343	6	337	3	380	50	89
A_123.FIN2	Plesovice	653	92	0.10	640	0.3990	0.0130	0.0544	0.0006	0.2315	0.0536	0.0017	341	9	341	3	343	68	99
A_174.FIN2	Plesovice	538	80	0.10	510	0.3930	0.0100	0.0530	0.0005	0.4152	0.0538	0.0013	336	8	333	3	349	54	95
A_222.FIN2	Plesovice	841	123	0.11	830	0.3930	0.0090	0.0533	0.0006	0.2783	0.0535	0.0012	336	7	335	4	337	50	99
A_310.FIN2	Plesovice	648	87	0.10	1020	0.3940	0.0110	0.0535	0.0006	0.2844	0.0536	0.0015	337	8	336	4	339	60	99
A_344.FIN2	Plesovice	720	100	0.10	790	0.3830	0.0140	0.0529	0.0006	0.5296	0.0526	0.0017	329	10	332	4	300	71	111
A_480.FIN2	Plesovice	683	99	0.10	380	0.3877	0.0056	0.0534	0.0003	0.1634	0.0528	0.0008	332	4	335	2	310	33	108
A_514.FIN2	Plesovice	540	75	0.10	620	0.3980	0.0062	0.0537	0.0004	0.2539	0.0540	0.0009	340	5	337	2	361	36	93
A_049.FIN2	M127	893	954	0.50	300	0.6770	0.0100	0.0842	0.0008	0.1808	0.0582	0.0009	524	6	521	5	532	35	98
A_099.FIN2	M127	809	877	0.52	700	0.6782	0.0084	0.0848	0.0005	0.2655	0.0582	0.0007	525	5	525	3	534	26	98
A_148.FIN2	M127	814	875	0.50	1400	0.6881	0.0074	0.0845	0.0006	0.2352	0.0593	0.0007	531	5	523	3	573	25	91
A_196.FIN2	M127	818	876	0.49	-500	0.6816	0.0089	0.0847	0.0006	0.4030	0.0583	0.0007	527	5	524	3	543	25	96
A_244.FIN2	M127	887	924	0.49	400	0.6749	0.0098	0.0840	0.0006	0.1309	0.0582	0.0009	523	6	520	4	531	34	98
A_293.FIN2	M127	770	846	0.50	600	0.6806	0.0075	0.0852	0.0005	0.3505	0.0580	0.0006	527	5	527	3	523	23	101
A_337.FIN2	M127	740	833	0.49	700	0.6700	0.0110	0.0840	0.0007	0.3196	0.0580	0.0009	520	7	520	4	527	33	99
A_385.FIN2	M127	876	902	0.49	1400	0.6710	0.0140	0.0838	0.0009	0.3480	0.0580	0.0011	521	9	519	5	526	43	99

Appendix 7.6: Summary of LA-SF-ICP-MS data of detrital zircons within Lakiri kaolins.

						RATIOS							AGES [Ma]						
Analysis	Sample	U [ppm][a]	Pb [ppm][a]	Th/U[a]	*206/204*	$^{207}Pb/^{235}U$[b]	2 σ[d]	$^{206}Pb/^{238}U$[b]	2 σ[d]	rho[c]	$^{207}Pb/^{206}Pb$[e]	2 σ[d]	$^{207}Pb/^{235}U$	2 σ	$^{206}Pb/^{238}U$	2 σ	$^{207}Pb/^{206}Pb$	2 σ	Conc.%
A_417.FIN2	LAKIRI	32	84	0.28	126	6.5900	0.1400	0.3788	0.0039	0.4061	0.1261	0.0025	2053	19	2070	18	2037	36	102
A_418.FIN2	LAKIRI	77	144	0.69	75	0.9600	0.0390	0.1042	0.0013	0.1385	0.0668	0.0027	679	20	639	8	796	91	80
A_419.FIN2	LAKIRI	220	1327	0.68	1330	6.1240	0.0580	0.3551	0.0027	0.5435	0.1246	0.0011	1993	8	1958	13	2021	15	97
A_420.FIN2	LAKIRI	120	547	0.51	780	7.1630	0.0830	0.3759	0.0029	0.4363	0.1379	0.0015	2130	10	2057	13	2197	19	94
A_421.FIN2	LAKIRI	116	143	0.21	360	5.8400	0.1200	0.3153	0.0045	0.7492	0.1336	0.0017	1947	17	1766	22	2143	23	82
A_422.FIN2	LAKIRI	209	1780	0.99	1240	6.6350	0.0750	0.3721	0.0036	0.7011	0.1288	0.0015	2063	10	2039	17	2083	19	98
A_423.FIN2	LAKIRI	481	592	0.15	3510	6.4390	0.0490	0.3523	0.0022	0.6157	0.1324	0.0008	2037	7	1945	10	2128	11	91
A_424.FIN2	LAKIRI	443	983	0.92	600	0.8560	0.0130	0.1021	0.0008	0.3451	0.0607	0.0009	627	7	627	5	618	31	101
A_425.FIN2	LAKIRI	454	746	0.20	3100	5.7810	0.0420	0.3377	0.0025	0.5739	0.1240	0.0009	1943	6	1875	12	2013	13	93
A_426.FIN2	LAKIRI	506	1946	0.44	3150	6.3350	0.0510	0.3624	0.0025	0.6558	0.1266	0.0009	2023	7	1993	12	2050	12	97
A_429.FIN2	LAKIRI	154	922	0.67	770	6.2600	0.1100	0.3386	0.0048	0.7360	0.1340	0.0016	2010	15	1879	23	2148	20	87
A_430.FIN2	LAKIRI	379	990	0.35	2000	5.4580	0.0580	0.3210	0.0025	0.6259	0.1232	0.0010	1893	9	1795	12	2005	14	90
A_431.FIN2	LAKIRI	66	316	1.99	117	0.7990	0.0370	0.0941	0.0013	0.0312	0.0613	0.0028	591	21	580	8	600	98	97
A_432.FIN2	LAKIRI	598	793	0.16	4500	7.0200	0.1200	0.3812	0.0050	0.8868	0.1336	0.0011	2111	15	2081	24	2144	14	97
A_433.FIN2	LAKIRI	681	4187	0.75	3900	6.3100	0.0470	0.3595	0.0026	0.6490	0.1271	0.0007	2019	7	1980	13	2059	10	96
A_434.FIN2	LAKIRI	207	444	0.24	1430	6.5120	0.0710	0.3589	0.0029	0.5342	0.1313	0.0011	2046	10	1976	14	2115	16	93
A_435.FIN2	LAKIRI	187	992	0.60	1090	7.0130	0.0930	0.3888	0.0042	0.6551	0.1312	0.0014	2111	12	2116	20	2111	19	100
A_436.FIN2	LAKIRI	755	1006	0.19	3700	5.4890	0.0620	0.3235	0.0027	0.8116	0.1230	0.0008	1897	10	1806	13	1998	12	90
A_437.FIN2	LAKIRI	366	795	0.30	600	5.5670	0.0870	0.3231	0.0040	0.7508	0.1249	0.0012	1909	13	1804	19	2027	18	89
A_438.FIN2	LAKIRI	323	2950	1.14	1150	6.2000	0.0830	0.3516	0.0036	0.8632	0.1280	0.0010	2003	12	1942	17	2069	14	94
A_439.FIN2	LAKIRI	523	1414	0.33	1700	5.7270	0.0470	0.3300	0.0023	0.6479	0.1261	0.0008	1935	7	1838	11	2042	11	90
A_440.FIN2	LAKIRI	122	183	0.59	260	0.8620	0.0230	0.0936	0.0010	0.0153	0.0668	0.0019	629	13	577	6	808	61	71
A_441.FIN2	LAKIRI	367	251	0.39	600	0.8120	0.0180	0.0949	0.0015	0.3196	0.0624	0.0014	602	10	585	9	669	48	87
A_442.FIN2	LAKIRI	47	79	0.69	70	0.9260	0.0430	0.1019	0.0015	0.0989	0.0670	0.0035	662	23	625	9	750	110	83
A_443.FIN2	LAKIRI	153	514	1.31	320	0.8310	0.0240	0.1009	0.0011	0.2526	0.0600	0.0017	612	13	620	6	574	60	108
A_446.FIN2	LAKIRI	283	3324	1.17	1300	8.6510	0.0780	0.4033	0.0033	0.5701	0.1554	0.0012	2301	8	2184	15	2404	13	91

A_447.FIN2	LAKIRI	647	3250	0.57	3400	6.2890	0.0630	0.3613	0.0034	0.7024	0.1260	0.0009	2016	9	1988	16	2042	13	97
A_448.FIN2	LAKIRI	506	3010	0.56	9400	10.3020	0.0920	0.4546	0.0040	0.6984	0.1638	0.0011	2462	8	2415	18	2497	12	97
A_449.FIN2	LAKIRI	421	1532	0.39	1200	5.8840	0.0680	0.3399	0.0033	0.6118	0.1256	0.0011	1958	10	1886	16	2036	15	93
A_450.FIN2	LAKIRI	36	81	0.77	59	1.4900	0.2000	0.1092	0.0038	0.3076	0.0970	0.0110	901	72	668	22	1430	210	47
A_451.FIN2	LAKIRI	255	689	1.03	390	0.8190	0.0200	0.0937	0.0009	0.3865	0.0632	0.0014	606	11	577	5	697	47	83
A_452.FIN2	LAKIRI	256	312	0.17	1570	5.3140	0.0510	0.3141	0.0026	0.5977	0.1226	0.0010	1870	8	1761	13	1992	15	88
A_453.FIN2	LAKIRI	336	195	0.07	2800	6.1110	0.0660	0.3505	0.0026	0.4628	0.1263	0.0012	1991	10	1937	12	2048	17	95
A_454.FIN2	LAKIRI	71	391	0.68	180	4.3790	0.0570	0.2939	0.0023	0.2649	0.1078	0.0014	1706	11	1661	11	1756	25	95
A_455.FIN2	LAKIRI	178	242	0.56	10	0.7730	0.0190	0.0934	0.0010	0.2779	0.0602	0.0015	580	11	576	6	592	55	97
A_456.FIN2	LAKIRI	175	451	1.07	1200	2.4440	0.0810	0.1848	0.0029	0.7212	0.0956	0.0023	1252	24	1093	16	1530	46	71
A_457.FIN2	LAKIRI	982	610	0.55	1350	0.7760	0.0130	0.0865	0.0009	0.7267	0.0651	0.0010	583	7	535	5	774	32	69
A_458.FIN2	LAKIRI	98	789	0.73	1200	9.0900	0.1000	0.4263	0.0035	0.4220	0.1545	0.0017	2346	10	2289	16	2393	19	96
A_459.FIN2	LAKIRI	227	129	0.06	3000	5.5790	0.0670	0.3210	0.0026	0.6018	0.1263	0.0012	1911	10	1795	12	2045	17	88
A_460.FIN2	LAKIRI	179	789	0.44	3700	7.1010	0.0740	0.3779	0.0028	0.6237	0.1364	0.0011	2123	9	2066	13	2180	14	95
A_463.FIN2	LAKIRI	346	264	0.09	4100	4.6810	0.0800	0.2826	0.0042	0.8545	0.1204	0.0011	1761	14	1603	21	1960	16	82
A_464.FIN2	LAKIRI	196	1379	2.85	400	0.7820	0.0180	0.0917	0.0010	0.2936	0.0617	0.0013	585	10	566	6	646	45	88
A_465.FIN2	LAKIRI	60	297	1.97	60	0.7840	0.0420	0.0942	0.0015	0.2757	0.0600	0.0030	582	24	580	9	560	110	104
A_466.FIN2	LAKIRI	56	275	1.98	61	0.8450	0.0430	0.0939	0.0014	0.2309	0.0656	0.0032	619	24	579	8	730	110	79
A_467.FIN2	LAKIRI	107	1329	1.35	1050	6.3800	0.0950	0.3599	0.0034	0.4030	0.1288	0.0019	2028	13	1982	16	2077	27	95
A_468.FIN2	LAKIRI	1212	1261	0.28	2600	4.1380	0.0600	0.2450	0.0039	0.9227	0.1231	0.0008	1660	12	1412	20	2001	11	71
A_469.FIN2	LAKIRI	123	595	0.61	570	3.9100	0.1100	0.2239	0.0041	0.8149	0.1271	0.0021	1611	22	1302	21	2052	29	63
A_470.FIN2	LAKIRI	118	266	0.79	190	0.7600	0.0180	0.0933	0.0010	0.2081	0.0594	0.0014	572	11	575	6	561	55	103
A_471.FIN2	LAKIRI	354	1255	0.40	2000	5.1950	0.0510	0.3051	0.0023	0.6649	0.1240	0.0009	1851	9	1716	11	2013	13	85
A_472.FIN2	LAKIRI	66	382	2.19	260	0.7650	0.0260	0.0952	0.0011	0.1562	0.0587	0.0020	576	15	586	6	519	74	113
A_473.FIN2	LAKIRI	196	1728	0.87	200	8.2770	0.0890	0.3982	0.0031	0.4599	0.1516	0.0015	2261	10	2160	14	2363	17	91
A_474.FIN2	LAKIRI	106	1375	1.23	1850	8.4270	0.0970	0.4027	0.0033	0.5781	0.1527	0.0015	2276	11	2181	15	2373	16	92
A_475.FIN2	LAKIRI	212	200	0.10	1600	6.2000	0.1200	0.3136	0.0048	0.7946	0.1442	0.0017	2005	16	1757	23	2280	19	77
A_476.FIN2	LAKIRI	402	673	0.66	1530	0.7680	0.0130	0.0940	0.0010	0.3939	0.0597	0.0009	578	7	579	6	584	34	99
A_477.FIN2	LAKIRI	61	745	1.29	330	6.4200	0.1000	0.3639	0.0034	0.3778	0.1288	0.0019	2034	14	2000	16	2073	26	96
A_481.FIN2	LAKIRI	310	626	0.22	1200	5.9740	0.0500	0.3478	0.0025	0.6463	0.1249	0.0008	1971	7	1924	12	2027	11	95
A_482.FIN2	LAKIRI	343	1104	0.41	2730	7.7590	0.0900	0.3852	0.0043	0.8409	0.1467	0.0009	2202	10	2099	20	2306	11	91
A_483.FIN2	LAKIRI	113	142	0.51	153	0.7920	0.0260	0.0933	0.0011	0.3460	0.0617	0.0019	589	15	575	7	628	67	92

A_484.FIN2	LAKIRI	770	689	0.44	1330	0.7670	0.0130	0.0883	0.0012	0.6099	0.0631	0.0009	577	8	546	7	705	30	77
A_485.FIN2	LAKIRI	671	336	0.06	5800	6.3510	0.0500	0.3503	0.0030	0.7142	0.1315	0.0008	2025	7	1936	14	2117	11	91
A_486.FIN2	LAKIRI	180	206	0.43	280	0.7720	0.0150	0.0943	0.0008	0.1734	0.0596	0.0012	581	9	581	5	567	44	102
A_487.FIN2	LAKIRI	43	179	1.59	158	0.8000	0.0340	0.0953	0.0014	0.0766	0.0613	0.0029	590	20	587	8	568	98	103
A_488.FIN2	LAKIRI	26	44	0.53	67	0.9940	0.0700	0.1037	0.0020	0.1274	0.0693	0.0049	686	35	636	12	770	150	83
A_489.FIN2	LAKIRI	174	1596	1.06	1160	6.0420	0.0820	0.3410	0.0035	0.6572	0.1280	0.0013	1982	11	1891	17	2068	18	91
A_490.FIN2	LAKIRI	207	1115	0.57	1760	6.5400	0.0720	0.3524	0.0030	0.6244	0.1341	0.0012	2051	10	1945	14	2150	16	90
A_491.FIN2	LAKIRI	314	1088	1.40	350	0.8080	0.0130	0.0961	0.0007	0.3164	0.0606	0.0009	601	7	592	4	614	33	96
A_492.FIN2	LAKIRI	19	62	0.34	88	5.4000	0.2000	0.2578	0.0058	0.4420	0.1503	0.0049	1886	29	1477	30	2362	51	63
A_493.FIN2	LAKIRI	124	357	1.15	177	0.7900	0.0240	0.0929	0.0011	0.3206	0.0613	0.0018	589	14	573	6	616	64	93
A_494.FIN2	LAKIRI	200	380	0.67	300	0.9580	0.0280	0.1083	0.0011	0.1698	0.0632	0.0017	680	14	663	7	705	61	94
A_497.FIN2	LAKIRI	42	82	0.81	70	0.8770	0.0570	0.0926	0.0017	0.1827	0.0683	0.0043	630	30	571	10	780	130	73
A_498.FIN2	LAKIRI	268	1577	0.60	2200	7.7470	0.0560	0.4006	0.0024	0.4737	0.1391	0.0010	2201	7	2171	11	2214	12	98
A_499.FIN2	LAKIRI	381	2099	0.69	2440	7.4050	0.0690	0.3674	0.0032	0.7228	0.1451	0.0010	2161	9	2016	15	2287	12	88
A_500.FIN2	LAKIRI	101	24	0.04	600	8.0600	0.1100	0.3985	0.0034	0.5397	0.1456	0.0017	2235	12	2161	16	2293	19	94
A_501.FIN2	LAKIRI	117	221	0.74	230	0.8470	0.0270	0.0970	0.0011	0.0491	0.0630	0.0021	623	16	597	6	681	74	88
A_502.FIN2	LAKIRI	235	729	0.36	1640	6.9260	0.0770	0.3654	0.0039	0.7932	0.1366	0.0010	2101	10	2007	18	2185	13	92
A_503.FIN2	LAKIRI	418	1461	1.55	840	0.8000	0.0200	0.0947	0.0008	0.2900	0.0610	0.0015	596	11	583	5	624	53	93
A_504.FIN2	LAKIRI	311	300	0.39	500	0.7770	0.0130	0.0942	0.0008	0.3824	0.0595	0.0009	583	7	580	5	574	33	101
A_505.FIN2	LAKIRI	99	287	1.20	156	0.7850	0.0250	0.0945	0.0010	0.0570	0.0602	0.0020	586	14	582	6	569	71	102
A_506.FIN2	LAKIRI	209	1348	0.78	1210	6.3980	0.0660	0.3616	0.0030	0.8994	0.1284	0.0012	2031	9	1990	14	2074	16	96
A_507.FIN2	LAKIRI	110	258	0.34	392	3.4000	0.1200	0.2201	0.0052	0.9166	0.1120	0.0018	1499	28	1280	28	1822	31	70
A_508.FIN2	LAKIRI	61	110	0.25	223	5.4400	0.3000	0.2820	0.0120	0.9224	0.1382	0.0032	1864	49	1596	59	2192	41	73
A_509.FIN2	LAKIRI	100	119	0.50	141	0.8700	0.0360	0.0970	0.0017	0.1970	0.0657	0.0028	636	20	597	10	752	91	79
A_510.FIN2	LAKIRI	256	1981	0.93	1350	7.2700	0.1500	0.3504	0.0057	0.9221	0.1503	0.0012	2140	18	1935	27	2347	14	82
A_511.FIN2	LAKIRI	376	1198	0.38	1550	6.0160	0.0480	0.3431	0.0023	0.6827	0.1273	0.0008	1977	7	1901	11	2059	11	92
A_515.FIN2	LAKIRI	282	1439	0.63	1660	6.0860	0.0520	0.3484	0.0023	0.5268	0.1272	0.0010	1988	8	1927	11	2058	13	94
A_516.FIN2	LAKIRI	1246	775	0.63	1960	1.6530	0.0200	0.1242	0.0011	0.6879	0.0968	0.0009	990	8	755	7	1562	17	48
A_517.FIN2	LAKIRI	367	772	0.90	820	0.7930	0.0200	0.0950	0.0009	0.3301	0.0605	0.0013	592	11	585	6	608	47	96
A_518.FIN2	LAKIRI	506	714	0.77	610	0.7780	0.0140	0.0906	0.0010	0.4934	0.0626	0.0010	584	8	559	6	690	33	81
A_519.FIN2	LAKIRI	749	1639	2.08	3100	4.2250	0.0800	0.2435	0.0048	0.9268	0.1264	0.0010	1676	16	1404	25	2047	13	69
A_520.FIN2	LAKIRI	283	350	0.38	1090	1.1500	0.0190	0.1256	0.0010	0.4311	0.0666	0.0010	776	9	763	6	815	31	94

A_521.FIN2	LAKIRI	290	5500	0.84	450	14.8000	1.9000	0.4780	0.0170	0.9658	0.2080	0.0160	2656	88	2515	72	2769	98	91
A_522.FIN2	LAKIRI	176	2546	1.54	1400	8.1550	0.0870	0.4057	0.0032	0.5139	0.1462	0.0014	2247	10	2195	15	2302	16	95
A_523.FIN2	LAKIRI	944	909	0.26	3050	3.3130	0.0830	0.1926	0.0045	0.9650	0.1251	0.0008	1477	20	1134	25	2029	11	56
A_524.FIN2	LAKIRI	308	821	0.34	2900	8.7500	0.1000	0.4041	0.0039	0.5732	0.1578	0.0015	2312	10	2188	18	2430	17	90
A_525.FIN2	LAKIRI	710	7060	1.42	1300	5.8300	0.1300	0.3321	0.0074	0.9597	0.1279	0.0008	1946	21	1846	36	2068	11	89
A_526.FIN2	LAKIRI	449	1060	0.28	4300	6.2840	0.0530	0.3580	0.0027	0.6712	0.1278	0.0008	2016	7	1972	13	2067	12	95
A_527.FIN2	LAKIRI	954	2940	0.94	3660	4.1300	0.1000	0.2348	0.0056	0.9748	0.1273	0.0007	1654	20	1366	31	2059	10	66
A_528.FIN2	LAKIRI	135	1755	1.35	1900	8.4000	0.1200	0.4136	0.0045	0.5244	0.1479	0.0019	2273	13	2231	21	2319	22	96
A_531.FIN2	LAKIRI	130	631	0.47	1340	9.5200	0.1000	0.4309	0.0039	0.4441	0.1611	0.0017	2388	10	2309	18	2464	18	94
A_532.FIN2	LAKIRI	145	317	0.88	190	0.7910	0.0200	0.0925	0.0010	0.2020	0.0624	0.0016	590	12	570	6	662	56	86
A_533.FIN2	LAKIRI	1044	418	0.97	850	0.7280	0.0099	0.0690	0.0006	0.3883	0.0766	0.0010	555	6	430	4	1109	26	39
A_534.FIN2	LAKIRI	683	2240	0.52	2800	6.7800	0.0550	0.3614	0.0030	0.7799	0.1366	0.0007	2082	7	1988	14	2185	9	91
A_535.FIN2	LAKIRI	388	885	0.26	4600	6.8110	0.0570	0.3618	0.0029	0.6688	0.1373	0.0010	2089	8	1990	14	2192	12	91
A_536.FIN2	LAKIRI	239	207	0.16	1510	3.6360	0.0770	0.2178	0.0036	0.8828	0.1213	0.0012	1553	17	1270	19	1972	18	64
A_537.FIN2	LAKIRI	198	410	0.91	160	0.7760	0.0210	0.0924	0.0011	0.3295	0.0612	0.0016	581	12	570	7	619	56	92
A_538.FIN2	LAKIRI	564	930	0.91	860	0.7890	0.0140	0.0885	0.0008	0.1999	0.0649	0.0012	590	8	547	5	763	39	72
A_539.FIN2	LAKIRI	478	3110	0.78	2700	5.9710	0.0570	0.3413	0.0027	0.6462	0.1273	0.0010	1971	8	1892	13	2059	13	92
A_540.FIN2	LAKIRI	173	965	0.56	1250	9.7100	0.1100	0.4346	0.0038	0.6640	0.1622	0.0014	2406	10	2326	17	2477	14	94
A_541.FIN2	LAKIRI	422	1620	0.43	2900	8.0700	0.1100	0.3798	0.0044	0.8453	0.1544	0.0011	2237	13	2075	20	2393	12	87
A_542.FIN2	LAKIRI	403	201	0.33	1220	0.7370	0.0180	0.0860	0.0008	0.3152	0.0618	0.0013	559	10	532	5	654	46	81
A_543.FIN2	LAKIRI	564	795	0.47	700	1.2030	0.0150	0.1096	0.0009	0.6047	0.0794	0.0008	801	7	671	5	1179	20	57
A_544.FIN2	LAKIRI	263	751	0.30	3300	5.8600	0.1400	0.3077	0.0054	0.9310	0.1378	0.0014	1949	22	1731	26	2196	19	79
A_545.FIN2	LAKIRI	300	531	0.66	520	0.9380	0.0170	0.1089	0.0009	0.1438	0.0625	0.0012	672	9	666	5	684	39	97

Appendix 7.7: Summary of LA-SF-ICP-MS data of detrital zircons within Eruku kaolins.

						RATIOS							AGES [Ma]						
Analysis	Sample	U [ppm][a]	Pb [ppm][a]	Th/U[a]	*206/204*	$^{207}Pb/^{235}U$[b]	2 σ[d]	$^{206}Pb/^{238}U$[b]	2 σ[d]	rho[c]	$^{207}Pb/^{206}Pb$[e]	2 σ[d]	$^{207}Pb/^{235}U$	2 σ	$^{206}Pb/^{238}U$	2 σ	$^{207}Pb/^{206}Pb$	2 σ	Conc.%
A_145.FIN2	ERUKU	182	665	1.51	121	0.8110	0.0200	0.0979	0.0009	0.0472	0.0605	0.0016	601	11	602	5	593	56	101
A_146.FIN2	ERUKU	183	834	0.54	680	7.8200	0.1100	0.3936	0.0035	0.3989	0.1451	0.0021	2209	13	2139	16	2287	25	94
A_147.FIN2	ERUKU	124	168	0.58	108	0.7910	0.0240	0.0958	0.0010	0.2245	0.0601	0.0018	589	14	591	6	572	64	103
A_149.FIN2	ERUKU	258	1302	0.71	950	6.0700	0.1000	0.3275	0.0038	0.6382	0.1348	0.0017	1984	14	1826	18	2160	22	85
A_150.FIN2	ERUKU	44	200	1.93	43	0.8200	0.0490	0.0937	0.0017	0.0654	0.0640	0.0038	603	28	577	10	670	130	86
A_151.FIN2	ERUKU	128	109	0.14	197	2.0540	0.0340	0.1508	0.0014	0.2153	0.0991	0.0017	1132	11	905	8	1600	32	57
A_152.FIN2	ERUKU	123	345	1.18	161	0.7630	0.0200	0.0938	0.0010	0.0597	0.0594	0.0017	574	11	578	6	566	64	102
A_153.FIN2	ERUKU	244	1027	0.46	1530	9.4500	0.0810	0.4225	0.0034	0.5989	0.1625	0.0012	2382	8	2272	15	2480	12	92
A_154.FIN2	ERUKU	132	1059	0.93	760	6.7330	0.0810	0.3776	0.0031	0.5398	0.1300	0.0013	2075	11	2065	14	2094	18	99
A_157.FIN2	ERUKU	194	329	0.67	263	0.8660	0.0220	0.1027	0.0010	0.0716	0.0615	0.0016	632	12	630	6	630	58	100
A_158.FIN2	ERUKU	110	400	0.42	680	6.7900	0.1000	0.3724	0.0037	0.4358	0.1326	0.0019	2083	13	2040	17	2129	25	96
A_159.FIN2	ERUKU	163	760	0.54	810	6.8680	0.0860	0.3680	0.0031	0.4129	0.1359	0.0016	2093	11	2020	15	2172	21	93
A_160.FIN2	ERUKU	316	231	0.09	1880	6.3040	0.0620	0.3468	0.0026	0.6447	0.1323	0.0010	2018	9	1919	12	2126	13	90
A_161.FIN2	ERUKU	196	1310	0.80	890	6.0920	0.0610	0.3326	0.0023	0.4660	0.1334	0.0012	1988	9	1851	11	2141	16	86
A_162.FIN2	ERUKU	153	312	0.84	250	0.8270	0.0290	0.0945	0.0013	0.0397	0.0644	0.0027	615	18	582	7	744	89	78
A_163.FIN2	ERUKU	195	603	0.36	1120	7.0610	0.0870	0.3764	0.0031	0.5232	0.1363	0.0014	2118	11	2059	14	2182	19	94
A_164.FIN2	ERUKU	336	1010	1.13	590	0.9280	0.0150	0.1075	0.0008	0.2237	0.0630	0.0010	666	8	658	5	695	32	95
A_165.FIN2	ERUKU	553	1767	0.35	3870	8.1000	0.1400	0.3863	0.0055	0.8234	0.1526	0.0014	2241	15	2105	26	2374	16	89
A_166.FIN2	ERUKU	59	202	1.47	90	0.7900	0.0340	0.0950	0.0016	0.0217	0.0606	0.0027	587	19	585	9	573	97	102
A_167.FIN2	ERUKU	472	1150	0.29	3250	6.5710	0.0550	0.3618	0.0026	0.5881	0.1323	0.0010	2056	8	1990	12	2127	13	94
A_168.FIN2	ERUKU	111	335	1.27	175	0.8000	0.0250	0.0957	0.0012	0.1850	0.0609	0.0020	595	14	589	7	606	69	97
A_169.FIN2	ERUKU	166	45	0.09	327	0.9500	0.0220	0.1104	0.0013	0.4332	0.0626	0.0014	676	12	675	8	676	48	100
A_170.FIN2	ERUKU	116	441	0.39	540	9.3400	0.1200	0.4211	0.0039	0.5833	0.1613	0.0018	2370	12	2265	18	2466	18	92
A_171.FIN2	ERUKU	65	307	1.99	112	0.8000	0.0340	0.0950	0.0013	0.1450	0.0613	0.0026	595	20	585	8	608	95	96
A_175.FIN2	ERUKU	97	189	0.29	390	4.9730	0.0850	0.2882	0.0029	0.1053	0.1257	0.0024	1813	14	1632	15	2031	34	80
A_176.FIN2	ERUKU	21	91	1.85	30	0.7520	0.0440	0.0921	0.0017	0.1433	0.0607	0.0037	569	27	568	10	530	120	107

A_177.FIN2	ERUKU	268	283	0.47	420	0.7420	0.0190	0.0907	0.0009	0.3022	0.0595	0.0014	562	11	560	6	565	51	99
A_178.FIN2	ERUKU	29	100	0.39	167	6.6100	0.2300	0.3377	0.0093	0.6412	0.1427	0.0041	2055	31	1872	45	2248	49	83
A_179.FIN2	ERUKU	141	464	0.37	960	6.9690	0.0940	0.3749	0.0045	0.5449	0.1350	0.0017	2106	12	2055	22	2161	21	95
A_180.FIN2	ERUKU	225	234	0.35	250	1.0430	0.0220	0.1179	0.0008	0.0280	0.0644	0.0014	724	11	718	5	738	48	97
A_181.FIN2	ERUKU	63	30	0.16	96	0.8840	0.0350	0.1013	0.0012	0.1694	0.0637	0.0025	637	19	622	7	669	84	93
A_182.FIN2	ERUKU	46	213	1.98	73	0.7910	0.0460	0.0939	0.0014	0.0864	0.0615	0.0036	585	25	578	8	570	120	101
A_183.FIN2	ERUKU	155	363	0.24	680	8.9740	0.0960	0.4142	0.0036	0.5507	0.1575	0.0015	2334	10	2233	16	2426	16	92
A_184.FIN2	ERUKU	99	850	0.86	570	8.6300	0.0880	0.4036	0.0032	0.2875	0.1554	0.0017	2301	9	2185	15	2405	18	91
A_185.FIN2	ERUKU	109	7	0.06	193	0.8690	0.0280	0.0984	0.0011	0.1686	0.0642	0.0021	632	15	605	7	716	69	85
A_186.FIN2	ERUKU	120	1637	1.53	750	7.5300	0.1800	0.3810	0.0074	0.8945	0.1432	0.0016	2168	24	2078	35	2266	19	92
A_187.FIN2	ERUKU	186	171	0.34	340	0.8830	0.0220	0.1052	0.0010	0.0502	0.0611	0.0016	641	12	645	6	617	58	104
A_188.FIN2	ERUKU	102	675	0.65	360	9.3200	0.1300	0.4374	0.0037	0.5150	0.1548	0.0019	2369	13	2338	17	2401	19	97
A_191.FIN2	ERUKU	174	323	0.57	270	1.1450	0.0240	0.1285	0.0013	0.1859	0.0646	0.0013	773	11	779	7	760	43	103
A_192.FIN2	ERUKU	10	16	0.59	17	0.9500	0.0960	0.0972	0.0029	0.1582	0.0715	0.0073	659	51	598	17	760	200	79
A_193.FIN2	ERUKU	50	299	0.81	219	4.6500	0.1100	0.3058	0.0041	0.3433	0.1105	0.0025	1754	20	1719	20	1796	41	96
A_194.FIN2	ERUKU	130	475	1.42	222	0.8900	0.0270	0.1038	0.0012	0.1881	0.0620	0.0018	643	14	637	7	650	65	98
A_195.FIN2	ERUKU	63	423	0.95	274	4.3550	0.0730	0.2914	0.0028	0.2388	0.1086	0.0019	1702	14	1648	14	1770	33	93
A_197.FIN2	ERUKU	513	2116	0.46	3500	7.5550	0.0820	0.3985	0.0038	0.6719	0.1376	0.0012	2179	10	2162	18	2196	15	98
A_198.FIN2	ERUKU	119	618	0.69	630	4.6360	0.0650	0.3127	0.0026	0.2354	0.1076	0.0015	1756	11	1754	13	1754	25	100
A_199.FIN2	ERUKU	216	412	0.71	261	0.9200	0.0220	0.1073	0.0011	0.4076	0.0623	0.0014	661	12	657	6	668	47	98
A_200.FIN2	ERUKU	405	1512	0.61	894	3.2620	0.0520	0.2014	0.0024	0.7747	0.1176	0.0012	1470	12	1182	13	1917	18	62
A_201.FIN2	ERUKU	106	50	0.16	171	0.9170	0.0260	0.1069	0.0011	0.1303	0.0626	0.0019	660	14	655	6	661	65	99
A_202.FIN2	ERUKU	332	637	0.76	510	0.8350	0.0140	0.0990	0.0009	0.1998	0.0613	0.0010	616	8	609	5	638	37	95
A_203.FIN2	ERUKU	763	455	0.07	4200	7.5890	0.0680	0.3842	0.0028	0.6778	0.1431	0.0010	2183	8	2095	13	2265	12	92
A_204.FIN2	ERUKU	335	834	0.93	620	0.8590	0.0140	0.1033	0.0008	0.2454	0.0604	0.0010	629	8	634	5	609	34	104
A_205.FIN2	ERUKU	570	325	0.07	2420	5.1700	0.0760	0.3019	0.0036	0.8417	0.1241	0.0010	1846	12	1700	18	2014	14	84
A_208.FIN2	ERUKU	44	216	2.05	67	0.7760	0.0410	0.0930	0.0016	0.1374	0.0608	0.0032	577	23	573	10	560	110	102
A_209.FIN2	ERUKU	224	1343	0.66	1550	7.3890	0.0670	0.3889	0.0026	0.4245	0.1378	0.0012	2159	8	2117	12	2198	15	96
A_210.FIN2	ERUKU	65	267	1.73	95	0.8180	0.0340	0.0955	0.0018	0.0339	0.0625	0.0028	606	20	588	10	648	97	91
A_211.FIN2	ERUKU	225	1156	0.50	1420	9.4660	0.0810	0.4300	0.0034	0.6087	0.1597	0.0012	2384	8	2305	15	2451	12	94
A_212.FIN2	ERUKU	68	260	0.39	290	8.1300	0.1500	0.3742	0.0042	0.1808	0.1577	0.0031	2242	17	2049	19	2424	34	85
A_213.FIN2	ERUKU	170	185	0.48	321	0.7600	0.0230	0.0913	0.0011	0.0544	0.0606	0.0021	572	13	563	7	588	71	96

A_214.FIN2	ERUKU	63	347	0.66	200	6.7600	0.1200	0.3513	0.0031	0.2078	0.1396	0.0025	2077	16	1941	15	2213	32	88
A_215.FIN2	ERUKU	370	42	0.03	1040	2.9430	0.0790	0.1937	0.0033	0.8962	0.1098	0.0015	1388	20	1141	18	1790	26	64
A_216.FIN2	ERUKU	30	89	1.14	44	0.9150	0.0470	0.1012	0.0017	0.1540	0.0653	0.0033	651	25	621	10	710	110	87
A_217.FIN2	ERUKU	46	198	1.71	64	0.7900	0.0380	0.0957	0.0013	0.0210	0.0600	0.0030	587	22	589	8	540	100	109
A_218.FIN2	ERUKU	109	84	0.29	197	0.9010	0.0320	0.1033	0.0010	0.1641	0.0631	0.0022	649	17	634	6	672	76	94
A_219.FIN2	ERUKU	266	2400	1.02	1650	6.2960	0.0610	0.3590	0.0029	0.6643	0.1271	0.0010	2017	8	1977	14	2057	13	96
A_220.FIN2	ERUKU	446	173	0.16	720	0.7830	0.0240	0.0972	0.0017	0.4081	0.0587	0.0015	586	14	598	10	544	56	110
A_221.FIN2	ERUKU	402	601	0.20	1790	5.0000	0.0730	0.2943	0.0029	0.8319	0.1229	0.0010	1817	12	1662	14	1996	15	83
A_225.FIN2	ERUKU	104	510	2.09	138	0.8630	0.0360	0.0949	0.0014	0.2428	0.0655	0.0026	628	20	584	8	764	86	76
A_226.FIN2	ERUKU	175	609	0.37	840	6.7890	0.0880	0.3709	0.0030	0.6752	0.1327	0.0013	2082	11	2033	14	2133	17	95
A_227.FIN2	ERUKU	120	147	0.51	149	0.7750	0.0280	0.0952	0.0011	0.1781	0.0591	0.0021	580	16	586	7	534	77	110
A_228.FIN2	ERUKU	192	359	0.82	289	0.7980	0.0270	0.0939	0.0014	0.1979	0.0617	0.0021	594	15	578	8	639	73	91
A_229.FIN2	ERUKU	45	98	0.88	61	0.8240	0.0340	0.0947	0.0014	0.1101	0.0630	0.0026	605	19	583	8	648	90	90
A_230.FIN2	ERUKU	319	459	0.54	432	0.7920	0.0150	0.0964	0.0007	0.3473	0.0595	0.0010	591	8	594	4	575	39	103
A_231.FIN2	ERUKU	91	127	0.57	79	0.7780	0.0250	0.0922	0.0008	0.0550	0.0611	0.0019	581	14	568	5	607	69	94
A_232.FIN2	ERUKU	352	1779	0.52	1610	9.1410	0.0740	0.4098	0.0027	0.6033	0.1618	0.0011	2351	7	2214	12	2473	12	90
A_233.FIN2	ERUKU	187	224	0.15	870	5.3260	0.0870	0.2996	0.0036	0.7696	0.1288	0.0013	1871	14	1689	18	2078	18	81
A_234.FIN2	ERUKU	479	1401	0.34	1970	6.3730	0.0520	0.3582	0.0024	0.6194	0.1289	0.0009	2028	7	1973	11	2082	12	95
A_235.FIN2	ERUKU	167	429	1.13	222	0.7520	0.0200	0.0916	0.0011	0.0195	0.0600	0.0018	568	11	565	7	575	64	98
A_236.FIN2	ERUKU	156	250	0.60	248	0.8740	0.0170	0.1033	0.0008	0.1583	0.0613	0.0012	636	10	634	5	630	44	101
A_237.FIN2	ERUKU	187	133	0.27	246	0.8630	0.0240	0.1021	0.0010	0.1629	0.0614	0.0019	630	13	627	6	624	67	100
A_238.FIN2	ERUKU	167	1550	1.02	830	7.3850	0.0840	0.3793	0.0030	0.5907	0.1409	0.0013	2158	10	2072	14	2238	16	93
A_239.FIN2	ERUKU	156	529	0.37	720	6.9600	0.0840	0.3741	0.0030	0.5833	0.1349	0.0013	2104	11	2048	14	2159	17	95
A_242.FIN2	ERUKU	121	504	1.77	154	0.7570	0.0210	0.0943	0.0009	0.1342	0.0582	0.0016	570	12	581	5	507	60	115
A_243.FIN2	ERUKU	62	122	0.76	97	0.8690	0.0360	0.1033	0.0015	0.1599	0.0606	0.0025	631	20	634	9	591	89	107
A_245.FIN2	ERUKU	193	588	1.20	287	0.8600	0.0260	0.1025	0.0011	0.2562	0.0608	0.0018	628	14	629	6	608	62	103
A_246.FIN2	ERUKU	55	62	0.41	73	0.8820	0.0480	0.1021	0.0018	0.2270	0.0628	0.0035	636	28	627	11	630	120	100
A_247.FIN2	ERUKU	25	28	0.43	32	0.8750	0.0540	0.1025	0.0017	0.1023	0.0622	0.0039	626	29	629	10	580	130	108
A_248.FIN2	ERUKU	242	417	0.66	370	0.8880	0.0180	0.1033	0.0010	0.1191	0.0623	0.0013	644	10	634	6	668	47	95
A_249.FIN2	ERUKU	97	207	0.86	79	0.7920	0.0320	0.0955	0.0014	0.0647	0.0598	0.0025	589	18	588	8	569	93	103
A_250.FIN2	ERUKU	199	542	1.14	201	0.7540	0.0190	0.0931	0.0008	0.1572	0.0590	0.0015	571	11	574	5	544	56	105
A_251.FIN2	ERUKU	121	305	0.96	187	0.8740	0.0200	0.1041	0.0009	0.0660	0.0608	0.0015	639	11	638	5	610	56	105

A_252.FIN2	ERUKU	366	14	0.01	650	0.7670	0.0110	0.0935	0.0007	0.2160	0.0596	0.0009	578	6	576	4	582	31	99
A_253.FIN2	ERUKU	74	1290	1.99	480	6.3200	0.1300	0.3531	0.0056	0.7042	0.1299	0.0020	2018	19	1948	27	2087	28	93
A_254.FIN2	ERUKU	181	488	1.21	288	0.7780	0.0240	0.0928	0.0012	0.2107	0.0608	0.0019	583	14	572	7	622	71	92
A_255.FIN2	ERUKU	247	277	0.42	380	0.8860	0.0180	0.1053	0.0009	0.1501	0.0611	0.0013	643	10	645	5	630	43	102
A_256.FIN2	ERUKU	185	564	0.32	1270	7.4850	0.0660	0.3958	0.0026	0.2882	0.1373	0.0013	2170	8	2149	12	2190	17	98
A_259.FIN2	ERUKU	300	248	0.36	490	0.7790	0.0190	0.0931	0.0012	0.0388	0.0609	0.0014	584	11	574	7	622	48	92
A_260.FIN2	ERUKU	95	445	2.10	100	0.7510	0.0370	0.0911	0.0015	0.0357	0.0598	0.0031	570	20	564	10	550	110	102
A_261.FIN2	ERUKU	81	286	1.51	83	0.8270	0.0310	0.0936	0.0012	0.3459	0.0638	0.0023	608	17	577	7	688	77	84
A_262.FIN2	ERUKU	145	200	0.60	20	0.7500	0.0180	0.0918	0.0009	0.0454	0.0594	0.0015	567	11	566	5	554	57	102
A_263.FIN2	ERUKU	300	760	1.01	360	0.8780	0.0180	0.1016	0.0010	0.4271	0.0627	0.0012	639	10	624	6	690	41	90
A_264.FIN2	ERUKU	646	826	0.36	1300	1.7650	0.0200	0.1648	0.0020	0.4762	0.0778	0.0010	1032	7	983	11	1138	24	86
A_265.FIN2	ERUKU	109	526	0.67	1180	4.5690	0.0730	0.3079	0.0027	0.2866	0.1079	0.0017	1742	13	1730	13	1762	28	98
A_266.FIN2	ERUKU	139	602	0.61	1230	4.5310	0.0680	0.3047	0.0026	0.3140	0.1080	0.0015	1735	13	1714	13	1764	26	97
A_267.FIN2	ERUKU	280	573	0.77	630	0.9090	0.0170	0.1071	0.0008	0.2447	0.0614	0.0011	655	9	656	5	651	39	101
A_268.FIN2	ERUKU	902	1335	0.19	1500	6.0260	0.0560	0.3521	0.0028	0.6732	0.1242	0.0009	1979	8	1944	13	2017	13	96
A_269.FIN2	ERUKU	213	441	0.69	590	1.1050	0.0240	0.1249	0.0012	0.4235	0.0642	0.0013	754	12	759	7	739	43	103
A_270.FIN2	ERUKU	942	3003	0.56	1400	6.6530	0.0710	0.3626	0.0034	0.8569	0.1332	0.0007	2065	10	1994	16	2139	10	93
A_271.FIN2	ERUKU	230	296	0.59	90	0.7880	0.0370	0.0915	0.0016	0.1618	0.0626	0.0031	588	21	564	9	660	100	86
A_272.FIN2	ERUKU	431	4239	0.94	4900	10.6780	0.0930	0.4710	0.0041	0.7320	0.1646	0.0011	2495	8	2488	18	2503	11	99
A_273.FIN2	ERUKU	218	221	0.45	250	0.7910	0.0240	0.0946	0.0015	0.2769	0.0609	0.0019	590	14	582	9	612	67	95
A_276.FIN2	ERUKU	23	86	1.08	140	1.5100	0.1200	0.1526	0.0038	0.2231	0.0720	0.0057	918	51	915	21	880	170	104
A_277.FIN2	ERUKU	244	1326	0.60	2300	8.5000	0.1100	0.3905	0.0044	0.6084	0.1581	0.0017	2285	12	2125	21	2434	19	87
A_278.FIN2	ERUKU	357	456	0.19	2400	3.6360	0.0520	0.2213	0.0024	0.7358	0.1193	0.0011	1555	11	1288	13	1943	17	66
A_279.FIN2	ERUKU	68	503	0.80	650	9.1100	0.1400	0.4400	0.0057	0.7776	0.1506	0.0016	2347	15	2349	26	2349	18	100
A_280.FIN2	ERUKU	459	627	0.16	2900	5.1020	0.0530	0.2773	0.0024	0.7356	0.1336	0.0009	1835	9	1577	12	2146	12	73

Appendix 7.8: Summary of LA-SF-ICP-MS data of detrital zircons within Awo-Omama kaolins.

						RATIOS							AGES [Ma]						
Analysis	Sample	U [ppm][a]	Pb [ppm][a]	Th/U[a]	*206/204*	$^{207}Pb/^{235}U$[b]	2 σ[d]	$^{206}Pb/^{238}U$[b]	2 σ[d]	rho[c]	$^{207}Pb/^{206}Pb$[e]	2 σ[d]	$^{207}Pb/^{235}U$	2 σ	$^{206}Pb/^{238}U$	2 σ	$^{207}Pb/^{206}Pb$	2 σ	Conc.%
A_005.FIN2	AWO	407	171	0.17	454	0.8100	0.0150	0.0981	0.0010	0.2358	0.0599	0.0010	602	8	603	6	588	38	103
A_006.FIN2	AWO	75	403	2.43	69	0.7600	0.0320	0.0910	0.0014	0.0516	0.0609	0.0027	570	19	561	8	583	96	96
A_007.FIN2	AWO	16	6	0.03	121	10.9700	0.2500	0.4754	0.0070	0.4071	0.1685	0.0037	2518	22	2505	31	2530	37	99
A_008.FIN2	AWO	34	187	0.69	209	5.3500	0.1300	0.3347	0.0044	0.3757	0.1158	0.0026	1875	20	1861	21	1893	40	98
A_009.FIN2	AWO	110	285	0.99	183	0.8380	0.0180	0.1009	0.0008	0.0920	0.0605	0.0014	617	10	619	5	592	50	105
A_010.FIN2	AWO	126	326	1.01	242	0.7790	0.0220	0.0960	0.0010	0.0321	0.0590	0.0017	583	12	591	6	535	64	110
A_011.FIN2	AWO	155	232	0.56	261	0.8760	0.0200	0.1041	0.0010	0.2063	0.0612	0.0014	637	11	639	6	623	50	102
A_012.FIN2	AWO	101	151	0.55	193	0.8580	0.0240	0.1026	0.0010	0.1152	0.0605	0.0017	626	13	630	6	596	61	106
A_013.FIN2	AWO	28	150	1.20	81	1.7860	0.0690	0.1707	0.0020	0.1132	0.0761	0.0031	1030	25	1016	11	1037	88	98
A_014.FIN2	AWO	146	329	1.04	213	0.7350	0.0350	0.0881	0.0013	0.0041	0.0608	0.0031	557	20	544	8	580	110	94
A_015.FIN2	AWO	124	685	0.59	800	9.0700	0.1300	0.4288	0.0050	0.3972	0.1532	0.0023	2345	13	2300	23	2379	26	97
A_016.FIN2	AWO	219	686	1.26	419	0.7900	0.0140	0.0969	0.0007	0.1849	0.0590	0.0010	590	8	596	4	559	39	107
A_017.FIN2	AWO	156	651	1.61	271	0.8180	0.0180	0.0981	0.0009	0.0694	0.0604	0.0013	605	10	603	5	601	49	100
A_018.FIN2	AWO	105	280	1.00	195	0.8590	0.0330	0.1026	0.0016	0.1327	0.0609	0.0024	627	18	630	9	603	87	104
A_022.FIN2	AWO	207	387	0.74	450	0.8380	0.0220	0.1000	0.0010	0.1816	0.0609	0.0016	616	12	614	6	613	57	100
A_023.FIN2	AWO	88	162	0.75	156	0.7860	0.0230	0.0954	0.0010	0.0760	0.0600	0.0018	588	13	587	6	567	65	104
A_024.FIN2	AWO	113	193	0.69	196	0.7860	0.0210	0.0950	0.0009	0.0336	0.0599	0.0017	587	12	585	5	577	62	101
A_025.FIN2	AWO	74	1179	2.01	430	5.2520	0.0960	0.3256	0.0033	0.5398	0.1168	0.0018	1859	16	1819	17	1903	28	96
A_026.FIN2	AWO	117	289	0.99	110	0.7770	0.0200	0.0952	0.0009	0.2168	0.0596	0.0016	584	12	586	6	553	59	106
A_027.FIN2	AWO	178	353	0.79	70	0.7760	0.0150	0.0949	0.0007	0.0030	0.0594	0.0013	583	9	584	4	557	47	105
A_028.FIN2	AWO	58	238	1.00	145	1.5910	0.0400	0.1599	0.0014	0.0495	0.0722	0.0018	962	16	956	8	955	56	100
A_029.FIN2	AWO	38	255	0.74	270	6.8100	0.1000	0.3733	0.0032	0.2317	0.1324	0.0020	2084	14	2044	15	2124	27	96
A_030.FIN2	AWO	93	438	1.04	320	1.5870	0.0360	0.1621	0.0013	0.0872	0.0712	0.0017	961	14	968	7	939	49	103
A_031.FIN2	AWO	55	82	0.52	125	0.9510	0.0310	0.1096	0.0011	0.2045	0.0628	0.0020	673	16	670	6	648	69	103
A_032.FIN2	AWO	51	3	0.62	2	0.0202	0.0056	0.0023	0.0002	0.0591	0.0730	0.0210	20	6	15	1	-160	460	-9

A_033.FIN2	AWO	141	179	0.51	187	0.7820	0.0180	0.0953	0.0007	0.1377	0.0595	0.0013	585	10	587	4	560	48	105
A_034.FIN2	AWO	248	809	1.39	550	0.8670	0.0210	0.1019	0.0009	0.0040	0.0617	0.0015	632	11	626	5	656	52	95
A_035.FIN2	AWO	13	24	0.73	21	0.8100	0.0560	0.0947	0.0021	0.0330	0.0629	0.0045	588	32	583	12	550	140	106
A_039.FIN2	AWO	249	232	0.41	590	0.7720	0.0190	0.0938	0.0009	0.1099	0.0597	0.0015	579	11	578	5	573	54	101
A_042.FIN2	AWO	123	176	0.62	216	0.7800	0.0260	0.0915	0.0010	0.0551	0.0618	0.0019	583	15	564	6	633	68	89
A_043.FIN2	AWO	43	142	1.40	68	0.7680	0.0530	0.0923	0.0017	0.0227	0.0605	0.0044	576	32	569	10	550	150	103
A_044.FIN2	AWO	196	194	0.42	400	0.7770	0.0210	0.0942	0.0011	0.2778	0.0598	0.0016	582	12	580	6	575	58	101
A_045.FIN2	AWO	265	115	0.18	340	0.8520	0.0160	0.1019	0.0010	0.2421	0.0606	0.0012	624	9	626	6	617	42	101
A_046.FIN2	AWO	33	82	0.98	97	0.7960	0.0380	0.0931	0.0014	0.0522	0.0622	0.0031	590	22	574	8	600	110	96
A_047.FIN2	AWO	180	167	0.40	280	0.7660	0.0260	0.0924	0.0009	0.4025	0.0605	0.0019	575	15	570	5	595	67	96
A_048.FIN2	AWO	148	262	0.74	185	0.7730	0.0190	0.0935	0.0009	0.1003	0.0599	0.0015	582	10	576	5	577	56	100
A_050.FIN2	AWO	240	612	1.22	260	0.6610	0.0110	0.0813	0.0007	0.1525	0.0589	0.0010	515	7	504	4	546	37	92
A_051.FIN2	AWO	50	101	0.86	80	0.8170	0.0550	0.0926	0.0019	0.0301	0.0641	0.0045	599	30	571	11	650	140	88
A_052.FIN2	AWO	360	364	0.23	950	1.8720	0.0260	0.1791	0.0015	0.4681	0.0757	0.0010	1070	9	1062	8	1082	26	98
A_056.FIN2	AWO	56	107	0.82	140	0.7470	0.0470	0.0886	0.0015	0.0534	0.0612	0.0040	562	28	547	9	590	140	93
A_057.FIN2	AWO	70	160	1.00	0	0.7760	0.0370	0.0916	0.0016	0.2329	0.0615	0.0030	580	21	565	9	610	100	93
A_058.FIN2	AWO	78	219	0.69	170	1.4020	0.0320	0.1468	0.0017	0.3250	0.0694	0.0016	886	14	883	10	887	48	100
A_059.FIN2	AWO	456	543	0.30	1350	1.4580	0.0160	0.1520	0.0010	0.3337	0.0694	0.0007	913	6	912	6	908	22	100
A_060.FIN2	AWO	152	258	0.64	240	0.8530	0.0180	0.1027	0.0011	0.1449	0.0607	0.0015	627	10	630	6	605	52	104
A_061.FIN2	AWO	173	322	0.79	170	0.7930	0.0250	0.0944	0.0013	0.2655	0.0608	0.0019	591	14	582	8	611	69	95
A_062.FIN2	AWO	178	596	1.40	50	0.8000	0.0200	0.0958	0.0012	0.3578	0.0604	0.0015	595	12	590	7	612	55	96
A_063.FIN2	AWO	283	843	1.15	540	0.8630	0.0140	0.1024	0.0009	0.1380	0.0611	0.0011	631	8	629	5	635	37	99
A_064.FIN2	AWO	129	1667	1.82	480	5.5330	0.0710	0.3219	0.0031	0.4524	0.1251	0.0017	1909	12	1799	15	2027	24	89
A_065.FIN2	AWO	438	180	0.18	1450	0.7400	0.0160	0.0896	0.0009	0.2545	0.0598	0.0012	562	9	553	5	587	45	94
A_066.FIN2	AWO	104	210	0.95	180	0.7390	0.0280	0.0894	0.0010	0.0141	0.0597	0.0026	559	17	552	6	574	89	96
A_067.FIN2	AWO	67	505	1.16	310	3.9120	0.0860	0.2821	0.0032	0.1955	0.1005	0.0023	1614	18	1602	16	1623	42	99
A_068.FIN2	AWO	29	29	0.43	65	0.7990	0.0600	0.0913	0.0022	0.0917	0.0640	0.0054	589	33	563	13	630	160	89
A_069.FIN2	AWO	141	757	2.28	170	0.8050	0.0260	0.0961	0.0012	0.2145	0.0607	0.0020	598	15	591	7	603	71	98
A_073.FIN2	AWO	50	157	0.34	340	7.0320	0.0910	0.3795	0.0033	0.3789	0.1341	0.0016	2113	12	2073	15	2146	21	97
A_074.FIN2	AWO	158	180	0.43	402	1.0830	0.0200	0.1197	0.0009	0.1033	0.0656	0.0013	743	10	729	5	774	42	94
A_075.FIN2	AWO	149	2430	0.80	85	10.8100	0.9500	0.2133	0.0079	0.9604	0.3390	0.0260	2300	140	1242	43	3300	220	38
A_076.FIN2	AWO	41	101	1.06	28	0.7900	0.0390	0.0936	0.0014	0.0239	0.0614	0.0032	588	23	576	8	590	110	98

A_077.FIN2	AWO	38	89	0.93	68	0.8310	0.0380	0.0991	0.0015	0.0960	0.0610	0.0029	607	21	609	9	576	99	106
A_078.FIN2	AWO	147	160	0.46	310	0.7570	0.0180	0.0924	0.0009	0.0878	0.0598	0.0016	572	11	570	5	568	58	100
A_079.FIN2	AWO	34	84	0.92	78	0.9690	0.0680	0.1062	0.0024	0.0001	0.0668	0.0049	685	37	650	14	750	160	87
A_080.FIN2	AWO	16	32	1.29	35	1.0690	0.0740	0.1016	0.0025	0.3247	0.0765	0.0050	729	37	623	15	1000	140	62
A_081.FIN2	AWO	217	591	1.14	360	0.8410	0.0240	0.0994	0.0010	0.1882	0.0614	0.0018	618	14	611	6	627	64	97
A_082.FIN2	AWO	131	135	0.43	301	0.8310	0.0250	0.0994	0.0010	0.0567	0.0607	0.0019	612	14	611	6	592	67	103
A_083.FIN2	AWO	116	88	0.28	213	0.9010	0.0390	0.0990	0.0013	0.2103	0.0661	0.0028	649	20	609	8	766	88	79
A_084.FIN2	AWO	70	142	0.92	77	0.7390	0.0350	0.0905	0.0012	0.1055	0.0594	0.0029	557	21	558	7	520	100	107
A_085.FIN2	AWO	267	319	0.53	490	0.7870	0.0170	0.0945	0.0009	0.0312	0.0605	0.0014	589	9	582	5	604	50	96
A_086.FIN2	AWO	166	182	0.46	299	0.8600	0.0250	0.0995	0.0010	0.2542	0.0628	0.0018	628	14	611	6	674	62	91
A_090.FIN2	AWO	65	117	0.46	185	1.6180	0.0420	0.1628	0.0019	0.2278	0.0723	0.0019	974	16	972	10	972	54	100
A_091.FIN2	AWO	110	191	0.69	239	0.8250	0.0230	0.0988	0.0009	0.0484	0.0609	0.0018	608	13	607	5	598	65	102
A_092.FIN2	AWO	166	570	1.43	170	0.8360	0.0230	0.0996	0.0009	0.0578	0.0611	0.0018	615	13	612	6	623	59	98
A_093.FIN2	AWO	213	644	0.86	560	1.4590	0.0380	0.1458	0.0017	0.5090	0.0727	0.0016	912	16	877	10	995	46	88
A_094.FIN2	AWO	46	166	1.57	148	0.7890	0.0410	0.0950	0.0017	0.1003	0.0614	0.0035	591	25	585	10	610	120	96
A_095.FIN2	AWO	115	1327	1.15	1000	10.7300	0.1200	0.4664	0.0043	0.3358	0.1678	0.0020	2501	11	2467	19	2534	20	97
A_096.FIN2	AWO	155	965	0.64	1280	10.5900	0.1600	0.4620	0.0052	0.5809	0.1668	0.0021	2487	14	2448	23	2524	21	97
A_097.FIN2	AWO	179	650	0.41	1080	7.3160	0.0930	0.3906	0.0033	0.6559	0.1361	0.0012	2149	11	2125	15	2180	16	97
A_098.FIN2	AWO	33	271	0.85	303	9.9700	0.2400	0.4566	0.0059	0.2868	0.1598	0.0039	2433	23	2424	26	2445	42	99
A_100.FIN2	AWO	15	195	1.69	10	6.0900	0.1600	0.3522	0.0049	0.0726	0.1265	0.0038	1982	23	1944	23	2026	54	96
A_101.FIN2	AWO	23	211	1.19	136	5.7500	0.1600	0.3486	0.0051	0.2962	0.1209	0.0034	1936	25	1931	23	1957	49	99
A_102.FIN2	AWO	125	190	0.44	287	1.3710	0.0270	0.1453	0.0013	0.1121	0.0687	0.0014	875	11	875	7	872	43	100
A_103.FIN2	AWO	47	79	0.71	174	0.8890	0.0420	0.1019	0.0015	0.0006	0.0639	0.0032	640	22	626	9	660	100	95
A_107.FIN2	AWO	33	333	1.30	310	5.0100	0.1500	0.2977	0.0056	0.6269	0.1222	0.0027	1814	25	1679	28	1982	41	85
A_108.FIN2	AWO	80	542	0.82	670	6.1090	0.0930	0.3492	0.0030	0.3394	0.1278	0.0019	1991	14	1930	15	2061	26	94
A_109.FIN2	AWO	151	261	0.75	275	0.8060	0.0220	0.0970	0.0009	0.1432	0.0606	0.0017	598	12	597	6	596	60	100
A_110.FIN2	AWO	176	157	0.41	282	0.7480	0.0280	0.0907	0.0013	0.2399	0.0602	0.0023	566	17	560	8	608	74	92
A_111.FIN2	AWO	37	75	0.86	54	0.8280	0.0440	0.0979	0.0015	0.0033	0.0615	0.0034	605	25	602	9	590	120	102
A_112.FIN2	AWO	154	579	0.98	370	1.5520	0.0330	0.1585	0.0014	0.4341	0.0713	0.0014	948	13	948	8	951	41	100
A_113.FIN2	AWO	88	194	0.92	166	0.8050	0.0250	0.0963	0.0011	0.1356	0.0611	0.0020	597	14	593	6	599	70	99
A_114.FIN2	AWO	219	610	0.87	420	1.2100	0.0220	0.1327	0.0011	0.1190	0.0666	0.0013	804	10	803	7	812	40	99
A_115.FIN2	AWO	145	333	0.93	274	0.8330	0.0240	0.1002	0.0009	0.2587	0.0608	0.0017	615	14	616	5	600	62	103

A_116.FIN2	AWO	54	235	0.61	331	5.0600	0.1200	0.3135	0.0037	0.1203	0.1180	0.0030	1827	21	1757	18	1914	48	92
A_117.FIN2	AWO	66	127	0.83	126	0.8550	0.0410	0.1005	0.0018	0.0813	0.0623	0.0031	622	22	617	11	630	100	98
A_118.FIN2	AWO	49	68	0.56	58	0.8720	0.0400	0.1028	0.0017	0.2906	0.0624	0.0029	635	23	631	10	630	99	100
A_119.FIN2	AWO	94	884	1.17	720	6.5500	0.1100	0.3714	0.0045	0.3644	0.1278	0.0021	2051	14	2036	21	2063	28	99
A_120.FIN2	AWO	99	112	0.46	129	0.9070	0.0320	0.1065	0.0015	0.1012	0.0618	0.0024	653	17	652	9	651	82	100
A_124.FIN2	AWO	61	148	1.13	49	0.7960	0.0400	0.0920	0.0013	0.2935	0.0630	0.0030	589	23	568	8	650	100	87
A_125.FIN2	AWO	36	184	2.34	61	0.7660	0.0430	0.0926	0.0016	0.0246	0.0606	0.0036	574	26	571	9	560	120	102
A_126.FIN2	AWO	64	111	0.72	83	0.7730	0.0320	0.0938	0.0012	0.0568	0.0595	0.0024	579	18	578	7	564	87	102
A_127.FIN2	AWO	32	56	0.74	44	0.9320	0.0580	0.1003	0.0022	0.3083	0.0678	0.0040	660	30	616	13	780	130	79
A_128.FIN2	AWO	153	202	0.56	262	0.8140	0.0240	0.0964	0.0009	0.0340	0.0615	0.0018	604	14	593	5	633	68	94
A_129.FIN2	AWO	218	858	1.71	408	0.7860	0.0230	0.0942	0.0011	0.2733	0.0609	0.0017	588	13	580	6	614	61	95
A_130.FIN2	AWO	115	529	1.87	211	0.8620	0.0270	0.1019	0.0012	0.1984	0.0618	0.0020	629	15	626	7	634	67	99
A_131.FIN2	AWO	170	195	0.51	203	0.7490	0.0180	0.0927	0.0008	0.2585	0.0592	0.0014	568	11	571	5	548	53	104
A_132.FIN2	AWO	523	614	0.62	720	0.7270	0.0100	0.0866	0.0006	0.1585	0.0612	0.0009	554	6	535	3	637	32	84
A_133.FIN2	AWO	70	356	0.69	283	6.7300	0.1300	0.3299	0.0044	0.6818	0.1481	0.0021	2071	17	1837	21	2320	24	79
A_134.FIN2	AWO	89	448	2.15	99	0.7890	0.0290	0.0965	0.0013	0.1808	0.0597	0.0022	587	16	594	7	548	79	108
A_135.FIN2	AWO	60	589	1.37	231	4.7180	0.0840	0.3140	0.0034	0.1966	0.1097	0.0021	1768	15	1760	17	1785	35	99
A_136.FIN2	AWO	138	821	0.83	690	4.6660	0.0610	0.3139	0.0027	0.3729	0.1086	0.0014	1760	11	1759	13	1776	23	99
A_137.FIN2	AWO	480	150	0.13	610	0.8250	0.0150	0.0990	0.0009	0.2619	0.0607	0.0011	610	8	609	5	621	38	98
A_140.FIN2	AWO	108	17	0.65	14	0.0860	0.0120	0.0091	0.0003	0.0464	0.0700	0.0110	83	12	59	2	620	280	9
A_141.FIN2	AWO	18	45	1.12	25	0.7950	0.0720	0.0934	0.0025	0.0876	0.0631	0.0063	580	40	575	15	550	190	105
A_142.FIN2	AWO	90	402	1.13	113	1.7860	0.0480	0.1728	0.0015	0.0939	0.0756	0.0020	1039	17	1027	8	1064	52	97
A_143.FIN2	AWO	74	165	0.92	69	0.8240	0.0420	0.0992	0.0013	0.0903	0.0607	0.0031	605	23	609	8	560	110	109
A_144.FIN2	AWO	162	789	0.56	850	7.3230	0.0930	0.3931	0.0038	0.4998	0.1357	0.0016	2151	11	2137	17	2171	20	98

XL

Appendix 7.9: Summary of LA-SF-ICP-MS data of detrital zircons within Ubulu-Uku kaolins.

						RATIOS							AGES [Ma]						
Analysis	Sample	U [ppm][a]	Pb [ppm][a]	Th/U[a]	*206/204*	$^{207}Pb/^{235}U$[b]	2 σ[d]	$^{206}Pb/^{238}U$[b]	2 σ[d]	rho[c]	$^{207}Pb/^{206}Pb$[e]	2 σ[d]	$^{207}Pb/^{235}U$	2 σ	$^{206}Pb/^{238}U$	2 σ	$^{207}Pb/^{206}Pb$	2 σ	Conc.%
A_281.FIN2	UBULU	187	493	1.04	140	0.8320	0.0210	0.0995	0.0008	0.0859	0.0609	0.0016	612	12	611	5	607	56	101
A_282.FIN2	UBULU	291	554	0.42	604	1.9490	0.0280	0.1834	0.0015	0.3309	0.0771	0.0010	1097	10	1085	8	1122	28	97
A_283.FIN2	UBULU	49	33	0.42	32	0.9050	0.0400	0.0930	0.0020	0.3135	0.0710	0.0030	656	21	573	12	944	86	61
A_284.FIN2	UBULU	176	444	1.04	244	0.8080	0.0270	0.0996	0.0010	0.2906	0.0594	0.0019	599	15	612	6	554	71	110
A_285.FIN2	UBULU	1735	2254	1.00	1580	0.6560	0.0140	0.0767	0.0018	0.8654	0.0624	0.0007	512	8	476	11	685	25	69
A_286.FIN2	UBULU	134	337	0.95	164	0.8830	0.0210	0.1005	0.0011	0.1450	0.0638	0.0015	642	12	617	7	729	52	85
A_287.FIN2	UBULU	195	885	1.67	350	0.9190	0.0190	0.1078	0.0008	0.1183	0.0621	0.0013	662	10	660	5	660	48	100
A_288.FIN2	UBULU	84	437	0.88	202	4.2350	0.0800	0.2268	0.0023	0.3309	0.1359	0.0025	1678	16	1318	12	2173	31	61
A_289.FIN2	UBULU	319	1170	0.43	2060	6.8250	0.0790	0.3693	0.0036	0.5996	0.1342	0.0013	2090	10	2026	17	2152	17	94
A_290.FIN2	UBULU	359	751	0.90	540	0.7900	0.0190	0.0923	0.0013	0.2013	0.0623	0.0015	590	11	569	8	672	51	85
A_294.FIN2	UBULU	123	62	0.16	242	0.8950	0.0270	0.1064	0.0013	0.2252	0.0616	0.0018	648	15	652	7	637	63	102
A_295.FIN2	UBULU	439	320	0.29	550	0.8770	0.0150	0.1042	0.0011	0.2438	0.0613	0.0011	639	8	639	6	639	39	100
A_296.FIN2	UBULU	155	768	1.33	174	1.8600	0.1800	0.1034	0.0019	0.9236	0.1240	0.0100	983	63	634	11	1670	160	38
A_297.FIN2	UBULU	383	46	0.03	480	0.8550	0.0200	0.0995	0.0011	0.6337	0.0632	0.0014	628	11	611	6	701	46	87
A_298.FIN2	UBULU	176	166	0.41	291	0.7960	0.0220	0.0958	0.0010	0.2613	0.0605	0.0016	594	13	590	6	600	59	98
A_299.FIN2	UBULU	249	322	0.58	400	0.9470	0.0240	0.1098	0.0011	0.1729	0.0628	0.0016	675	13	671	7	692	53	97
A_300.FIN2	UBULU	219	1130	1.25	670	1.6200	0.0320	0.1639	0.0019	0.4285	0.0719	0.0013	977	13	978	11	976	38	100
A_301.FIN2	UBULU	1191	810	0.33	1490	0.7300	0.0120	0.0881	0.0011	0.7813	0.0602	0.0006	556	7	544	7	611	22	89
A_302.FIN2	UBULU	176	586	1.26	50	0.8540	0.0190	0.1025	0.0008	0.2529	0.0605	0.0013	625	10	630	5	598	47	105
A_303.FIN2	UBULU	166	413	0.95	291	0.8870	0.0240	0.1025	0.0011	0.2207	0.0630	0.0017	642	13	629	7	681	59	92
A_304.FIN2	UBULU	270	408	0.53	270	1.0440	0.0200	0.1155	0.0011	0.1840	0.0658	0.0013	725	10	705	7	789	41	89
A_305.FIN2	UBULU	166	579	1.43	260	0.8170	0.0180	0.0985	0.0008	0.0998	0.0603	0.0014	605	10	605	5	591	52	102
A_306.FIN2	UBULU	320	53	1.00	28	0.0511	0.0039	0.0053	0.0001	0.2739	0.0718	0.0055	51	4	34	1	760	140	4
A_307.FIN2	UBULU	197	420	0.89	354	0.8650	0.0240	0.0996	0.0012	0.2060	0.0632	0.0017	631	13	612	7	696	58	88
A_311.FIN2	UBULU	142	272	0.74	209	0.8750	0.0320	0.0947	0.0009	0.3596	0.0671	0.0023	634	16	583	5	797	63	73
A_312.FIN2	UBULU	106	257	1.12	280	0.7450	0.0270	0.0905	0.0011	0.1816	0.0599	0.0022	562	16	558	7	559	75	100
A_313.FIN2	UBULU	364	57	0.02	3200	4.7180	0.0590	0.2813	0.0027	0.7449	0.1217	0.0010	1769	10	1597	13	1979	14	81

A_314.FIN2	UBULU	287	340	0.46	610	0.8970	0.0220	0.1057	0.0010	0.4677	0.0616	0.0013	649	12	648	6	646	47	100
A_315.FIN2	UBULU	204	115	0.22	490	2.2250	0.0640	0.1455	0.0030	0.7061	0.1111	0.0019	1184	20	875	17	1816	30	48
A_316.FIN2	UBULU	247	887	1.60	260	0.7870	0.0160	0.0962	0.0010	0.1794	0.0600	0.0013	590	9	592	6	584	47	101
A_317.FIN2	UBULU	205	583	0.50	1300	5.3100	0.0640	0.2937	0.0025	0.5740	0.1314	0.0013	1869	10	1659	13	2114	17	78
A_318.FIN2	UBULU	480	246	0.21	670	0.8980	0.0140	0.1042	0.0008	0.3029	0.0626	0.0009	650	7	639	5	687	32	93
A_319.FIN2	UBULU	111	172	0.19	500	5.4560	0.0770	0.3028	0.0032	0.6469	0.1307	0.0013	1892	12	1705	16	2105	18	81
A_320.FIN2	UBULU	453	634	0.64	680	0.8180	0.0210	0.0889	0.0012	0.6494	0.0669	0.0013	606	12	549	7	821	42	67
A_321.FIN2	UBULU	253	741	0.78	400	1.2070	0.0290	0.1295	0.0020	0.6228	0.0675	0.0012	802	13	785	11	844	37	93
A_322.FIN2	UBULU	457	873	0.74	890	0.8720	0.0150	0.1005	0.0008	0.2925	0.0631	0.0010	636	8	617	5	704	34	88
A_323.FIN2	UBULU	477	952	0.69	110	1.4390	0.0230	0.1445	0.0015	0.3921	0.0729	0.0012	904	10	870	8	1003	34	87
A_324.FIN2	UBULU	292	409	0.55	50	0.8820	0.0210	0.1023	0.0011	0.1860	0.0627	0.0016	641	11	628	7	683	53	92
A_327.FIN2	UBULU	226	512	0.87	50	0.8060	0.0150	0.0970	0.0007	0.2616	0.0605	0.0011	599	8	597	4	599	39	100
A_328.FIN2	UBULU	101	247	1.03	202	0.8350	0.0320	0.0947	0.0012	0.1212	0.0640	0.0024	612	18	583	7	702	82	83
A_329.FIN2	UBULU	53	208	1.64	170	0.8840	0.0650	0.0960	0.0015	0.0708	0.0674	0.0052	633	34	591	9	760	160	78
A_330.FIN2	UBULU	618	705	0.47	1900	0.8360	0.0140	0.0994	0.0009	0.2677	0.0610	0.0010	616	8	611	5	632	36	97
A_331.FIN2	UBULU	51	78	0.63	93	0.8210	0.0370	0.0966	0.0016	0.1827	0.0621	0.0028	604	21	594	9	614	96	97
A_332.FIN2	UBULU	356	737	0.85	190	0.8910	0.0190	0.1042	0.0010	0.2043	0.0622	0.0013	646	10	639	6	669	47	96
A_333.FIN2	UBULU	88	179	0.80	136	0.8610	0.0330	0.0948	0.0014	0.2512	0.0666	0.0026	630	19	584	8	781	84	75
A_334.FIN2	UBULU	371	226	0.24	450	0.7970	0.0140	0.0968	0.0007	0.4196	0.0598	0.0009	594	8	596	4	586	35	102
A_335.FIN2	UBULU	107	106	0.27	260	1.6770	0.0570	0.1541	0.0030	0.5574	0.0791	0.0023	999	21	923	17	1165	55	79
A_336.FIN2	UBULU	221	249	0.47	250	0.7770	0.0200	0.0935	0.0010	0.1820	0.0605	0.0016	582	11	576	6	598	57	96
A_338.FIN2	UBULU	182	660	0.42	2200	6.0110	0.0820	0.3446	0.0034	0.6529	0.1268	0.0013	1976	12	1908	16	2051	19	93
A_339.FIN2	UBULU	397	427	0.12	5900	6.4560	0.0660	0.3652	0.0032	0.7312	0.1285	0.0011	2039	9	2006	15	2076	15	97
A_340.FIN2	UBULU	81	230	1.10	100	0.8390	0.0330	0.0967	0.0011	0.2236	0.0631	0.0024	614	18	595	7	650	80	92
A_341.FIN2	UBULU	103	237	0.86	76	0.8440	0.0270	0.0941	0.0009	0.3925	0.0653	0.0021	618	15	580	6	739	68	78
A_345.FIN2	UBULU	99	164	0.71	210	0.7790	0.0280	0.0928	0.0012	0.1878	0.0609	0.0022	584	17	572	7	603	80	95
A_346.FIN2	UBULU	399	674	0.87	650	0.8860	0.0160	0.0966	0.0013	0.2962	0.0670	0.0013	644	9	595	8	826	39	72
A_347.FIN2	UBULU	107	334	1.25	220	0.8460	0.0270	0.0991	0.0011	0.2349	0.0622	0.0019	620	15	609	7	643	66	95
A_348.FIN2	UBULU	167	468	0.98	70	0.9630	0.0240	0.1127	0.0011	0.0813	0.0621	0.0016	683	12	688	6	652	57	106
A_349.FIN2	UBULU	296	715	1.09	160	0.7930	0.0180	0.0935	0.0009	0.1927	0.0617	0.0015	592	10	576	5	647	51	89
A_350.FIN2	UBULU	248	308	0.44	480	0.9640	0.0250	0.1099	0.0016	0.6734	0.0636	0.0012	683	13	672	9	717	40	94
A_351.FIN2	UBULU	124	274	0.59	232	1.2060	0.0660	0.1227	0.0013	0.6987	0.0715	0.0034	798	28	746	7	909	82	82

A_352.FIN2	UBULU	88	173	0.86	80	0.7550	0.0320	0.0890	0.0013	0.0580	0.0619	0.0028	567	18	550	8	613	91	90
A_353.FIN2	UBULU	184	29	0.04	40	0.8690	0.0300	0.0991	0.0012	0.4952	0.0636	0.0019	632	16	609	7	704	64	87
A_354.FIN2	UBULU	162	627	1.61	208	0.8310	0.0260	0.0983	0.0009	0.4297	0.0617	0.0018	612	15	604	5	650	61	93
A_355.FIN2	UBULU	208	726	1.32	381	0.9060	0.0220	0.1061	0.0010	0.3442	0.0617	0.0013	653	12	650	6	650	49	100
A_356.FIN2	UBULU	285	659	0.86	400	0.9070	0.0190	0.1065	0.0009	0.3520	0.0619	0.0012	654	10	653	6	655	42	100
A_357.FIN2	UBULU	192	303	0.67	272	0.7380	0.0180	0.0898	0.0008	0.3626	0.0596	0.0013	560	10	554	5	580	48	96
A_358.FIN2	UBULU	140	307	0.86	240	0.8560	0.0250	0.1017	0.0013	0.1873	0.0614	0.0018	626	14	624	8	618	64	101
A_361.FIN2	UBULU	430	662	0.64	550	0.7910	0.0150	0.0946	0.0009	0.3349	0.0608	0.0011	591	9	583	5	618	40	94
A_362.FIN2	UBULU	105	277	0.56	355	2.5600	0.1000	0.1775	0.0047	0.8574	0.1043	0.0025	1279	31	1052	26	1684	46	62
A_363.FIN2	UBULU	150	186	0.54	262	1.0770	0.0270	0.1175	0.0013	0.2984	0.0665	0.0016	740	13	716	8	802	51	89
A_364.FIN2	UBULU	42	79	0.73	63	0.8550	0.0420	0.0918	0.0016	0.0143	0.0694	0.0038	621	23	566	10	830	120	68
A_365.FIN2	UBULU	93	127	0.69	125	0.7140	0.0360	0.0811	0.0013	0.1854	0.0640	0.0031	543	21	503	8	684	99	73
A_366.FIN2	UBULU	145	246	0.80	130	0.7010	0.0280	0.0855	0.0013	0.2775	0.0601	0.0025	540	18	529	8	572	87	92
A_367.FIN2	UBULU	514	316	0.20	950	0.9760	0.0150	0.1113	0.0010	0.3179	0.0637	0.0010	692	8	680	6	729	32	93
A_368.FIN2	UBULU	201	379	0.78	322	0.7680	0.0160	0.0943	0.0008	0.2655	0.0593	0.0012	577	9	581	5	564	42	103
A_369.FIN2	UBULU	317	2081	1.78	626	1.3370	0.0170	0.1386	0.0010	0.2185	0.0701	0.0009	861	7	837	6	926	26	90
A_370.FIN2	UBULU	127	261	0.77	162	0.8950	0.0350	0.1011	0.0012	0.4148	0.0645	0.0024	647	18	621	7	746	73	83
A_371.FIN2	UBULU	137	500	1.53	220	0.8840	0.0410	0.0995	0.0015	0.1204	0.0645	0.0030	640	22	611	9	720	100	85
A_372.FIN2	UBULU	122	329	1.00	212	0.8950	0.0220	0.1064	0.0011	0.1000	0.0612	0.0016	647	12	652	7	616	56	106
A_373.FIN2	UBULU	134	288	0.78	200	0.9250	0.0220	0.1070	0.0010	0.1969	0.0631	0.0016	663	12	655	6	683	54	96
A_374.FIN2	UBULU	109	257	1.07	141	0.7370	0.0310	0.0888	0.0012	0.1172	0.0603	0.0025	558	18	549	7	572	89	96
A_375.FIN2	UBULU	325	760	0.62	540	1.4510	0.0280	0.1490	0.0019	0.3126	0.0707	0.0014	909	11	895	10	942	40	95
A_378.FIN2	UBULU	134	261	0.74	190	0.8440	0.0200	0.1003	0.0010	0.0715	0.0611	0.0015	619	11	616	6	614	54	100
A_379.FIN2	UBULU	146	435	1.15	330	0.8720	0.0230	0.1010	0.0012	0.2234	0.0627	0.0017	635	12	620	7	691	53	90
A_380.FIN2	UBULU	90	139	0.67	129	1.0880	0.0450	0.1133	0.0025	0.3899	0.0693	0.0025	743	21	692	15	899	80	77
A_381.FIN2	UBULU	990	920	0.25	2910	2.8300	0.1600	0.1875	0.0080	0.9906	0.1075	0.0019	1339	43	1104	43	1748	32	63
A_382.FIN2	UBULU	257	558	0.30	1000	4.9090	0.0510	0.2859	0.0021	0.3834	0.1245	0.0013	1803	9	1621	11	2018	18	80
A_383.FIN2	UBULU	277	235	0.35	240	2.1070	0.0270	0.1558	0.0013	0.4400	0.0980	0.0012	1150	9	933	7	1582	22	59
A_384.FIN2	UBULU	283	290	0.35	495	1.5410	0.0280	0.1378	0.0010	0.3179	0.0812	0.0014	947	11	832	6	1216	34	68
A_386.FIN2	UBULU	1111	1997	1.35	376	0.7570	0.0230	0.0620	0.0016	0.8798	0.0884	0.0013	571	13	388	10	1385	28	28
A_387.FIN2	UBULU	424	1235	1.34	480	0.8270	0.0150	0.0947	0.0009	0.4440	0.0633	0.0010	611	8	583	5	706	35	83
A_388.FIN2	UBULU	572	865	0.91	540	0.7960	0.0120	0.0831	0.0010	0.2863	0.0694	0.0011	594	7	514	6	904	34	57

A_389.FIN2	UBULU	768	56	0.04	1020	0.8730	0.0120	0.1014	0.0008	0.3762	0.0624	0.0008	637	7	622	5	681	27	91
A_390.FIN2	UBULU	39	90	0.66	40	1.2680	0.0890	0.0927	0.0017	0.3902	0.0985	0.0062	812	37	571	10	1490	120	38
A_391.FIN2	UBULU	25	45	0.81	18	0.8000	0.0500	0.0845	0.0019	0.0951	0.0693	0.0043	590	29	523	11	790	130	66
A_392.FIN2	UBULU	585	768	0.58	930	0.7720	0.0160	0.0932	0.0009	0.2150	0.0600	0.0013	580	9	575	5	590	46	97
A_395.FIN2	UBULU	50	131	0.96	151	0.9750	0.0440	0.1098	0.0015	0.3126	0.0642	0.0027	687	23	671	9	713	87	94
A_396.FIN2	UBULU	192	247	0.44	470	0.9520	0.0440	0.0999	0.0010	0.1311	0.0687	0.0028	673	21	614	6	842	73	73
A_397.FIN2	UBULU	260	548	0.80	30	0.8730	0.0160	0.1027	0.0008	0.1373	0.0615	0.0012	636	9	630	5	644	41	98
A_398.FIN2	UBULU	237	476	0.80	430	0.8030	0.0170	0.0965	0.0008	0.2200	0.0602	0.0013	597	10	594	5	598	48	99
A_399.FIN2	UBULU	221	344	0.70	460	0.8000	0.0220	0.0924	0.0009	0.1783	0.0627	0.0017	595	12	570	5	674	61	85
A_400.FIN2	UBULU	383	513	0.57	720	0.7780	0.0130	0.0931	0.0009	0.3268	0.0604	0.0010	585	7	574	5	615	35	93
A_401.FIN2	UBULU	503	1090	1.14	580	0.8600	0.0150	0.0957	0.0009	0.1589	0.0650	0.0012	630	8	589	5	766	39	77
A_402.FIN2	UBULU	1627	1086	1.85	491	0.2832	0.0064	0.0230	0.0004	0.7510	0.0889	0.0013	253	5	146	3	1396	28	10
A_403.FIN2	UBULU	223	435	0.79	830	0.8750	0.0220	0.1013	0.0010	0.2921	0.0625	0.0015	636	12	622	6	671	52	93
A_404.FIN2	UBULU	96	178	0.70	270	0.8800	0.0290	0.1024	0.0012	0.0280	0.0621	0.0022	638	16	628	7	641	77	98
A_405.FIN2	UBULU	91	256	1.16	230	0.8800	0.0420	0.0947	0.0012	0.3334	0.0670	0.0030	636	22	583	7	798	98	73
A_406.FIN2	UBULU	62	119	0.73	43	0.9560	0.0620	0.0945	0.0016	0.1441	0.0733	0.0045	671	30	582	10	930	120	63
A_407.FIN2	UBULU	701	205	0.05	2400	3.1070	0.0230	0.2041	0.0015	0.5828	0.1102	0.0007	1435	6	1197	8	1801	12	66
A_408.FIN2	UBULU	614	509	0.80	520	0.7680	0.0110	0.0847	0.0007	0.4110	0.0658	0.0009	578	6	524	4	792	28	66
A_409.FIN2	UBULU	132	382	1.12	620	0.8670	0.0310	0.1026	0.0012	0.0336	0.0609	0.0021	631	16	629	7	611	78	103
A_412.FIN2	UBULU	275	796	1.11	1180	0.8530	0.0180	0.1025	0.0010	0.3248	0.0602	0.0012	625	10	629	6	595	44	106
A_413.FIN2	UBULU	63	123	0.71	270	0.8870	0.0320	0.1049	0.0015	0.1485	0.0616	0.0026	641	17	643	9	604	88	106
A_414.FIN2	UBULU	138	310	0.94	60	0.8130	0.0240	0.0944	0.0010	0.3116	0.0619	0.0017	601	14	581	6	643	61	90
A_415.FIN2	UBULU	101	86	0.29	180	0.8870	0.0270	0.1009	0.0011	0.3326	0.0636	0.0019	641	15	620	7	707	66	88
A_416.FIN2	UBULU	342	1624	0.70	1900	4.9850	0.0790	0.2858	0.0039	0.8816	0.1260	0.0009	1813	14	1619	20	2043	13	79

Chapter One

Introduction

This chapter gives the background information, problem statement, motivation, hypotheses, objectives, study areas, climate, and delimitations of the study.

1.1 Background

The continental drift hypothesis championed by German meteorologist Alfred Wegener in 1912 was revitalised in the 1960s with the emergence of the plate tectonic theory and the discovery of seafloor spreading (Carey, 1958). The emergence demonstrated that the separation of continental masses with the subsequent formation of ocean basins cannot be simply considered as a hypothesis lacking geological mechanism to explain the drifting of the continents (Torquato and Cordani, 1981) but a fact (Cordani *et al*., 2010). During the early Cretaceous (130 Ma), the South American plate began to drift westwards from the African plate as well as the opening up of the South Atlantic Ocean (Du Toit, 1921). Complementary shapes along the margin of the continents were first recognized by Dutch scientist Ortenus in 1596 and these striking similarities in their coastlines in the South Atlantic Ocean have stimulated several scientific, geological, and geochronological research to validate the fact that it is more than just a simple coincidence (Du Toit, 1921, 1937; Bullard *et al*., 1965; Allard and Hurst, 1969; Colbert, 1973, Rogers and Santosh, 2004; Ernst *et al*., 2013).

Comparative quantitative tests have been made between the two continental masses with the advent of radiometric dating (Hurley *et al*., 1967; Almeida *et al*., 1973; Torquato, 1975; and Guadagnin *et al*., 2013). Hurley *et al*. (1967) substantiated the geochronological evolution of the similarities between basement rocks in Liberia and Sierra Leone in West Africa to analogous rocks in Venezuela, Guayana and Surinam in South America. This is attributed to the strong episode of orogeny in the middle Precambrian called Eburnean in Africa and Transamazonian in South America which was later corroborated by Tugarinov (1967). Furthermore, the induced granitisation processes associated with these orogenies leading to the formation of granitic rocks of different types on both regions were

later identified as a means for pre-drift reconstruction such as pegmatitic provinces or Tin (Sn) mineralisation in both continents despite the structural trends and geochronological line of evidences (Almeida, 1968). Parana Basin in South America and Karoo Basin in Southern Africa have been correlated based on geology, stratigraphy, paleontology, and paleoecology. Extensive continental glaciations covering both parts and sedimentary sequences in the two basins have been easily correlated due to very similar faunas and floras (Colbert, 1973). The international community, through the United Nations Educational, Scientific and Cultural Organization (UNESCO) support programmes funded cross-Atlantic correlations (International Geological Correlation programme, projects numbers 108 and 144 between 1975 and 1984). Margin basins from prolific hydrocarbon provinces with oil habitats have been correlated as indicated by paleogeographic ties (Schiefelbem *et al*., 2000). More than five predicted matches have been validated between West African basin from Rio Muni to Angola and the Brazillian conjugate basins from Recôncavo to Santos based on oil geochemical family characterisation (Schiefelbem *et al*., 2003).

Despite these findings above, Ernst *et al*. (2013) stated that pre-Pangaea paleocontinental reconstructions is an unfinished business needing an integrated multi-disciplinary approach. Hence, from the foregoing, it is clear that the knowledge of the use of clays particularly kaolins in the cross-Atlantic correlations is lacking and hereby creating a gap in the clays and clay minerals body of knowledge (CCMBK) since such pioneering work is rare in Africa. Chivas and Bird (1995) investigated the large translations between Australia and India based on the $\delta^{18}O$ of weathering clays. The work is imperative considering the enormous thick clay deposits occurring on both continents (Tardy *et al*., 1991 and Sousa *et al*., 2007a). The current research is part of the Cretaceous-Tertiary Clay deposits and argillaceous sediments project within the wider clays and clay minerals in Africa programme. The project involves kaolins in South America (Brazil and Argentina) and parts of Africa (South Africa, Botswana, Namibia, Angola, Democratic Republic of Congo, Gabon, Cameroon, and Nigeria) aimed at contributing to the knowledge of clays and clay minerals in Africa. This study in Nigeria where much has not yet been done is necessary in filling the gaps in the overall interpretation of findings from the clays and clay minerals in Africa programme.

Nigeria is endowed with abundant deposits and widespread distribution of the clay minerals, especially kaolin. Data from the Federal Ministry of Solid Minerals Development shows that an estimated reserve of three (3) billion tonnes of good kaolinitic clay have been identified in many localities within the basement complex and sedimentary basins in Nigeria (Onyemaobi, 2002). Kaolin ($Al_2Si_2O_5(OH)_4$) group consisting of minerals such as kaolinite, dickite, nacrite, and halloysite is important and is widely used in various industrial applications, such as raw material in ceramics, paper, filling, coating, refractory, fiberglass, cement, rubber and plastics, paints, catalyst, pharmaceutics and agriculture (Ekosse, 2010). The physical and chemical characteristics of kaolin determine its ultimate application. Some of these characteristics are dependent on the environment of formation, geological origin, tectonic settings, geographic location and the method of processing (Murray and Kogel, 2005).

Studies have revealed that the composition of parent rocks affect the geochemistry and mineralogy of the clay type that is eventually formed in any given environment (Nesbitt and Young, 1989). Various studies have been carried out on the distribution, applications and occupational potentials of non-metallic mineral resources in Nigeria (Elueze, 1989, Ogunseiju, 1989, and Elueze and Bolarinwa, 1995). However, quite a number of the kaolinitic clay bodies which form the bulk of these mineral resources have not been adequately studied in detail with respect to their geochemical and mineralogical characteristics (Ajayi and Agagu, 1981; Onyemaobi, 2002). One of the important issues still open for research is to decipher the paleoenvironmental conditions and tectonic settings under which they were formed by exploring new physico-chemical, mineralogical, geochemical, isotopic, and geochronological data since they are valuable indicators of past climates and environment (Singer, 1980).

1.2 Problem Statement

Large continental kaolinitic deposits occur on either side of the South Atlantic Ocean, both within Africa and South America (Ekosse, 2010) and hitherto, there has never been any formal attempt to correlate them since both were together before and shared similar

geologic history until their breakup into separate continents during the Cretaceous period. This is creating a great gap in the knowledge of clay minerals in Africa even though several works have been done across both continents as earlier stated. Hence, there is still much uncertainty in correlations between the two continents as far as clay and clay minerals is concerned (Pankhurst *et al*., 2008 and Ernst *et al*., 2013). The continents of Africa and South America occupy strategic places in global tectonic understanding and have attracted geoscientific interest since the beginning of the studies on the continental drift (Torquato and Cordani, 1981). Hence, integration of new data will allow re-evaluation of the geological framework of the two domains and provide new insights for correlations between them. This research is directed towards filling the knowledge gap as the resulting information will be very useful in understanding more about the evolution of the Gondwana.

Geochronological timing of kaolinisation of kaolin deposits around the world is not known, leaving the whole of Mesozoic and early Cenozoic as possible times of kaolin formation (Gilg and Frei, 1997 and Gilg, 2000). Hence, there is need to explore and evaluate possible methods that can provide unambiguous true kaolinisation ages.

Kaolin is an important industrial mineral which has played a very important role in the economic and technological development of many industrialised nations (Murray, 2007). Nigeria is a mono-economic nation with petroleum contributing the largest percentage of her foreign exchange earnings and revenues. Considering the current dwindling of oil prices and the gradual reduction of its oil reserve, diversifying the economy of Nigeria will therefore call for the systematic investigation and characterisation of her vast occurrence of kaolinitic clays (Raw Materials Research and Development Council (RMRDC) Multidisciplinary Committee Techno-Economic Survey (MCTS) Report, 2003 and Ekosse, 2010). Hence, the proper documentation of physico-chemical, mineralogical, and industrial applications will be inevitable in boosting the nation's economy.

1.3 Motivation

The opening up of the Atlantic Ocean during the Mesozoic led to the breakup of the Pangaea and the subsequent individualisation of the South American and African

continents (Du Toit, 1921). Several studies have been carried out to establish the pre-drift geological correlations between the two continents based on the rock associations, tectonic links, geochronological data, mineralisation and structural patterns which are traceable across the Atlantic Ocean (Du Toit, 1937; Torquato and Cordani, 1981; Caby, 1989; Castaing *et al*., 1994; Trompette, 1997; Neves, 2003, Chaves and Neves, 2005; Dickson *et al*., 2005; Cordani *et al*., 2010; and Ernt *et al*., 2013). None of the studies evaluated the use of continental argillaceous sediments such as kaolins in pre-drift reconstructions which are good paleo-climatic and paleo-environmental indicators (Tabor *et al*., 2002) except Petschnick *et al*. (1996) whose work was limited to marine argillaceous sediments of the South Atlantic. Hence, the current research on the Cretaceous-Tertiary Kaolins in Nigeria is part of a wider project (National Research Foundation (NRF) Competitive Programme for Rated Researchers (CPRR) UID 91559): "Cretaceous-Tertiary clay deposits and argillaceous sediments" which involves parts of South America (Brazil and Argentina) and parts of Africa (South Africa, Botswana, Namibia, Angola, Democratic Republic of Congo, Gabon, Cameroon, and Nigeria). It is one of the pioneering research in using argillaceous sediments in the elucidation of correlation and theories regarding the assembly and dispersal of the two continental bodies.

The dynamic nature of the earth's climatic system is also a motivation for this research. Alverson *et al*. (2000) advocated for a deeper exploration of past climatic and environmental conditions as a means to enhance our ability to peer into the future. In addition, Stern *et al*. (1997) also emphasised that the place of documenting past climatic and environmental conditions in geologic record is critical for understanding factors associated with climate change. This will create better understanding to predict and respond to current and future climatic and environmental challenges.

The demand for kaolin which is also referred to as "white gold" (Ekosse, 2010) in the world market consistently continues to increase (Murray, 2007). Hence, the need for economic potential assessments of promising kaolin deposits.

1.4 Hypotheses

a) The geochemical characteristics of Cretaceous – Tertiary kaolins are influenced by their provenance and tectonic settings.
b) The oxygen and hydrogen isotopic compositions of the waters in which kaolins are formed vary systematically with paleoclimatic and paleoenvironmental conditions.
c) The dating of detrital minerals will provide geochronological information to constrain the timing of kaolinisation.
d) The African and South American Continents evolved from the break-up of Gondwana during the Cretaceous period.
e) The physico-chemical, mineralogical, geochemical compositions of kaolins determine its ultimate industrial application.

1.5 Objectives

1.5.1 Main Objective

The main objective of this study is to evaluate the environment of formation and tectonic settings of Cretaceous-Tertiary kaolins within the Eastern Dahomey and Niger Delta Basins in Nigeria.

1.5.2 Specific Objectives

The major objectives of this study are summarised below:

a) To determine the provenance and tectonic settings of the Cretaceous-Tertiary kaolins within the Eastern Dahomey and Niger Delta Basins in Nigeria.
b) To evaluate paleoenvironmental conditions under which the selected kaolins were formed.
c) To carry out geochronological dating of detrital zircon minerals in the kaolins.
d) To correlate the results from this study with selected Cretaceous African and South American kaolins and document the evolution of the Gondwana kaolins with particular emphasis on mineralogical, geochemical, isotopic and geochronogical characteristics.

e) To assess industrial applications of the kaolins.

1.6 Study Areas

The research involves the study of four selected Cretaceous-Tertiary kaolin deposits in Nigeria, namely:

i. The Cretaceous Lakiri and Eruku kaolins which are two of the study areas occur within the Abeokuta Group of the Eastern Dahomey Basin (Fig. 1.1). The stratigraphy of the Dahomey Basin can broadly be packaged into two – the Cretaceous Abeokuta Group and the Cenozoic Units (Ewekoro, Akinbo, Oshosun, Ilaro Formations, Coastal plain sands, and Alluvium) (Table 1.1) (Nwajide, 2013). The Abeokuta Group has been further subdivided by Omatsola and Adegoke (1981) into three formations: Ise Formation (oldest), Afowo Formation, and Araromi Formation (youngest).

The Ise Formation: this is a sequence of continental sands, grits and siltstones with a basal conglomerate overlying the Basement Complex. Interbedded kaolinitic clays occur up to metres in some places. Sporomorohs recovered from the shell-BP paleontologists including *Cicatricosisporites* sp. cf. *C. mohrioides, Pilosisporites trichopapillosus, Klukisporites pseudoreticulatus, Aequitriradites* aff. *verucosus* and *Stapilinisporites caminus* indicate a Neocomian (probably Valanginian – Barremian) age for the formation.

The Afowo Formation: This Formation, according to Omatsola and Adegoke (1981) is equivalent to the outcropping unit referred to as the “Abeokuta Formation”. It is mainly composed of coarse to medium-grained sandstones with variable, but thick, interbedded shales, siltstones and clays, with the shale component progressively increase towards the top. Its lower part is constituted of an alternation of brackish to loose fluviatile sands. Intense pyritisation of some horizons is common. On the basis of its palynomorph content (Billman, 1976) and the marine foraminifera and ammonites (e.g. Sphenodiscus and Pachydiscus) it bears (Omatsola and Adegoke, 1981), the formation has been dated Turonian to Maastrichtian. Its maximum recorded thickness is 2,300 metres.

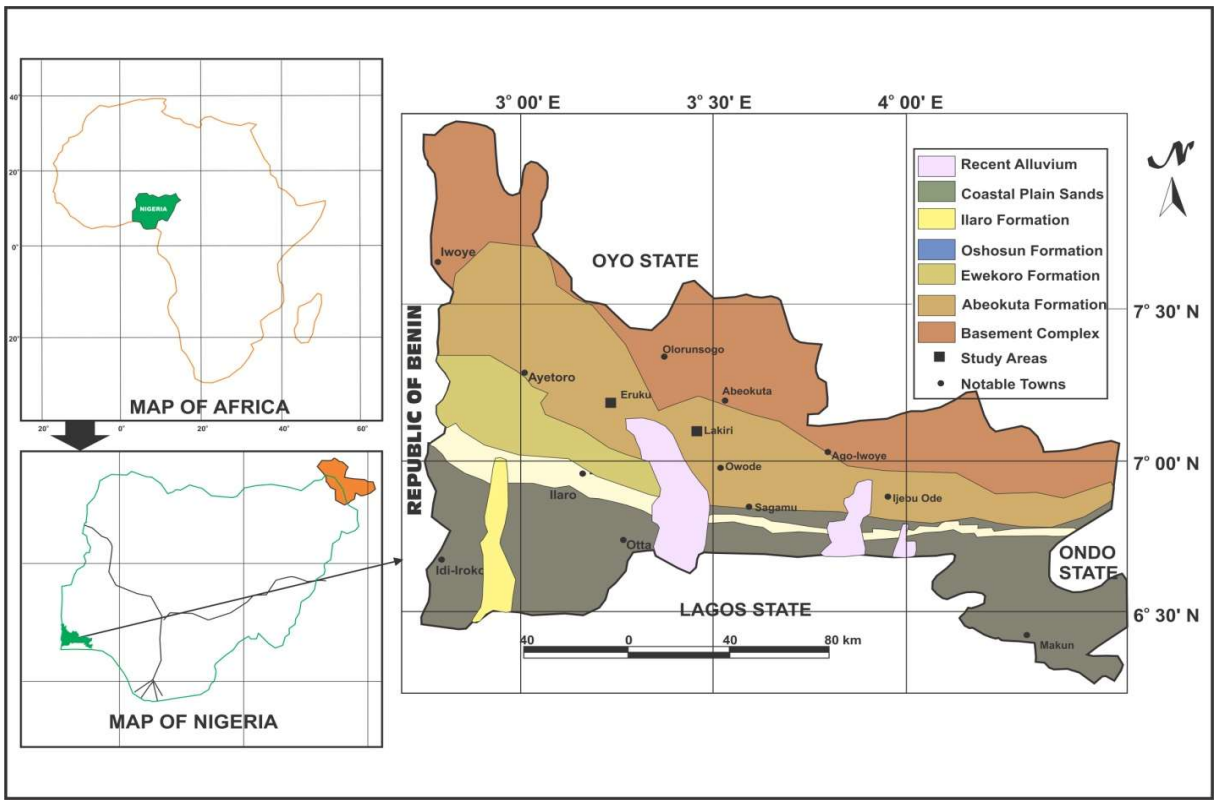

Figure 1.1: Geologic Map of Eastern Dahomey Basin showing the study areas (Modified after Billman, 1976).

Table 1.1: Summary of Formations within the Eastern Dahomey Basin (Modified from Nwajide, 2013).

Geologic Age (Ma)	**Formation**	**Lithology**
Recent (0.01 - 0)		Alluvium
Oligocene – Pleistocene (5.3 - 0.01)		Coastal plain sands
Middle-Upper Miocene (15.9 – 5.3)	Ilaro	Sands, phosphatic beds with intercalation of shales and clays
Middle Eocene (38.0 – 41.3)	Oshosun	Mudstones, claystones with interbeds of pebbly sandstones
Lower-Middle Eocene (41.3 – 56.2)	Akinbo	Shale with silty, glauconitic marl and conglomerate
Upper Paleocene (56.2 – 59.2)	Ewekoro	Thinly bedded glauconitic and sandy limestones
Maastrichtian-Paleocene (65 – 59.2)	Araromi	Sands underlain with shale and siltstones with thin interbeds of limestones and marls
Turonian- Maastrichtian (95 – 65)	Afowo	Sandstones with interbeds of shales, siltstones,and clays
Valanginian – Barremian (140 – 125)	Ise	Gritty sands and siltstones with interbeds of kaolinitic clays
Precambrian Basement Complex		

The Araromi Formation: This formation is composed of fine to medium-grained sands at the base, overlain by shale and siltstones with thin interbedded limestones and marls. Thin lignitic bands are also common. The shales are light grey to black, mostly marine and with very high organic content. The formation is richly fossiliferous, bearing abundant foraminifera, ostracodes, and palynomorphs. On the basis of this rich fossil contents, it has been dated Maastrichtian to Paleocene (Adegoke *et al*., 1980).

ii. The Tertiary Ubulu-Uku and Awo-Omama kaolins are the other two which occur within the Ogwashi-Asaba Formation of Niger Delta Basin (Fig. 1.2). The stratigraphy of the Niger Delta Basin can broadly be packaged into two – the subsurface and surface (Outcropping) Formations (Table 1.2) (Nwajide, 2013).

The **Ogwashi-Asaba Formation** consists of white, blue, and pink clays, cross-bedded sands, carbonaceous mudstones, shales and seams of lignite. The type locality is at Eke Mgbalimgba in Ogwashi-Asaba, Delta State but extends from Okitipupa Ridge through Onitsha, Ozubulu, Nnewi, Ikot Ekpene, Uyo, and Calabar where it is overlapped by the Benin Formation. Ogwashi-Asaba Formation contains some plant remains, which indicate an Oligocene – Miocene age and a continental environment of deposition for it (Nwajide, 2013).

1.7 Climate

Nigeria can be divided into four climatic regions: the subequatorial region, tropical hinterland, tropical continental north, and the highlands (Nwajide, 2013). The study areas fall within the subequatorial region in the south from coast inland for 130-150 km characterised by 1500-3000 mm rain, with double maxima, and daily relative humidity over 60-90% (Nwajide, 2013). In this region, there are four seasons – long wet season from mid-March to July, short dry season in August (except in the southern fringe of the delta), short wet season from August to October, and long dry season from November to mid-March (Iloeje, 1981).

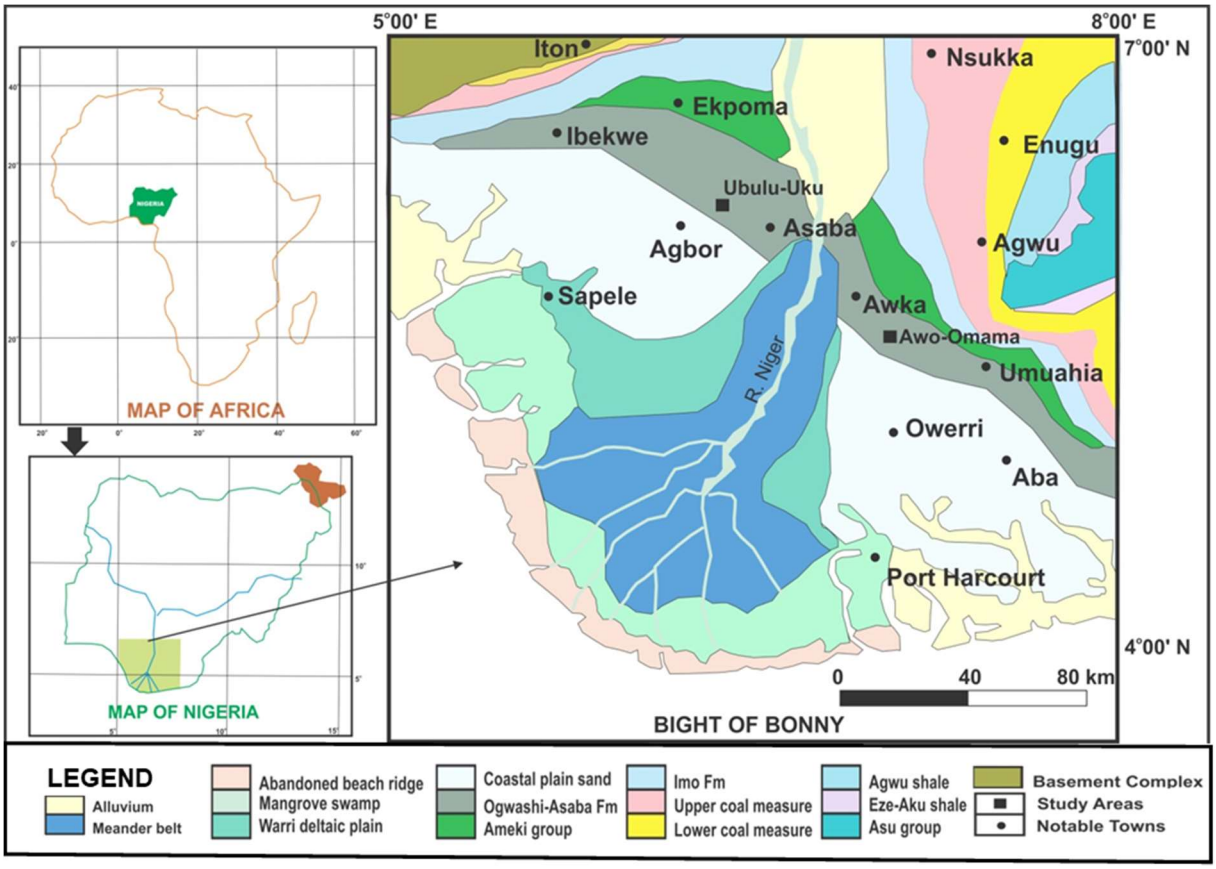

Figure 1.2: Geologic Map of Niger Delta Basin showing the study areas (Modified after Nwajide, 2013).

Table 1.2: Summary of Surface and Subsurface Formations within the Niger Delta (After Nwajide, 2013).

Geologic Age (Ma)	**Surface (Outcrop) Formations**	**Lithology**	**Subsurface Formations**	**Lithology**
Oligocene – Present (28 – 0)	Benin	Cross-bedded sands with clay lenses and lignites	Benin	Sands
Oligocene - Miocene (28.1 – 5.3)	Ogwashi-Asaba	Clays, silts, sands and thin to thick lignite seams	Agbada	Alternating sands/mudrock
Eocene – Early Oligocene (47.8 – 28.1)	Ameki	Clays and silts with thin shelly Limestones.		
Paleocene – Early Eocene (66 – 47.8)	Imo	Shales with sand lenses, marls and fossiliferous limestones.	Akata	Marine shales with sandy and silty beds

1.8 Delimitations

The current research focuses on selected kaolins in Nigeria within the Cretaceous (165 - 66 Ma) during the Mesozoic to Tertiary (66 - 23.03 Ma) during the Cenozoic periods. The study does not discuss the timing and sequence of paleoenvironmental changes across the Cretaceous-Tertiary boundary even though it remains controversial at the moment, nor look into the impact-mass extinction and multiple impact-mass extinction across the boundary hypotheses (Alvarez *et al.,* 1980). Furthermore, flora and fauna records during this period was not discussed. The study does not consider kaolins in South America but infer from literature.

Chapter Two
Literature Review

This chapter reviews available literature on kaolins, regional geologic settings of Nigeria, Cretaceous to Tertiary kaolins in Nigeria, provenance and tectonic settings of kaolins, kaolins in paleoclimatic and paleoenvironmental studies, dating of kaolins, applications and beneficiation of kaolins.

2.1 Kaolins

2.1.1 Kaolin group

Kaolin minerals include kaolinite ($Al_2Si_2O_5(OH)_4$), dickite ($Al_2Si_2O_5(OH)_4$), nacrite ($Al_2Si_2O_5(OH)_4$), and halloysite ($Al_2Si_2O_5(OH)_4.2H_2O$) respectively (Murray, 2007). Kaolinite is by far the most common kaolin mineral with the theoretical chemical composition: 46.54% SiO_2, 39.50% Al_2O_3, and 13.96% H_2O (Murray, 2007), whereas the remaining three are relatively uncommon.

Kaolins are two layered clays consisting of 1:1 ratio of tetrahedral and octahedral layers continuous in the z- and x- axes direction, respectively, and stacked one above one another in the y-direction (Figs. 2.1 – 2.4). The four tips of tetrahedral are occupied by oxygen ions whilst the center is occupied by silicon which shares its four positive charges with four oxygen at the tips. The center of the octahedral sheet is occupied by Al^{3+} whilst the tips are occupied by oxygen and hydroxyl ions. It is the combination of one octahedral sheet and a tetrahedral sheet that makes one kaolinite unit. The thickness of each unit is 7.13 Å (Murray, 2007).

Halloysite, unlike the other kaolins has a single layer of water molecule between its sheets. The basal spacing is about 10.25 Å (Fig. 2.4) but when heated, the water is lost and the basal spacing reduces to 7.13 Å which is equivalent to kaolinite basal spacing.

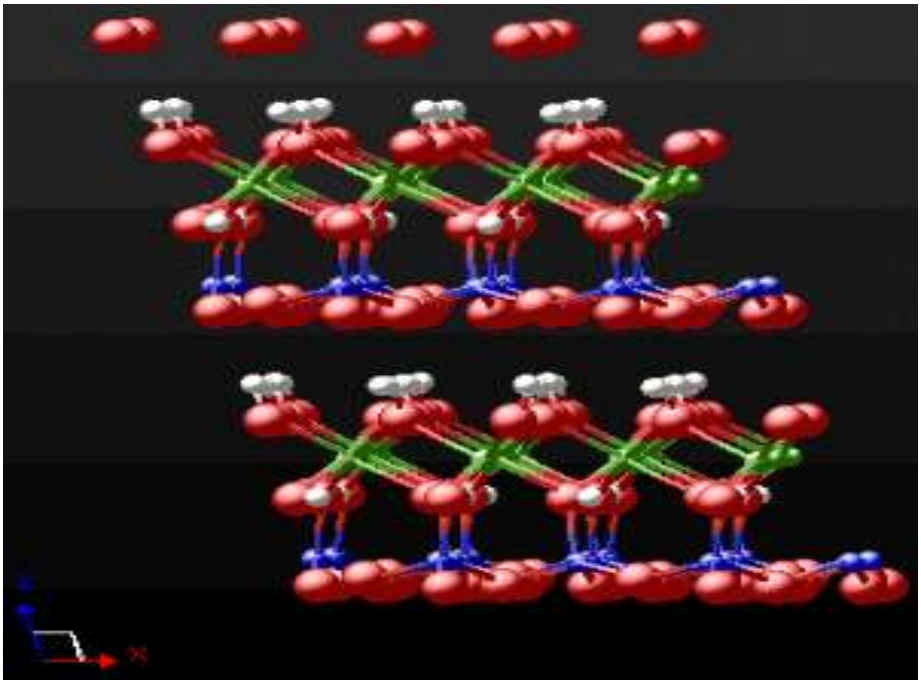

Figure 2.1: Crystal structure of Kaolinite (Green: Al, Red-White: OH, Red: O, and Dark blue: Si) (After Downs and Hall-Wallace, 2003).

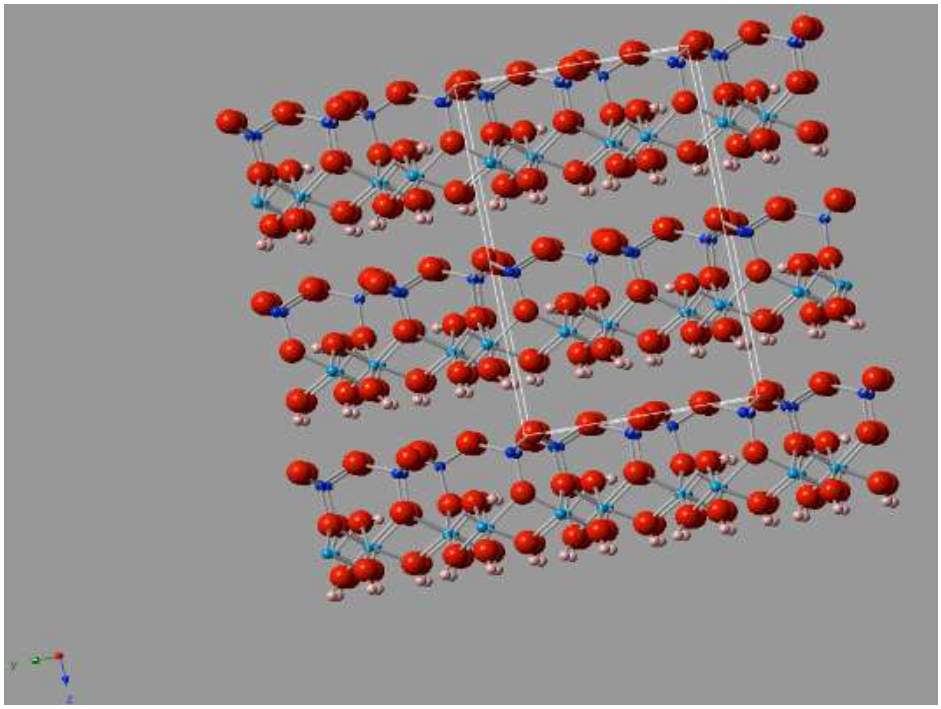

Figure 2.2: Crystal structure of Dickite (Light blue: Al, Red-Orange: OH, Red: O, and Dark blue: Si) (After Downs and Hall-Wallace, 2003).

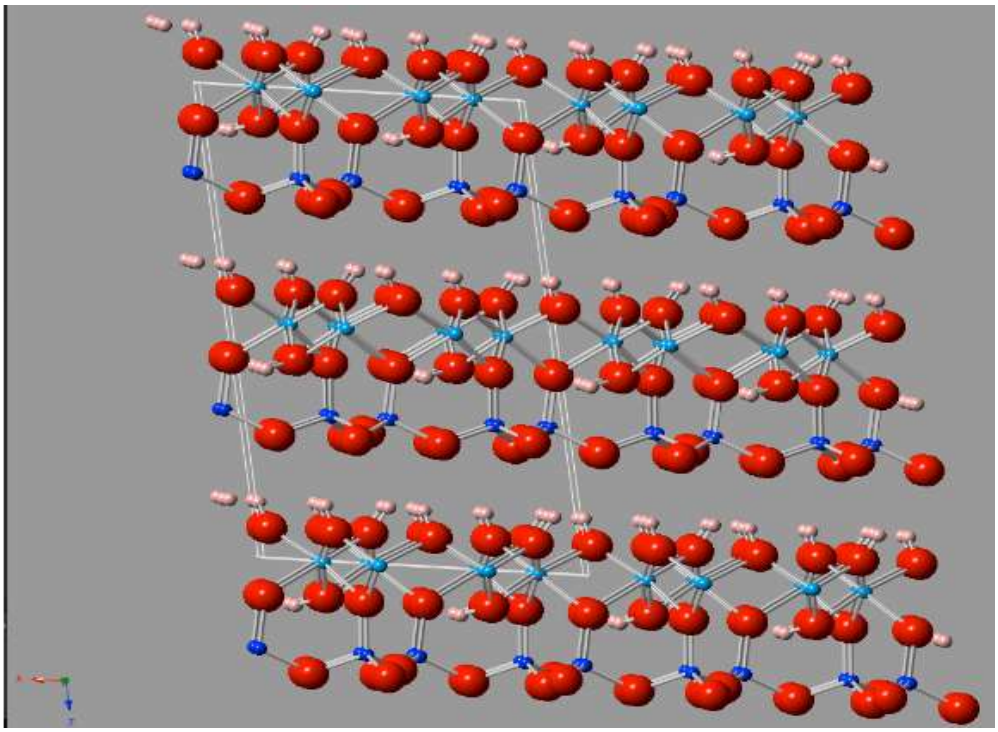

Figure 2.3: Crystal structure of Nacrite (Light blue: Al, Red-Orange: OH, Red: O, and Dark blue: Si) (After Downs and Hall-Wallace, 2003).

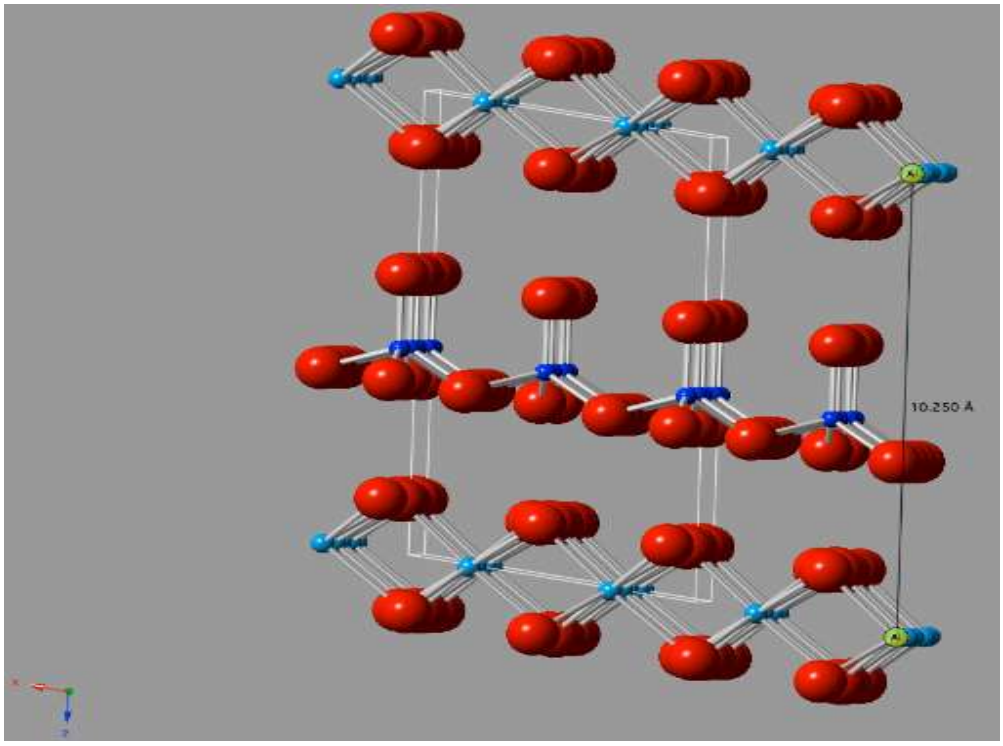

Figure 2.4: Crystal structure of hydrated Halloysite (Light blue: Al, Red: O, and Dark blue: Si) (After Downs and Hall-Wallace, 2003).

The Association Internationale Pour l'Etude des Argiles (AIPEA) Nomenclature Committee recommended the term 7 Å halloysite and 10 Å halloysite for hydrated and dehydrated halloysites, respectively, to designate the two forms (Murray, 2007). Apart from halloysite, no other kaolin show swelling characteristics (Millot, 1970). A summary of the lattice parameters for the kaolin minerals are given in Table 2.1.

Table 2.1: Lattice parameters for kaolin minerals (After Haq *et al.,* 2008).

	Kaolinite		**Hydrated Halloysite**	**Dehydrated Halloysite**	**Dickite**	**Nacrite**
a	5.155 Å	**a**	5.14 Å	5.14 Å	5.1474 Å	8.906 Å
b	8.945 Å	**b**	8.90 Å	8.90 Å	8.939 Å	5.146 Å
c	7.405 Å	**c**	20.7 Å	14.9 Å	14.390 Å	15.664 Å
α	91.7°	**β**	99.7°	101.9°	96.483°	113.58°
β	104.862°					
γ	89.822°					

2.1.2 Kaolin genesis

Kaolins commonly form either as direct product of the weathering or as products of hydrothermal alteration of pre-existing rocks and minerals. They can thus be classified geologically on the basis of their origin into two major groups, namely:

a. Primary or Residual kaolins, and
b. Secondary or sedimentary kaolins.

Primary or Residual kaolin formation is favoured in a relatively humid climate where rainfall exceeds evaporation and downward percolation and lateral movements of groundwater results in the leaching of K, Na, Mg, Ca and other trace metals. They are those formed as a result of insitu weathering or hydrothermal alteration of parent rocks such as granites, gneisses, pegmatites, etc. In the majority of rocks, feldspars and micas

are easy targets of chemical weathering, which alters these minerals into kaolins with inclusions of chemically resistant quartz and ferric oxides (Figure 2.5). Both the quartz and the iron oxides may be subsequently leached away, leaving behind a pure/clean residual kaolin product. In many cases, however, the quartz contents of the kaolins are not effectively removed and this makes quartz (apart from muscovite, tourmaline, and zircon) one of the common co-existing minerals in kaolinitic deposits. Where the iron oxides in the kaolin is not effectively removed, it can impart different colours like greenish, brownish or in some cases blackish colouration (depending on the state of iron in the kaolin). Organic content of the kaolinitic deposit is also influential in the overall colouration of the deposit.

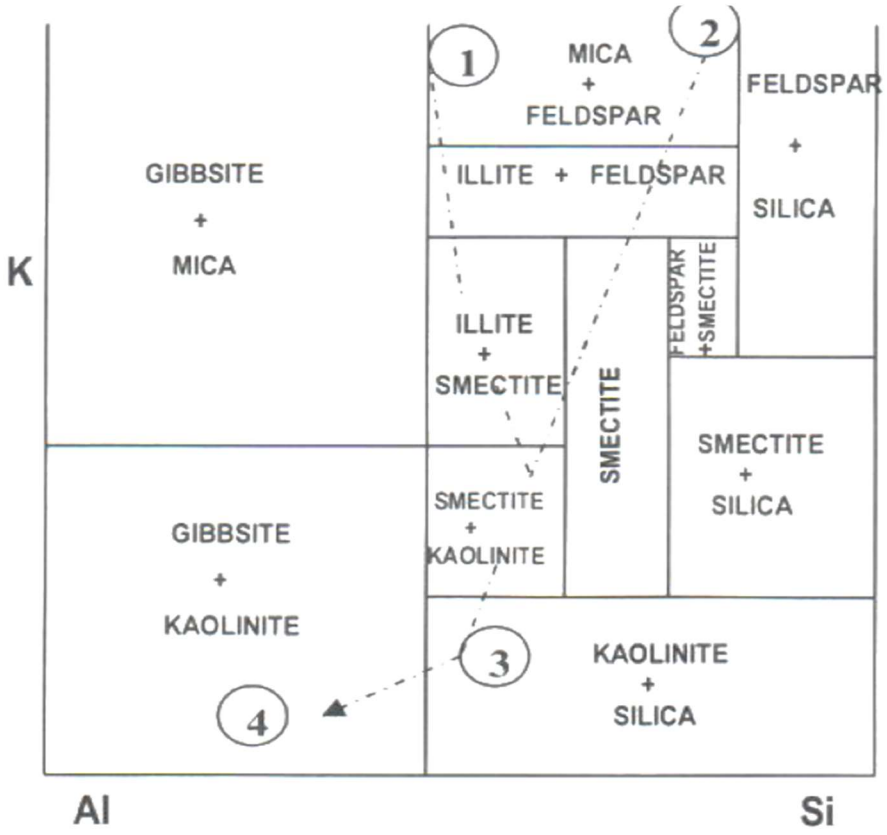

Figure 2.5: Phase diagram applicable to chemical weathering of mica and feldspar (Murray and Keller, 1993).

Since residual kaolins are products of direct weathering or hydrothermal alteration processes, it is essential that they have to be emplaced and protected from forces of erosion and transportation. In cases where they could not be so protected they are eroded, transported, and deposited in the sedimentary environments where they form the transported/sedimentary kaolin deposits. These deposits are found in lacustrine, paludal, deltaic, and lagoonal environments (Murray and Keller, 1993). They have commonly low concentrations of unstable minerals form the parent rocks. The composition of the parent rock, nature of environment of formation, and tectonic settings have notable effect on the clay product formed as a result of weathering processes. Acidic rocks as well as acidic environments tend to produce kaolins, whilst basic rocks and alkaline environments tend to produce clay minerals of smectite group. Some of the factors believed to control the geochemistry of sedimentary kaolins include: (1) the detrital minerals like quartz, feldspars, zircon, rutile, and leucoxene that reflect the source area composition, (2) the newly formed minerals during weathering including kaolinite and non-clay minerals such as anatase, and (3) post-depositional alterations such as diagenesis and weathering (Baioumy, 2014). Secondary kaolins are believed to be purer than primary kaolin (Murray, 1980).

2.2 Regional Geologic Settings of Nigeria

The geology of Nigeria comprises of the crystalline Basement Complex (Precambrian (>600 Ma)), younger granites (Jurassic (200-145 Ma)), and the Mesozoic – Cenozoic sediments (Cretaceous - recent (<145 Ma). The Basement complex covers about half of the surface area of the country with strong structural control on the architecture and evolution of the sedimentary basins (Fig. 2.6) (Obaje, 2009).

2.2.1 The Basement Complex

The Basement Complex of Nigeria constitutes parts of upper proterozoic mobile belts sandwiched between West African and Congo-Kasai Cratons. Obaje (2009) recognised the following four (4) main petrological groups within the Nigeria Basement Complex:

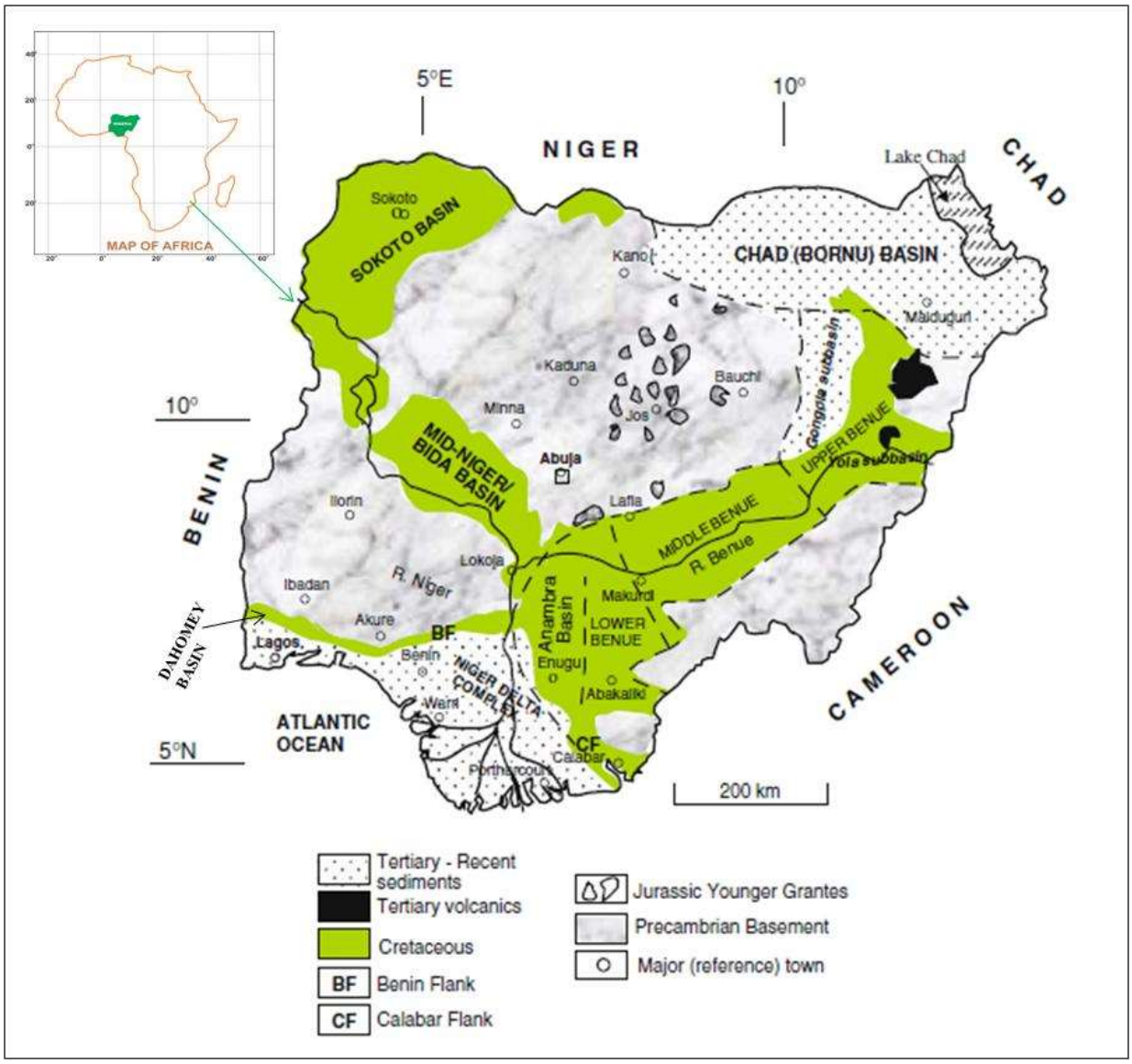

Figure 2.6: Geologic Map of Nigeria showing the Basement complex and the Sedimentary Basins (Adapted from Obaje, 2009).

(i) **Migmatite-gneiss complex**, which were often referred to as **Migmatite-gneiss-quartzite complex** (Rahaman, 1976; 1988).

This covers over 30% of the total surface area of Nigeria. According to Dada (2006), it is a heterogenous rock group in which the following components are distinguished:

a. Early (Grey) gneiss which constitute the oldest recognisable rock. It is grey foliated biotite/hornblende gneiss of granodioritic to tonalitic composition.

b. Mafic to Ultramafic components which are commonly present as amphibolites, biotite and biotite-hornblende schists.
c. Felsic components usually of granitic composition with texture varying from aplitic to granitic to pegmatitic. The coarse grained granite gneiss which often occurs as mappable units within the basement complex is a prominent member of this group.

This group of rocks is believed to have experienced a rugged tectonic cycle of formation with four orogenies namely Liberian (2800 ± 200 Ma), Eburnean (2000 ± 200 Ma), Kibaran (1100 ± 200 Ma), and Pan-African (600 ± 150 Ma) (Grant, 1978; Ajibade, 1980; Ogezi, 1977). The Pan-African event is well documented by the numerous ages obtained from different radiometric techniques that fall within the limits quoted for this orogeny.

(ii) **Schist belts (Slightly Migmatised to Non-Migmatised metasedimentry and metaigneous rocks),** which are often referred to as **Newer Metasediments** (Oyawoye, 1964), or **Younger Metasediments** (McCurry, 1976).

They consist of metamorphosed sediments (pelitic to semi-pelitic rocks, quartzite, calc-silicate rocks, metaconglomerates and pebbly schists, greywackes) and associated amphibolites and other metavolcanic rocks.

(iii) Older granites (Pan African Granitoids).

The term “Older granite” was introduced by Falconer (1911) which was later referred to as “Pan African Granitoids” by Dada (2006). They range widely in age (750 – 450 Ma) and composition from tonalities, diorite through granodiorites to true granites and syenites. Charnockites were emplaced during this period as well (Tubosun *et al.,* 1984; Olarewaju, 2006). However, on the basis of their textural characteristic, Rahaman (1988) discarded the earlier classification and recognized the following members of this suite:

a) Migmatic granite
b) Granite gneiss
c) Early pegmatite and fine grained granite

d) Homogenous to coarse porphyritic granite

e) Slightly deformed pegmatites, aplites and vein quartz

f) Undeformed pegmatites, two-mica granites and vein quartz

(iv) Undeformed acid and basic dykes

They are widespread in the basement complex and have been described in association with the gneisses and older granites. According to most authors, they occur as the youngest members of the basement complex regarding the crosscutting relationship with the host rock (Rahaman, 1988). They range in thickness from about a few millimeters to half a meter and composition from felsic pegmatites, microgranites, aplites and syenite to basic dolerite and lamprophyric dykes (Dada, 2006)

2.2.2 Sedimentary Basins in Nigeria

There are seven sedimentary basins in Nigeria, namely: Dahomey, Niger Delta, Benue, Anambra, Bida (Nupe / Mid-Niger), Chad, and Sokoto Embayment. They are distributed so that they form an imperfect X-shaped configuration (Fig. 2.6). Onshore, they cover a total area of 500,000 km^2 i.e. roughly half the surface area of Nigeria. To this must be added to the offshore part of the coastal basins whose extent is unknown. Apart from the Niger delta and Bida Basins, these basins transgress the Nigerian border extending into neighbouring countries: Benin, Niger, Chad and Cameroon Republics. The Nigerian Sedimentary Basin *sensu lato* is filled with Cretaceous – Recent sediments. The sediments range from continental to marine through transitional. The basins can be classified on the basis of their position (location) relative to the West African Craton as: (i) Intracratonic, (ii) Peri-cratonic and (iii) "Aulacogen".

(i) Intracratonic Basins are formed by depressions within the craton. They are Bida, Sokoto and Chad Basins. They are broad downwarps along the margin of the Nigerian shield (Basement Complex). Except for the Bida Basin, they constitute the Southern

edges of major epeirogenic basins that lie mainly in the neighbouring countries (Niger and Chad).

(ii) Peri-Cratonic Basins are formed at the periphery of and marginal to the West African Craton. They are the Niger delta and Dahomey Basins. They may also be called peri-oceanic basins because of their coastal location.

(iii) “Aulacogen”: This is a basin formed as a result of the opening of the continental crust. The Benue “Trough” which eventually formed the Benue Basin is the only example of an aulacogen in Nigeria. It is also sometimes considered as an example of a coastal basin. This is because (like the peri-oceanic basins) it is genetically related to the initiation of the Nigerian continental margin during the Mesozoic.

The study areas fall within the peri-oceanic Dahomey and Niger Delta Basins located in the southern part of Nigeria (Fig. 2.6).

Dahomey Basin

The Dahomey Basin, also called the Dahomey Embayment, Benin Basin, or West Nigerian Basin in older literature, extends from southeastern Ghana in the West, through Southern Togo and southern Benin Republic (formerly Dahomey) to Southwest Nigeria (The western flank of the Niger Delta) (Figs. 2.7 and 2.8). The Basin (together with other West African coastal sedimentary basins) was initiated during the Mesozoic in response to the separation of the African – South American land masses and the subsequent opening of the Atlantic Ocean. Deposition was initiated in fault-controlled depressions on the crystalline Basement Complex. The depressions were a result of rift-generated basement subsidence during the Early Cretaceous (Neocomian) (Billman, 1976; Omatsola and Adegoke, 1981).

The axis of the basin and the thickest sediments occur slightly west of the border between Nigeria and Benin Republic. The basin is bounded on the west by faults and other tectonic structures. Its eastern limit is marked by the Benin Hinge line, a major fault structure marking the western limit of the Niger Delta Basin.

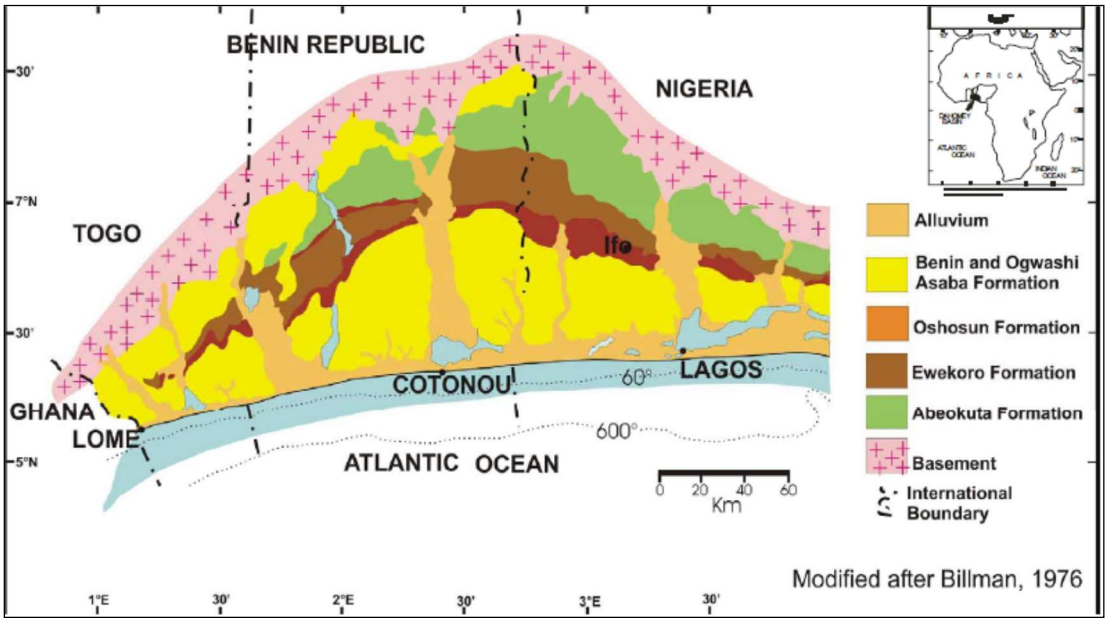

Figure 2.7: Outcrop Geology of the Dahomey Basin.

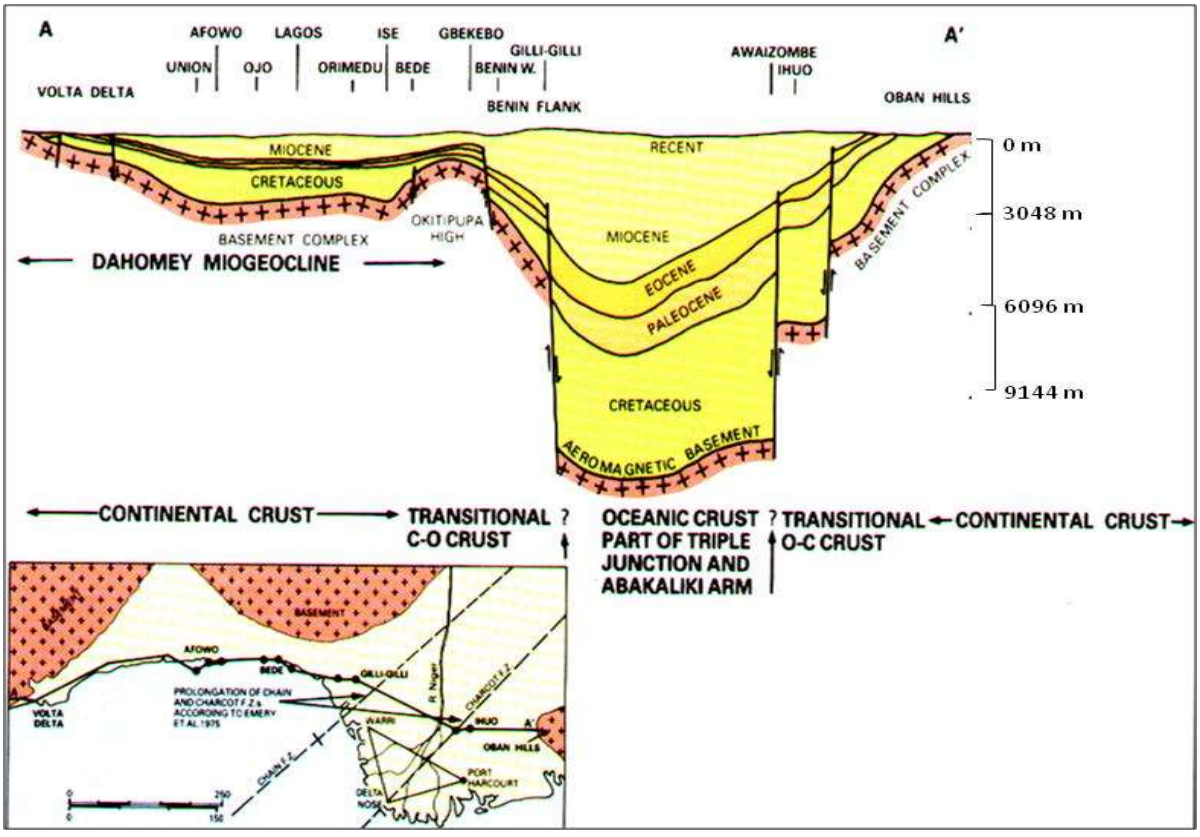

Figure 2.8: East-West Geological Section showing the Dahomey and Niger Delta Basins (After Whiteman, 1982).

To the west of the Benin Hinge line is the Okitipupa Ridge (Adegoke, 1969). The tertiary sediments of the Dahomey Basin thin out and are partially cut off from the sediments of the Niger Delta Basin against this ridge of basement rocks. The basin's offshore limit is not well defined.

Niger Delta Basin

The Niger Delta is the most important sedimentary basin in Nigeria both in size and thickness of sediments. It is also the most important, from the economic point of view as its petroleum reserves provide a large part of the country's foreign exchange earnings. The delta covers a land area in excess of 105,000 km^2 (Avbovbo, 1978). To this must be added a larger offshore part. It extends in an East-West direction from S.W. Cameroon to the Okitipupa Ridge. Its apex is situated southeast of the confluent of the Niger and Benue Rivers.

It lies mainly in the Gulf of Guinea to the Southwest of the Benue Trough and constitutes the most important Cenozoic construction in the South Atlantic. It is generally agreed that the modern Niger delta is built on an oceanic crust. Supporting arguments come from the pre-continental drift reconciliation (Carey, 1958; Stoneley, 1966) – which indicates an important overlap of NE Brazil on the present Niger delta; and from a series of geological and geographical observations, for example, the presence of a series of linear subdued and alternatively positive and negative anomalies beneath the Niger delta, which was interpreted as seafloor spreading lineations (Burke *et al.*, 1971).

2.3 Cretaceous to Tertiary Kaolins in Nigeria

Most of the sedimentary kaolins in the world, geologically occur as Cretaceous and Tertiary argillaceous sediments (Murray, 1998). Ekosse (2010) with these in mind advocated that kaolin exploration in Africa should be focused on investigating Cretaceous and Tertiary argillaceous sediments. In Nigeria, many of the Cretaceous-Tertiary kaolin deposits occur within the sedimentary basins which are believed to be filled with Cretaceous-Recent sediments except for some Tertiary kaolin occurring within the Jos Plateau in areas underlain by the younger granites (Table 2.2).

Table 2.2: Notable Kaolinitic Clay deposits within the Sedimentary basins in Nigeria.

Basin	State	Geographic locations	Northings	Eastings
Dahomey	Ogun	Onibode	7° 8' 0"	3° 27' 0"
		Ayetoro	7° 59' 0"	6° 0' 0"
		Lakiri	7° 5' 21"	3° 27' 26"
		Sokelu	7° 8' 17"	3° 26' 17"
		Kepe	7° 7' 2"	3° 15' 55"
		Eruku	7° 10' 20"	3° 15' 0"
	Lagos	Ikorodu	6° 37' 0"	3° 31' 0"
Niger Delta	Akwa Ibom	Eket	4° 39' 0"	7° 56' 0"
		Ikot-Ekpene	5° 11' 0"	7° 56' 0"
		Uyo	5° 3' 0"	7° 56' 0"
	Abia	Ibere	5° 30' 0"	7° 38' 0"
	Delta	Ukwu-Nzu	6°14'44"	6° 29' 0"
		Ubulu-Uku	6° 24' 0"	6°25'18"
	Rivers	Buan	4° 37' 0"	7° 29' 0"
	Imo	Awo-Omama	5° 39' 23"	6° 56' 4"
Sokoto	Kebbi	Illo	11° 33' 0"	3° 42' 0"
		Kaoje	11° 11' 0"	4° 7' 0"
Chad	Borno	Maiduguri	11° 50' 42"	13° 9' 36"
Anambra	Anambra	Ozubulu	5° 57' 0"	6° 51' 0"
	Enugu	Enugu	4° 35' 23"	7° 49' 12"
Bida	Kogi	Felele	7° 48' 0"	6° 44' 0"
	Niger	Gbako	9° 30' 0"	6° 6' 0"
Lower Benue	Ebonyi	Abakaliki	6° 20' 0"	8° 6' 0"
		Afikpo	5° 53' 0"	7° 55' 0"
Middle Benue	Benue	Apa	7° 45' 0"	7° 58' 0"
		Iga Okpaya	7° 33' 0"	7° 52' 0"

Source: Modified from RMRDC MCTS Report (2003) and Ekosse (2010).

The only previous works on the Ubulu-Uku and Awo-Omama deposits were those conducted by the Geological Consultancy Unit (G.C.U.) of the Department of Geology, University of Ife (now Obafemi Awolowo University) on behalf of the National Fertilizer Company of Nigeria Limited in 1986 which was published by Emofurieta *et al*. (1992). The investigation was directed mainly at assessing the suitability of the clays as coating agent in the manufacture of Nitrogen, Phosphorous, and Potassium (NPK) fertilizer; the objective therefore is different from that of the present study. The mineralogy of the two

deposits indicated that the kaolinite content ranges from 81-85 % with the amount of quartz ranging from 11-26 %. The chemistry of the Ubuku-Uku with average contents of 59.97 %, 24.66 %, and 7.11 % for SiO_2, Al_2O_3, and H_2O^+, respectively, is similar to the corresponding values of 60.84 %, 24.37 %, and 7.15 % obtained for the Awo-Omama kaolins (Emofurieta *et al*., 1992). They concluded that the chemistry reveals that both deposits are siliceous but beneficiation would yield very high quality kaolinite suitable for various industrial uses and applications.

2.4 Provenance and Tectonic Settings of Kaolins

Labile minerals like feldspars under surficial environment gradually loses calcium (Ca), potassium (K), and sodium (Na) due to chemical weathering to form more stable minerals while degradation of rocks into smaller sizes without possibly any geochemical and mineralogical changes are associated with physical weathering (Fedo *et al*., 1995). Climatic factors such as rainfall and temperature govern weathering conditions and reactions which control the mineralogical and geochemical composition of the resulting material (Dingle and Lavelle, 1998). Hence, geochemical variations of major, trace and rare earth elements (REEs) can be good geochemical proxies in paleoclimatic, paleoenvironmental, provenance analyses, and tectonic settings considerations (Bhatia, 1983; Roser and Korch, 1986; and Nesbitt and Young, 1989).

Several studies on the various methods for the determination of major, trace and rare earth elements in various matrices with satisfactory sensitivity, selectivity, and reliability have been carried out (Bulska and Ruszczynska, 2017). The inductively coupled mass spectrometry (ICP-MS) is widely used in routine multielemental determination at the trace and ultratrace level in liquid samples with different matrix composition. The ICP-MS analytical procedure require previous digestion of solid samples. However, the recent development in ICP-MS has led to the advent of the introduction of the laser ablation (LA) application. The LA-ICP-MS allows direct solid sampling which avoids wet decomposition of the sample as well as risk of contamination during sample preparation (Bulska and Ruszczynska, 2017).

The geochemistry of sediments can be altered by post-depositional processes such as weathering and diagenesis since some minerals containing Ca, Na, magnesium (Mg), Iron (Fe), and manganese (Mn) degrade quickly during weathering to form Al-rich clays such as kaolins (Cox *et al*., 1995). Hence, the distribution of trace elements, which display relatively immobile behavior such as REEs, yttrium (Y), scandium (Sc), cobalt (Co), zirconium (Zr), and chromium (Cr) have been used as provenance indicators (Taylor and McLennan, 1985). However, the minerals in which these elements are hosted can as well determine the extent of occasional modifications by effect of weathering, hydraulic sorting, and diagenetic processes on the chemical signature of the source rock (Bock *et al*., 1998).

The REEs are generally believed not to be affected by fractionation during sedimentation processes and are readily insoluble in most natural waters and thereby provide relevant information concerning the provenance of the sediments. They are well concentrated in the clay fraction especially the kaolinite as the principal carrier (Prudêncio *et al*., 1989) but lower in the silt and sand fractions due to the dilution effect of quartz with low REE content (Cullers et al., 1988). The REEs with atomic numbers 57-71 are the lanthanide series elements, which are divided based on mass into light REE (LREE) with atomic masses <153 (Lanthanum (La), Cerium (Ce), Praseodymium (Pr), Neodymium (Nd), Samarium (Sm), and Europium (Eu)) and heavy REE (HREE) with atomic masses >153 (Gadolinium (Gd), Terbium (Tb), Dysprosium (Dy), Holmium (Ho), Erbium (Er), Thulium (Tm), Ytterbium (Yb), Lutetium (Lu)). The REE concentration values are usually normalised relative to common standard such as chondritic meteorites (Nakamura, 1974), Post-Achaean Australian Shale (PAAS) (Taylor and McLennan, 1985), North American Shale Composite (NASC) (Li, 2000). Gromet *et al*. (1984) and McLennan (1989) postulated that a deviation of the LREE enrichment relative to HREE and a negative Eu anomaly in a chondrite-normalised diagram for PAAS is indicative of intense weathering in the source area, diagenetic or hydrothermal overprint.

Discrimination plots, functions, indices, and elemental ratios of major and trace elements have been developed (For example by Bhatia, 1983, Nesbitt and Young, 1982; Roser and Korch, 1988; and Hofmann *et al*., 2001). Ohta and Arai (2007) and Price and Velbel

(2003) presented a critical review of the criteria in evaluating the utility of weathering indices. They concluded that an ideal chemical weathering index should be applicable for comparison of studies on different parent materials, locations, and ages. This implies, it should have wide application and maximum comparison with other studies taking into account behaviours of multiple elements with minimum risk of obtaining biased results based on restrictive assumptions (Ohta and Arai, 2007).

The Chemical Index of Alteration (CIA) was proposed by Nesbitt and Young (1982) using major element geochemistry in inferring Early Proterozoic climates and plate motions. It has also been applied in evaluating weathering history of modern and ancient sediments (Selvaraj and Chen, 2006). Cox *et al.* (1995) and Potter *et al.* (2005) applied the index of compositional variability (ICV) to discriminate source rock types based on major element geochemistry. They concluded that variability in the ICV values could be due to variations in source rock composition or to differences in weathering intensity.

Dill *et al*. (1997) used trace elements and mineralogical data in discriminating between hypogene and supergene kaolinisation of clay deposits in Western Peru. The distinction was possible based on the fact that sulphur (S), barium (Ba), and strontium (Sr) are considerably enriched in kaolin during hydrothermal alteration whereas chromium (Cr), niobium (Nb), titanium (Ti), and REEs are concentrated during weathering.

Dombrowski (1982) and Dombrowski and Murray (1984) in resolving the controversies regarding the origins of the soft (predominantly Cretaceous) and hard (Tertiary) Georgia sedimentary kaolins applied Th and Co trace element geochemistry. They distinguished the soft Tertiary kaolin deposits derived from granite and gneiss and the hard Cretaceous derived from phyllite and schist. The immobility of Th under supergene conditions and its concentration in alteration products is vital in source material analyses.

Baioumy *et al*. (2012) interpreted that the positive correlation observed between the total REE and P_2O_5 contents in the clay fractions of sedimentary kaolin deposits from Sinai, Egypt is indicative of the occurrence of most of the REEs in the phosphate minerals. They further inferred the heterogeneity and less maturity of Carboniferous kaolin deposits relative to the homogenous and matured Cretaceous kaolins from their respective

mineralogical and geochemical compositions. They therefore concluded that the Carboniferous kaolins have local sources and did not travel far before deposition while the Cretaceous kaolins have common source and deposited in remote basins. Baioumy (2014) based on the integration of major, trace, and REE geochemistry of clay fractions of the Cretaceous sedimentary kaolins, Red Sea, Egypt concluded that they were from a mixture of mafic (with relatively high TiO_2 and Ni content), granitic (with REE pattern with negative Eu anomaly as well as high Zr and Y contents), and alkaline (with abnormally high Nb contents) rocks.

Ekosse (2001) in determining the provenance of the Kgwakgwe kaolin deposits in Southeastern Botswana concluded based on the TiO_2/Al_2O_3 plot that the source of the materials was predominantly granite/rhyolite. Furthermore, the K/Rb ratios between 268 and 337 were interpreted based on the findings of Zawada (1988) and Campbell and Williams (1965) to represent freshwater to brackish conditions of deposition of the sediments. In addition, kaolin formation within Kgwakgwe Basin was attributed to fluid acidity by circulation of meteoric water and groundwater activity rather than fluid temperature due to the absence of high temperature minerals usually associated with kaolins of hypogene origin.

The characterisation of two Cretaceous kaolin facies from Ediki, Southwest Cameroon as having low alumina content, CIA, and high Si_2O_3/Al_2O_3 ratio with relative K enrichment over the alkali was interpreted to represent partial kaolinisation processes, low to moderate degrees of crystallinity and significant quartz contamination in both facies (Diko and Ekosse, 2013).

Through Earth's history, continents have spilt and have reassembled. Continental rifts are due to extensional processes within the continents which bring about 'thinning' of the continental crust surrounding the rift with increased extension. Such extension in oceans occur in mid-ocean ridges leading to the generation of new oceanic crust through the process of ocean floor spreading. Eventually, two margins separated by an ocean are called passive margins (Kearey and Vine, 1990; Verma and Armstrong, 2013).

Bhatia (1983) applied major element geochemistry of Paleozoic Sandstone suites of Eastern Australia in discriminating plate tectonic settings for sedimentary basins by proposing a discrimination plot based on first and second discriminant functions of the major element analyses. He concluded from the study that sedimentary basins may be assigned to oceanic arc, continental island arc, active continental margin, and passive continental margin. Based on this work, Valiani and Rezaee (2014) determined the tectonic settings of clay deposits within the Kahrizak Formation in East of Tehran, Iran as active continental margin. Bhatia and Crook (1986) reported decrease in V, Sc, and the Ba/Rb, K/Th, and K/U ratios with corresponding increase in the light rare earth elements (LREE) for trace elements from oceanic island arc (OIA) to continental island arc (CIA) to active continental margin (ACM) to passive margin (PM) settings. Roser and Korsch (1986) proposed a bivariate diagram of SiO_2–K_2O/Na_2O for sandstone-mudstone suites, which discriminates oceanic island arc (ARC), active continental margin (ACM), and passive continental margin (PM). However, due to lack of coherent statistical treatment of compositional data and insufficient representative average data used in the development of these existing discriminating schemes, Verma and Armstrong (2016) developed a new discriminant function based on isometric log-ratio transformation in discriminating between active and passive margin settings.

2.5 Kaolins in Paleoclimatic and Paleoenvironmental Studies

Clay minerals in sedimentary basins can be detrital or authigenic in origin (Chamley, 1989; Fagel, 2007). Authigenic clay minerals are formed *in situ* by post-depositional diagenetic changes and hydrothermal alteration, whereas the detrital clay minerals are weathering products of the initial rocks or the source area which were transported and deposited as detrital grains (Singer, 1984; Chamley, 1989; Weaver, 1989). Clay minerals of detrital origin are useful tools to study provenance of sediments on the hinterland, transport, and paleoenvironment. Only detrital clays can represent important proxy of paleoclimatic and paleoenvironmental conditions. However, post-formational diagenetic

changes can obliterate the climatic signal (Girard *et al*., 2000) and lead to incorrect paleoclimatic interpretations (Lacoviello *et al*., 2012). In order to constrain the reliability of the paleoclimatic inferences made from detrital clays, an integrated approach based on combined examination of the Oxygen (O) and Hydrogen (H) isotopic compositions is crucial and correlation with documented inferences from other paleoclimatic proxies (if available) (Girard *et al*., 2000; Baioumy *et al*., 2013).

Various autonomous parameters such as fossil content, mineralogy, and geochemistry have been applied in paleoenvironmental assessment of ancient sedimentary successions. Interpretation of fossils (flora and fauna) paleoecological evidences also provides information regarding depositional environments and paleoclimate (Brenchley and Harper, 1998). The study of stable isotope of O and H ratios (D/H and $^{18}O/^{16}O$) for kaolins in paleoenvironmental and paleoclimatic evaluations date back to 1960s (Savin and Epstein, 1970).

Kaolinite has been identified as a useful isotopic indicator of ancient continental climate (Singer, 1984). The isotopic composition of the kaolinite is a function of the following:

(i) Isotopic composition of the various waters with which the kaolinite may have interacted during and after its formation;
(ii) Temperature of the environment at any given time during which the kaolinite was subject to isotopic exchange; and
(iii) Whether the kaolinite reached isotopic equilibrium with its environment (Savin and Epstein, 1970).

The latter is critical for it to be considered as a good paleoclimatic and paleoenvironmental indicator by reaching a state of equilibrium with the contemporaneous environment.

The isotopic H and O compositions of the meteoric waters vary proportionately with climatic variables such as rainfall and temperature. Hence, there exists the likelihood to obtain paleoclimatic information from stable isotopic composition of ancient kaolinite. Thiry (2000) supported the stability of kaolinite over other clay minerals as paleoclimatic indicators because once formed, they remain stable for a long time. It can retain the original isotopic signatures for over 100 Ma (Gilg *et al*., 2013). Post-depositional isotopic exchange between kaolinite and water for oxygen is virtually rare but for hydrogen isotopic exchange can occur under certain conditions (O'Neil and Kharaka, 1976 and Bird and Chivas, 1988) like recrystallization or increase in temperature above formation temperature even at temperatures as low as 40°C (Longstaffe and Ayalon, 1990).

Savin and Epstein (1970) postulated that kaolinite formed at the Earth surface conditions would plot on a straight linear array (kaolinite line) on a graph of δD and $\delta^{18}O$. The 'meteoric water line' approximately parallel to the 'kaolinite line' defines the distribution of the O and H isotope ratios of meteoric waters on the Earth surface (Fig. 2.9). Hence, we can compare the climate during kaolinisation with that of the present by determining changes in the isotopic compositions of the meteoric waters. A scatter of isotopic compositions about the 'kaolinite line' is interpreted as incomplete post-formational isotopic exchange.

Shephard *et al*. (1969), Marumo *et al*. (1982), and Shephard and Gilg (1996) proposed the use of stable isotope geochemistry of kaolinite in distinguishing between supergene (S) and hypogene (H) kaolins by defining a line (S/H) (Fig. 2.9). It is believed that hydrothermal kaolinite (hypogene) will typically plot left to the S/H line (Shephard *et al*., 1969). Keller (1976a, 1976b) reported that kaolinite formed by hydrothermal processes have unique textures from those formed by weathering. He postulated that the former are fine grained, tightly packed from scanning electron micrographs. Furthermore, Giral-Kacmarcik *et al*. (1998) demonstrated that kaolinite may show distinct isotopic compositions for different size fractions in relation to different 'populations' formed at different times and under different environmental conditions.

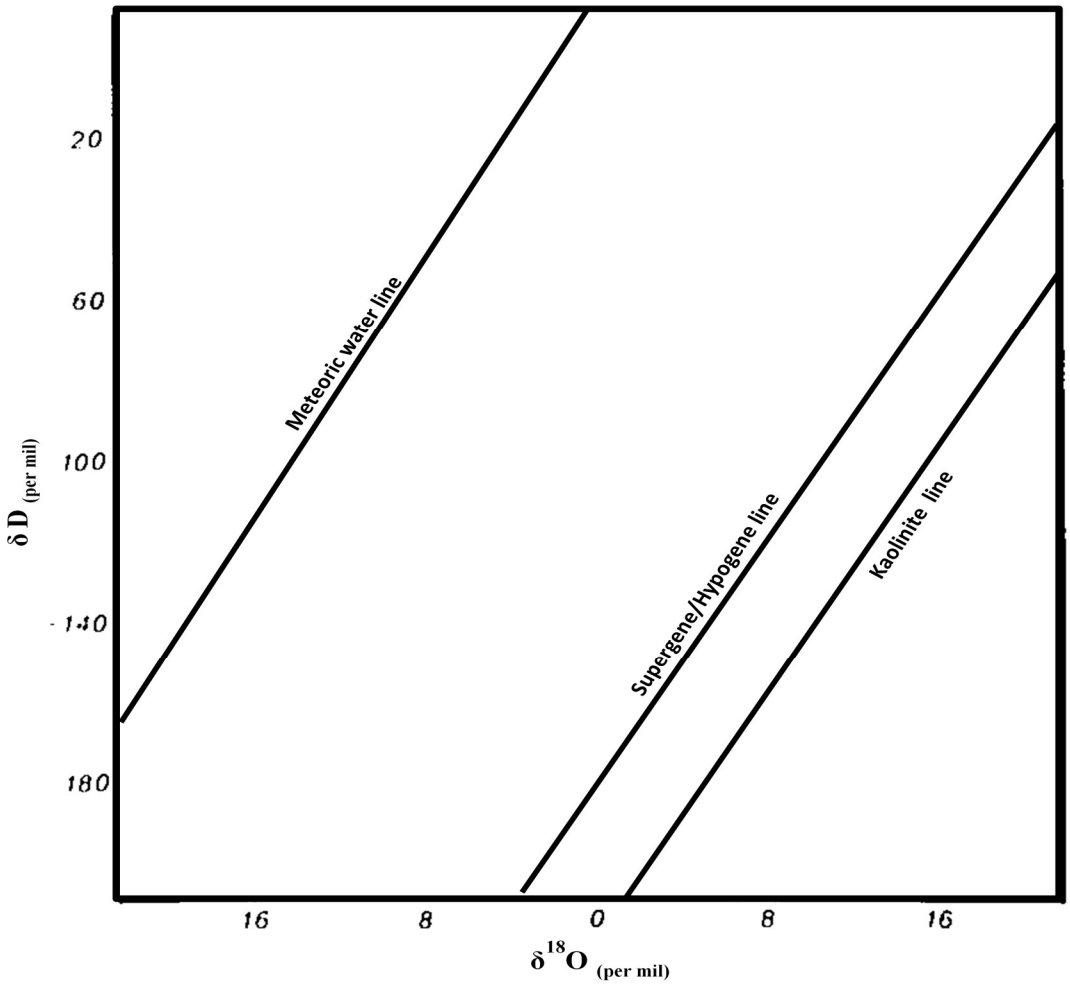

Figure 2.9: The meteoric water, supergene/hypogene, and kaolinite lines (Modified after Bird and Chivas, 1988).

The equation for oxygen and hydrogen isotopic fractionation between kaolinite and water according to Gilg and Shephard (1996) from both experimental and empirical data is given as:

Oxygen: $1000 \ln \alpha_{kaolinite\text{-}water} = -2.2 (10^6) (T^{-2}) - 7.7$ (2.1)

Hydrogen: $1000 \ln \alpha_{kaolinite\text{-}water} = 2.76 (10^6) (T^{-2}) - 6.75$ (2.2)

Where $\alpha_{kaolinite\text{-}water}$ is the fractionation factors for oxygen and hydrogen and T is the temperature.

Gilg *et al*. (1999) when studying the Lastarria kaolin deposit in South-central Chile obtained the hydrogen and oxygen isotopic compositions of the meteoric waters during kaolinisation from the isotopic compositions of kaolinite using the point of intersection of the meteoric water line ($\delta D = 8\ \delta^{18}O + 10$) with curve of waters in equilibrium with this kaolinite. They observed a major decrease from ~ 12°C paleotemperature during kaolinisation to the present day ~9.4°C annual mean air temperatures and in the δD value of local meteoric waters from -39 to -54‰ which was interpreted to represent a significant evolution in the climate from warmer and probably more humid during kaolinisation (Parrish *et al*., 1982) to the present temperate-humid one with up to 2100 mm rainfall (Weischet, 1970). Gilg *et al*. (2013) from hydrogen and oxygen isotopic studies on kaolinite concluded based on the results obtained that the kaolins in Finland formed at mean annual temperatures (MATs) of 13-15°C and are isotopically distinct from Mesozoic kaolins formed in the rest of Europe under tropical environment.

Bird and Chivas (1988) in resolving the problem associated with Permian climates in eastern Australia reported that the depletion of isotopic values obtained for the kaolinite analysed reflects an isotopically depleted ocean during the early Permian times and that paleoweathering that formed the kaolinite occurred at low temperatures. The later was similar to the report by Mizota and Longstaffe (1996) that the lower $\delta^{18}O$ values obtained from the stable isotope geochemistry of Iwaizumi kaolinite clay deposit, Japan indicate that weathering occurred at lower average temperatures (< 20°C) during the Cretaceous than in the Oligocene or younger times.

Ekosse (2007) in paleoenvironmental considerations of Makoro and Kgwakgwe kaolins in Botswana based on stable isotope compositions inferred lower kaolinisation temperatures for the Makoro kaolinite and established Makoro kaolins to be of sedimentary origin while the Kgwakgwe was primary but residual.

2.6 Dating of Kaolins

Age constraint for kaolins have relied greatly on relative dating with respect to their location within the stratigraphic profile (Bird and Chivas, 1988). Absolute geochronological information using conventional radiometric techniques in dating the

timing of kaolinisation is currently a major problem in geochronology. This is so because suitable radiogenic isotope systems such as K, Rb, or U are highly depleted in kaolins (Gilg, 2003). Several attempts have been made using such techniques which have yielded ambiguous dates which many researchers in the geosciences community are skeptical to accept as probable timing of kaolinisation (Gilg and Frei, 1997).

Gilg *et al*. (2003) in trying to unravel the genesis of illite-smectite (I-S) in the Saxonian kaolin deposits in Germany emphasised that the consistent $^{87}Rb/^{86}Sr$ model ages between 104 and 116 Ma obtained represent a good timing for I-S crystallisation but not necessarily for kaolinisation. This was due to the observation that the kaolinite has low Rb content with Sr isotope compositions close to that of the initial Sr composition of the I-S bearing samples. The K-Ar data for the pure kaolinite gave incorrect geological dates of 285±6 Ma, which was attributed to the presence of excess or inherited ^{40}Ar in kaolinite from weathering environments (Clauer and Chaudhuri, 1995 and Gilg and Frei, 1997), while for the I-S bearing samples gave significantly higher dates between 147 to 167 Ma. Clauer and Chaudhuri (1995) argued against the use of a method in dating fine-grained clay minerals due to ^{39}Ar recoil during irradiation and alteration changes. Obradovich (1965) interpreted preferential loss of radiogenic ^{40}Ar to be due to particle size reduction with the smallest crystals being often the 'youngest'. Thompson and Hower (1973) related those unexpected ages from ^{40}Ar-^{39}Ar to be due to variations in the mineral compositions contrary to Obradovich's earlier interpretation. In addition, the slow accumulation of K and Ar during illitisation is believed to yield ages theoretically closer to the end of the process than to the start because clay minerals have been shown to precipitate during slow and long-lasting crystallisation processes leading to a progressive increase of K content and therefore of radiogenic ^{40}Ar (Clauer, 2013)

Indirect dating system of clay minerals based on hydrogen and oxygen ratios have been demonstrated (Shephard *et al*., 1969; Bird and Chivas, 1988; and Gilg, 2000). This was possible because the D/H and $^{18}O/^{16}O$ values of clay minerals formed in weathering environments show the temperatures of crystallisation as well as the isotopic compositions of groundwater with which they equilibrate. Therefore, if the local meteoric waters isotopic compositions vary systematically with time due to paleoclimatic or

paleogeographic variations, the calibration of this isotopic change can be applied to date paleoweathering as long as the clay minerals retain their initial isotopic compositions (Gilg, 2000). Bird and Chivas (1989 and 1993) distinguished distinctly between kaolinitic sediment profiles formed in the Late Paleozoic and Late Mesozoic – Early Tertiary from those formed during Mid-Tertiary during the northward drift of the Australian continent based on their oxygen isotopic compositions.

Gilg and Frei (1997) employed a combined radiogenic (K-Ar and Rb-Sr) and stable (H) isotope study in direct dating of kaolinite and associated K-bearing minerals (Illite or 'mica clay mineral' and alunite) from two European residual deposits in Germany and France. The pure kaolinite K-Ar and Rb-Sr calculated ages obtained as 651±6 Ma and 858±32 Ma, respectively, were in excess of the age of the parent rocks (Pegmatite and Leucogranites of St Yrieix, France) of Carboniferous age. The Precambrian calculated ages could not be ascribed as a probable timing of kaolinisation. The 'excess' calculated K-Ar age has been attributed to inherited ^{40}Ar in kaolins. However, since the kaolin and alunite were observed not to have re-equilibrated their D/H ratios with present day meteoric waters, the Eocene K-Ar age (45.5±1.2 Ma) for pure alunite was interpreted to be the timing of kaolin formation.

Sousa *et al*. (2007a) in elucidating the controversies regarding the possible sources of the soft and flint kaolin facies of the Capim River, Northern Brazil applied the Pb-Pb single zircon direct evaporation geochronology. Such findings will give crystallisation ages and not kaolinisation ages but can be used to constrain geochronological information obtained from stable isotopic studies of the kaolins. Four (4) morphological zircon crystal types were identified for the study (Types I-IV) and four (4) major zircon age plateaus of the Capim kaolin district (CKD) were observed for the two facies and were interpreted to mean that both have a common source. Two among the four age plateaus (2.15 and 2.02 Ga) are considered as the best defined age intervals for the Capim kaolin zircons. Hence, they identified two main sediment sources for the Capim River kaolin which have also been corroborated by previous paleocurrent measurements (Santos and Rossetti, 2003).

Zircon applied to geochronology is of great value for investigation on the provenance, evolution and the age of the rocks because of its resistance to isotopic resetting and high

U/Pb ratios. Pb-Pb single zircon isotopic analyses using thermal ion mass spectrometry (ThIMS) was first applied in 1965 (Kosztolanyi, 1965). Gentry *et al*. (1982) proposed the mounting of 'ungrinded zircon' as against the grinded fine grained zircons used by Kosztolanyi (1965) because of the high proximity to cross-contamination between subsequently processed samples and the eventual contamination of the instrument. The single zircon evaporation technique depends on the conversion of zircon ($ZrSiO_4$) to ZrO_2 on stepwise heating from temperatures of about 1400 to ~1650°C thereby releasing SiO_2 and Pb, which are deposited on a second filament to be analysed for its isotopic composition (Kober,1986 and 1987). Although in this approach, information about U/Pb ratio is lost which have been established not to be a problem since comparable concordant ages have been obtained between $^{207}Pb/^{206}Pb$ ages and the conventional U-Pb ages (Kober, 1986 and 1987). The presence of internal heterogeneity, growth zones, and fluid inclusions in zircons calls for caution in constraining the geological significance of the $^{207}Pb/^{206}Pb$ ages obtained because Pb can be released from the different domains within the zircons at different temperatures (Ansdell *et al*., 1991). Kober (1987) postulated that since Pb from most retention sites are released at highest temperature, the $^{207}Pb/^{206}Pb$ ratio obtained from higher temperature steps should be considered as accurate indicator of the age of the zircon.

2.7 Applications and Beneficiation of Kaolins

Kaolinite which is the dominant mineral in the kaolin group is one of the most important industrial clay minerals useful to man with a wide range of applications because of its relatively low cost and easy availability. Kaolin application is a function of its physical and chemical characteristics in relation to requirements of the end user (Murray, 2007). There are many kaolin deposits in the world that are mined and processed for industrial uses such as the Cretaceous – Tertiary Georgia and South Carolina sedimentary kaolin in United States of America, which has been explored since the 1750s (Virta, 2004), the Cornwall and Devon in Southwestern England, which is believed to host the world's largest and highest primary kaolin deposit, the Amazon region of Northern Brazil hosting

large Tertiary sedimentary kaolins at the Jari and Capim Rivers among others (Murray, 2007). Some of the industrial uses of kaolin include:

a. Paper production: It is applied to make the paper sheet smoother and brighter with improved printability (Bundy, 1993). The significant properties required for the kaolins include whiteness, particle size < 2 μm, non-abrasiveness, and low viscosity (Murray, 2007).
b. Paint production: It is used as a pigment extender in water-based interior latex paints and also in oil-based exterior industrial primers. It enhances the brushability (i.e the resistance of the paint to brushing or scrubbing), washability (i.e the ease of removing stains from the surface of the paints by washing), and leveling of the paints. The particle size of these fine kaolins used in paint is about 98% less than 2 mm (Bundy, 1993).
c. Ceramic industry: It is perhaps one of the early applications by man in making earthenware for cooking, production of dinner wares, sanitary wares, tiles, pottery, and refractories. These applications depend mainly on the plasticity, strength, shrinkage, refractoriness, and colour of the kaolins (Murray, 2007)
d. Rubber production: in the production of rubber, the reinforcing and stiffening properties of the hard kaolin variety gives a wear-resistance to non-black rubber goods while the soft kaolin variety are used when the abrasion resistance is not too vital such as in the production of rubber toys (Bundy, 1993). Roskill (1979) advocated for the absence of metals like iron, manganese, and copper because they are deleterious to rubber durability.
e. Plastic Industry: kaolin is used as a filler in plastics to aid surface finishing as well as reducing cracking and shrinkage during curing. The most important use of kaolin is in polyvinyl chloride (PVC) coatings on wire and cable. Fine particle kaolins can substantially increase the impact strength of plastics, for example, in polypropylene and PVC (Trivedi and Hagemeyer, 1995).
f. Catalyst carrier: the refractory character of kaolin allows it to be used in the catalytic cracking of petroleum. The purity of kaolin with respect to low iron, titanium and alkali is preferred since the carrier in catalytic cracking must be composed of alumina and silica solely (Bundy, 1993). Kaolin is converted to zeolite

in the preparation of the cracking catalyst support to increase the surface area of the catalyst. The catalyst allows the breaking down of heavy petroleum fractions to gasolines even at a lower temperature and pressure (Bundy, 1993).

g. Portland cement production: kaolin is an ideal source of alumina and silica since cements contain mixtures of lime, silica, alumina, iron oxide, and gypsum as retardant (Bundy, 1993).
h. Pharmaceutical industry: kaolin is used as an adsorptive for gastro-intestinal disorders, as a tablet or capsule diluent, and for dusting in surgical operations (Russell, 1988). The kaolin to be used must be free from toxic metals, grit, and be sterilized to remove pathogenic micro-organisms (Murray, 2007).
i. Cosmetic industry: kaolin with a scent additive is used as powder in the production of baby or body powder. About 75% of the body powder formulation can be made up of sterilized delaminated kaolin because of its covering power, excellent grease resisting properties and good adhesion to the skin (Cochrane, 1996).
j. Fertilizers: kaolins are applied as diluents so as to provide optimum relative concentration elements particularly in prilling to coat particles of ammonium nitrate, a major component of many fertilizers (Murray, 2007).
k. Insecticide and pesticide carriers: The kaolin moisture content must be less than 1%. It is treated with selected pesticides or insecticides and sprayed as a slurry onto fruit trees and other garden products (Murray, 2007).

Kaolins are beneficiated for most industrial applications because relatively pure and commercially useable deposits based on standard and specifications for individual applications are few (Murray, 2007). Therefore, beneficiation entails processes that are used in generally increasing the relative concentration of principal components in the kaolins and the removal of impurities (such as quartz, micaceous minerals, illite, smectite, feldspar, goethite, hematite, pyrite, anatase, rutile, ilmenite, and trace quantities of tourmaline, zircon among others) so as to produce a marketable end-product without alteration of the physical and chemical identity of the mineral (Fuerstenau, 1986). Two major processes in the beneficiation of kaolins are the dry and wet processing. The dry processing aimed at refining, degritting, and desanding involves the drying and pulverizing the crude kaolin and further air classified using air currents to remove grit size

particles before packaging for customers (Fig. 2.10). It is cost effective especially for refractory and ceramic applications where the bulk chemistry may be less stringent (Pickering and Murray, 1995). On the other hand, the wet processing is less cost effective and entails greater complex procedures (Fig. 2.11) in meeting application requirements with low tolerance (Murray, 2007).

Poorni and Natarajai (2013) advocated for the use of bio-beneficiation through the use of micro-organism by biological processes in avoiding technical, economic, and environmental issues associated with reductive leaching and bleaching techniques (Andrade *et al*. (2011) and Guo *et al.* (2010)). The bio-beneficiation approach will preserve the kaolin structure and its chemistry in the safest environmental and economic manner (Ajayi and Adefila, 2012; and Hosseini and Ahmadi, 2015). This method involves bio-leaching using bacteria such as Agrobacter sp. or Bacillus sp. and fungi such as Aspergillus niger in transforming solid compounds into soluble and extractable elements which can be subsequently recovered. Other techniques include bio-flocculation and bio-flotation (Hosseini and Ahmadi, 2015).

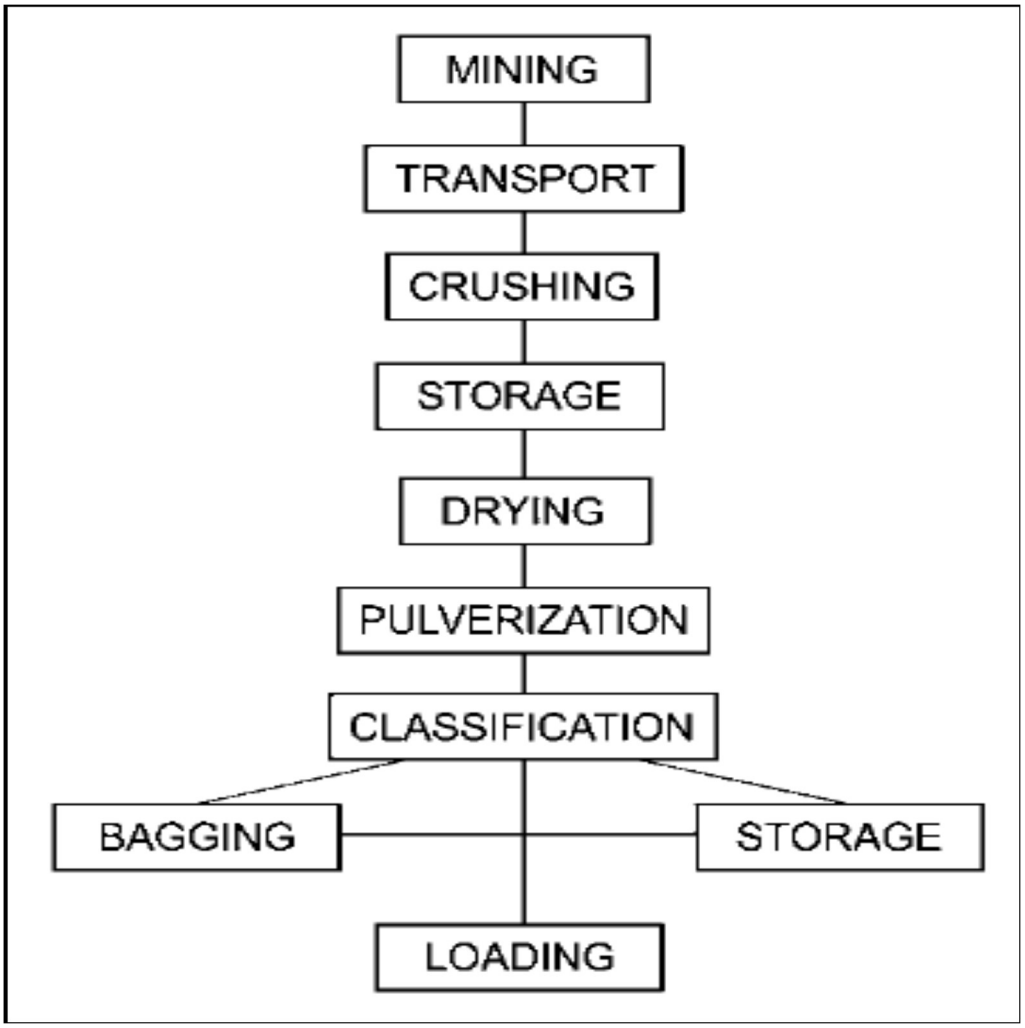

Figure 2.10: Dry Process Flow sheet for Kaolin (After Murray, 2007).

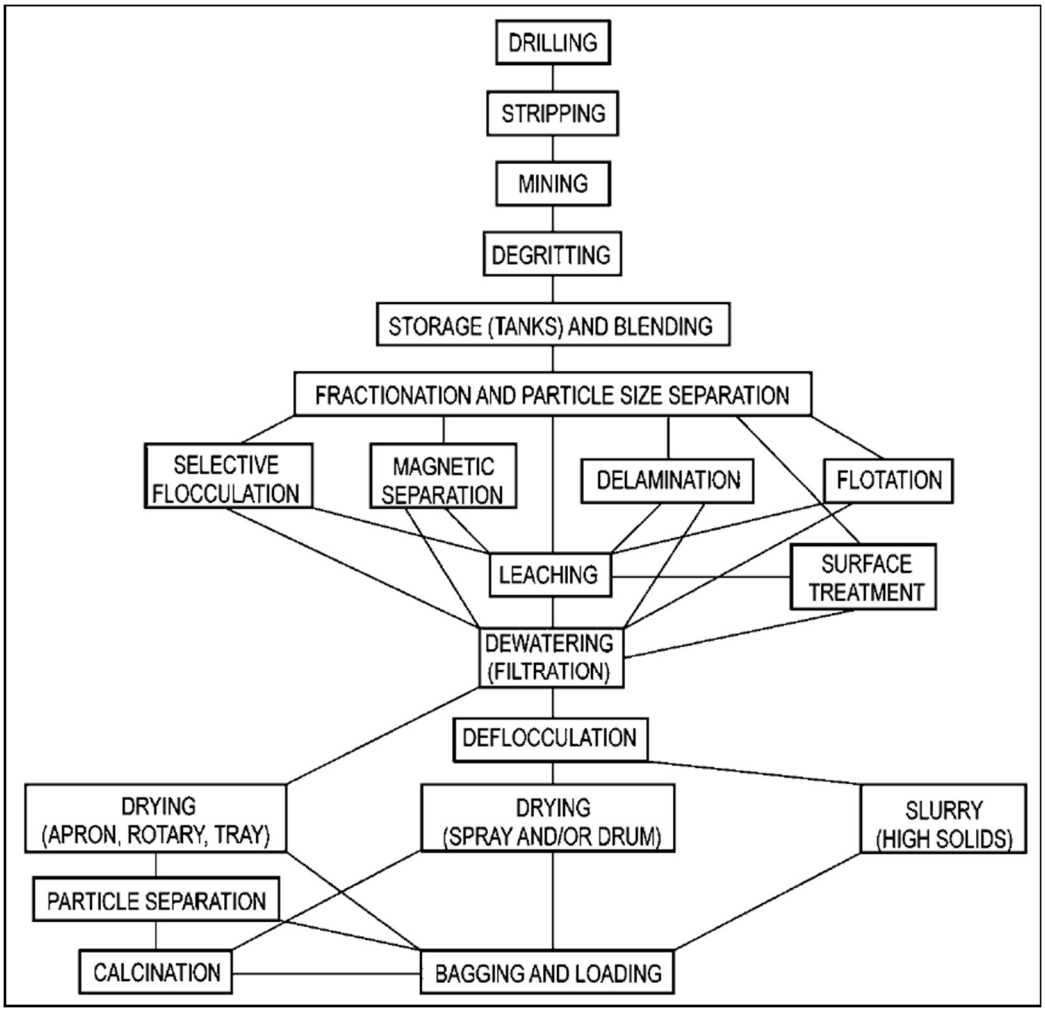

Figure 2.11: Wet Process Flow sheet for Kaolin (After Murray, 2007).

Chapter Three

Methodology

This chapter presents the general methodology followed in the fieldwork, sample preparation, laboratory analyses, data analyses and interpretation employed for this study.

3.1 Fieldwork

3.1.1 Reconnaissance Visits

Preliminary visits to the sites to evaluate both vertical and lateral stratigraphic relationships within the deposits allowed proper description and observation of lithologies and textural variations. The geographic locations of the selected kaolin deposits were determined using a global positioning system (GPS). A measuring tape was used in determining the outcrop dimensions and sampling depths.

3.1.2 Field Descriptions

A. Cretaceous Kaolin Deposits

i. The Lakiri kaolin deposit outcrops within the Lakiri village in Obafemi-Owode Local Government area (LGA) of Ogun State. The kaolin is dominantly purple to creamy-white with thicknesses up to 5 m with no distinct horizon and overburden up to 2 m (Fig. 3.1). The deposit is quite extensive beyond the study site with estimated thickness based on geoelectrical vertical sounding (VES) varying from 0.4 m to 17 m (Badmus and Olatinsu, 2009).

ii. The Eruku kaolin deposit outcrops within the Eruku village in Ado-Odo LGA of Ogun State. The deposit is generally reddish yellow with height of about 5 m and more than 35 m wide with overburden top sandy soil of 1.5 m (Figs. 3.2 and 3.3).

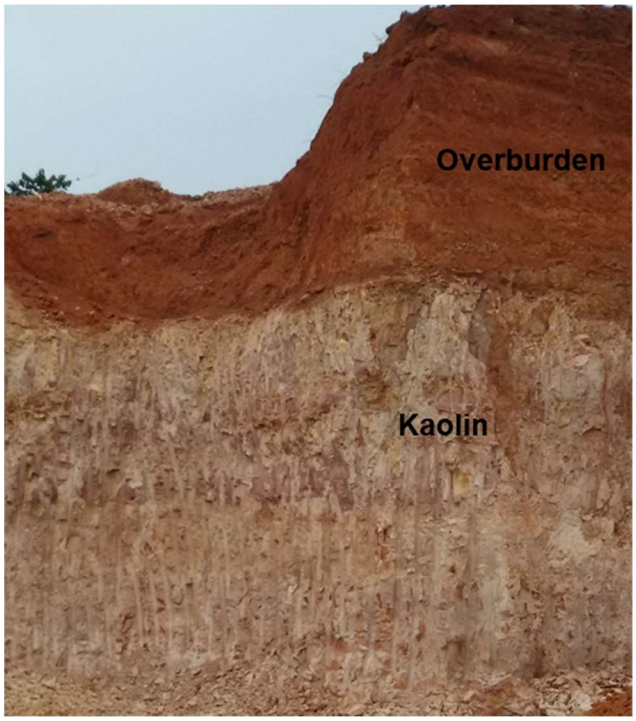

Figure 3.1: Profile view of the Lakiri kaolin deposit.

Figure 3.2: Profile view of the Eruku kaolin deposit.

Figure 3.3: Aerial view of Eruku kaolin deposit.

B. Tertiary Kaolin Deposits

i. The Ubulu-Uku kaolins outcrop along Agokun River near Anioma village, east of Agbor, Delta State. It extends for a distance of more than 2.5 km and thickness varies from 10 m to 40 m with an estimated reserve of more than 15.5 x 10^6 metric tonnes (Emofurieta *et al*., 1992). It is overlain by a brown-reddish ferricretic layer from which iron is leached by percolating water giving rise to purplish colour at the contact zone between the base of the ferricretic layer and the upper horizon of the kaolin deposit (Fig. 3.4).

ii. The Awo-Omama kaolin deposit outcrops along the western wall of the Njiagba river valley near Awo-Omama village in the Orlu LGA of Imo State. Exposures of this deposit are also known to occur along the Onitsha-Owerri road (about 5 km south of the main outcrop and quarry site). The deposit grades from creamy-white downwards to purplish-yellow at the base (Fig. 3.5). The deposit is embedded within a friable cross-bedded sandstone deposit with herringbone structures at some spots (Figs. 3.6 and 3.7). Large sub-angular to rounded pebbles were also found within the sandstone (Fig. 3.8). The estimated thickness of the deposit based on geoelectrical vertical sounding (VES) varied from 30 m to 90 m with an estimated reserve of 3.92 x 106 mT (Emofurieta *et al*., 1992).

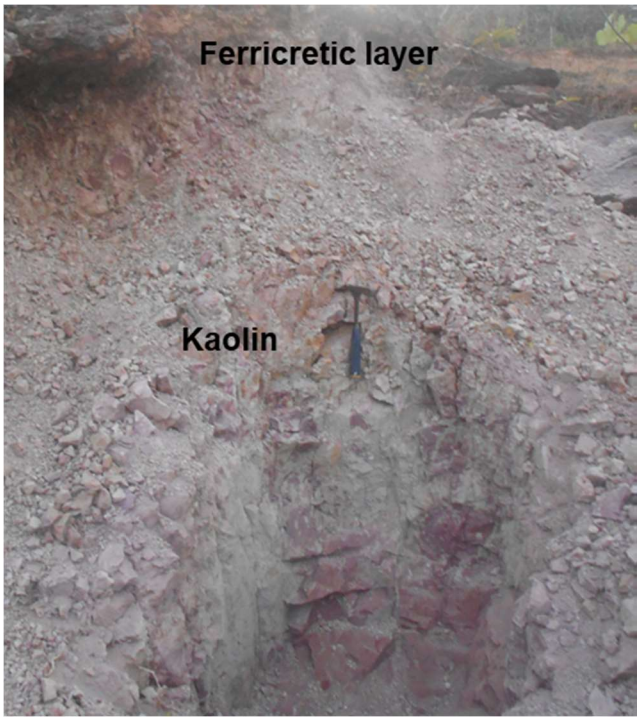

Figure 3.4: Profile view of the Ubulu-Uku kaolin deposit.

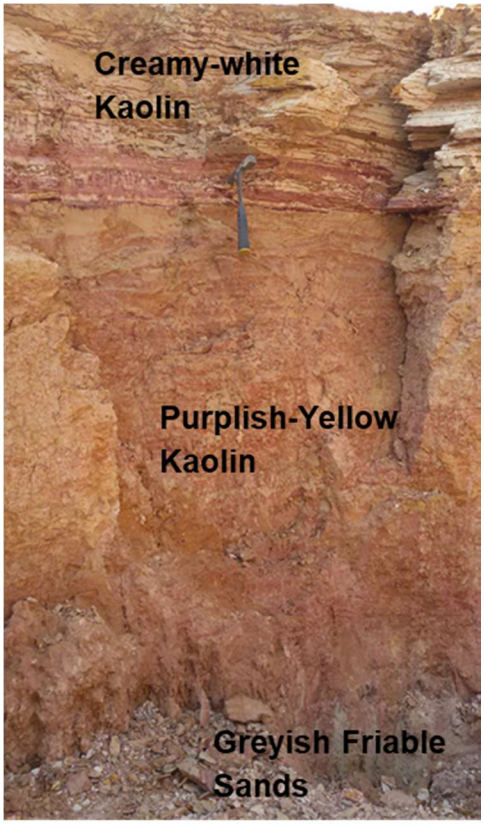

Figure 3.5: Profile view of the Awo-Omama kaolin deposit.

Figure 3.6: Cross-bedding within the friable sandstone of Ogwashi Asaba Formation.

Figure 3.7: Herringbone structure within the friable sandstone of Ogwashi Asaba Formation.

Figure 3.8: Large sub-angular to rounded pebbles within the friable sandstone of Ogwashi Asaba Formation.

3.1.3 Sampling

Representative samples from the kaolin deposits were collected along lateral and vertical exposed profiles with the aid of an auger, hand trowel, chisel, and geologic hammer. The sampling intervals were judgmental (Tan, 1996). To avoid contaminations from recent weathering products or external leached materials, the outcrop faces were dug back to at least 60 cm to gain access to fresh surface for proper description and sampling of the kaolins (Deepthy, 2008). A total of twenty-eight (28) kaolin samples composed of nine (9) from Eruku (EP), and six (6) from Lakiri (LP) deposits at 2 m interval, respectively; six (6) from Awo-Omama (AL), seven (7) from Ubulu Uku (UL) deposits at 1 m interval, respectively were collected. The samples were coded for ease of handling as EP, LP, AL, and UL respectively with numbers added to these codes (e.g EP1, LP1, AL1, UL1) to differentiate the profiles within specific sites (Fig. 3.9).

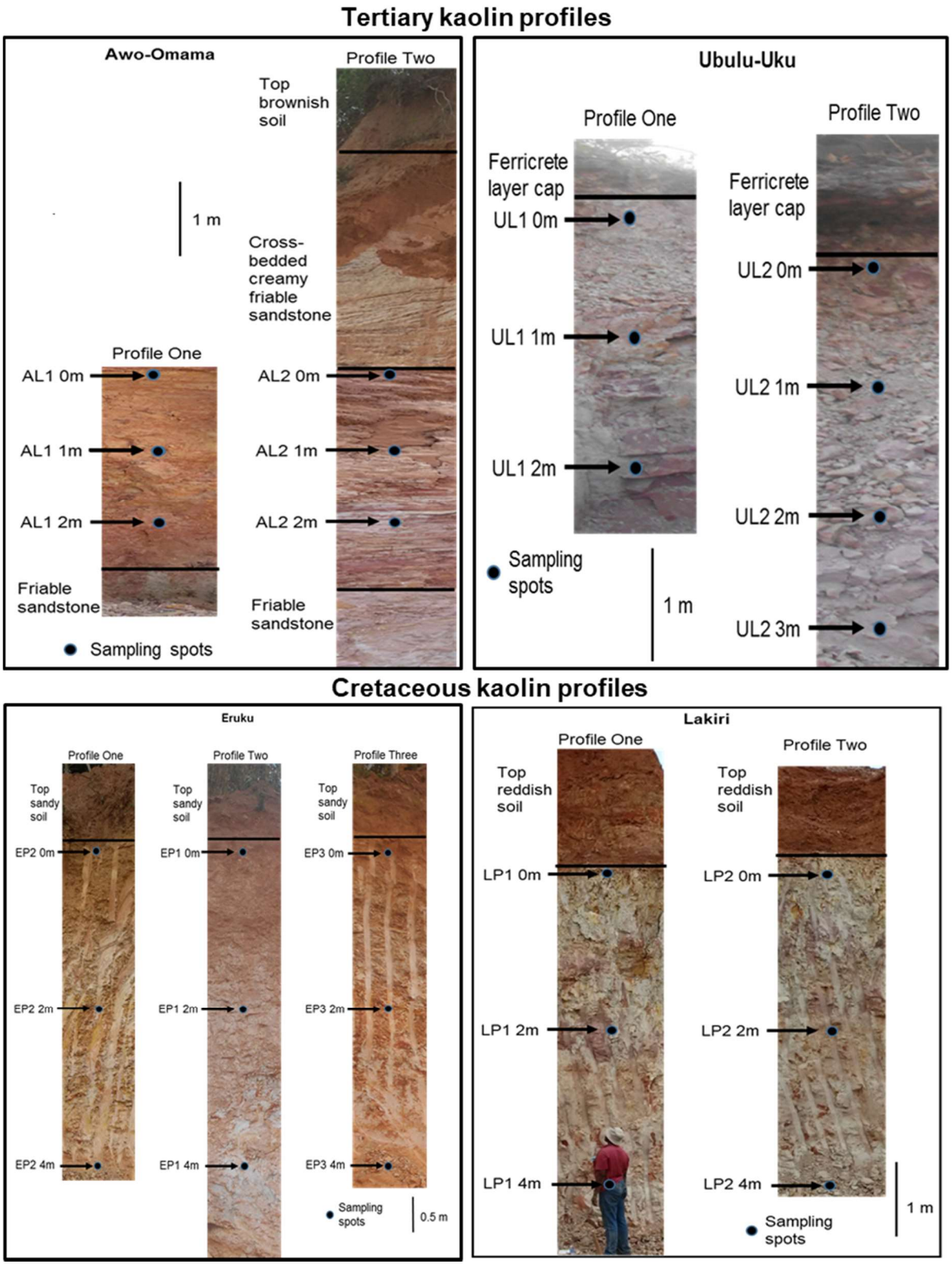

Figure 3.9: Vertical profiles showing sampling spots and lithologic units of the studied kaolin deposits.

3.2 Sample Preparation

Disaggregation of air-dried samples was done gently using a mortar and pestle without grinding them so that coarse grained non-clay minerals will not be reduced to the clay-size range. This was also to ensure that the internal structure of the particles were not destroyed (Deepthy, 2008). The disaggregated samples were transferred into a nest of sieves comprising of 2 mm (top), 1 mm, 125 µm, 105 µm, 63 µm sizes and the collection plate (bottom) and placed on a vibratory Fritsch Spartan Analysette 3 – Pulverisette sieve shaker in the Soil Science Laboratory, School of Agriculture, University of Venda (UNIVEN) for 10 minutes where an electromagnetic drive causes vertical oscillation of the sieves. The <2 mm fraction was taken as the bulk (van Reeuwijk, 2002). The <63 µm fraction (silt + clay) were collected from which the clay (<2 µm) fraction was later separated from the silt (between 2 µm and 63 µm) fraction.

To ensure easy sample dispersion and to avoid x-ray diffraction broadening peaks and increased background, organic matter was removed from the samples by oxidation with 30% hydrogen peroxide (H_2O_2) as described by Bird and Chivas (1988) and van Reeuwijk (2002) in the Soil Science Laboratory, School of Agriculture, UNIVEN. Fifty grams of each bulk samples were transferred into 500 ml beakers and 20 ml of H_2O_2 were added to the samples. To make up to 300 ml, distilled water was added to each of the beakers and placed on a sand bath for approximately four hours at a temperature of 200 ˚C until the supernatant is clear when all the organic matter has been decomposed. The samples were washed thoroughly with distilled water after this treatment. After the removal of organic matter from the bulk samples, they were oven-dried at 105 ˚C and gently crushed and packaged for mineralogical and geochemical analyses.

3.2.1 Separation of Clay and Silt Fractions

The clay fractions were obtained by centrifuge method (Tan, 1996). However, prior to this, 20 ml of calgon dispersing agent solution prepared from 40 grams of sodium hexametaphosphate $(NaPO_3)_6$ and 10 grams of soda (Na_2CO_3) was added to the sample

beakers from which organic matter have been removed (van Reeuwijk, 2002). The resulting solutions were transferred into a dispersion cup and stirred for 15 minutes using an Eijelkamp mechanical milkshake mixer in the Soil Science Laboratory, School of Agriculture, UNIVEN. The soil suspensions were either transferred into sedimentation cylinders for particle size determination or into polyethylene bottles for particle size separation by centrifugation. In order to separate the clay fractions from the <63 µm, the soil suspensions within the polyethylene bottles were allowed to stand undisturbed for 4 hours (van Reeuwijk, 2002) to allow the silt fraction to settle out of the suspension. The supernatants were decanted and transferred into centrifuge tubes whereas the residues which represent the silt fractions in the polyethylene bottles were transferred into petri dishes and oven-dried at 105 ˚C for 4 hours. The centrifuge tubes were centrifuged at a speed of 2500 rpm twice for about 40 minutes using a Grant-bio LMC 3000 centrifuge in the department of Hydrology and Water Resources, School of Environmental Sciences, UNIVEN. The clear water was siphoned and the clay fraction from the centrifuge tubes were oven-dried at 105 ˚C for 4 hours. The oven-dried clay and silt fractions were gently crushed and packaged for laboratory analyses.

3.3 Laboratory Analyses

The various size fractions were analysed to generate physico-chemical, mineralogical, geochemical, isotopic, and geochronological data (Table 3.1). Samples for stable isotope analyses were chosen based on their high kaolinite content (≥ 90 wt%) and less amount of other minerals. One sample per profile was chosen. Composite samples of each of the kaolin deposit were used for U/Pb dating of zircons, this gave a total of 4 samples (one sample per kaolin deposit). Composite samples of each of the kaolin profiles were used for Atterberg limit, this gave a total of 9 samples (one sample per kaolin profile).

Table 3.1: Summary of the various analyses done, size fractions, number of samples and laboratory where it was carried out.

S/N	Analyses		Particle size fraction	Number of samples	Laboratory
1.	Physico-chemical	Colour, particle size distribution (PSD), pH and EC	Bulk	28	Department of Soil Science, University of Venda (UNIVEN)
		Atterberg limits (Liquid limit (LL), plastic limit (PL), and plasticity index (PI))	<425 µm	09	Department of Mining and Environmental Geology, UNIVEN
2.	Mineralogical	X-ray diffraction	Bulk Silt Clay	28+01* 04 28	Ithemba LABS, Cape Town and XRD Analytical and Consulting cc, Pretoria
		Fourier transform infrared spectroscopy	Clay	28	Department of Ecology and Resource Management, UNIVEN
		Thermogravimetric analysis and Differential scanning calorimetry	Clay	28	Department of Chemistry, University of Johannesburg (UJ)
		Scanning electron microscopy	Clay	28	Central Analytical Facilities, Stellenbosch University (SU).
3.	Geochemical	X-ray fluorescence spectroscopy and Laser ablation inductively coupled plasma mass spectroscopy	Bulk Silt Clay	28+01* 04 28	Central Analytical Facilities, SU.
		Energy-dispersive X-ray spectroscopy	Clay	28	Central Analytical Facilities, SU.
4.	Stable isotope	Oxygen and Hydrogen	Clay	09	Department of Geological Sciences, University of Cape Town (UCT).
5.	Zircon dating	U/Pb	Bulk	04	Central Analytical Facilities, SU.

*duplicate sample.

3.3.1 Physico-chemical analyses

3.3.1.1 Hydrogen Ion Concentration (pH)

Following the procedures outlined by van Reeuwijk (2002), about 20 g of the <2 mm fractions of the kaolin and 50 ml of water was weighed into 100 ml polythene wide-mouth type bottle. The bottle was subsequently capped and shaken for 2 hours. Prior to the determination of the pH, the bottle was shaken by hand once or twice before opening. The pH meter electrode probe was immersed in the upper part of the suspension. Measurements were made using a Crison BasiC 20 pH meter twice and the average recorded for each sample. Commercial buffer solutions of pH 7.0 and 4.0 were used for calibration of the pH meter.

3.3.1.2 Electrical Conductivity (EC)

Following the procedures outlined by van Reeuwijk (2002), about 20 g of the <2 mm fractions of the kaolin and 50 ml of water was weighed into 100 ml polythene wide-mouth type bottle. The bottle was subsequently capped and shaken for 2 hours. Prior to the determination of the pH, the bottle was shaken by hand once or twice before opening. A Crison BasiC 30 conductivity meter calibrated using a conductivity standard (1413 µS/cm at 25 ˚C) electrode probe was immersed in the upper part of the suspension. The measurements were taken twice and the average recorded for each sample.

3.3.1.3 Colour

Visual colour assessment provided a rapid means of simply comparing different samples but the use of a Munsell soil colour chart with separate notations for hue, value, and chroma (HVC) gave an objective assessment. These three variables represent all visible colours in equally distributed increments, represented by colour chips. Dry <2 mm kaolin fractions were used since moisture can significantly affect whiteness (Soil Survey Staff,

2014). The HVC characteristics and colour of each sample was obtained by making visual comparison with the soil colours in the Munsell soil colour chart (Ruck and Brown, 2015).

3.3.1.4 Particle Size Distribution

The determination of three fractions (sand, silt, and clay) by hydrometer followed the procedures described by van Reeuwijk (2002). The method is based on the Stoke's law (Eqn. 3.1) governing the rate of sedimentation of particles suspended in water (Gaspe *et al.,* 1994).

$$V = 2\ g\ r^2\ (d_1-d_2)/9\eta \qquad (3.1)$$

Where V = rate of settling particles (cm/s), g is the acceleration due to gravity (981 cm/s^2), r is the radius of the particles (cm), d_1 is density of the particles g/cm^3, d_2 is the density of fluid (water) (g/cm^3), and η is the viscosity (g/cms).

50 grams of dispersed sample (section 3.2.1) was transferred into sedimentation cylinder and filled to 1000 ml mark with deionized waster and allowed to stand overnight to equilibrate. In addition, 100 ml of 5% calgon dispersion solution was mixed with 880 ml of deionized water in a 1000 ml cylinder to prepare a blank solution. At the beginning of each set, the temperature was recorded and the hydrometer reading of the blank was taken. The density was determined by inserting the plunger into suspension and carefully mixed for 30 secs until a uniform suspension was obtained. The hydrometer reading was taken by inserting the ASTM 152H soil hydrometer after 40 secs. This represents the amount of silt plus clay suspended since the sand has settled to the bottom of the cylinder by this time. The temperature was taken again and the hydrometer reading was measured again after 6 hours, 52 minutes. This is the amount of clay in suspension. The silt has settled to the bottom of the cylinder by this time. Temperature and density corrections were made by adding 0.2 unit for every 1 ˚C above 20 ˚C, and subtraction of 0.2 unit for every 1 ˚C below 20 ˚C. The density of the blank at each reading was subtracted from the corresponding density readings for each of the samples.

The percentages of clay, silt, and sand were determined as follows:

P_{clay} = (corrected hydrometer reading at 6 hrs, 52 mins/ wt of sample) x 100 (3.2)

P_{silt} = ((corrected hydrometer reading at 40 secs/ wt of sample) x 100) - (P_{clay}) (3.3)

P_{sand} = 100 % - P_{silt} - P_{clay} (3.4)

The P_{clay}, $P_{silt,}$ and P_{sand} are plotted on the textural triangle (Fig. 3.10) to determine the sample textures.

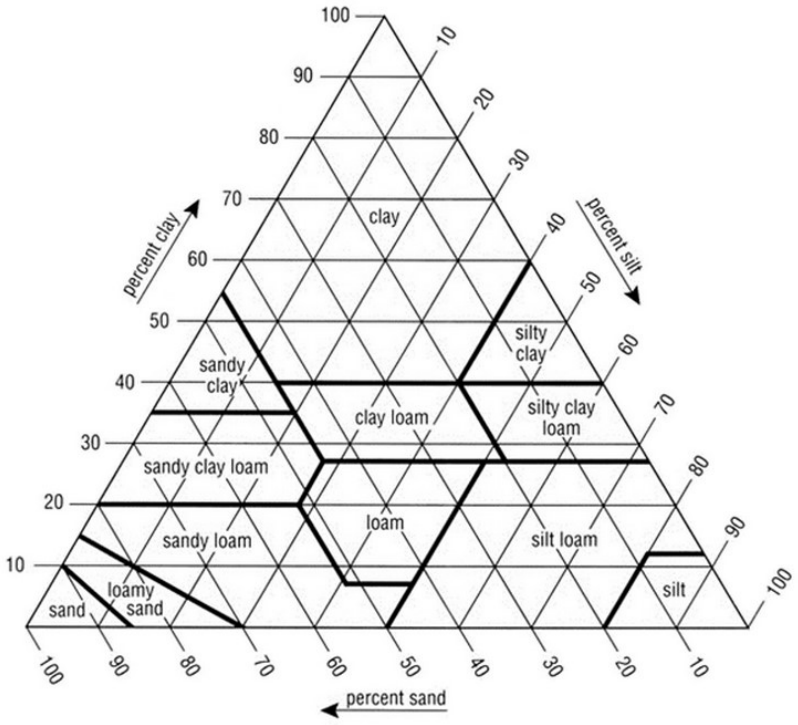

Figure 3.10: Soil Textural classification triangle based on their sand, silt, and clay percentages (After Brady and Weil, 1999).

3.3.1.5 Atterberg Limits

Atterberg limit tests were determined for the <425 µm fraction. The tests conducted were the liquid limit (LL) and plastic limit (PL). The plasticity index (PI) was calculated based on the arithmetic difference of the LL and PL of the samples. The LL and PL tests were carried out using the method described by Casagrande (1948), Grim (1962), Minapuye (1981), and also described by Ekosse (1990).

Liquid Limit (LL): About 50 grams of the <425 µm fraction of each sample selected was mixed with water thoroughly until the uniformity of paste was attained. The paste was then transferred into the LL cup and leveled using a spatula. A grooving tool was then used to cut a clean and sharp groove on the paste into two halves. The cup was lifted and dropped at a rotational speed of 2 drops per second continuously until the groove closes over a length of about 13 mm. This procedure was repeated four to five times at different moisture contents until the number of blows required to close the groove was somewhere around 25 blows. The paste corresponding to the closed groove was removed and weighed to get the weight of sample at that particular moisture content. The weighed paste was dried in an oven at 105 ˚C to remove the water content. The dried paste was weighed again and recorded. The LL which is the water content expressed as a percentage was calculated as follows:

$$LL = ((W_1-W_2) / (W_1-W_3)) \times 100 \quad (3.5)$$

Where: W_1 is the weight of the container plus wet sample, W_2 is the weight of the container plus dry sample, and W_3 is the weight of container.

Plastic Limit (PL): About 50 grams of the <425 µm fraction of each sample selected was mixed with water thoroughly until it becomes plastic enough to be moulded. Using the palm, small sample paste was rolled on a flat surface until the thread of the small paste crumble just before reaching a thread of 3 mm diameter. The crumbled threads are collected and placed in a container of known mass and weighed before been oven-dried at 105 ˚C. The dried mass of the sample was weighed and recorded. The PL was expressed as a percentage by weight following equation (3.5).

3.3.2 Mineralogical Analyses

3.3.2.1 X-ray Diffraction (XRD) analysis

The XRD qualitative analysis was carried using a Bruker AXS D8 Advance PSD system operated at 40 kV and 40 mA, with Cu-Kα radiation at the Ithemba LABS, Cape Town. Samples were scanned from 0.02˚ 2θ to 85˚ 2θ at a counting time of 0.5 secs. The

diffraction peaks occur when the paths of the diffracted x-ray is equal to an integer multiple of the path difference expressed by Bragg's equation as follows:

$$n\lambda = 2d\sin\theta \quad (3.6)$$

Where; n = integer, λ = wavelength, d = interactive spacing in Angstroms (Á), and θ = diffraction angle.

The mineral phases were identified using X'Pert Highscore Plus Software and compared with data and patterns available in the mineral powder diffraction file (ICDD, 2002) for confirmation. The quantitative relative phase amounts (weight %) were estimated using the Rietveld method at XRD Analytical and Consulting cc, Pretoria.

The crystallinity of the clay fractions were evaluated using the Hinckley Index (HI) (Aparicio and Galan, 1999; Hinckley, 1963) as illustrated in Figure 3.11. Normal HI values ranges from <0.5 (disordered) to 1.5 (ordered) (Aparicio and Galan, 1999).

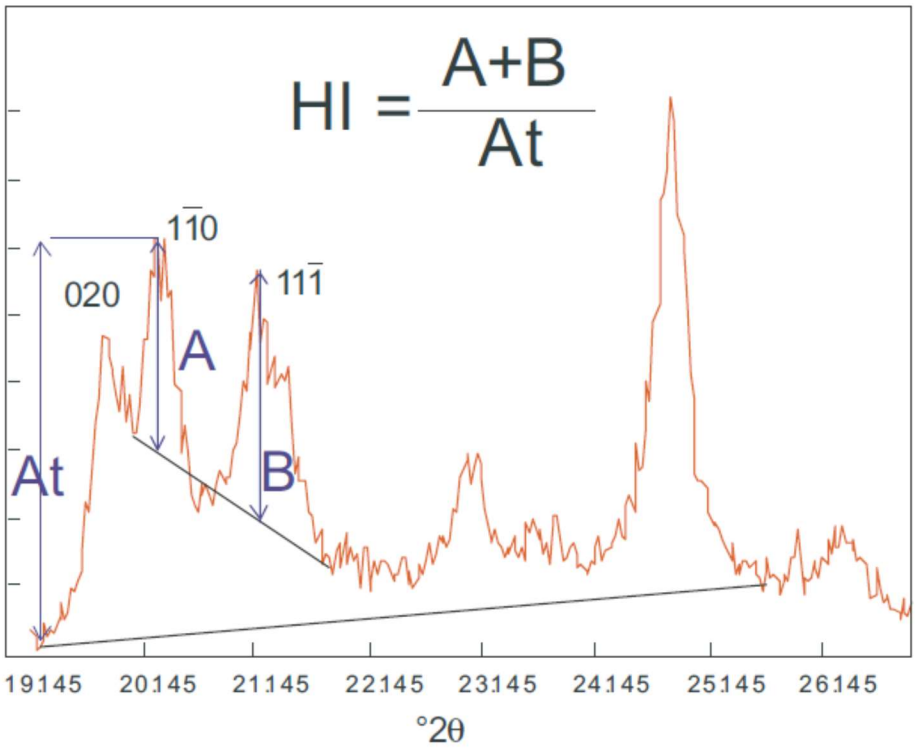

Figure 3.11: Calculation of the HI from the ratio of the height above background of the $\mathbf{1\bar{1}0}$ (A) and $\mathbf{11\bar{1}}$ (B) peaks above the band of overlapping peaks occurring between 20-23 ~ compared to the total height of the $\mathbf{1\bar{1}0}$ above background (At). The abscissa is in terms of 2 theta and the ordinate is on a relative scale (After Aparicio *et al.*, 2006).

3.3.2.2 Fourier Transform Infrared (FTIR) Spectrophotometry

The FTIR in clay mineralogy has the ability to characterise the functional group in clays and fingerprint regions of very small quantities of samples (Tan, 1998). The clay size fraction was used in order to minimise the dispersion of the Infrared spectra (IR) beam, scattering of radiant IR, and the distortion and broadening of absorption bands which arises from sample size heterogeneity with coarse particles causing interferences (Deepthy, 2008). The IR (400 to 4000 cm^{-1} with a resolution of 4 cm^{-1}) were obtained using a Bruker Alpha Platinum – Attenuated total reflectance (ATR) Spectrometer at Department of Ecology and Resource Management, UNIVEN (Fig. 3.12) following the procedures outlined by Madejova and Komadel (2001). To achieve high quality spectra, good contact between the sample and the ATR crystal (ZnSe) was ensured. The Bruker's spectroscopy software, OPUS, allowed real time monitoring of the spectral quality after applying pressure on the sample. The IR peaks were reported based on % transmittance to given wavelengths.

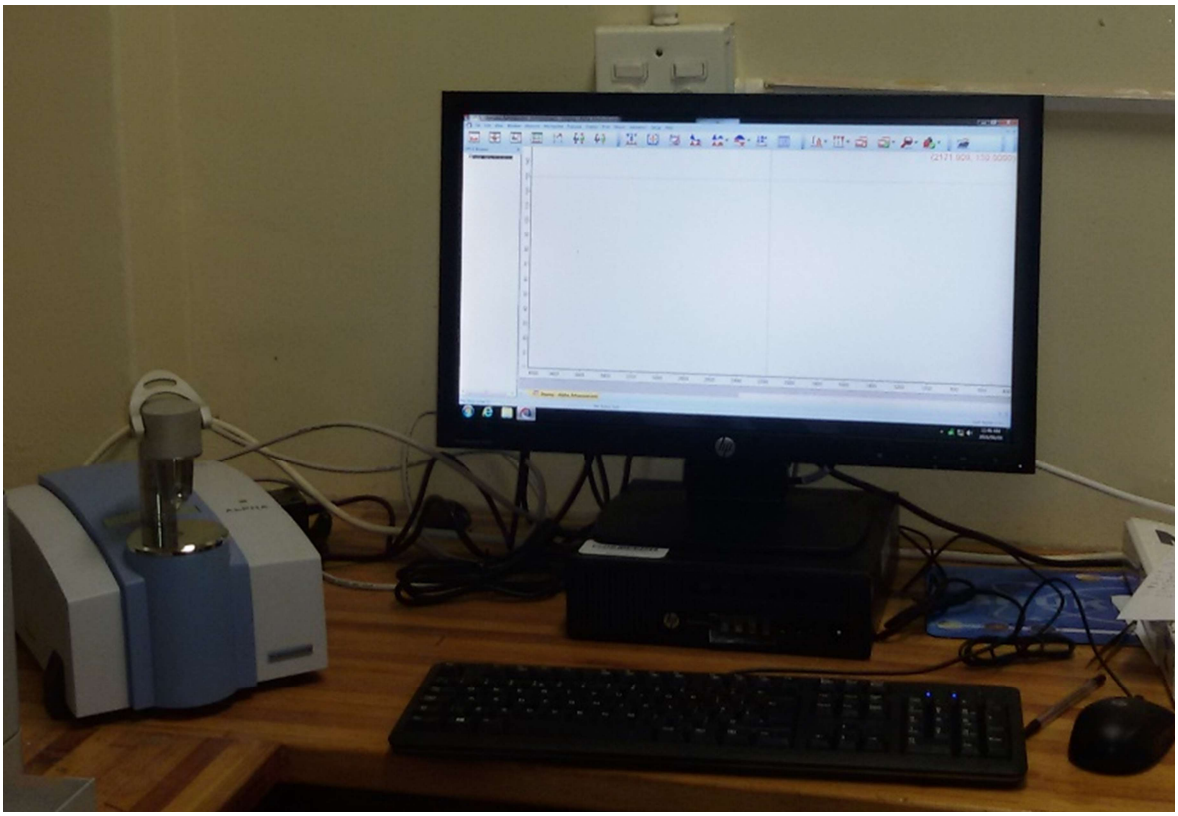

Figure 3.12: Bruker Alpha Platinum – Attenuated total reflectance (ATR) Spectrometer.

The FTIR is an alternative method in the determination of kaolinite disorder (crystallinity) degree based on differences in the position and relative intensity of OH stretching and bending bands in IR spectrum (Madejova *et al.,* 1997). Vaculikova *et al.* (2011) proposed two approaches in determining the degree of structural disorder of kaolinites from IR spectra namely, empirical approach (IR-E) and numerical approach (IR-N). The IR-E is based on resolution and relative intensities of bands in OH stretching and bending region whereas IR-N is based on crystallinity indices (CI) calculated from the intensities selected vibration modes structural OH bands.

3.3.2.3 Scanning Electron Microscopy with an Energy Dispersive X-ray Spectrum (SEM-EDX)

The morphological and microchemical analyses of the clay fractions were carried out using a Zeiss MERLIN Field Emission Scanning Electron Microscope at the Central Analytical Facilities, SU with the images obtained by backscattered electron detector (Fig. 3.13). The procedure followed the descriptions by Leonard *et al.* (2012). Backscattered electron images provide a qualitative representation of composition of a sample and its phases. The brightness of a phase is proportional to the atomic mass of the phase. Therefore a phase which appears brighter has an atomic mass greater than the surrounding or adjacent phase. Prior to imaging, the samples were mounted on aluminium stubs with double sided carbon tape. The samples were then coated with a thin (~10nm thick) layer of gold, using an Edwards S150A Gold Sputter Coater. This is done in order to make the sample surface electrically conductive to avoid electron build-up on the sample surface which can cause electron charge. A Zeiss 5-diode Back Scattered Electron (BSE) Detector (Zeiss NTS BSD) and Zeiss Smart SEM software were used to generate BSE images. The samples were chemically quantified by semi-quantitative Energy Dispersive X-Ray Spectrometry (EDX) using an Oxford Instruments® X-Max 20 mm^2 detector and Oxford Aztec software.

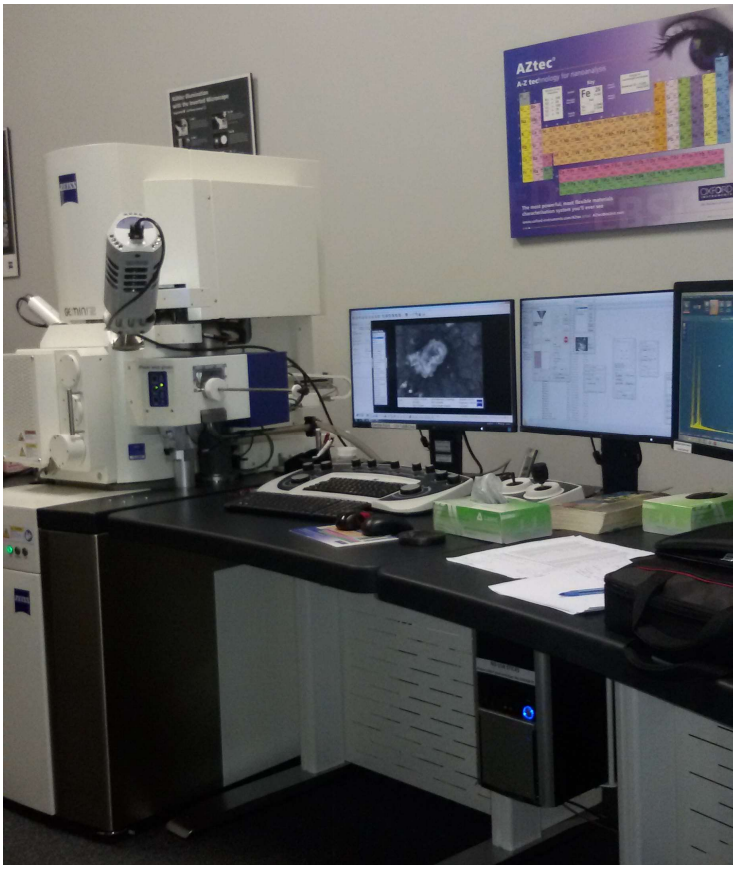

Figure 3.13: Zeiss MERLIN Field Emission Scanning Electron Microscope.

Beam conditions during the quantitative analysis and backscattered electron image analysis on the Zeiss MERLIN were 20 kV accelerating voltage, 16 nA probe current, with a working distance of 9.5 mm and a beam current of 11nA. The counting time was 10 seconds live-time. Gold was automatically excluded from analysis due to sample coating with gold. The physical limitations of EDX do not allow for the analysis of elements lighter than boron therefore the elements hydrogen, helium, lithium and beryllium were not analysed.

3.3.2.4 Thermogravimetric Analysis and Differential Scanning Calorimetry (TGA-DSC)

The TGA-DSC techniques were the methods used in investigating the thermal characteristics of the clay fractions. TGA measures change in weight during heating or cooling whereas

DSC measures heat absorbed or liberated during heating or cooling. The endothermic and exothermic reactions occurring during the heating of the kaolin were recorded by a differential thermal analyzer. The operating principle is based on the Kissinger (1957) equation (Eqn. 3.7) from which the peak temperature was calculated.

$$\ln (\Theta T_m^{-2}) = C - E (RT_m^{-1}) \quad (3.7)$$

Where: Θ = Heating rate, T_m = Peak temperature, C = Integrating constant, E = Activation energy, and R = Gas constant.

A TA instrument SDT Q600 TGA-DSC analyser in the Department of Chemistry, UJ was used for the thermal analysis. The sample (10 mg) was heated from room temperature (25˚C) to 1100°C, at a rate of 10˚C/min (Ekosse, 2007; Diko *et al*., 2016).

3.3.3 Geochemical Analyses

3.3.3.1 X-ray Fluorescence (XRF) Spectrometry

For the major element compositions, glass disks were prepared for XRF analysis using 7 g of high purity trace element and Rare Earth Element (REE)-free flux ($LiBO_2$ = 32.83%, $Li_2B_4O_7$ = 66.67%, LiI = 0.50%) mixed with 0.7g of the powder sample following the procedures described by Verma *et al*. (1996). Whole-rock major element compositions were determined by XRF spectrometry on a PANalytical Axios Wavelength Dispersive spectrometer at the Central Analytical Facilities, SU, South Africa. The spectrometer is fitted with an Rh tube and with the following analysing crystals: LIF200, LIF220, PE 002, Ge 111 and PX1. The instrument is fitted with a gas-flow proportional counter and a scintillation detector. The gas-flow proportional counter uses a 90% Argon-10% methane mixture of gas. Major elements were analysed on a fused glass disk using a 2.4kW Rhodium tube. Matrix effects in the samples were corrected for by applying theoretical alpha factors and measured line overlap factors to the raw intensities measured with the SuperQ PANalytical software. The concentration of the control standards that were used in the calibration procedures for major element analyses fit the range of concentration of the samples. Amongst these standards were NIM-G (Bushveld Granite from the Council

for Mineral Technology, South Africa) and BE-N (Basalt from the International Working Group).

The Loss on Ignition (LOI) was determined by oven-drying the samples at 105 ˚C overnight to remove the moisture. About 2.0 g of the samples were taken in a silica crucible and placed inside a muffle furnace at 1000 ˚C for 2 hours. Then it was allowed to cool to room temperature inside a dessicator to avoid adsorption of moisture and weighed again. LOI was calculated using equation 3.8 (van Reeuwijk, 2002).

$$LOI\ (wt\ \%) = ((W_2-W_3) / (W_2-W_1)) \times 100 \qquad (3.8)$$

Where: W_1 is the weight of the empty crucible, W_2 is the total weight of the crucible plus sample before keeping inside furnace, and W_3 is the total weight of the crucible and sample after heating to 1000 ˚C.

3.3.3.2 Laser Ablation – Inductively Coupled Plasma – Mass Spectrometry (LA-ICP-MS)

Inductively Coupled Plasma – Mass Spectrometry (ICP-MS) is widely used for the analysis of trace elements, including rare earth elements in solution. However, LA-ICP-MS allows direct analysis of solid samples with minimal sample treatment using sample introduction system including laser and spark ablation (Gunther and Hattendorf, 2005). A Resolution 193 nm Excimer laser from ASI connected to an Agilent 7700 ICP-MS was used in the analysis of trace elements in the samples (Fig. 3.14). Ablation was performed in He gas at a flow rate of 0.35 L/min, then mixed with argon (0.9 L/min) and Nitrogen (0.004 L/min) just before introduction into the ICP. The procedure followed the descriptions by Gunther and Hattendorf (2005).

For traces in fusions, 2 spots of 100 µm is ablated on each sample using a frequency of 10 Hz and 2 mJ energy. Fusion disks prepared for XRF analysis by an automatic Claisse M4 Gas Fusion instrument and ultrapure Claisse Flux, using a ratio of 1:10 sample:flux, were coarsely crushed and a chip of sample mounted along with up to 12 other samples in a 2.4 cm round resin disk. The mount was mapped, and then polished for analysis.

Figure 3.14: Laser 193 nm Excimer interfaced to the Agilent 7700 ICP-MS.

Trace elements were quantified using National Institute of Standards and Technology (NIST) 612 glass standard reference material for calibration and the % SiO_2 from XRF measurement as internal standard, using standard – sample bracketing. Two replicate measurements were made on each sample. The calibration standard was repeated after every 12 samples. A quality control standard was run in the beginning of the sequence as well as with the calibration standards throughout. BCR-2 or BHVO 2G, both basaltic glass certified reference standards produced by USGS (Wilson, 1997), was used for this purpose. A fusion control standard from certified basaltic reference material (BCR-2, from USGS) was also analysed in the beginning of a sequence to verify the effective ablation of fused material. Data was processed using Glitter software, distributed by Access Macquarie Ltd., Macquarie University, USA. The analyses were carried out at the Central Analytical Facilities, SU, South Africa.

3.3.3.3 Stable Isotopic Analyses

All analytical data for oxygen and hydrogen isotope ratios for nine (9) selected samples were determined using a Finnigan Delta XP Mass Spectrometer at the Department of Geological Sciences, UCT, South Africa. The samples were selected based on their enriched kaolinite content (> 85 wt %) with less of other minerals. One sample per profile with the highest kaolinite content was chosen. The analytical procedure followed that earlier described by Diamond and Harris (1997) and Harris *et al*. (1999).

About 20 mg of each kaolinite enriched clay fraction of the samples was placed in a sealed glass container attached to a vacuum line and the content frozen in liquid nitrogen. The air was then pumped away and all the absorbed water was cryogenically distilled into a second glass container by heating the sample at 150 ˚C with an air gun. The weight percent of absorbed water was determined from the measured mass of the original material and the water produced.

The oxygen isotope ratios were determined after drying the samples in an oven at 110 ˚C and degassing under vacuum on the silicate line at 200 ˚C for 2 hours and then reacted with ClF_3 at approximately 560 ˚C for 12-16 hours (Borthwick and Harnon, 1982). The liberated O_2 was converted to CO_2 quantitatively in the presence of hot graphite (carbon) rod. The $\delta^{18}O$ ($^{18}O/^{16}O$) of the CO_2 was then measured using the Finnigan Delta XP Mass Spectrometer (Fig. 3.15). Duplicate splits of the Murchison Quartz (MQ) in-house standard were ran with each batch of eight samples and used to normalize the raw data to the SMOW scale using a value of $\delta^{18}O$ = 10.1 ‰ for the MQ standard.

The hydrogen isotope analyses of the absorbed water extracted was carried out using the variation of the closed tube Zn reduction method of Coleman *et al*. (1982). This method involve the conversion of the absorbed water extracted to hydrogen gas prior to measurement on the Finnigan Delta XP Mass Spectrometer. Internal water standards (CTMP2010 and RMW, exactly 2mg) were used to calibrate the raw data to the SMOW scale and were also normalised against SLAP. In order to correct the raw data relative to the reference gas value, the CTMP2010 was adjusted to -7.4 and “stretched” so that the RMW = - 131.4.

Figure 3.15: Finnigan Delta XP Mass Spectrometer with a dual gas inlet.

In addition, the silicates were adjusted so that kaolinite = -57 wt% (average δd value obtained for the SB8 kaolinite standard). Three analyses of Bulk Serina Kaolin (SB8, Kaolinite standard) from Serina Mine near Cape Town, gave structural water content values of 10.80, 11.75, and 10.62 wt% and a mean δd value of -57 wt% (See appendix 3.1). Analytical precision was estimated ±0.2 ‰ for $\delta^{18}O$ and ±2 ‰ for δD.

3.3.3.4 U/Pb Zircon Dating

Four composite samples representing each of the kaolin deposits (Eruku, Lakiri, Ubulu-Uku and Awo-Omama) were analysed. Samples (2-5 kg) were crushed and sieved through a 350 µm sieve, followed by panning and magnetic separation using a Frantz Isodynamic Separator based on the intensity of current generated (Table 3.2). The non-magnetic fraction was further separated by a heavy liquid technique, using 99% Methyleniodide with a density of 3.325 g/cm^3. After drying of the heavy mineral fraction, zircon picking of about 120 grains were done by hand, using a Wild M3Z microscope.

Table 3.2: Magnetic separation by a Frantz Isodynamic Separator based on the intensity of current generated.

Magnetic at 0.4 A	Magnetic at 0.8 A	Magnetic at 1.5 A	Non-Magnetic at 1.5 A
Garnet	Biotite	Muscovite	Zircon
Ilmenite	Hornblende	Spinel	Rutile
Chromite	Hypersthene	Enstatite	Sphene
Chloritoid	Augite	Tourmaline	Leucoxene
Olivine	Actinolite	Clinozoisite	Apatite
	Staurolite	Diopside	Corundum
	Epidote	Tremolite	Barite
	Chlorite		Fluorite
			Sillimanite
			Kyanite

Zircons were mounted in an epoxy mould that was ground down and then polished using a 1-micron pad and a 1-micron diamond paste using a Struers Rotopol-35 equipment to expose grain centres. The mould was gold coated using a S150A sputter coater and cathodoluminescence (CL) and backscatter (BS) images scanned with a Zeiss MERLIN Field Emission Scanning Electron Microscope (FE-SEM) (Fig. 3.13). The CL images were used to identify different internal zoning patterns within the individual zircon grains (core and rim); whereas the BS images were used to constrain the spots to be ablated in order to avoid parts with fractures and holes which can affect the quality of result generated. All U-Pb age data obtained at the Central Analytical Facility, SU, were acquired by laser ablation – single collector – magnetic sectorfield – inductively coupled plasma – mass spectrometry (LA-SFICP-MS) employing a Thermo Finnigan Element 2 mass spectrometer coupled to a NewWave UP213 laser ablation system (Fig. 3.16). Data were obtained by single spot analyses with a spot diameter of 30 µm and a crater depth of approximately 15 to 20 µm.

The methods employed for U-Pb isotope analysis are described in detail by Gerdes and Zeh (2006) and Frei and Gerdes (2009). The processing of U-Pb data was done using the LA-ICP-MS data reduction software package Iolite v.3.1 (Paton *et al*., 2011), combined with VizualAge (Petrus and Kamber, 2012).

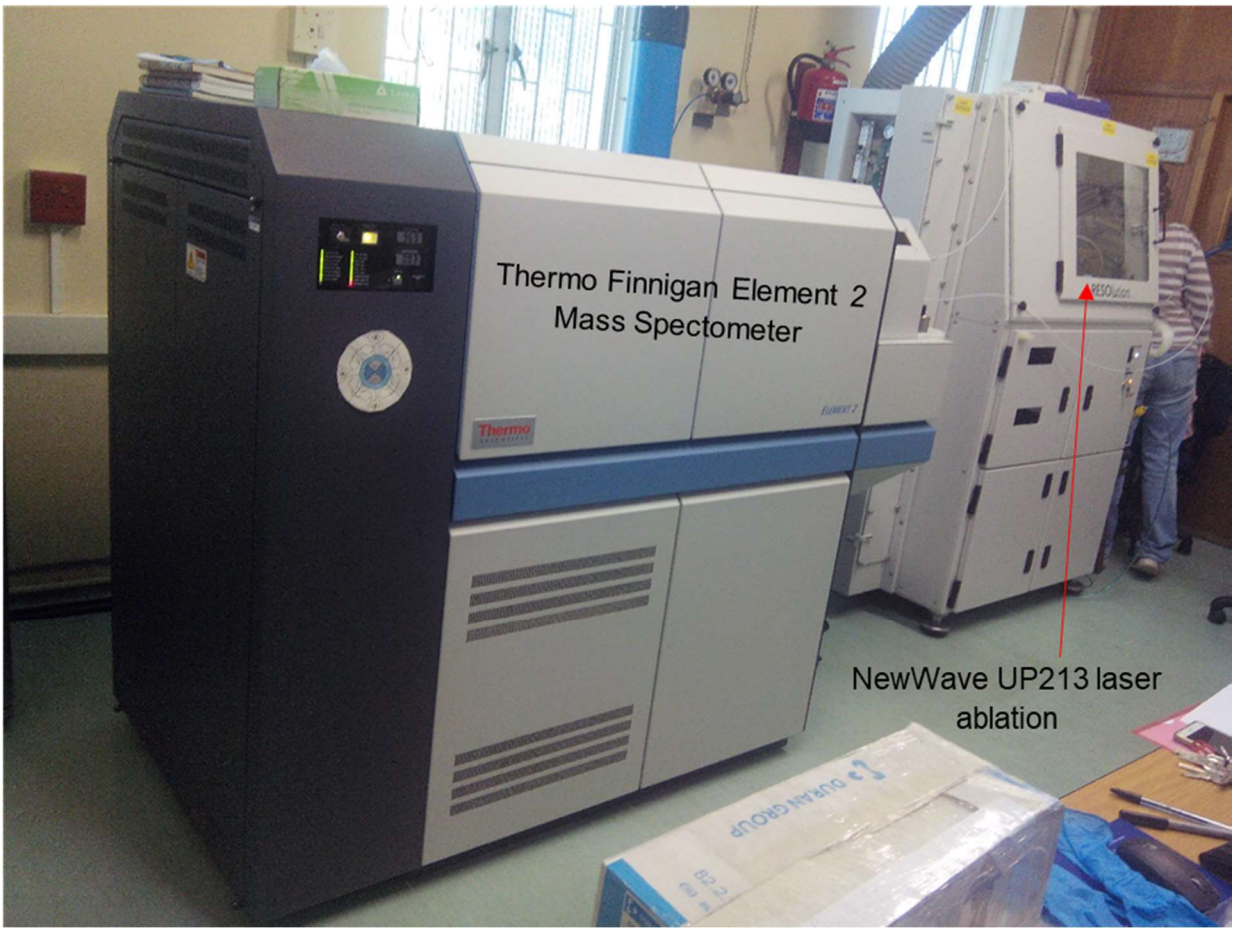

Figure 3.16: LA-SFICP-MS comprising of the Thermo Finnigan Element *2* mass spectrometer coupled to a NewWave UP213 laser ablation system.

For quality control, primary zircon reference material, GJ1 (608±1 Ma) (Jackson *et al*., 2004), secondary zircon reference materials Plešovice (Sláma *et al*., 2008) and M127 (524±1 Ma) (Nasdala *et al*., 2016) secondary zircon reference materials were analysed to correct for uncertainties due to elemental fractionation and instrumental mass discrimination on measured isotopic ratios (Taylor *et al*., 2016). The results were consistently in excellent agreement with the published ID-TIMS age. The calculation of concordia ages, and plotting of concordia diagrams, was performed using Isoplot/Ex 3.0 (Ludwig, 2003). The data were filtered using various concordance levels (Table 3.3).

Table 3.3: Concordance levels used in filtering the raw U/Pb Zircon data.

Diagrams	Concordance Acceptance level	Discordance Rejection level
Concordia for zircons in the samples	None (All data were plotted both concordant and discordant)	None (All data were plotted both concordant and discordant)
Concordia for reference materials	97 – 103	>3%
Probability density plots for zircons in the samples	90 – 110	>10%
Weighted average plots for zircons in the samples	95 – 105	>5%

3.3.4 Validation of Analytical Methods

The quality of data generated in the laboratory depends on the integrity of the samples collected from the field. Standard field precautions and procedures were followed during field sampling in order to avoid sample contamination. In evaluating laboratory accuracy, duplicate samples were analysed. During all the laboratory analyses, all apparatus were thoroughly cleansed with distilled water and in some cases acetone to avoid sample contamination. In addition, standard reagents and chemicals used were supplied by MERCK (Pty) Ltd., Johannesburg, South Africa.

3.4 Data Interpretation

(i) Weathering Indices

The CIW and CIA indices were calculated (equations 3.9 and 3.10) in assessing the extent of chemical weathering/alteration based on the molecular proportions of element oxides.

- The Chemical Index of weathering (CIW) (Harnois, 1988)

  $CIW = [(Al_2O_3) / (Al_2O_3+CaO+Na_2O)] \times 100$ (3.9)

- The Chemical Index of Alteration (CIA) (Nesbitt and Young, 1982)
  $CIA = [(Al_2O_3) / (Al_2O_3+CaO+Na_2O+K_2O)] \times 100$ (3.10)

(ii) Elemental Ratios

Geochemical proxies for assessing sediment provenance and paleoenvironmental interpretations (Hofer *et al*., 2013) used include the following ratios:

- Th/Sc, Zr/Sc, and SiO_2/Al_2O_3 in identifying sediment recycling and sorting processes (McLennan *et al*., 1993; and Roser *et al*., 1996).
- Cr/Ni, Cr/V in sediment provenance and paleoenvironmental considerations (McLennan *et al*., 1993).
- U/Th, Ni/Co, and V/Cr in evaluating paleoredox conditions (Jones and Manning, 1994).
- Th/Co, Th/Cr, Cr/Th, and Eu/Eu* differentiating between felsic and mafic sources (Cullers (1994, 2000); and Cullers and Podkovyrov (2000)). Also, comparison to the average compositions of the upper continental crust (UCC) and the post-Archean Australian Shale (PAAS) (Taylor and McLennan, 1985).

(iii) Discrimination Diagrams

Binary and ternary diagrams were used in evaluating the weathering geochemical trends and tectonic settings such as

- A-CN-K, (Nesbitt and Young, 1984 and 1989) with CIA values;
- Source area composition (La/Sc versus Th/Co, and La-Th-Sc plots (Lopez *et al*., 2005) and TiO_2 versus Al_2O_3 (Paikaray *et al.,* 2001); and
- Discriminant function diagrams using major and trace elements for tectonic settings (Bhatia, 1983; Verma and Armstrong, 2016).

(iv) Statistical Methods

Multivariate statistical analysis (MSA) such as factor analysis (FA) was employed in identifying inter-elemental relationships that best discriminates the studied kaolins. The advanced IBM Statistical Package for Social Sciences (SPSS) version 23 was used. The FA allows the identification of the underlying structure that is presumed to exist within a

set of multivariate observations (Davis, 2002). This structure is expressed in the pattern of variances and covariances between variables and the similarities between observations. Variables with concentrations below detection limit were excluded (Hofer *et al*., 2013).

Chapter Four

Results

This chapter presents the physico-chemical, mineralogical, and geochemical data for the Cretaceous – Tertiary kaolins within the Eastern Dahomey and Niger Delta Basins in Nigeria.

4.1 Physico-chemical Properties of Studied Cretaceous – Tertiary Kaolins

4.1.1 Colour

Natural kaolin contain various levels of impurities which greatly affect its colour. These impurities include quartz, micas, feldspar, iron oxides, and titanium oxides. Among these, iron is the main contaminating element in kaolins (Zhou *et al*., 2014).

The Eruku kaolin had varying shades of colour from light grey to pinkish grey (56 %), light pink (22 %), and reddish yellow (22 %) (Table 4.1). The presence of pinkish, reddish, yellowish, and greyish colours are indicative of the presence of anatase, hematite, goethite, and organic matter, respectively in the samples (Ekosse, 2001; Fernandez-Caliani and Cantano, 2010; Diko *et al*., 2011). Lakiri kaolins have varying shades of colour from light grey to pinkish grey (50 %), pale red (33 %), and pinkish white (17 %). The presence of anatase and hematite is responsible for the pinkish and reddish colour in the Lakiri kaolins (Ekosse, 2001; Fernandez-Caliani and Cantano, 2010; Diko *et al*., 2011). From the percentage colour distributions for the Cretaceous kaolins, increasing dominance is pinkish white (least) < light pink, reddish yellow and pale red < light grey and pinkish grey (dominant) (Figure 4.1).

The Awo-Omama kaolin with dominant pale red colour (except AL2 1m) is indicative of the presence of predominantly hematite. However, Ubulu-Uku kaolins show varying shades of colour from pale red (57 %), light brown to reddish brown (29 %), and pinkish grey (14 %). The presence of reddish, brownish, pinkish, and greyish colours are suggestive of the presence of hematite, goethite, anatase, and organic matter,

respectively in the Ubulu-Uku kaolins (Ekosse, 2001; Fernandez-Caliani and Cantano, 2010; Diko *et al*., 2011). From the percentage colour distributions for the Tertiary kaolins, increasing dominance is light brown and reddish brown (least) < pinkish grey < pale red (dominant) (Figure 4.1).

Table 4.1: Hue, Value, Chroma, and Colour of the studied Cretaceous – Tertiary kaolins.

Age	Deposit	Sample ID	Hue/Value/Chroma	Colour
Cretaceous	Eruku	EP1 0m	7.5R/8/4	Light pink
		EP1 2m	5R/8/3	Light pink
		EP1 4m	10R/7/1	Light grey
		EP2 0m	7.5YR/7/6	Reddish yellow
		EP2 2m	7.5YR/7/2	Pinkish grey
		EP2 4m	5YR/7/6	Reddish yellow
		EP3 0m	5YR/7/2	Pinkish grey
		EP3 2m	5R/7/1	Pinkish grey
		EP3 4m	5YR/7/1	Light grey
	Lakiri	LP1 0m	7.5YR/8/2	Pinkish white
		LP1 2m	7.5R/7/2	Pale red
		LP1 4m	7.5R/7/1	Pinkish grey
		LP2 0m	7.5R/7/3	Pale red
		LP2 2m	7.5YR/7/1	Light grey
		LP2 4m	7.5YR/7/1	Light grey
Tertiary	Awo-Omama	AL1 0m	5R/7/2	Pale red
		AL1 1m	7.5R/7/3	Pale red
		AL1 2m	7.5R/7/3	Pale red
		AL2 0m	7.5R/6/4	Pale red
		AL2 1m	7.5YR/7/2	Pinkish grey
		AL2 2m	7.5R/7/3	Pale red
	Ubulu-Uku	UL1 0m	7.5R/7/2	Pale red
		UL1 1m	7.5YR/6/3	Light brown
		UL1 2m	7.5R/6/3	Pale red
		UL2 0m	2.5YR/7/2	Pale red
		UL2 1m	7.5YR/6/2	Pinkish grey
		UL2 2m	7.5R/6/2	Pale red
		UL2 3m	2.5YR/4/4	Reddish brown

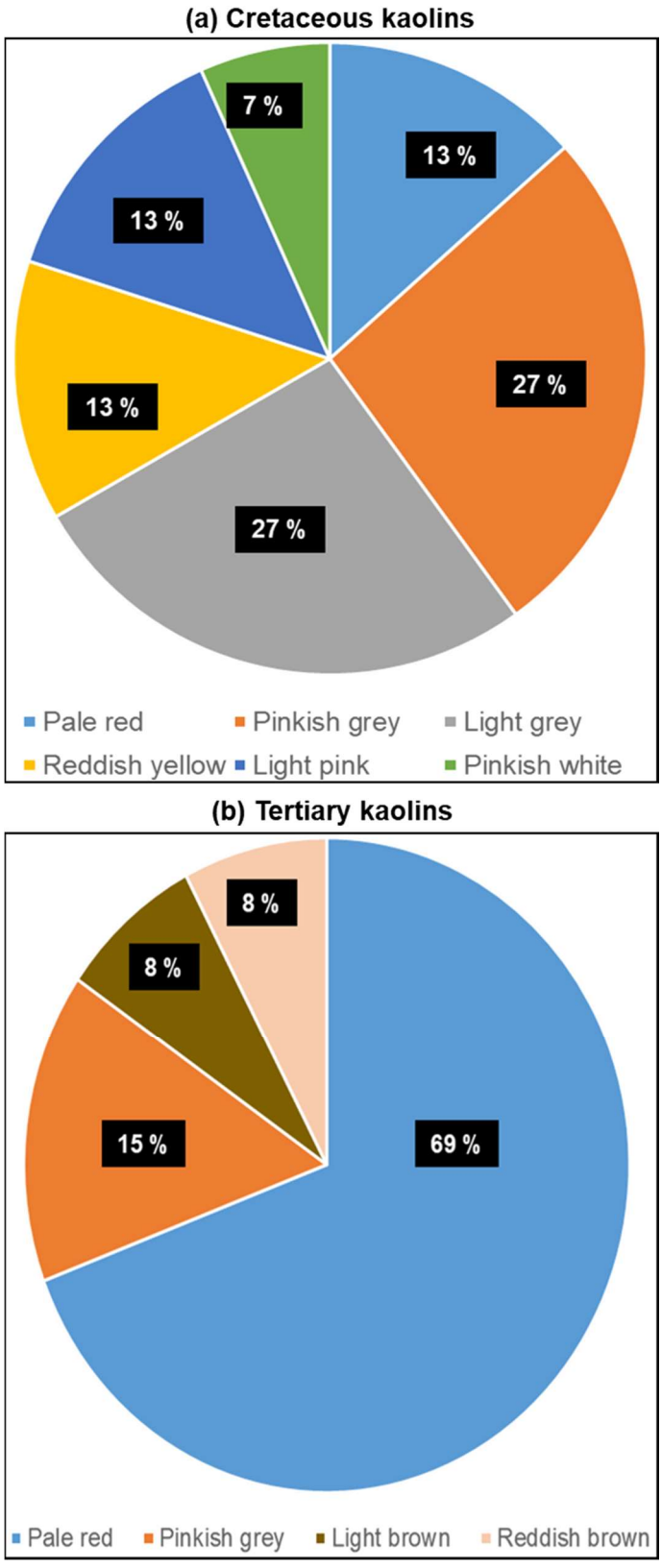

Figure 4.1: Colour distribution of the studied kaolins: (a) Cretaceous and (b) Tertiary.

4.1.2 Electrical Conductivity (EC)

The EC of Eruku kaolins were between 0.2 and 8.1 µS/cm with a mean value of 2.4 µS/cm, whereas EC of Lakiri kaolins were between 0.5 and 9.1 µS/cm with a mean value of 4.1 µS/cm. The EC of Awo-Omama kaolin samples varied from 0.2 to 13.1 µS/cm with a mean value of 3.3 µS/cm, whereas EC of Ubulu-Uku kaolins were between 0.7 and 9.7 µS/cm with a mean value of 3.17 µS/cm. From the EC plot for the Cretaceous-Tertiary kaolins, most of the samples (82 %) had values between 0.2 and 5.0 µS/cm (Figure 4.2). In addition, 18 % (EP2 0m, LP1 2m, LP2 0m, AL1 1m, and UL2 2m) had EC values > 8.0 µS/cm.

4.1.3 Hydrogen Ion Concentration (pH)

The pH of Eruku kaolins were between 4.27 and 4.87 with a mean value of 4.65, whereas pH of Lakiri kaolins were between 4.35 and 5.21 with a mean value of 4.78. The pH of Awo-Omama kaolin samples ranged from 4.63 to 4.96 with a mean value of 4.79, whereas pH of Ubulu-Uku kaolins were between 4.27 and 5.29 with a mean value of 4.77. The pH values of the studied Cretaceous – Tertiary kaolins were generally acidic with values < 7 (4.27 to 5.29) (Figure 4.3).

4.1.4 Texture

Figures 4.4a and b show the relative abundances of the sand, silt, and clay fractions within each of the samples. The Cretaceous kaolins predominantly have clay textures (Figure 4.4c), whereas the Tertiary kaolins have textures varying from clay (85 %) to sandy clays (15 %) (Figure 4.4d).

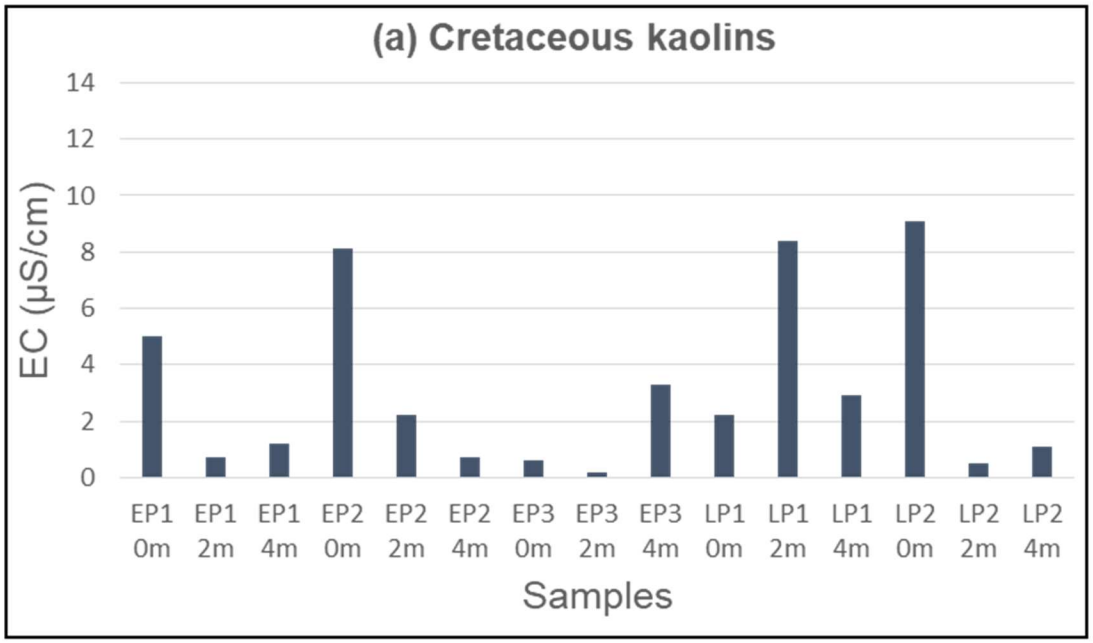

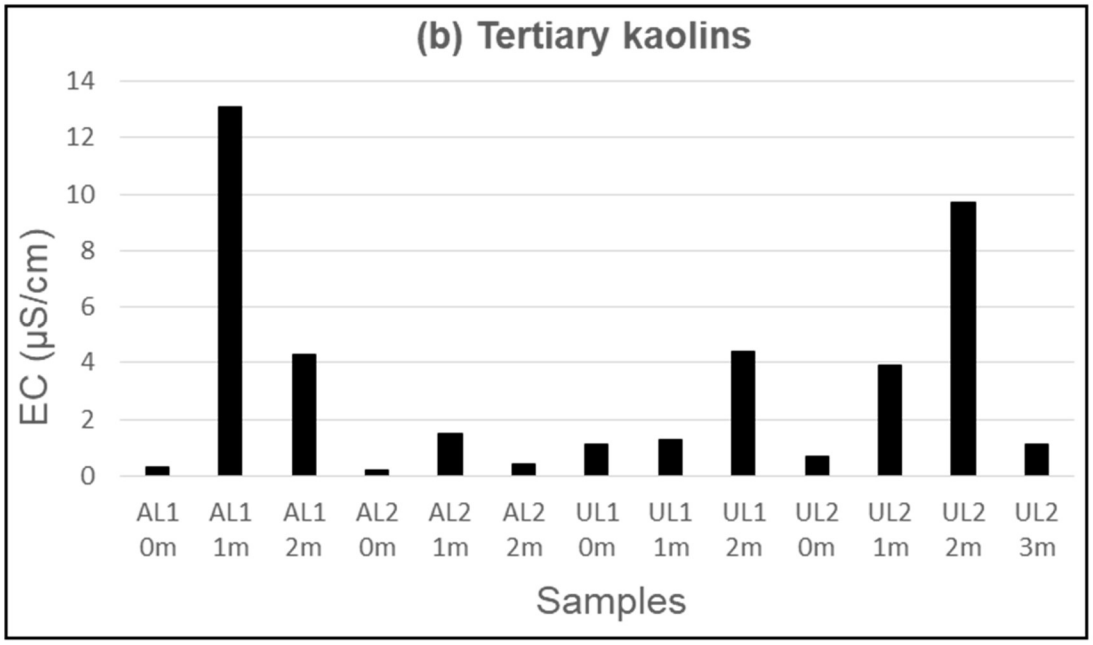

Figure 4.2: EC values of studied kaolins: (a) Cretaceous and (b) Tertiary.

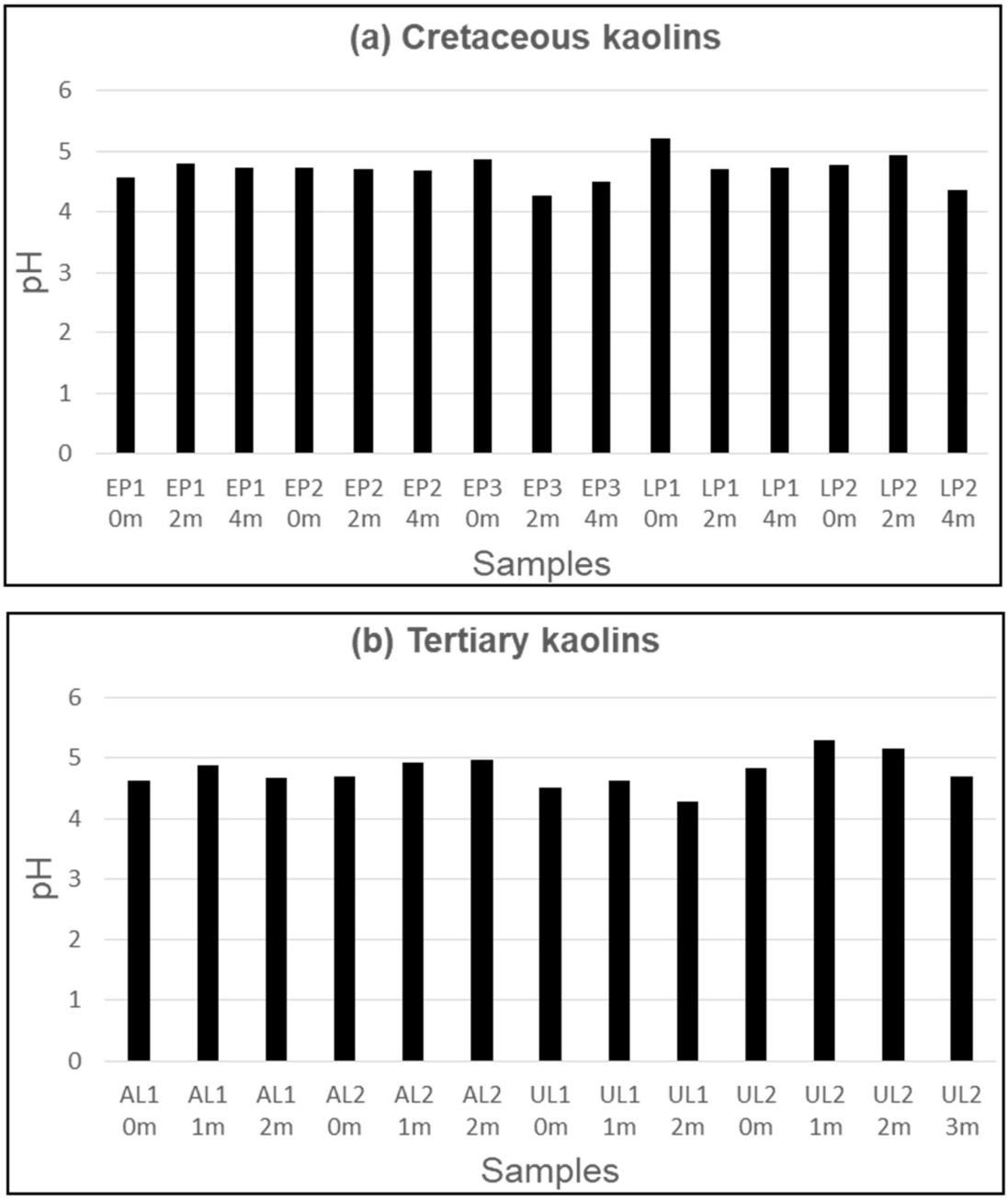

Figure 4.3: pH values of studied kaolins: (a) Cretaceous and (b) Tertiary.

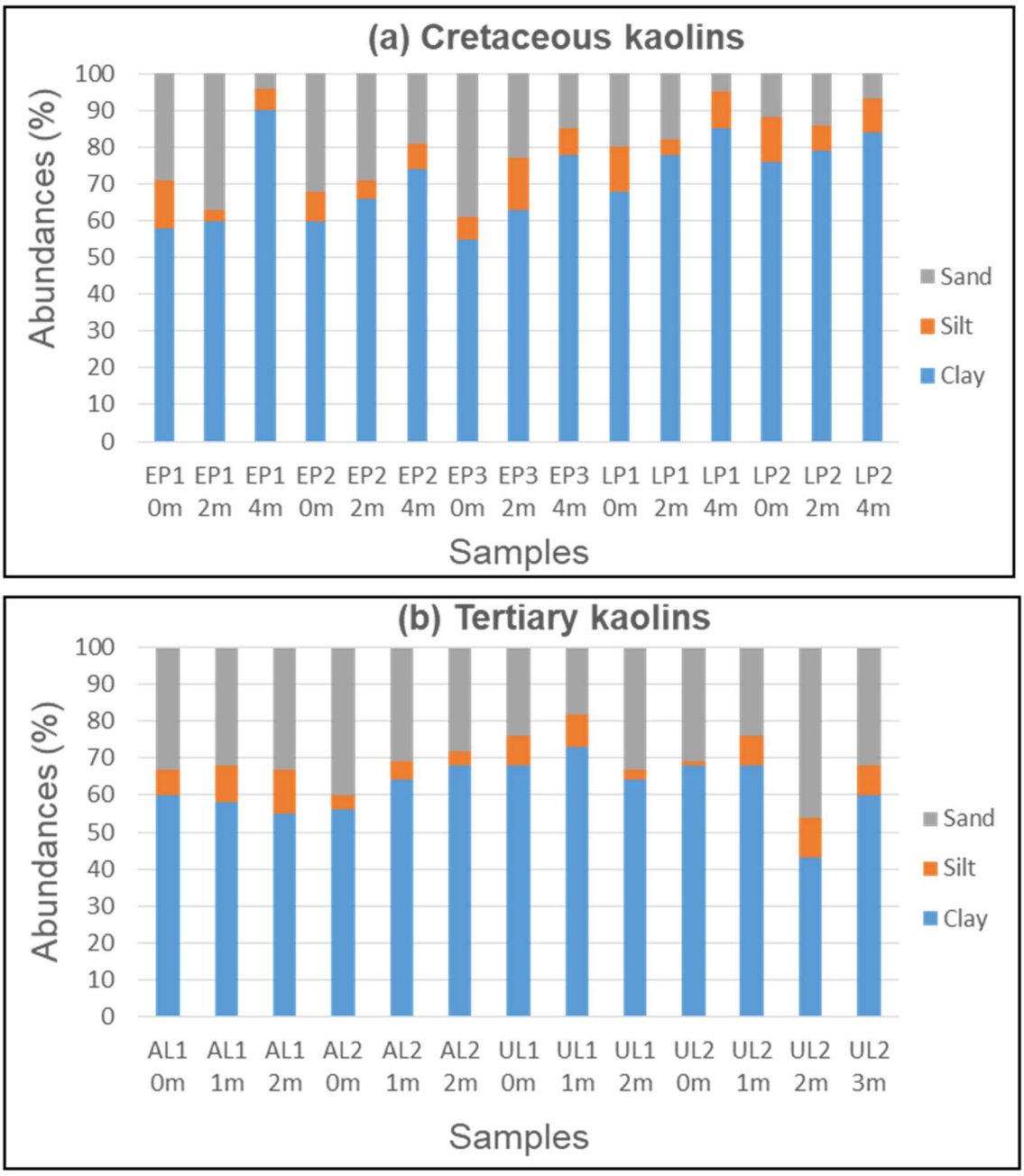

Figure 4.4a: Relative abundances of the Sand, Silt, and Clay fractions within the studied Cretaceous - Tertiary kaolins.

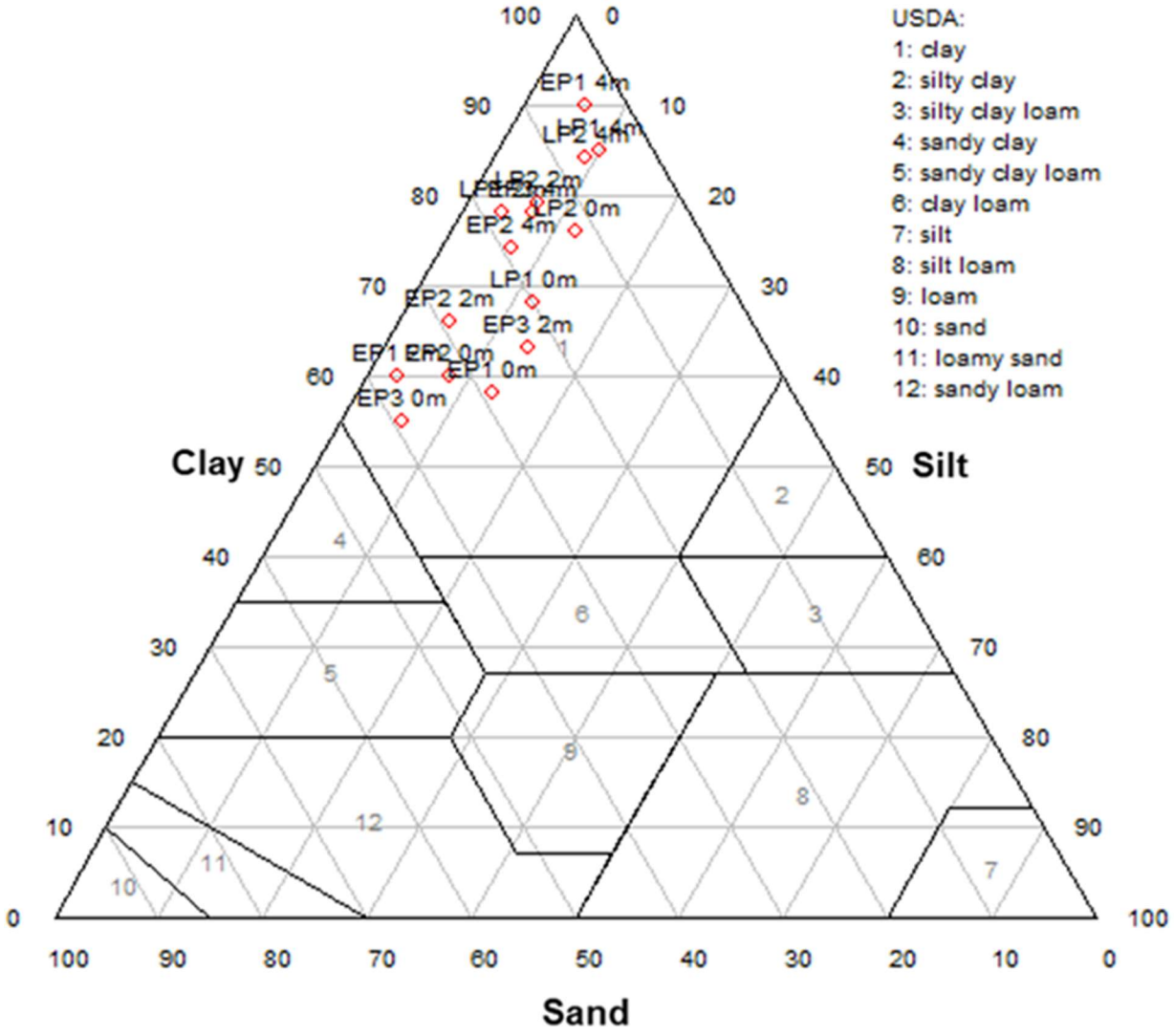

Figure 4.4c: Textural ternary plot for the studied Cretaceous kaolins.

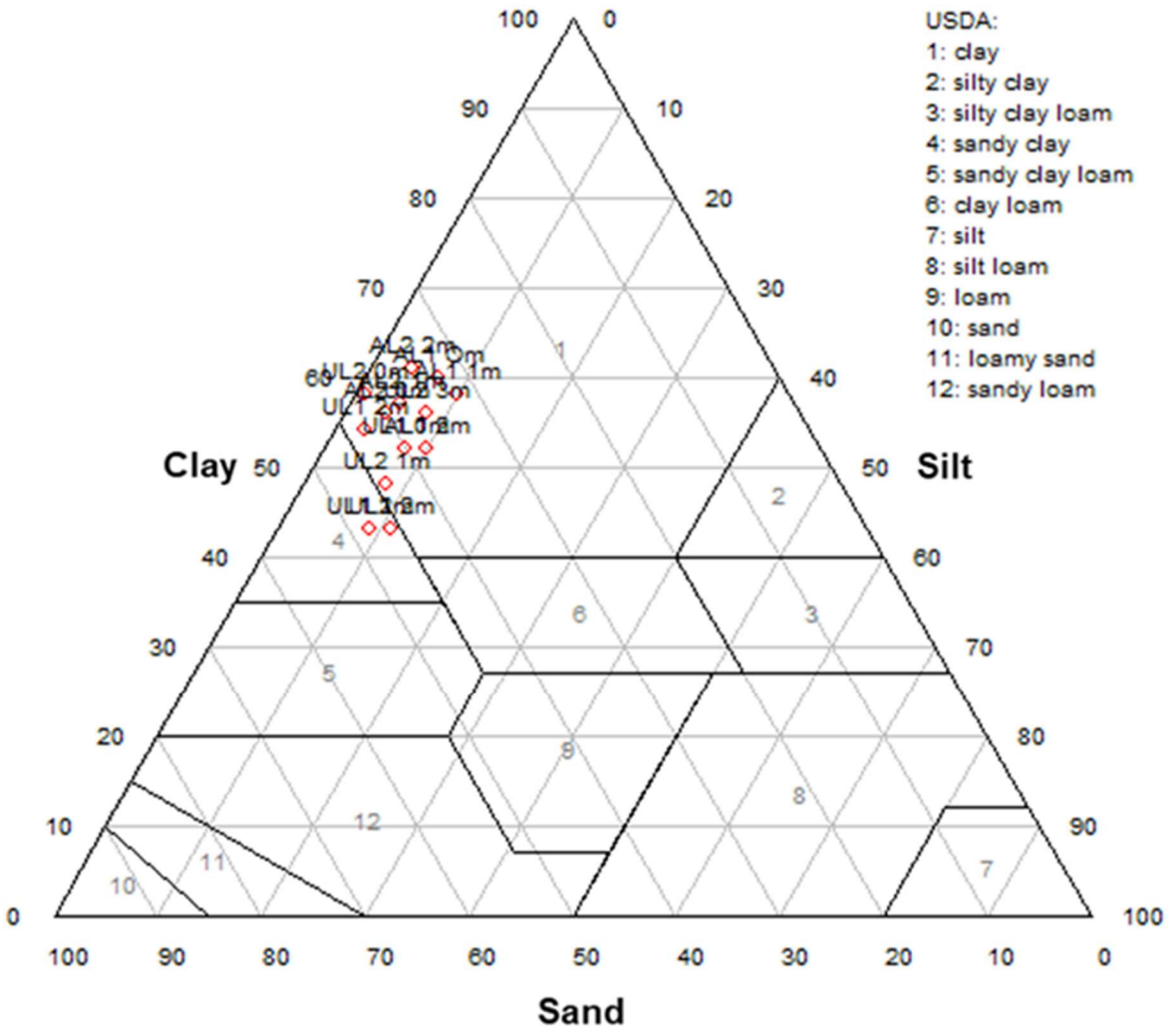

Figure 4.4d: Textural ternary plot for the studied Tertiary kaolins.

4.1.5 Atterberg Limits

The Atterberg limits for the studied Cretaceous – Tertiary kaolins are presented in Table 4.2 and Figure 4.5.

The liquid limit (LL) of Eruku kaolins were between 43 and 49 wt % with a mean value of 47 wt %, whereas LL of Lakiri kaolins were between 45 and 51 wt % with an average of 48 wt %. The LL of Awo-Omama kaolin samples varied from 23 to 33 wt % with a mean value of 28 wt %, whereas LL of Ubulu-Uku kaolins were between 48 and 56 wt % with an average of 52 wt %.

Table 4.2: Atterberg limits of the studied Cretaceous – Tertiary kaolins.

Age	Deposit	Sample ID	LL	PL	PI
Cretaceous	Eruku	EP1	48	29	19
		EP2	51	38	13
		EP3	49	32	17
	Lakiri	LP1	33	18	15
		LP2	48	28	20
Tertiary	Awo-Omama	AL1	43	32	11
		AL2	56	34	22
	Ubulu-Uku	UL1	23	13	10
		UL2	45	34	11

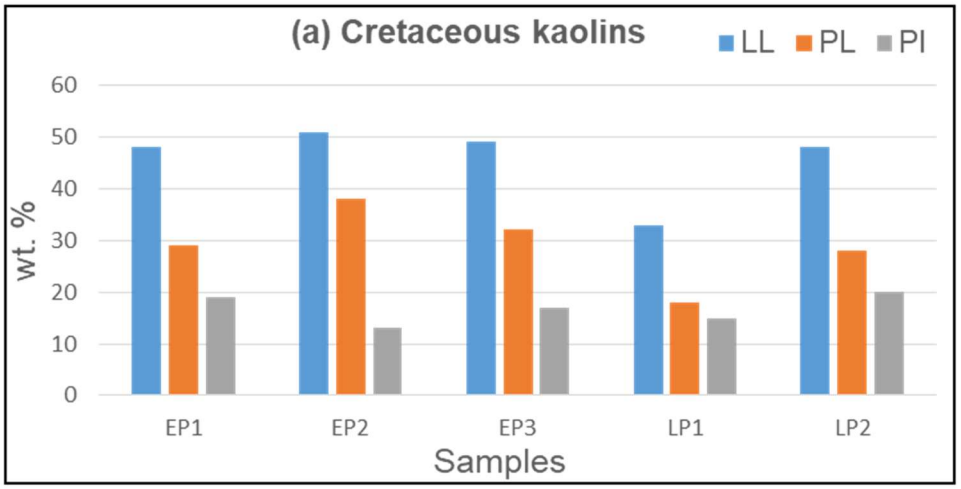

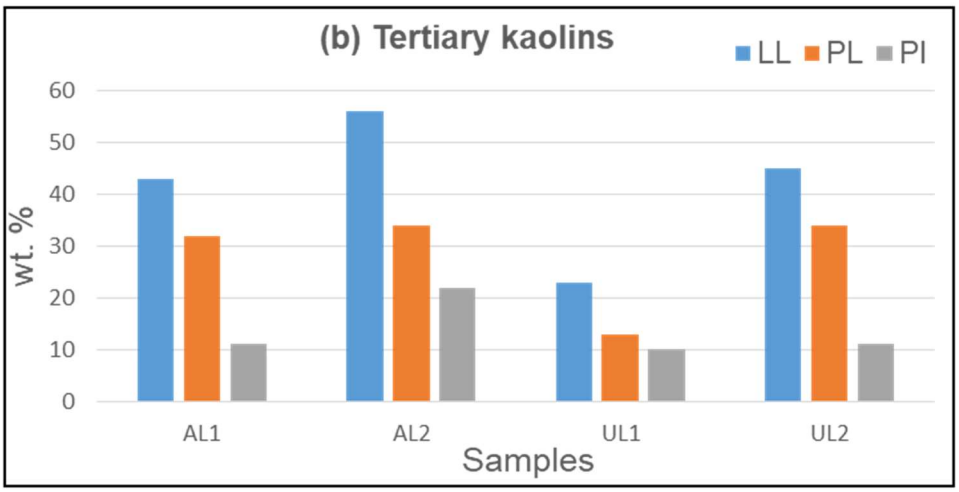

Figure 4.5: Atterberg limits of the studied kaolins: (a) Cretaceous and (b) Tertiary.

The plastic limit (PL) of Eruku kaolins were between 28 and 32 wt % with a mean value of 31 wt %, whereas PL of Lakiri kaolins were between 34 and 38 wt % with an average of 36 wt %. The PL of Awo-Omama kaolin samples varied from 13 to 18 wt % with a mean value of 16 wt %, whereas PL of Ubulu-Uku kaolins were between 29 and 34 wt % with an average of 32 wt %.

The plastic index (PI) of Eruku kaolins were between 11 and 20 wt % with a mean value of 16 wt %, whereas PI of Lakiri kaolins were between 11 and 13 wt % with an average of 12 wt %. The PI of Awo-Omama kaolin samples ranged from 10 to 15 wt % with a mean value of 13 wt %, whereas PI of Ubulu-Uku kaolins were between 19 and 22 wt % with an average of 21 wt %.

4.2 Mineralogical Properties of Studied Cretaceous – Tertiary Kaolins

4.2.1 X-ray Diffraction (XRD) Studies

4.2.1.1 Qualitative Analyses

The qualitative analyses of the studied Cretaceous-Tertiary kaolins were based on the identification of known characteristic mineral peaks. Kaolinite peaks were observed at 7.13 Å, 4.36 Å, 4.16 Å, and 3.57 Å whereas peaks at 4.25 Å and 3.34 Å were assigned to quartz. Peaks observed at 3.51 Å, 4.15 Å, 2.71 Å, and 10.01 Å were assigned to anatase, goethite, hematite, and muscovite respectively. Figures 4.6 – 4.24 shows the X-ray diffraction patterns of the studied Cretaceous – Tertiary kaolins confirming the presence of the different mineral phases.

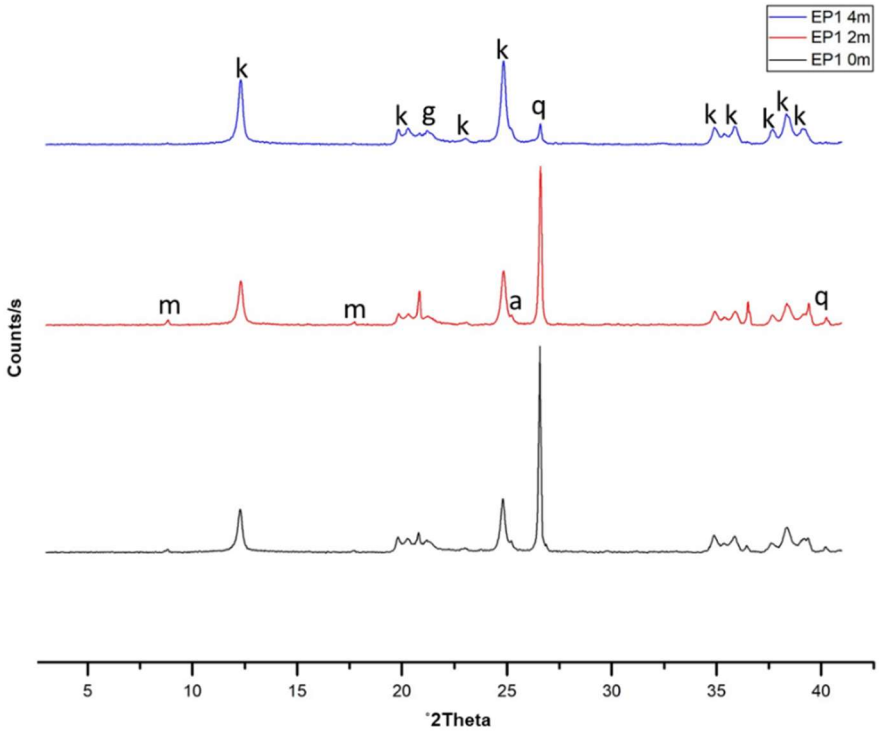

Figure 4.6: Mineral phases as determined by XRD of Eruku bulk samples: k= kaolinite; m= muscovite; q= quartz; a= anatase; g= goethite.

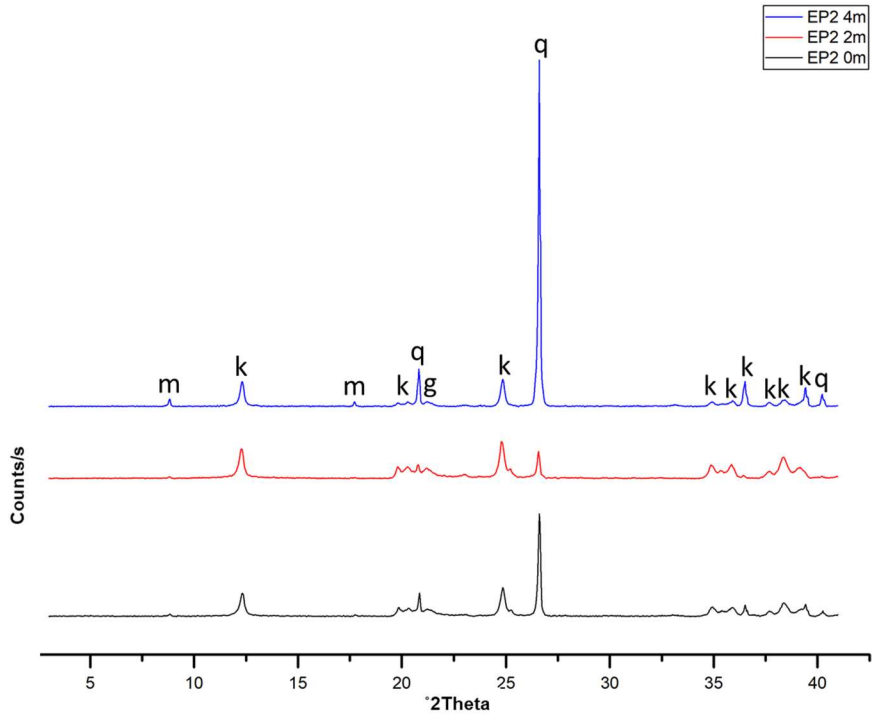

Figure 4.7: Mineral phases as determined by XRD of Eruku bulk samples: k= kaolinite; m= muscovite; q= quartz; g= goethite.

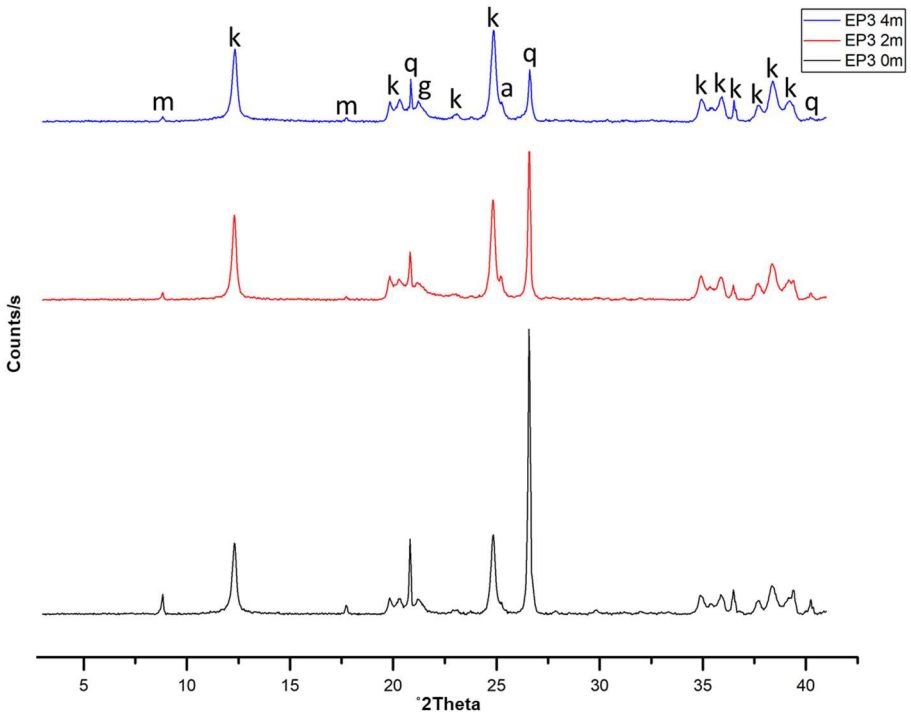

Figure 4.8: Mineral phases as determined by XRD of Eruku bulk samples: k= kaolinite; m= muscovite; q= quartz; a= anatase; g= goethite.

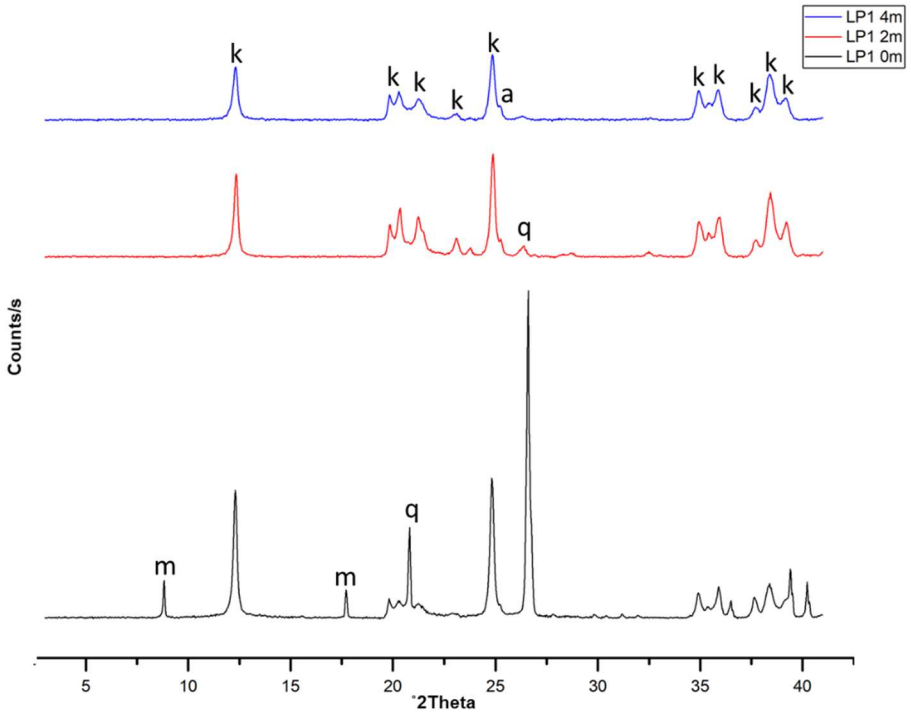

Figure 4.9: Mineral phases as determined by XRD of Lakiri bulk samples: k= kaolinite; q= quartz; a= anatase.

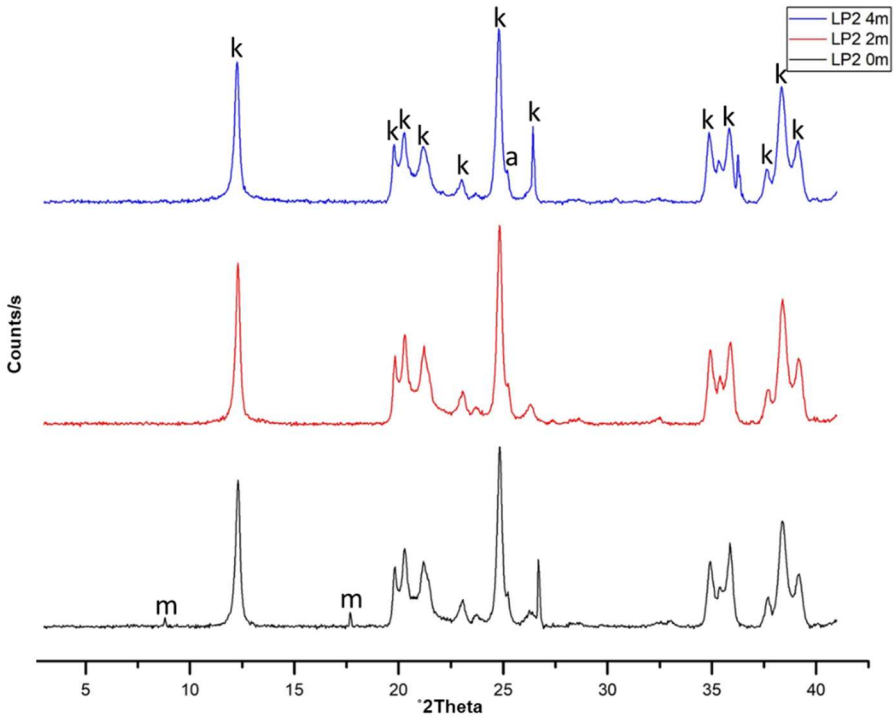

Figure 4.10: Mineral phases as determined by XRD of Lakiri bulk samples: k= kaolinite; m= muscovite; a= anatase.

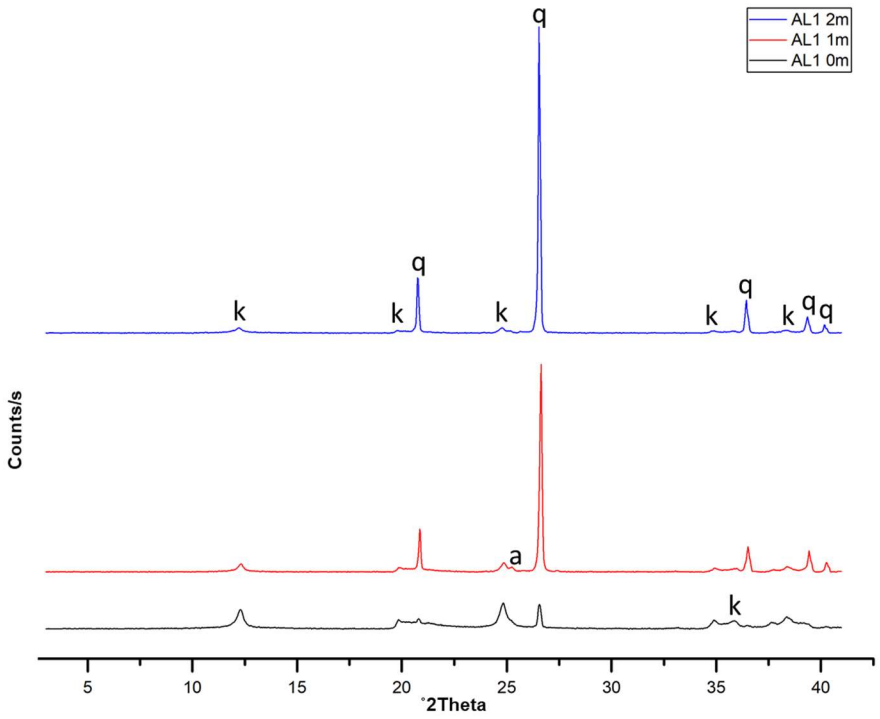

Figure 4.11: Mineral phases as determined by XRD of Awo-Omama bulk samples: k= kaolinite; q= quartz; a= anatase.

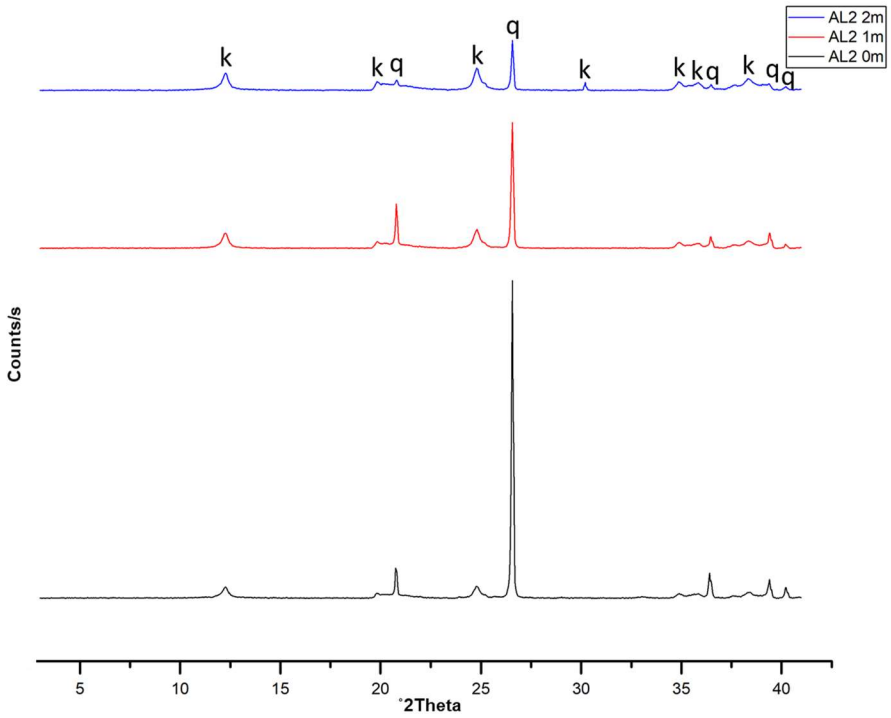

Figure 4.12: Mineral phases as determined by XRD of Awo-Omama bulk samples: k= kaolinite; q= quartz.

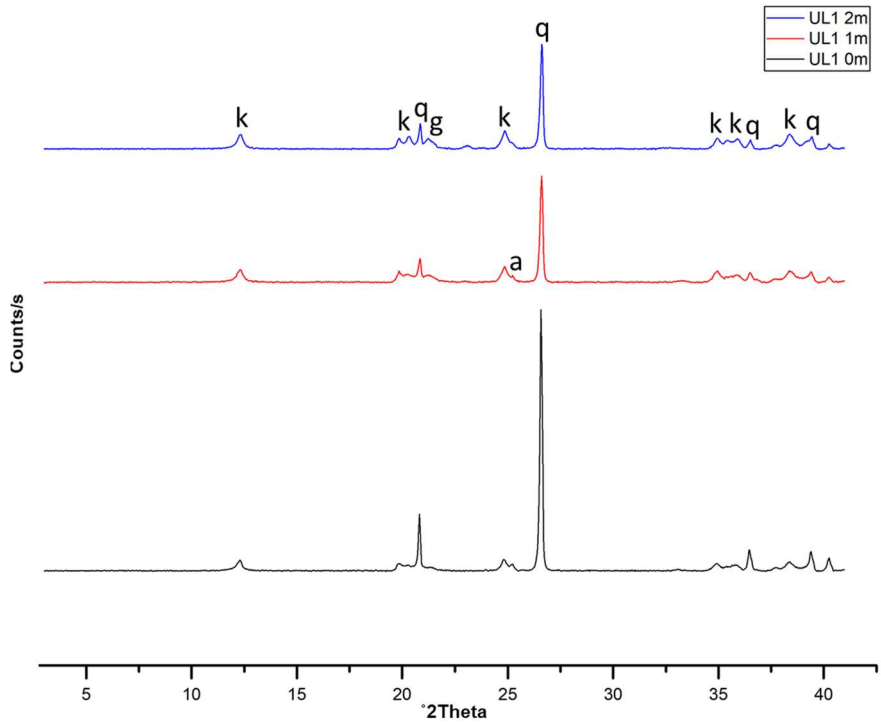

Figure 4.13: Mineral phases as determined by XRD of Ubulu-Uku bulk samples: k= kaolinite; q= quartz; a= anatase; g= goethite.

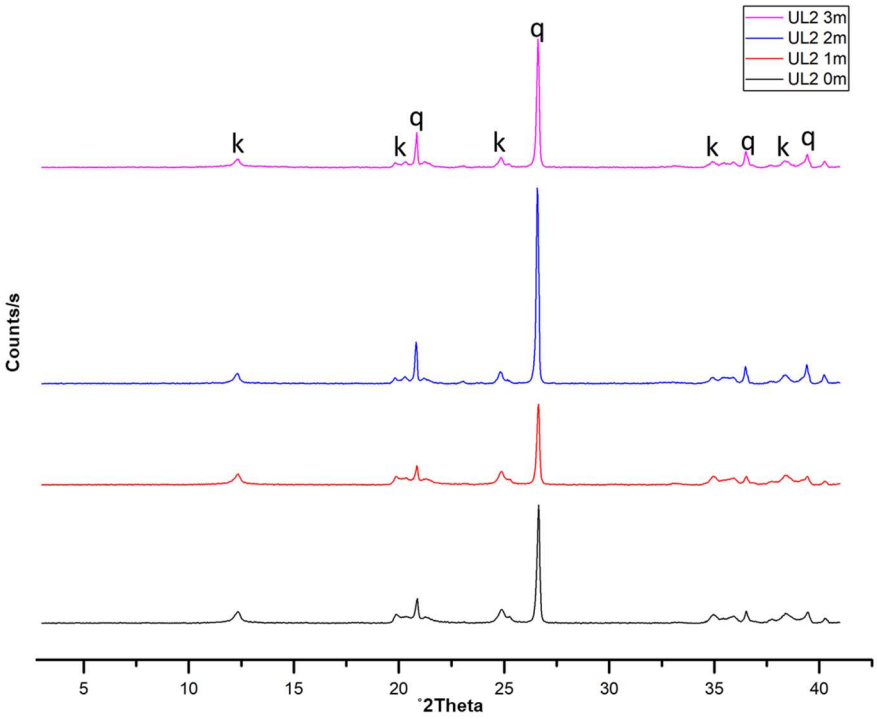

Figure 4.14: Mineral phases as determined by XRD of Ubulu-Uku bulk samples: k= kaolinite; q= quartz.

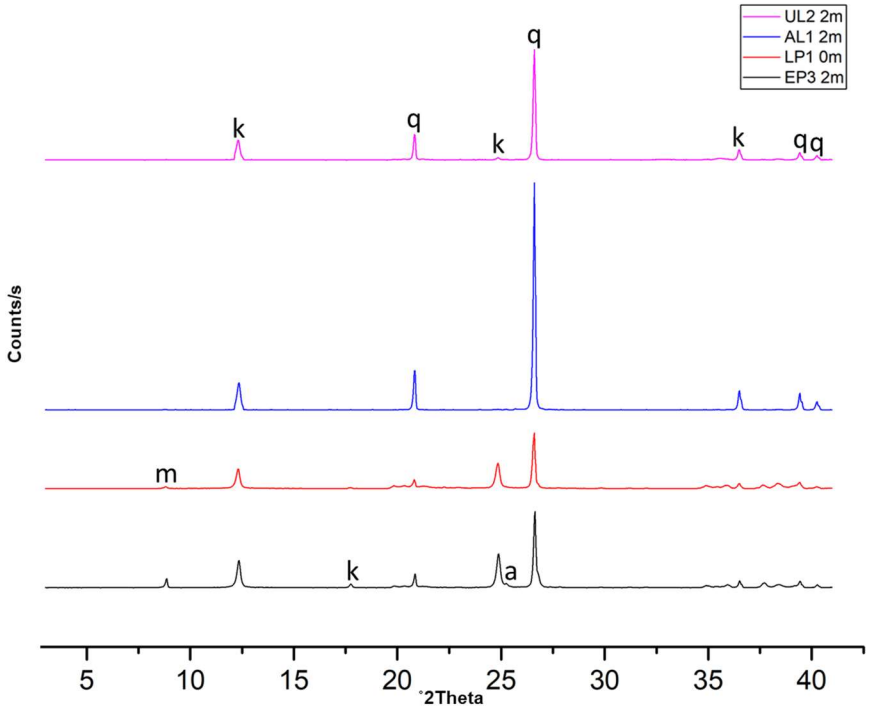

Figure 4.15: Mineral phases as determined by XRD of Eruku, Lakiri, Awo-Omama, and Ubulu-Uku Silt fractions: k= kaolinite; q= quartz; m= muscovite; a= anatase.

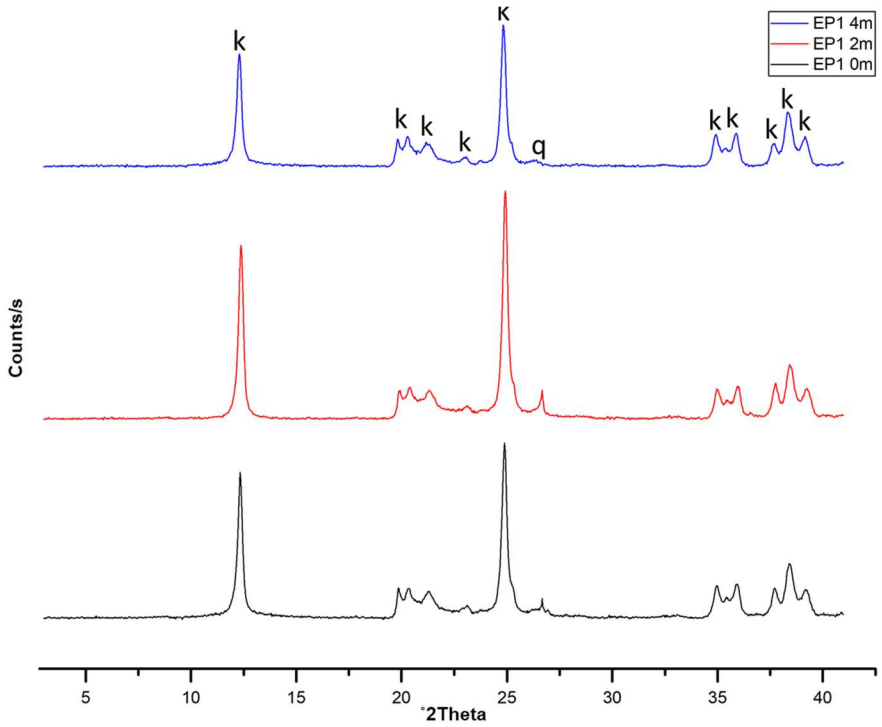

Figure 4.16: Mineral phases as determined by XRD of Eruku Clay fraction: k= kaolinite; q= quartz.

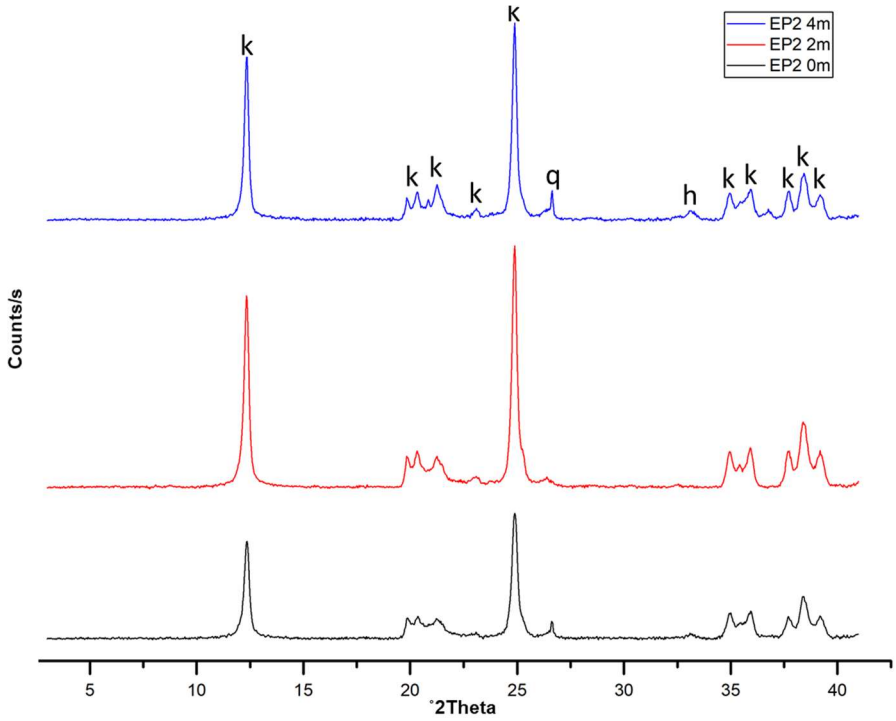

Figure 4.17: Mineral phases as determined by XRD of Eruku Clay fraction: k= kaolinite; q= quartz; h=hematite.

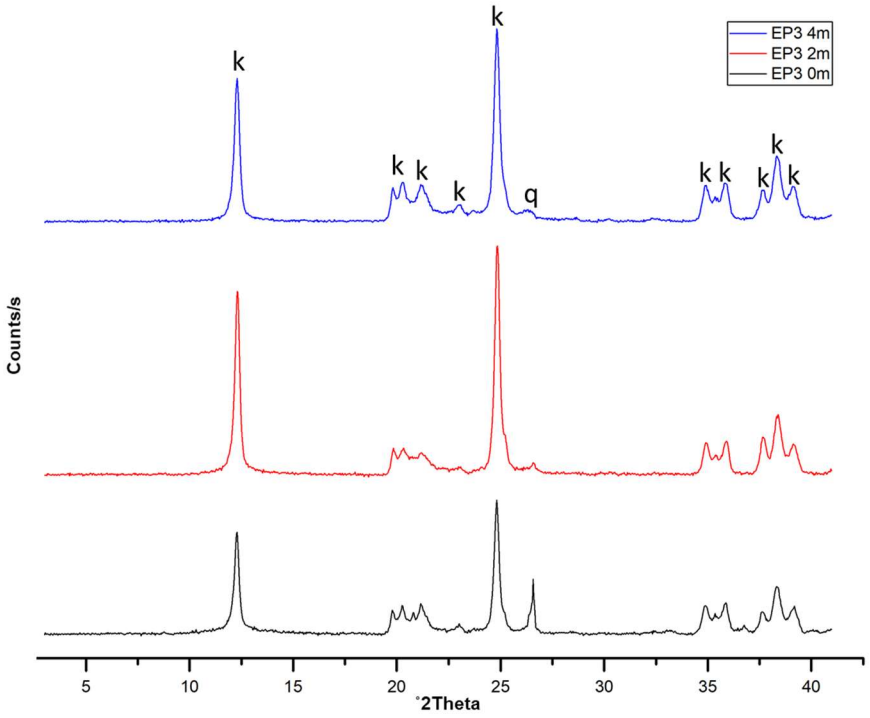

Figure 4.18: Mineral phases as determined by XRD of Eruku Clay fraction: k= kaolinite; q= quartz.

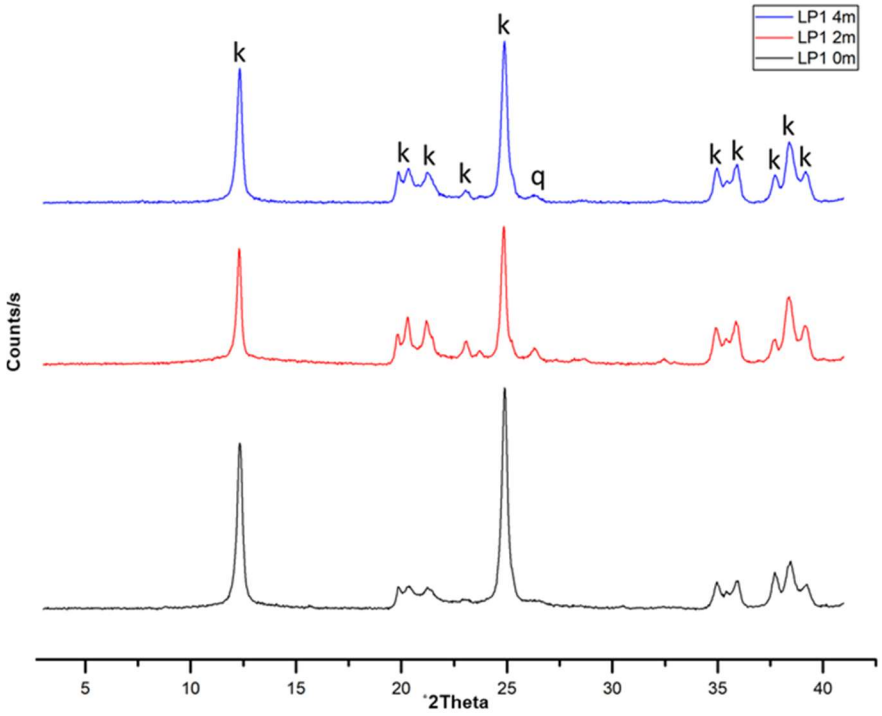

Figure 4.19: Mineral phases as determined by XRD of Lakiri Clay fraction: k= kaolinite; q= quartz.

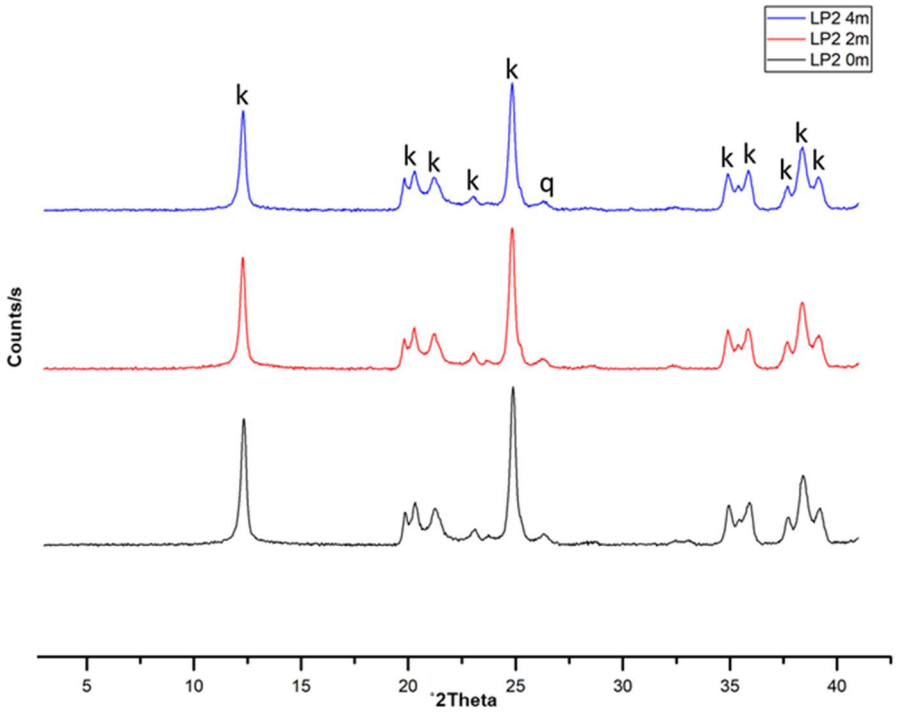

Figure 4.20: Mineral phases as determined by XRD of Lakiri Clay fraction: k= kaolinite; q= quartz.

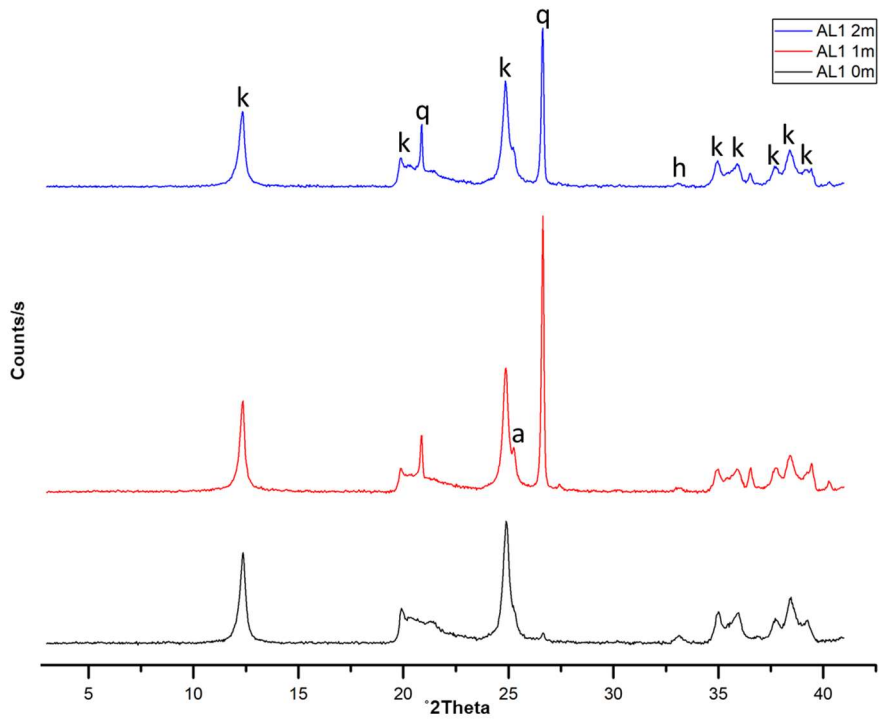

Figure 4.21: Mineral phases as determined by XRD of Awo-Omama Clay fraction: k= kaolinite; q= quartz; h=hematite; a=anatase.

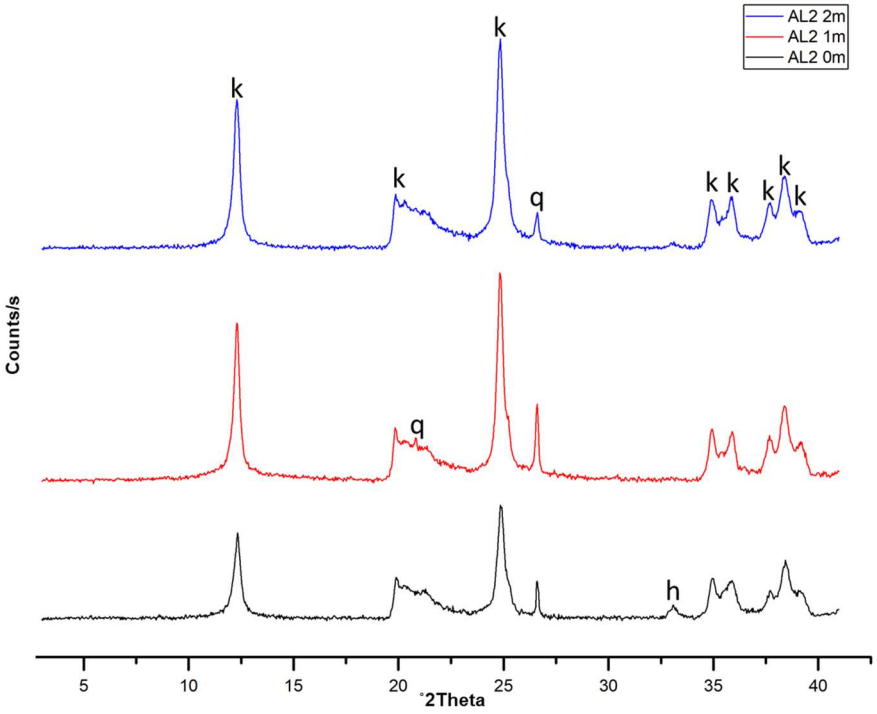

Figure 4.22: Mineral phases as determined by XRD of Awo-Omama Clay fraction: k= kaolinite; q= quartz.

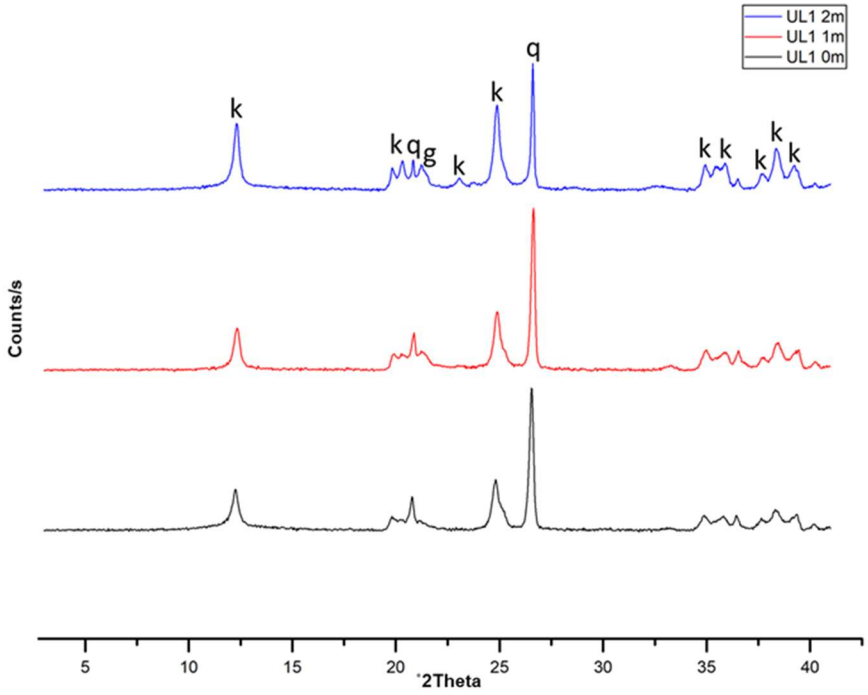

Figure 4.23: Mineral phases as determined by XRD of Ubulu-Uku Clay fraction: k= kaolinite; q= quartz; g= goethite.

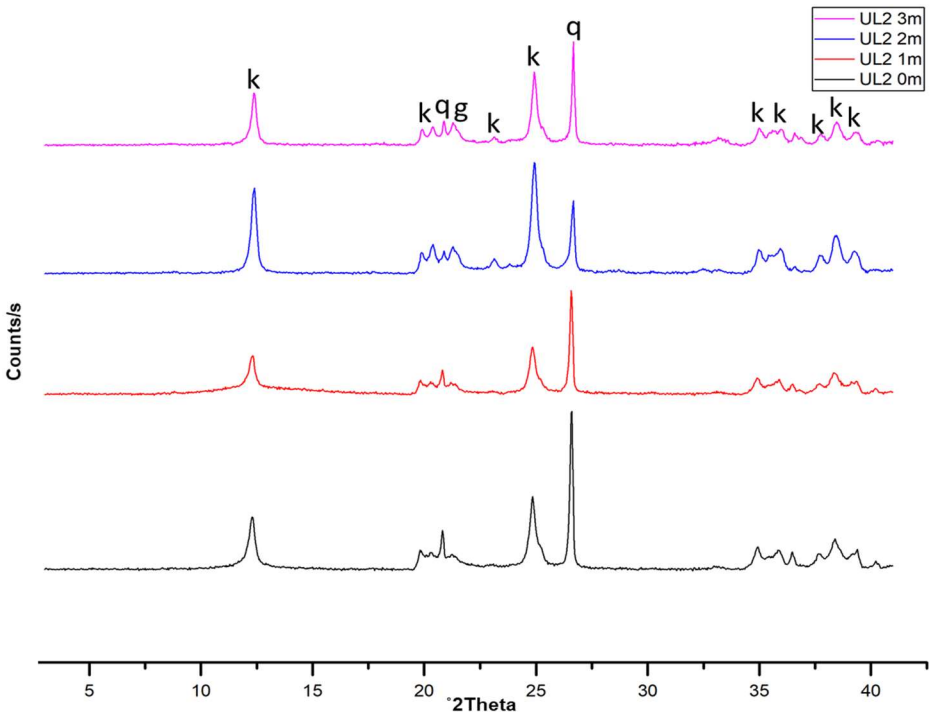

Figure 4.24: Mineral phases as determined by XRD of Ubulu-Uku Clay fraction: k= kaolinite; q= quartz; g= goethite.

4.2.1.2 Quantitative Analyses

- **Bulk (<2 mm) Samples**

The results of quantitative analyses of the various mineral present in the bulk fractions are presented in Table 4.3.

The Eruku kaolins had kaolinite and quartz as the most dominant mineral constituents with combined abundances ranging from 49 to 94 wt % whereas anatase, muscovite, hematite, and goethite were present in minor quantities except for muscovite having up to 9 wt % in EP3 0m. In the Lakiri kaolins, kaolinite was the dominant mineral phase with abundances ranging from 64 to 99 wt %, whereas quartz, anatase, muscovite, hematite, goethite were present in minor quantities except for quartz and muscovite with 29 wt % and 7 wt % in sample LP1 0m.

Table 4.3: Results of Quantitative Analyses of Minerals present (wt %) in the Bulk samples of the studied Cretaceous-Tertiary Kaolins.

Age	Deposit	Sample ID	Kaolinite	Quartz	Anatase	Muscovite	Hematite	Goethite
Cretaceous	Eruku	BK EP1 0m	71	23	2	4	-	tr
		BK EP1 2m	72	23	1	4	-	tr
		BK EP1 4m	94	5	1	-	-	tr
		BK EP2 0m	75	24	tr	1	-	tr
		BK EP2 2m	92	4	1	3	-	-
		BK EP2 4m	49	47	tr	3	-	1
		BK EP3 0m	61	29	-	9	-	1
		BK EP3 2m	76	15	1	7	tr	1
		BK EP3 4m	85	7	2	5	-	1
	Lakiri	BK LP1 0m	64	29	-	7	tr	-
		BK LP1 2m	99	tr	tr	-	-	1
		BK LP1 4m	99	-	tr	-	-	1
		BL LP2 0m	98	-	1	1	tr	-
		BL LP2 2m	98	1	1	-	-	-
		BK LP2 4m	98	2	tr	-	-	-
		Min	49	1	1	1	-	1
		Max	99	57	2	9	-	1
		Average	83	21	1	5	-	1
Tertiary	Awo-Omama	BK AL1 0m	93	6	1	-	-	-
		BK AL1 1m	40	59	1	-	-	-
		BK AL1 2m	25	74	1	-	-	-
		BK AL2 0m	47	52	1	-	-	-
		BK AL2 1m	63	37	tr	-	-	-
		BK AL2 2m	84	15	1	-	-	-
	Ubulu-Uku	BK UL1 0m	58	42	tr	-	-	tr
		BK UL1 1m	74	24	1	-	-	1
		BK UL1 2m	76	23	1	-	-	tr
		BK UL2 0m	71	28	1	-	-	tr
		BK UL2 1m	74	25	1	-	-	tr
		BK UL2 2m	46	54	1	-	-	tr
		BK UL2 3m	57	42	1	-	-	1
		Min	25	6	1	-	-	1
		Max	93	74	1	-	-	1
		Average	62	37	1	-	-	1

(tr) Trace, (-) Not detected

The Awo-Omama kaolin samples had kaolinite and quartz as the most dominant mineral constituents with combined abundances ranging from 96 to 100 wt % whereas anatase was present with abundances ranging from 1 to 4 wt %. Muscovite, hematite, and goethite were not detected. In the Ubulu-Uku kaolins, kaolinite and quartz were the dominant mineral phases with combined abundances ranging from 98 to 100 wt % whereas anatase and goethite were present in trace quantities.

On average weight percentages, bulk samples of the Cretaceous kaolin deposits have kaolinite, quartz, and muscovite present in decreasing order with anatase, goethite, and hematite in traces whereas Tertiary kaolin deposits have kaolinite and quartz present in decreasing order with anatase and goethite in traces.

- **Silt (2 – 63 µm) Fractions**

The results of quantitative analyses of the various mineral present in the silt fractions are presented in Tables 4.4 and Figure 4.25.

In the Cretaceous kaolins, kaolinite was the dominant mineral constituent with abundance between 54 and 56 wt % followed by quartz with 35 wt %. Muscovite and anatase were present in minor quantities. Hematite and goethite were present in traces. For Tertiary kaolins, quartz was the dominant mineral phase with abundance between 51 and 58 wt % followed by kaolinite with abundance ranging from 42 to 49 wt %. Anatase was present in trace quantities whereas muscovite, hematite, and goethite were absent.

- **Clay (<2 µm) Fractions**

The results of quantitative analyses of the various mineral present in the clay fractions are presented in Table 4.5 and Figures 4.26 – 4.27.

The Cretaceous kaolin samples had kaolinite as the dominant mineral constituent with abundances between 93 and 99 wt % whereas quartz, anatase, hematite and goethite were present in trace to minor quantities ranging from 1 to 6 wt %. Muscovite was absent (Fig. 4.26).

Table 4.4: Results of Quantitative Analyses of Minerals present (wt %) in the Silt fractions of the studied Cretaceous-Tertiary Kaolins.

Age	Deposit	Sample ID	Kaolinite	Quartz	Anatase	Muscovite
Cretaceous	Eruku	ST EP3 2m	54	35	1	10
	Lakiri	ST LP1 0m	56	35	tr	9
Tertiary	Awo-Omama	ST AL1 2m	42	58	tr	-
	Ubulu-Uku	ST UL2 2m	49	51	-	-

(tr) Trace, (-) Not detected

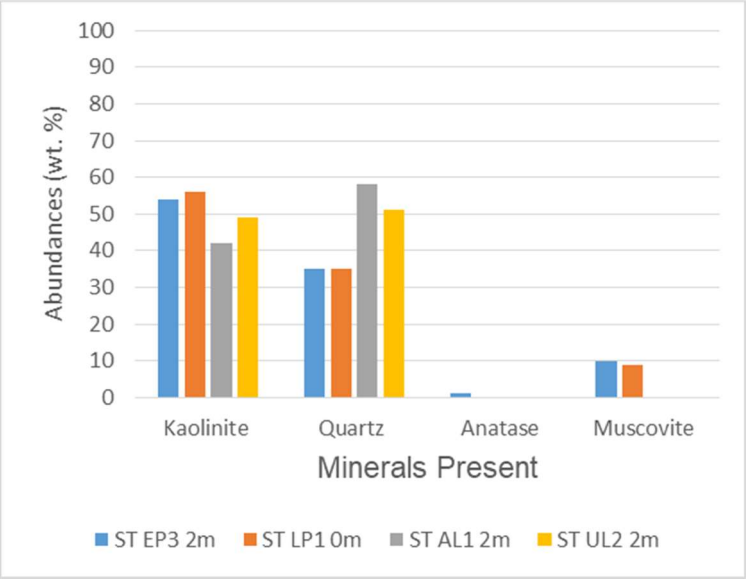

Figure 4.25: Mineral Abundance (wt %) in the Silt fractions of the studied Cretaceous-Tertiary Kaolins.

The Tertiary kaolins had kaolinite and quartz as the dominant mineral phases with combined abundance ranging from 93 to 99 wt % whereas anatase, hematite, and goethite were present in trace to minor quantities ranging from 1 to 2 wt % (Fig. 4.27).

In the Cretaceous – Tertiary kaolins, the dominant clay mineral was kaolinite accounting for 69 and 99 wt % whereas the non-clay minerals like quartz, anatase, hematite and goethite accounted for percentages between 1 and 28 wt % (Tables 4.5).

Table 4.5: Results of Quantitative Analyses of Minerals present (wt %) in the Clay fractions of the studied Cretaceous-Tertiary Kaolins.

Age	Deposit	Sample ID	Kaolinite	Quartz	Anatase	Hematite	Goethite
Cretaceous	Eruku	CF EP1 0m	97	2	1	-	tr
		CF EP1 2m	96	3	1	-	tr
		CF EP1 4m	98	2	tr	-	tr
		CF EP2 0m	97	1	1	1	tr
		CF EP2 2m	98	1	1	-	tr
		CF EP2 4m	94	4	tr	1	1
		CF EP3 0m	93	6	tr	tr	2
		CF EP3 2m	94	3	1	1	2
		CF EP3 4m	97	1	tr	tr	1
	Lakiri	CF LP1 0m	99	1	tr	-	-
		CF LP1 2m	99	1	tr	-	-
		CF LP1 4m	99	1	tr	-	-
		CF LP2 0m	99	1	tr	-	-
		CF LP2 2m	99	1	tr	-	-
		CF LP2 4m	99	1	tr	-	-
		Min	93	1	1	1	1
		Max	99	6	1	1	1
		Average	98	2	1	1	1
Tertiary	Awo-Omama	CF AL1 0m	91	7	1	1	-
		CF AL1 1m	69	28	2	1	-
		CF AL1 2m	75	23	1	1	-
		CF AL2 0m	89	9	1	1	-
		CF AL2 1m	79	20	1	-	-
		CF AL2 2m	90	9	1	tr	-
	Ubulu-Uku	CF UL1 0m	70	28	1	-	1
		CF UL1 1m	76	22	-	-	2
		CF UL1 2m	90	9	tr	-	1
		CF UL2 0m	74	24	1	-	1
		CF UL2 1m	84	15	tr	-	1
		CF UL2 2m	90	9	1	-	-
		CF UL2 3m	88	11	tr	-	1
		Min	69	7	1	1	1
		Max	91	28	2	1	2
		Average	82	18	1	1	1

(tr) Trace, (-) Not detected

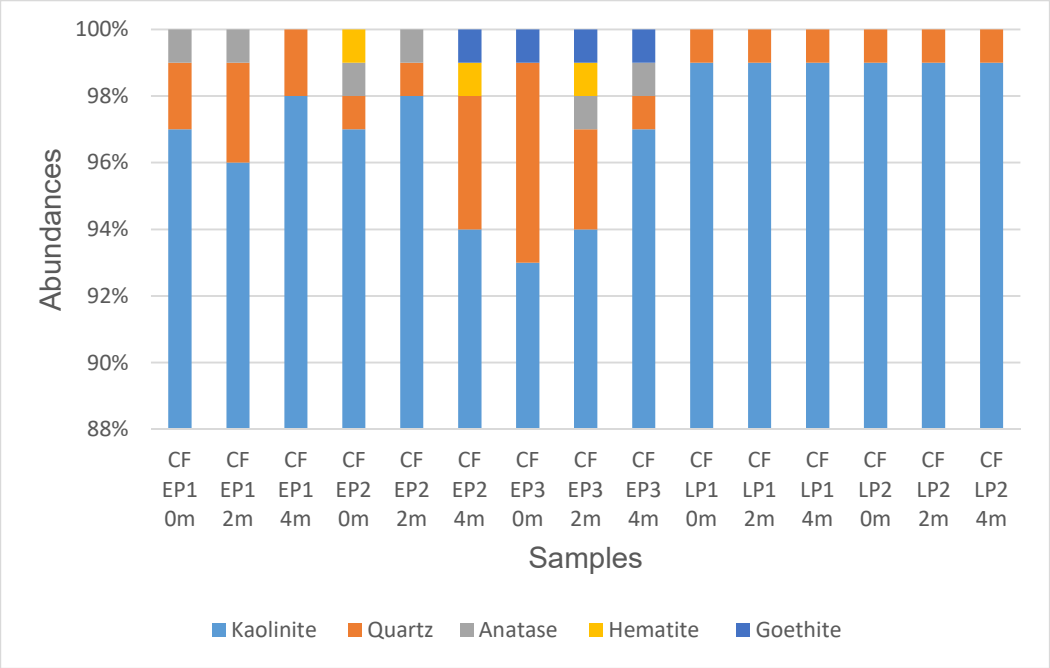

Figure 4.26: Mineral Abundances (wt %) in the Clay fractions of the studied Cretaceous Kaolins.

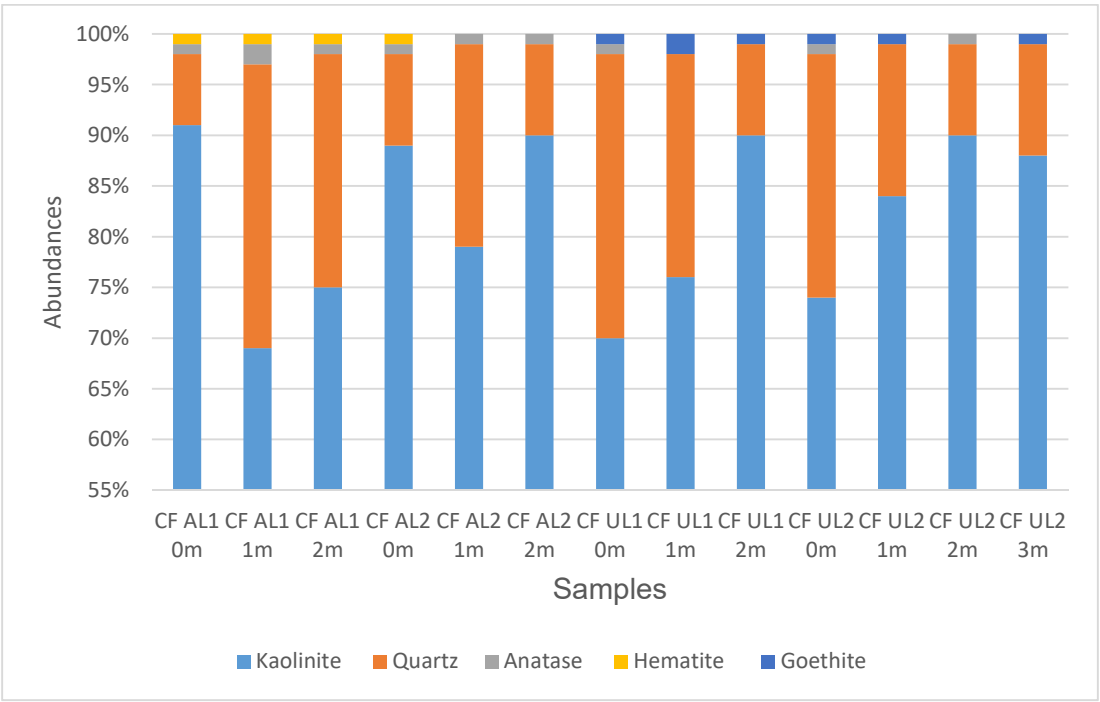

Figure 4.27: Mineral Abundances (wt %) in the Clay fractions of the studied Tertiary Kaolins.

4.2.2 Fourier Transform Infrared Spectroscopy

The Infrared (IR) spectra for the clay fractions of the studied Cretaceous – Tertiary kaolins are presented in Figures 4.28 – 4.35. The summary of the assignment of the adsorption bands in measured IR are presented in Appendix 4.1.

The four distinguishable bands in the hydroxyl stretching region (3695, 3670, 3650, and 3620 cm^{-1}) unique to kaolin minerals (Vaculikova *et al*., 2011) were all present in the Cretaceous-Tertiary kaolins except for the 3670 cm^{-1} which had low intensity. These bands were identified within regions 3686 – 3688 cm^{-1}, 3669 – 3670 cm^{-1}, 3651 – 3653 cm^{-1}, and 3619 – 3621 cm^{-1} respectively in the Cretaceous kaolin deposits, whereas in the Tertiary kaolin deposits, they were identified within regions 3688 – 3692 cm^{-1}, 3667 – 3670 cm^{-1}, 3649 – 3652 cm^{-1}, and 3619 – 3621 cm^{-1} respectively (Figures 4.28, 4.30, 4.32, and 4.34).

The Si-O stretching bands (1114 – 1115 cm^{-1}, 1027 – 1028 cm^{-1}, and 1004 – 1005 cm^{-1}) were also present in the Cretaceous – Tertiary kaolins. For the Cretaceous kaolins, the Si-O stretching (longitudinal mode) was identified within region (1114 – 1116 cm^{-1}) whereas the Si-O stretchings (in-plane) were identified within regions 1023 – 1026 cm^{-1} and 998 – 1002 cm^{-1} respectively. The Tertiary kaolins have Si-O stretching (longitudinal mode) band within region 1116 – 1118 cm^{-1} whereas Si-O stretchings (in-plane) were identified within regions 1024 – 1028 cm^{-1} and 997 – 1002 cm^{-1} respectively (Figures 4.29, 4.31, 4.33, and 4.35).

The OH deformation of inner-surface hydroxyl groups (935 – 937 cm^{-1}) and OH deformation of inner hydroxyl groups (912 cm^{-1}) were present in all the samples. The Cretaceous kaolins have OH deformation of inner-surface hydroxyl groups and OH deformation of inner hydroxyl groups present within regions 936 – 940 cm^{-1} and 910 – 914 cm^{-1} respectively. For Tertiary kaolins, they occur within regions 936 – 938 cm^{-1} and 910 – 914 cm^{-1} respectively.

The Si-O bands perpendicular (750 -751 cm^{-1} and 681 - 684 cm^{-1}) were identified at 749 – 753 cm^{-1} and 683 – 696 cm^{-1} for both the Cretaceous and Tertiary kaolins.

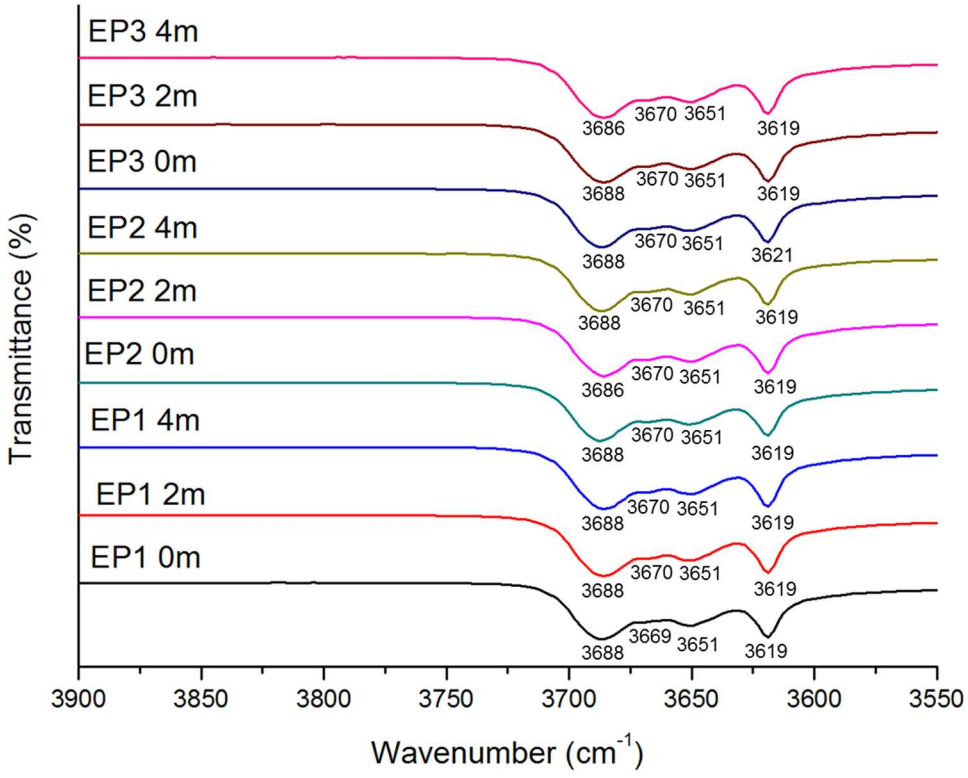

Figure 4.28: The IR spectra of Eruku Kaolin Clay fraction between 3900 to 3550 cm^{-1}.

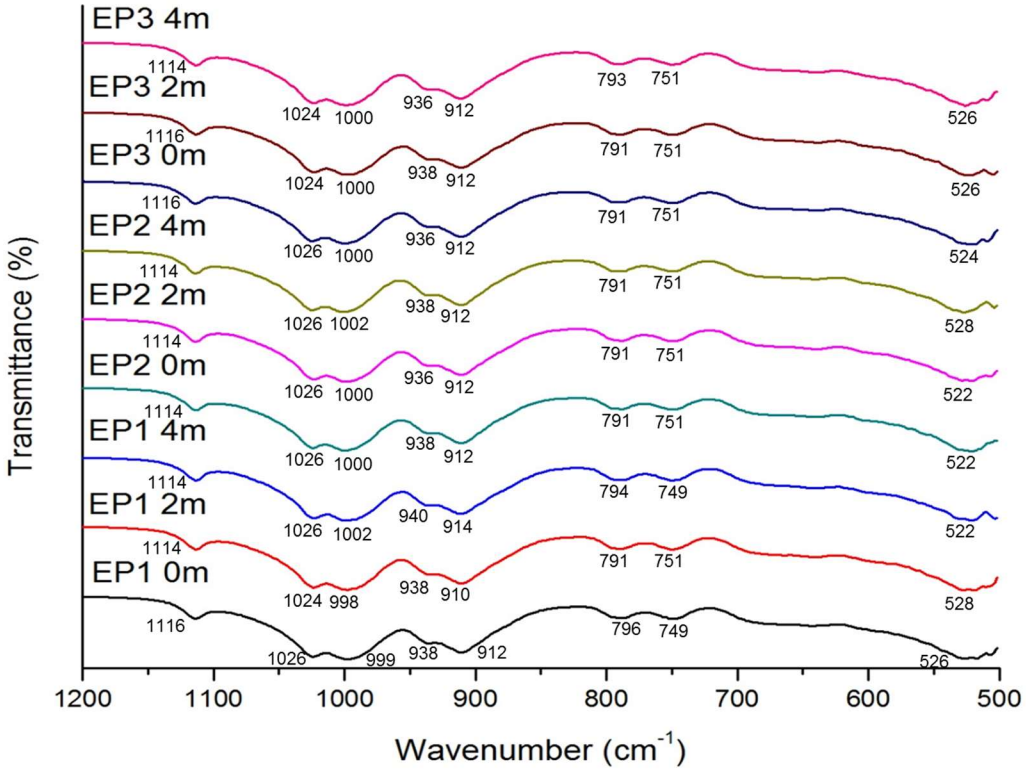

Figure 4.29: The IR spectra of Eruku Kaolin Clay fraction between 1200 to 500 cm^{-1}.

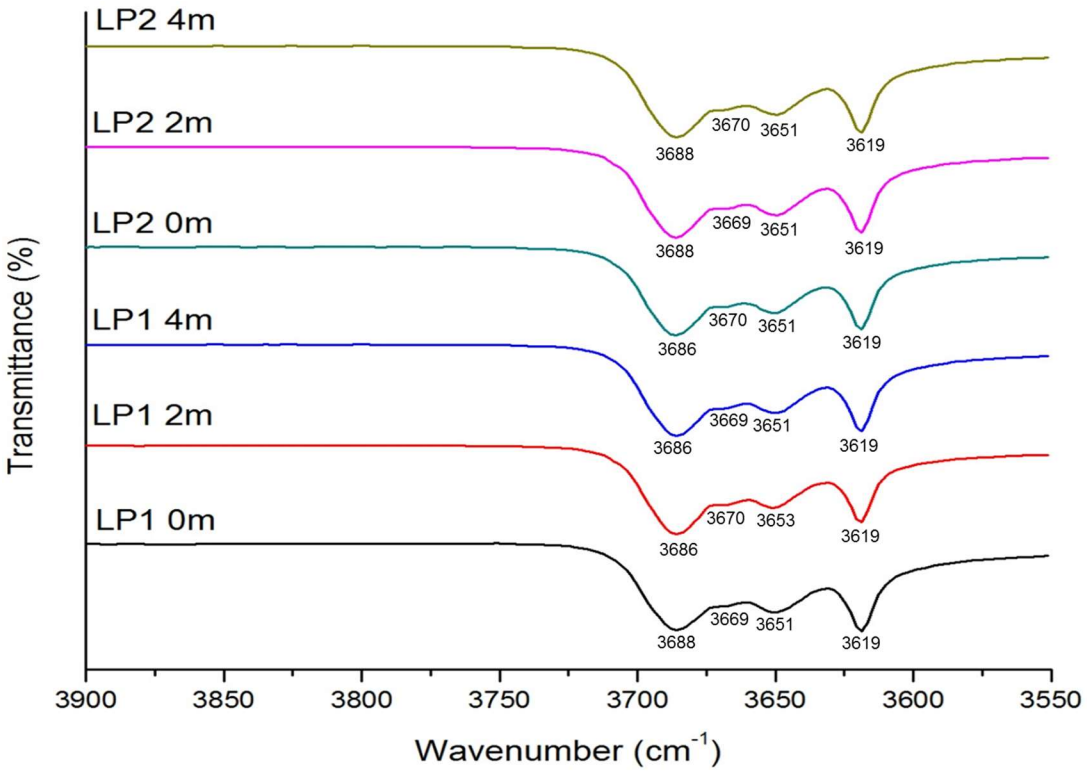

Figure 4.30: The IR spectra of Lakiri Kaolin Clay fraction between 3900 to 3550 cm^{-1}.

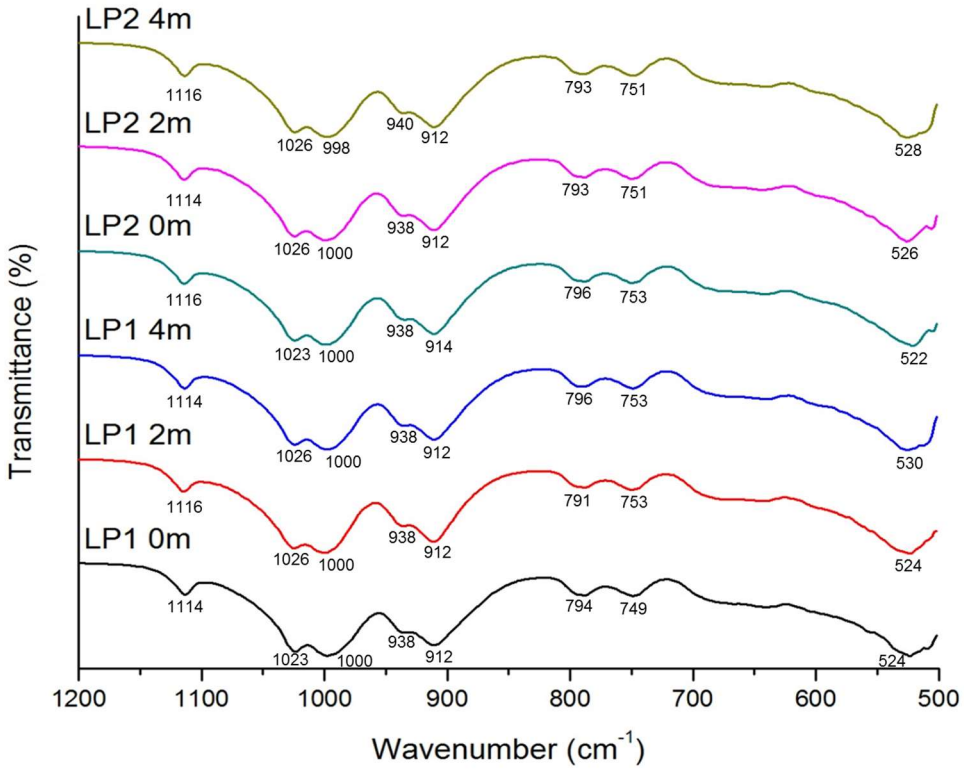

Figure 4.31: The IR spectra of Lakiri Kaolin Clay fraction between 1200 to 500 cm^{-1}.

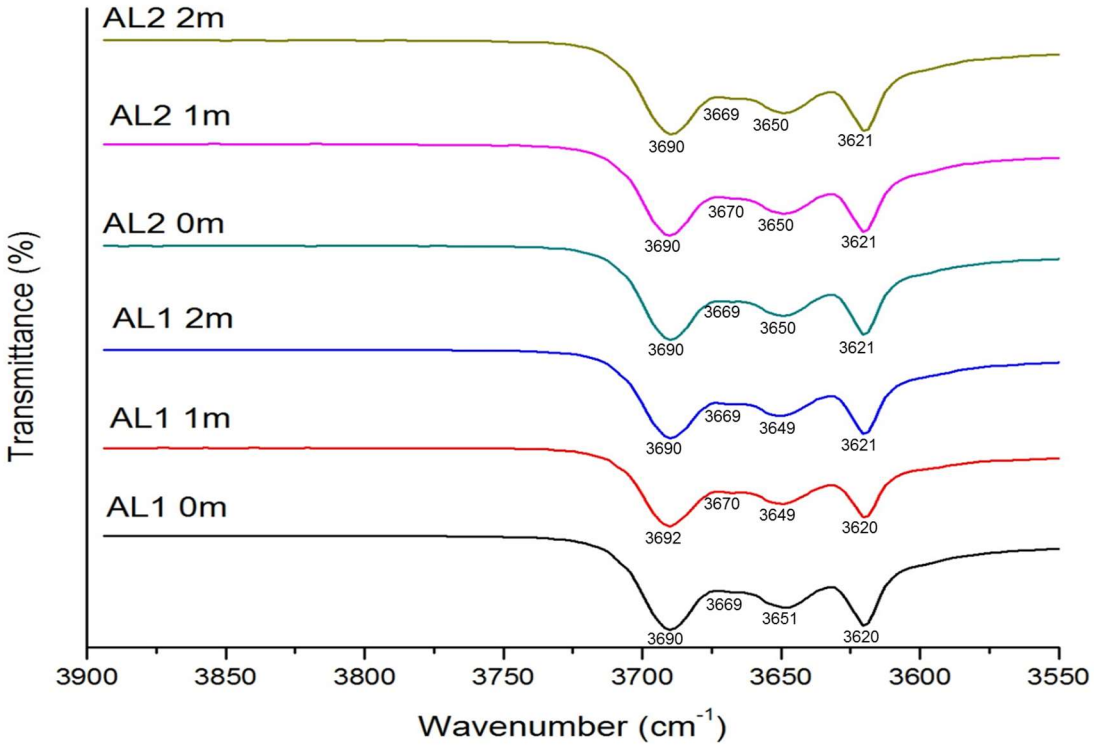

Figure 4.32: The IR spectra of Awo-Omama Kaolin Clay fraction between 3900 to 3550 cm^{-1}.

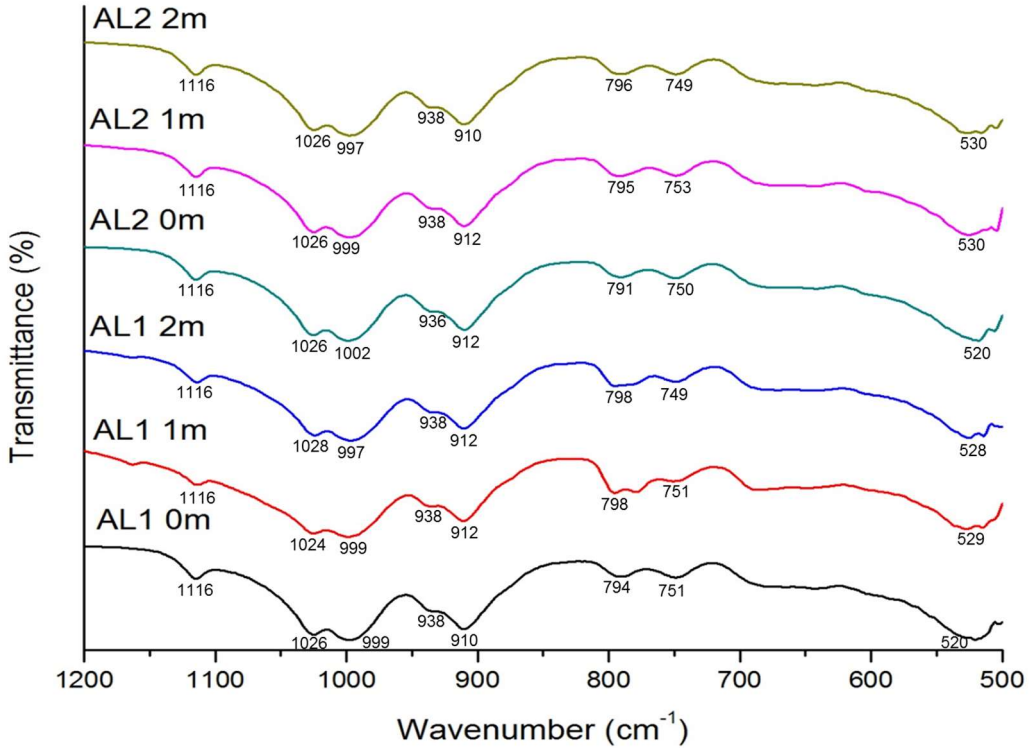

Figure 4.33: The IR spectra of Awo-Omama Kaolin Clay fraction between 1200 to 500 cm^{-1}.

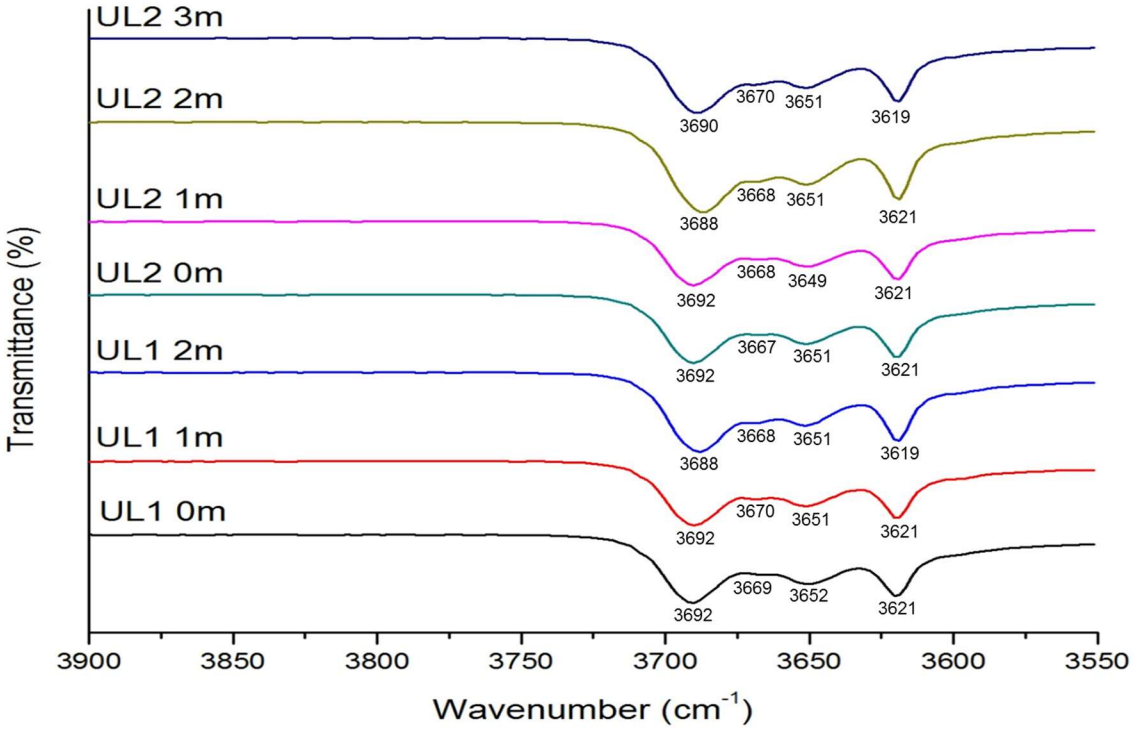

Figure 4.34: The IR spectra of Ubulu-Uku Kaolin Clay fraction between 3900 to 3550 cm^{-1}.

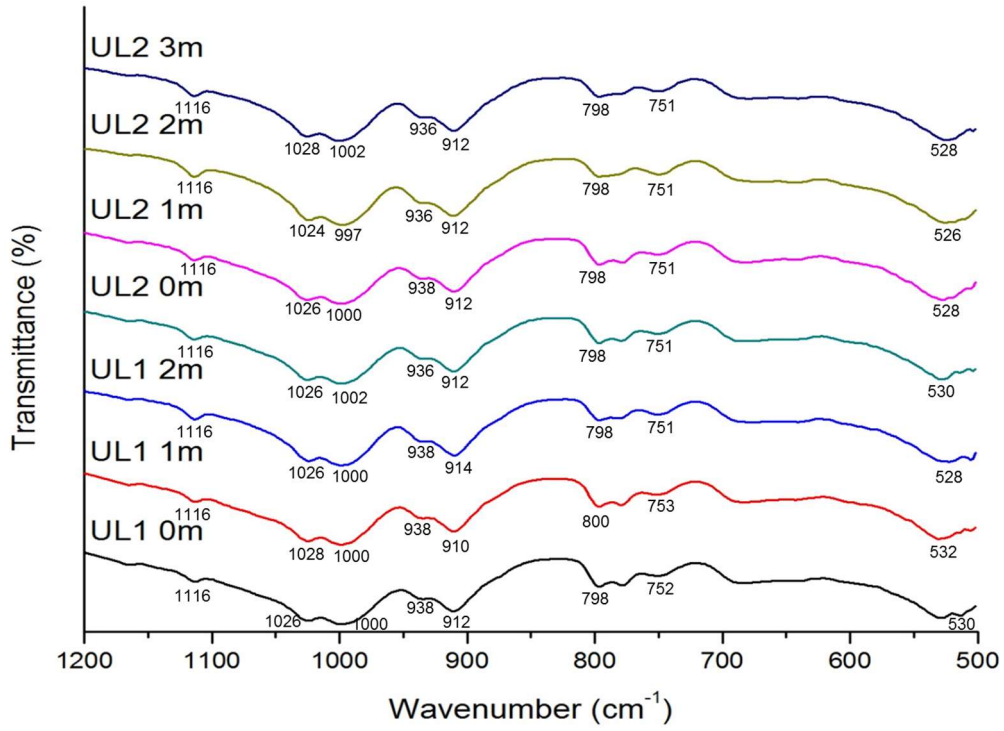

Figure 4.35: The IR spectra of Ubulu-Uku Kaolin Clay fraction between 1200 to 500 cm^{-1}.

Fe-O, Fe_2O_3, Ti-O, Si-O-Al stretching observed at 541 cm^{-1} for KGa kaolinites (Madejova and Komadel, 2001) were identified within regions 522 – 530 cm^{-1} and 520 – 532 cm^{-1} for Cretaceous and Tertiary kaolins respectively.

Characteristic bands at 1114 – 1118 cm^{-1} and 683 – 696 cm^{-1} are indicative of quartz interference in all the samples. Muscovite interference was identified at bands between 1023 – 1028 cm^{-1} whereas the 520 – 532 cm^{-1} were taken to indicate the presence of iron oxides and Ti-O bond vibrations (Gao *et al*., 2003). It therefore means that the IR spectra showed the presence of kaolinite, quartz, muscovite, hematite, goethite, and anatase in the samples, most of which had earlier been identified by XRD in some of the samples.

4.2.3 Thermogravimetric Analyses (TGA) and Differential Scanning Calorimetry (DSC)

The exposure of raw kaolin material to the hot environment in a calciner with increasing temperature is accompanied by a number of reactions (Equations 4.1 – 4.2), including dihydroxylation and phase transformations (Teklay *et al*., 2014).

- Reactions:

Between 450 – 700 ˚C: endothermic: dehydroxylation:

$Al_2Si_2O_5(OH)_4 \rightarrow Al_2O_3.2SiO_2$ (metakaolinite) + H_2O (4.1)

Between 900 – 1000 ˚C: exothermic: transformation into crystalline phases:

$Al_2O_3.2SiO_2 \rightarrow 2Al_2O_3.3SiO_2$ (primary mullite or pseudomullite: Si-Al spinel with mullite - like composition) + amorphous SiO_2 (4.2)

However, dehydration occurs at temperature (T) < 100 ˚C due to the presence of free bound water (Teklay *et al*., 2014) and pre-dehydroxylation at T between 200 ˚C and 450 ˚C (Ilic *et al*., 2010). The TGA-DSC characteristic patterns and data for the studied Cretaceous – Tertiary kaolins are presented in Figures 4.36 – 4.63 and Table 4.6.

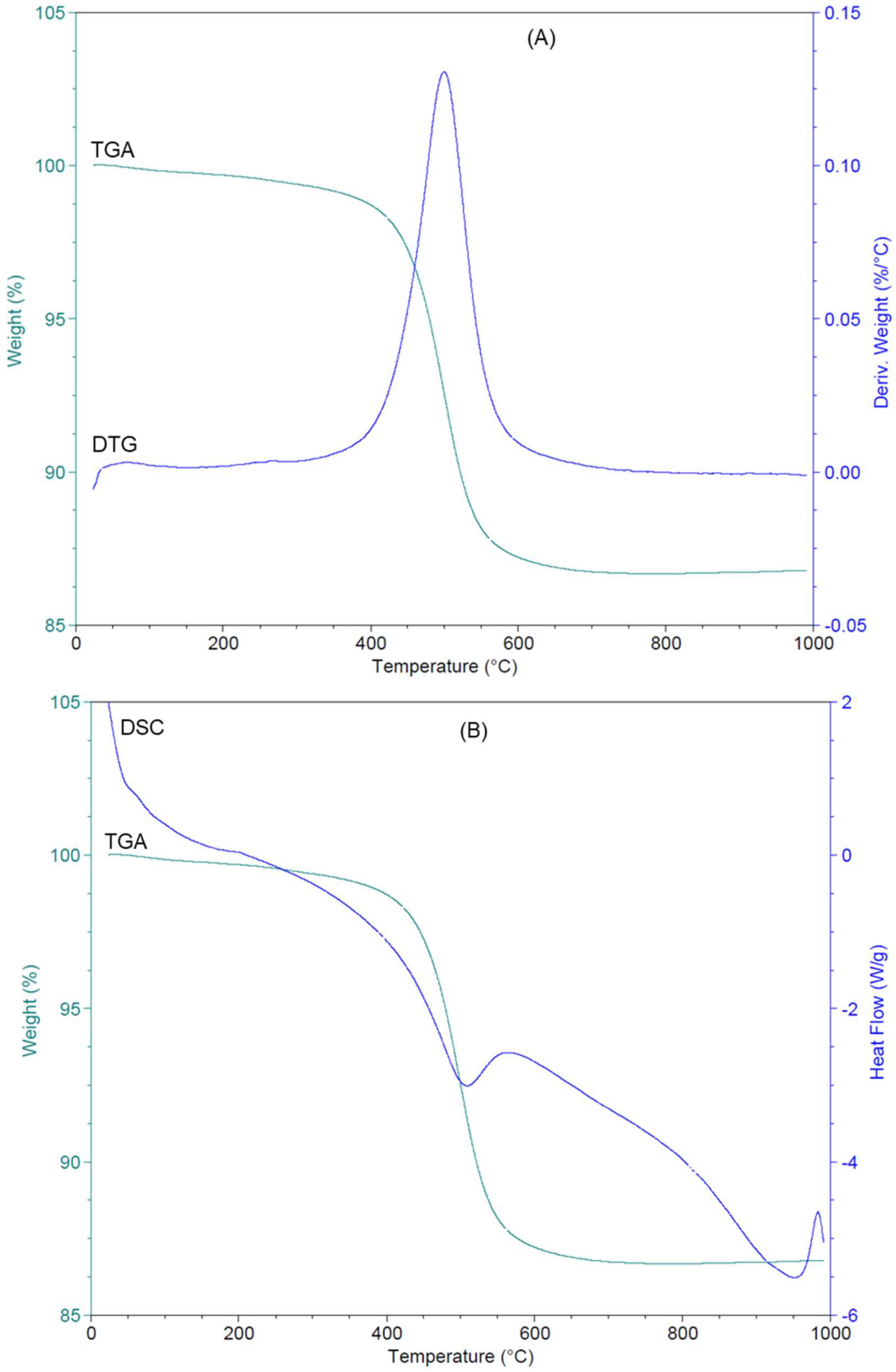

Figure 4.36: Thermal analyses of EP1 0m showing: (a) TGA/DTG and (b) DSC/TGA curves.

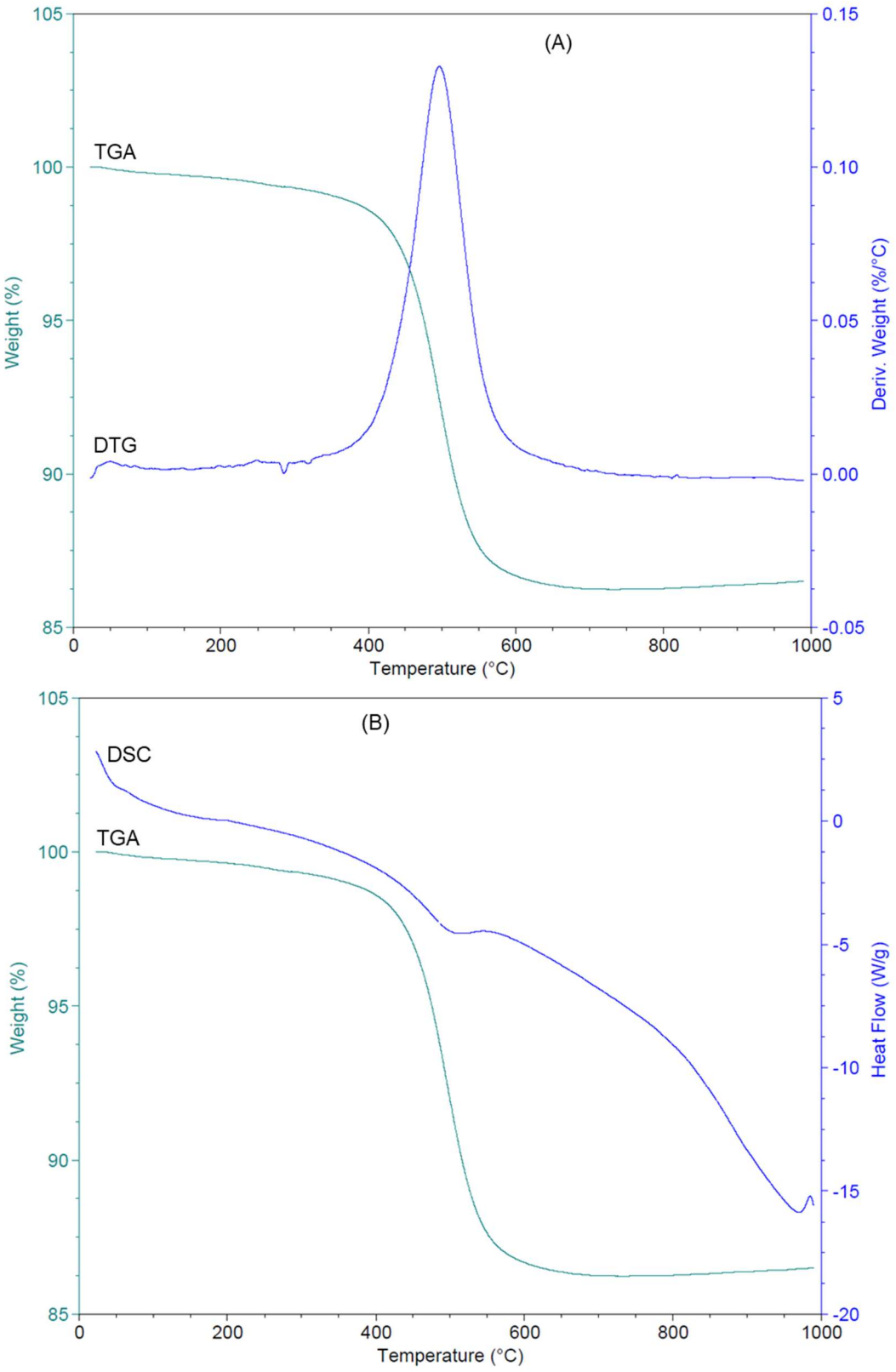

Figure 4.37: Thermal analyses of EP1 2m showing: (a) TGA/DTG and (b) DSC/TGA curves.

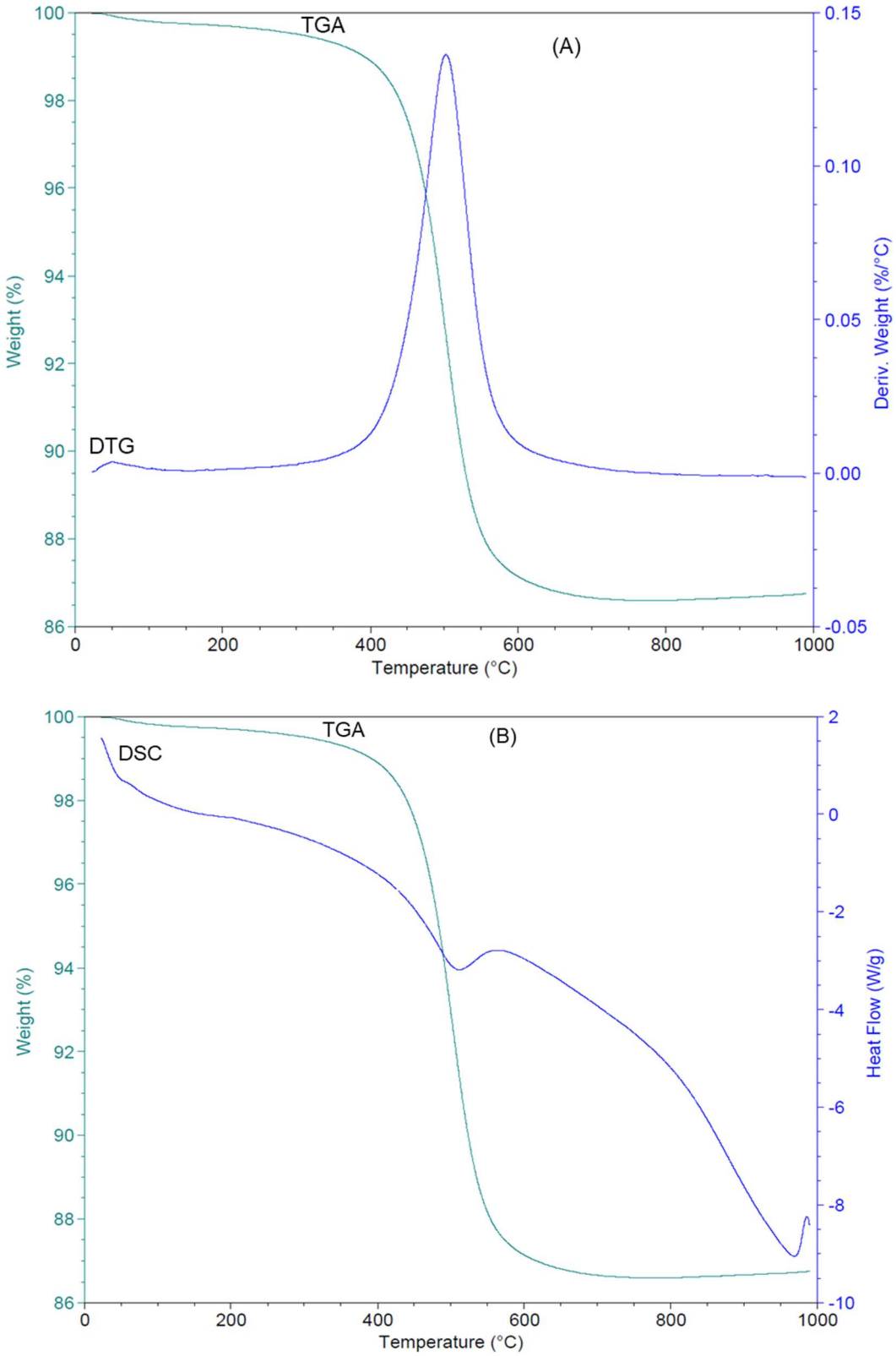

Figure 4.38: Thermal analyses of EP1 4m showing: (a) TGA/DTG and (b) DSC/TGA curves.

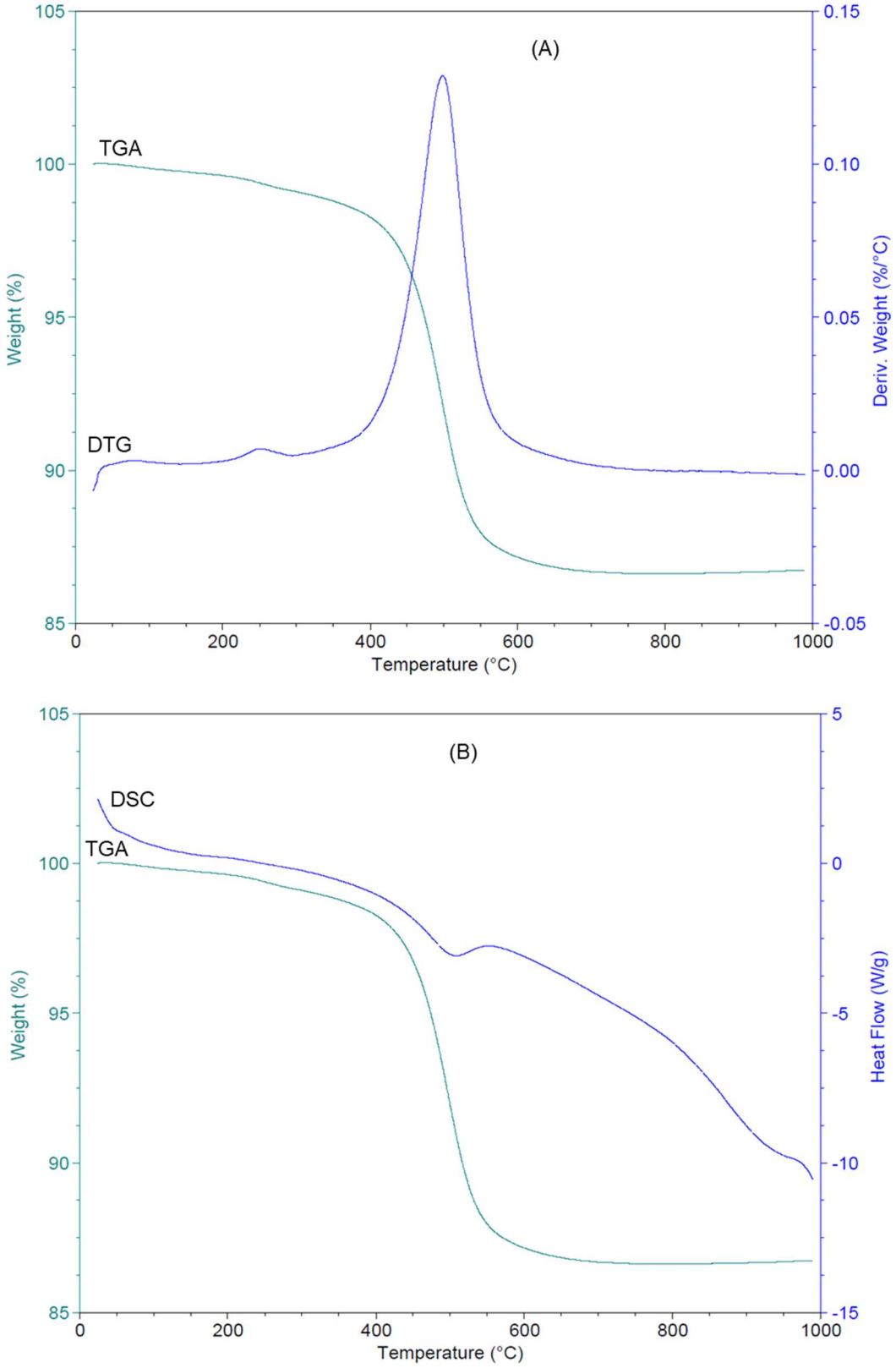

Figure 4.39: Thermal analyses of EP2 0m showing: (a) TGA/DTG and (b) DSC/TGA curves.

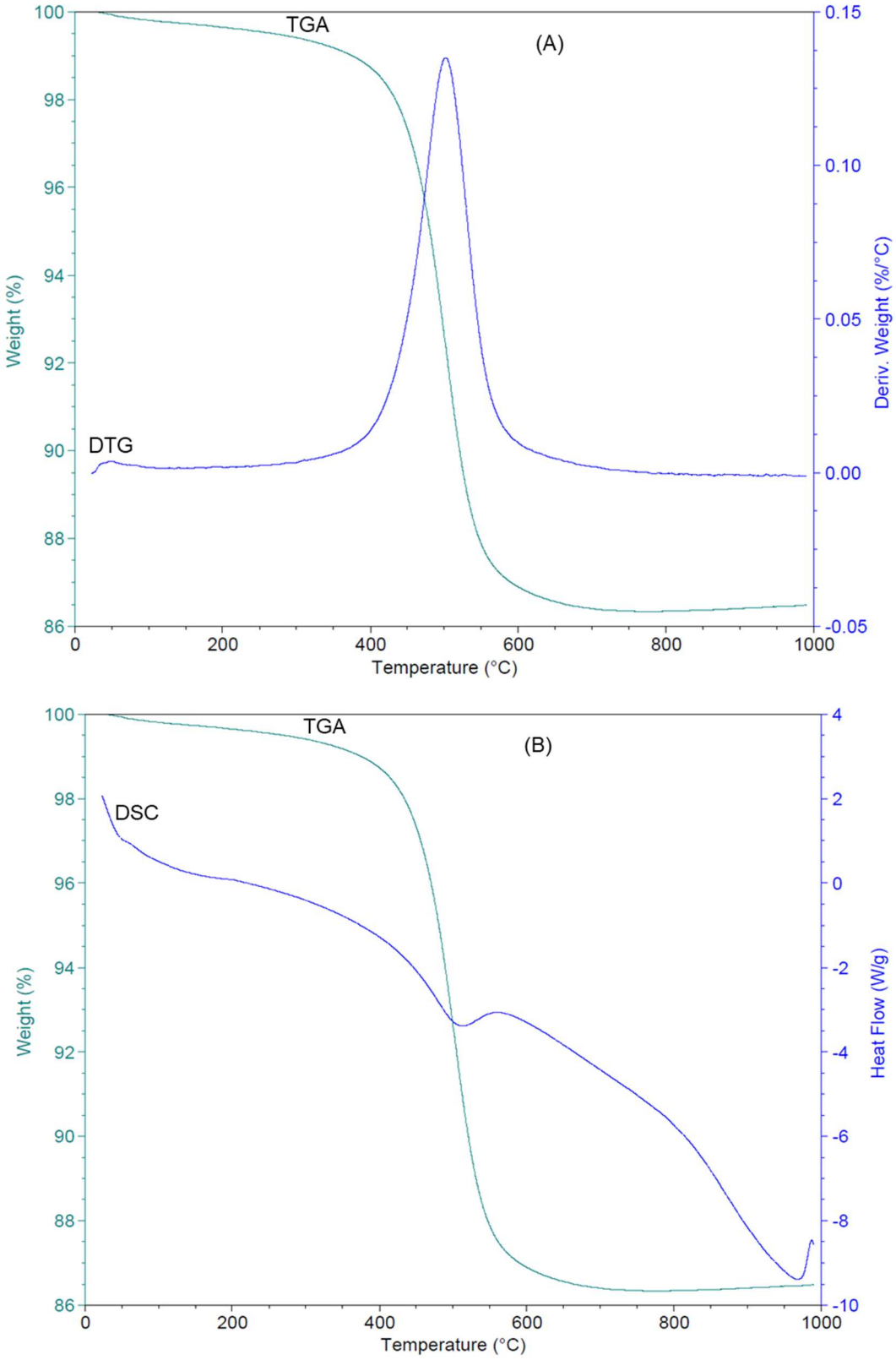

Figure 4.40: Thermal analyses of EP2 2m showing: (a) TGA/DTG and (b) DSC/TGA curves.

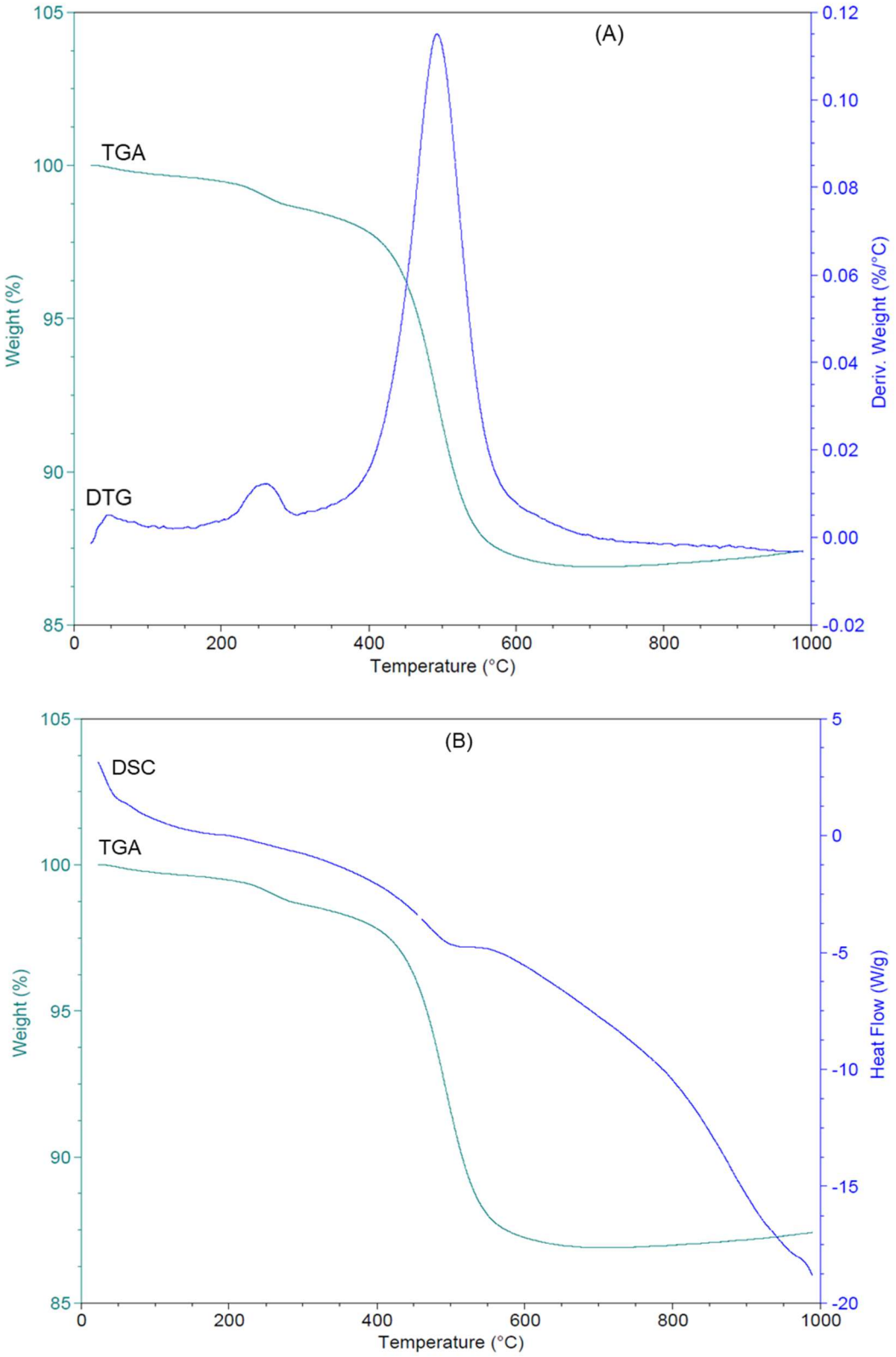

Figure 4.41: Thermal analyses of EP2 4m showing: (a) TGA/DTG and (b) DSC/TGA curves.

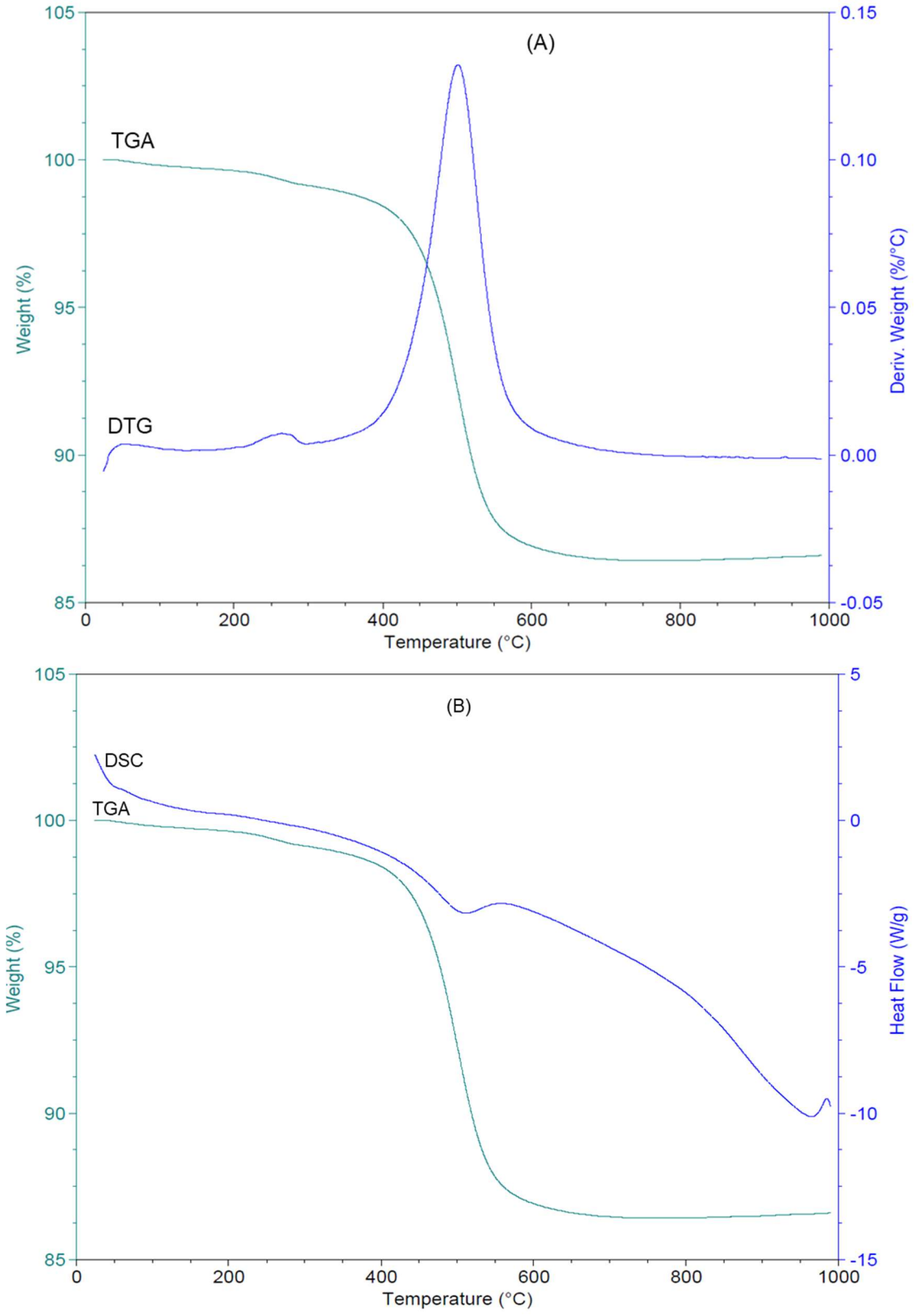

Figure 4.42: Thermal analyses of EP3 0m showing: (a) TGA/DTG and (b) DSC/TGA curves.

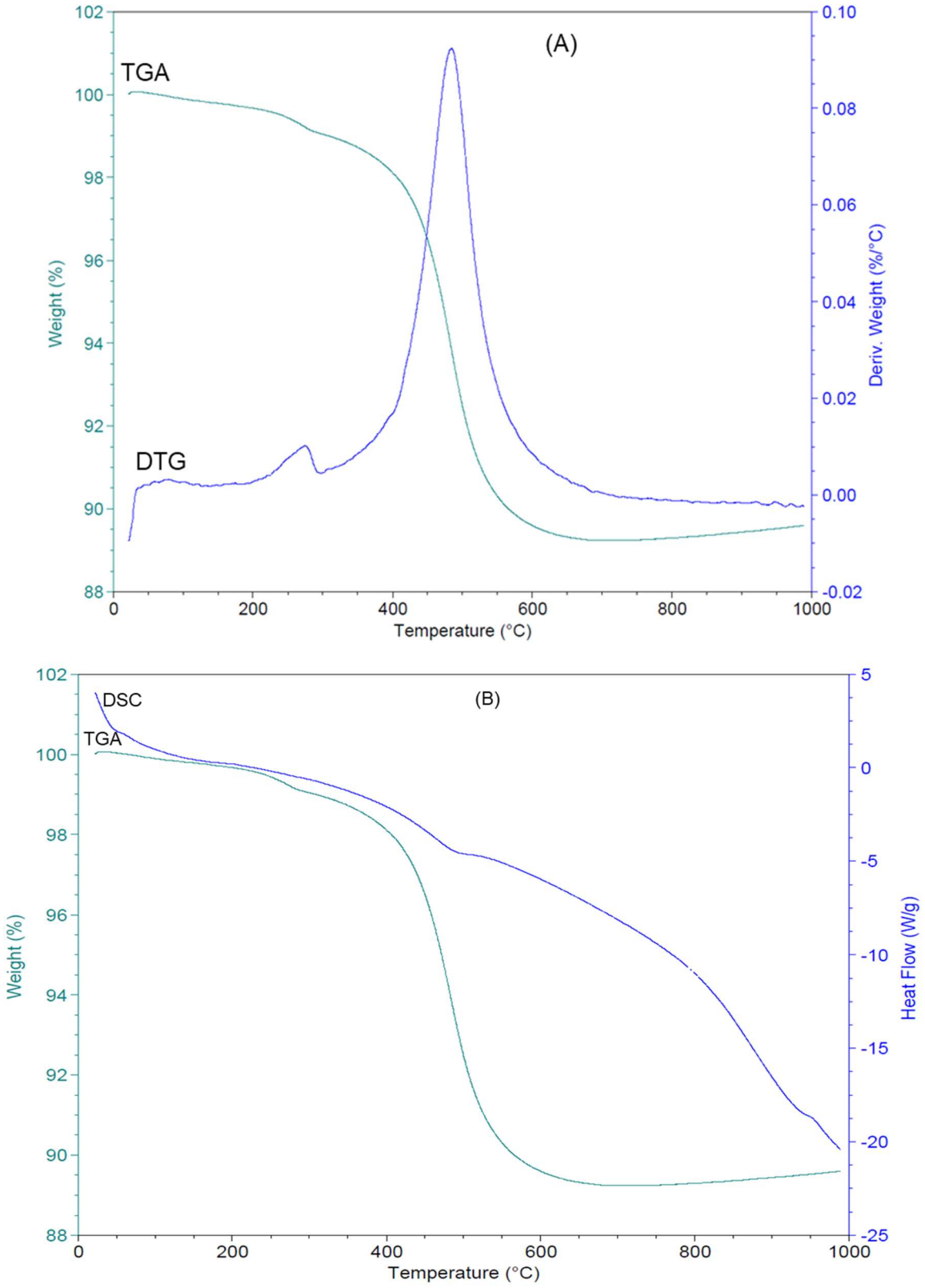

Figure 4.43: Thermal analyses of EP3 2m showing: (a) TGA/DTG and (b) DSC/TGA curves.

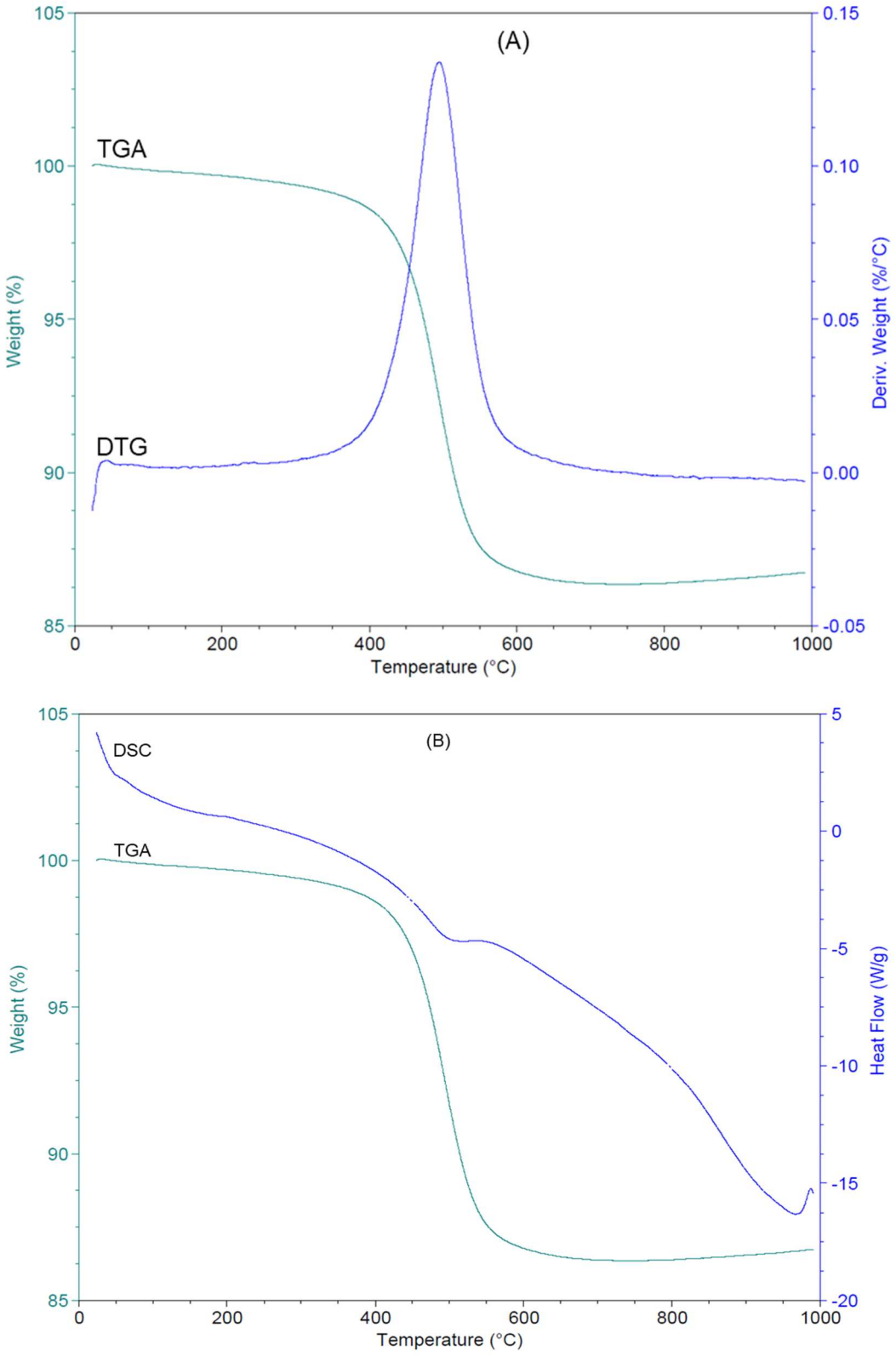

Figure 4.44: Thermal analyses of EP3 4m showing: (a) TGA/DTG and (b) DSC/TGA curves.

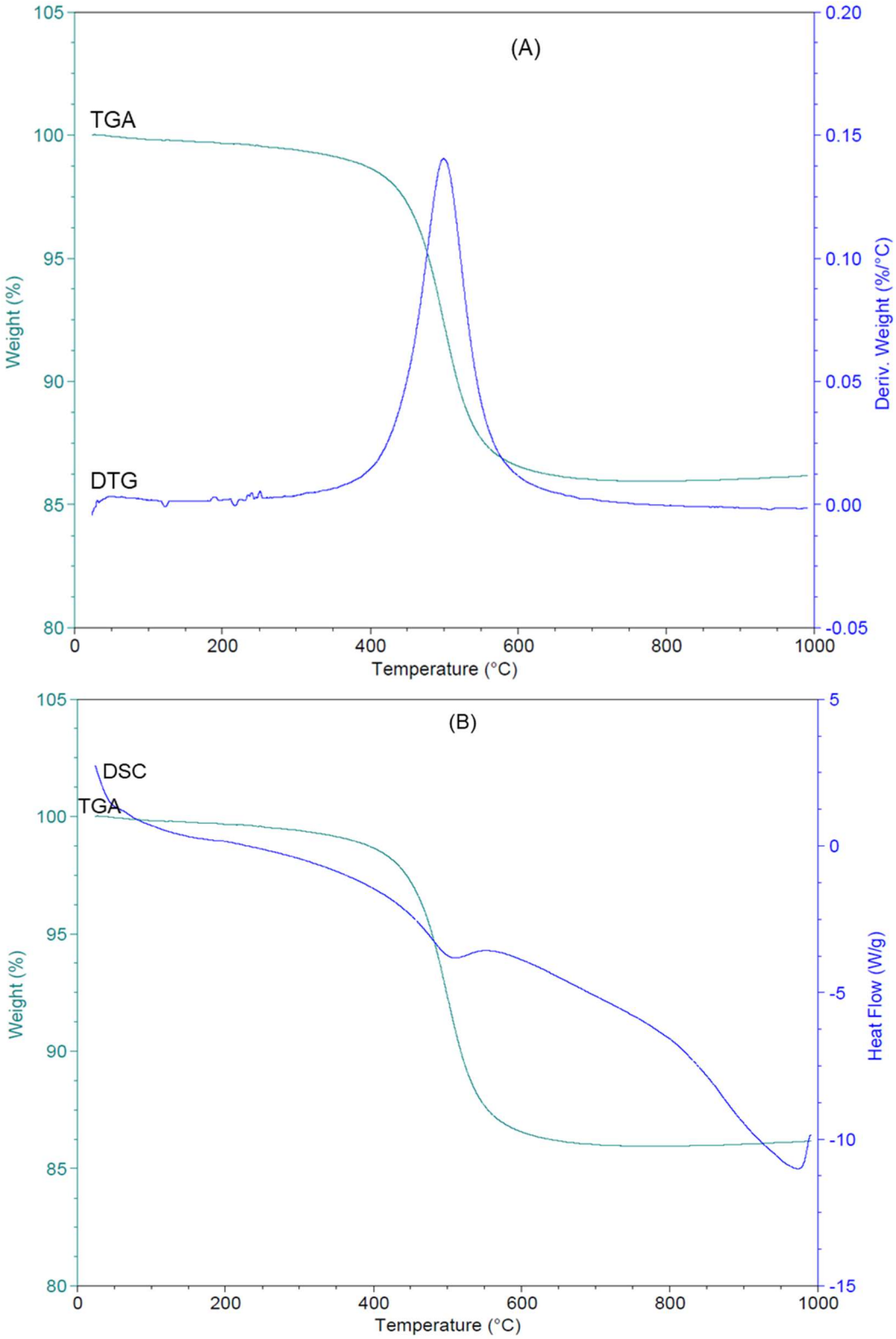

Figure 4.45: Thermal analyses of LP1 0m showing: (a) TGA/DTG and (b) DSC/TGA curves.

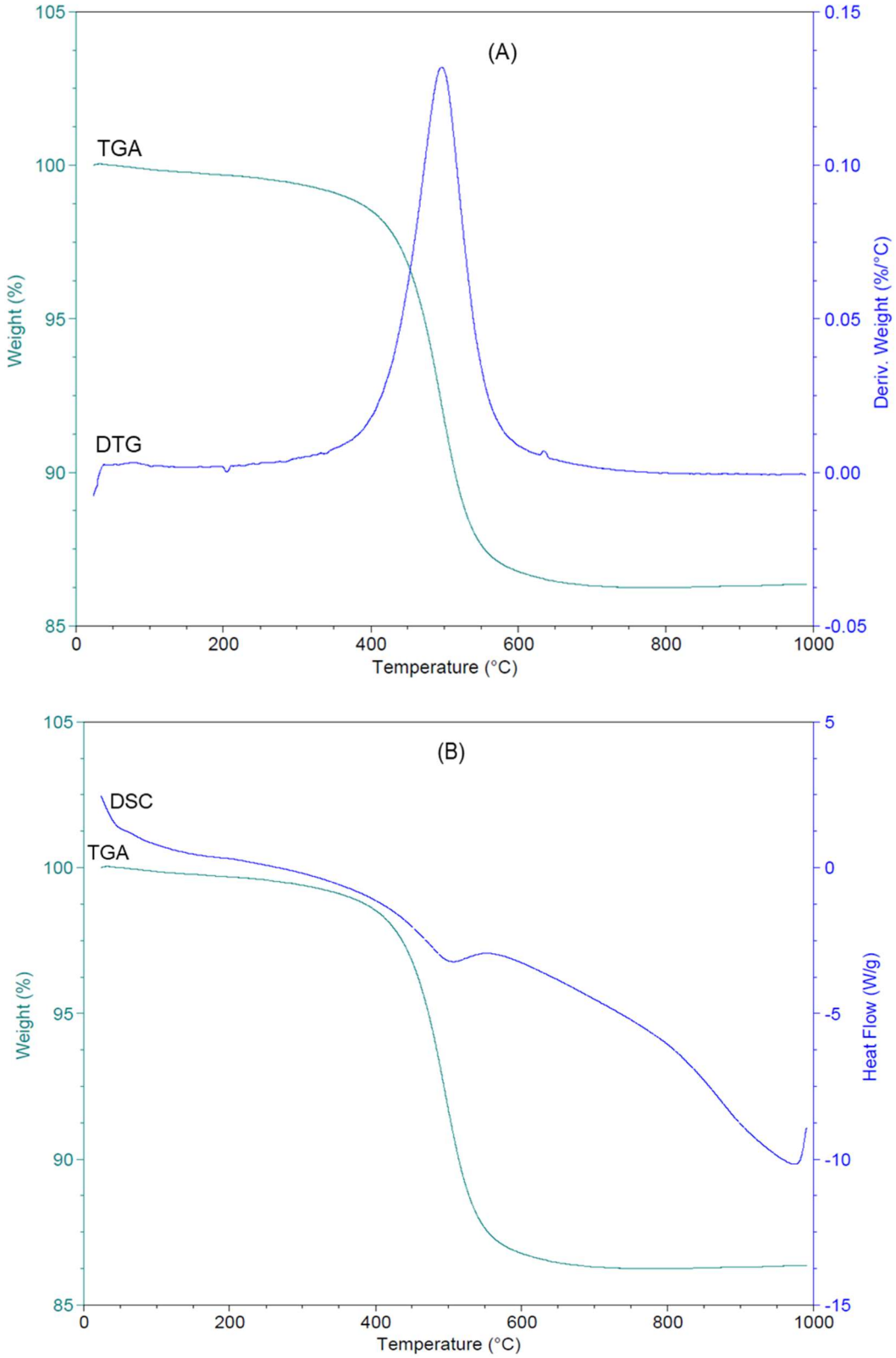

Figure 4.46: Thermal analyses of LP1 2m showing: (a) TGA/DTG and (b) DSC/TGA curves.

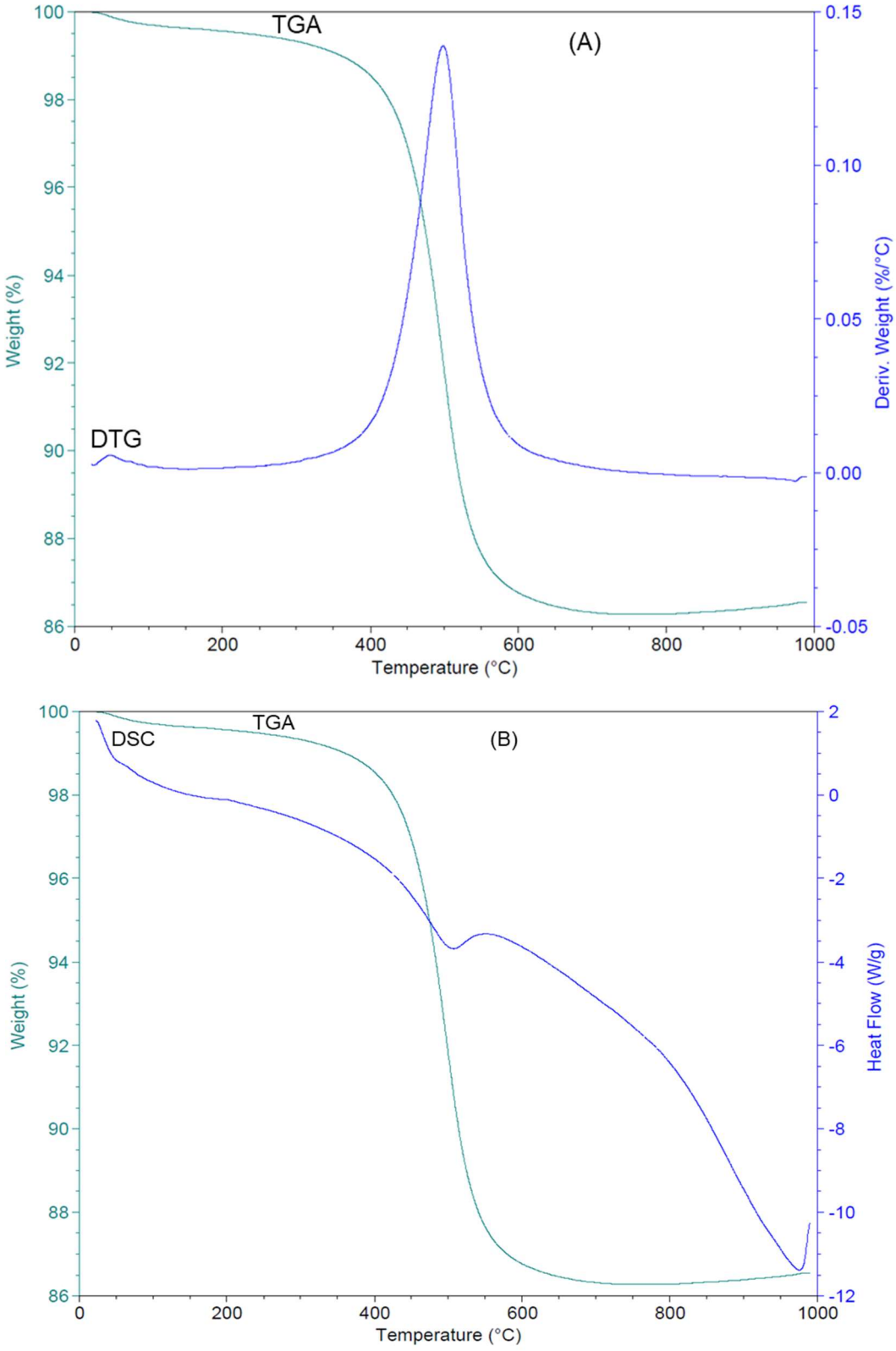

Figure 4.47: Thermal analyses of LP1 4m showing: (a) TGA/DTG and (b) DSC/TGA curves.

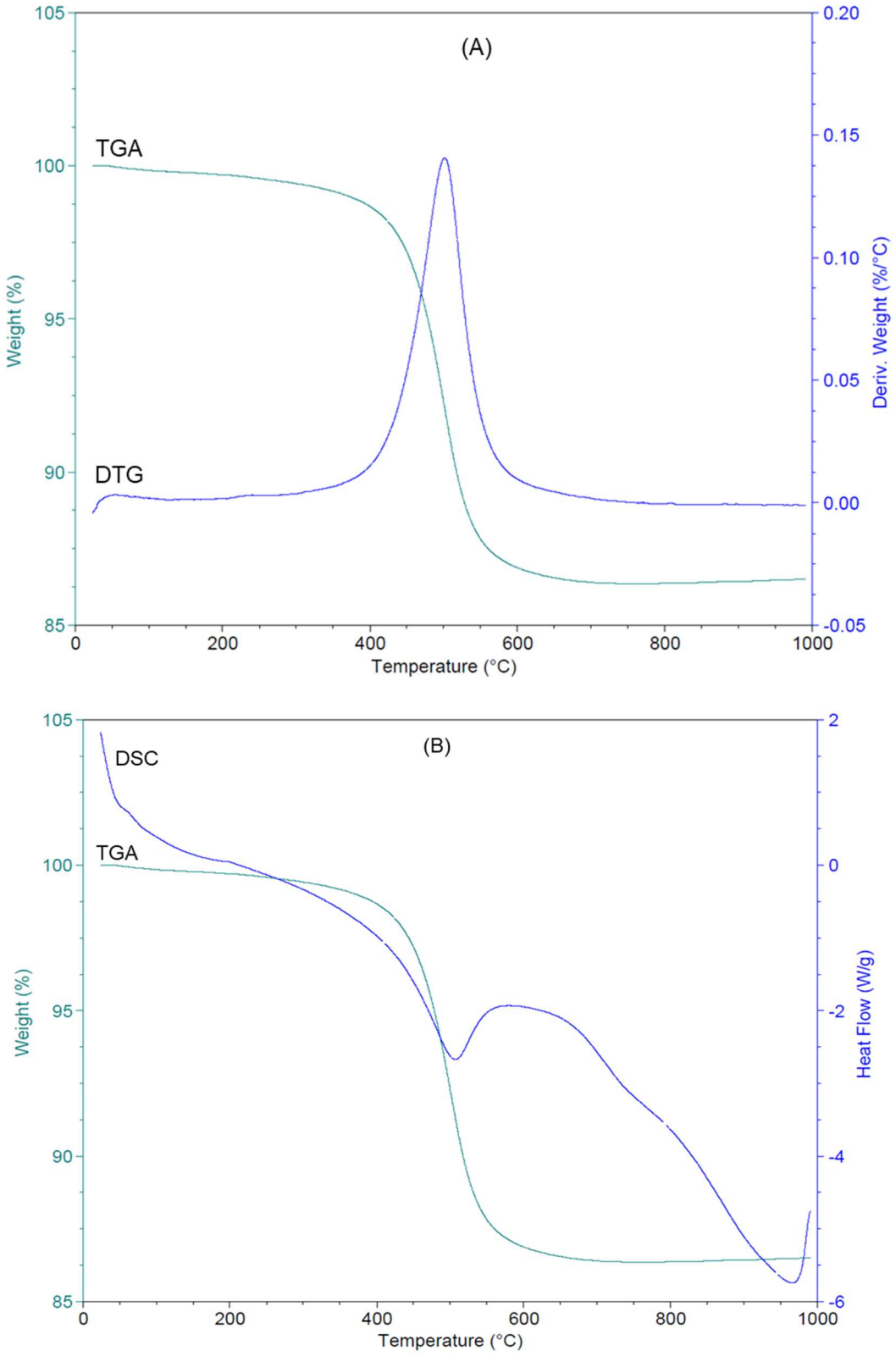

Figure 4.48: Thermal analyses of LP2 0m showing: (a) TGA/DTG and (b) DSC/TGA curves.

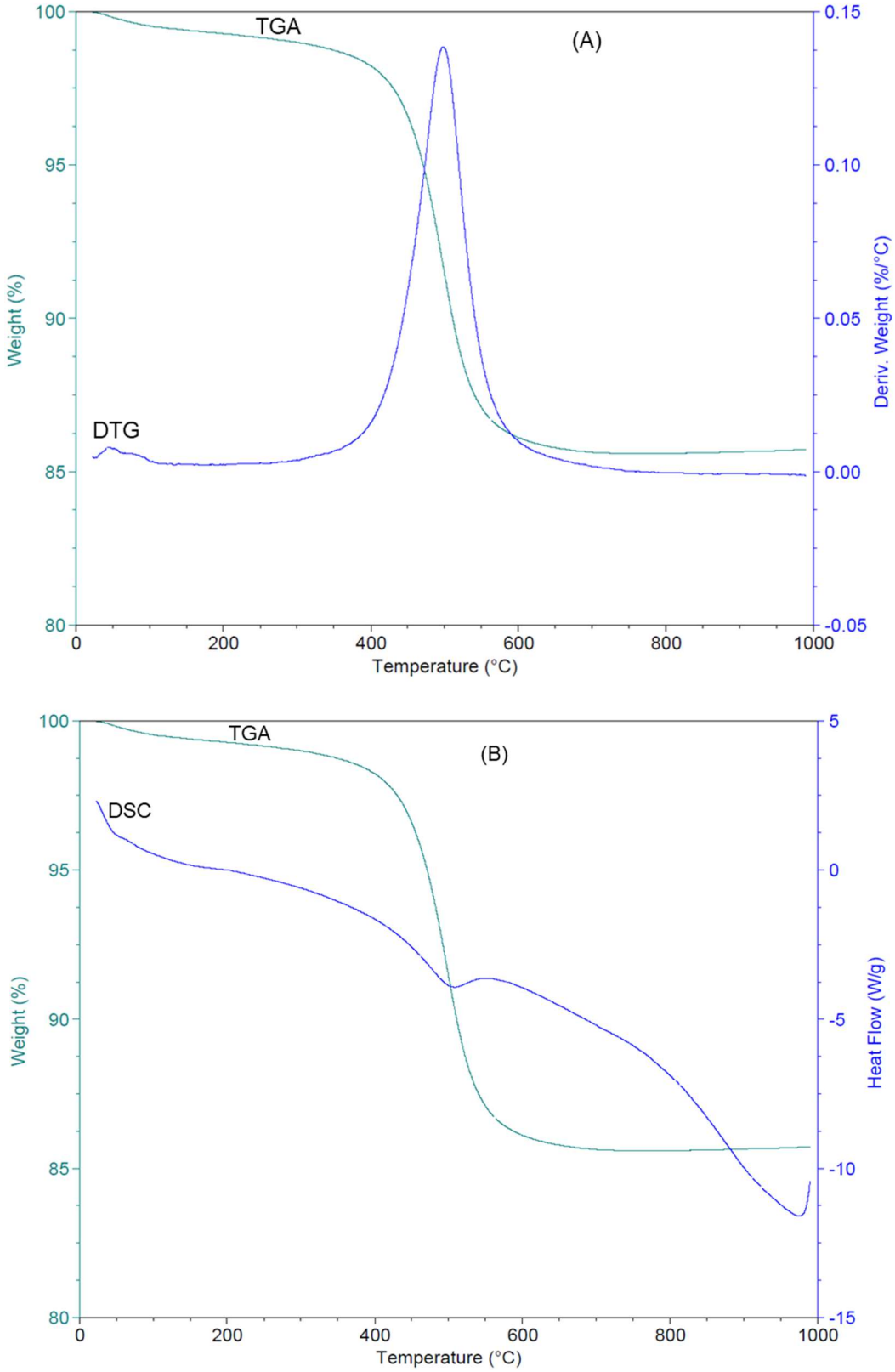

Figure 4.49: Thermal analyses of LP2 2m showing: (a) TGA/DTG and (b) DSC/TGA curves.

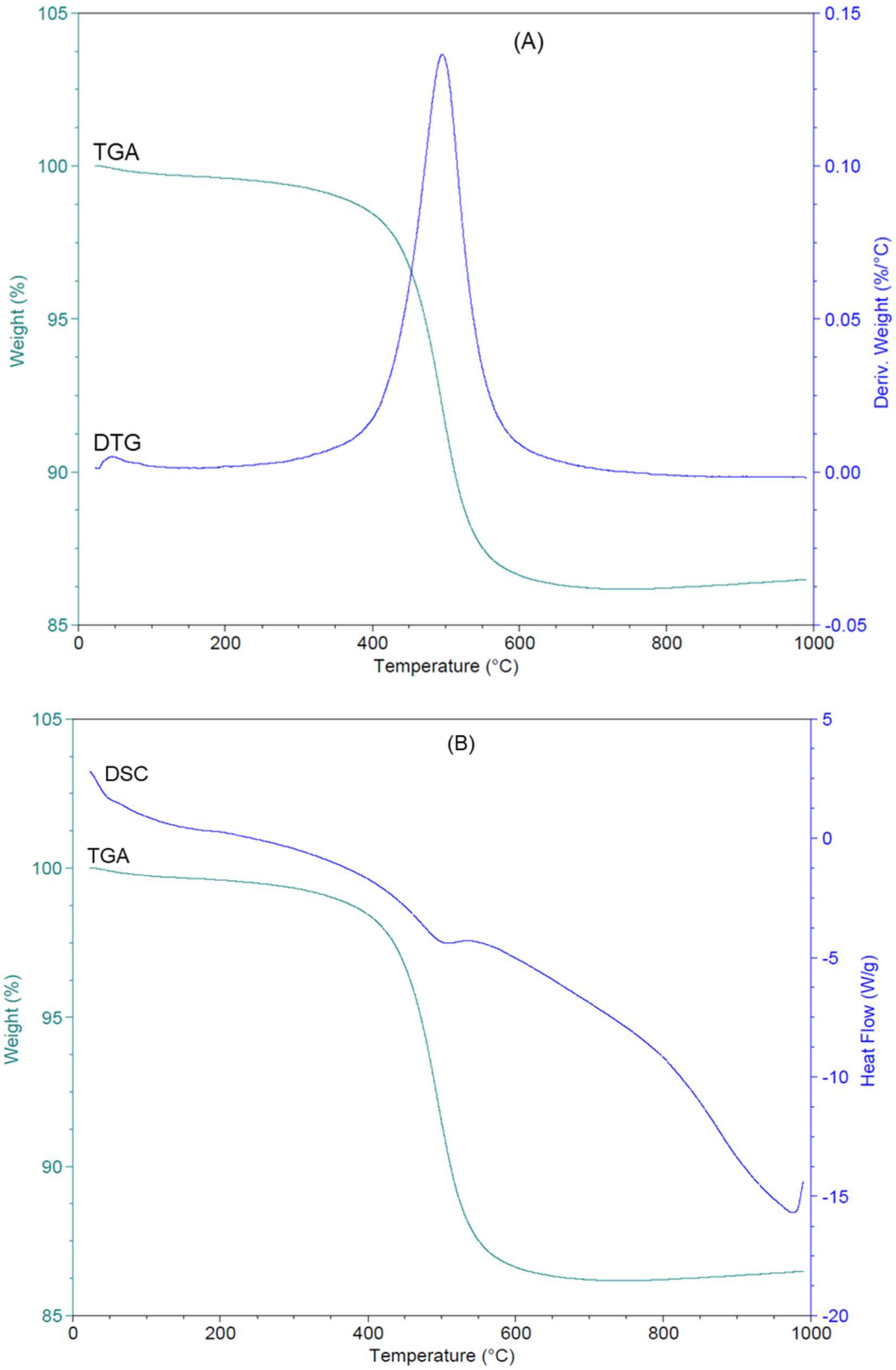

Figure 4.50: Thermal analyses of LP2 4m showing: (a) TGA/DTG and (b) DSC/TGA curves.

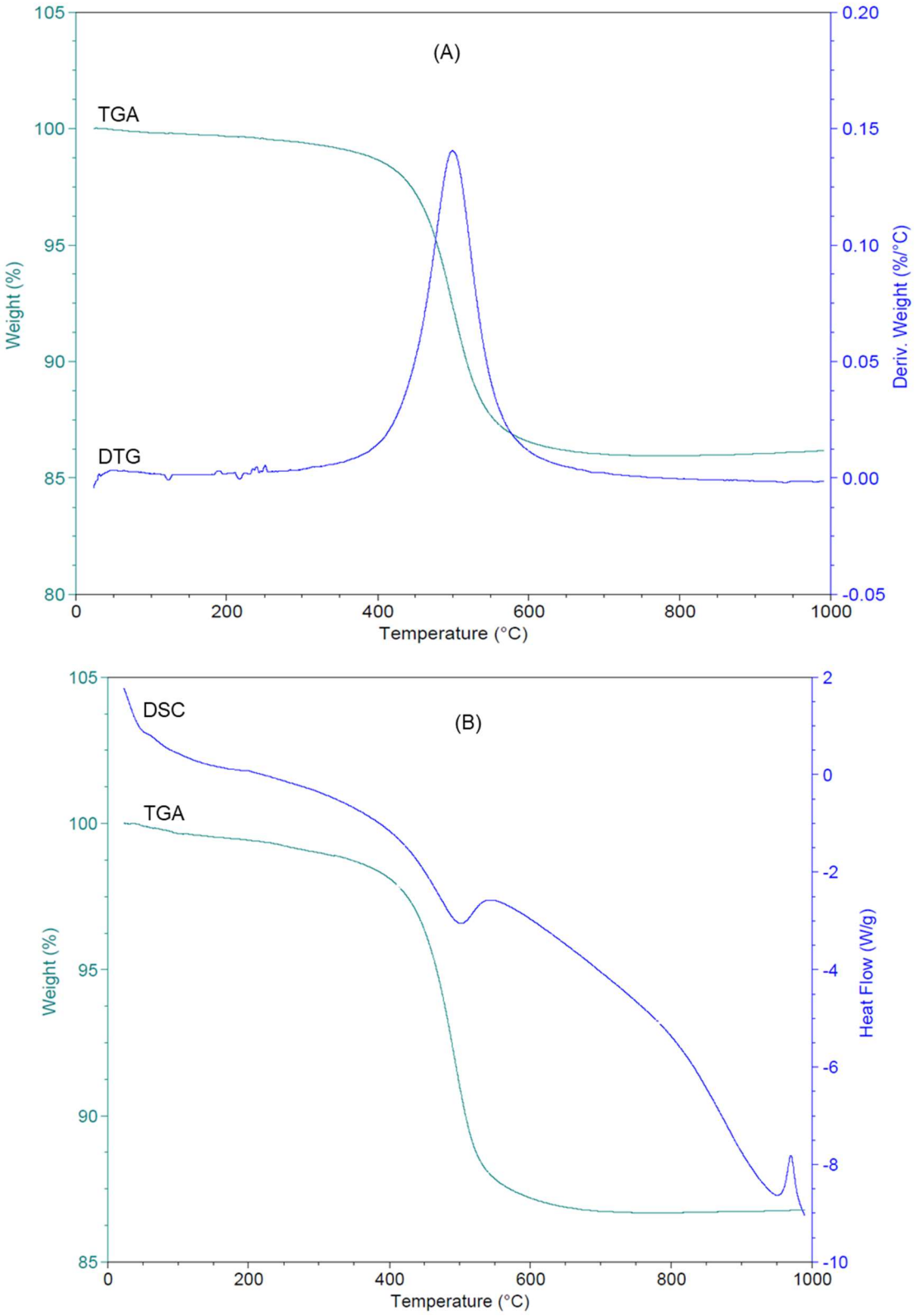

Figure 4.51: Thermal analyses of AL1 0m showing: (a) TGA/DTG and (b) DSC/TGA curves.

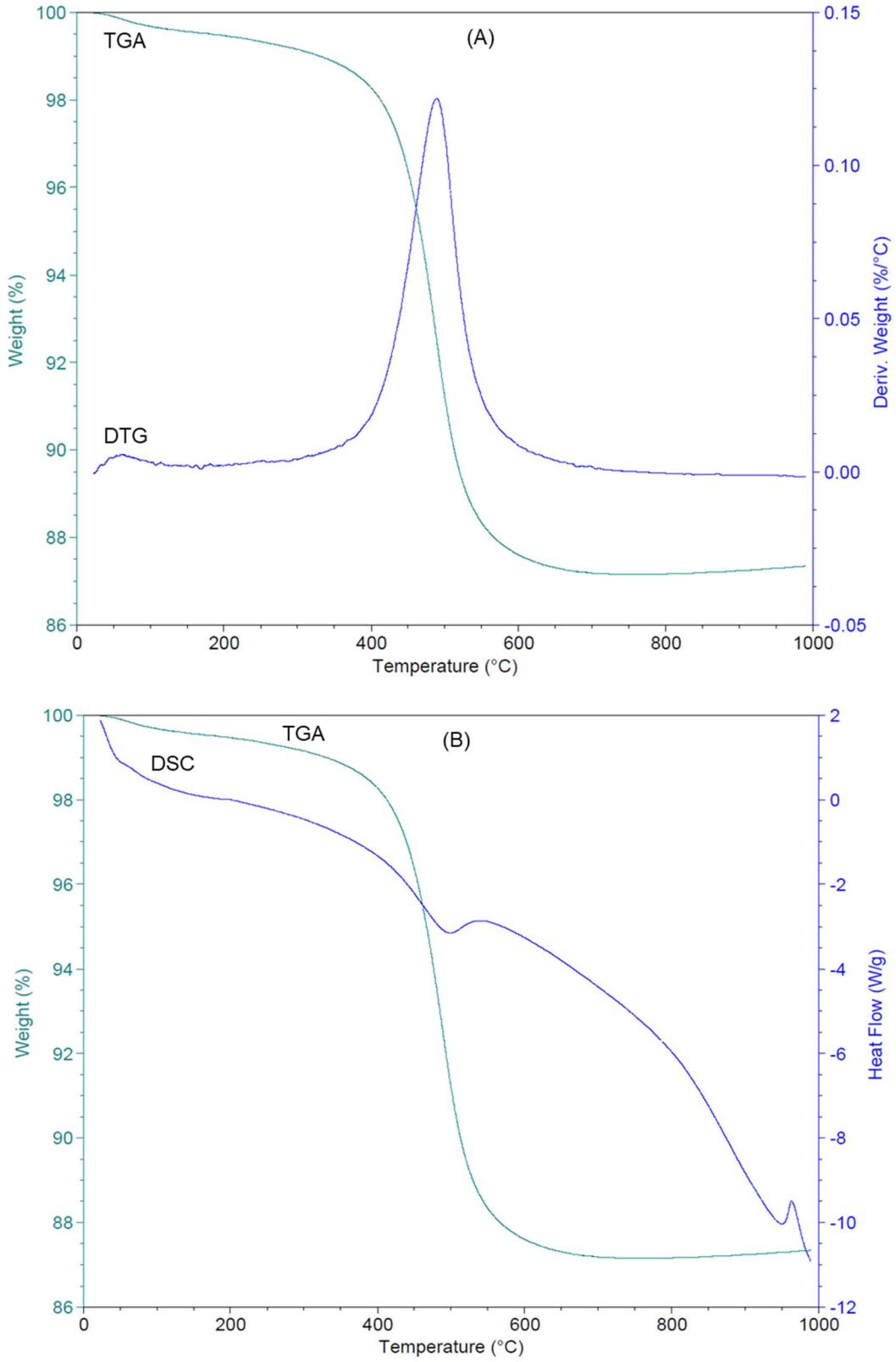

Figure 4.52: Thermal analyses of AL1 1m showing: (a) TGA/DTG and (b) DSC/TGA curves.

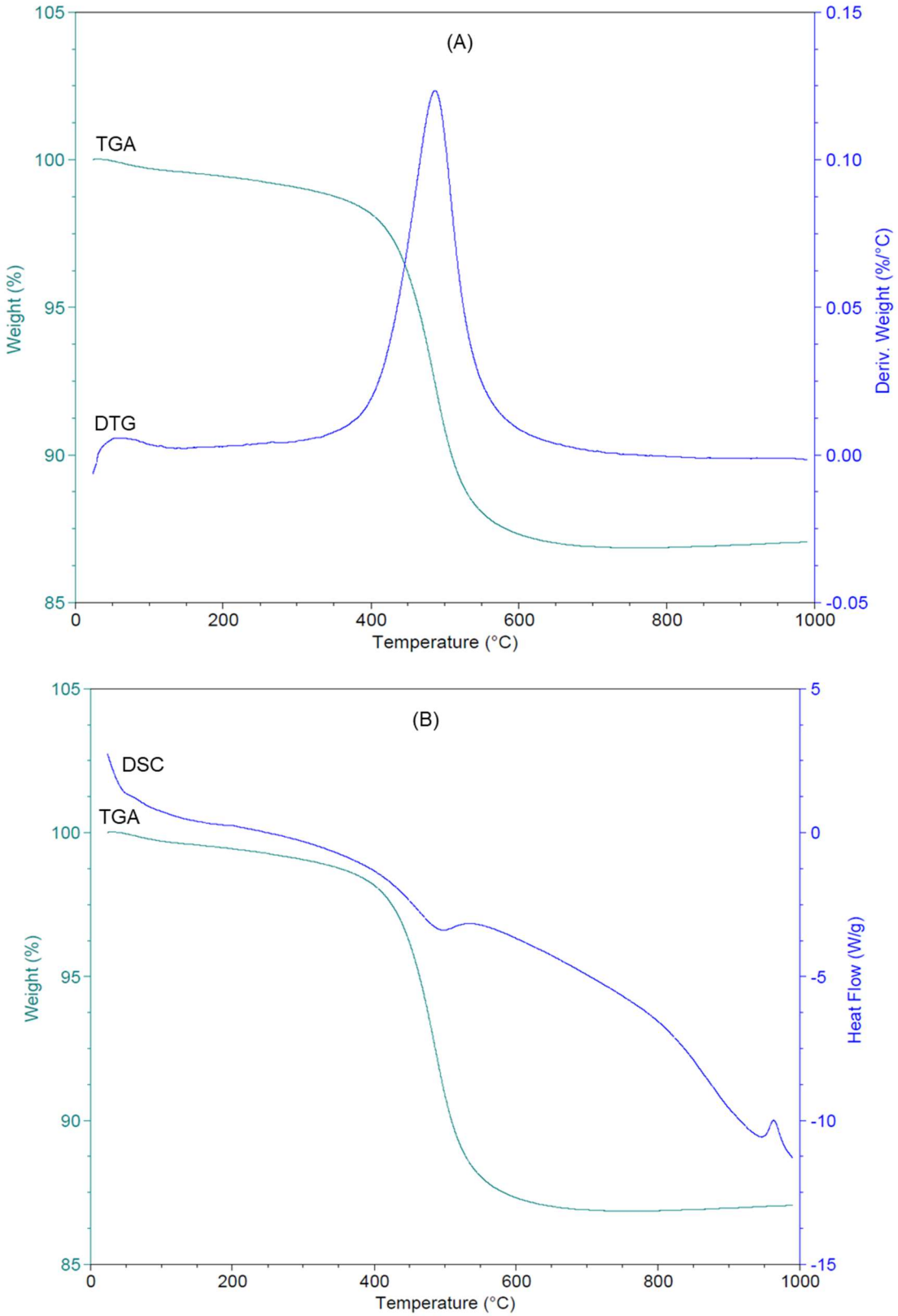

Figure 4.53: Thermal analyses of AL1 2m showing: (a) TGA/DTG and (b) DSC/TGA curves.

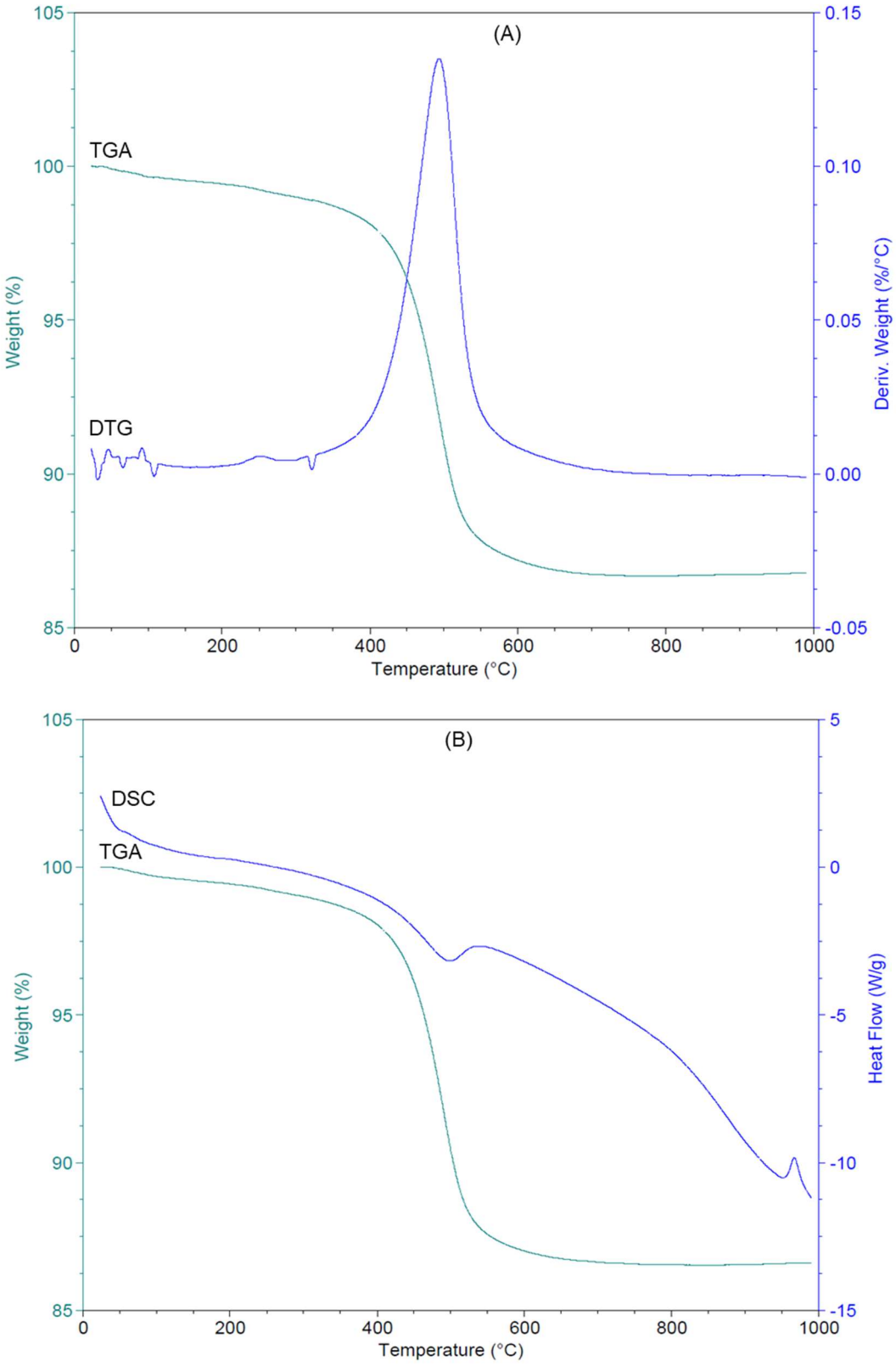

Figure 4.54: Thermal analyses of AL2 0m showing: (a) TGA/DTG and (b) DSC/TGA curves.

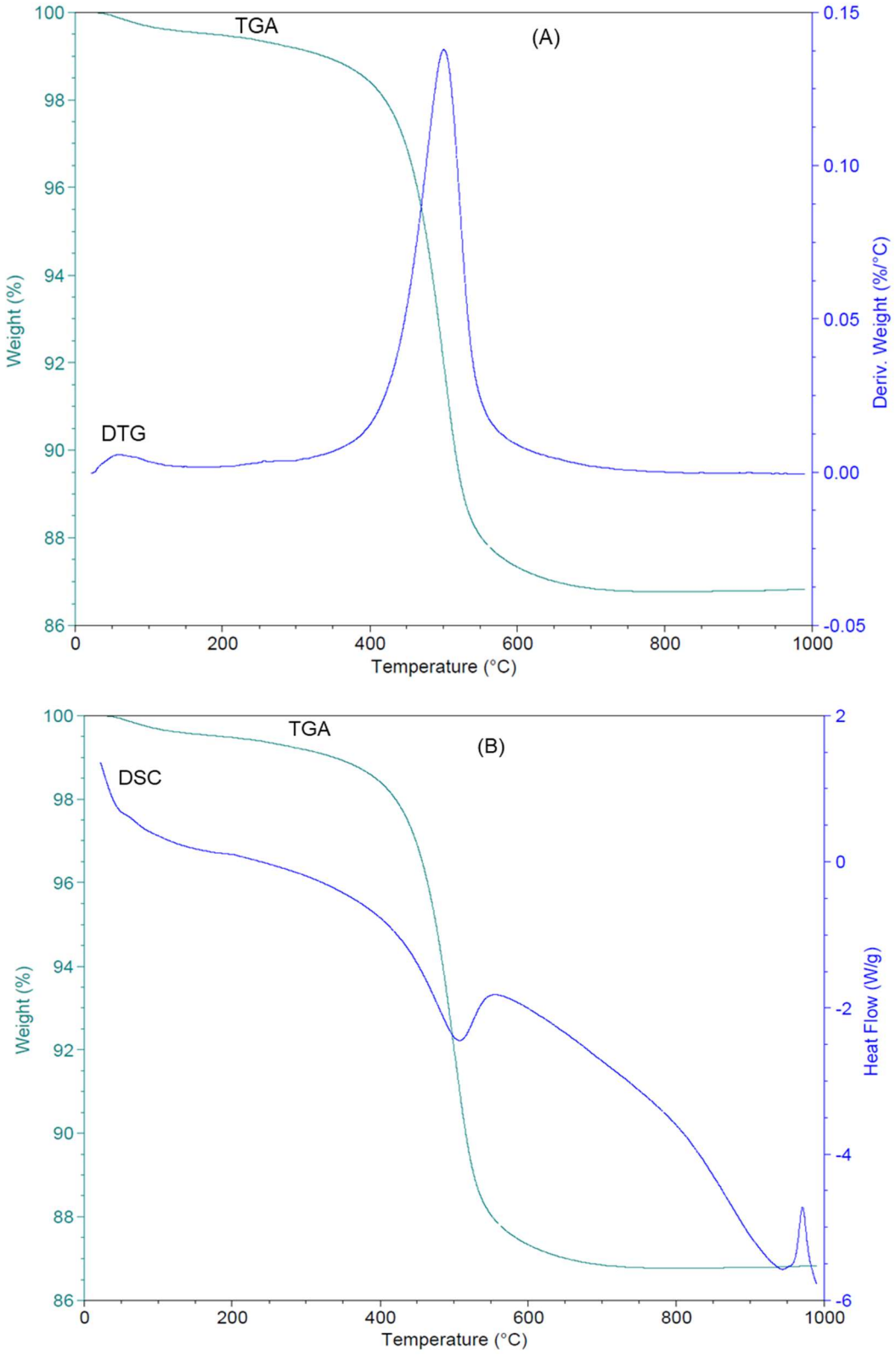

Figure 4.55: Thermal analyses of AL2 1m showing: (a) TGA/DTG and (b) DSC/TGA curves.

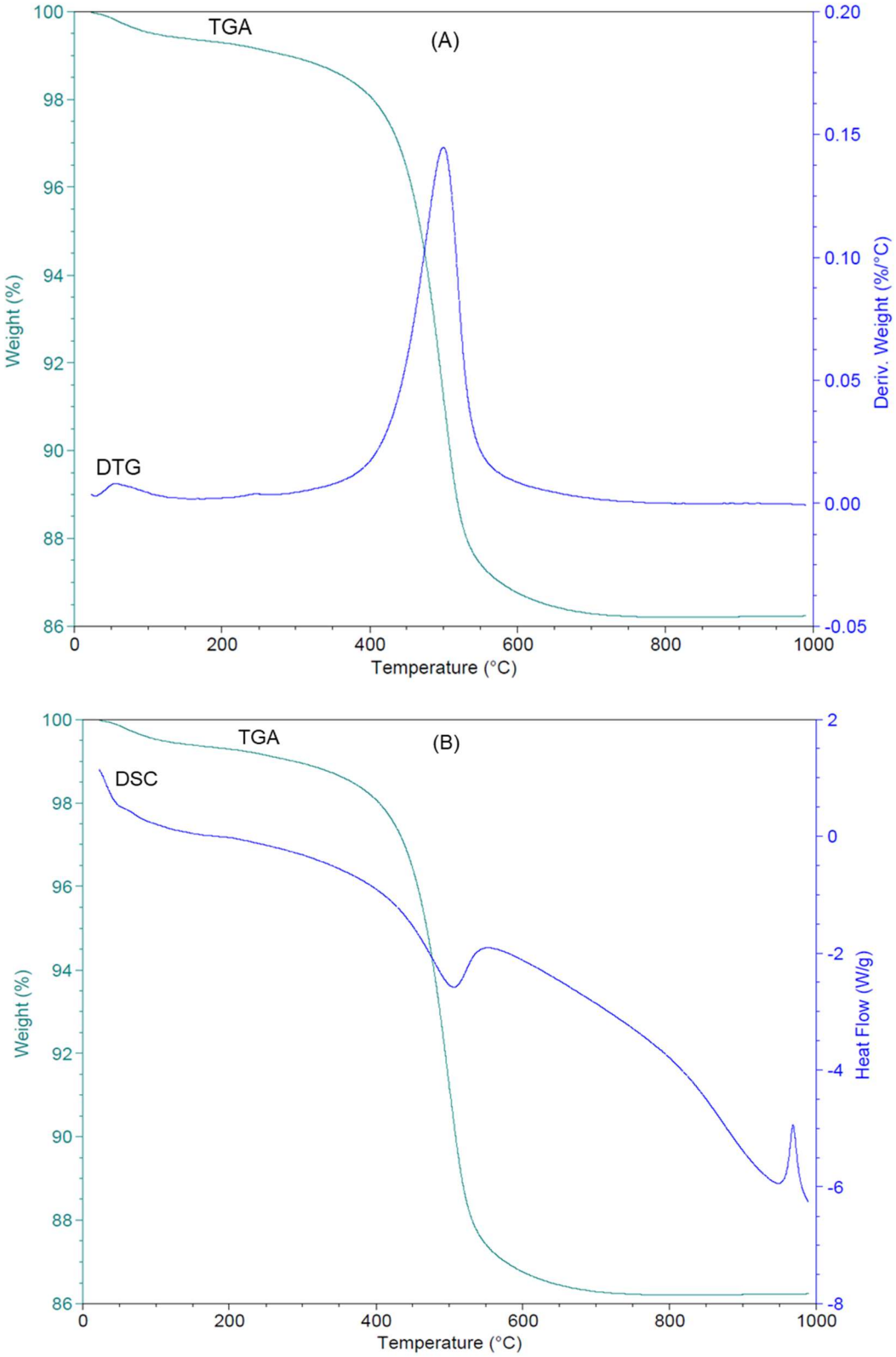

Figure 4.56: Thermal analyses of AL2 2m showing: (a) TGA/DTG and (b) DSC/TGA curves.

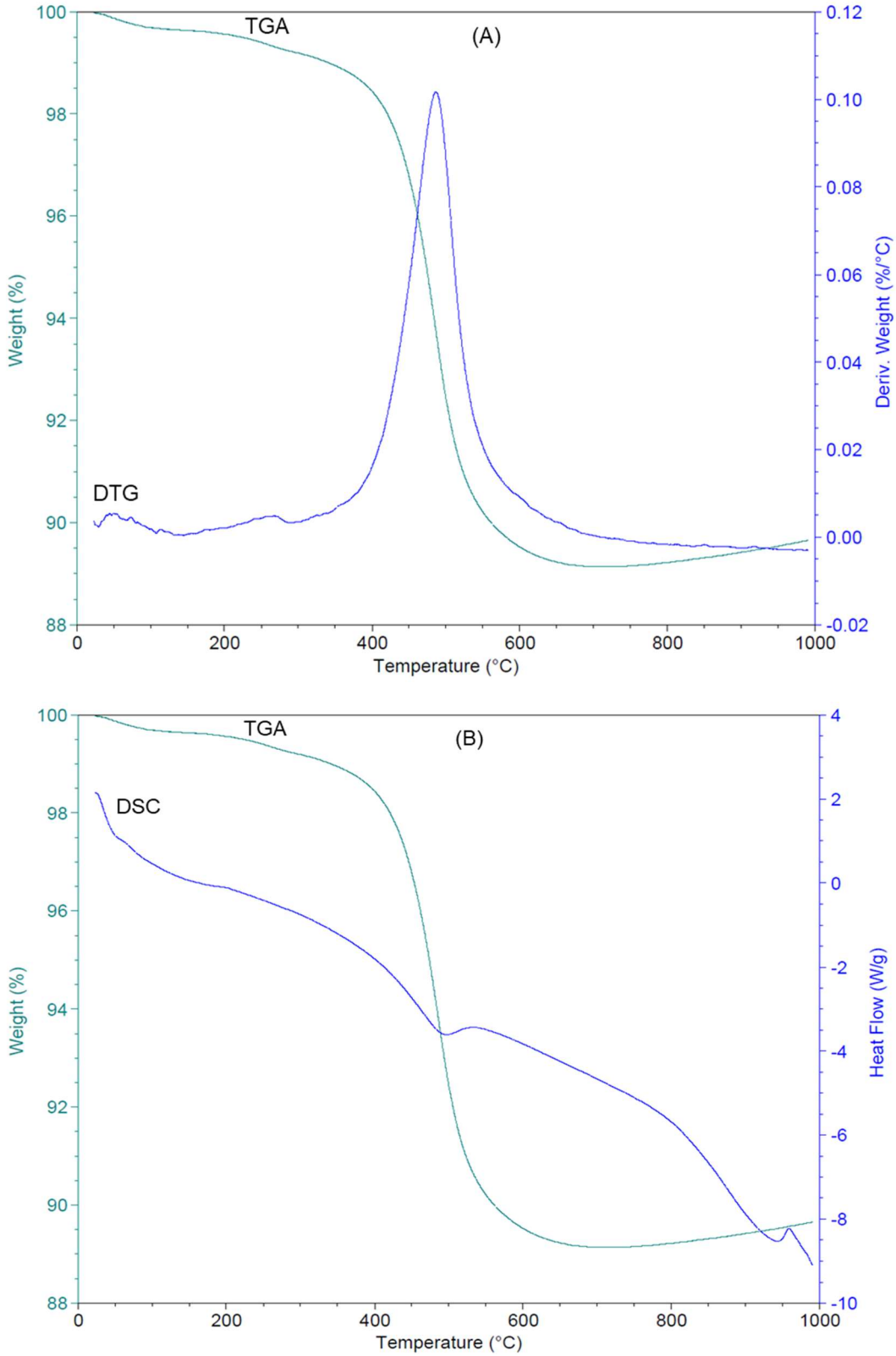

Figure 4.57: Thermal analyses of UL1 0m showing: (a) TGA/DTG and (b) DSC/TGA curves.

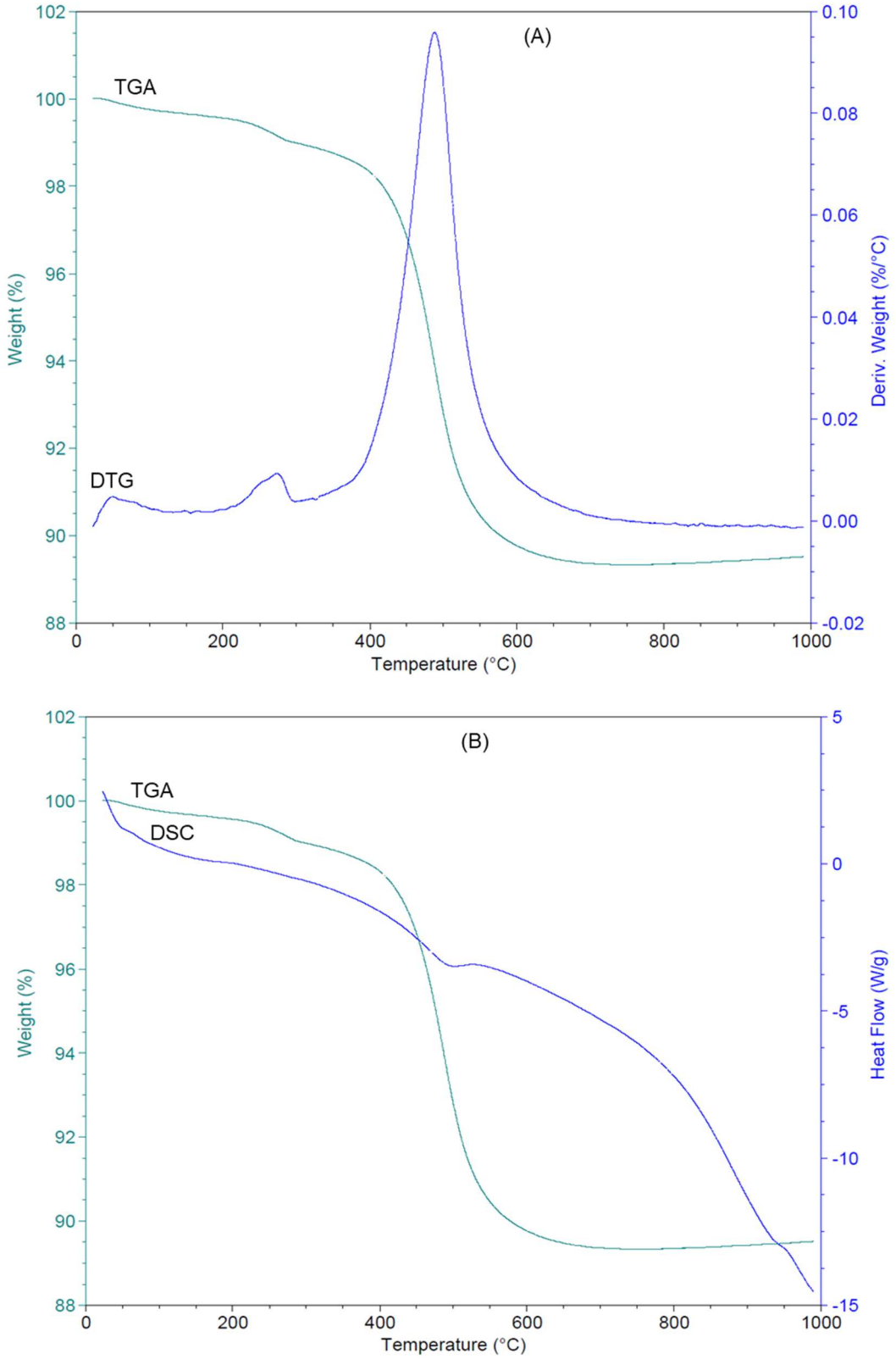

Figure 4.58: Thermal analyses of UL1 1m showing: (a) TGA/DTG and (b) DSC/TGA curves.

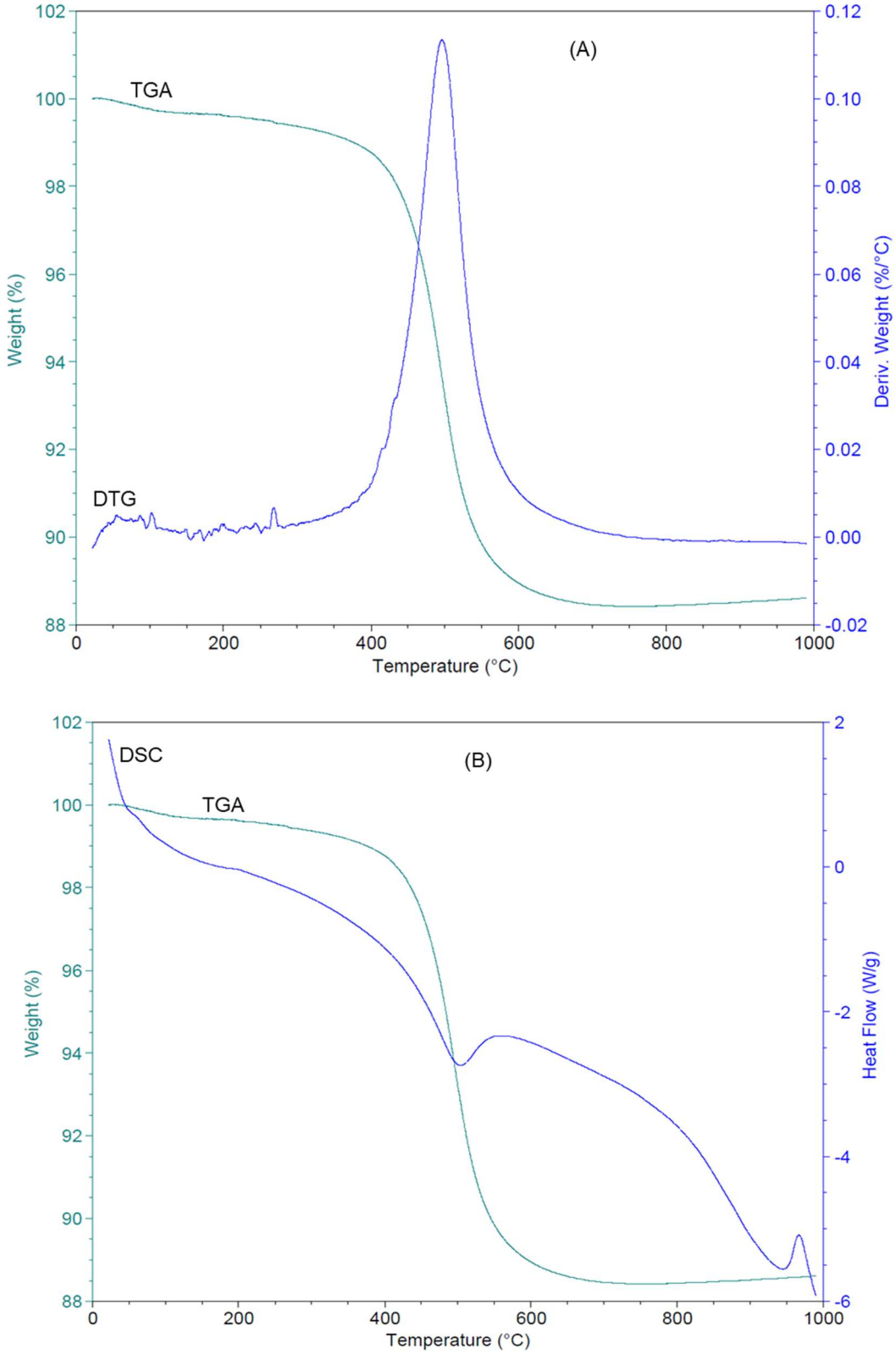

Figure 4.59: Thermal analyses of UL1 2m showing: (a) TGA/DTG and (b) DSC/TGA curves.

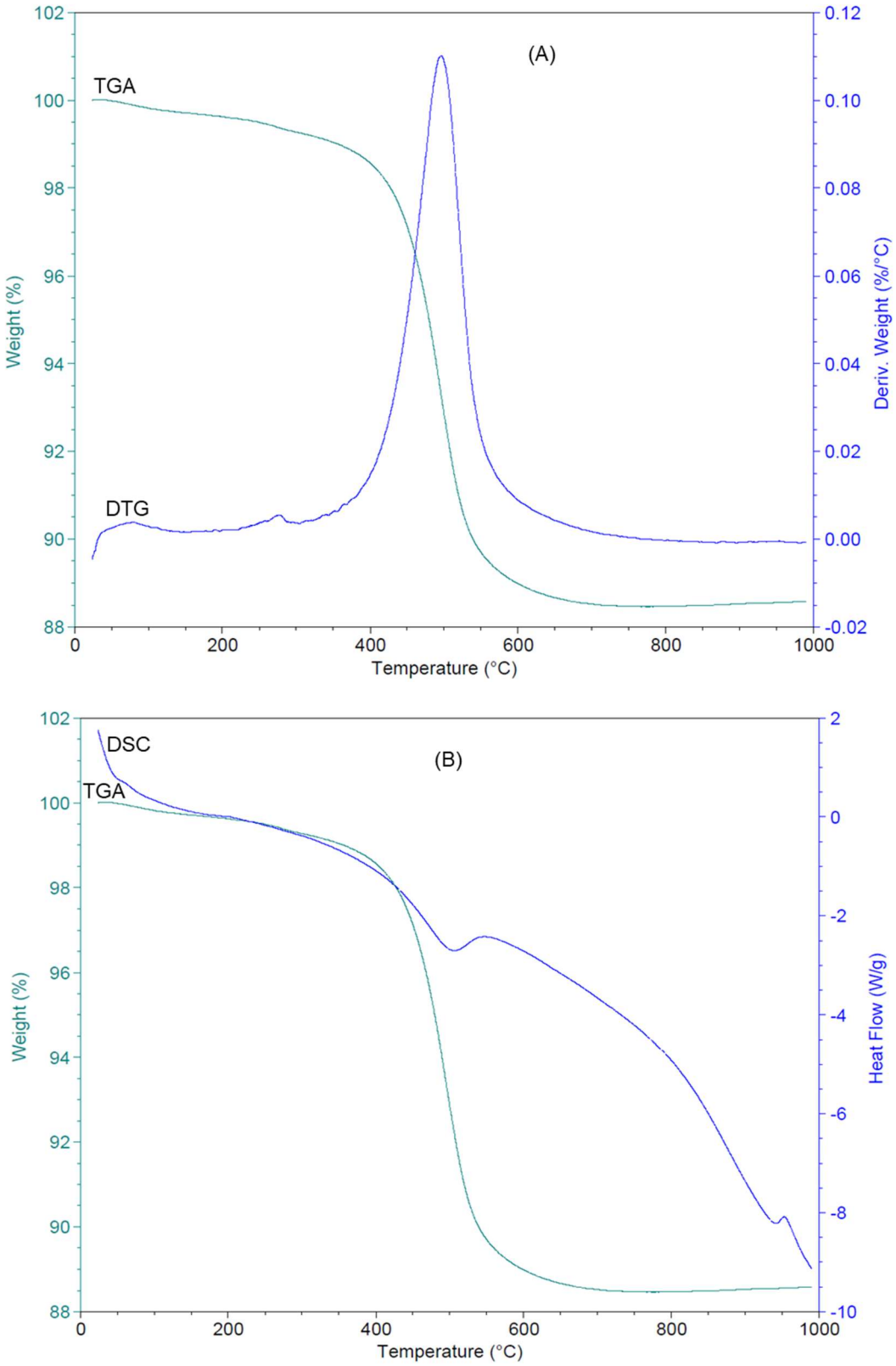

Figure 4.60: Thermal analyses of UL2 0m showing: (a) TGA/DTG and (b) DSC/TGA curves.

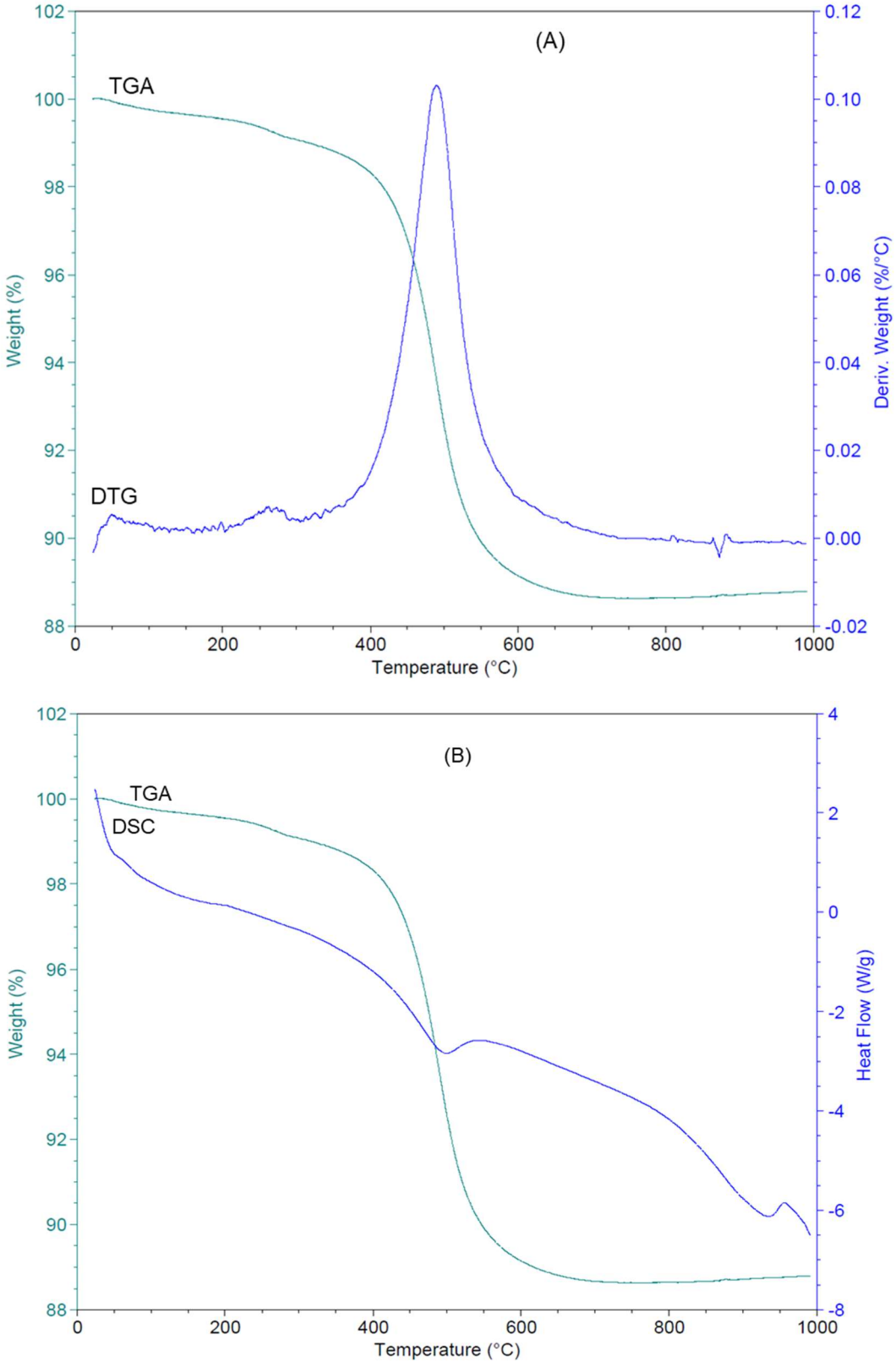

Figure 4.61: Thermal analyses of UL2 1m showing: (a) TGA/DTG and (b) DSC/TGA curves.

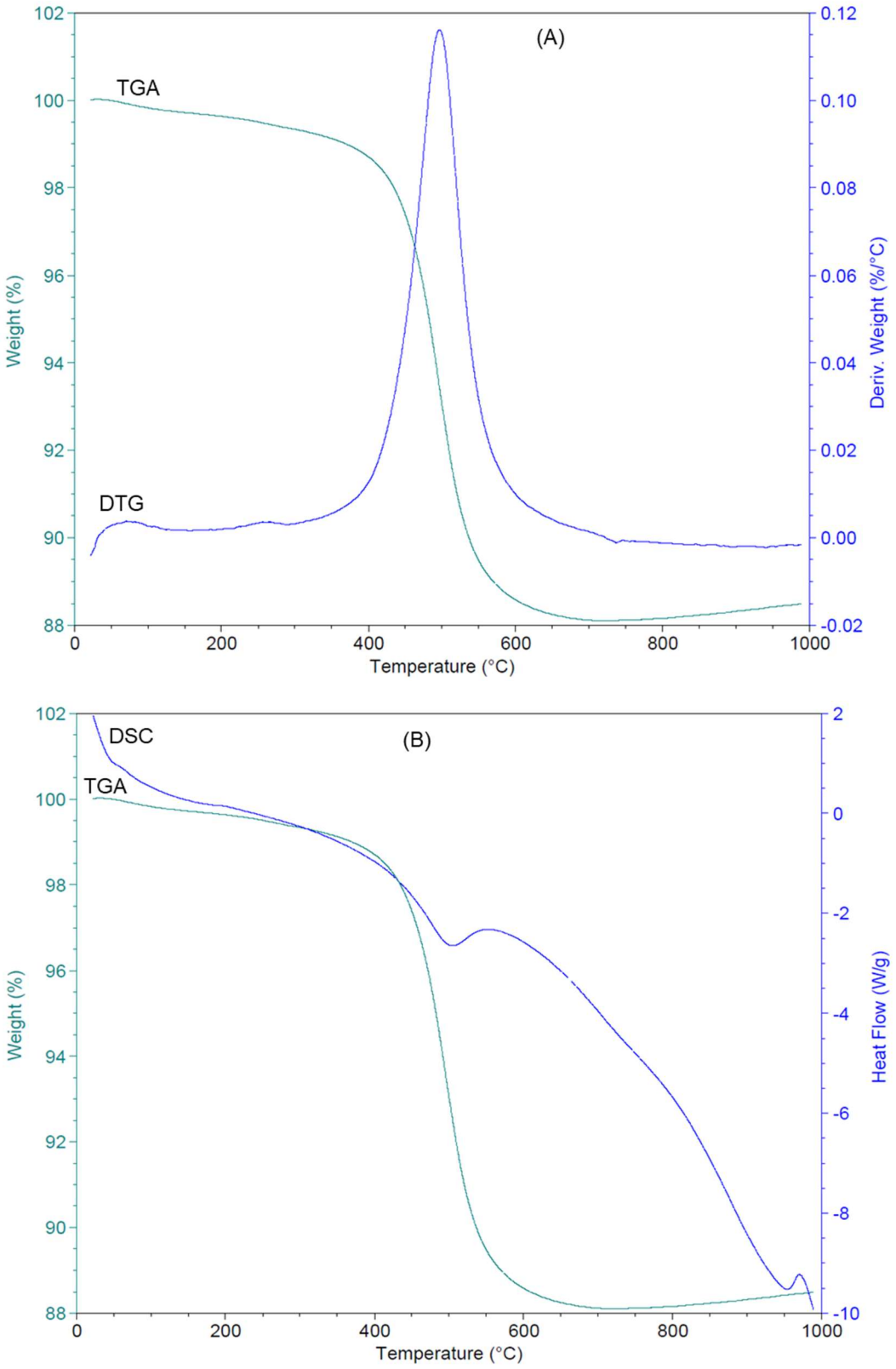

Figure 4.62: Thermal analyses of UL2 2m showing: (a) TGA/DTG and (b) DSC/TGA curves.

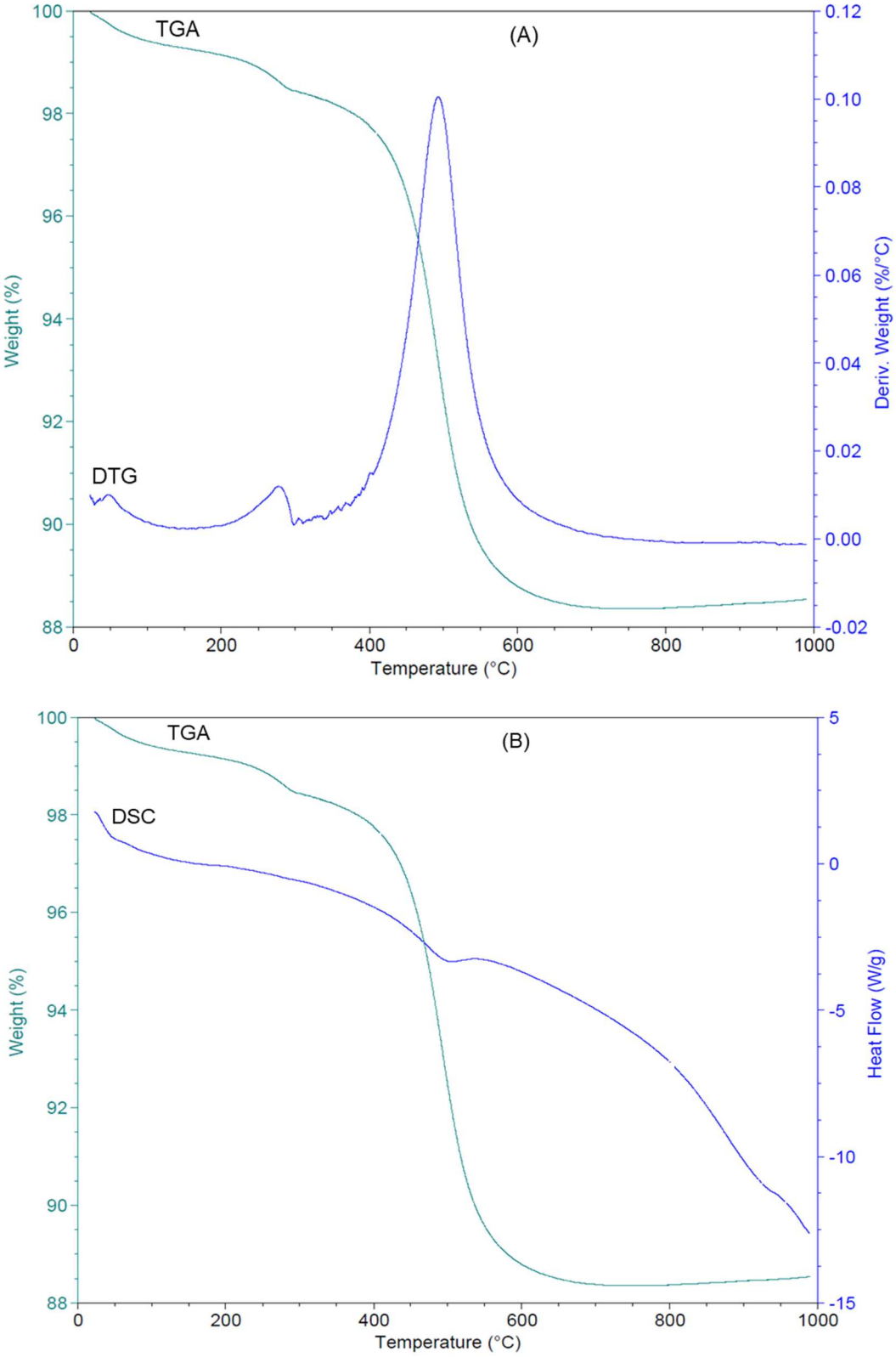

Figure 4.63: Thermal analyses of UL2 3m showing: (a) TGA/DTG and (b) DSC/TGA curves.

The Cretaceous kaolins had three endothermic reaction peaks at temperatures between 40 – 75 ˚C (Dehydration) with an average of 53.1 ˚C, 250 – 275 ˚C (Pre-dehydroxylation in Lakiri Kaolins only) with an average of 263.8 ˚C, and 488 – 517 ˚C (Dehydroxylation) with an average of 511 ˚C and exothermic reaction peak at temperatures between 980 – 985 ˚C (Mullite formation) with an average of 981.9 ˚C. The reactions were accompanied with total weight losses ranging from 13.1 - 14.4 % with an average of 13.6 %.

The Tertiary kaolins had three endothermic reaction peaks at temperatures between 50 – 80 ˚C (Dehydration) with an average of 57.4 ˚C, 250 – 280 ˚C (Pre-dehydroxylation) with an average of 267.9 ˚C, and 500 – 514 ˚C (Dehydroxylation) with an average of 505 ˚C and exothermic reaction peak at temperatures between 951 – 970 ˚C (Mullite formation) with an average of 964.3 ˚C. The reactions were accompanied with total weight losses ranging from 10.7 - 13.8 % with an average of 12.2 %.

4.2.4 Kaolinite Morphology

The different morphologies for the studied Cretaceous – Tertiary kaolins are presented in Figures 4.64 – 4.78.

The Eruku kaolins were characterised by pseudohexagonal stacks (Figure 4.64) and thin platy particles (Figure 4.65). Texturally, the kaolinite crystals were subhedral to corroded-edged anhedral flakes with finer sizes (Figure 4.66). Morphologically, the Lakiri kaolins occur as pseudohexagonal plates (Figure 4.67) and thin platy particles (Figure 4.68). Texturally, the kaolinite crystals were subhedral to ragged-edged anhedral flakes and were of comparatively finer sizes (< 2 µm) (Figure 4.69).

The observed morphologies of the Awo-Omama kaolins ranged from pseudohexagonal stacks to books (Figure 4.70) and thin platy particles (Figure 4.71). Texturally, the kaolinite crystals were euhedral to subhedral with cerrated boundaries (Figure 4.72) with coarser sizes (Figure 4.73). The Ubulu-Uku kaolins were characterised by pseudohexagonal stacks (Figure 4.74) and thin platy kaolinites (Figure 4.75). Texturally, the kaolinite crystals were subhedral (Figure 4.76) to anhedral with ragged boundaries (Figure 4.77) with coarser sizes (Figure 4.78).

Table 4.6: DTG/DSC/TGA Endothermic and Exothermic Peak Temperatures (with main reactions) and Total Weight Loss for the Clay fractions of the studied Cretaceous – Tertiary Kaolins.

Age	Deposit	Sample ID	Endothermic Temperature Peaks			Exothermic Temperature Peaks⁺	Total Weight Loss (%)#
			Dehydration* (T < 100 ˚C)	Pre-dehydroxylation* (200 - 400 ˚C)	Dehydroxylation⁺ (450 - 700 ˚C)	Mullite Formation (900 - 1000 ˚C)	
Cretaceous	Eruku	CF EP1 0m	70	-	512	980	13.2
		CF EP1 2m	50	-	510	980	13.8
		CF EP1 4m	50	-	517	980	13.8
		CF EP2 0m	75	250	510	-	13.1
		CF EP2 2m	50	-	517	980	13.7
		CF EP2 4m	50	260	513	-	13.1
		CF EP3 0m	50	270	513	980	13.6
		CF EP3 2m	75	275	488	-	13.1
		CF EP3 4m	45	-	517	983	13.6
	Lakiri	CF LP1 0m	50	-	510	985	13.9
		CF LP1 2m	40	-	510	983	13.8
		CF LP1 4m	50	-	510	983	13.8
		CF LP2 0m	50	-	512	983	13.7
		CF LP2 2m	45	-	516	983	14.4
		CF LP2 4m	47	-	510	983	13.8
		Min	40	250	488	980	13.1
		Max	75	275	517	985	14.4
		Average	53.1	263.8	511	981.9	13.6
Tertiary	Awo-Omama	CF AL1 0m	-	-	500	967	13.1
		CF AL1 1m	51	-	500	966	12.8
		CF AL1 2m	50	-	500	966	13.1
		CF AL2 0m	-	250	500	967	13.5
		CF AL2 1m	60	-	512	970	13.2
		CF AL2 2m	55	-	512	965	13.8
	Ubulu-Uku	CF UL1 0m	50	275	500	962	10.8
		CF UL1 1m	55	275	500	-	10.7
		CF UL1 2m	60	-	512	963	11.6
		CF UL2 0m	80	280	514	951	11.5
		CF UL2 1m	50	260	500	960	11.4
		CF UL2 2m	70	260	510	970	11.9
		CF UL2 3m	50	275	505	-	11.7
		Min	50	250	500	951	10.7
		Max	80	280	514	970	13.8
		Average	57.4	267.9	505	964.3	12.2

* From DTG curves, ⁺ From DSC curves, # From TGA curves, (-): No peak

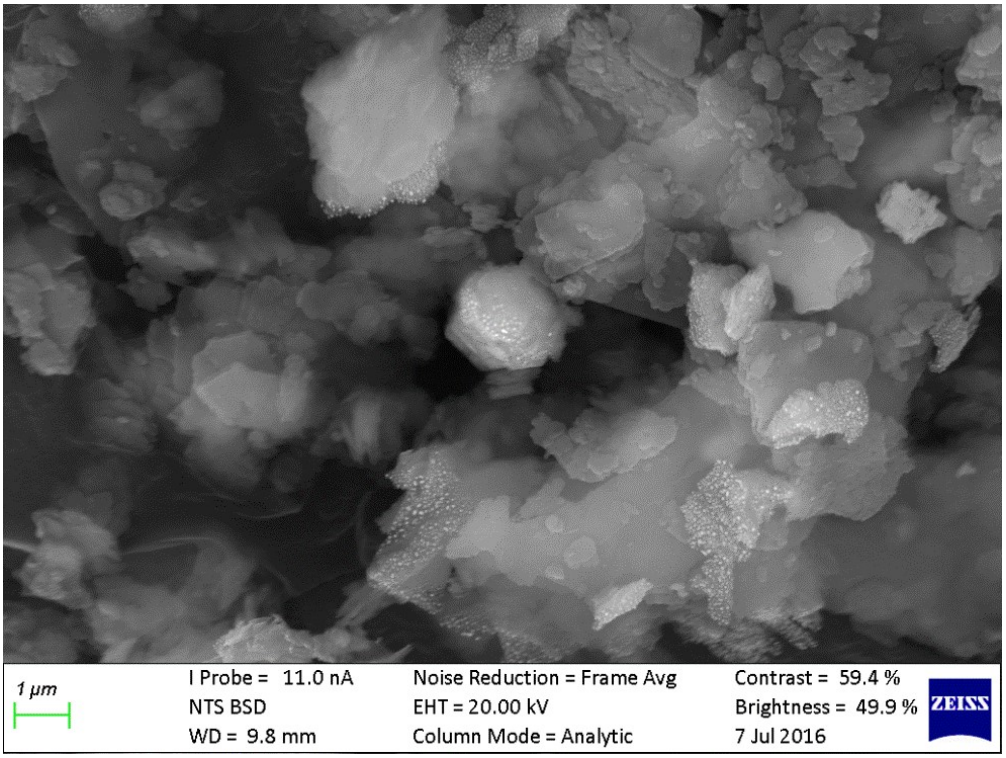

Figure 4.64: SEM Photomicrograph of representative sample from Eruku kaolin deposit showing pseudohexagonal plates.

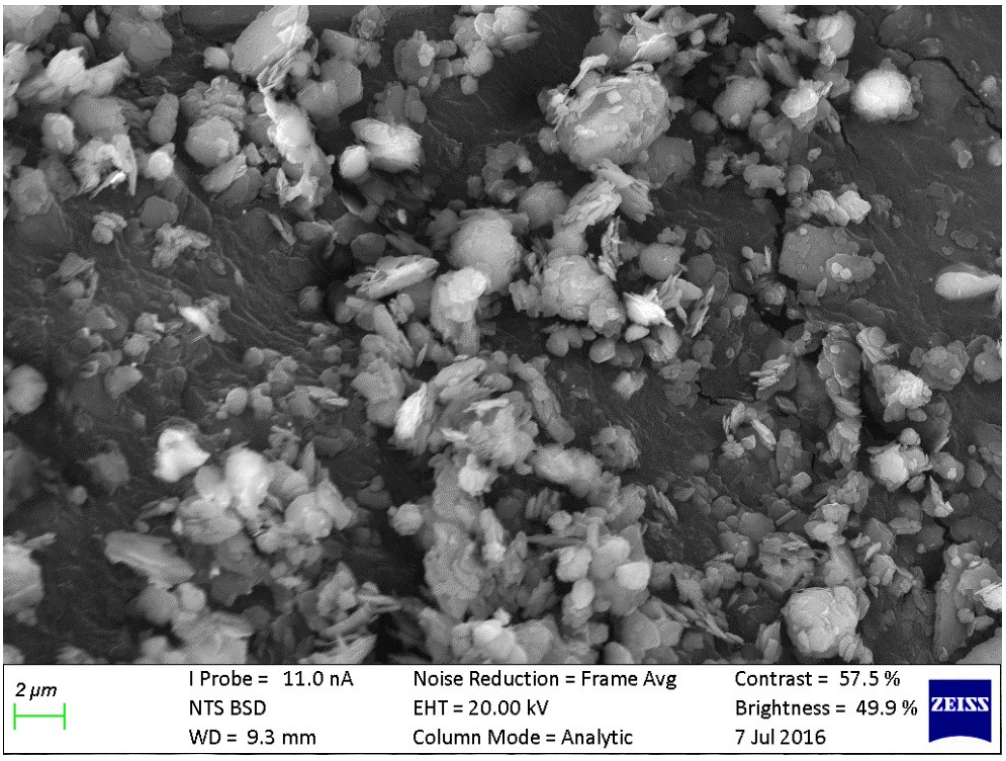

Figure 4.65: SEM Photomicrograph of representative sample from Eruku kaolin deposit showing thin platy particles.

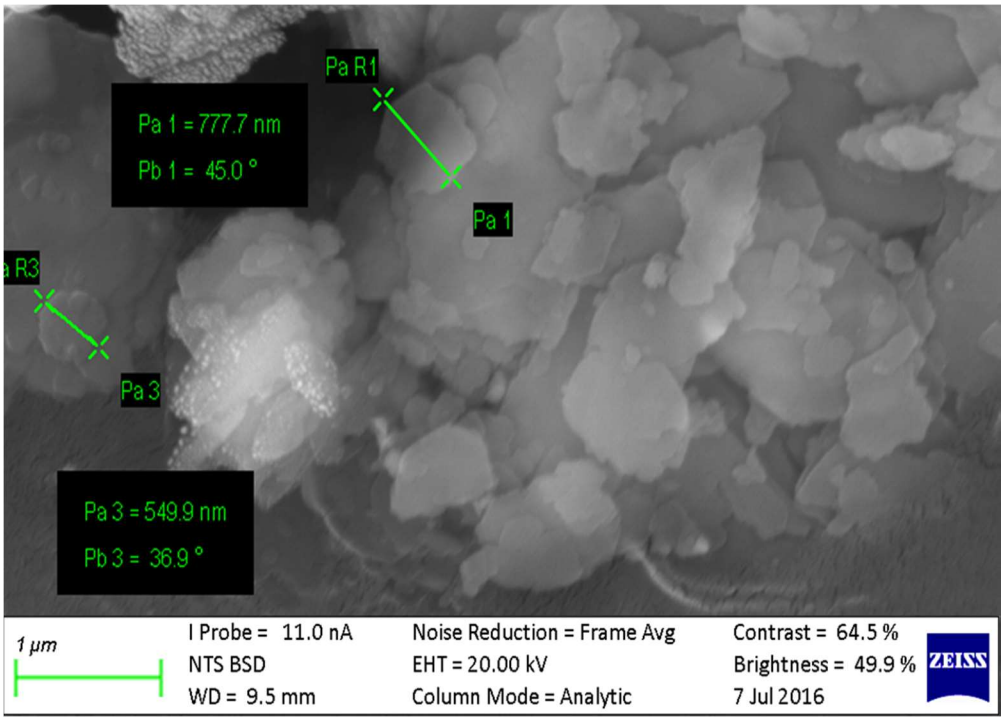

Figure 4.66: SEM Photomicrograph of representative sample from Eruku kaolin deposit showing various size dimensions.

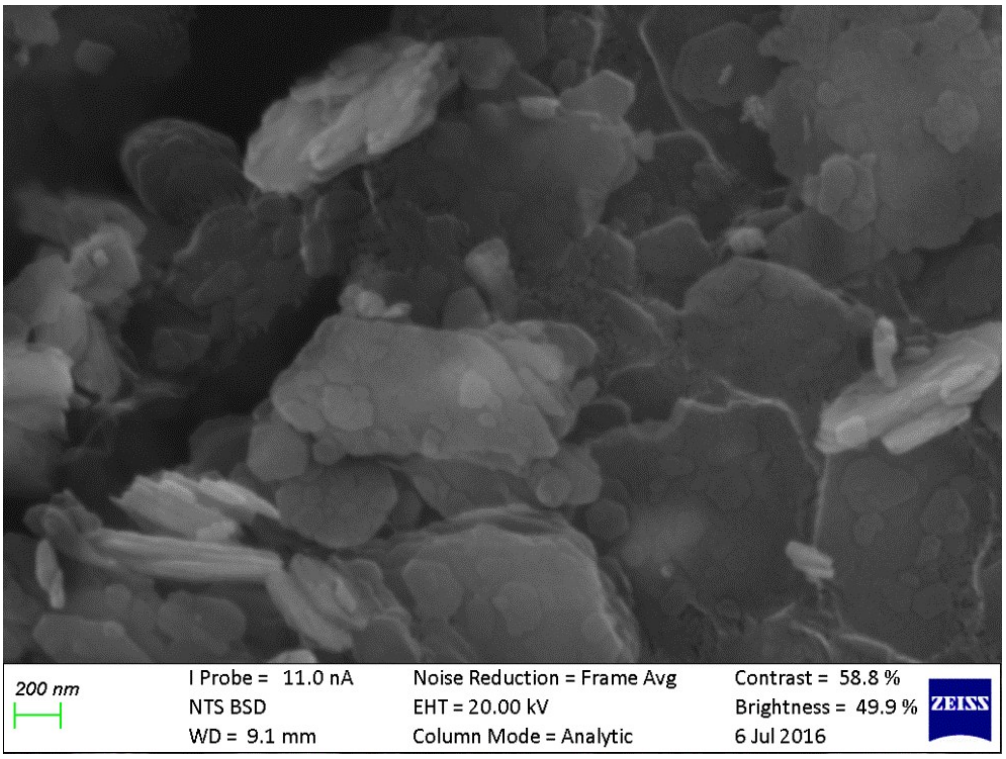

Figure 4.67: SEM Photomicrograph of representative sample from Lakiri kaolin deposit showing pseudohexagonal plates.

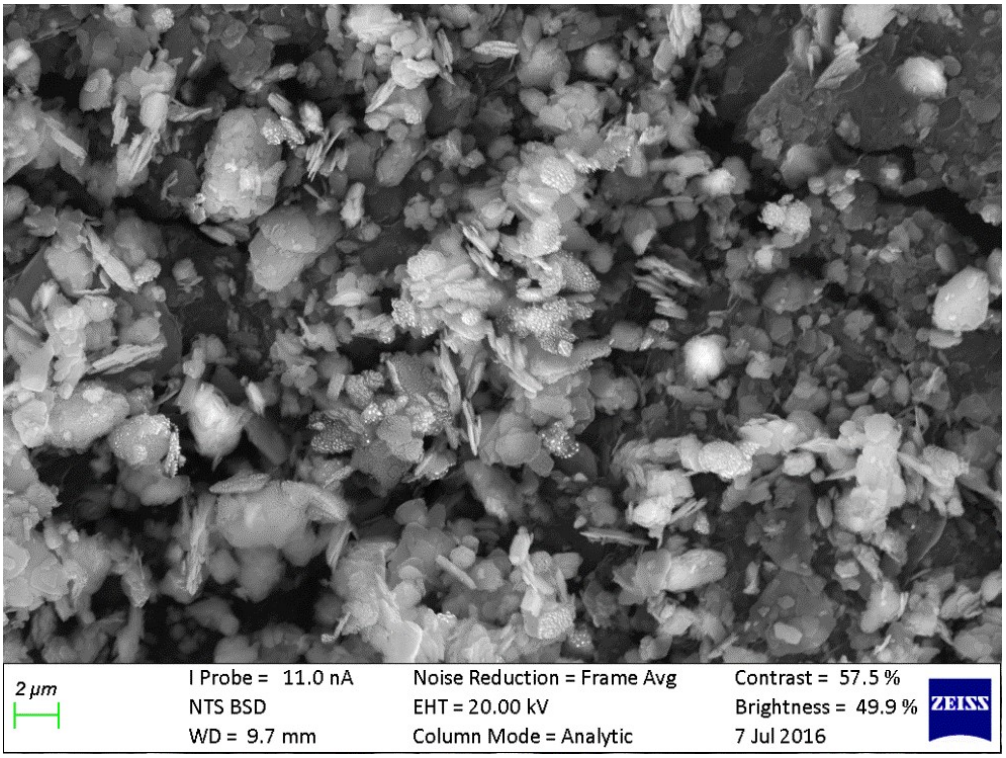

Figure 4.68: SEM Photomicrograph of representative sample from Lakiri kaolin deposit showing thin platy particles.

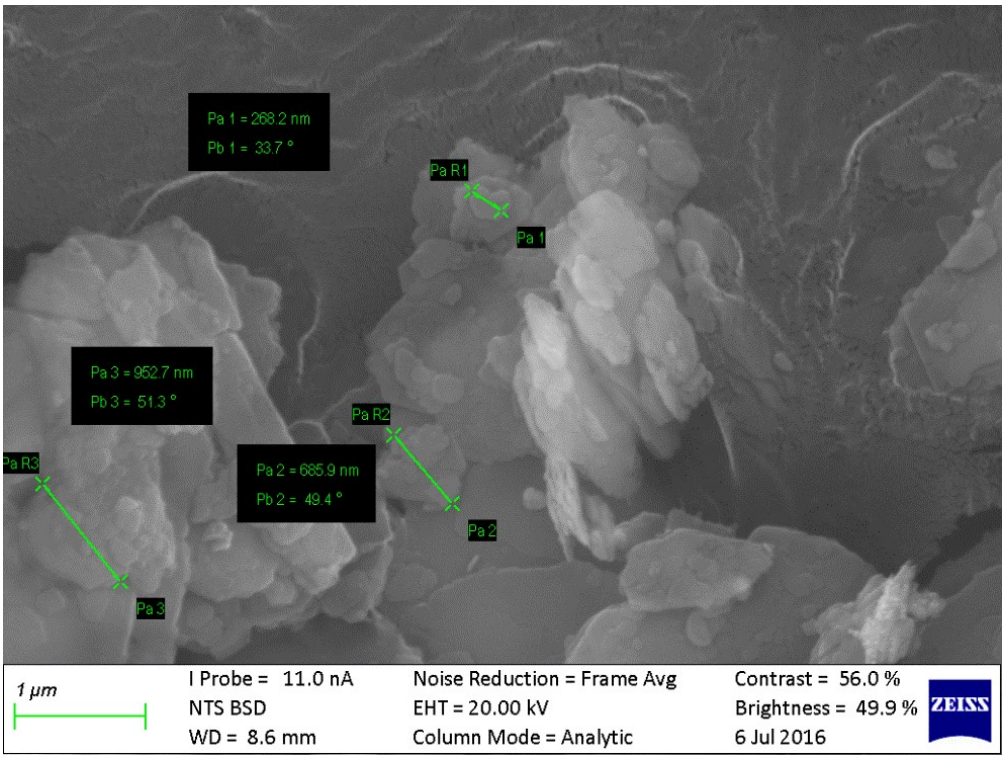

Figure 4.69: SEM Photomicrograph of representative sample from Lakiri kaolin deposit showing various size dimensions.

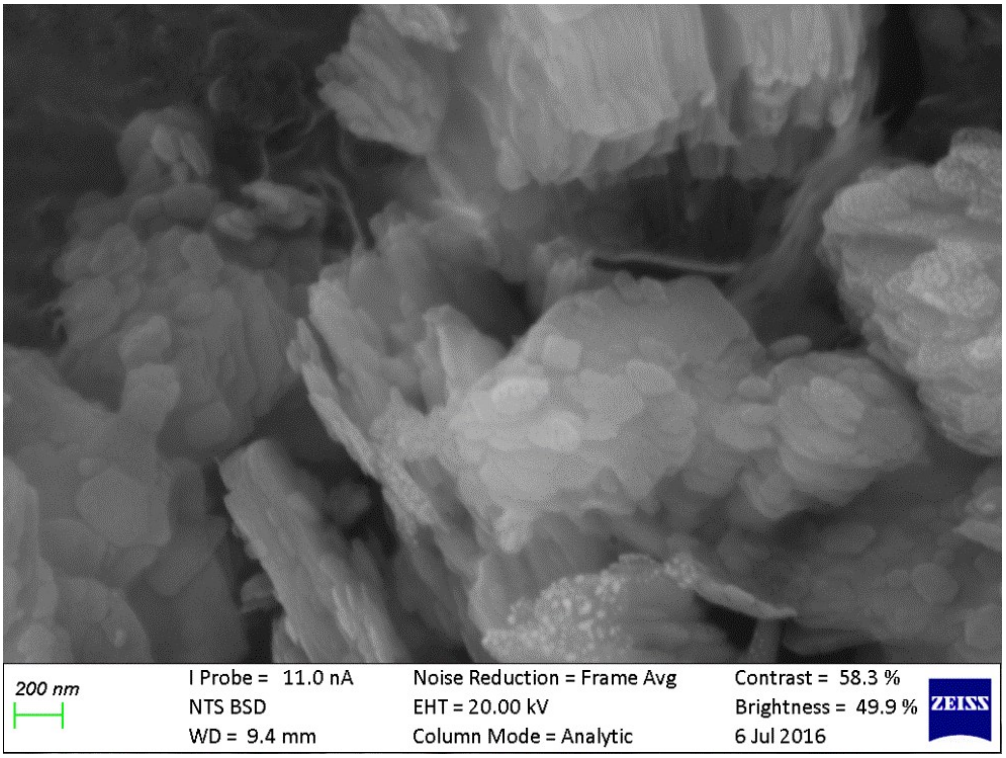

Figure 4.70: SEM Photomicrograph of representative sample from Awo-Omama kaolin deposit showing pseudohexagonal stacks and books.

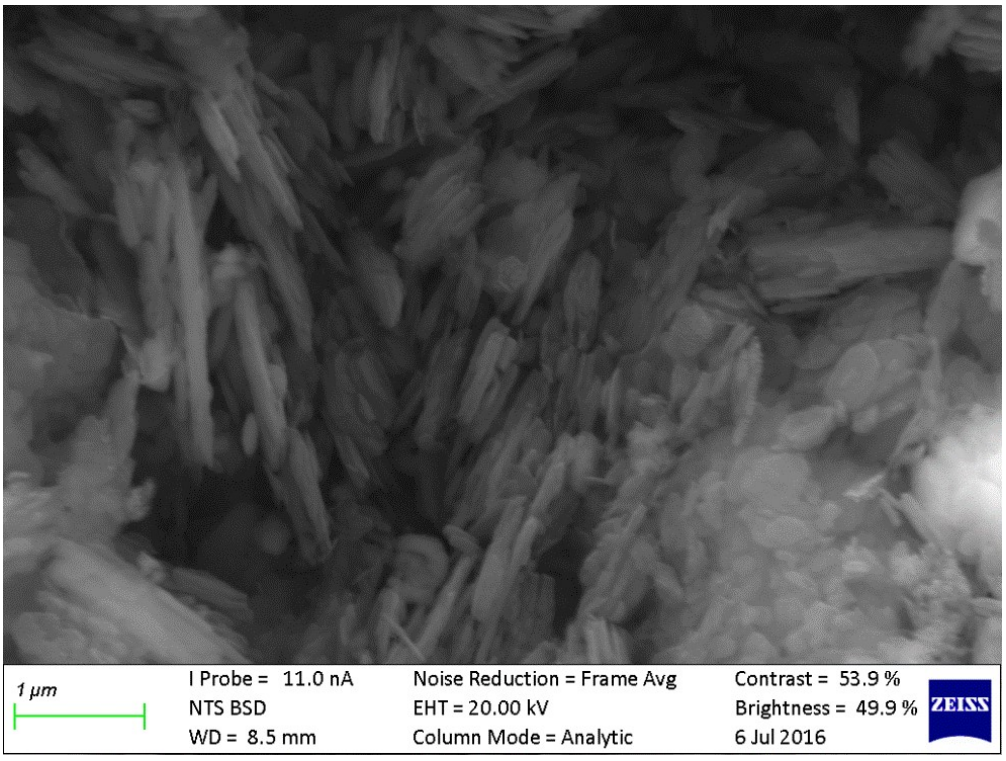

Figure 4.71: SEM Photomicrograph of representative sample from Awo-Omama kaolin deposit showing thin platy particles.

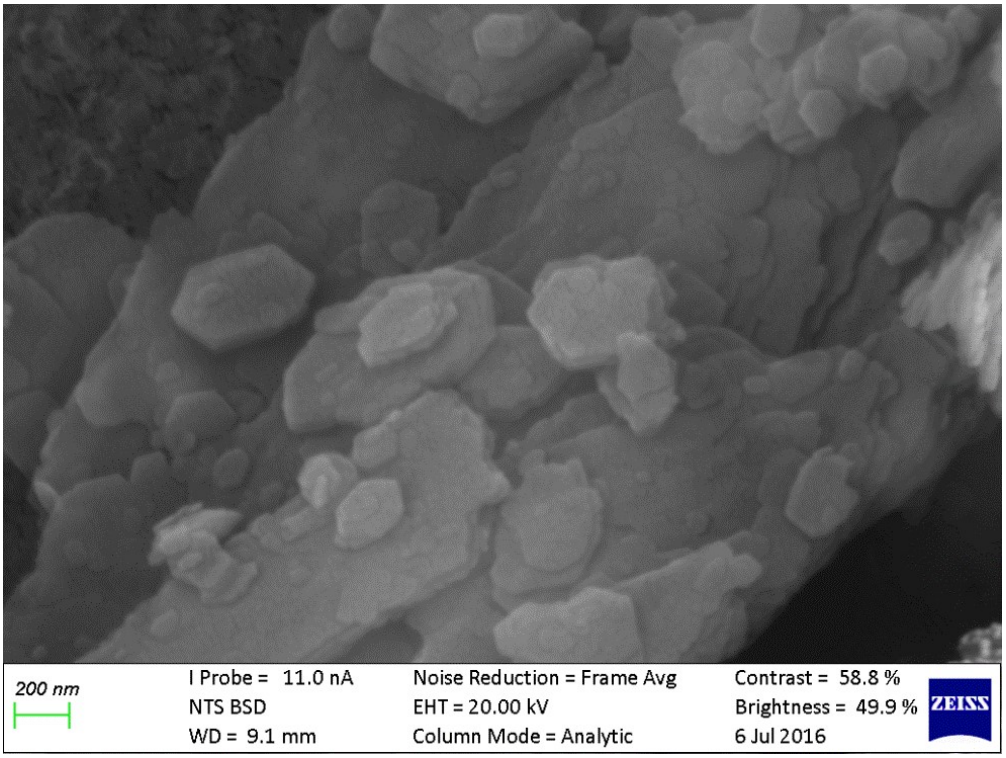

Figure 4.72: SEM Photomicrograph of representative sample from Awo-Omama kaolin deposit showing euhedral kaolinite crystals.

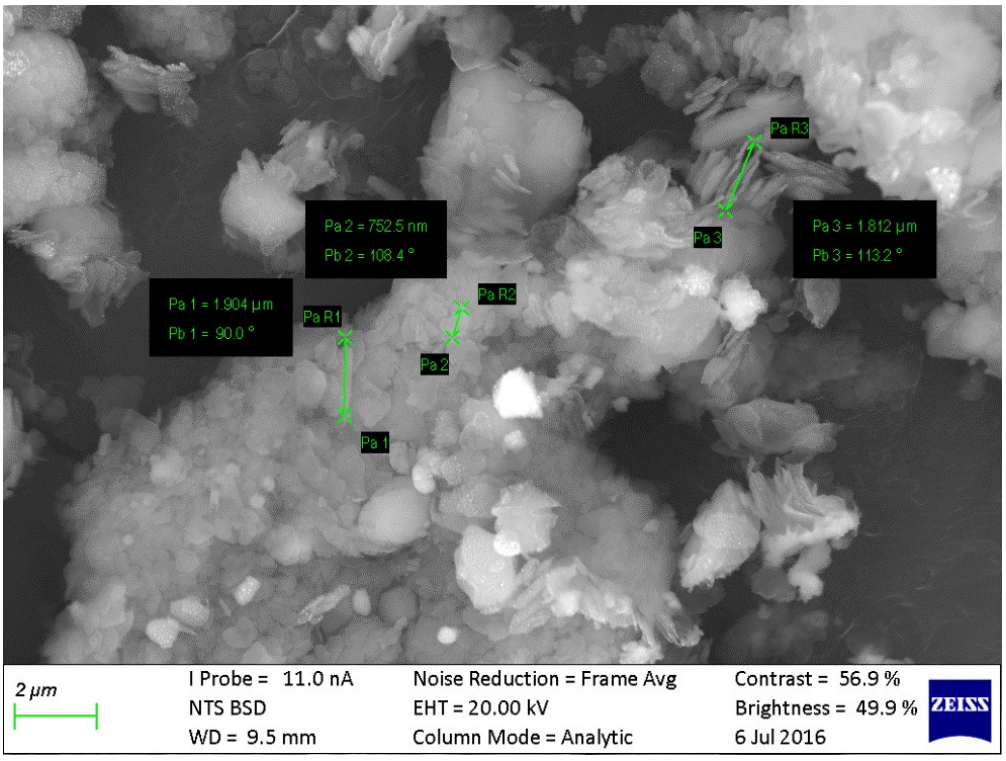

Figure 4.73: SEM Photomicrograph of representative sample from Awo-Omama kaolin deposit showing various size dimensions.

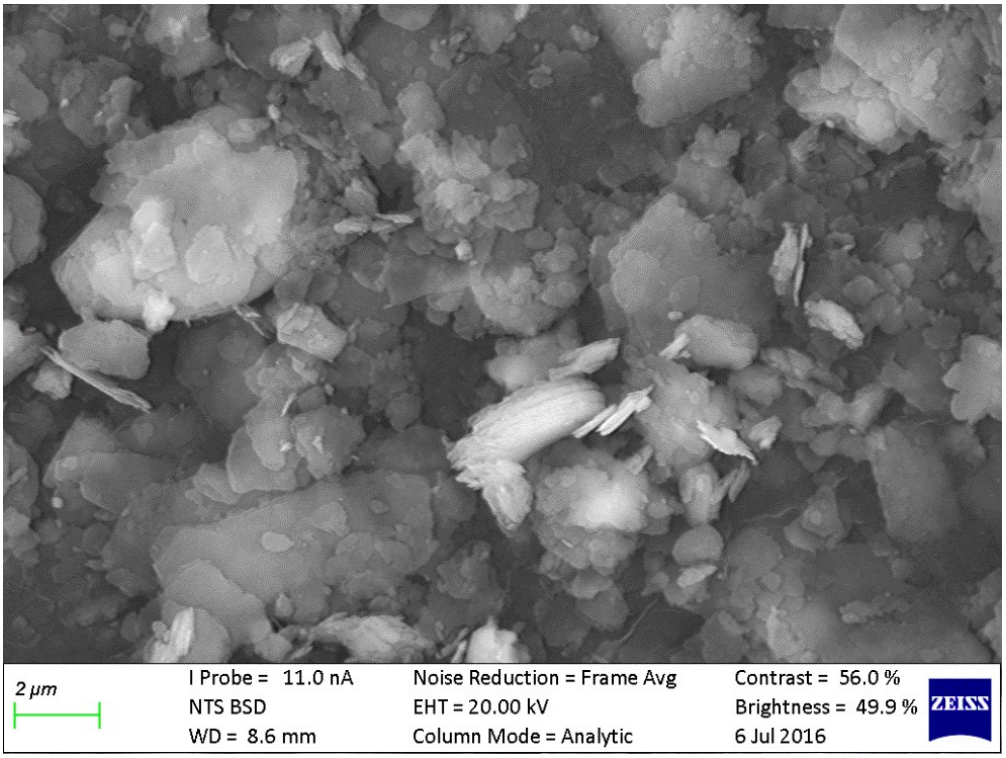

Figure 4.74: SEM Photomicrograph of representative sample from Ubulu-Uku kaolin deposit showing pseudohexagonal stacks.

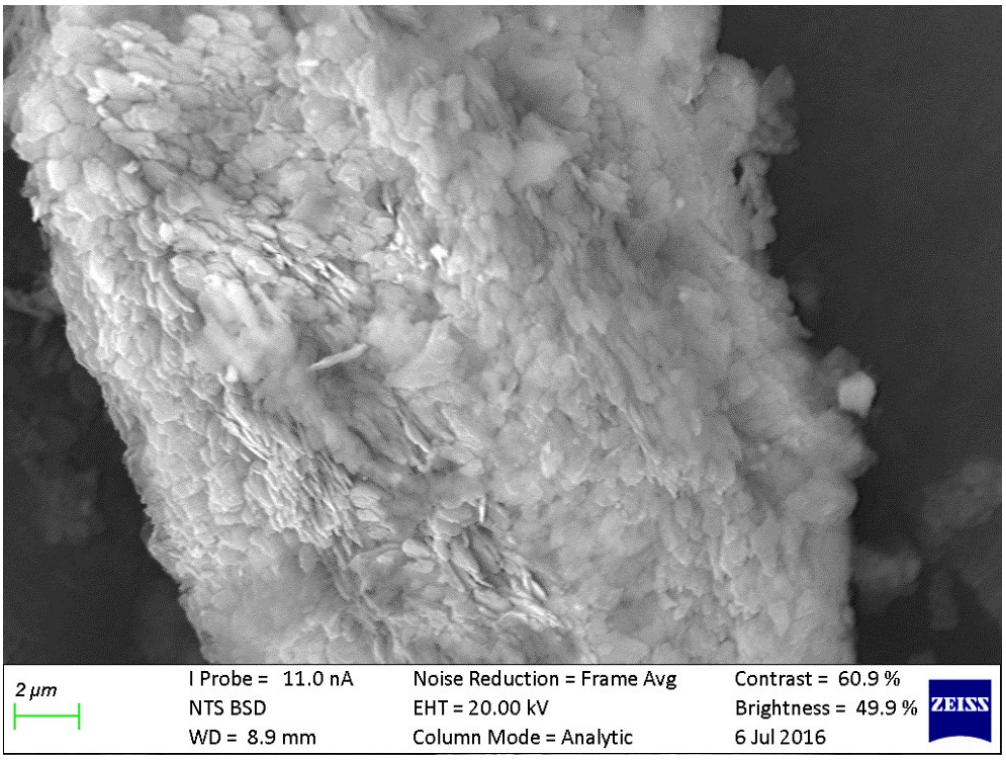

Figure 4.75: SEM Photomicrograph of representative sample from Ubulu-Uku kaolin deposit showing thin platy particles.

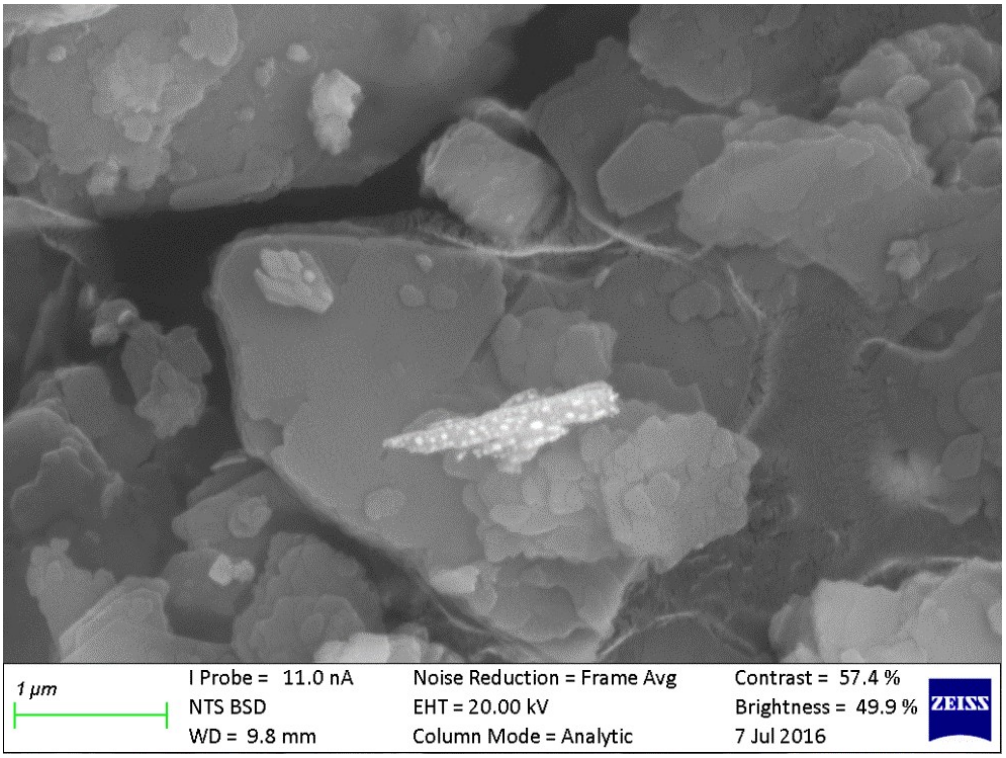

Figure 4.76: SEM Photomicrograph of representative sample from Ubulu-Uku kaolin deposit showing subhedral kaolinite crystals.

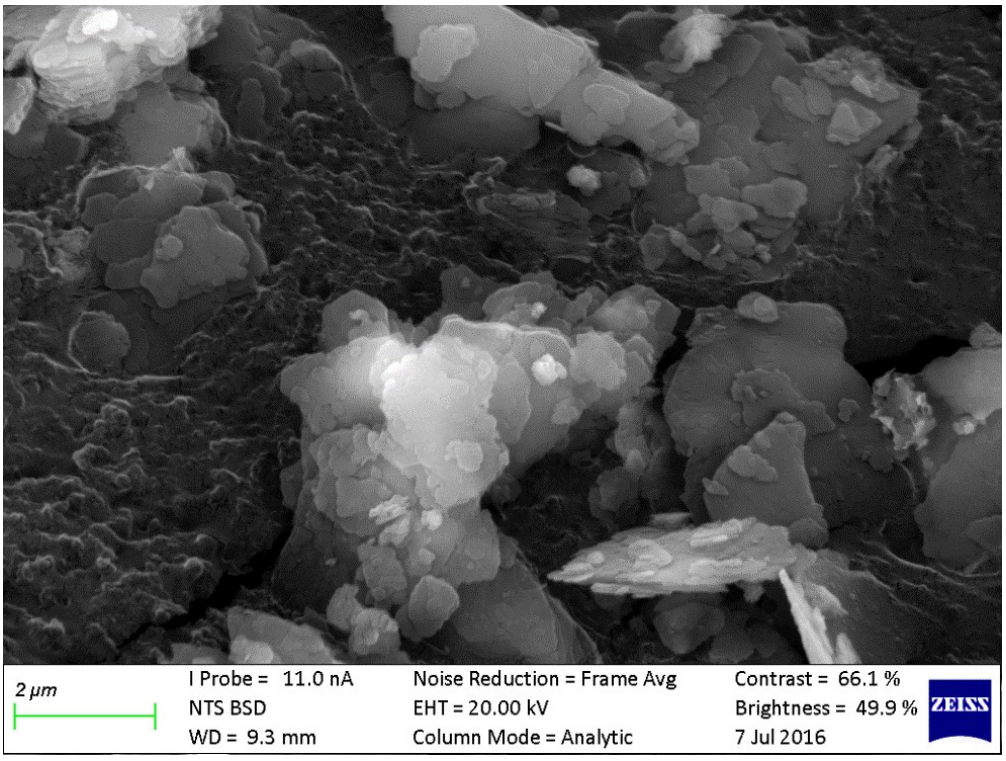

Figure 4.77: SEM Photomicrograph of representative sample from Ubulu-Uku kaolin deposit showing anhedral kaolinite crystals with ragged boundaries.

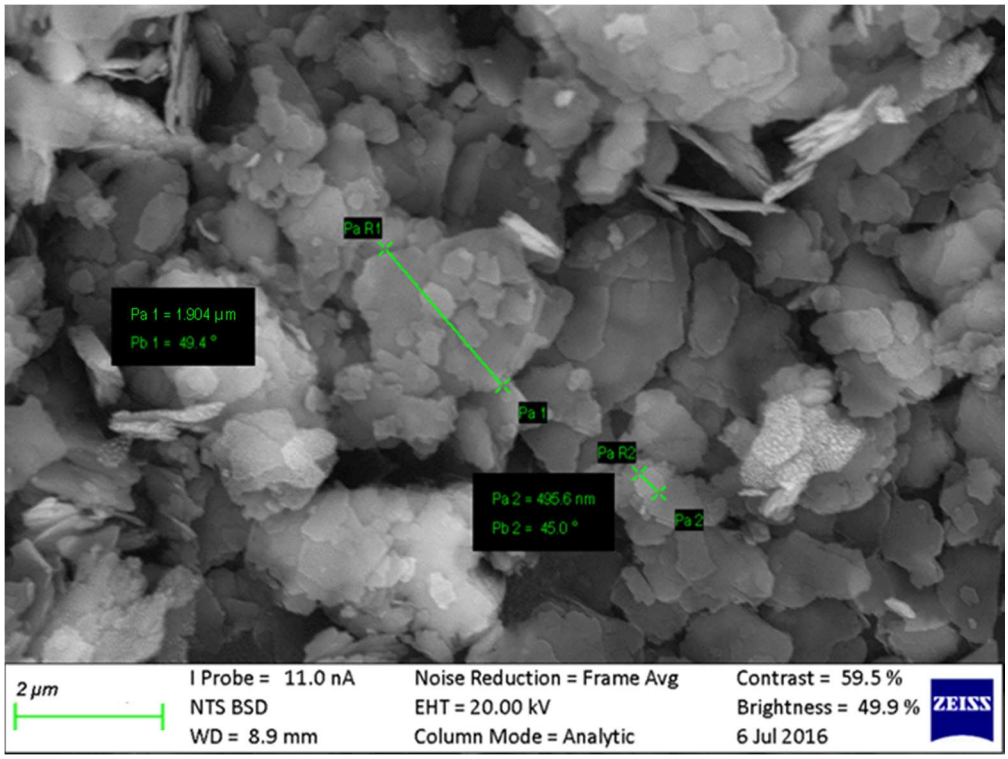

Figure 4.78: SEM Photomicrograph of representative sample from Ubulu-Uku kaolin deposit showing various size dimensions.

4.3 Geochemical Properties of Studied Cretaceous – Tertiary Kaolins

4.3.1 Major Element Oxides

Major element oxide data for the bulk, silt, and clay fractions for the studied Cretaceous – Tertiary kaolins are presented in Appendix 4.2

- **Bulk (<2 mm) Samples**

The Eruku kaolin deposit has SiO_2 concentrations varying between 47.22 and 58.06 wt % (except for EP2 4m with 80.30 wt %) and Al_2O_3 concentrations from 26.99 to 36.64 wt % (except for EP2 4m with 11.44 wt %). Fe_2O_3 and TiO_2 concentrations ranged from 1.48 to 5.04 wt % and 1.07 to 2.84 wt %, respectively. The concentrations of K_2O, CaO, Cr_2O_3, MgO, MnO, Na_2O, and P_2O_5 were generally below 0.7 wt % in the Eruku kaolins. The LOI were between 9.46 and 12.89 wt % (except for EP2 4m with 4.03 wt %).

The Lakiri kaolins have SiO_2 concentrations ranging between 44.63 and 69.60 wt % and Al_2O_3 concentrations from 21.40 to 39.90 wt %. Fe_2O_3 and TiO_2 concentrations ranged from 0.59 to 2.70 wt % and 1.14 to 2.0 wt %, respectively. The concentrations of K_2O, CaO, Cr_2O_3, MgO, MnO, Na_2O, and P_2O_5 were generally below 0.56 wt % in the Lakiri kaolins. The LOI were between 7.42 and 13.92 wt %.

The Awo-Omama kaolin samples have SiO_2 concentrations varying between 50.11 and 87.99 wt % and Al_2O_3 concentrations from 10.86 to 32.09 wt %. Fe_2O_3 and TiO_2 concentrations ranged from 0.85 to 4.24 wt % and 0.83 to 1.99 wt %, respectively. The concentrations of K_2O, CaO, Cr_2O_3, MgO, MnO, Na_2O, and P_2O_5 were generally below 0.27 wt % in the Awo-Omama kaolins. The LOI were between 2.83 and 11.97 wt %.

The Ubulu-Uku kaolin samples have SiO_2 concentrations between 55.11 and 67.63 wt % and Al_2O_3 concentrations from 17.80 to 26.83 wt %. Fe_2O_3 and TiO_2 concentrations ranged from 4.63 to 8.30 wt % and 1.67 to 2.38 wt %, respectively. The concentrations of K_2O, CaO, Cr_2O_3, MgO, MnO, Na_2O, and P_2O_5 were generally below 0.60 wt % in the Ubulu-Uku kaolins. The LOI values were between 6.81 and 10.02 wt %.

- **Silt (2 – 63 µm) Fractions**

The Cretaceous kaolin deposits have SiO_2 contents varying from 61.68 to 62.35 wt % and Al_2O_3 concentrations from 22.98 to 25.39 wt %. Fe_2O_3 and TiO_2 concentrations ranged from 1.09 to 1.88 wt % and 2.04 to 4.11 wt %, respectively. The concentrations of K_2O, CaO, Cr_2O_3, MgO, MnO, Na_2O, and P_2O_5 were generally below 0.87 wt %. The LOI were between 7.88 and 8.83 wt %.

The Tertiary kaolin deposits have SiO_2 contents varying from 80.88 to 94.99 wt % and Al_2O_3 concentrations from 1.38 to 6.23 wt %. Fe_2O_3 and TiO_2 concentrations ranged from 0.64 to 7.72 wt % and 1.75 to 2.14 wt %, respectively. The concentrations of K_2O, CaO, Cr_2O_3, MgO, MnO, Na_2O, and P_2O_5 were generally below 0.16 wt %. The LOI were between 0.59 and 2.57 wt %.

- **Clay (<2 µm) Fractions**

The concentrations of SiO_2 in the Eruku and Lakiri kaolins varied from 42.35 to 47.52 wt % and 44.19 to 44.78 wt %, respectively. The range of Fe_2O_3 and TiO_2 concentrations in Eruku kaolins were 1.38 to 3.96 wt % (except for EP2 0m and EP2 4m with 5.23 and 7.53 wt %, respectively) and 1.28 to 2.52 wt %, respectively. For Lakiri kaolins, the concentrations of Fe_2O_3 and TiO_2 ranged from 0.63 to 2.11 wt % and 1.29 and 1.54 wt %, respectively. The concentrations of K_2O, CaO, Cr_2O_3, MgO, MnO, Na_2O, and P_2O_5 in the Eruku and Lakiri kaolins were generally below 0.58 and 0.35 wt % respectively. The LOI values obtained for Eruku and Lakiri kaolins were between 12.90 to 13.54 wt % and 13.70 to 13.91 wt%, respectively.

The Awo-Omama kaolin samples have SiO_2 contents varying between 43.47 and 51.01 wt % and Al_2O_3 concentrations from 30.11 to 36.76 wt %. Fe_2O_3 and TiO_2 concentrations ranged from 2.67 to 5.14 wt % and 1.63 to 3.95 wt %, respectively. The concentrations of K_2O, CaO, Cr_2O_3, MgO, MnO, Na_2O, and P_2O_5 were generally below 0.49 wt % in the Awo-Omama kaolins. The LOI were between 11.20 and 13.47 wt %.

The SiO_2 and Al_2O_3 concentrations were between 44.90 and 53.85 wt % and 28.57 to 33.87 wt % in the Ubulu-Uku kaolins. Fe_2O_3 and TiO_2 concentrations ranged from 4.32 to 6.75 wt % and 1.89 to 2.68 wt %, respectively. The concentrations of K_2O, CaO, Cr_2O_3, MgO, MnO, Na_2O, and P_2O_5 were generally below 0.65 wt % in the Ubulu-Uku kaolins. The LOI values were between 10.24 and 11.99 wt %.

4.3.2 Trace Elements

The results of the trace element concentrations for the bulk, silt, and clay fractions for the studied Cretaceous – Tertiary kaolins are presented in Appendix 4.3.

4.3.2.1 The Compatible Trace Elements (Sc, V, Cr, Co, and Ni)

These are trace elements whose preference is in the mineral phase usually with partition coefficient greater than 1.

- **Bulk (<2 mm) Samples**

The values obtained for Sc, V, Cr, Co, and Ni in the Cretaceous kaolins ranged from 11.15 to 37.7 ppm, 67.78 to 172.13 ppm (except for LP2 0m with 305.35 ppm), 49.65 to 156.07 ppm (except for LP2 0m with 218.84 ppm), 2.20 to 12.18 ppm, and 18.02 to 50.13 ppm (except for LP2 0m with 164.23 ppm), respectively. In the Tertiary kaolins, the Sc, V, Cr, Co, and Ni concentrations varied from 12.87 to 22.81 ppm, 45.82 to 214.78 ppm, 40.13 to 163.06, 1.17 to 7.25 ppm, and 12.61 to 32.48 ppm, respectively.

- **Silt (2 – 63 µm) Fractions**

The Sc, V, Cr, Co, and Ni concentrations within the studied Cretaceous – Tertiary kaolins ranged from 10.81 to 28.26 ppm, 36.29 to 131.43 ppm, 45.97 to 148.57 ppm, 1.52 to 5.72 ppm, and 13.11 to 28.37 ppm, respectively.

- **Clay (<2 µm) Fractions**

The values obtained for Sc, V, Cr, Co, and Ni in the Cretaceous kaolins ranged from 13.6 to 19.13 ppm, 96.69 to 209.85 ppm, 124.18 to 160.39 ppm, 5.93 to 12.19 ppm, and 40.76 to 61.53 ppm, respectively. In the Tertiary kaolins, the Sc, V, Cr, Co, and Ni concentrations varied from 12.18 to 22.73 ppm, 98.21 to 197.50 ppm, 83.18 to 177.37, 2.03 to 6.10 ppm, and 18.70 to 36.18 ppm, respectively.

4.3.2.2 The Incompatible Trace Elements (Rb, Sr, Y, Zr, Nb, Ba, Th, and U)

- **Bulk (<2 mm) Samples**

The concentrations of Rb, Y, Th, Nb (except for Ubulu-Uku kaolins), and U were generally less than 50 ppm in the Cretaceous - Tertiary kaolins whereas Sr (except for Lakiri and Awo-Omama kaolins), Zr, and Ba (except for Lakiri kaolins) were more than 50 ppm in the Cretaceous - Tertiary kaolins.

- **Silt (2 – 63 µm) Fractions**

The concentrations of Rb, Th, U, Sr (except for Eruku kaolins), Y (except for Awo-Omama and Ubulu-Uku kaolins), and Nb (except for Eruku and Ubulu-Uku kaolins) were generally less than 50 ppm in the Cretaceous - Tertiary kaolins whereas Zr and Ba were more than 50 ppm in the Cretaceous - Tertiary kaolins.

- **Clay (<2 µm) Fractions**

The concentrations of Rb, Y, Th, and U were generally less than 50 ppm in the Cretaceous - Tertiary kaolins whereas Zr, Ba (except for Lakiri kaolins), Sr (except for Lakiri kaolins), and Nb (except for Eruku and Lakiri kaolins) were generally more than 50 ppm in the Cretaceous - Tertiary kaolins.

4.3.3 Rare Earth Elements (REEs)

The light REEs (LREE) are the low atomic number members of the REE series from La – Sm, while the higher atomic number members from Gd – Yb are referred to as the heavy REEs (HREE). The results of the REE concentrations for the bulk, silt, and clay fractions for the studied Cretaceous – Tertiary kaolins are presented in Appendix 4.4.

- **Bulk (<2 mm) Samples**

The absolute LREE concentrations were generally more than 10 ppm (except for Pr in samples AL1 1m, AL1 2m, AL2 0m, and EP2 4m) in the Cretaceous - Tertiary kaolins whereas the HREE concentrations were generally less than 10 ppm (except for Gd and Dy in samples UL1 2m, EP1 2m, EP2 2m, EP3 2m, EP3 4m) in the Cretaceous - Tertiary kaolins. The Eu concentrations were between 0.55 and 4.47 ppm in the Cretaceous - Tertiary kaolins.

- **Silt (2 – 63 µm) Fractions**

The absolute LREE concentrations were generally more than 10 ppm (except for Sm in all the samples, Pr in Awo-Omama and Ubulu-Uku samples, and Nd in Awo-Omama samples) in the Cretaceous - Tertiary kaolins whereas the HREE concentrations were

generally less than 10 ppm (except for Er and Yb in Eruku samples) in the Cretaceous - Tertiary kaolins. The Eu concentrations were between 0.48 and 1.55 ppm in the Cretaceous - Tertiary kaolins.

- **Clay (<2 µm) Fractions**

The absolute LREE concentrations were generally more than 10 ppm (except for Sm in some Eruku, Lakiri, Awo-Omama, and Ubulu-Uku samples and Pr in samples LP1 2m, LP1 4m, LP2 0m, and LP2 2m) in the Cretaceous - Tertiary kaolins whereas the HREE concentrations were generally less than 10 ppm (except for Gd in samples UL1 2m and UL2 3m) in the Cretaceous - Tertiary kaolins. The Eu concentrations were between 0.61 and 5.04 ppm in the Cretaceous - Tertiary kaolins.

Concluding Remarks

In this chapter, the physico-chemical, mineralogical, and geochemical results for the Cretaceous – Tertiary kaolins within the Eastern Dahomey and Niger Delta Basins in Nigeria have been presented.

Chapter Five

Provenance and Tectonic Settings of the Cretaceous-Tertiary kaolins within the Eastern Dahomey and Niger Delta Basins in Nigeria.

This chapter aimed to establish the provenance and tectonic settings of the Cretaceous-Tertiary kaolins within the Eastern Dahomey and Niger Delta Basins in Nigeria (Specific Objective 1) based on Hypothesis 1. The geochemical characteristics of the studied kaolins were used to achieve specific objective 1.

5.1 Provenance

5.1.1 Major Elements

Table 5.1 shows the mean values and ranges of the major element concentrations. The chemical compositions of the clay fractions of Eruku, Lakiri, Awo-Omama, and Ubulu-Uku kaolin deposits are identical to hydrated alumino-silicates based on the dominance of SiO_2, Al_2O_3 and LOI in the clays. The Cretaceous Eruku and Lakiri deposits show higher Al_2O_3 contents relative to the Tertiary Awo-Omama and Ubulu-Uku kaolin deposits which is a reflection of the mineralogy of the clays. The mineralogy of the Cretaceous kaolin deposits showed higher mean kaolinite content (98 %) relative to the Tertiary kaolin deposits (82) (Table 5.2). The presence of impurities like anatase, hematite, and goethite (Table 5.2) are evident from the TiO_2 and Fe_2O_3 contents. The contents of Cr_2O_3, CaO, MgO, MnO, Na_2O, K_2O, and P_2O_5 are comparatively lower than the other oxides in the kaolin samples. The Lakiri deposit with average SiO_2, Al_2O_3, and LOI contents of 44.55 %, 39.19 %, and 13.81 %, respectively, is generally similar to the theoretical kaolin mineral chemical composition with corresponding values of 46.54 %, 39.50 %, and 13.90 % (Murray, 2007).

The Cretaceous and Tertiary kaolin deposits from the study show lower averages in SiO_2, Fe_2O_3, CaO, MgO, MnO, Na_2O, and K_2O when compared with the Upper Continental Crust (UCC).

Table 5.1: Major element oxides (wt %) and weathering indices (CIA and CIW) of the <2 µm fractions of Cretaceous - Tertiary kaolins from Eastern Dahomey and Niger Delta Basins, Nigeria and for average Upper Continental Crust (UCC) and Cretaceous Red Sea kaolin deposits (Egypt).

Deposit		SiO_2	TiO_2	Al_2O_3	Cr_2O_3	Fe_2O_3	CaO	MgO	MnO	Na_2O	K_2O	P_2O_5	L.O.I.	CIA	CIW
Awo-Omama	Average	46.13	2.34	34.75	0.02	3.8	0.02	-	-	0.25	0.31	0.44	12.69	98.34	99.21
(n=6)	Max	51.01	3.95	36.73	0.02	5.14	0.04	bdl	0.02	0.32	0.4	0.49	13.47	98.64	99.35
	Min	43.47	1.63	30.11	0.01	2.67	0.01	bdl	bdl	0.2	0.21	0.41	11.2	97.89	98.98
Ubulu-Uku	Average	49.69	2.05	30.65	0.01	5.97	0.02	-	-	0.27	0.51	0.38	11.1	97.42	99.05
(n=7)	Max	53.85	2.68	33.87	0.01	6.75	0.02	bdl	0.01	0.36	0.58	0.65	11.99	98.01	99.16
	Min	44.9	1.89	28.57	0.01	4.32	0.02	bdl	bdl	0.23	0.38	0.31	10.24	96.98	99.01
Eruku	Average	44.73	1.69	37.19	0.02	2.98	0.02	-	-	0.21	0.25	0.38	13.54	98.71	99.39
(n=9)	Max	47.52	2.52	38.6	0.1	7.53	0.03	bdl	0.01	0.38	0.41	0.58	13.54	98.97	99.89
	Min	42.35	1.28	35.48	0.01	1.38	0.01	bdl	bdl	0.02	0.18	0.14	12.9	98.4	98.95
Lakiri	Average	44.55	1.41	39.19	0.01	1.02	0.02	-	-	0.2	0.11	0.32	13.81	99.19	99.46
(n=6)	Max	44.78	1.54	39.36	0.02	2.11	0.02	bdl	0.01	0.23	0.19	0.35	13.91	99.39	99.54
	Min	44.19	1.29	38.25	0.01	0.63	0.01	bdl	bdl	0.17	0.05	0.26	13.7	99.06	99.39
UCC[1]	Average	65.89	0.5	15.17	-	4.49	4.19	2.2	0.07	3.89	3.39	0.2	-	-	-
Cretaceous Red Sea[2]	Average	47.64	2.06	34.6	-	1.72	0.1	0.28	0	0.1	0.1	0.1	13.1	-	-

[1] Taylor and McLennan (1985), [2] Baioumy (2014) and bdl = below detection limit

Table 5.2: Mineralogy of the <2 µm fractions of studied Cretaceous - Tertiary kaolins.

Age		Kaolinite %	Quartz %	Anatase %	Hematite %	Goethite %
Cretaceous	Average	98	2	1	1	1
(n=15)	Max	99	6	1	1	1
	Min	93	1	1	1	1
Tertiary	Average	82	18	1	1	1
(n=13)	Max	91	28	2	1	2
	Min	69	7	1	1	1

However, they show relative enrichments in Al_2O_3, Fe_2O_3, Na_2O, K_2O, and P_2O_5 and relative depletions in SiO_2, MgO, and CaO when compared with the average clay fractions from Cretaceous Red Sea Kaolin deposit, Egypt (Baioumy, 2014) (Table 5.1).

During weathering and transportation processes, Al and Ti exhibit low solubility (Paikaray *et al*., 2008) and can strongly affect the source rock characteristics. Bivariate diagram of TiO_2 versus Al_2O_3 for the samples (Fig. 5.1) indicates that the Cretaceous kaolin deposits mostly originated from granitic to granodioritic source rocks while the Tertiary kaolin deposits were likely to have originated from granodioritic to gabbroic source rocks.

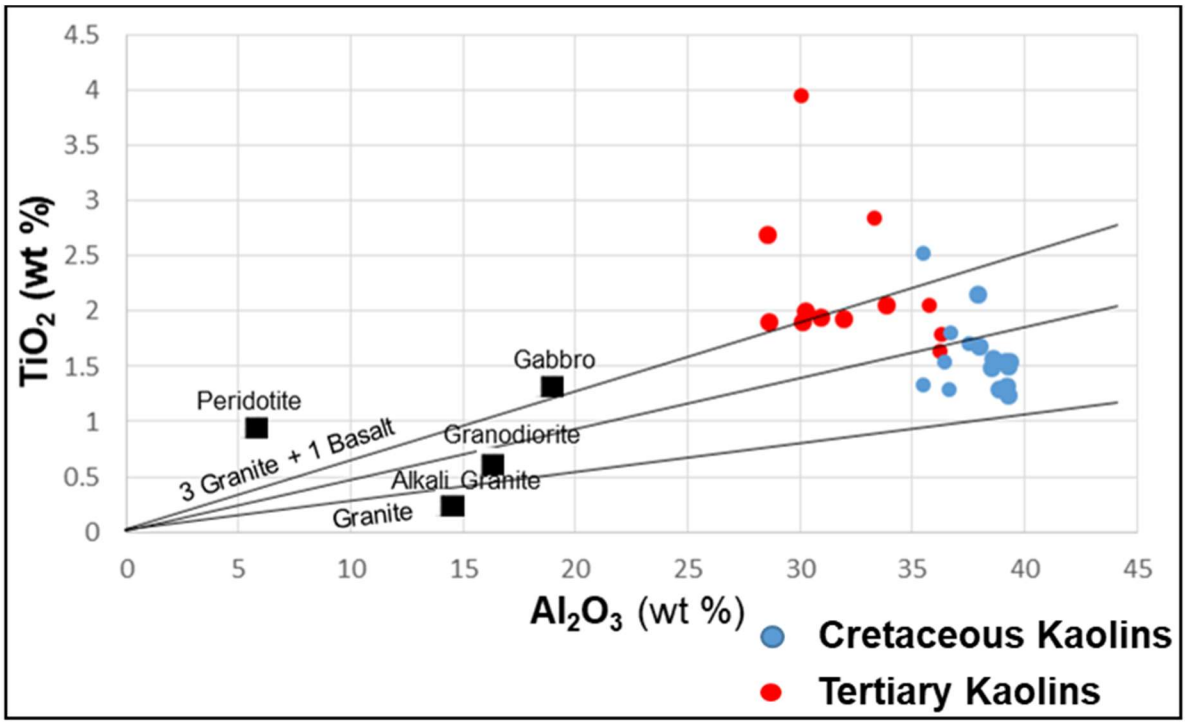

Figure 5.1: TiO_2 versus Al_2O_3 bivariate plot of the <2 µm fractions of the studied Cretaceous – Tertiary kaolins (Fields after Paikaray *et al*., 2008).

Discrimination diagrams proposed by Roser and Korsch (1988) (Figs. 5.2 and 5.3) in distinguishing the source area compositions of sedimentary rocks into four provenance zones (mafic, intermediate, felsic igneous, and quartzose sedimentary provenance) suggest predominantly source rocks with mafic rocks for both the Cretaceous and Tertiary

kaolin deposits. The use of ratios of TiO_2, Fe_2O_3, MgO, Na_2O, and K_2O all to Al_2O_3 is to circumvent the problem of biogenic CaO and $CaCO_3$ and also biogenic SiO_2 (Oni *et al*., 2014). Mafic rocks have been proposed to be responsible for high Ti and Ni contents in sediments (Floyd *et al*., 1989). However, ilmenite from granite has been indicated to be the source of high TiO_2 in Scotian Basin sediments due to the positive correlation between Zr and both Ti and Ni (Pe-Piper *et al*., 2008). Therefore, weak correlation between TiO_2 and Zr (Fig. 5.4) excludes the possibility of mafic rocks as the sole source rocks for the kaolin deposits but rather a combination of contributions of both felsic and mafic rocks as indicated by the TiO_2 versus Al_2O_3 plot.

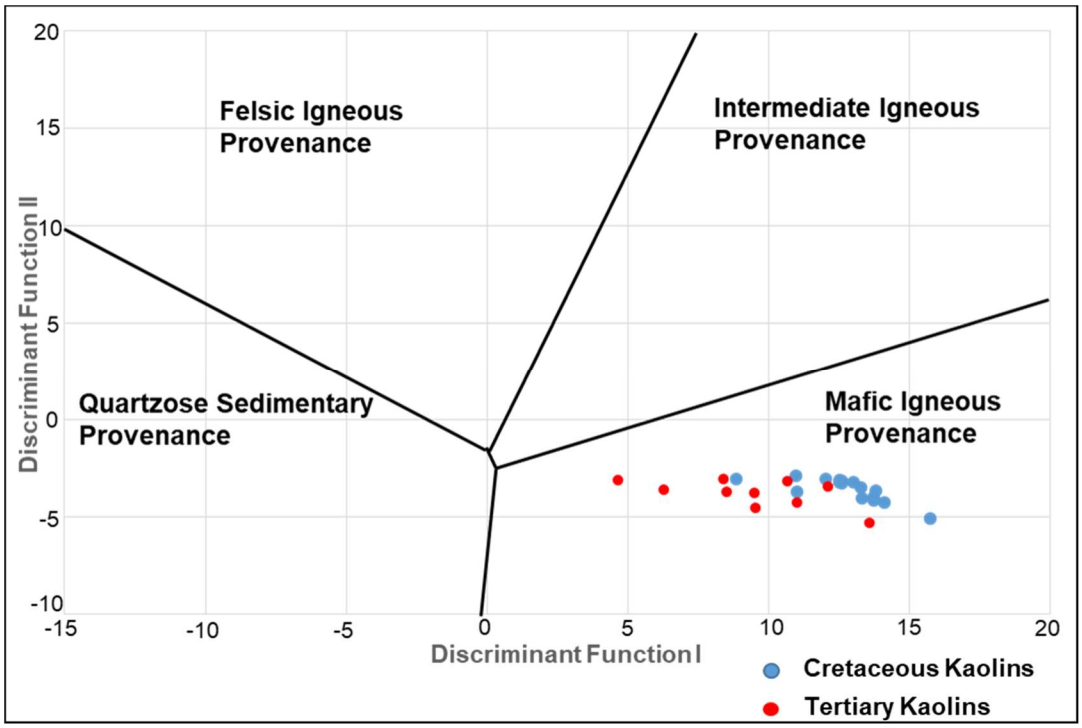

Figure 5.2: Discrimination diagrams for the provenance of the <2 µm fractions of the studied Cretaceous – Tertiary kaolins using raw major oxide concentrations, DFI= 0.445 TiO_2+ 0.070 Al_2O_3 - 0.250 Fe_2O_3- 1.142 MgO + 0.438 CaO + 1.475 Na_2O + 1.426 K_2O - 6.861; DFII = -1.773 TiO_2+ 0.607 Al_2O_3 + 0.760 Fe_2O_3- 1.500 MgO + 0.616 CaO + 0.509 Na_2O - 1.224 K_2O -9.090 (Fields after Roser and Korsch, 1988).

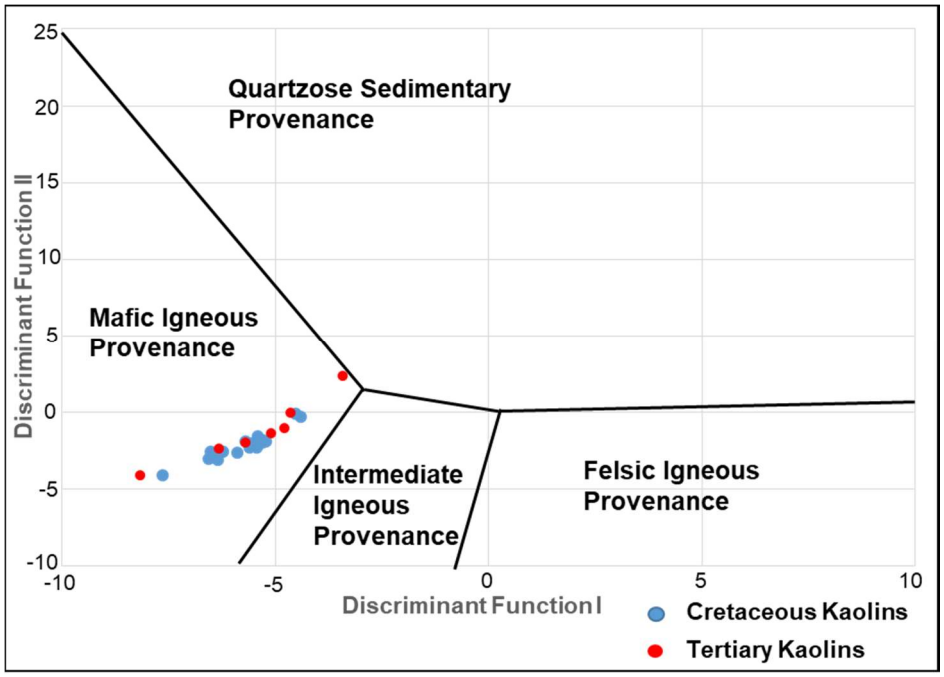

Figure 5.3: Discrimination diagrams for the provenance of the <2 µm fractions of the studied Cretaceous – Tertiary kaolins using ratios of major oxides to Al_2O_3, DFI = 56.500 TiO_2/Al_2O_3 - 10.879 Fe_2O_3/Al_2O_3 + 30.875 MgO/Al_2O_3 - 5.404 Na_2O/Al_2O_3 + 11.112 K_2O/Al_2O_3 - 3.89; DFII = 30.638 TiO_2/Al_2O_3 - 12.541 Fe_2O_3/Al_2O_3 + 7.329 MgO/Al_2O_3 + 12.031 Na_2O/Al_2O_3 + 35.402 K_2O/Al_2O_3 - 6.382 (Fields after Roser and Korsch, 1988).

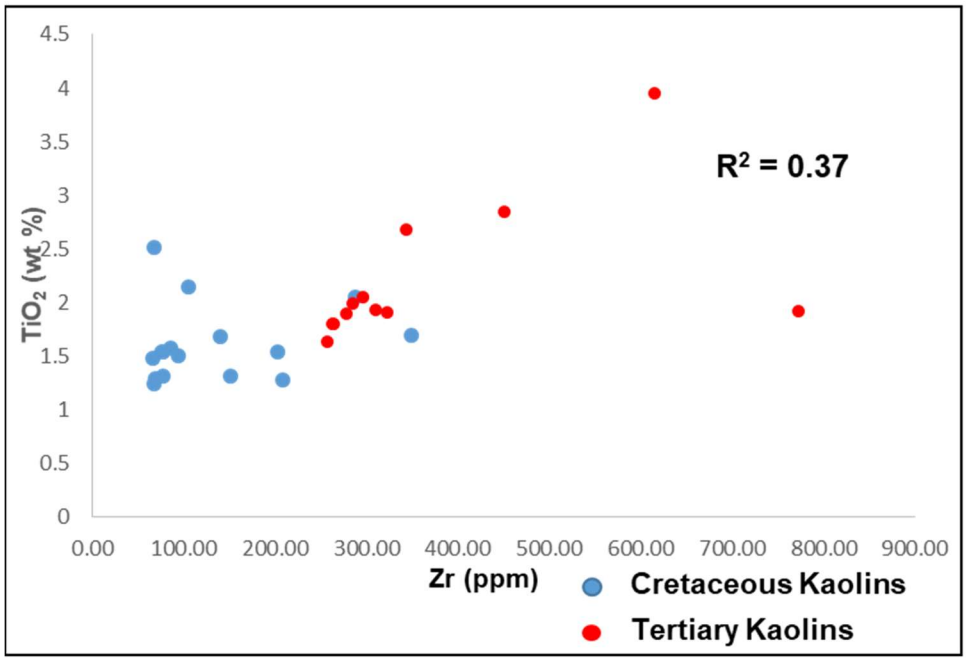

Figure 5.4: TiO_2 versus Zr of the <2 µm fractions of the studied Cretaceous – Tertiary kaolins.

Hence, the exclusive 'mafic igneous provenance' for the kaolins as inferred from the discriminant functions diagram of Roser and Korsch (1988) will not be considered.

Major element compositional variations in sedimentary rocks are strongly affected by chemical weathering. The degree of chemical weathering in the source area can be evaluated in terms of the chemical index of alteration (CIA) proposed by Nesbitt and Young (1982). The index is expressed as:

$$CIA = [(Al_2O_3) / (Al_2O_3+CaO^*+Na_2O+K_2O)] \times 100 \text{ in molecular proportions} \quad (5.1)$$

Where, CaO* represents CaO associated with the silicate fraction of the sample. McLennan *et al*. (1993) proposed that CaO values should be accepted if $CaO<Na_2O$ and when $CaO > Na_2O$, it is assumed that the concentration of CaO equals that of Na_2O. The CIA values for the Cretaceous kaolin deposits range from 98.40 to 99.39, and 96.98 to 98.64 for the Tertiary kaolin deposits (Table 5.1). The $Al_2O_3 – (CaO^* + Na_2O) – K_2O$ (A-CN-K) ternary plot with CIA shows that the source rocks have experienced intense chemical weathering under wet humid climatic condition (Fig. 5.5).

The chemical index of weathering (CIW) proposed by Harnois (1988) is similar to CIA except for the exclusion of K_2O and hence not sensitive to post-depositional K-enrichment. It is defined as:

$$CIW = [(Al_2O_3) / (Al_2O_3+CaO^*+Na_2O)] \times 100 \text{ in molecular proportions} \quad (5.2)$$

Where, CaO* is as defined in equation (5.1). The CIW values range from 98.95 to 99.89 and 98.98 to 99.35 for the Cretaceous and Tertiary kaolin deposits, respectively (Table 5.1). These values are supportive of the earlier conclusion that the chemical weathering in the source area was intense as indicated by CIA.

5.1.2 Trace Elements

Mean values and ranges of trace element compositions are presented in Table 5.3. Trace elements such as Ba, Cr, Sr, V, and Zr have concentrations more than 100 ppm in most of the samples except for Lakiri deposits having values less than 100 ppm for Ba, Sr, and Zr.

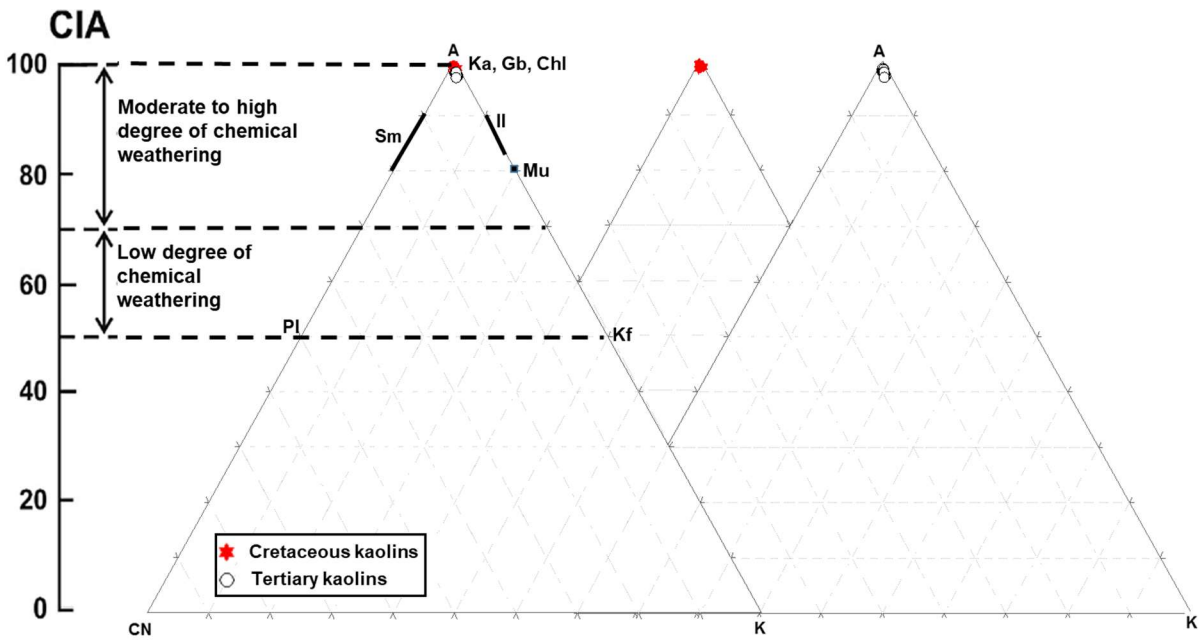

Figure 5.5: A-CN-K (Al_2O_3 – CaO* + Na_2O – K_2O) ternary diagram of the <2 µm fractions of the studied Cretaceous to Tertiary kaolins combined with CIA (Fields after Nesbitt and Young, 1982; Hofer *et al*., 2013).

The clay fractions were enriched in Cr, Nb, Sc, Th, U, V, and Zr and depleted in Ba, Co, Rb, and Sr respectively relative to the average Upper Continental Crust (UCC) (Table 5.3). Comparison with the clay fractions of the Red Sea Cretaceous sedimentary kaolin deposits (Egypt) show that the kaolin deposits from this study show relative enrichments in Ba, Co, Cr, Rb, Sr, and Th, and depletions in Ni, U, V, Y, and Zr (Table 5.3).

Immobile element ratios such as La/Sc, Th/Sc, Zr/Sc are good provenance indicators (Mishra and Sen, 2012). The ratios of Th/Sc, La/Sc, and Th/Cr are significantly different in felsic and mafic rocks and may allow constraints on the average source rock composition (Cullers, 1994; Cox *et al.*, 1995). The Th/Sc, La/Sc, and Th/Cr ratios fall within the range of values obtained for sediments from felsic rocks (Table 5.4). In a plot of elemental ratios, such as La/Sc versus Th/Co (Fig. 5.6), all data plot in the field of felsic rock provenance.

Table 5.3: Trace elements concentrations (ppm) of the <2 µm fractions of Cretaceous to Tertiary kaolins from Eastern Dahomey and Niger Delta Basins, Nigeria, and for average Upper Continental Crust (UCC) and Cretaceous Red Sea kaolin deposits (Egypt).

Deposit		Ba	Co	Cr	Nb	Ni	Rb	Sc	Sr	Th	U	V	Y	Zr
Awo-Omama	Average	209.09	3.51	150.11	77.23	30.16	18.12	19.09	125.19	25.74	4.3	157.88	22.23	356.82
(n=6)	Max	254.68	3.9	177.37	125.3	34.88	23.74	22.73	157.2	28.38	5.9	197.5	34.74	616.18
	Min	153.32	3.25	122.48	73.69	26.41	9.23	17.04	91.94	22.27	2.77	140.87	13.26	257.75
Ubulu-Uku	Average	339.02	3.53	109.76	99.72	26.31	35.8	16.32	195.27	26.47	5.36	136.19	25.79	373.64
(n=7)	Max	428.32	6.1	125.41	202.6	36.18	39.1	18.57	211.4	31.8	6.39	190.77	37.73	773.9
	Min	285.34	2.03	83.18	73.69	18.7	28.19	12.18	170.22	19.92	4.42	98.21	16.55	278.67
Eruku	Average	231.48	8.5	136.02	37.77	46.7	10.2	16.84	162.34	29.6	4.07	131.77	16.58	153.13
(n=9)	Max	366.87	10.6	149.46	48.26	54.01	13.55	19.13	315.37	38.07	5.98	182.52	26.66	348.65
	Min	113.16	5.93	103.46	33.72	42.72	7.42	14.63	59.78	12.65	2.94	103.86	10.16	67.21
Lakiri	Average	78.47	9.31	138.79	34.57	49.73	5.11	17.51	48.88	28.8	2.56	130.23	10.75	76.91
(n=6)	Max	174.48	12.2	160.39	36.1	61.53	8.4	20.14	132.75	40.55	3.09	209.85	18.21	94.26
	Min	37.92	6.71	124.18	29.33	40.76	2.74	15.67	18.02	20.61	2.23	96.69	7.49	67.69
UCC[1]	Average	550	17	83	12	44	112	13.6	350	10.7	2.8	107	22	190
K. Red Sea[2]	Average	92.2	3.82	123.6	97.6	103	0.92	-	118.8	11.48	7.01	159.4	67.4	630.8

[1] McLennan (2001), [2] Baioumy (2014), and K = Cretaceous

Table 5.4: Elemental ratios for the <2 µm fractions of Cretaceous to Tertiary kaolins from Eastern Dahomey and Niger Delta Basins, Nigeria compared to the ratios in similar fractions derived from felsic and mafic rocks.

Deposit		Eu/Eu*	Th/Sc	La/Sc	Th/Cr	Ni/Co	Th/U	V/Cr	LREE/HREE	LaN/SmN	CeN/YbN
Awo-Omama	Average	0.72	1.35	6.68	0.17	8.63	6.28	1.07	23.78	6.75	21.02
(n=6)	Max	0.78	1.52	8.21	0.19	10.75	8.29	1.38	27.5	7.49	26.23
	Min	0.68	1.21	5.97	0.15	7.26	4.41	0.85	15.35	5.88	10.55
Ubulu-Uku	Average	0.75	1.63	7.79	0.24	7.78	4.98	1.25	20.72	5.62	20.35
(n=7)	Max	0.8	1.82	9.1	0.34	9.23	6.35	0.92	24.86	6.42	25.88
	Min	0.7	1.35	6.25	0.21	5.94	4.23	1.73	17.7	4.63	14
Eruku	Average	0.77	1.76	7.42	0.22	5.32	7.44	0.99	25.8	5.45	42.55
(n=9)	Max	0.86	2.3	9.74	0.27	7.37	10.27	0.77	35.49	6.56	80.39
	Min	0.7	0.77	3.93	0.09	4.52	3.73	1.76	22.45	3.67	29.62
Lakiri	Average	0.76	1.65	7.52	0.21	5.39	11.47	0.93	38.24	8.75	60.98
(n=6)	Max	0.97	2.32	19.96	0.27	6.08	16.48	1.31	77.87	12.74	167.92
	Min	0.66	1.32	2.24	0.13	4.98	7.29	0.7	18.34	4.78	19.41
Felsic Rocks[1]	Max	0.83	18.1	27.7	4						
	Min	0.32	0.64	0.7	0.067						
Mafic Rocks[1]	Max	1.02	0.4	1.1	0.045						
	Min	0.7	0.05	0.4	0.002						

[1] Cullers (2000); $Eu/Eu^* = Eu_N / (Sm_N x Gd_N)^{0.5}$

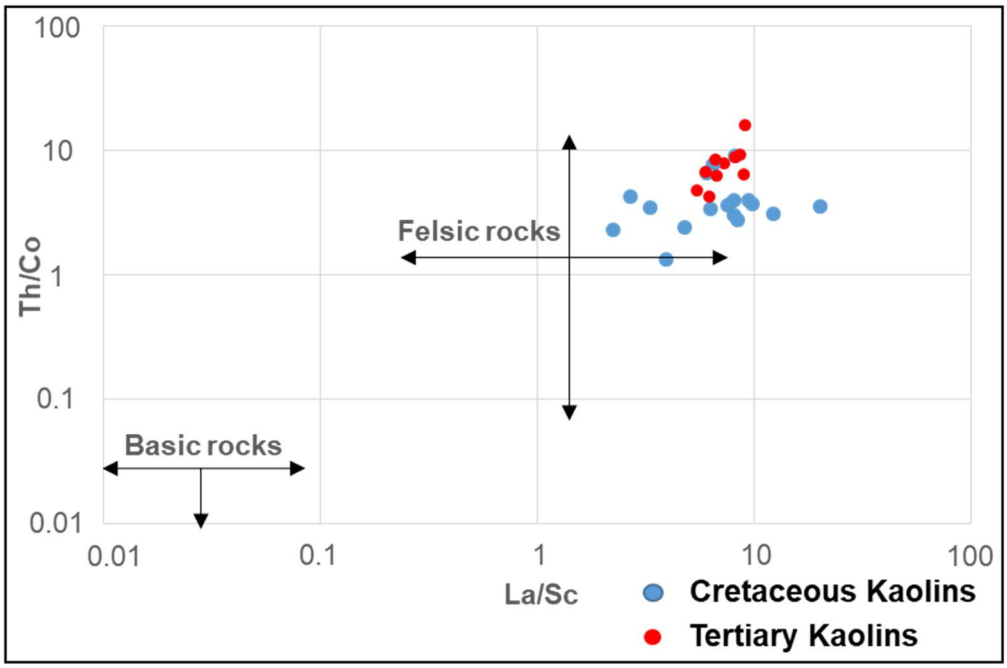

Figure 5.6: La/Sc versus Th/Co plot for the <2 µm fractions of the studied Cretaceous to Tertiary kaolins (Fields after Lopez *et al*., 2005).

Furthermore, the ternary La-Th-Sc diagram shows that the data plotted in the field corresponding to felsic rocks (Fig. 5.7) predominantly granitic with some data plotting between granite and granodiorite compositions. This suggests that the kaolins could as well have source rocks with granodiorite compositions similar to the earlier deductions from the TiO_2 versus Al_2O_3 plot.

The average Th/U ratios of 7.44, 11.47, 6.28, and 4.98 obtained for Eruku, Lakiri, Awo-Omama, and Ubulu-Uku kaolin deposits, respectively, are relatively higher than 3.5 for UCC (McLennan, 2001). This indicates more intense weathering in the source areas or sediment recycling because both weathering and sediment recycling typically result in the loss of U, leading to an increase in the Th/U ratios. Sediment recycling increases the Zr/Sc ratios with zircon enrichment (Tao *et al*., 2013). It is therefore a useful measure of heavy metal concentration (McLennan, 1989).

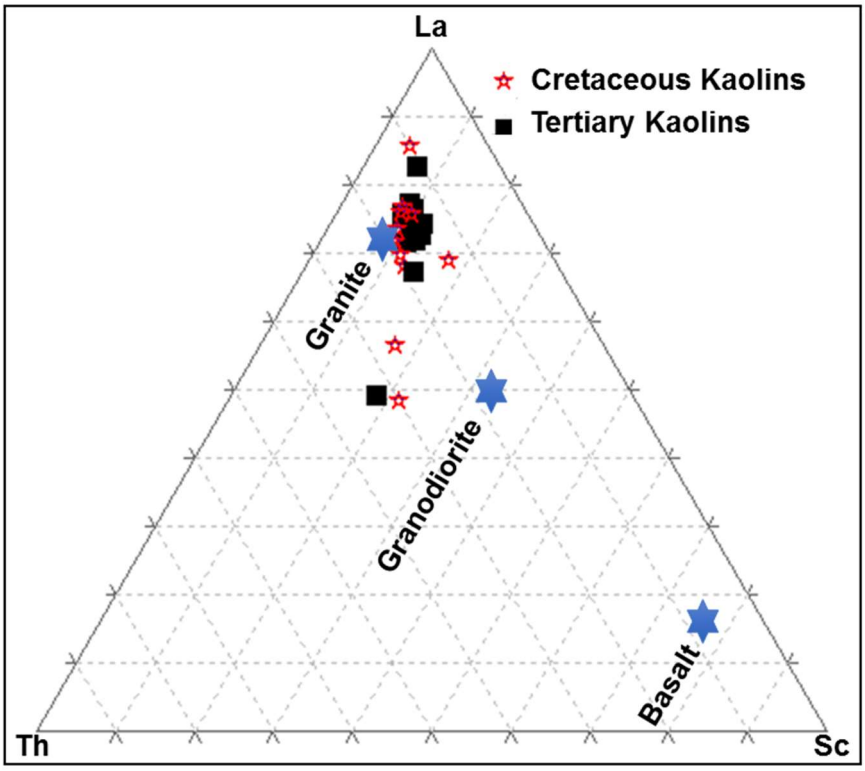

Figure 5.7: La-Th-Sc plot for the <2 µm fractions of the studied Cretaceous to Tertiary kaolins (Fields after Lopez *et al*., 2005).

The bivariate Th/Sc versus Zr/Sc plot (Fig. 5.8) indicates that the provenance was not only controlled by source composition but also by sediment recycling. This is evident because in the first-cycle sediments, Th/Sc ratios will show a positive correlation with Zr/Sc, depending on the nature of the source rock, whereas Zr/Sc ratios in mature or recycled sediments display considerable variation with little or no corresponding change in the Th/Sc ratio (McLennan *et al*., 1993). The influence of sediment recycling is more conspicuous in the Tertiary kaolin deposits.

In evaluating paleoredox conditions, Ni/Co ratios > 5 represent suboxic and anoxic environments, whereas ratios < 5 suggest oxic environments (Jones and Manning, 1994). In addition, Gross (1964) and Landergreen and Manhem (1963) obtained V/Cr ratios of 1.1 and 0.75 respectively for anoxic recent marine to brackish water sediments and higher values between 2 and 10 for oxic environments. The Ni/Co ratios obtained for the kaolins vary from 4.52 to 10.75 (Table 5.4), indicating that they were deposited in a dysoxic to

anoxic depositional environment. The V/Cr ratios for the kaolins vary from 0.70 to 1.76, suggesting that they were deposited in an anoxic environment of deposition. In addition, the V versus Ni diagram is suggestive of a marine anoxic depositional environment (Fig. 5.9).

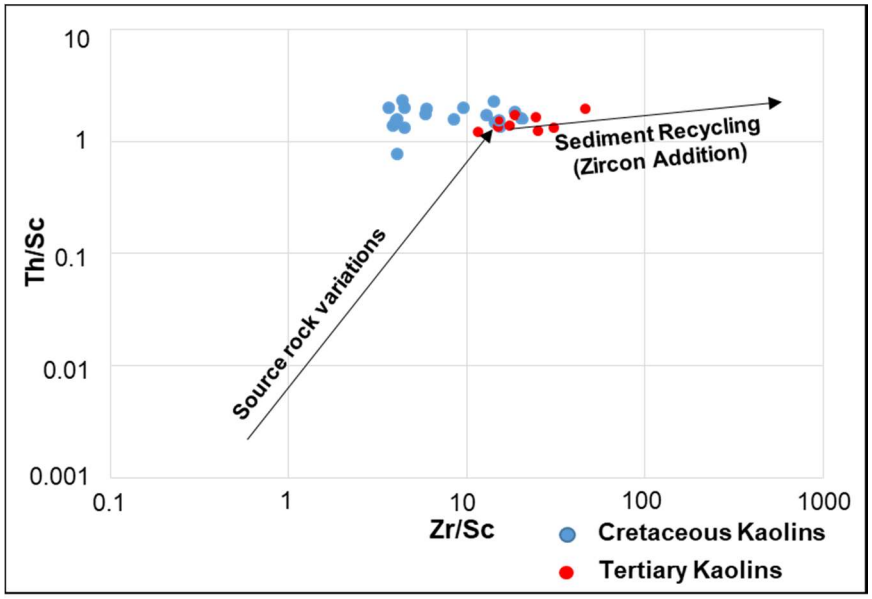

Figure 5.8: Bivariate Th/Sc versus Zr/Sc plot for the <2 µm fractions of the studied Cretaceous to Tertiary kaolins (Fields after McLennan *et al*., 1993).

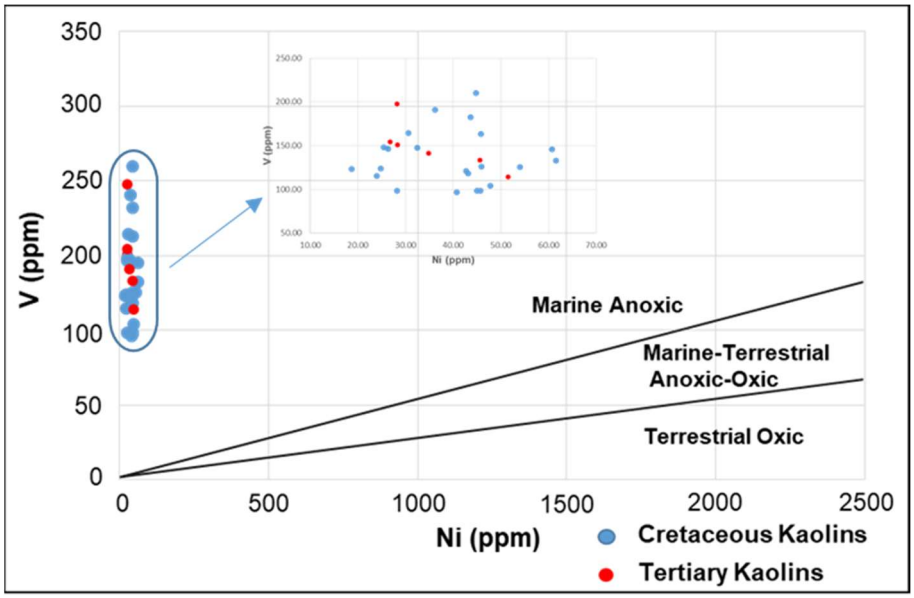

Figure 5.9: Cross plot of V versus Ni for the <2 µm fraction of the studied Cretaceous to Tertiary kaolins (Fields after Akinlua *et al.,* 2010).

From the foregoing, it is clear that the kaolins were formed in a restricted oxygen-poor (anoxic) depositional environment which can be explained in relation to the series of horst and graben structural framework models of the Eastern Dahomey and Niger Delta Basins (Whiteman, 1982; Onuoha, 1999; Ajayi *et al*., 2006).

5.1.3 Rare Earth Elements (REEs)

The REE absolute mean and range values are presented in Table 5.5. The absolute mean REE concentrations were in decreasing order of Eruku > Lakiri > Awo-Omama > Ubulu-Uku kaolin deposits, respectively. The average LREE obtained from this study show relative enrichment in comparison to the UCC and clay fractions of the Red Sea Cretaceous sedimentary kaolin deposits (Egypt) and depletion in average HREE relative to the clay fractions of the Red Sea Cretaceous sedimentary kaolin deposits (Egypt) (Table 5.5). The absolute REE values were chondrite-normalised using chondrite REE concentrations provided by Haskin *et al*. (1971) (Appendix 5.1). The average chondrite-normalised REE patterns for the clay fractions of the Cretaceous and Tertiary kaolin deposits are plotted (Fig. 5.10).

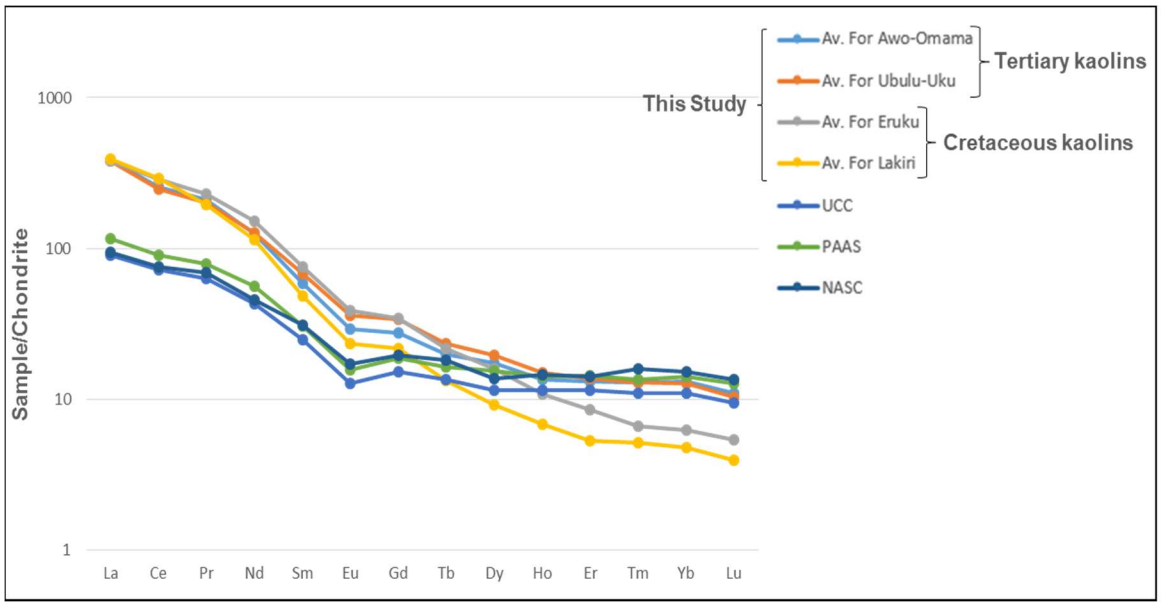

Figure 5.10: Chondrite-normalised REE pattern of average of the <2 µm fractions of Cretaceous to Tertiary kaolins from Eastern Dahomey and Niger Delta Basins, Nigeria, and for average Upper Continental Crust (UCC), average post-Archean Australian Shale (PAAS), and average North American Shale (NASC).

Table 5.5: Rare earth element (REE) concentrations (ppm) of the <2 μm fractions of Cretaceous to Tertiary kaolins from Eastern Dahomey and Niger Delta Basins, Nigeria, and for average Upper Continental Crust (UCC) and Cretaceous Red Sea kaolin deposits (Egypt).

Deposit		**La**	**Ce**	**Pr**	**Nd**	**Sm**	**Eu**	**Gd**	**Tb**	**Dy**	**Ho**	**Er**	**Tm**	**Yb**	**Lu**	**ΣREE**
Awo-Omama	Average	127.5	224.98	23.41	74.92	10.58	2.02	6.9	0.93	5.27	0.94	2.61	0.39	2.64	0.38	483.5
(n=6)	Max	153.63	285.92	31.77	106.06	14.34	2.79	8.55	1.18	7.34	1.4	4.06	0.62	4.23	0.61	616.71
	Min	127.5	169.76	16.98	53.28	7.49	1.46	4.85	0.65	3.3	0.56	1.61	0.23	1.63	0.24	364.18
Ubulu-Uku	Average	125.52	219.65	22.53	76.69	12.35	2.48	8.44	1.1	5.91	1.05	2.75	0.39	2.56	0.35	481.8
(n=7)	Max	150.92	248.62	24.39	84.12	13.75	2.97	9.76	1.3	7.83	1.51	4.17	0.56	4.04	0.53	546.74
	Min	109.24	191.9	18.65	61.15	9.45	2	6.26	0.72	4.17	0.72	1.75	0.25	1.69	0.23	408.16
Eruku	Average	125.37	253.17	25.94	90.99	13.61	2.67	8.55	1.03	4.79	0.76	1.72	0.2	1.25	0.18	530.23
(n=9)	Max	180.92	412.07	44.59	169.8	27.03	5.04	15.13	1.67	7.65	1.04	2.75	0.29	2.06	0.3	868.62
	Min	64.72	108.64	11.19	38.36	5.43	1.36	4.34	0.56	2.43	0.43	1.1	0.13	0.82	0.13	239.87
Lakiri	Average	129.53	254.99	21.85	68.41	8.81	1.6	5.44	0.63	2.79	0.48	1.07	0.16	0.96	0.13	496.85
(n=6)	Max	348.14	727.78	63.27	209.52	28.21	5.01	17.76	1.75	6.04	0.85	1.47	0.21	1.2	0.18	1413.1
	Min	42.66	82.4	6.56	21.03	3.17	0.61	1.91	0.33	1.58	0.33	0.91	0.09	0.81	0.1	163.24
UCC[1]	Average	30	64	7.1	26	4.5	0.88	3.8	0.64	3.5	0.8	2.3	0.33	2.2	0.32	146.37
Crt. Red Sea[2]	Average	61.64	119.8	12.78	43.32	8.16	1.64	7.04	1.28	8.04	1.58	4.58	0.68	4.4	0.64	275.76

[1] McLennan (2001) and [2] Baioumy (2014)

The pattern shows REE fractionation in the source area. Fractionation of REE during sedimentary processes is intensified under intense chemical weathering conditions (Dypvik and Brunfelt, 1976). The LREE are enriched relative to the HREE and the former constitute a large part of the ΣREE. The REE patterns are useful in provenance determination.

Low LREE/HREE ratio and no Eu anomalies reflect mafic source area composition, while high LREE/HREE and Eu anomalies reflect felsic source area composition (Cullers and Graf, 1983; Cullers, 1994). Hence, the high LREE/HREE ratios and EU anomalies in the clay fraction of the Cretaceous and Tertiary kaolin deposits suggest felsic source rocks for these deposits. In addition, the Eu/Eu* ratios also indicate that the kaolins were derived from felsic rocks (Table 5.4). Felsic rocks usually have negative Eu anomaly (Eu/Eu* < 0.85) due to lithospheric or intercrustal feldspar fractionation or breakdown of feldspars during weathering processes (Condie *et al.,* 1992). The fractionation indices measuring the enrichment of LREE to HREE such as LaN/SmN and CeN/YbN ratios show a wide range of variation from 3.67 to 12.74 and 10.55 to 167.92 respectively. These further suggest LREE fractionation relative to HREE (Ajayi *et al.,* 2006; Oyebanjo *et al.,* 2014).

5.2 Tectonic Settings

Several researchers (Bhatia, 1983; Bhatia and Crook, 1986; Roser and Korsch, 1986, 1988; McLennan *et al*., 1990; and Verma and Armstrong-Altrin, 2016) have used the chemical compositions of sediments to discriminate tectonic settings. The major-element based bivariate plots by Bhatia (1983) and Roser and Korsch (1986) are commonly used. They involve the use of immobile (such as Al_2O_3, TiO_2 and Fe_2O_3) and variably mobile major elements, including Na_2O and K_2O. To avoid the uncertainties associated with this variability, the Bhatia (1983) approach was used in this study which is based on the use of discriminant functions with constant factors as against Roser and Korsch (1986) which is based on the concentrations of the highly mobile major elements (Na and K). The consistency of the Bhatia (1983) classification of tectonic settings for the studied kaolins was further tested using the Verma and Armstrong-Altrin (2016) approach which is based

on the use of both major and trace elements. The bivariate discrimination plot (DF2 versus DF1) of Bhatia (1983) favours passive continental margins (Fig. 5.11). High CaO as carbonate correction was not necessary due to the low concentration of CaO in all the clay fractions of the kaolin deposits.

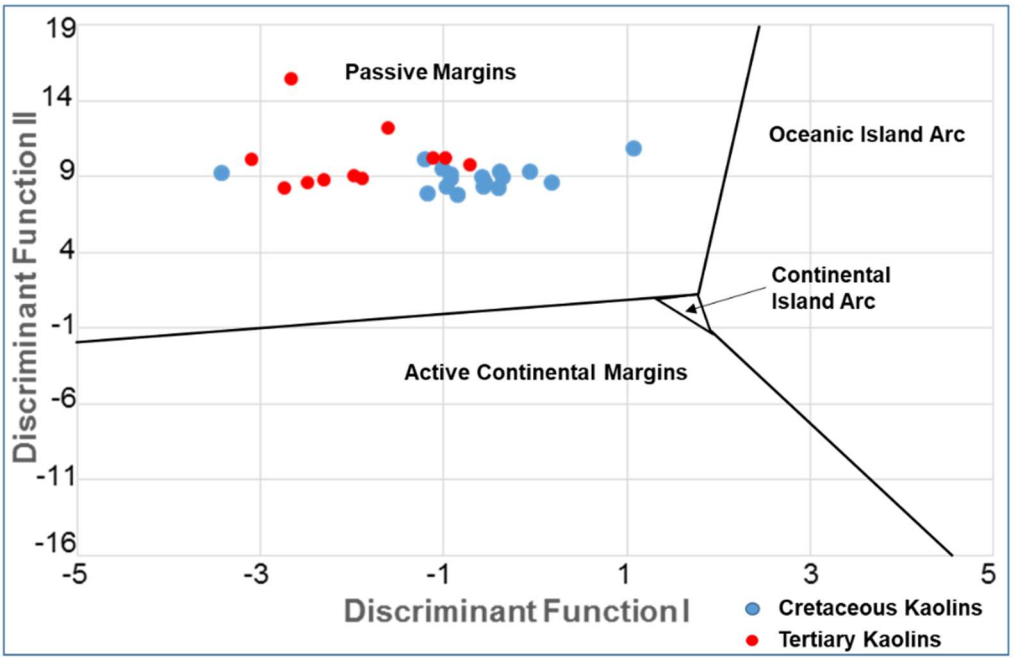

Figure 5.11: Discrimination function diagram for sedimentary tectonic settings of the <2 µm fractions of the studied kaolin deposits (Fields after Bhatia, 1983). DFI = −0.0447SiO_2 − 0.972TiO_2 + 0.008Al_2O_3 − 0.267Fe_2O_3 + 0.208FeO − 3.082MnO + 0.140MgO + 0.195CaO + 0.719Na_2O − 0.032K_2O + 7.510P_2O_5 + 0.303; DFII = −0.421SiO_2 + 1.998TiO_2 − 0.526Al_2O_3 − 0.551Fe_2O_3 − 1.610FeO + 2.720MnO + 0.881MgO − 0.907CaO − 0.177Na_2O − 1.840K_2O + 7.244P_2O_5 + 43.57.

Verma and Armstrong-Altrin (2016) treated several geochemical data with isometric log-ratio transformation (ilr) to provide a new way of discriminating the active and passive margin settings. Two new discriminant function-based multidimensional diagrams were proposed for the discrimination of active and passive margin settings from the ilr of major and trace elements. The discrimination function based on major element oxides, $DF_{(A\text{-}P)M}$ is given as:

$$DF_{(A\text{-}P)M} = (3.005 \times ilr1_{Tim}) + (2.8243 \times ilr2_{Alm}) + (-1.596 \times ilr3_{Fem}) + (-0.7056 \times ilr4_{Mnm}) + (-0.3044 \times ilr5_{Mgm}) + (0.6277 \times ilr6_{Cam}) + (-1.1838 \times ilr7_{Nam}) + (1.5915 \times ilr8_{Km}) + (0.1526 \times ilr9_{Pm}) - 5.9948 \quad (5.3)$$

Ten major element oxides (SiO_2, TiO_2, Al_2O_3, Fe_2O_3, MnO, MgO, CaO, Na_2O, K_2O, and P_2O_5) were first adjusted to 100 % on an anhydrous basis (SiO_2A to P_2O_5A) and then transformed to nine isometric log-ratios ($ilr1_{TiM}$ to $ilr9_{PM}$). The group centroid were as follows: for active margin C_{AM} = -1.00378 and for passive margin C_{PM} = 0.84703 with an average of these two values of -0.078376 taken as the tectonic boundary $(A\text{-}P)_{boundary}$. The discrimination function based on combined major element oxides and trace elements, $DF_{(A\text{-}P)MT}$ is given as:

$$DF_{(A\text{-}P)MT} = (3.2683 \times ilr1_{TiMT}) + (5.3873 \times ilr2_{AlMT}) + (1.5546 \times ilr3_{FeMT}) + (3.2166 \times ilr4_{MnMT}) + (4.7542 \times ilr5_{MgMT}) + (2.0390 \times ilr6_{CaMT}) + (4.0490 \times ilr7_{NaMT}) + (3.1505 \times ilr8_{KMT}) + (2.3688 \times ilr9_{PMT}) + (2.8354 \times ilr10_{CrMT}) + (0.9011 \times ilr11_{NbMT}) + (1.9128 \times ilr12_{NiMT}) + (2.9094 \times ilr13_{VMT}) + (4.1507 \times ilr14_{YMT}) + (3.4871 \times ilr15_{ZrMT}) - 3.2088 \quad (5.4).$$

The ten major element oxides (SiO_2 to P_2O_5) and six trace elements (Cr, Nb, Ni, V, Y, and Zr) were selected and adjusted to sum to 100 % (SiO_2 MT to Zr MT) and then transformed to 15 isometric log-ratios ($ilr1_{TiMT}$ to $ilr15_{ZRMT}$). The group centroid were as follows: for active margin C_{AMT} = -1.37443 and for passive margin C_{PMT} = 1.10752 with an average of these two values of -0.13345 taken as the tectonic boundary $(A\text{-}P)_{boundary}$.

The discrimination function values for major (M) and combined major and trace elements (MT) for clay fractions of each sample was calculated (Appendix 5.2) and plotted (Table 5.6 and Fig. 5.12) using equations 5.3 and 5.4. All the samples plot in the passive margin field.

The tectonic settings inferred for the studied Cretaceous and Tertiary kaolins is in agreement with the tectonic evolutionary history of the sedimentary basins in Nigeria. The passive margin comprises of Atlantic-type rifted continental margins developed along the

edges of the continent, ocean basins adjacent to collision orogens, and inactive or extinct convergent.

Table 5.6: Discriminant functions for major (M) and major and trace elements (MT) of the <2 μm fractions of the studied Cretaceous to Tertiary kaolins.

Deposit		Function (M)	Function (MT)
Awo-Omama (n=6)	Average	-14.34	10.28
	Max	-16.16	13.26
	Min	-9.34	9.19
Ubulu-Uku (n=7)	Average	-14.04	11.93
	Max	-15.36	17.62
	Min	-10.46	9.97
Eruku (n=9)	Average	-12.39	12.79
	Max	-21.08	14.11
	Min	-9.62	9.83
Lakiri (n=6)	Average	-11.75	14.29
	Max	-12.56	15.1
	Min	-9.94	12.97

Figure 5.12: Discriminant function diagrams for the <2 μm fractions of the studied Cretaceous to Tertiary kaolins: a. Major element oxides (M) based diagram; b. Combined major and trace element (MT) based diagram (Fields after Verma and Armstrong-Altrin, 2016).

Intra-cratonic and rift-bounded grabens (e.g the Benue Trough) formed on a thick continental crust are also categorized under the passive margin type (Okunlola and Idowu, 2012). The Eastern Dahomey and Niger Delta Basins are referred to as peri-oceanic basins formed at the periphery of the West African Craton (Omatsola and Adegoke, 1981).

5.4 Statistical Analyses of Geochemical Data

A correlation matrix indicating the correlation coefficients (r) between the major element oxides and LOI is presented in Table 5.7. Correlation coefficient values ($r > 0.5$) were considered significant. Significant positive correlations between Al_2O_3 and LOI; Fe_2O_3 and CaO; Fe_2O_3 and MnO; K_2O and TiO_2; Na_2O and P_2O_5 as well as significant negative correlations between Al_2O_3 with CaO, Fe_2O_3, K_2O, and MnO; Fe_2O_3 with SiO_2 and LOI; K_2O and LOI; Na_2O and MnO; and SiO_2 and TiO_2 were identified for the Cretaceous kaolins. For the Tertiary kaolins, there were significant positive Al_2O_3 and LOI; Fe_2O_3 and MgO; MgO and P_2O_5; MnO and TiO_2; and Na_2O with MgO and P_2O_5 as well as significant negative correlations between Al_2O_3 with K_2O and SiO_2; K_2O with Cr_2O_3 and LOI; and SiO_2 and TiO_2. These correlation pairs provided meaningful insights into the relationships among the variables. However, to establish the nature of these relationships, dimensional reduction through factor analyses using principal component method is needed. This allowed the reduction of redundant information into few factors that can explain the whole variability (Cravero *et al*., 2010).

Factor analyses was extended to include the major element oxides, LOI, trace elements, LREE, HREE, and Eu data. Based on the Scree plots (Figures 5.13 and 5.14), the first two components accounted 94.2 % of the data variability in the Cretaceous kaolins, whereas the first three components accounted for 96.8 % of the data variability in the Tertiary kaolins (Tables 5.8 and 5.9). Hence, the first two components for the Cretaceous kaolins and the first three components for the Tertiary kaolins were retained. This decision is consistent with the suggestion of Davis (2002) that components with total variance less than 4 % should not be considered.

Table 5.7: Pearson correlation matrix of the major element oxides and LOI of the studied Cretaceous - Tertiary kaolins.

	Al_2O_3	CaO	Cr_2O_3	Fe_2O3	K_2O	MnO	Na_2O	P_2O_5	SiO_2	TiO_2	L.O.I.	
Cretaceous												
Al_2O_3	1.000											
CaO	**-.547**	1.000										
Cr_2O_3	.071	-.404	1.000									
Fe_2O_3	**-.778**	**.589**	-.103	1.000								
K_2O	**-.686**	.272	.035	.231	1.000							
MnO	**-.738**	.327	-.065	**.507**	.405	1.000						
Na_2O	.200	.021	-.109	.088	-.331	**-.508**	1.000					
P_2O_5	-.176	.427	-.340	.487	-.149	-.107	**.817**	1.000				
SiO_2	-.003	-.337	.152	**-.603**	.431	.102	-.384	**-.593**	1.000			
TiO_2	-.387	.058	-.027	-.185	**.787**	.401	-.486	-.383	**.648**	1.000		
L.O.I.	**.923**	-.467	.044	**-.697**	**-.782**	-.485	.002	-.259	-.045	-.375	1.000	
	Al_2O_3	**CaO**	**Cr_2O_3**	**Fe_2O_3**	**K_2O**	**MgO**	**MnO**	**Na_2O**	**P_2O_5**	**SiO_2**	**TiO_2**	**L.O.I.**
Tertiary												
Al_2O_3	1.000											
CaO	-.014	1.000										
Cr_2O_3	.365	.245	1.000									
Fe_2O_3	-.388	.095	-.402	1.000								
K_2O	**-.617**	.037	**-.627**	.453	1.000							
MgO	-.237	.000	-.192	**.844**	.330	1.000						
MnO	-.216	.239	.460	-.087	-.225	.047	1.000					
Na_2O	-.423	-.191	-.050	.468	.286	**.676**	.208	1.000				
P_2O_5	.064	.038	.319	.479	-.159	**.781**	.201	**.605**	1.000			
SiO_2	**-.843**	-.046	-.261	-.145	.480	-.277	.191	.106	-.461	1.000		
TiO_2	-.382	.028	.450	-.342	-.321	-.136	**.673**	.342	.157	.483	1.000	
L.O.I.	**.984**	-.031	.404	-.344	**-.656**	-.164	-.148	-.406	.156	**-.868**	-.347	1.000

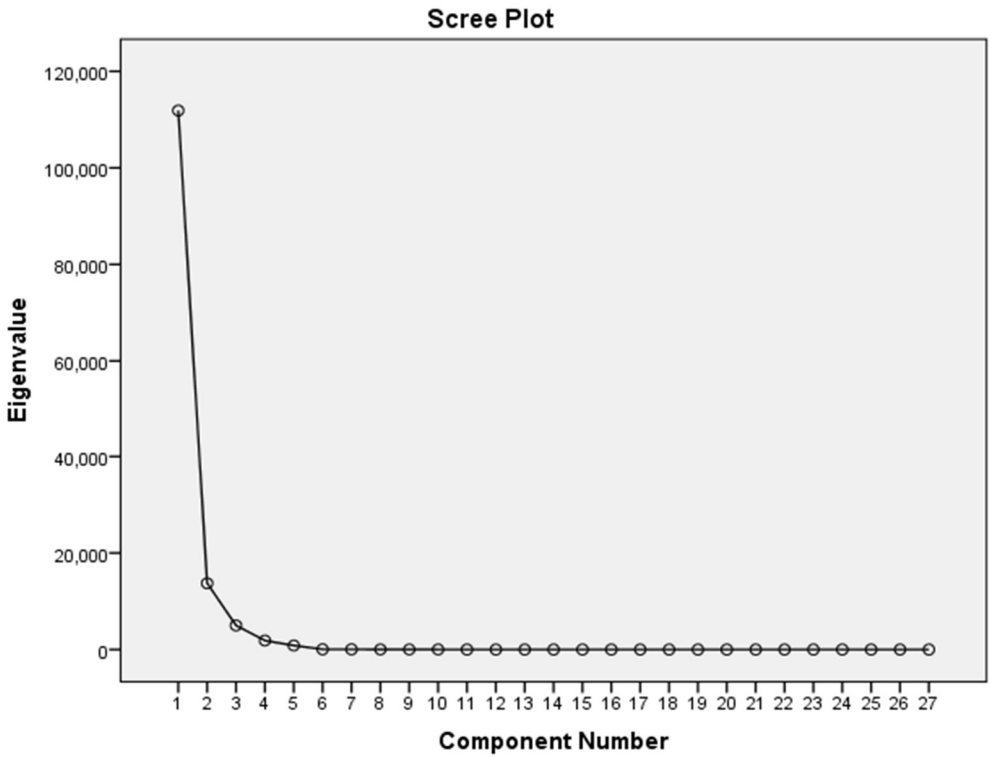

Figure 5.13: Scree plot of the studied Cretaceous kaolins.

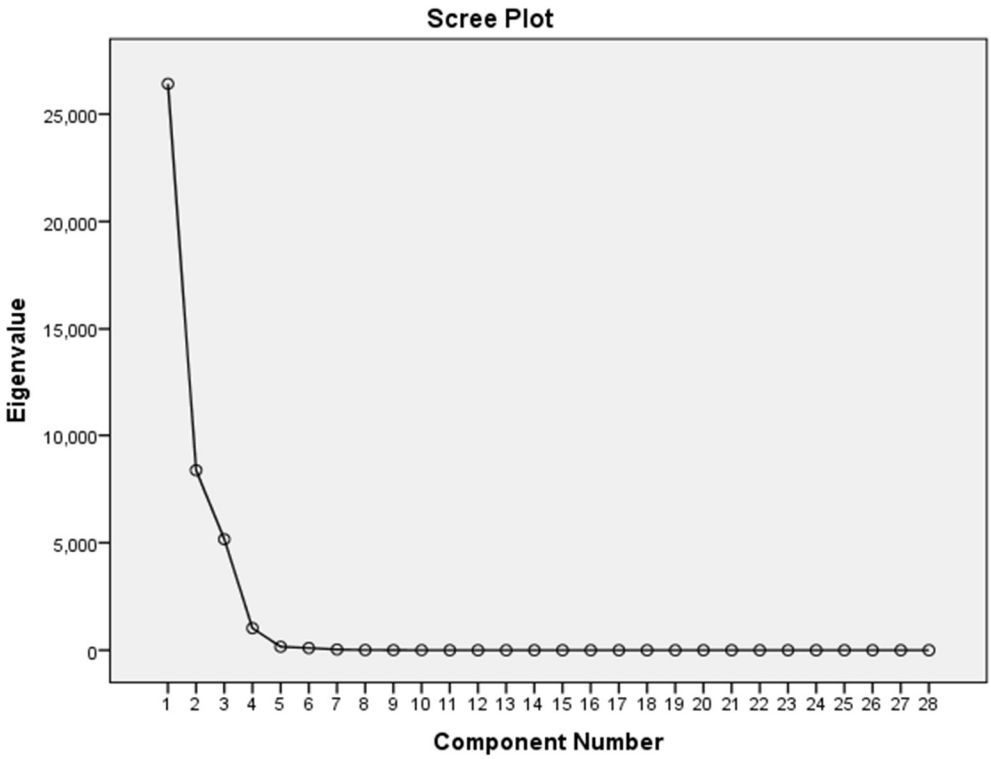

Figure 5.14: Scree plot of the studied Tertiary kaolins.

Table 5.8: Factor Loadings obtained from Principal Component Analysis of the studied Cretaceous kaolins.

	Components	
	1	2
Al_2O_3	**-.517**	.411
CaO	**.597**	-.383
Cr_2O_3	-.182	-.095
Fe_2O_3	.357	-.448
K_2O	**.598**	-.032
MnO	.350	-.289
Na_2O	-.037	-.107
P_2O_5	.377	-.156
SiO_2	-.015	.235
TiO_2	.458	-.032
L.O.I.	**-.551**	.307
Sc	.180	-.002
V	-.005	-.271
Cr	-.142	.305
Co	-.012	.468
Ni	-.047	**.508**
Rb	**.601**	-.030
Sr	**.942**	-.125
Y	**.728**	.177
Zr	.273	-.229
Nb	.347	-.155
Ba	**.955**	-.032
Th	**.532**	.459
U	**.838**	-.407
LREE	**.572**	**.820**
HREE	**.820**	.234
Eu	**.800**	.482
% of Variance	83.900	10.300

For the Cretaceous kaolins, the calculated components 1 and 2 explained 83.9 % and 10.3 % of the variance. Component 1 shows significant positive factor loadings (Table 5.8: bold numbers indicate significant factor loadings > 0.500) with CaO, K_2O, Rb, Sr, Y, Ba, Th, U, LREE, HREE, and Eu, and negative factor loadings with Al_2O_3 and LOI. Component 2 groups only Ni and LREE with positive loading values.

Table 5.9: Factor Loadings obtained from Principal Component Analysis of the studied Tertiary kaolins.

	Components		
	1	2	3
Al_2O_3	**-.764**	-.301	.154
CaO	.004	.006	.071
Cr_2O_3	**-.646**	.103	-.038
Fe_2O_3	**.642**	-.014	-.101
K_2O	**.842**	-.252	.196
MgO	**.513**	-.063	.030
MnO	.017	.467	.106
Na_2O	**.515**	.227	-.294
P_2O_5	.009	-.063	-.029
SiO_2	.488	.278	-.093
TiO_2	-.077	.479	-.310
L.O.I.	**-.774**	-.241	.234
Sc	-.472	.012	.415
V	-.090	.073	.106
Cr	**-.688**	-.310	.369
Co	.358	-.331	-.087
Ni	-.091	**-.569**	.095
Rb	**.866**	-.208	.167
Sr	**.893**	.142	.361
Y	.279	**.852**	.285
Zr	-.048	**.997**	-.054
Nb	.103	**.958**	.009
Ba	**.982**	.052	.152
Th	-.054	.408	**.710**
U	.494	**.631**	.189
LREE	-.061	.036	**.996**
HREE	-.060	**.708**	.200
Eu	**.600**	.114	**.760**
% of Variance	64.000	20.300	12.500

The component 1 for the Cretaceous kaolins represents the kaolinite factor which shows the inverse relationship between Al_2O_3 and CaO, K_2O, Rb, Sr, Y, Ba, Th, U, LREE, HREE, and Eu. These elements are related to input from felsic minerals. The positive correlation between Ni and LREE from component 2 suggest that the input from ferromagnesian minerals have influence on the total LREE contents.

The calculated components 1, 2, and 3 for the Tertiary kaolins explained 64 %, 20.3 %, and 12.5 % of the variance respectively. Component 1 shows significant positive factor loadings with Fe_2O_3, K_2O, MgO, Na_2O, Rb, Sr, Ba, and Eu, and negative significant factor loadings with Al_2O_3, Cr_2O_3, and Cr. Component 2 shows significant positive factor loadings with Y, Zr, Nb, U, and HREE, and negative significant factor loading with Ni. Component 3 groups only Th, LREE, and Eu with significant positive loading values (Table 5.9).

The component 1 for the Tertiary kaolins represents the kaolinite factor which shows the inverse relationship between Al_2O_3 and Fe_2O_3, K_2O, MgO, Na_2O, Rb, Sr, Ba, and Eu. These elements are related to input from both ferromagnesian and felsic minerals. Component 2 shows that the variations in the concentrations of associated trace elements are related to enhance survival of abrasion-resistant accessory minerals such as zircon rich in Zr and Y compared to less stable mafic phases such as pyroxene and amphiboles rich in Ti, Cr, and Ni (Ishiga *et al*., 1999). The positive correlation between Th, LREE, and Eu suggests the influence of felsic input on their contents since they are usually concentrated preferentially in residual liquids.

5.3 Conclusions

Based on the mineralogical and geochemical considerations, the following deductions have been made:

a) The geochemical evaluation show that the kaolins were predominantly derived from felsic (granitic) rocks in addition to contributions from intermediate (granodioritic) and mafic (gabbroic) rocks. In addition, factor analyses in geochemical provenance analysis also indicated a mixed provenance (felsic and mafic) for the kaolins.
b) The kaolins were formed under intense chemical weathering with influence of sediment recycling due to the enrichment in Zr particularly for the Tertiary kaolins. The geochemical parameters V/Cr, Ni/Co ratios and V versus Ni plot demonstrate that the kaolins were deposited under anoxic depositional paleoenvironment which

is consistent with the horst and graben structural geotectonic settings of the Eastern Dahomey and Niger Delta Basins.

c) The provenance characteristics suggest that the kaolins were deposited in passive margin settings.

Chapter Six

Paleoenvironmental Conditions of Formation of the Cretaceous-Tertiary kaolins within the Eastern Dahomey and Niger Delta Basins in Nigeria.

This chapter aimed to determine the paleoenvironmental conditions under which the Cretaceous-Tertiary kaolins within the Eastern Dahomey and Niger Delta Basins in Nigeria were formed (Specific Objective 2) based on Hypothesis 2. The oxygen and hydrogen stable isotope geochemistry of the studied kaolins were used to achieve specific objective 2.

6.1 Stable Isotope Signature

The isotopic data obtained for the nine (9) selected <2 μm fraction of the studied Cretaceous – Tertiary kaolins along with their respective quantitative estimates of the minerals present in them from XRD are presented in Table 6.1.

The XRD analyses of the selected samples show that they contain predominantly kaolinite (≥ 90 %) followed by quartz and to a less extent anatase, goethite, and hematite (Table 6.1a). The potential impact of contaminant minerals, notably quartz, on the stable isotope signature of the Paleogene/Neogene kaolins cannot be ascertained without knowing the $\delta^{18}O$ of the quartz. However, if this is authigenic quartz, its $\delta^{18}O$ could be quite high, whereas if it is detrital quartz, the $\delta^{18}O$ could be around 10 ‰ (Lawrence and Meaux, 1993). Therefore, if the quartz is 10 ‰ less than the kaolinite, 10 % quartz will lower the $\delta^{18}O$ of the kaolinite by about 1 ‰. Similarly, if quartz is 30 ‰, 10 % quartz will raise the $\delta^{18}O$ of the kaolinite by 1 ‰. Hence, we assume that the presence of quartz is unlikely to affect the measured kaolinite value by >1 ‰ and the shift will not make any difference to the interpretation. The δD values of the Cretaceous kaolins ranged between – 49 and – 57 ‰, whereas the values for the Tertiary deposits were between – 54 and – 66 ‰. The average of the δD values for the Cretaceous kaolins (- 52 ‰) is higher than that of the Tertiary (- 60 ‰).

Table 6.1a: Minerals present (wt %) of the studied Cretaceous – Tertiary kaolins.

Age	Deposit	Sample ID	Kaolinite	Quartz	Anatase	Hematite	Goethite
Cretaceous	Eruku	EP1	98	1	tr	-	tr
		EP2	98	1	1	-	tr
		EP3	97	1	1	tr	1
	Lakiri	LP1	99	1	-	-	-
		LP2	99	1	-	-	-
		Min	97	1	1	-	1
		Max	99	1	1	-	1
		Average	98.2	1	1	-	1
Tertiary	Awo-Omoma	AL1	91	7	1	1	-
		AL2	90	9	1	tr	-
	Ubulu-Uku	UL1	90	9	tr	-	-
		UL2	90	9	1	-	-
		Min	90	7	1	1	-
		Max	91	9	1	-	-
		Average	90.25	8.5	1	-	-

(tr) Trace, (-) Not detected

The $\delta^{18}O$ values of the Cretaceous kaolins ranged from 19.1 to 19.8 ‰, whereas the values for the Tertiary kaolins ranged from 20 to 21.5 ‰. The average of the $\delta^{18}O$ values for the Cretaceous kaolins (19.4 ‰) is lower than that of the Tertiary kaolins (20.8 ‰) (Table 6.1b). The $\delta^{18}O$ values between 19.1 and 21.5 ‰ were within the values for kaolinites of sedimentary origin which is usually between 19 and 23 ‰ as against 15 and 19 ‰ for kaolinites from residual deposits (Savin and Lee, 1988; Baioumy, 2013).

The δD and $\delta^{18}O$ values of the studied Cretaceous – Tertiary kaolins are plotted in Figure 6.1. In the δD - $\delta^{18}O$ diagram, the samples scatter between the kaolinite line (KL) of Savin and Espein (1970) (Eqn. 6.1) and the supergene – hypogene line (SHL) of Sheppard *et al.* (1969) (Eqn. 6.2) except for a sample from Awo-Omama plotting slightly to the right of the KL. The slight deviation below the KL is suggestive of post-formational modifications of the isotopic compositions of the sample (Gilg, 2000; Baioumy, 2013).

Table 6.1b: Measured δD and $\delta^{18}O$ isotopic compositions of the studied Cretaceous – Tertiary kaolins.

Age	Deposit	Sample ID	$\delta^{18}O$	δD
Cretaceous	Eruku	EP1	19.2	-57
		EP2	19.5	-49
		EP3	19.1	-52
	Lakiri	LP1	19.5	-51
		LP2	19.8	-52
		Min	19.1	-57
		Max	19.8	-49
		Average	19.4	-52
Tertiary	Awo-Omama	AL1	20.0	-66
		AL2	21.1	-64
	Ubulu-Uku	UL1	21.6	-54
		UL2	20.7	-54
		Min	20.0	-66
		Max	21.6	-54
		Average	20.8	-60

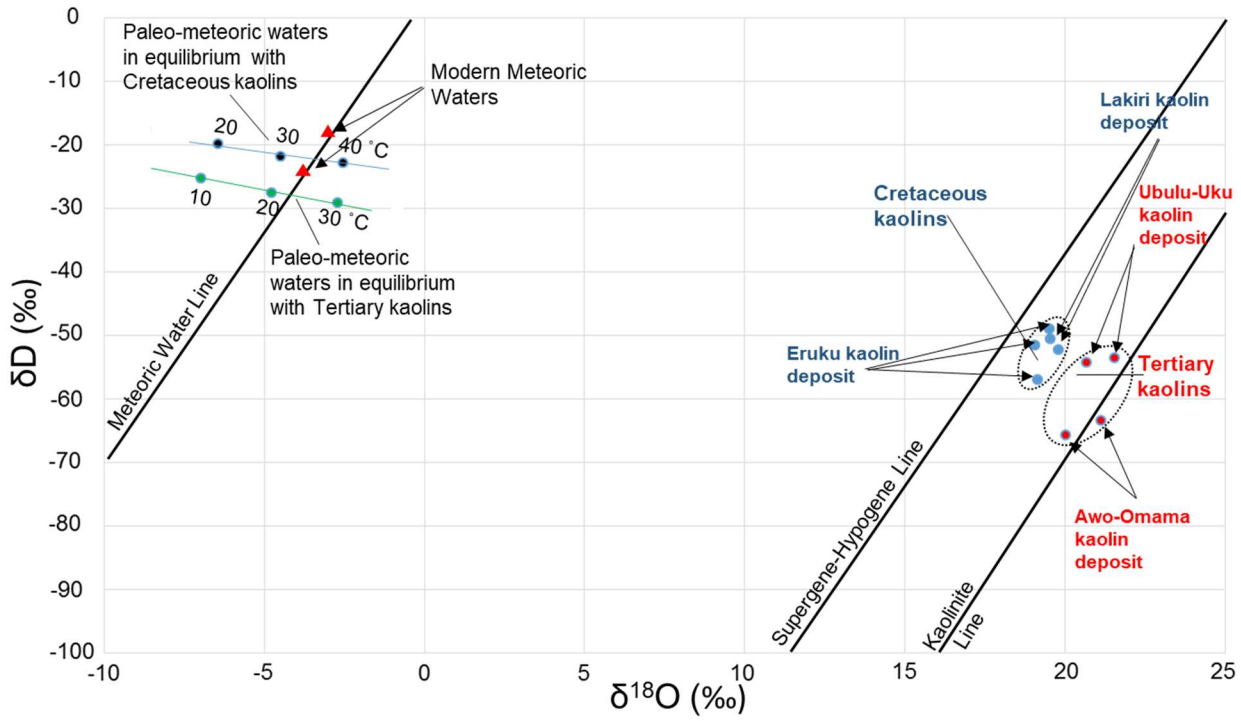

Figure 6.1: δD versus $\delta^{18}O$ isotopic compositions diagram of the studied Cretaceous – Tertiary kaolins. The paleometeoric waters in equilibrium with the kaolinites at temperatures between 10 – 40 ˚C were also plotted.

The global meteoric water line (GMWL) of Craig (1961) was used (Eqn. 6.3).

KL: $\delta D = 7.5\delta^{18}O - 220$ (6.1)

SHL: $\delta D = 7.5\delta^{18}O – 185$ (6.2)

GMWL: $\delta D = 8\delta^{18}O + 10$ (6.3)

Detailed inspection indicates that the Tertiary samples plotted around the KL, whereas the Cretaceous samples were systematically displaced to the left close to the SHL. All samples plotting to the right of the SHL clearly suggest a supergene origin for the studied Cretaceous – Tertiary kaolins formed at surficial temperatures. Several published works have been documented in the literature explaining post-formational diagenetic transformations in kaolinites with respect to variations in isotopic compositions (Singer, 1984; Chamley, 1989; Savin and Hsieh, 1998; Girard *et al*., 2000; Tabor and Montanez, 2002, 2005; Feng and Yapp, 2009; Sheldon and Tabor, 2009). Variations in intraprofile isotopic compositions may not necessarily be interpreted as a record of changes in weathering-climatic conditions through time but may arise due to continuous process of dissolution and precipitation (Girard *et al*., 2000). Savin and Hsieh (1998) argued that the conversion of kaolinite with high to low crystallinity in a pedogenic profile could be a subtle indication of mineralogical alteration after the formation of the kaolinite. They also attributed it to the continuous dissolving and reprecipitation as the weathering profile progressively deepens. In addition, diagenetic alterations have been recognized from dissimilarities between pedogenic kaolinites and geological deposits. In the modern soil kaolinites, finer grain size, greater degree of disorder, and small amount of isomorphous substitution of Fe for Al have been indicated (Herbillon *et al*., 1976; Sheldon and Tabor, 2009). In the light of the possibility of post-formational diagenetic transformations in the studied kaolinites, we conclude that diagenesis has little or no effect on the measured isotopic values for the following reasons (though further arguments could be considered). First, no significant intraprofile variations in the O and H isotopic values were observed. Instead the isotopic data obtained showed a reasonable level of linearity (Feng and Yapp, 2009). Second, the kaolinite crystallinity indices obtained for the kaolinites did not show

any evidence of intraprofile conversion from high degree of structural order to low degree of structural order. Hence, we assume that the measured isotopic compositions for the kaolinites represent the isotopic signal during their formation before transport and deposition.

The two most important factors that influence the δD and $\delta^{18}O$ values of kaolins are the O and H isotopic composition of the meteoric water in which they were formed and the temperature of formation (Tabor and Montanez, 2005). To infer paleoenvironmental conditions through the use of isotopic data, it must be preceded by the evaluation of the imprint of the modern meteoric water that might have been in contact with the deposits (dos Santos *et al*., 2007).

Up-to-date isotopic long term data in Nigeria is scarce. The only available long term (1961 – 1973) weighted annual mean values of δD and $\delta^{18}O$ in Nigeria were -27.7±10.86 ‰ and -4.28±1.81 ‰ for rainfall at Kano State (IAEA/WMO, 2017). However, the closest short term measurement is from Ore-Agbabu with $\delta^{18}O$ value of -3 ‰ for year 1979 (Loehnert, 1988). This value is comparable to -3.1 ‰ from Ekiti State (Talabi and Tijani, 2013). Therefore, to avoid 'continental effect' that preferentially removes heavy isotopes causing more negative $\delta^{18}O$ values with increasing distance from the coast (Rozanski *et al*.,1993; Taupin *et al*., 2000), $\delta^{18}O$ = -3 ‰ will be used for this study. This is crucial due to the slight negative increase in $\delta^{18}O$ value with increasing distance from the coast observed from -3 ‰ at Ore-Agbabu to -4.28 ‰ at Kano as moisture is gradually removed from air masses moving inland and condensation processes preferentially removing heavy isotopes.

Substituting $\delta^{18}O$ = -3 ‰ into eqn. 6.3, δD gives -14 ‰. To determine the isotopic composition of kaolinite in equilibrium with the modern meteoric water in the Eastern Dahomey and Niger Delta Basins, the equilibrium fractionation factor equations (6.4 and 6.5) between kaolinite and water given by Savin and Epstein were used.

For oxygen: $$\propto^{O}_{K-W} = \frac{\delta^{18}O_K + 1000}{\delta^{18}O_W + 1000} \quad (6.4)$$

For hydrogen: $$\propto^{D}_{K-W} = \frac{\delta D_K + 100}{\delta D_W + 1000} \quad (6.5)$$

Taking $\propto^{O}_{K-W}$ = 1.027 and $\propto^{D}_{K-W}$ = 0.97 (Lawrence and Taylor, 1972), the kaolinites in equilibrium with the modern meteoric water should have $\delta^{18}O_K$ = 23.9 ‰ and δD_K = - 44 ‰ isotopic compositions. The $\delta^{18}O_K$ and δD_K values obtained were much heavier than those measured for any of the studied kaolinite samples from the Eastern Dahomey and Niger Delta Basins respectively. Hence, the studied Cretaceous – Tertiary kaolins from the Eastern Dahomey and Niger Delta Basins are not in equilibrium with the modern meteoric water. Thus, the measured isotopic values should reflect the isotopic composition of the paleometeoric water during formation, unless further mineralogical transformation took place after it was formed.

6.1.1 Paleometeoric Water

The H- and 0- isotope compositions meteoric water during kaolinisation were calculated from the measured isotopic compositions of the kaolinite using the plot intersection of the meteoric water line with the curves of waters in equilibrium with this kaolinite based on Gilg *et al*. (1999) approach. Using the average $\delta^{18}O$ and δD values for the studied Cretaceous – Tertiary kaolins by equating equations 6.4 to 6.6 and 6.5 to 6.7 between 10 and 40 ˚C, the data obtained (Table 6.2) were plotted (Fig. 6.1). This gave meteoric water with $\delta^{18}O$ and δD values of – 3.9 and – 23 ‰ for Cretaceous kaolins and – 4.7 and – 28 ‰ for Tertiary kaolins.

Oxygen: $1000 \ln \alpha_{k\text{-}w} = -2.2 (10^6) (T^{-2}) - 7.7$ (6.6)

Hydrogen: $1000 \ln \alpha_{k\text{-}w} = 2.76 (10^6) (T^{-2}) - 6.75$ (6.7)

Where, $\alpha_{k\text{-}w}$ is the fractionation factor for oxygen and hydrogen and T is the temperature.

Using the isotopic compositions for the paleometeoric water, the equilibrium fractionation factors (Eqns. 6.4 and 6.5) for oxygen were 1.023 and 1.026, and for hydrogen were 0.969 and 0.967 for the studied Cretaceous and Tertiary kaolins, respectively. These fractionation values are comparable to those expected in weathering environments (Savin and Epstein, 1970; Lawrence and Taylor, 1972) given as 1.027 and 0.97 for oxygen and hydrogen, respectively. Hence, the studied Cretaceous – Tertiary kaolins can be

associated to paleoweathering. In addition, a comparison of the $\delta^{18}O$ and δD values for the paleometeoric water from Cretaceous – Tertiary – Recent shows that the meteoric water during the Tertiary became slightly depleted (lighter) in $\delta^{18}O_w$ and δD_w, whereas moving from Tertiary to recent, the meteoric water became enriched (heavier) in $\delta^{18}O_w$ and δD_w using – 3 and – 14 ‰ for present day values.

Table 6.2: Calculated $\delta^{18}O$ and δD values for the paleometeoric waters in equilibrium with the studied Cretaceous – Tertiary kaolins between 10 – 40 ˚C.

Age	Temperature (˚C)	$\delta^{18}O$ (‰)	δD (‰)
Cretaceous	10	-8.4	-18
	20	-6.4	-20
	30	-4.5	-22
	40	-2.5	-23
Min	10	-8.4	-23
Max	40	-2.5	-18
Average	25	-5.5	-21
Tertiary	10	-7.0	-25
	20	-4.8	-28
	30	-2.7	-29
	40	-0.8	-31
Min	10	-7.0	-31
Max	40	-0.8	-25
Average	25	-3.8	-28

6.1.2 Paleotemperature during Kaolinisation

To use kaolin minerals as proxies of paleotemperature, it requires the application of relatively well-known O- and H- isotope mineral-water fractionation factors as a function of temperature. The proposed Sheppard and Gilg (1996) revised equations (6.6 and 6.7) are commonly used. However, from the intercept of the paleometeoric waters in equilibrium with the Cretaceous – Tertiary kaolinites, average paleotemperatures (T_G) can be extrapolated which gave approximately 32.5 and 21.5 ˚C for the temperature of kaolinisation of the Cretaceous and Tertiary kaolins, respectively. These values show that

the Cretaceous kaolins were formed at temperatures about 11 ˚C hotter than the temperatures under which the Tertiary kaolins were formed. Isotopic paleotemperatures from marine records have shown that the world during transition between the Cretaceous period and Tertiary period experienced global cooling as much as 8 to 10 ˚C (Savin, 1977; Gilg, 2000). Thus, the 11 ˚C temperature difference between the Cretaceous and Tertiary kaolins is consistent with that obtained earlier from marine records.

In addition, Clauer *et al*. (2015) and Galan *et al*. (2016) combined equations 6.6 and 6.7 of Sheppard and Gilg (1996) by eliminating $\delta^{18}O_w$ and δD_w using eqn. 6.3 to develop a single-mineral geothermometer (Eqn. 6.8) for kaolin minerals similar to the one proposed by Delgado and Reyes (1996) for smectite minerals.

$$3.04*10^6T^{-2} = \delta^{18}O_K - 0.125\delta D_K + 7.04 \quad (6.8)$$

The calculated temperature of kaolinisation (T_C) obtained by applying eqn. 6.8 are presented in Table 6.3. The calculated average T_C values indicated about 10.2 ˚C temperature difference from Cretaceous to Tertiary periods. This is similar to the earlier observation from the T_G values. From the foregoing, it is obvious that the Cretaceous kaolins formed under warmer conditions than the Paleogene/Neogene kaolins, whereas the temperature during the formation of the Paleogene/Neogene kaolins is slightly cooler than the recent mean annual surface temperature of 26.1 ˚C in Kano State, Nigeria based on data gathered between 1961 – 1973 (IAEA/WMO, 2017). The paleotemperatures obtained for both the Cretaceous and Paleogene/Neogene kaolins are characteristic of formation under tropical climate. Palymorphs recovered from Araromi Formation of the Abeokuta Group (Eastern Dahomey Basin) indicated the dominance of palm pollens. This suggest a warm tropical humid climate (Vadja-Santivanez, 1999; Durogbo and Aroyewun, 2011). In addition, due to the proliferation of palms and wet climate indicators in the fossil record, Durogbo and Olayiwola (2017) also gave credence to a humid tropical climate for the formation of the kaolin-bearing Ogwashi-Asaba Formation (Niger Delta Basin) during the middle Miocene.

Table 6.3: Calculated temperature of kaolinisation (T_C) of the studied Cretaceous – Tertiary kaolins.

Age	Deposit	Sample ID	Temperature
Cretaceous	Eruku	EP1	29.3
		EP2	32.1
		EP3	32.2
	Lakiri	LP1	30.9
		LP2	28.9
		Min	28.9
		Max	32.2
		Average	30.7
Tertiary	Awo-Omoma	AL1	20.5
		AL2	17.0
	Ubulu-Uku	UL1	20.5
		UL2	23.9
		Min	17.0
		Max	23.9
		Average	20.5

Several studies on the causes of climate change have focused on the effect of tectonic motions since the development of plate tectonic model provided the framework to examine temperature variations of the past in relation to the present (Hassinpak and Eslinger, 1985; Bird and Chivas, 1988; Gilg, 2000; Gilg *et al*., 2013). The southward movement of Nigeria away from the equator during the Cretaceous to Tertiary (Fig. 6.2) could have contributed to the decrease in temperature and also the interaction of the kaolins with lighter meteoric waters during the Tertiary (Gilg, 2000; Gilg *et al*., 2013). In addition, the evidence of global cooling from marine record (Savin, 1977) since Cretaceous may also have contributed to the shift in isotopic compositions with time. Gilg *et al*. (1999) in explaining the systematic changes of isotopic compositions argued that since the Southern South America have experienced barely any change in paleolatitude since the opening of the South Atlantic (Parrish *et al*., 1982; Scotese *et al*., 1988), it can be concluded that the changes could only be related to global cooling. However, a single theory cannot explain the variations because climatic changes are the result of many factors (Savin, 1977).

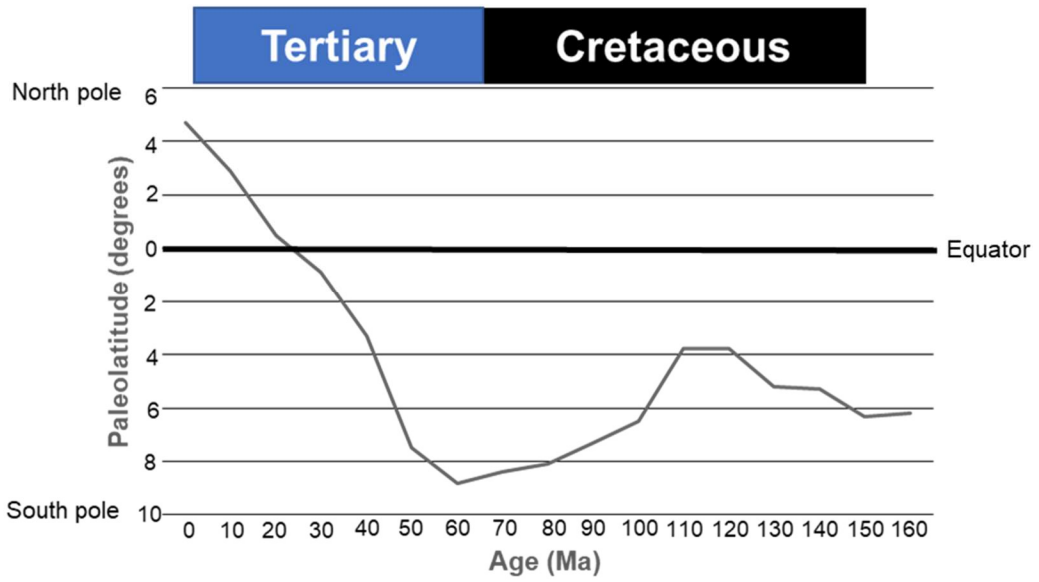

Figure 6.2: Paleolatitude history of the sample localities within Eastern Dahomey and Niger Delta Basins, Nigeria since Cretaceous to Recent. The plot is based on the paleolatitude calculator developed by van Hinsbergen *et al*. (2015).

6.2 Conclusions

Based on the stable isotopic considerations, the following deductions have been made:

a) The δD and $\delta^{18}O$ values of the studied Cretaceous – Tertiary kaolins suggest that they were sedimentary kaolins formed by weathering, rather than by hydrothermal alteration.
b) The $\delta^{18}O$ and δD values for the paleometeoric water for the Cretaceous kaolins – Tertiary kaolins – Recent shows that the meteoric water during the formation of the Tertiary kaolins became slightly depleted (lighter) in $\delta^{18}O_w$ and δD_w, whereas moving to recent, the meteoric water became enriched (heavier) in $\delta^{18}O_w$ and δD_w.
c) The paleotemperatures indicated a warmer conditions during the formation of the Cretaceous kaolins (32.5 ˚C) relative to the Tertiary kaolins (21.5 ˚C), whereas the temperature during the formation of the Tertiary kaolin was cooler relative to the Recent (26.1˚C). The paleotemperatures were characteristic of kaolinisation under a tropical climate.

Chapter Seven

Detrital Zircon Geochronology of the Cretaceous-Tertiary kaolins within the Eastern Dahomey and Niger Delta Basins in Nigeria.

This chapter aimed to date the detrital zircon minerals in the Cretaceous – Tertiary kaolins within the Eastern Dahomey and Niger Delta Basins in Nigeria (Specific Objective 3) based on Hypothesis 3. The U-Pb radiogenic dating of the zircon minerals within the studied kaolins were used to achieve specific objective 3.

7.1 Zircon Morphology and Origin

The cathodoluminescence (CL) images of the zircons were used essentially for the morphological descriptions based on Corfu *et al*. (2003). The backscattered (BSE) images of the zircon minerals in each of the kaolin deposits are presented in Appendices 7.1 – 7.4.

7.1.1 Lakiri Kaolins

Figure 7.1 shows CL images of the representative zircons within the Lakiri kaolin deposit.

Most of the zircons were subhedral with a few euhedral crystals. Crystal fragments were also identified. The grains were predominantly subrounded to rounded with few needle-like crystals. The sizes of the zircons ranged between 70 and 300 µm. The euhedral grains suggest little sedimentary transport, whereas the rounded grains suggest input of materials that underwent prolonged and possibly multicycle transport (Xu *et al*., 2013). The zircon textures were dominated by xenocrystic cores with rims followed by homogeneous unzoned cores. The xenocrystic cores have varying colour domains (lighter or darker) depending on the differences in the U-content. Few sector and chaotic zoning were observed. The growth or oscillatory zonings were not too common. The needle-like acicular zircon crystals are suggestive of rapid crystallization, whereas xenocrystic cores themselves does not yield useful clues as to their origin (Corfu *et al*., 2003).

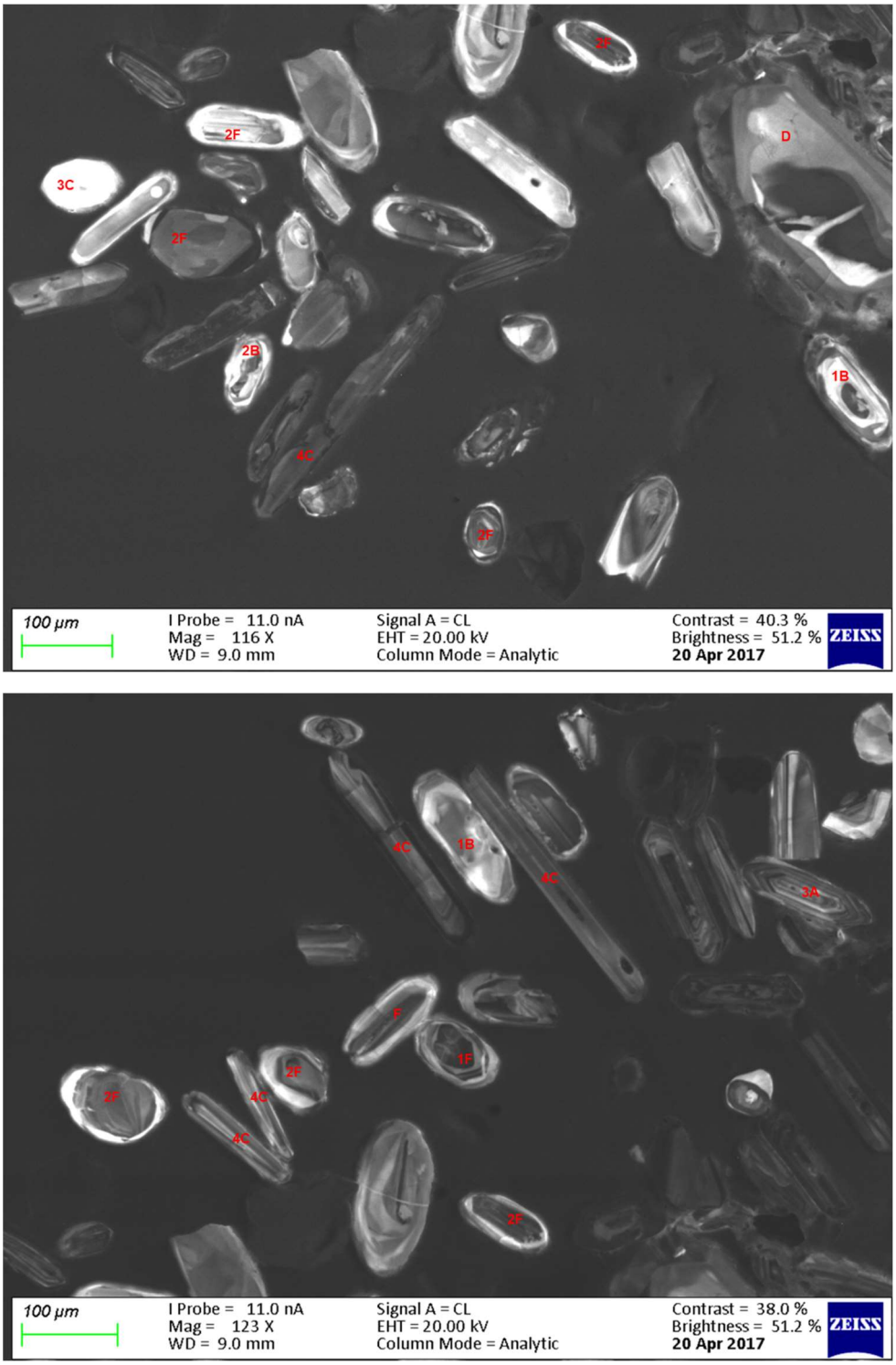

Figure 7.1a: CL images of some of the representive zircons showing main types of internal structures within the studied Lakiri kaolins where, 1: Euhedral; 2: Subhedral to subrounded grains; 3: Oval to rounded grains; 4: Needle-like grains; A: Oscillatory/growth zoning; B: Sector zoning; C: Homogeneous unzoned; D: Chaotic texture; and F: Xenocrystic cores.

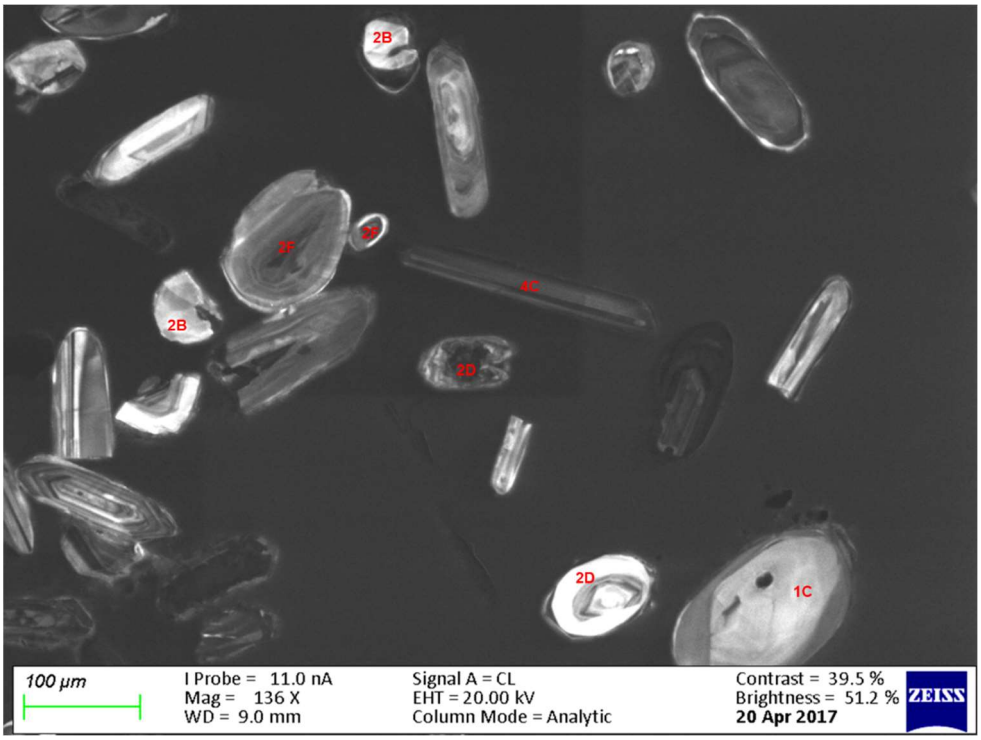

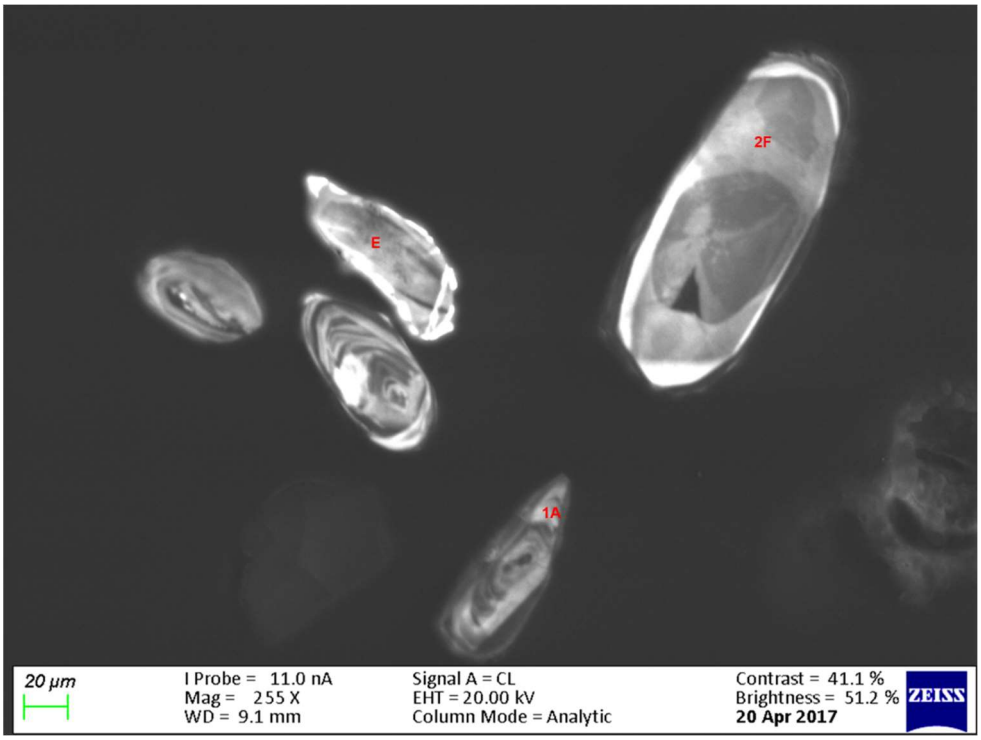

Figure 7.1b: CL images of some of the representive zircons showing main types of internal structures within the studied Lakiri kaolins where, 1: Euhedral; 2: Subhedral to subrounded grains; 4: Needle-like grains; A: Oscillatory/growth zoning; B: Sector zoning; C: Homogeneous unzoned; D: Chaotic texture; E: Irregular concentric zoning; and F: Xenocrystic cores.

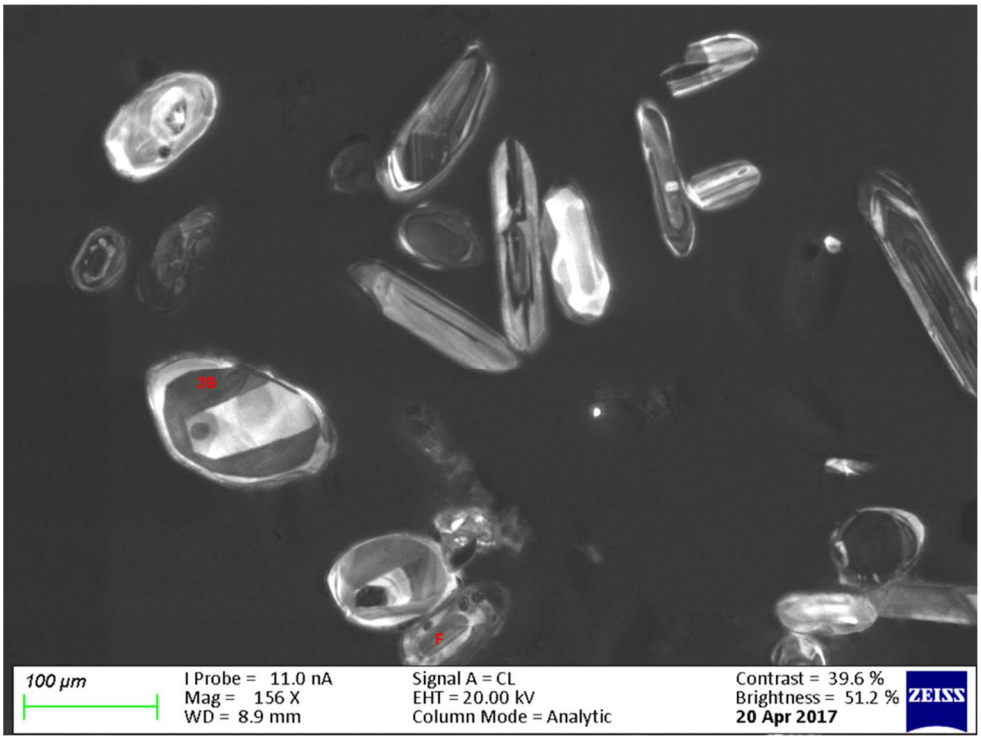

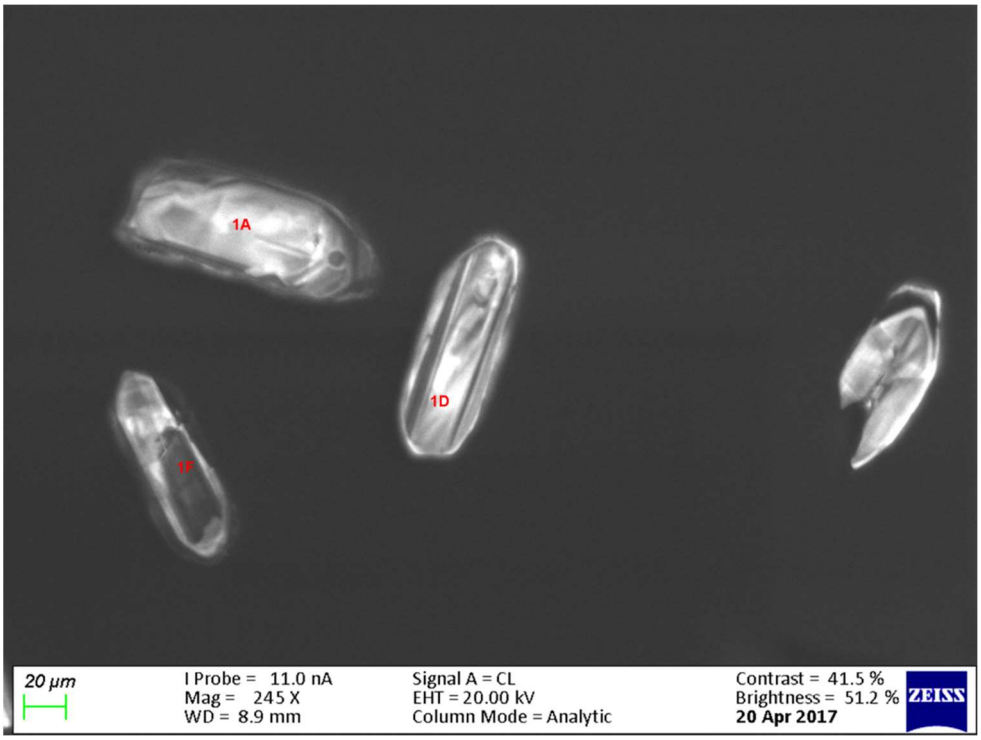

Figure 7.1c: CL images of some of the representive zircons showing main types of internal structures within the studied Lakiri kaolins where, 1: Euhedral; 2: Subhedral to subrounded grains; A: Oscillatory/growth zoning; B: Sector zoning; D: Chaotic texture; and F: Xenocrystic cores.

The Th/U ratios of the zircons ranged from 0.04 to 1.99, though most zircons had ratios >0.3 (Fig. 7.2). Wanniarachchi *et al*. (2016) identified 3 groups of zircon origins based on the Th/U ratios. Th/U >0.3, 0.3 – 0.1, and <0.1 represents those of igneous origin, igneous or metamorphic origin, and metamorphic origin, respectively. The Th/U ratios obtained for the zircons within the Lakiri kaolins were suggestive of predominantly magmatic origin.

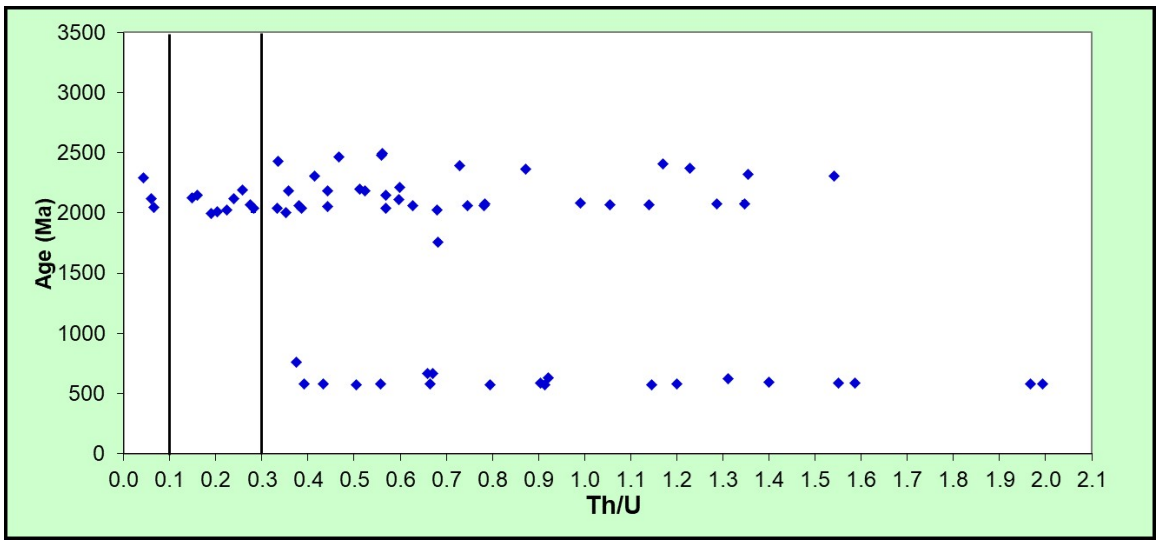

Figure 7.2: Th/U variation with age (Ma) in the studied Lakiri kaolins; the 0.1 and 0.3 black lines mark the upper and lower limits of zircon of metamorphic or magmatic origin, respectively (Wanniarachchi *et al*., 2016).

7.1.2 Eruku Kaolins

Figure 7.3 shows CL images of the representative zircons within the Eruku kaolin deposit. Most of the zircons were euhedral to subhedral with a few oval to rounded grains. The sizes of the zircons ranged between 50 and 200 µm. The euhedral grains suggest little sedimentary transport, whereas the rounded grains suggest input of materials that underwent prolonged and possibly multicycle transport (Xu *et al*., 2013). The zircon textures were dominated by xenocrystic cores with some having oscillatory zones followed by homogeneous unzoned cores.

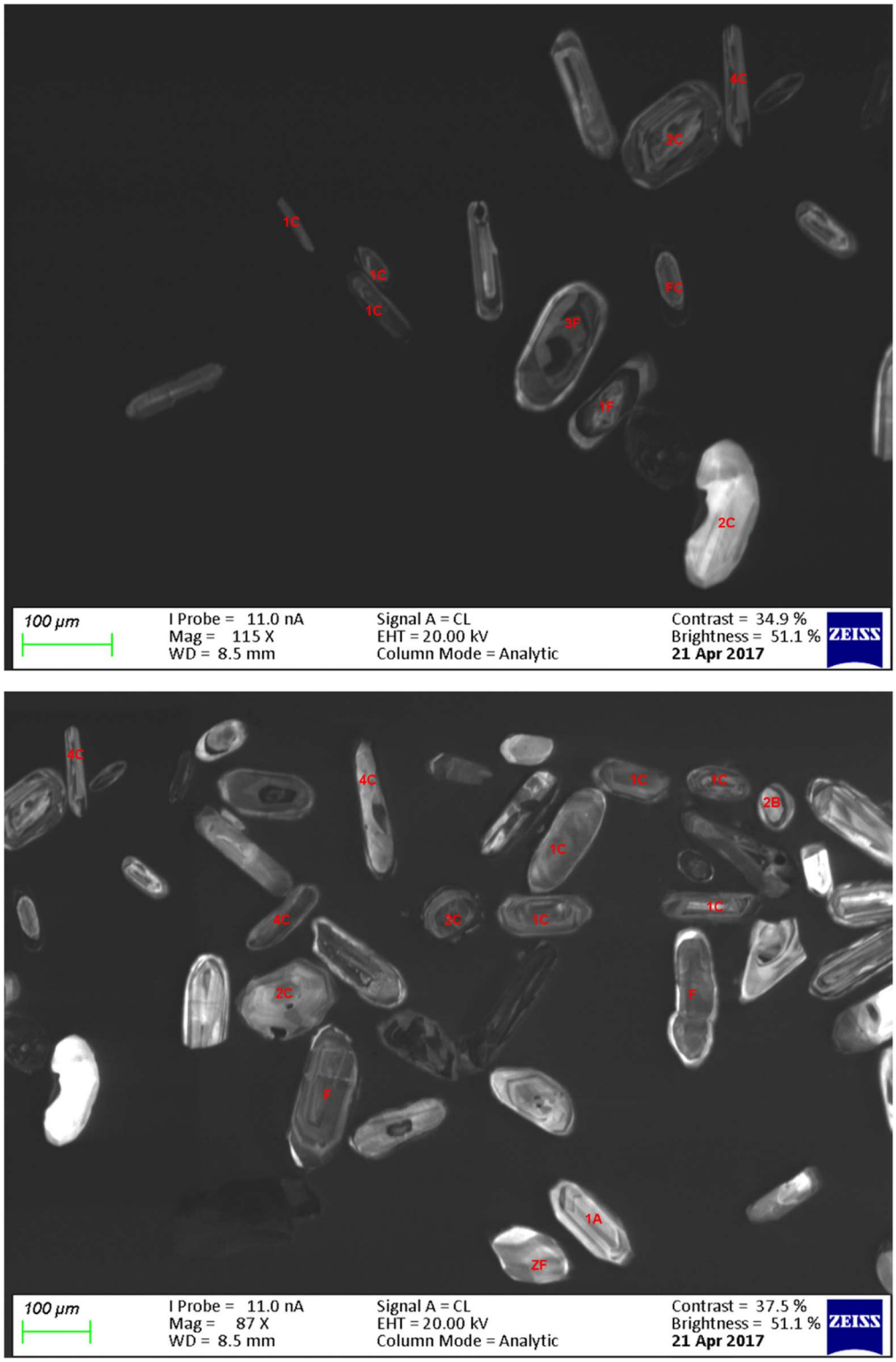

Figure 7.3a: CL images of some of the representive zircons showing main types of internal structures within the studied Eruku kaolins where, 1: Euhedral; 2: Subhedral to subrounded grains; 3: Oval to rounded grains; 4: Needle-like grains; A: Oscillatory/growth zoning; B: Sector zoning; C: Homogeneous unzoned; and F: Xenocrystic cores.

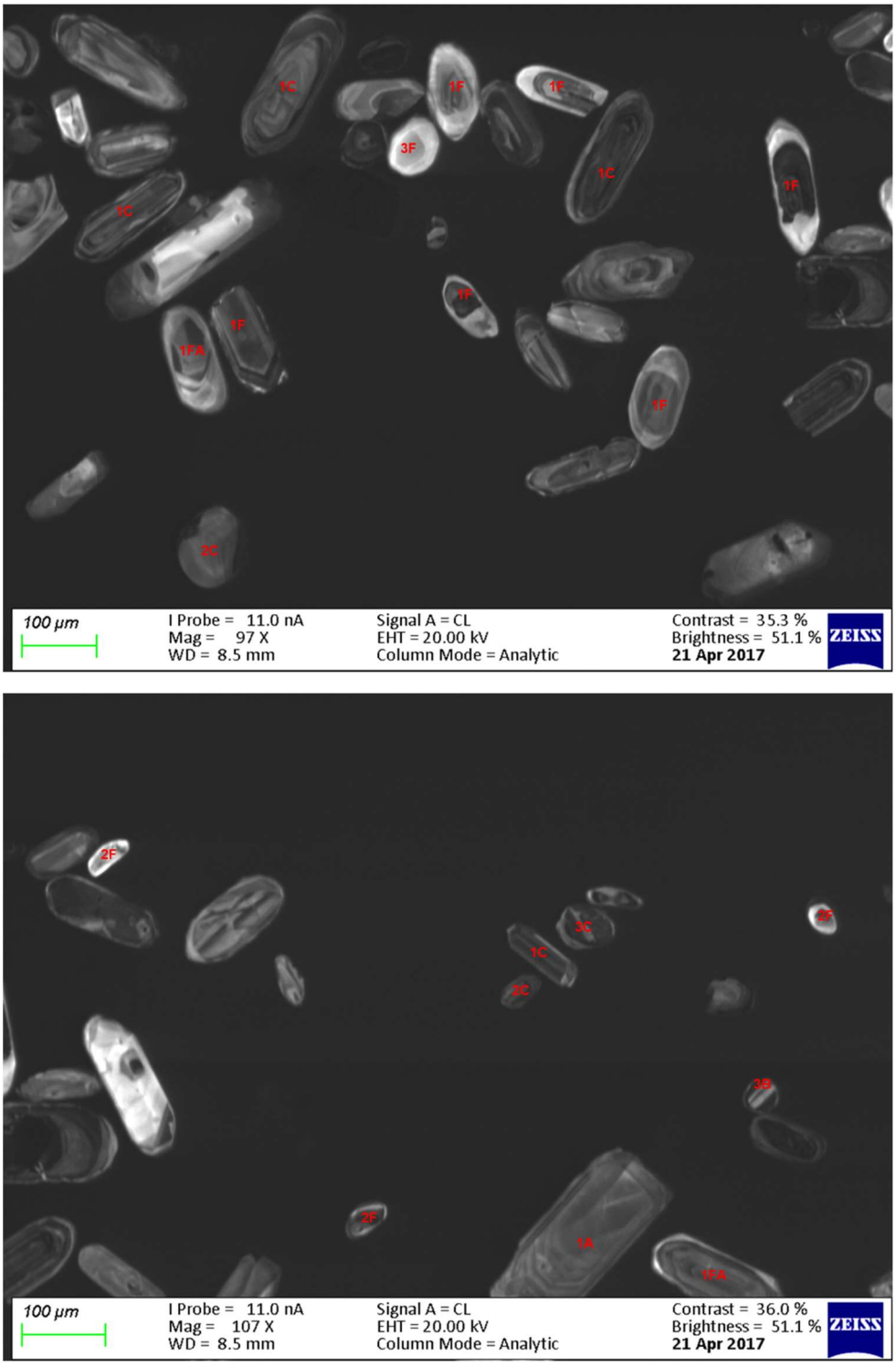

Figure 7.3b: CL images of some of the representive zircons showing main types of internal structures within the studied Eruku kaolins where, 1: Euhedral; 2: Subhedral to subrounded grains; 3: Oval to rounded grains; A: Oscillatory/growth zoning; B: Sector zoning; C: Homogeneous unzoned; and F: Xenocrystic cores.

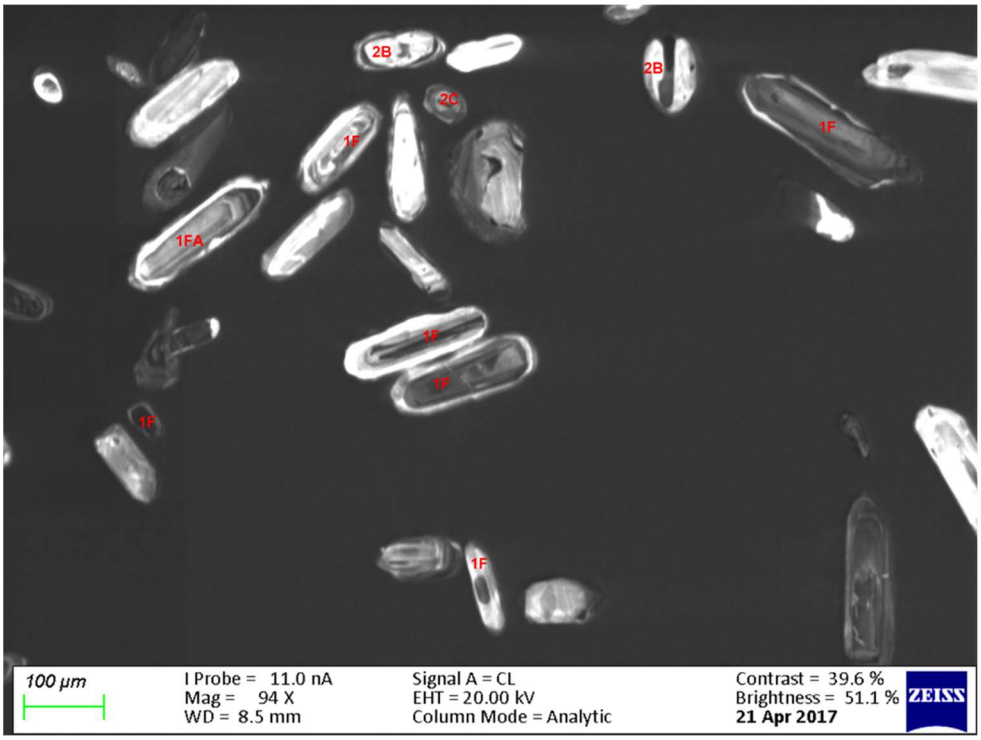

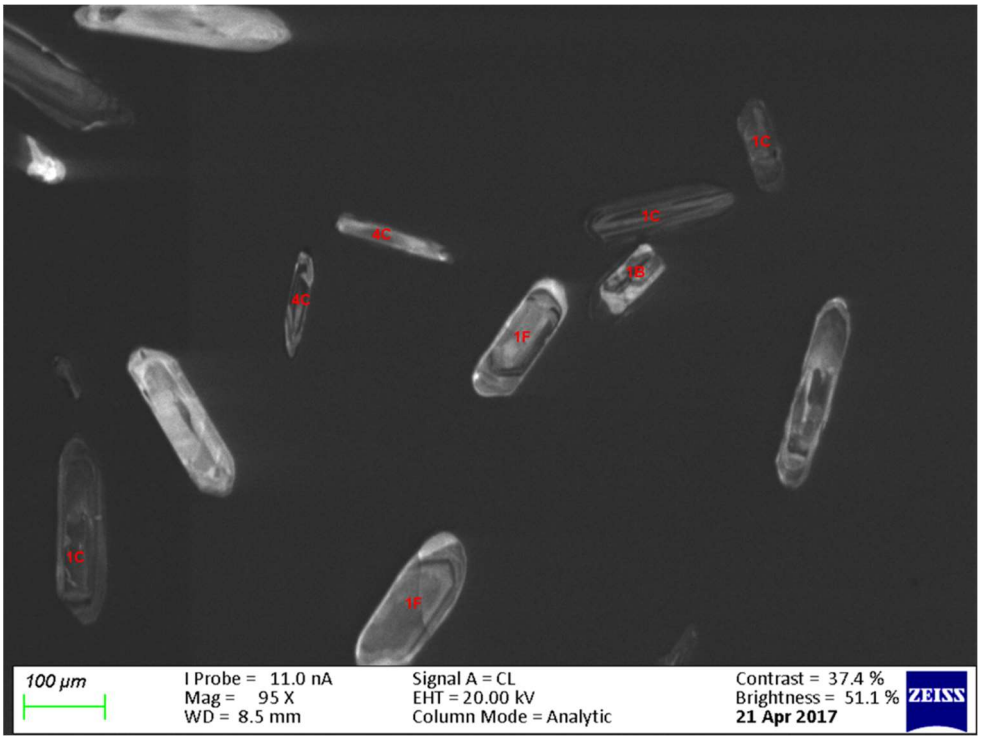

Figure 7.3c: CL images of some of the representive zircons showing main types of internal structures within the studied Eruku kaolins where, 1: Euhedral; 2: Subhedral to subrounded grains; 4: Needle-like grains; A: Oscillatory/growth zoning; B: Sector zoning; C: Homogeneous unzoned; and F: Xenocrystic cores.

The xenocrystic cores have varying colour domains (lighter or darker) depending on the differences in the U-content. Few sector zonings were observed.

The Th/U ratios of the zircons ranged from 0.01 to 2.10, though most zircons had ratios >0.3 (Fig. 7.4). The Th/U ratios obtained for the zircons within the Eruku kaolins were suggestive of predominantly magmatic origin (Wanniarachchi *et al*., 2016).

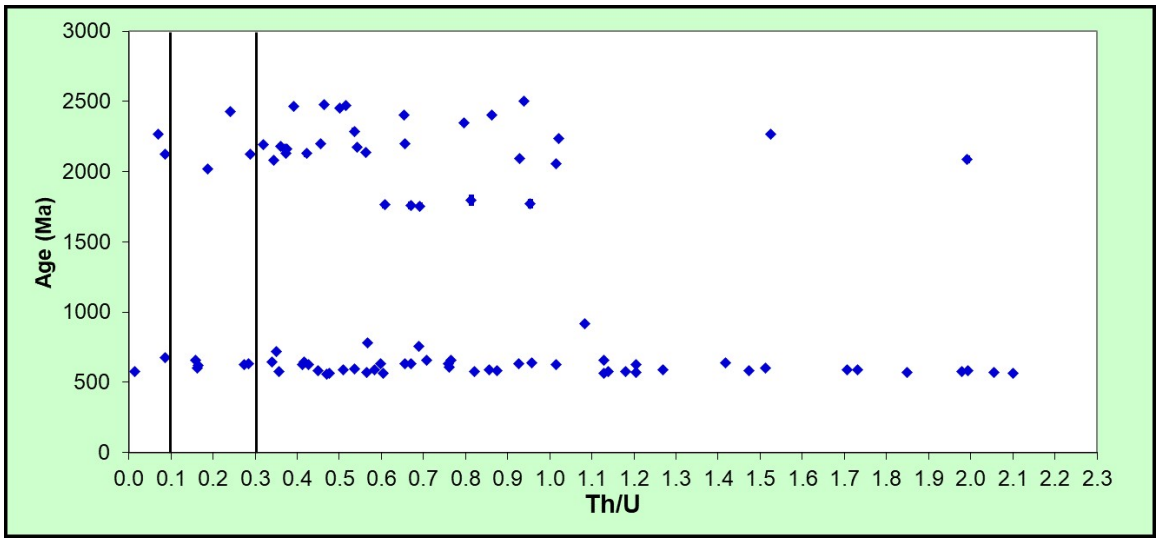

Figure 7.4: Th/U variation with age (Ma) in the studied Eruku kaolins; the 0.1 and 0.3 black lines mark the upper and lower limits of zircon of metamorphic or magmatic origin, respectively (Wanniarachchi *et al*., 2016).

7.1.3 Awo-Omama Kaolins

Figure 7.5 shows CL images of the representative zircons within the Awo-Omama kaolin deposit. Most of the zircons were euhedral with few subhedral to subrounded grains. The sizes of the zircons ranged between 60 and 200 µm. The predominantly euhedral grains suggest little sedimentary transport, whereas the subhedral to subrounded grains suggest input of materials that underwent a little prolonged transport (Xu *et al*., 2013). The zircon textures were dominated by oscillatory/growth zoning followed by those with xenocrystic cores.

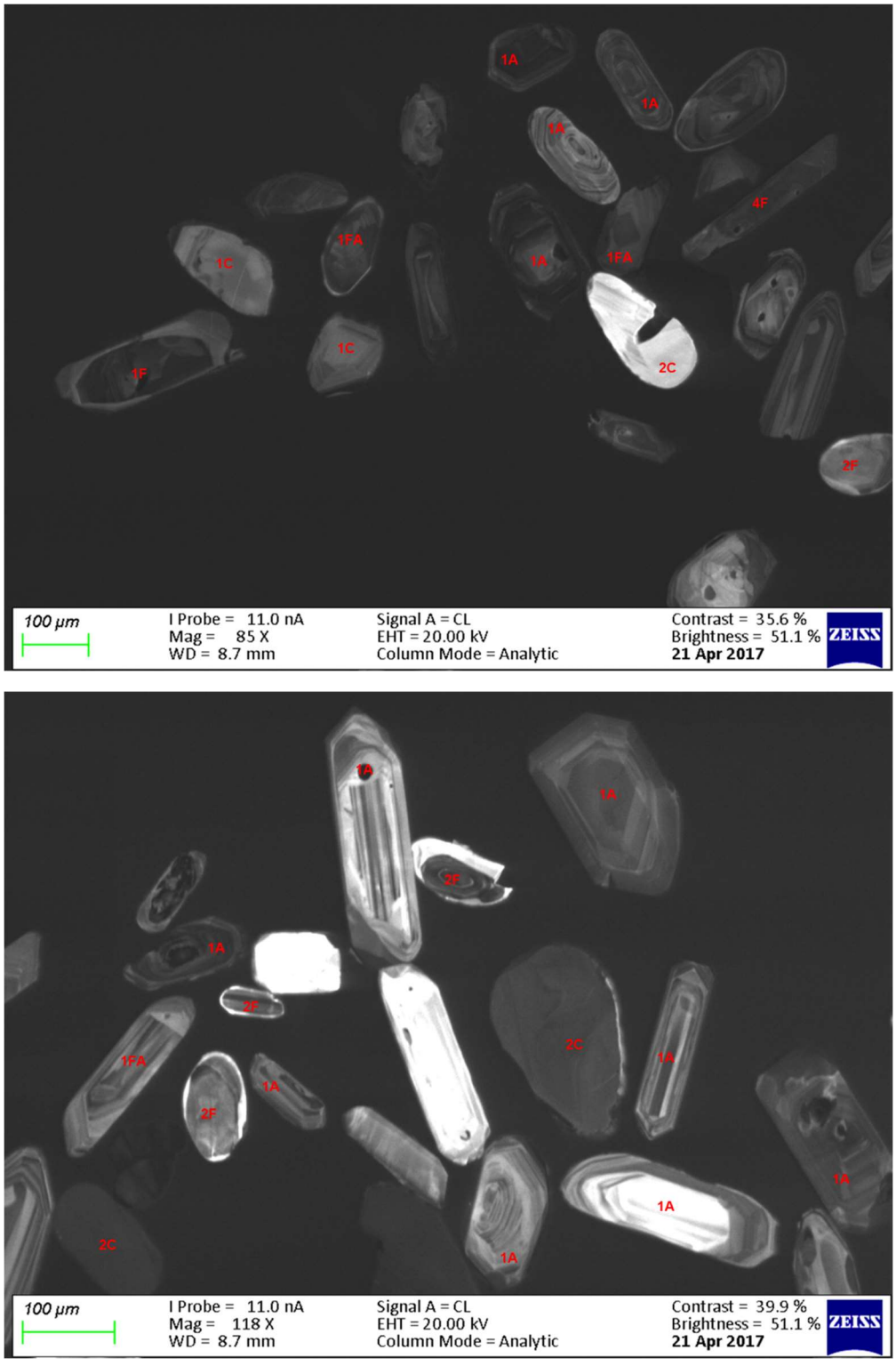

Figure 7.5a: CL images of some of the representive zircons showing main types of internal structures within the studied Awo-Omama kaolins where, 1: Euhedral; 2: Subhedral to subrounded grains; A: Oscillatory/growth zoning; C: Homogeneous unzoned; and F: Xenocrystic cores.

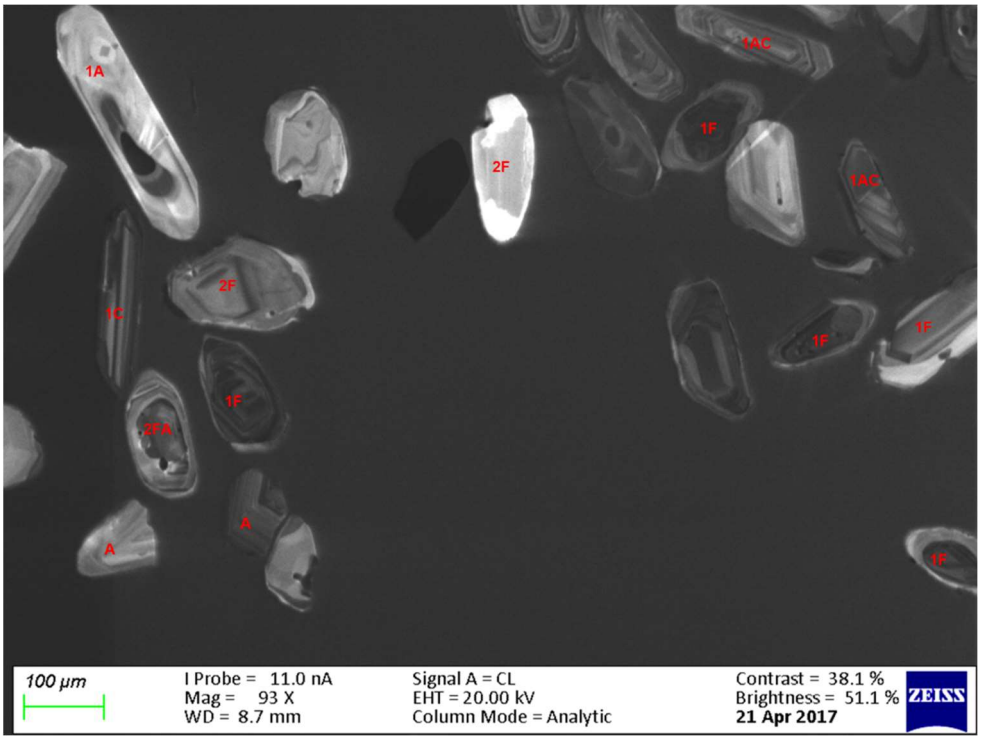

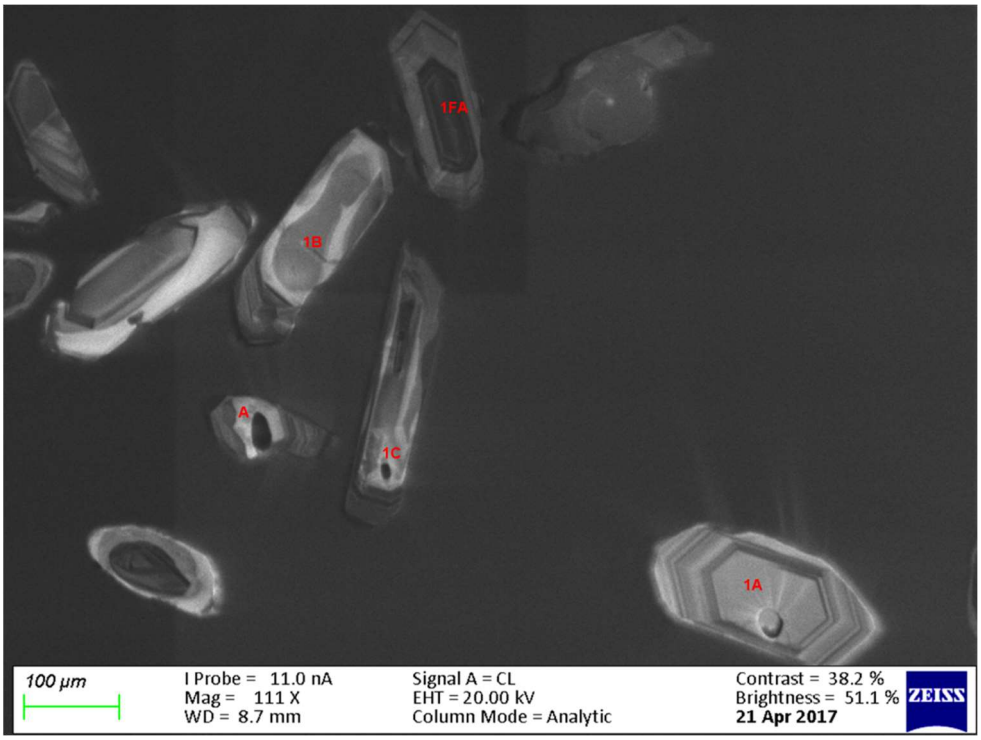

Figure 7.5b: CL images of some of the representive zircons showing main types of internal structures within the studied Awo-Omama kaolins where, 1: Euhedral; 2: Subhedral to subrounded grains; A: Oscillatory/growth zoning; B: Sector zoning; C: Homogeneous unzoned; and F: Xenocrystic cores.

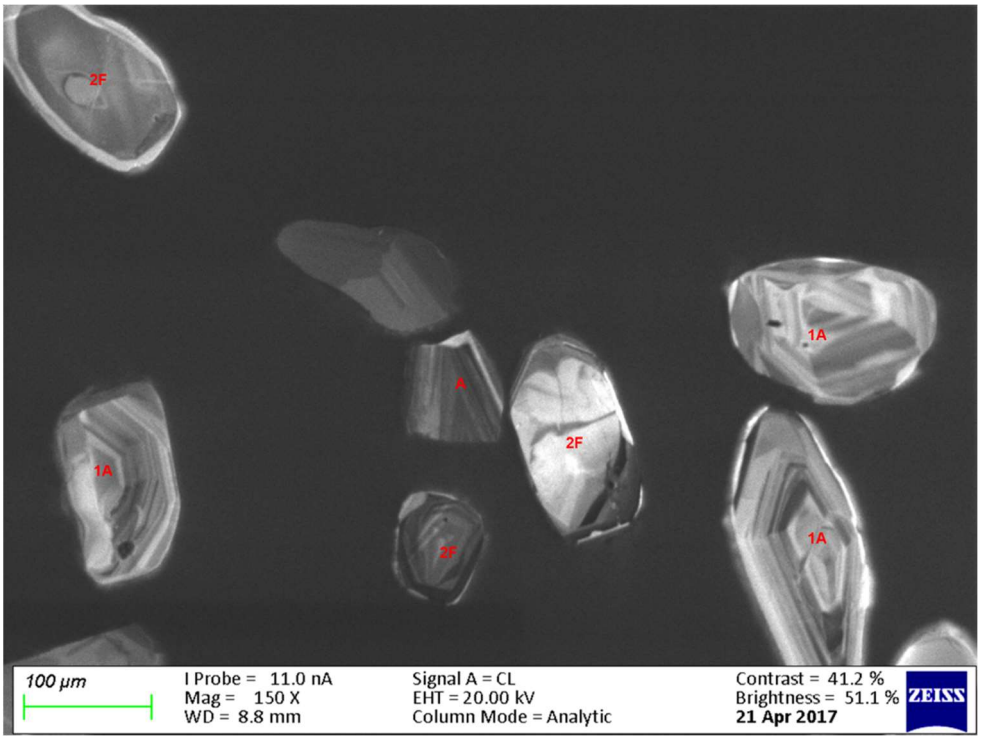

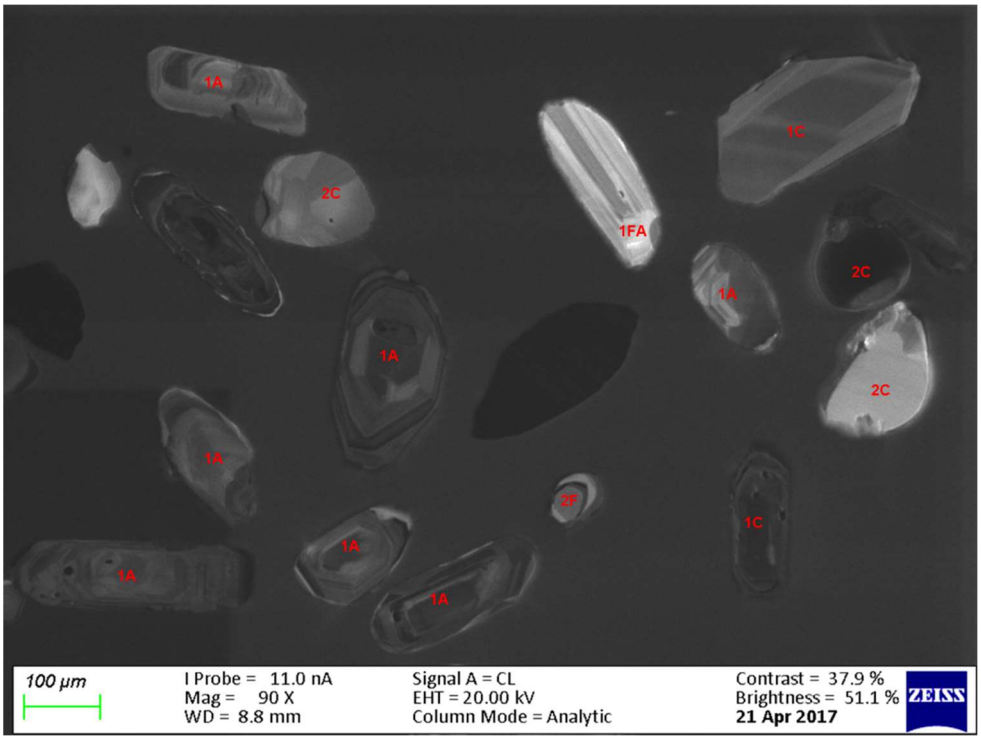

Figure 7.5c: CL images of some of the representive zircons showing main types of internal structures within the studied Awo-Omama kaolins where, 1: Euhedral; 2: Subhedral to subrounded grains; A: Oscillatory/growth zoning; C: Homogeneous unzoned; and F: Xenocrystic cores.

The xenocrystic cores have varying colour domains (lighter or darker) depending on the differences in the U-content. Oscillatory/growth zonings are considered as evidence of magmatic origin (Corfu *et al*., 2003).

The Th/U ratios of the zircons ranged from 0.03 to 2.43, though most zircons had ratios >0.3 (Fig. 7.6). The Th/U ratios obtained for the zircons within the Awo-Omama kaolins were suggestive of predominantly magmatic origin (Wanniarachchi *et al*., 2016).

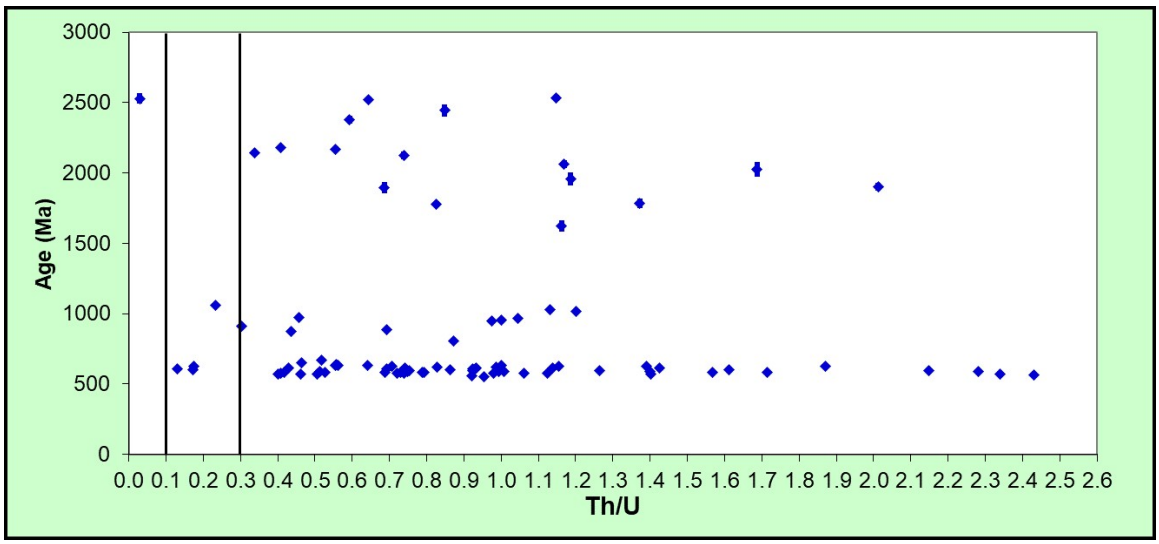

Figure 7.6: Th/U variation with age (Ma) in the studied Awo-Omama kaolins; the 0.1 and 0.3 black lines mark the upper and lower limits of zircon of metamorphic or magmatic origin, respectively (Wanniarachchi *et al*., 2016).

7.1.4 Ubulu-Uku Kaolins

Figure 7.7 shows CL images of the representative zircons within the Ubulu-Uku kaolin deposit.

Most of the zircons were euhedral with few subhedral to subrounded and oval to rounded grains. The sizes of the zircons ranged between 50 and 200 µm. The predominantly euhedral grains suggest little sedimentary transport, whereas the rounded grains suggest input of materials that underwent prolonged and possibly multicycle transport (Xu *et al*., 2013).

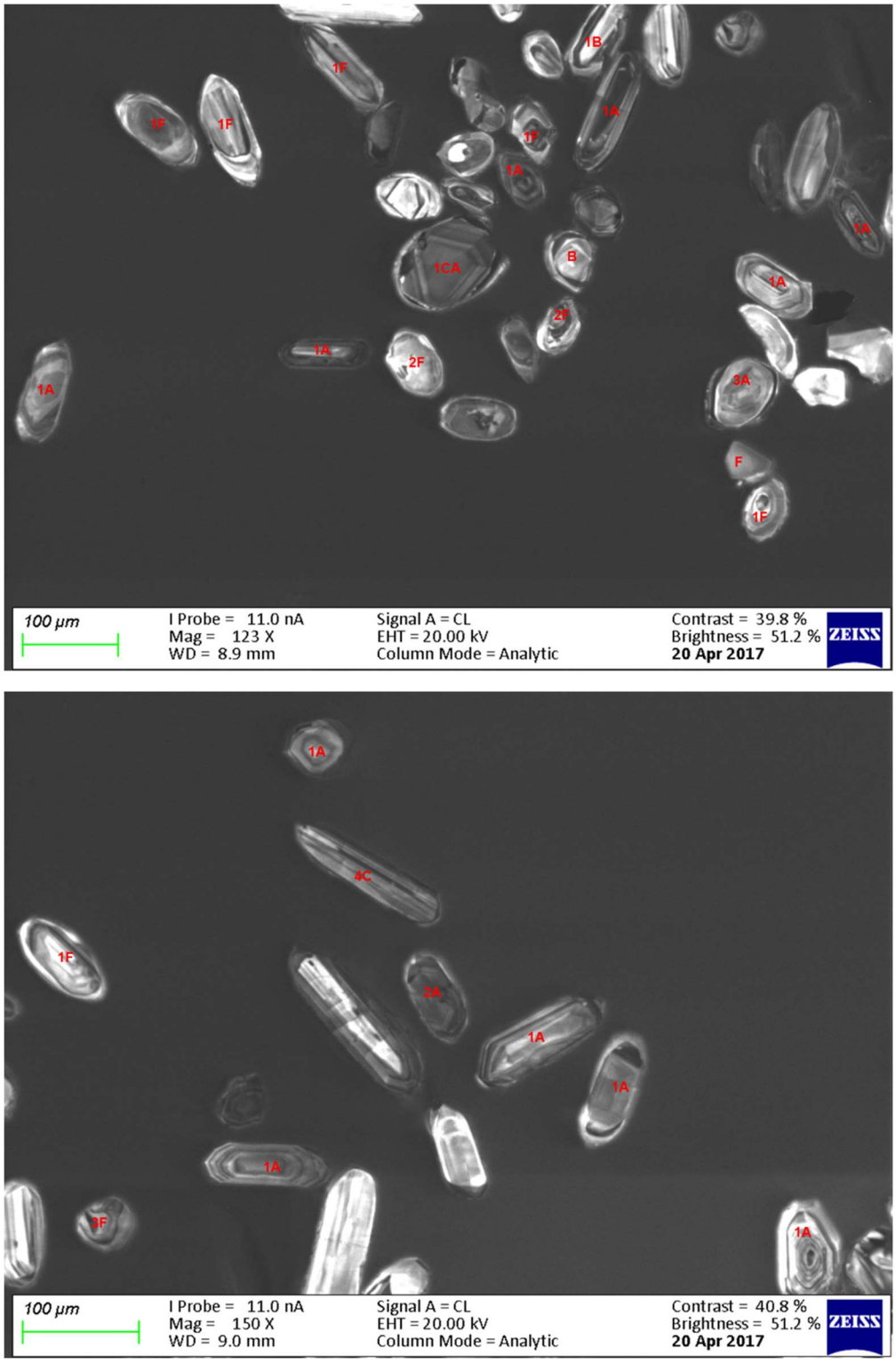

Figure 7.7a: CL images of some of the representive zircons showing main types of internal structures within the studied Ubulu-Uku kaolins where, 1: Euhedral; 2: Subhedral to subrounded grains; 3: Oval to rounded grains; A: Oscillatory/growth zoning; B: Sector zoning; C: Homogeneous unzoned; and F: Xenocrystic cores.

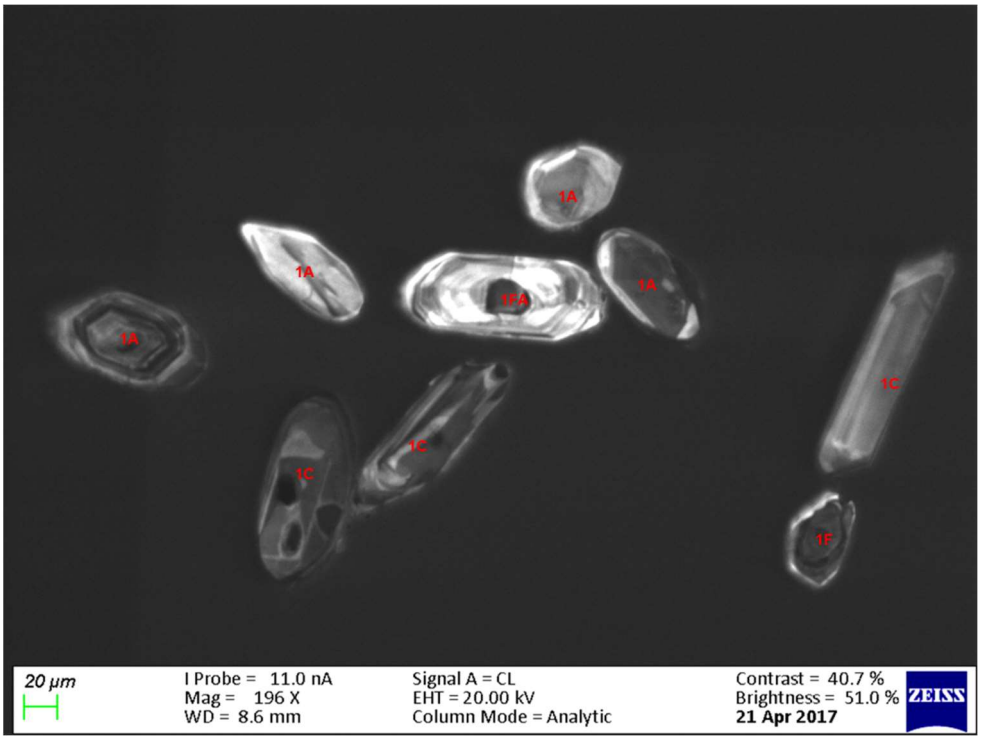

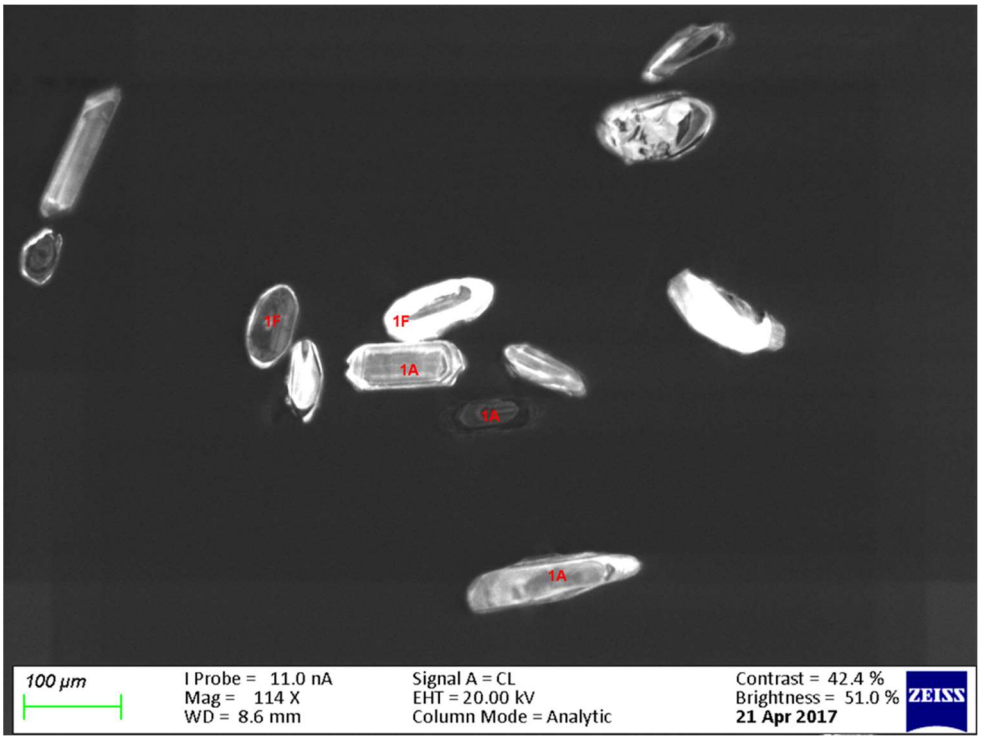

Figure 7.7b: CL images of some of the representive zircons showing main types of internal structures within the studied Ubulu-Uku kaolins where, 1: Euhedral; A: Oscillatory/growth zoning; and F: Xenocrystic cores.

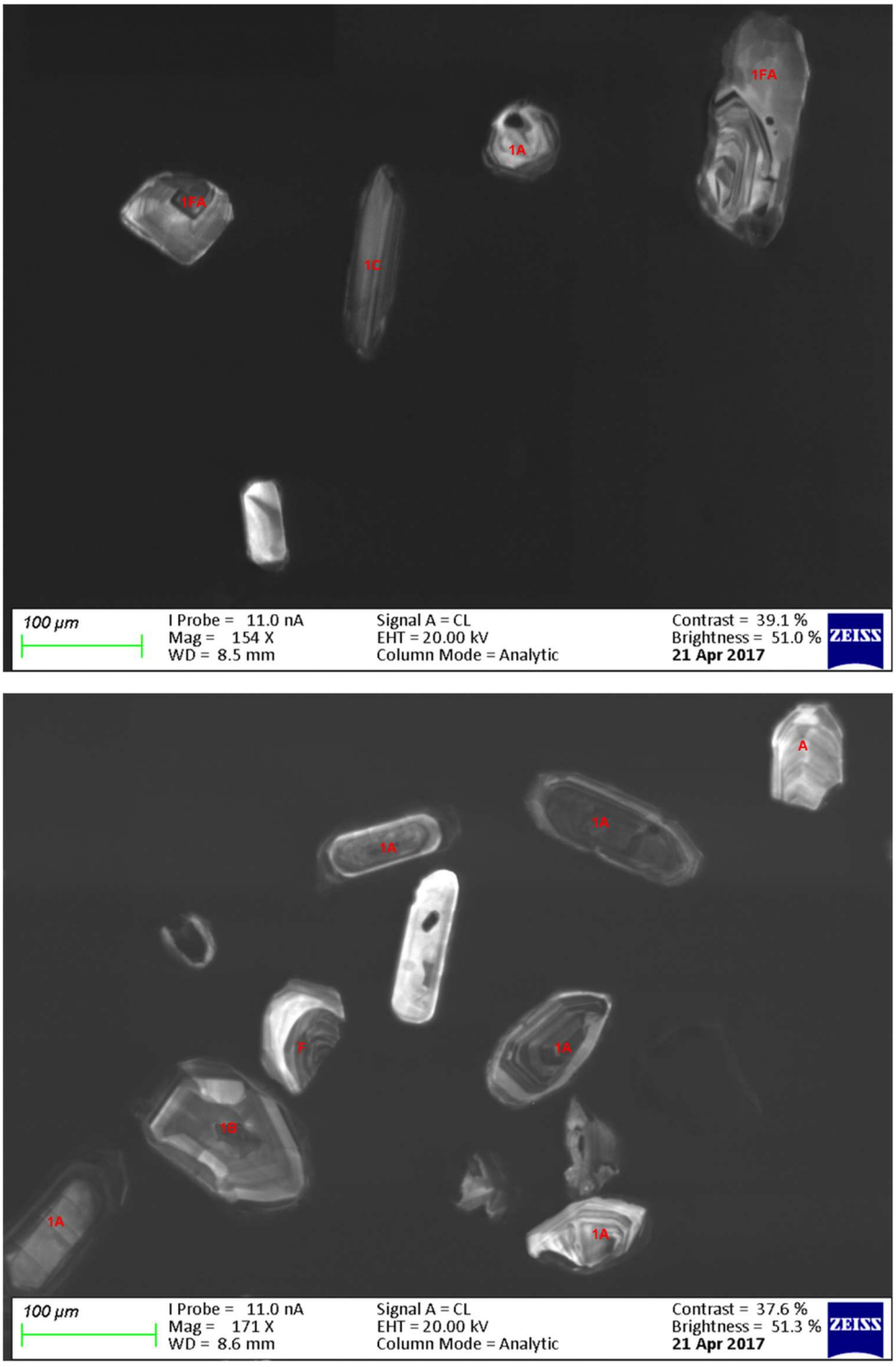

Figure 7.7c: CL images of some of the representive zircons showing main types of internal structures within the studied Ubulu-Uku kaolins where, 1: Euhedral; A: Oscillatory/growth zoning; B: Sector zoning; C: Homogeneous unzoned; and F: Xenocrystic cores.

The zircon textures were dominated by oscillatory/growth zoning followed by those with xenocrystic cores. Few grains showed sector zonings. Oscillatory/growth zonings are considered as evidence of magmatic origin (Corfu *et al*., 2003).

The Th/U ratios of the zircons ranged from 0.04 to 1.78, though most zircons had ratios >0.3 (Fig. 7.8). The Th/U ratios obtained for the zircons within the Ubulu-Uku kaolins were suggestive of predominantly magmatic origin (Wanniarachchi *et al*., 2016).

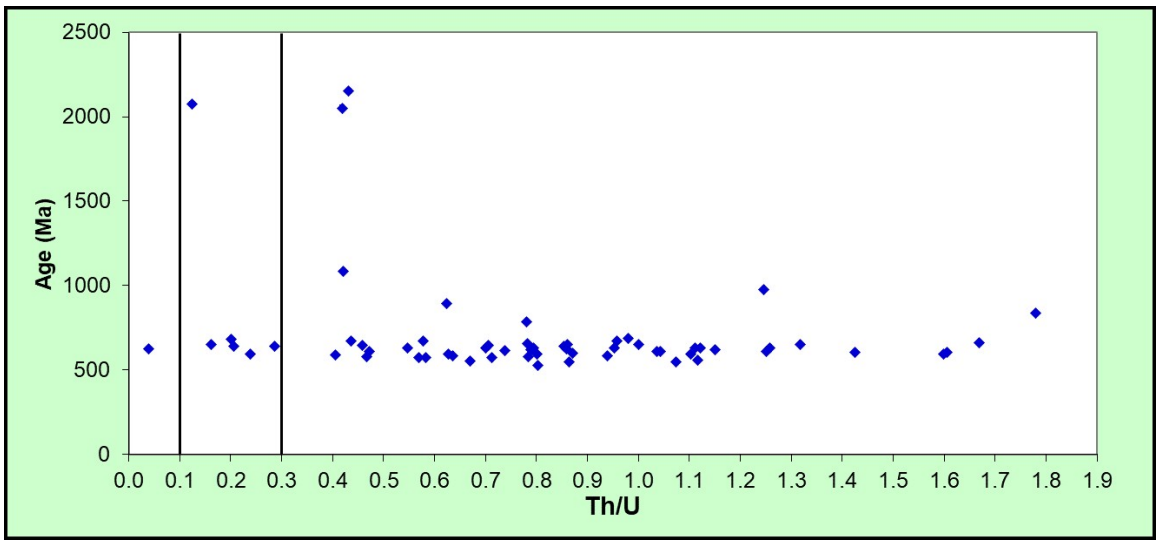

Figure 7.8: Th/U variation with age (Ma) in the studied Ubulu-Uku kaolins; the 0.1 and 0.3 black lines mark the upper and lower limits of zircon of metamorphic or magmatic origin, respectively (Wanniarachchi *et al*., 2016).

7.2 Detrital Zircon U-Pb Ages

The results of the analyses of zircon minerals selected in each of the kaolin deposits are presented in Appendices 7.5 – 7.9. Most ablation spots were located in the core and rim region of the grains. Ages less than 1300 Ma were based on the $^{206}Pb/^{238}U$ ratios, whereas older ages (> 1300 Ma) were based on the $^{207}Pb/^{206}Pb$ ratios. This is because $^{207}Pb/^{206}Pb$ ages become increasingly imprecise below 1300 Ma due to small amounts of ^{207}Pb usually due to the effect of possible Pb loss (Meinhold *et al*., 2010).

7.2.1 Lakiri Kaolins

A total of 101 analyses were undertaken and results are shown on concordia plots (Figures 7.9 and 7.10). Figure 7.9 for ages <1300 Ma show cluster around 570 Ma, whereas Figure 7.10 for ages >1300 Ma show cluster around 2000 Ma. Analyses plotting away from the concordia (line connecting equal ages) are believed to have lost common lead (^{204}Pb). These results show that 35 % of the analyses had >10 % discordance.

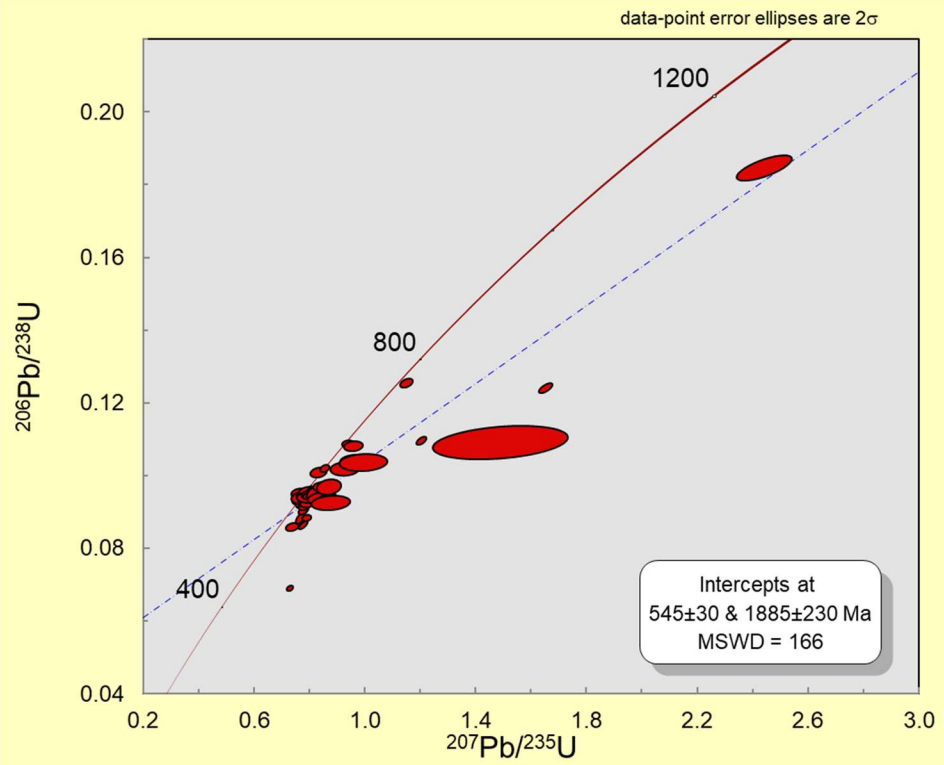

Figure 7.9: U-Pb concordia diagram of detrital zircons (Ages < 1300 Ma) in the studied Lakiri kaolins.

- **Description of Probability Density Plot**

The probability density plot shows the distribution of age frequencies for zircon ages with ≤ 10 % discordance. The largest peaks center within the Neoproterozoic (1000 – 541 Ma) (19 grains, several peaks) and Paleoproterozoic (2500 - 1600 Ma) (45 grains, several peaks) with smaller peaks observed close to them (Fig. 7.11). In addition, small peak can be identified within the Archean ages (4000 - 2500 Ma).

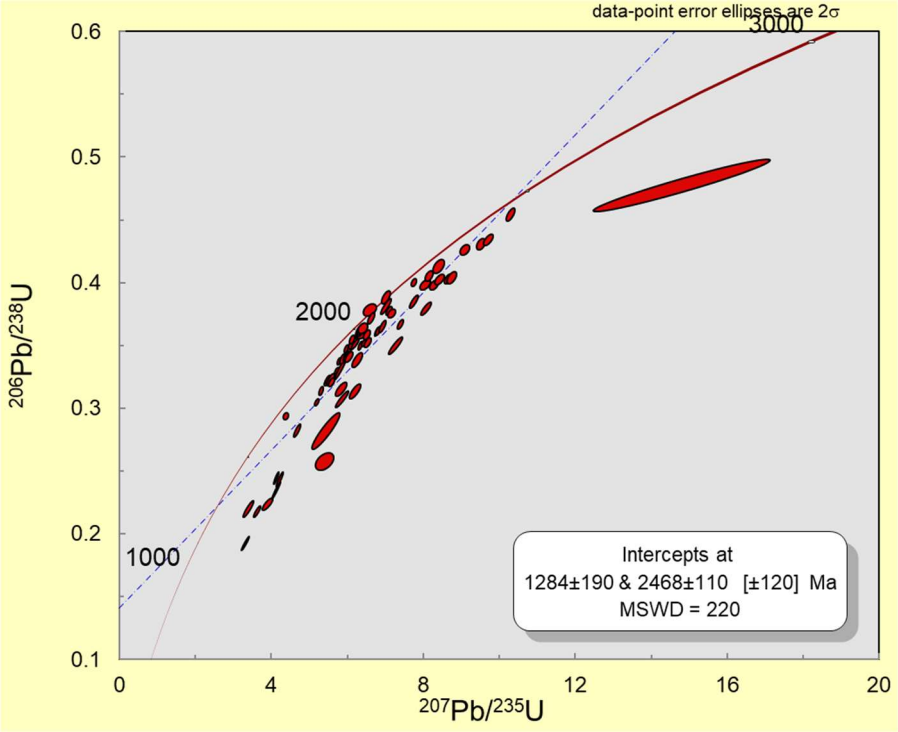

Figure 7.10: U-Pb concordia diagram of detrital zircons (Ages > 1300 Ma) in the studied Lakiri kaolins.

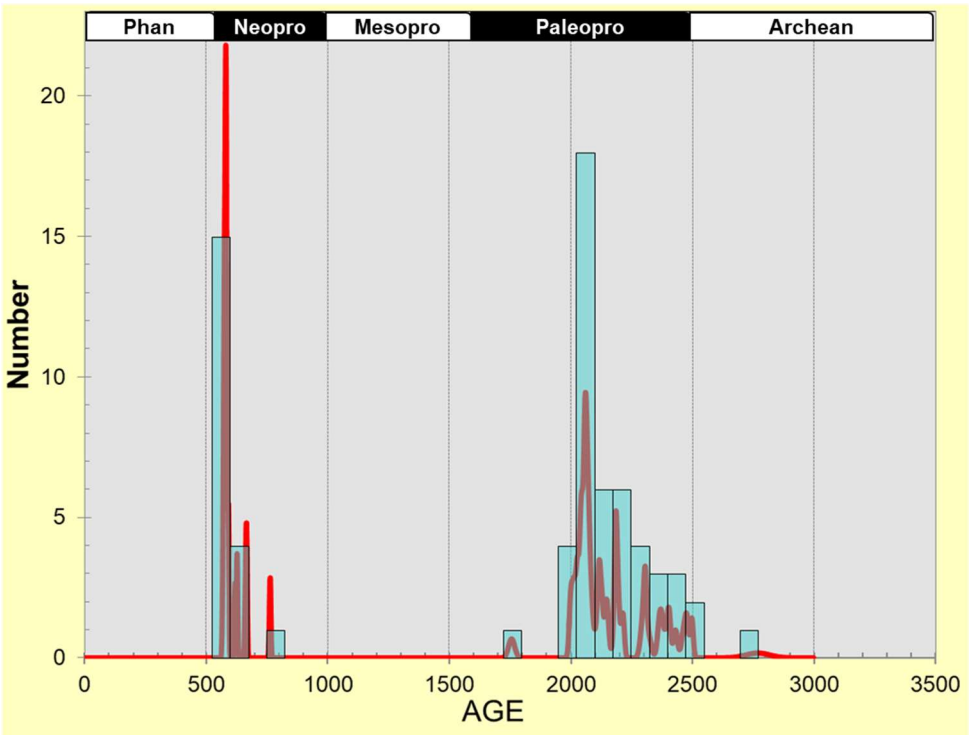

Figure 7.11: Probability density diagram of detrital zircon ages with concordance between 90 and 110 % in the studied Lakiri kaolins.

- **Weighted Averages of Zircon Population Groups**

Five zircon age population groups with ≤ 10 % were obtained (Fig. 7.12 and Table 7.1).

Table 7.1: Weighted Averages of Zircon Population Groups within the studied Lakiri Kaolins.

Group	Weighted Average (Ma)	MSWD	N
1	579.7± 2.3	1.7	13
2	2054.7±6.1	2.0	11
3	2120±12	1.2	4
4	2186.5±5.4	0.79	5
5	2304.8±7.5	1.1	4

7.2.2 Eruku Kaolins

A total of 114 analyses were undertaken and results are shown on concordia plots (Figures 7.13 and 7.14). Figure 7.13 for ages <1300 Ma show cluster around 580 Ma, whereas Figure 7.14 for ages >1300 Ma show cluster around 1750 Ma. Analyses plotting away from the concordia (line connecting equal ages) are believed to have lost common lead (^{204}Pb). These results show that 22 % of the analyses had >10 % discordance.

- **Description of Probability Density Plot**

The probability density plot shows the distribution of age frequencies for zircon ages with ≤ 10 % discordance. The largest peaks center within the Neoproterozoic (1000 - 541 Ma) (54 grains, several peaks) with smaller peaks observed close to them. In addition, smaller peaks can be identified within the Paleoproterozoic (2500 - 1600 Ma) (35 grains, several peaks) (Fig. 7.15).

- **Weighted Averages of Zircon Population Groups**

Nine zircon age population groups with ≤ 10 % were obtained (Fig. 7.16 and Table 7.2).

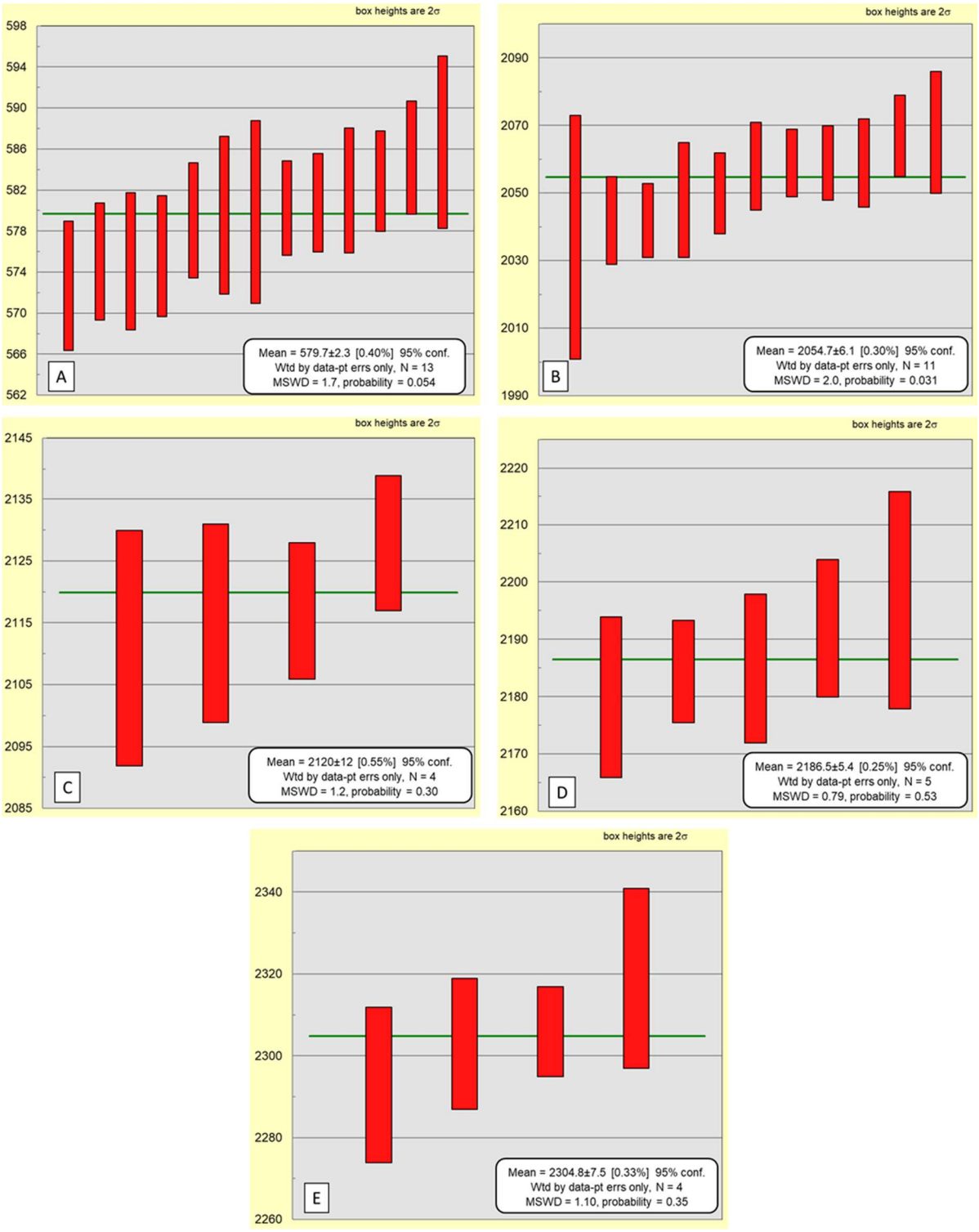

Figure 7.12: Weighted Averages of Zircon Population Groups in the studied Lakiri kaolins from the youngest (A): G1 to the Oldest (E): G5. Ages are in Ma and N = Number of analyses.

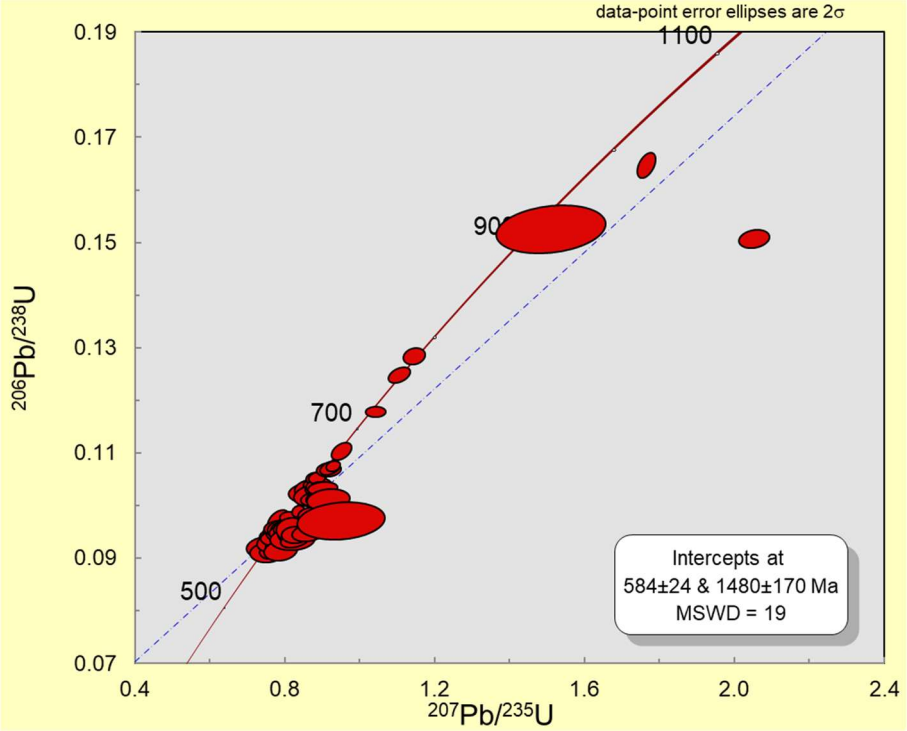

Figure 7.13: U-Pb concordia diagram of detrital zircons (Ages < 1300 Ma) in the studied Eruku kaolins.

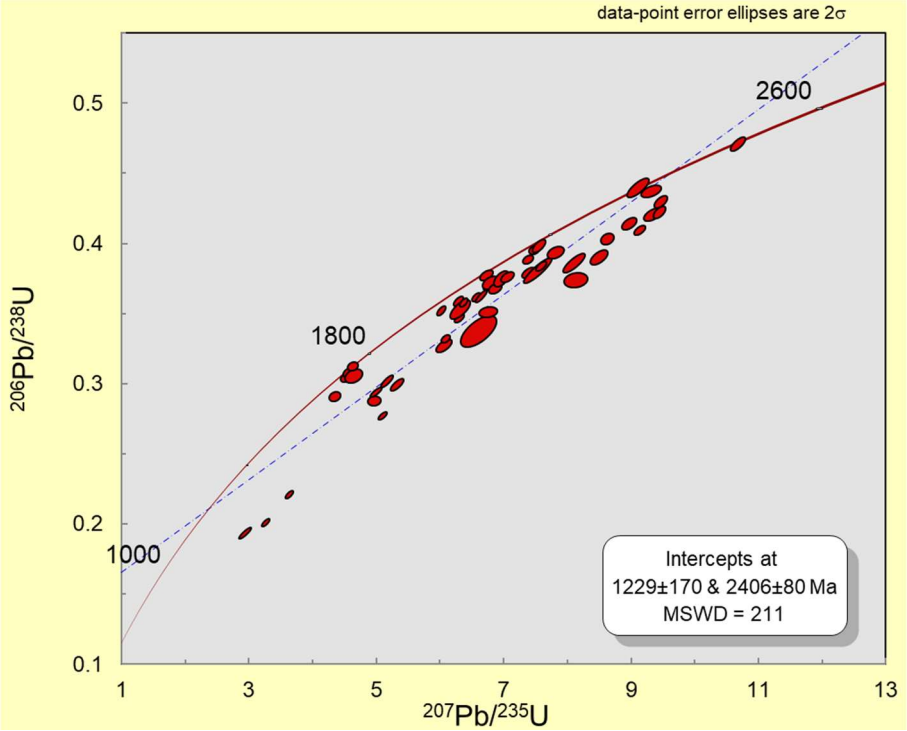

Figure 7.14: U-Pb concordia diagram of detrital zircons (Ages > 1300 Ma) in the studied Eruku kaolins.

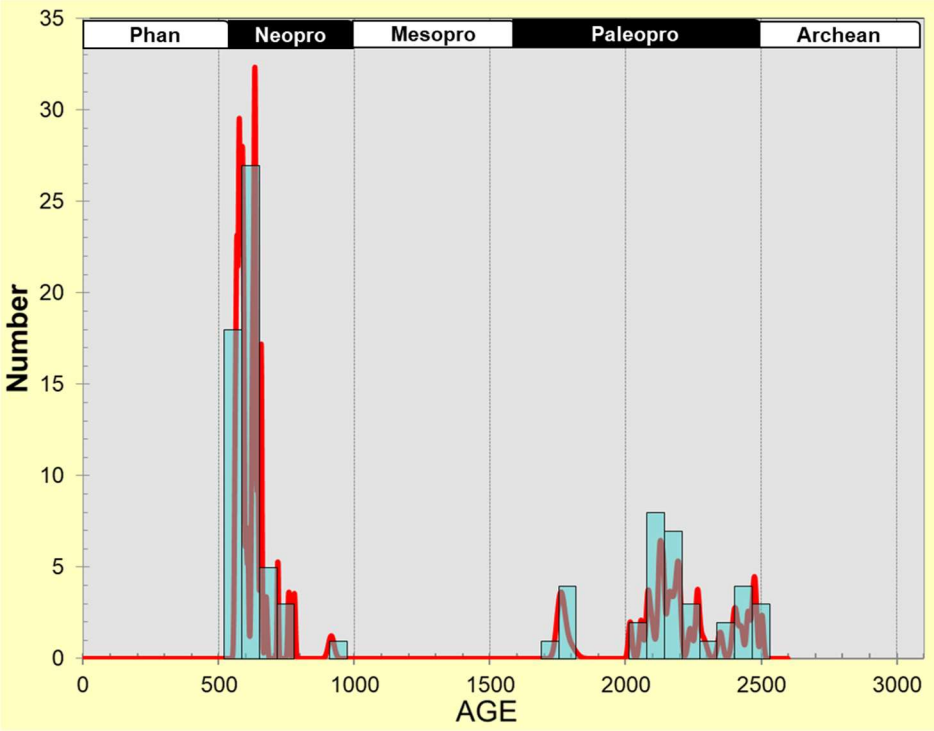

Figure 7.15: Probability density diagram of detrital zircon ages with concordance between 90 and 110 % in the studied Eruku kaolins.

Table 7.2: Weighted Averages of Zircon Population Groups within the studied Eruku Kaolins.

Group	Weighted Average (Ma)	MSWD	N
1	577.9± 2.8	1.9	13
2	632.1±2.6	2.0	13
3	656.6±2.6	0.31	4
4	1762±13	0.22	4
5	2085.8±9.2	0.62	4
6	2132.4±5.9	0.93	5
7	2190±12	1.4	5
8	2268±23	1.3	3
9	2474.6±7.5	0.9	3

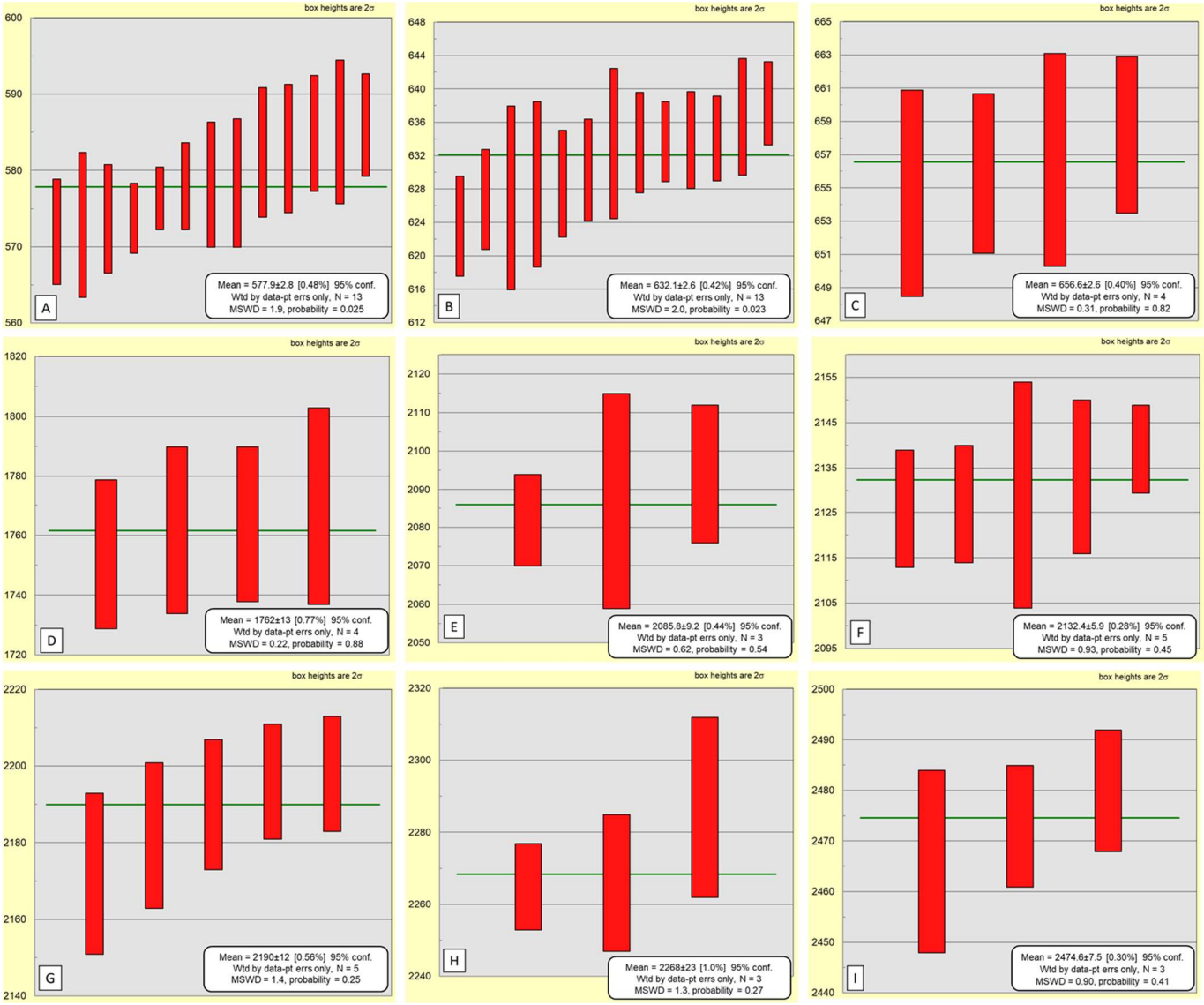

Figure 7.16: Weighted Averages of Zircon Population Groups in the studied Eruku kaolins from the youngest (A): G1 to the Oldest (I): G9. Ages are in Ma and N = Number of analyses.

7.2.3 Awo-Omama Kaolins

A total of 112 analyses were undertaken and results are shown on concordia plots (Figures 7.17 and 7.18). Figure 7.17 for ages <1300 Ma show a big cluster around 580 Ma with smaller clusters around 800 and 900 Ma, whereas Figure 7.18 for ages >1300 Ma show no cluster. Analyses plotting away from the concordia (line connecting equal ages) are believed to have lost common lead (^{204}Pb). These results show that 15 % of the analyses had >10 % discordance.

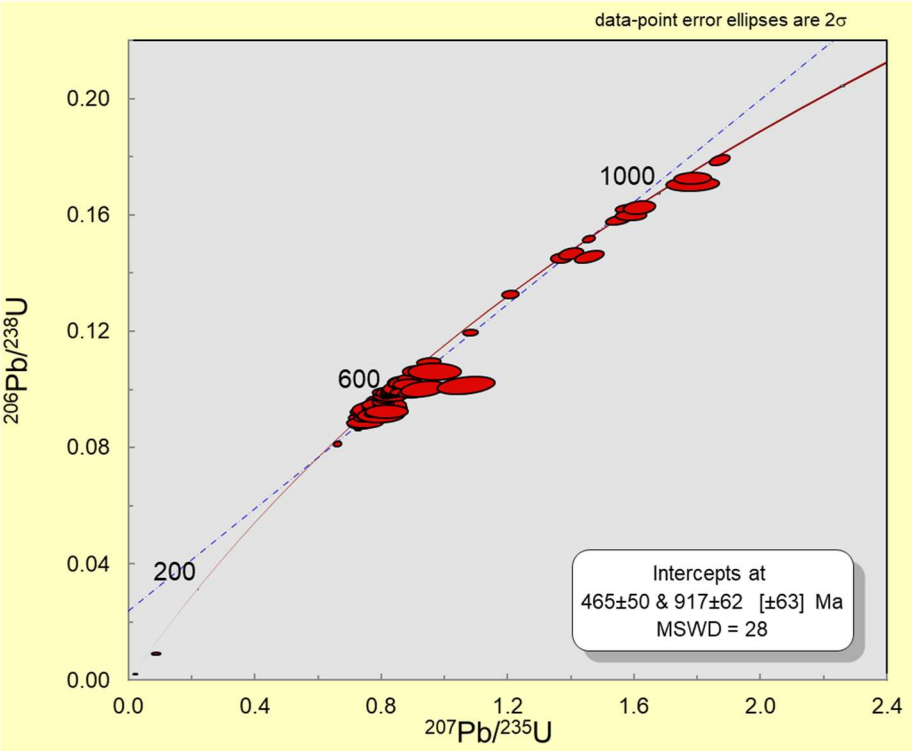

Figure 7.17: U-Pb concordia diagram of detrital zircons (Ages < 1300 Ma) in the studied Awo-Omama kaolins.

- **Description of Probability Density Plot**

The probability density plot shows the distribution of age frequencies for zircon ages with ≤ 10 % discordance. The largest peaks center within the Neoproterozoic (541 – 1000 Ma) (76 grains, several peaks) with smaller peaks observed close to them. In addition, smaller

peaks were identified within the Paleoproterozoic (2500 - 1600 Ma) (16 grains, several peaks) and Archean (4000 - 2500 Ma) (3 grains, one peak) (Fig. 7.19).

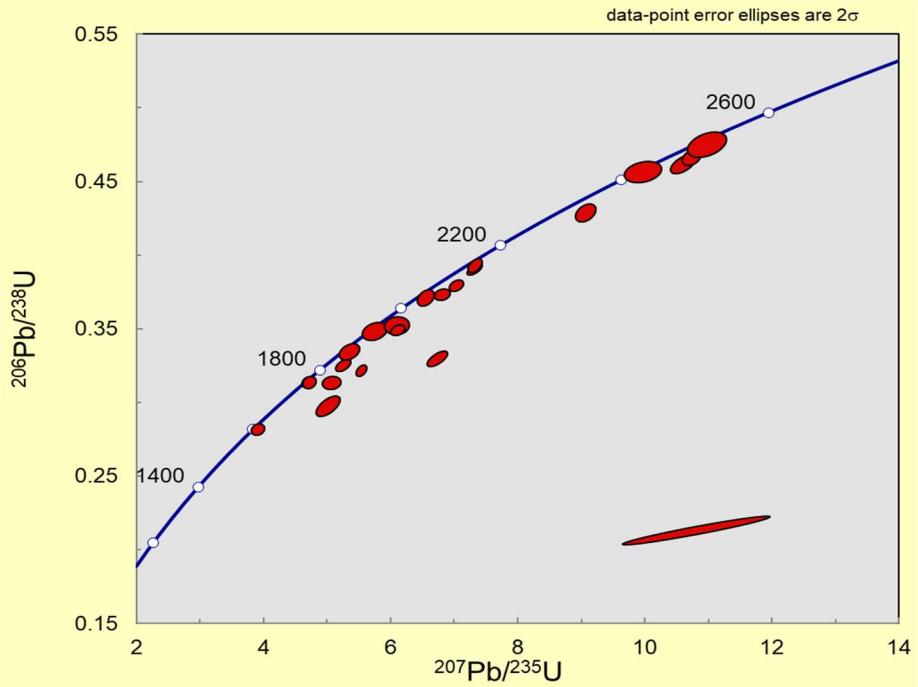

Figure 7.18: U-Pb concordia diagram of detrital zircons (Ages > 1300 Ma) in the studied Awo-Omama kaolins.

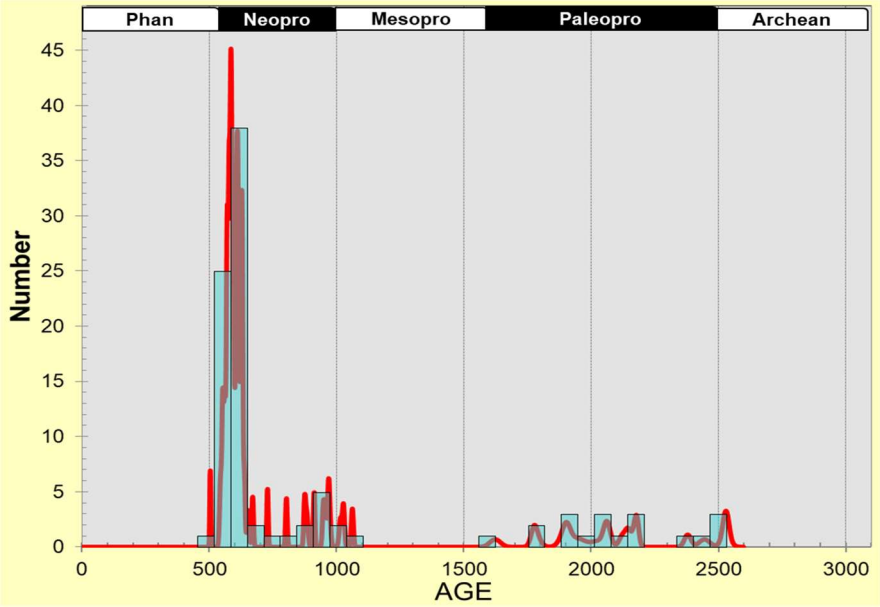

Figure 7.19: Probability density diagram of detrital zircon ages with concordance between 90 and 110 % in the studied Awo-Omama kaolins.

- **Weighted Averages of Zircon Population Groups**

Five zircon age population groups with $\leq 10\ \%$ were obtained (Fig. 7.20 and Table 7.3).

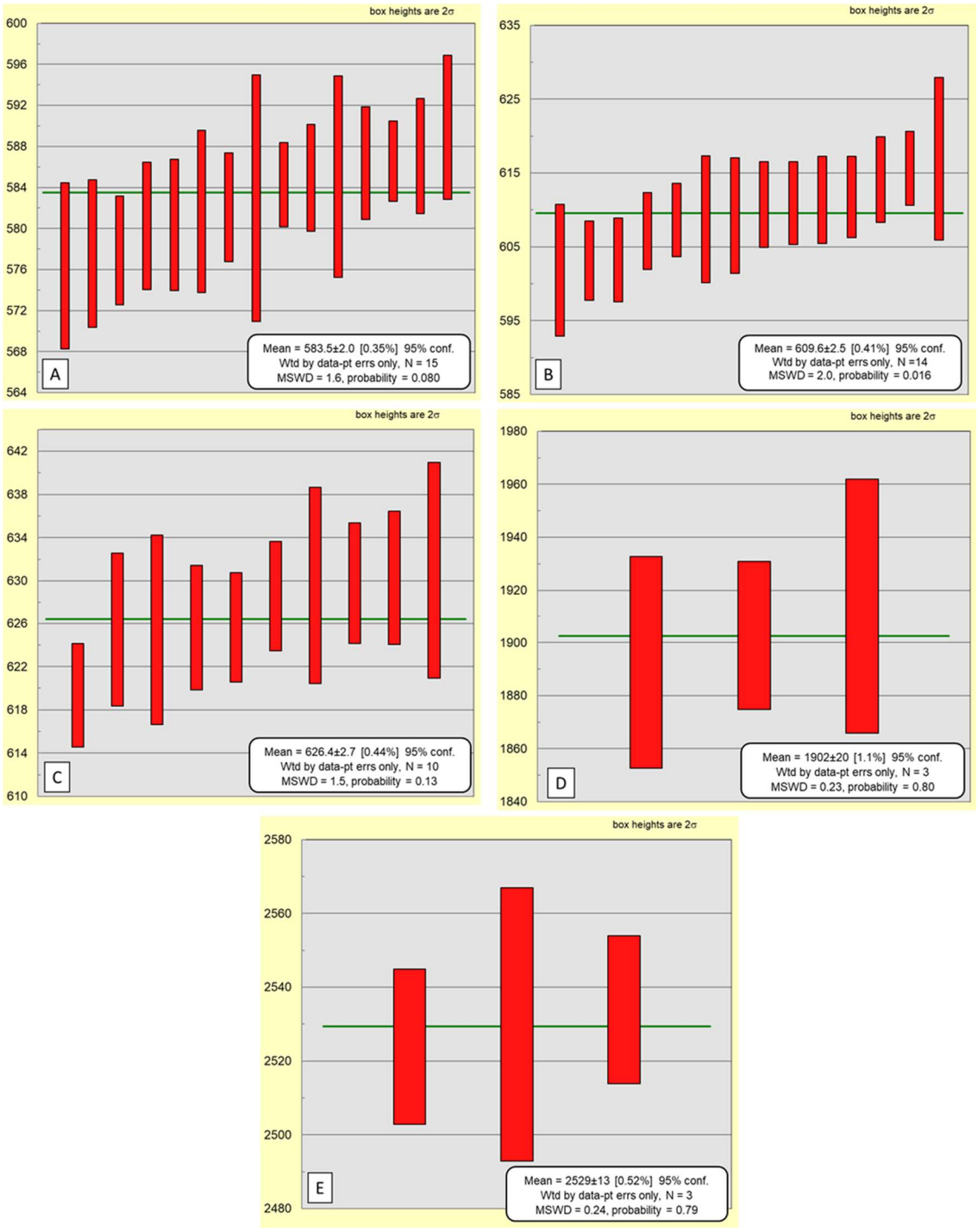

Figure 7.20: Weighted Averages of Zircon Population Groups in the studied Awo-Omama kaolins from the youngest (A): G1 to the Oldest (E): G5. Ages are in Ma and N = Number of analyses.

Table 7.3: Weighted Averages of Zircon Population Groups within the studied Awo-Omama Kaolins.

Group	Weighted Average (Ma)	MSWD	N
1	583.5± 2.0	1.6	15
2	609.6±2.5	2.0	14
3	626.4±2.7	1.5	10
4	1902±20	0.23	3
5	2529±13	0.24	3

7.2.4 Ubulu-Uku Kaolins

A total of 114 analyses were undertaken and results are shown on concordia plots (Figures 7.21 and 7.22). Figure 7.21 for ages <1300 Ma show a big cluster around 570 Ma, whereas Figure 7.22 for ages >1300 Ma show no cluster. Analyses plotting away from the concordia (line connecting equal ages) are believed to have lost common lead (^{204}Pb). These results show that 47 % of the analyses had >10 % discordance.

- **Description of Probability Density Plot**

The probability density plot shows the distribution of age frequencies for zircon ages with ≤ 10 % discordance. The largest peaks center within the Neoproterozoic (1000 – 541 Ma) (56 grains, several peaks) with smaller peaks observed close to them. In addition, smaller peaks were identified within the Paleoproterozoic (2500 - 1600 Ma) (4 grains, several peaks) (Fig. 7.23).

- **Weighted Averages of Zircon Population Groups**

Seven zircon age population groups with ≤ 10 % were obtained (Fig. 7.24 and Table 7.4).

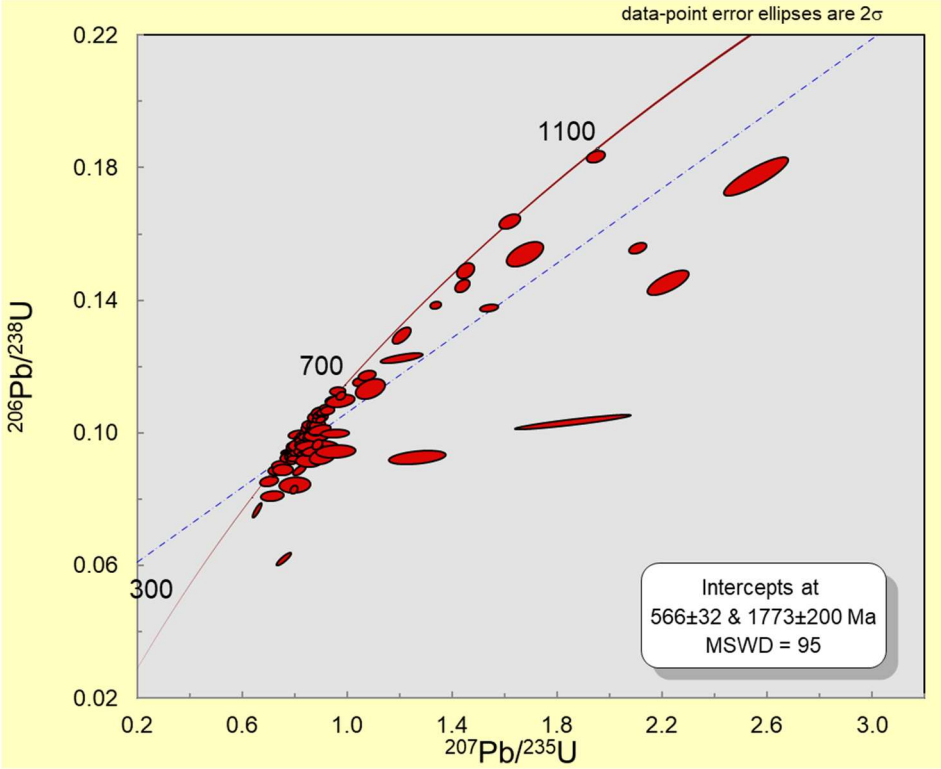

Figure 7.21: U-Pb concordia diagram of detrital zircons (Ages < 1300 Ma) in the studied Ubulu-Uku kaolins.

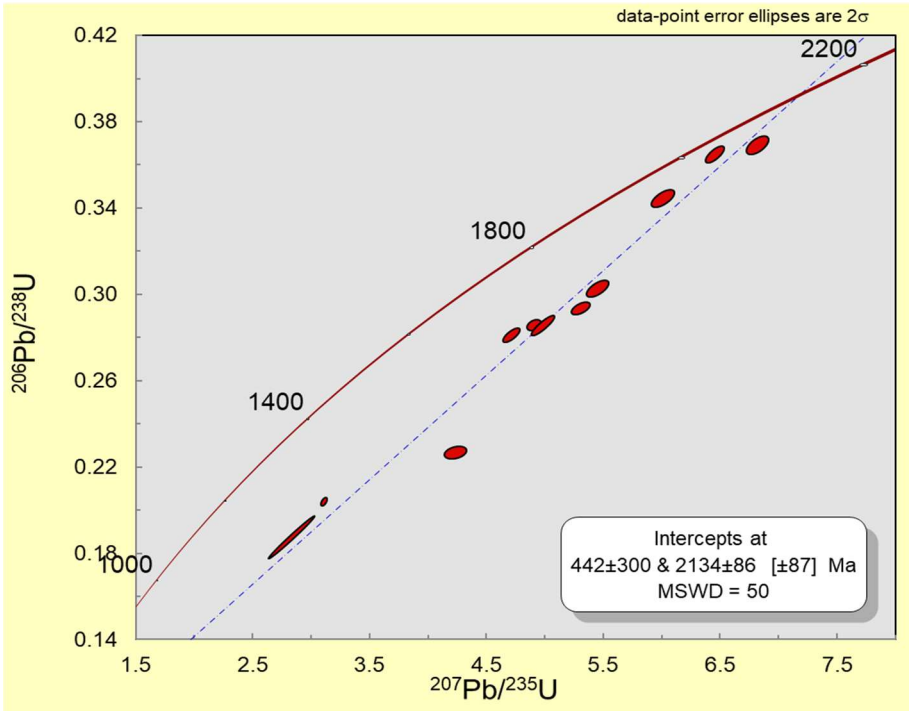

Figure 7.22: U-Pb concordia diagram of detrital zircons (Ages > 1300 Ma) in the studied Ubulu-Uku kaolins.

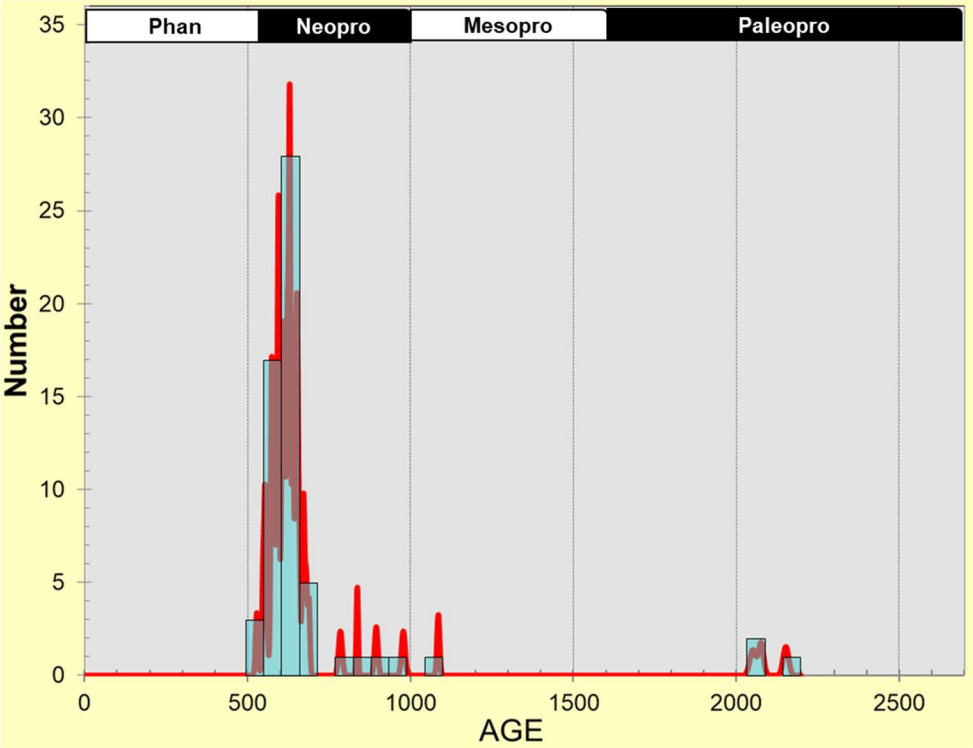

Figure 7.23: Probability density diagram of detrital zircon ages with concordance between 90 and 110 % in the studied Ubulu-Uku kaolins.

7.3 Maximum Depositional Age of the Cretaceous – Tertiary Kaolins

The most commonly used approach to determine the maximum age of deposition is from the youngest U-Pb zircon population age (Fedo *et al*., 2003; Dickinson and Gehrels, 2009). To place limits on the maximum age of deposition of geological formations, the maximum age of deposition must be younger than the age of the youngest detrital zircon provided no disturbance occurred in the U-Pb isotopic system.

However, both the minimum and maximum age brackets for deposition can be determined when the detrital zircon geochronology is linked with geochronology of cross-cutting younger igneous rocks or metamorphic ages (Fedo *et al*., 2003).

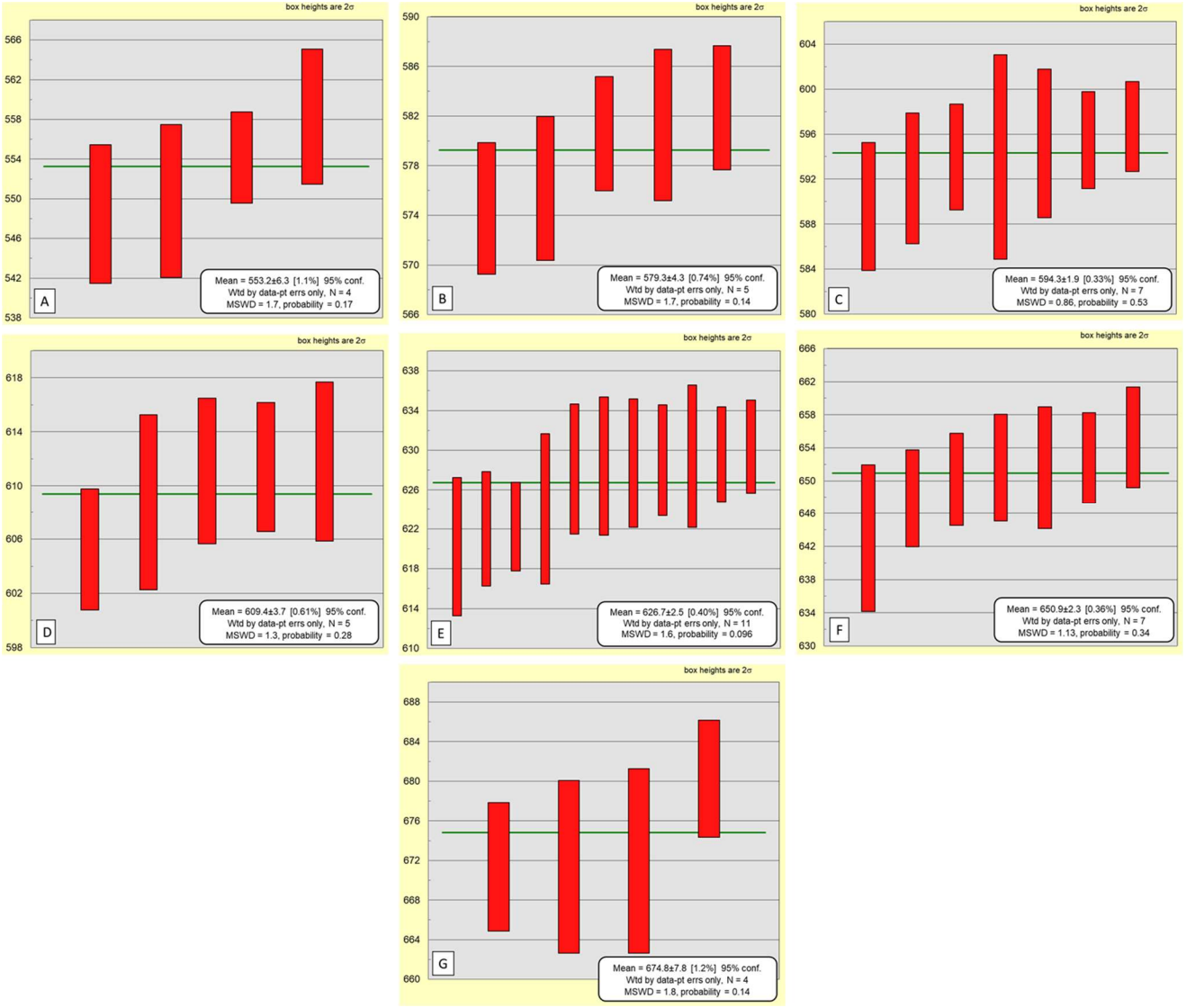

Figure 7.24: Weighted Averages of Zircon Population Groups in the studied Ubulu-Uku kaolins from the youngest (A): G1 to the Oldest (G): G7. Ages are in Ma and N = Number of analyses.

Table 7.4: Weighted Averages of Zircon Population Groups within the studied Ubulu-Uku Kaolins.

Group	Weighted Average (Ma)	MSWD	N
1	553.2±6.3	1.7	4
2	579.3±4.3	1.7	5
3	594.3±1.9	0.86	7
4	609.4±3.7	1.3	5
5	626.7±2.5	1.6	11
6	650.9±2.3	1.1	7
7	674.8±7.8	1.8	4

In this study in order to obtain the most accurate representation of the maximum depositional age of the kaolins, three alternate measures were used to determine the youngest age varying from least to most statistically robust (Tucker *et al*., 2013; Maksaev *et al*., 2015) as follows:

i. Youngest single grain (YSG) age;
ii. Youngest graphic peak (YGP) age from the probability density plot; and
iii. Weighted average (WA) age of the youngest zircon population group.

Results of the approaches are presented in Table 7.5. It is obvious that the maximum depositional age estimates for the Cretaceous - Tertiary kaolins in the Eastern Dahomey and Niger Delta Basins in Nigeria corresponds to the Ediacaran Period (645 – 541 Ma) of the Neoproterozoic Era (1000 – 541 Ma) except for the YSG ages 504±4.1 and 528.6±7.7 Ma for Awo-Omama and Ubulu-Uku kaolins, respectively. The YSG ages may be erroneous to be considered as the maximum depositional ages for the kaolin deposits since it only represents a single data point (Dickinson and Gehrels, 2009). Hence, the YSG ages will not be considered.

Table 7.5: Age of Maximum Deposition (Ma) Interpretations for the studied Cretaceous – Tertiary kaolins.

Age	Deposit	YSG Age	YGP Age	WA Age	Period	Era
Cretaceous	Lakiri	569.6±6.5	580.5	579.7±2.3	Ediacaran	Neoproterozoic
	Eruku	559.8±5.6	633.1	577.9±2.8	(645 – 541)	(1000 – 541)
Tertiary	Awo-Omama	504±4.1	586.3	583.5±2	Ediacaran	Neoproterozoic
	Ubulu-Uku	528.6±7.7	629.2	553.2±6.3	(645 – 541)	(1000 – 541)

7.3.1 Implications for Timing of Kaolinisation

The Ediacaran Period (645 – 541 Ma) of the Neoproterozoic Era (1000 – 541 Ma) determined as the maximum depositional age for the Cretaceous – Tertiary kaolins is highly unlikely. The Neoproterozoic Era in the Earth's history is believed to be a time when the Earth entered a 'snowball' state characterised by periods of widespread glaciation of global extent (Kirschvink, 1992; Gyollai *et al.,* 2014). One of the postulates of the snowball Earth hypothesis is that during glaciation, chemical weathering on the continents were shut down (Dobrzinski *et al*., 2004). In addition, considering the conditions favourable for the formation of kaolins such as high rainfall and temperate to tropical climate (Murray and Keller, 1993), the studied Cretaceous to Tertiary kaolins could not have been formed under the Neoproterozoic environmental conditions. Furthermore, the Neoproterozoic maximum depositional ages for the Cretaceous to Tertiary kaolins is not consistent with the earlier palynological studies of the Abeokuta Group (host of the Cretaceous kaolins) by Jan du Chene *et al.,* (1979) who indicated a Late Albian – Early Cenomanian age. However, Omatsola and Adegoke (1981) dated the Ise Formation within the Abeokuta Group to be Neocomian (probably Valanginian – Barremian) based on pollen and spores present in them. The Ogwashi - Asaba Formation (host of the Tertiary kaolins) have also been dated Oligo-Miocene using pollen data (Okezie and Onuogu, 1988; Nwajide, 2013).

Alternatively, stable isotope data of the Cretaceous - Tertiary kaolins can yield useful timing constraints by comparing the hydrogen isotope ratios with those of sedimentary kaolins of known age. Gilg (2000) reported that, the Upper Oligocene to Miocene kaolins have δD values, ranging from – 77 to – 90 ‰, compared to the Middle Jurassic and Mid

- Late Cretaceous kaolins with δD values from – 59 to – 66 ‰, and Late Triassic kaolin (-50 ‰). Comparing the δD values of the Cretaceous (– 48.95 to – 57.02 ‰) and Tertiary (– 53.64 to – 65.71 ‰) kaolins, these values are comparable to the Late Triassic – Late Cretaceous (237 – 72 Ma) sedimentary kaolins formed during the Mesozoic Era. However, no stable isotope geochronology exist for Western Africa compared to Australia and Europe since values of isotopic compositions may be identical for different continents. An established stable isotopic geochronological system is required for West Africa to corroborate the correctness of the kaolinisation timing constraints based on the stable isotopic data.

Hence, the Neoproterozoic maximum depositional age obtained from the U-Pb detrital zircon dating most likely refer to the provenance ages of the rocks from which they were derived. Thus, considering the Early Cretaceous age for the Ise Formation (host for the Cretaceous kaolins), it can be inferred that the probable timing of kaolinisation for the Cretaceous kaolins lies between the Ediacaran (645 – 541 Ma) and Early Cretaceous Periods. In addition, the probable timing of kaolinisation for the Tertiary kaolins will be between the Ediacaran Period (645 – 541 Ma) and Oligo – Miocene age considering the Oligo – Miocene age obtained for the Ogwashi – Asaba Formation (host for Tertiary kaolins).

7.3.2 Implications for Provenance of the Cretaceous - Tertiary Kaolins

Provenance ages obtained from the U-Pb dating of the detrital zircons present within the Cretaceous – Tertiary kaolins can be used to identify specific sediment sources. A detailed inspection of the probability density plots reveal that U-Pb detrital zircon ages in the range of 1000 – 541 Ma (Neoproterozoic Era) constituted 48 % and 85 % of the Cretaceous and Tertiary kaolins, respectively. Ages within 2500 – 1600 Ma (Paleoproterozoic Era) constituted 52 % and 13 % of the Cretaceous and Tertiary detrital zircons, whereas the Tertiary kaolins (particularly Awo-Omama kaolins) had 2 % of U-Pb detrital zircon ages within 4000 – 2500 Ma (Archean).

The Nigeria basement complex had undergone four (4) major orogenies, the Liberian (2700 – 2500 Ma); the Eburnean (2500 – 2000 Ma); the Kibaran (2000 – 1100 Ma); and

the Pan African (750 – 450 Ma) (Oyinloye, 2011). The U-Pb ages of the detrital zircons with the studied Cretaceous – Tertiary kaolins reflect major inputs of zircon grains from predominantly the Eburnean and Pan African orogenies with little contributions from the Liberian and Kibaran orogenies (Table 7.6).

Table 7.6: Percentages of U-Pb Ages of Detrital Zircons (using ≤ 10 discordance) within the studied Cretaceous – Tertiary Kaolins.

Orogeny*	**Ages (Ma)***	**Deposits**			
		Lakiri (n=68)	**Eruku (n=89)**	**Awo-Omama (n=97)**	**Ubulu-Uku (n=61)**
Liberian (Archean)	2700 - 2500	2%	-	4%	-
Eburnean (Mid - Late Paleopro)	2500 - 2000	67%	34%	10%	5%
Kibaran (Early Mesopro - Mid Paleopro)	2000 - 1100	3%	6%	8%	-
Pan African	750 - 450	28%	60%	78%	95%

*Oyinloye, 2011.

Paleocurrent data for the Abeokuta Group within the Eastern Dahomey Basin is not available but the most probable sediment source will be from the West African Massif located north of the basin (Figure 7.25), whereas paleocurrent analysis of the Ogwashi-Asaba Formation within the Niger Delta Basin (Oboh-Ikuenobe *et al*., 2005) gave paleocurrent direction of approximately 150˚ (Figure 7.26). Thus, the azimuth and the rose diagram suggest that the provenance direction of the sediment source for the Ogwashi-Asaba Formation is confined to the Northwest of the Niger Delta Basin. This will correspond to sediment sources from the West African and Northern Nigerian Massifs (Figure 7.25).

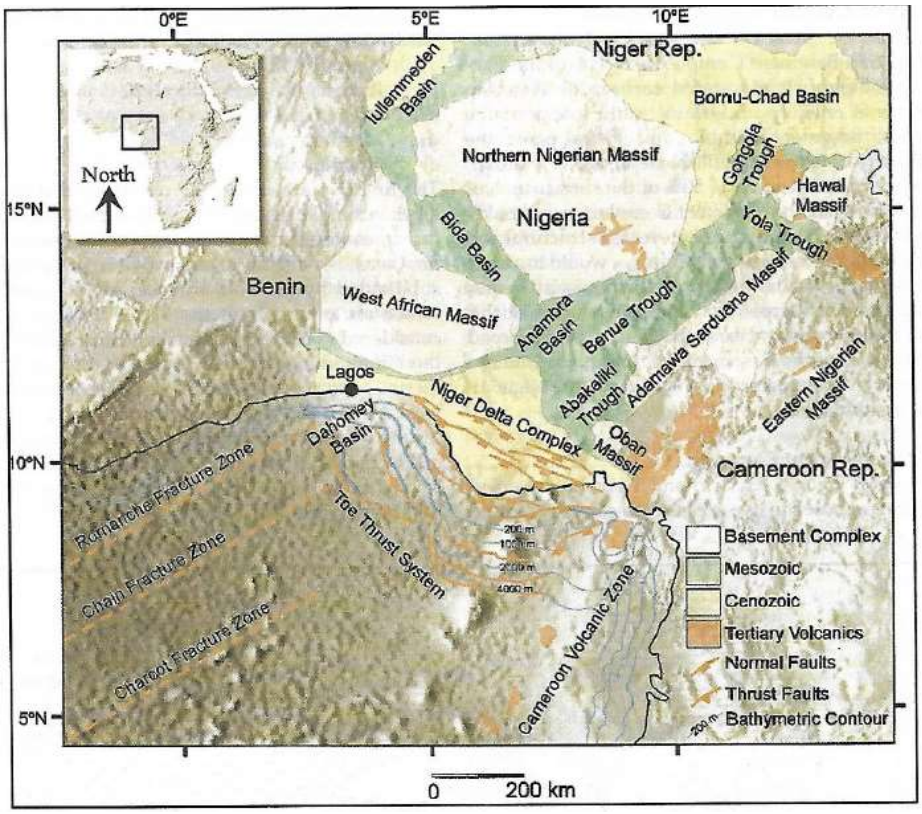

Figure 7.25: Map of Nigeria showing the probable source regions for the sediments within the Eastern Dahomey and Niger Delta Basins vis a vis – the West African Massif, the Northern Nigerian Massif, and the Eastern Nigerian Massif, respectively (After Nwajide, 2013).

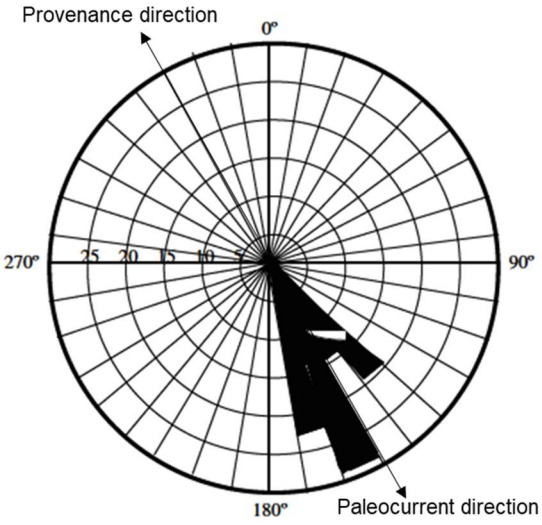

Figure 7.26: Rose diagram illustrating Paleocurrent and Provenance directions in the Ogwashi-Asaba Formation (Modified after Oboh-Ikuenobe, *et al*., 2005).

The Massifs are made up of the Migmatite-Gneiss Complex (MGC) (Migmatite, Gneisses, and Granite Gneisses) which accounted for 60 % of the surface area of the Nigerian Basement (Rahaman and Ocan, 1978). The banded Ibadan Grey Gneiss (within the West African Massif) of mantle origin was dated 2500 Ma (Archean) followed by the Eburnean Ibadan type Granite Gneisses. The MGC rocks are well exposed but not limited to Abuja, Keffi, Akwanga, Bauchi,Kaduna, Kano, Funtua, Okenne, Egbe, Ajaokuta (within the Northern Nigerian Massif); Ibadan, Ile-Ife, Akure, Ikere (within the West African Massif); and Obudu and the Oban Massif (within the Eastern Nigerian Massif) (Obaje, 2009).

The Older Granites (OG) are the most obvious manifestation of the Pan African orogeny in Nigeria with a wide range in age (750 -450 Ma) and composition (Rahaman, 1988). The OG suite are classified compositionally as biotite granites, biotite-muscovite granites, syenites, charnockites, serpentinites, and anorthosites. They occur intricately associated with the MGC and the Schist Belts in which they generally intruded. Hence, they occur in most places where rocks of the MGC and the Schist Belts occur such as in and around Wusasa (Zaria), Abuja, Bauchi, Akwanga (within the Northern Nigerian Massif); Ado-Ekiti, Akure (within the West African Massif); and Obudu areas (within the Eastern Nigerian Massif) (Obaje, 2009).

Representation of the Kibaran Orogeny is scarce in Nigeria because during that time, the West African Craton was stable. Hence, the little contributions from the Liberian and Kibaran orogenic rock can probably be from the Banded Ibadan Grey Gneiss (Archean age) and minor mafic volcanics (Kibaran age) in the large Iseyin-Oyan River Schist Belt, respectively, both within the West African Massif (Turner, 1983; Obaje, 2009).

7.4 Conclusions

Based on the U-Pb radiogenic dating of the zircon minerals within the studied kaolins, the following deductions have been made:

a. The studied zircon minerals were generally characterised by euhedral – subhedral – rounded – subrounded shapes.

b. The maximum depositional age estimates for the Cretaceous - Tertiary kaolins in the Eastern Dahomey and Niger Delta Basins in Nigeria correspond to the Ediacaran Period (645 – 541 Ma) of the Neoproterozoic Era (1000 – 541 Ma). Lack of consistency with previous studies throw doubt on this estimated age. In addition, the environmental conditions during Neoproterozoic Era is very unlikely to favour kaolin formation. Hence, the Ediacaran Period (645 – 541 Ma) of the Neoproterozoic Era (1000 – 541 Ma) is taken as part of the provenance ages of rocks from which the sediments were derived. However, considering the ages of the host formations for the studied Cretaceous - Tertiary kaolins, it can be inferred that the probable timing of kaolinisation for the Cretaceous kaolins lies between the Ediacaran (645 – 541 Ma) and Early Cretaceous Periods. In addition, the probable timing of kaolinisation for the Tertiary kaolins will be between the Ediacaran Period (645 – 541 Ma) and Oligo – Miocene age.
c. Combined geochronological and paleocurrent information strongly demonstrate that the sediment sources for the studied Cretaceous – Tertiary kaolins were predominantly from rocks of Eburnean and Pan African ages located in the West African Massif for the Cretaceous kaolins, whereas for the Tertiary kaolins were from both the West African and Northern Nigerian Massifs with little contributions from rocks of Liberian and Kibaran ages.

Chapter Eight

Correlation between Selected Cretaceous African and South American Kaolins: Implications on the Evolution of the Gondwana Kaolins

This chapter aimed to correlate the results from this study with selected Cretaceous African and South American kaolins (Specific Objective 4) based on Hypothesis 4 with particular emphasis on their mineralogical, geochemical, isotopic and geochronogical characteristics as proxy signals.

8.1 Geology of the selected Cretaceous kaolin deposits

8.1.1 Lakiri and Eruku kaolin deposits (Nigeria)

Detailed geology of these deposits have been discussed earlier in chapter one (subsection 1.6) and chapter two (subsection 2.2.2) (Table 8.1).

Table 8.1: Summary of the selected Cretaceous kaolin deposits.

Country	Deposits	Geologic Age (Ma)	Basin	Host Formations	References
Nigeria	Lakiri	Valanginian – Barremian (140 – 125)	Eastern Dahomey	Ise	This study
	Eruku	Valanginian – Barremian (140 – 125)	Eastern Dahomey	Ise	This study
Egypt	Teeh*	Aptian - Albian (125 - 100)	Gulf of Suez	Malha	Baioumy *et al.*, 2012; 2013.
Brazil	Capim River*	Campanian - Maastrichtian (84 - 66)	Cameta	Ipixuna	Sousa *et al.*, 2007 a and b; dos Santos *et al.*, 2007; Pruett, 2016

(*): These sedimentary kaolin deposits were chosen because their mineralogical, geochemical, isotopic and geochronogical (except for Teeh) characteristics are available in literature.

8.1.2 Teeh kaolin deposit (Egypt)

In the Sinai Peninsula, the Teeh kaolin deposit occur within the Lower Cretaceous Malha Formation of the Gulf of Suez Basin (Baioumy, 2013). The Malha Formation is composed predominantly of gray, ferruginous cross-bedded sandstones with few interbeds of green silty shales and calcareous sandstones (Abu-Zied, 2008) (Fig. 8.1).

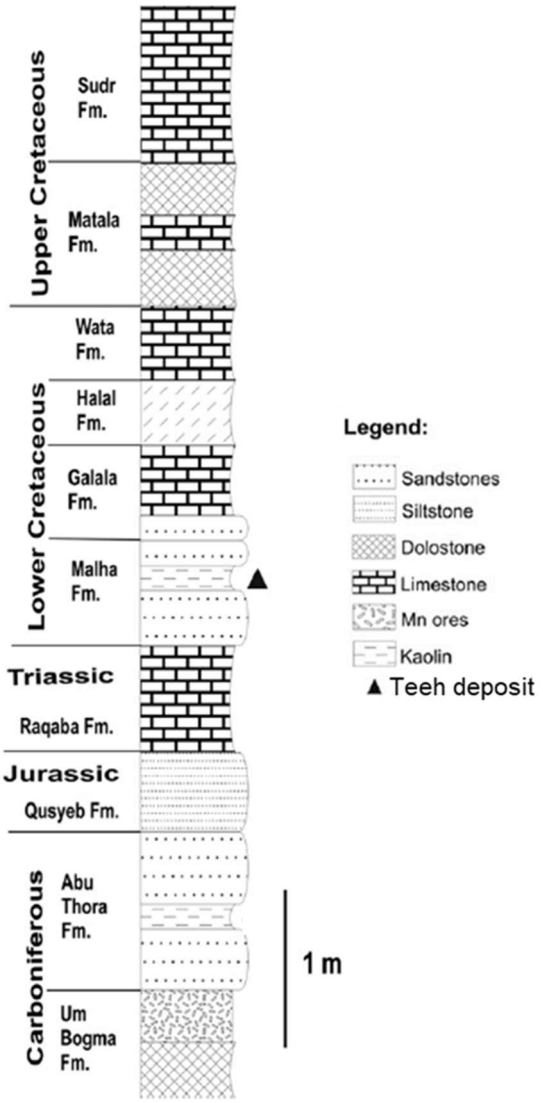

Figure 8.1: Generalised stratigraphy of the Gulf of Suez Basin in Egypt (After Baioumy, 2013).

8.1.3 Capim River kaolin deposit (Brazil)

The Capim River kaolin deposit occurs within the Ipixuna Formation belonging to the Cameta Sub-basin (Fig. 8.2). The Ipixuna Formation consists of strongly deferruginised, kaolinised sandstones and intercalated kaolinitic argillites. The lower part of the formation consist of the soft kaolin unit whereas the upper part corresponds to the flint kaolin unit (also referred to as 'semi-flint' or 'hard' kaolin) (Kotschoubery *et al*., 1996; Carneiro *et al*., 2002). The soft kaolins are believed to be Late Cretaceous, whereas the flint kaolin unit were probably of Oligo-Miocene age. Hence, the study only considered the soft kaolin unit.

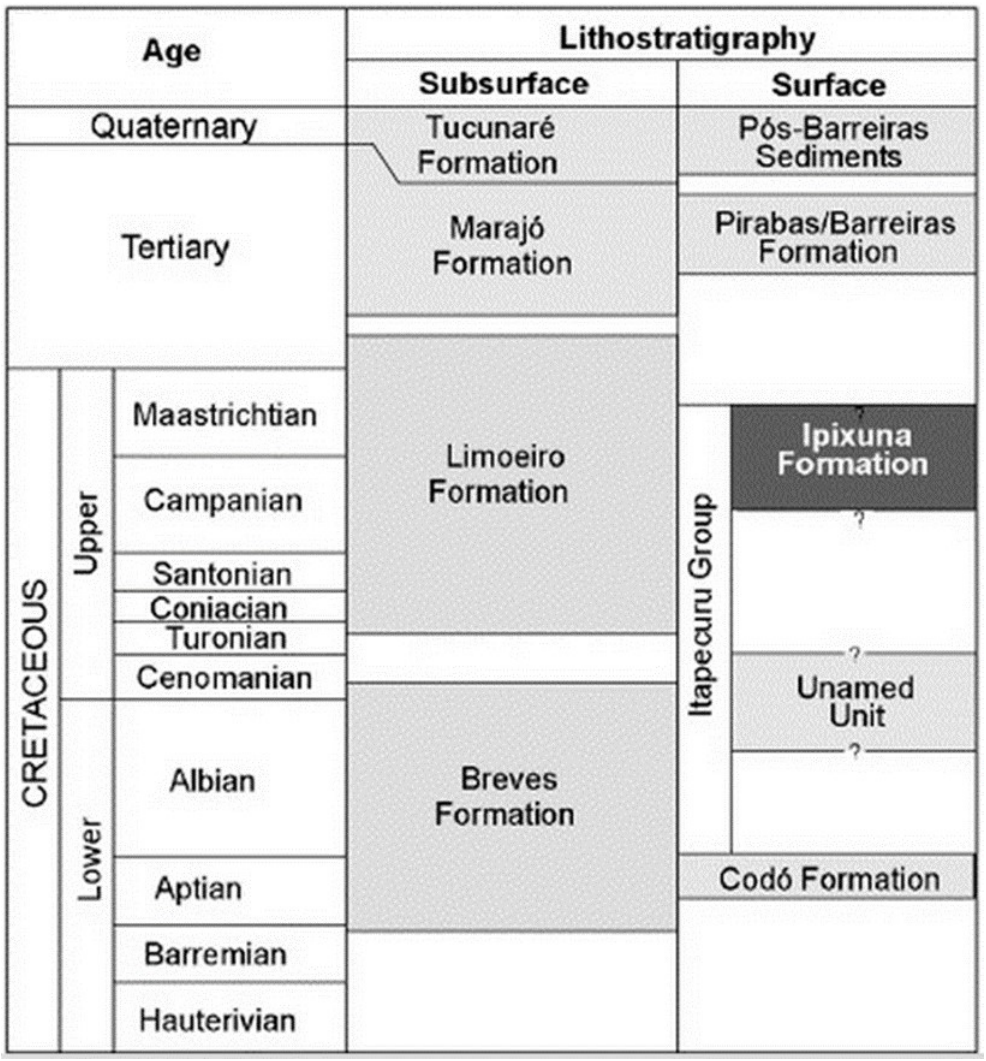

Figure 8.2: Generalised stratigraphy of the Cameta Sub-basin (Brazil), both in subsurface and surface (After Santos and Rossetti, 2006).

8.2 Mineralogical Considerations

8.2.1 XRD Studies

In the bulk samples, the Lakiri and soft Capim River kaolins contained greater amounts of kaolinites (averages of 99 and 98 wt %, respectively) and less quartz (average of 1 wt % for both, respectively) when compared to the Eruku and Teeh kaolins (kaolinite contents of 78 and 75 wt %, respectively, and quartz contents of 16 and 22 wt %, respectively) (Table 8.2 and Figure 8.3). The Lakiri and soft Capim River kaolins both have an average of 1 wt % for the titania and iron oxides, whereas the Eruku and Teeh both have averages of 2 and 3 wt %, respectively. In addition, no mica was identified in the kaolin deposits except for Eruku kaolin deposit (average of 4 wt %) (Table 8.2).

Table 8.2: Average mineralogical compositions (wt %) of the bulk selected Cretaceous kaolin deposits.

Country	Deposit	Kaolinite	Quartz	Mica	Titania + Iron oxides	HI
Nigeria	Lakiri	99	1	-	1	0.99
	Eruku	78	16	4	2	0.98
Egypt	Teeh[1]	75	22	-	3	0.7
Brazil	Soft Capim River[2]	98	1	-	1	1.11*

[1] Baioumy *et al*. (2012), [2] Pruett (2016) and * dos Santos *et al*. (2012).

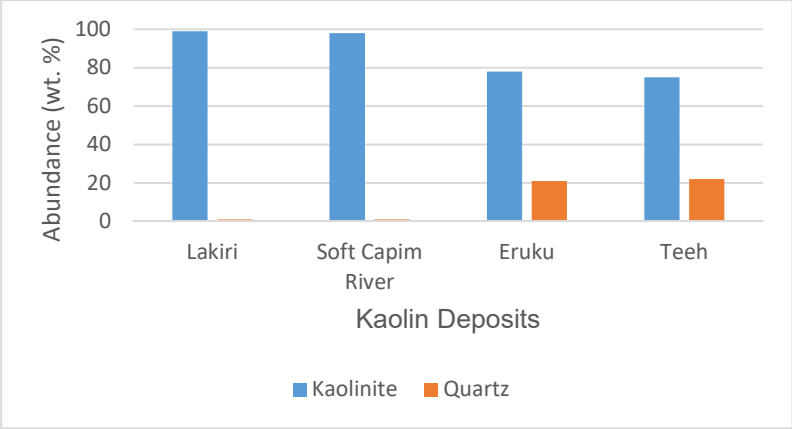

Figure 8.3: Kaolinite and quartz abundance (wt %) in the selected Cretaceous kaolins.

A plot of the average percentages of minerals present in each of the deposits on the ternary diagram for general mineralogical classification of economic kaolin deposits categorized the deposits in kaolin types (Fig. 8.4). The Lakiri and soft Capim River kaolins with more average kaolinite abundances plotted in the region of pure kaolin, whereas the Eruku and Teeh kaolins with lower average kaolinite with more quartz contents plotted in the region of sandy kaolins.

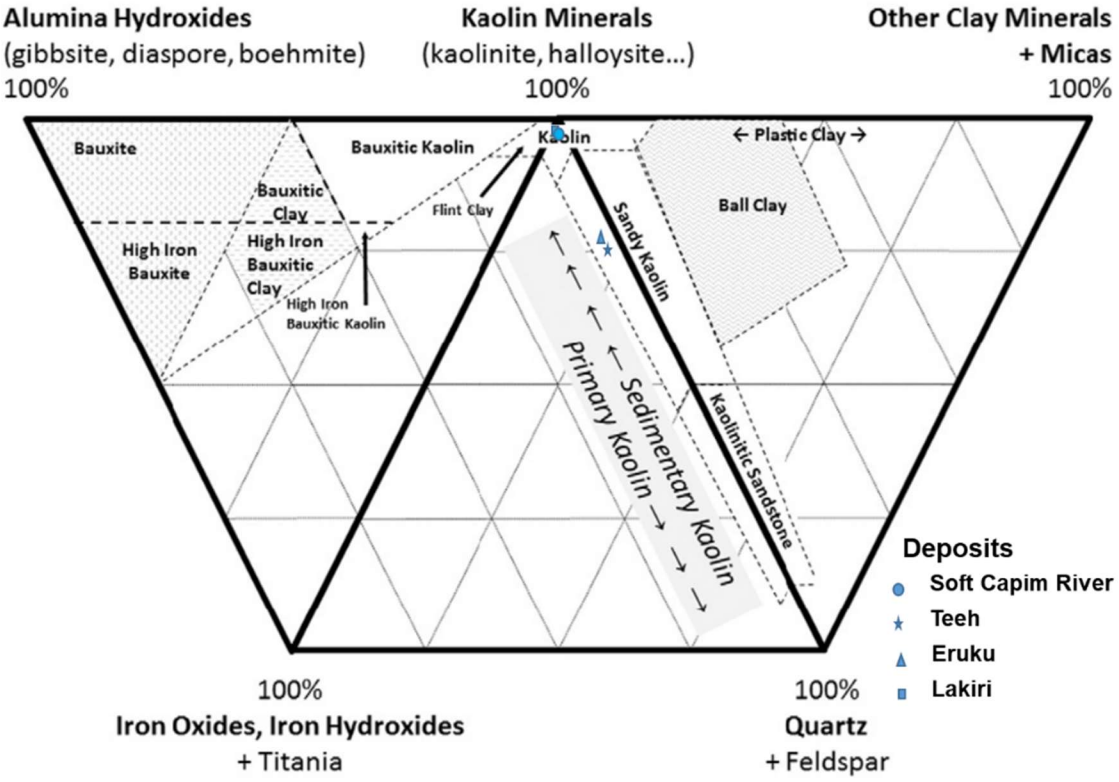

Figure 8.4: Bulk kaolin type mineralogical classification for the selected Cretaceous kaolins (Fields after Pruett, 2016).

The Hinckley index (HI) average values ranged from 0.70 (Teeh kaolins) to 1.11 (Soft Capim River kaolins) indicating a moderate kaolinite structural order for all the deposits. From the HI averages (Table 8.2), increasing kaolinite structural order is Teeh (with least orderliness) < Eruku < Lakiri < Soft Capim River kaolins (with best orderliness).

8.2.2 Kaolinite Morphology

The SEM images display the various morphologies and textures of the selected Cretaceous kaolins (Figs. 8.5 and 8.6). Morphologically, the Nigerian Lakiri and Eruku kaolins were similar to the Brazilian soft Capim River kaolins. Figure 8.5 shows that the kaolins from Nigeria have kaolinite crystals occurring as thin platy particles and pseudohexagonal plates which were comparable with the soft Capim River kaolins from Brazil (Figs. 8.6 a and b).

In addition, the Nigerian kaolins appear to have less microporosity between grains than observed between grains in the Brazilian soft Capim River kaolins. This could be attributed to the coarser kaolinite with paucity of ultra-fine (< 0.1 μm) particles in the matrix between the stacks in the soft Capim River kaolins. Texturally, the kaolinite plates in the Nigerian kaolins have euhedral – subhedral – anhedral external forms with irregular edges, whereas the soft Capim River kaolinite crystals were euhedral with flat edges. The Egyptian Teeh kaolin deposit under the SEM have anhedral flakes with the occurrence of pockets of anatase as uniform very fine-grained and rounded crystals within the kaolinite mass (Figs. 8.6 c and d). This SEM observation for the Egyptian Teeh kaolin deposit is not similar to any of the Cretaceous Nigerian and Brazilian kaolins.

8.3 Geochemical Considerations

The average major element oxides in the clay fraction of the selected Cretaceous kaolin deposits indicated that SiO_2, Al_2O_3, TiO_2, and Fe_2O_3 occur as major constituents. Other oxides (MnO, MgO, CaO, Na_2O, K_2O, and P_2O_5) occur as minor constituents. The average SiO_2 contents does not show significant variation among the kaolins, whereas average Al_2O_3 (39.19 and 39.35 wt %) for the Lakiri and soft Capim River kaolins were more than the Eruku and Teeh kaolin deposits (Table 8.3).

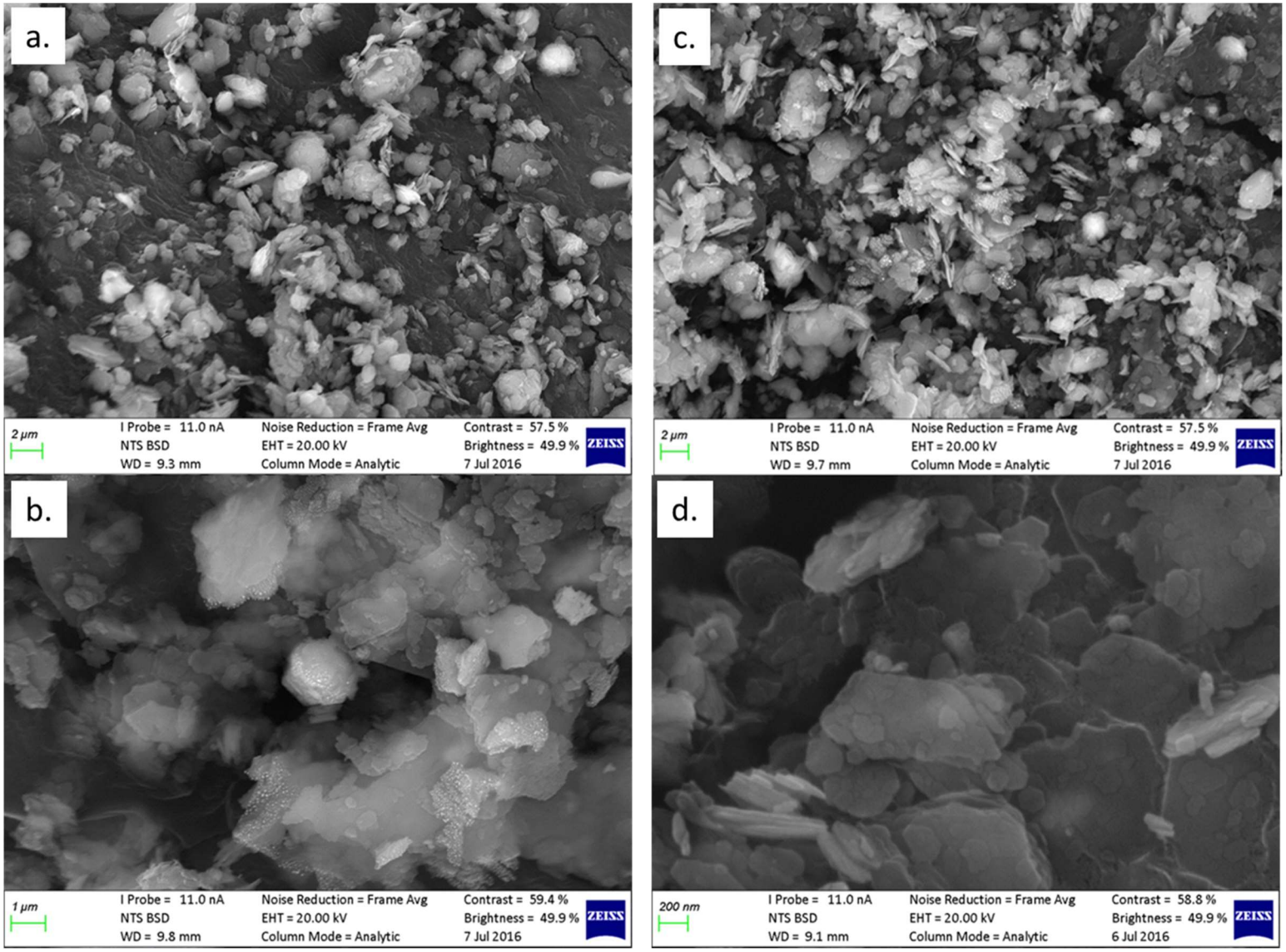

Figure 8.5: SEM micrographs of Cretaceous Eruku (a and b) and Lakiri kaolins (c and d) in Nigeria. Micrographs a and c show thin platy particles, whereas b and d shows pseudohexagonal stacks.

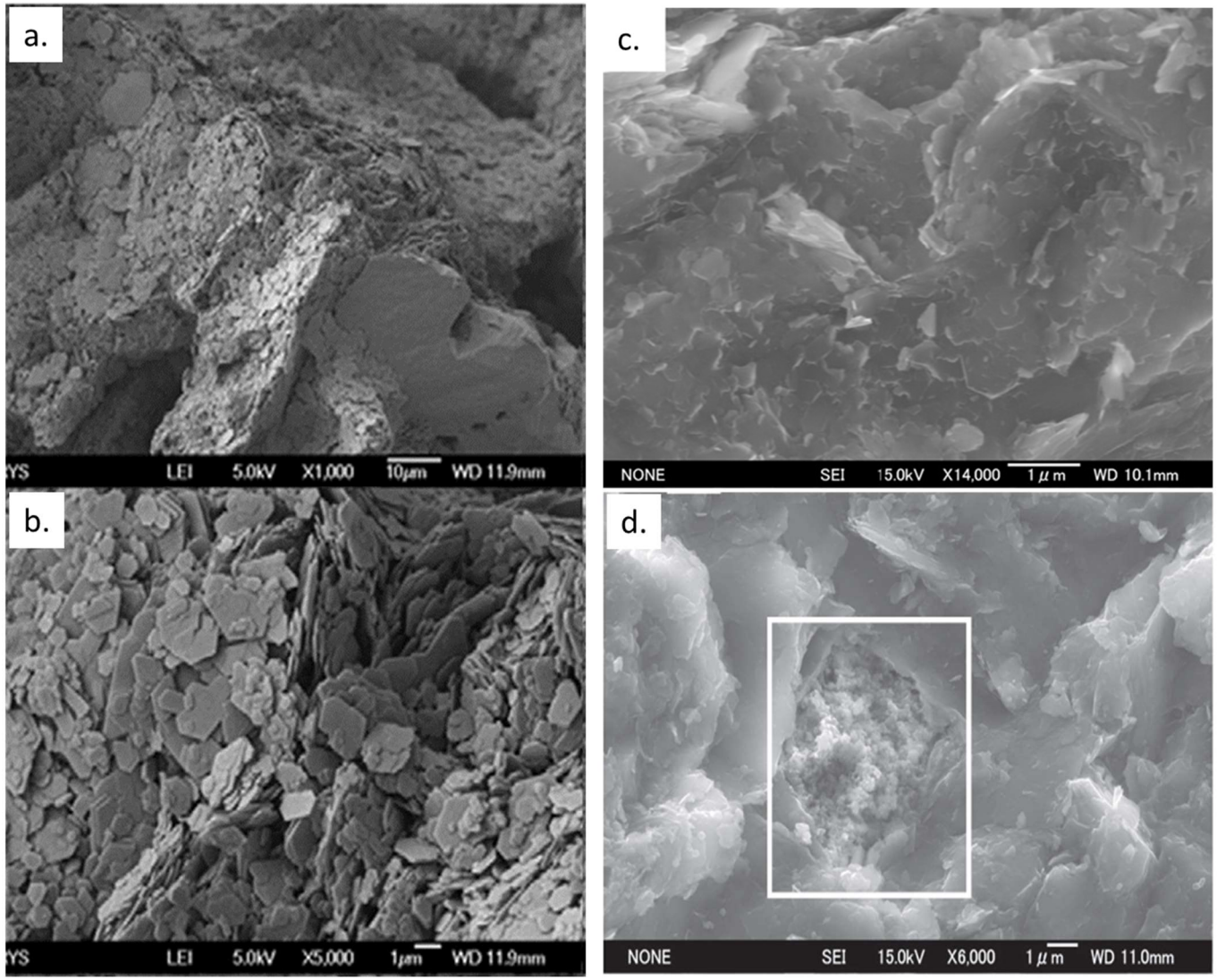

Figure 8.6: SEM micrographs of Cretaceous soft Capim River (a and b) and Teeh kaolins (c and d) in Brazil and Egypt respectively. Micrographs a shows thin platy particles, whereas b shows pseudohexagonal stacks. Micrographs c shows anhedral flakes, whereas d shows anatase clusters in pockets within the kaolinite mass.

Table 8.3: Average geochemistry of major element oxides (wt %), CIA, and trace elemental ratios of the Clay fractions of selected Cretaceous kaolin deposits.

	Nigeria		Egypt	Brazil
	Lakiri	Eruku	Teeh	Soft Capim River
SiO_2	44.55	44.73	45.5	44.3
TiO_2	1.41	1.69	2.1	0.44
Al_2O_3	39.19	37.19	35.8	39.35
Fe_2O_3	1.02	2.98	1.5	0.66
CaO	0.02	0.02	0.12	<0.02
MgO	-	-	0.25	0.04
MnO	-	-	0.01	-
Na_2O	0.2	0.21	0.06	<0.06
K_2O	0.11	0.25	0.07	0.02
P_2O_5	0.32	0.38	0.12	<0.09
L.O.I.	13.51	13.54	13.98	14.15
CIA	99.19	98.71	99.31	99.75
V/Cr	0.93	0.99	1.5	1.04
Ni/Co	5.39	5.32	13.46	8.37

In assessing the paleoweathering conditions, the average chemical index of alteration (CIA) values for the soft Capim River kaolin (99.75) was the highest, whereas the Eruku (98.71) has the lowest (Table 8.3). The Al_2O_3 – (CaO* + Na_2O) – K_2O (A-CN-K) ternary plot with CIA shows that the source rocks have experienced intense chemical weathering under tropical climatic condition (Fig. 8.7) with all plotting in the kaolinite field with high CIA values.

The provenance for the Nigerian Eruku and Lakiri kaolins were predominantly derived from felsic rocks in addition to contributions from intermediate and mafic rocks as presented in Chapter five. In contrast, the Brazilian soft Capim River kaolin source rocks were granitic and gneissic with accessory ilmenite (Sousa *et al*., 2007b), whereas the Egyptian Teeh kaolins were considered to have been sourced from medium-to high grade metamorphic, mafic, granitic rocks (Baioumy *et al*., 2012). These suggest remarkable heterogeneity in their sources with influence on their mineralogical and geochemical characteristics.

In evaluating the paleoredox conditions under which the kaolins were formed, Ni/Co ratios greater than 5 represent suboxic and anoxic environments, whereas ratios less than 5 suggest oxic environments (Jones and Manning, 1994). In addition, Gross (1964) and Landergreen and Manhem (1963) obtained V/Cr ratios of 1.1 and 0.75 respectively for anoxic recent marine to brackish water sediments and higher values between 2 and 10 for oxic environments. The average Ni/Co ratios obtained for the Cretaceous kaolins vary from 5.32 to 13.46 (Table 8.3), suggesting that they were deposited in anoxic environments.

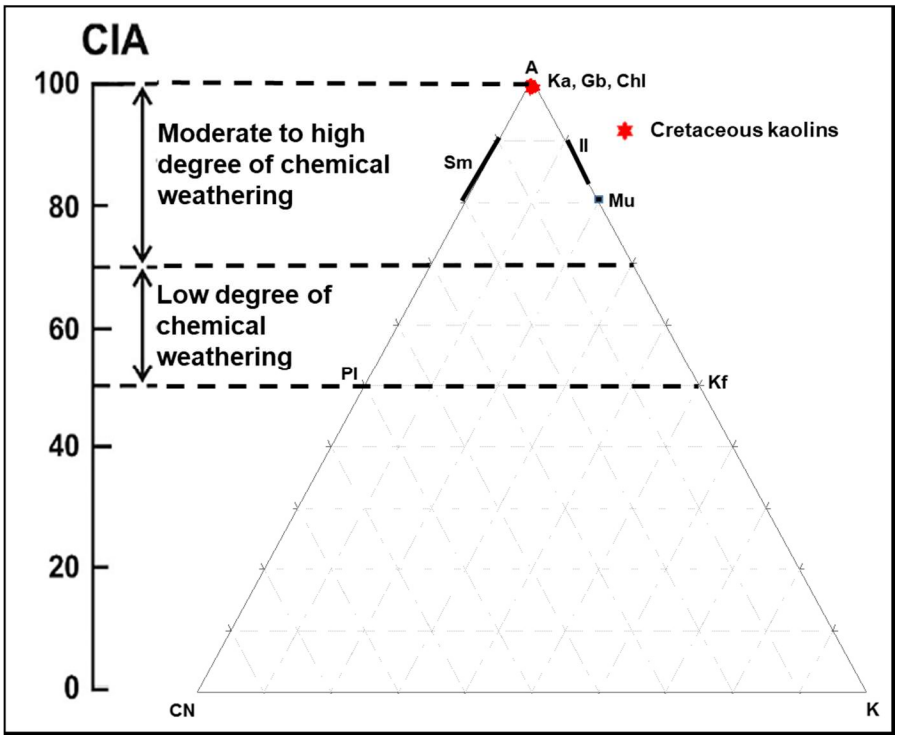

Figure 8.7: A-CN-K (Al_2O_3 – CaO* + Na_2O – K_2O) ternary diagram of the clay fractions of the selected Cretaceous kaolins combined with CIA (Fields after Nesbitt and Young, 1982; Hofer *et al*., 2013).

Furthermore, the V/Cr ratios between 0.93 to 1.50 also indicated deposition in anoxic environments (Table 8.3). This observation that the kaolins were formed in a restricted oxygen-poor (anoxic) depositional environment is consistent with the horst and graben structural systems for the Eastern Dahomey Basin (Whiteman, 1982; Ajayi *et al*., 2006)

in Nigeria, Cameta Sub-basin (Sousa *et al*., 2007b) in Brazil, and Gulf of Suez Basin (Omran and El Sharawy, 2014) in Egypt.

8.4 Hydrogen and Oxygen Stable Isotopic Considerations

The average hydrogen and oxygen compositions of the selected Cretaceous kaolins from Nigeria, Egypt and Brazil are presented in Table 8.4 and plotted in Figure 8.8.

In general, the average $\delta^{18}O$ (19.2 and 19.7 ‰) and δD (-53 and -52 ‰) values obtained for the Nigerian Eruku and Lakiri kaolins displayed similar contents. The average $\delta^{18}O$ values obtained for all the selected Cretaceous kaolins were within the +19 and +23 ‰ values for kaolinites of sedimentary origin except for the Brazilian soft Capim River kaolin with 15.65 ‰ which corresponds to kaolinites from residual deposits with values between +15 and +19 ‰ (Murray and Jansen, 1984) (Table 8.4). dos Santos *et al*. (2007) attributed the low $\delta^{18}O$ for the soft Capim River kaolin to mineralogical contaminations from framework grains rather than just post-formational modifications due to interactions with meteoric waters depleted in $\delta^{18}O$. They further concluded that the $\delta^{18}O$ values reflect a low isotopic composition of the parent minerals such as feldspars and micas with variable rates of replacements by kaolinites.

The Nigerian Eruku and Lakiri kaolins have higher average δD values relative to the Brazilian soft Capim River (-69 ‰) and Egyptian Teeh (-74 ‰) kaolins. This suggests that the meteoric water isotopic composition during the formation of the Nigerian kaolins were heavier, whereas the latter might have interacted with paleometeoric waters more depleted of $\delta^{18}O$ and δD (Mizota and Longstaffe, 1996).

In Figure 8.8, all the average $\delta^{18}O$ and δD values of the selected Cretaceous kaolins plotted between the kaolinite line (KL) of Savin and Espein (1970) and the supergene – hypogene line (SHL) of Sheppard *et al*. (1969) except for the Egyptian Teeh kaolin deposit plotting slightly to the right of the KL. The plot below the KL is suggestive of post-formational modifications of the isotopic compositions of the Egyptian Teeh kaolinites (Gilg, 2000; Baioumy, 2013).

Table 8.4: Average $\delta^{18}O$ and δD values (in ‰) and calculated temperature of kaolinisation (in ˚C) for the selected Cretaceous kaolins

Country	Deposit	$\delta^{18}O$	δD	Temperature
Nigeria	Eruku	19.2	-53	31.2
	Lakiri	19.7	-52	29.9
Egypt	Teeh	19.9	-74	16.8
Brazil	Soft Capim River	15.7	-69	38.4

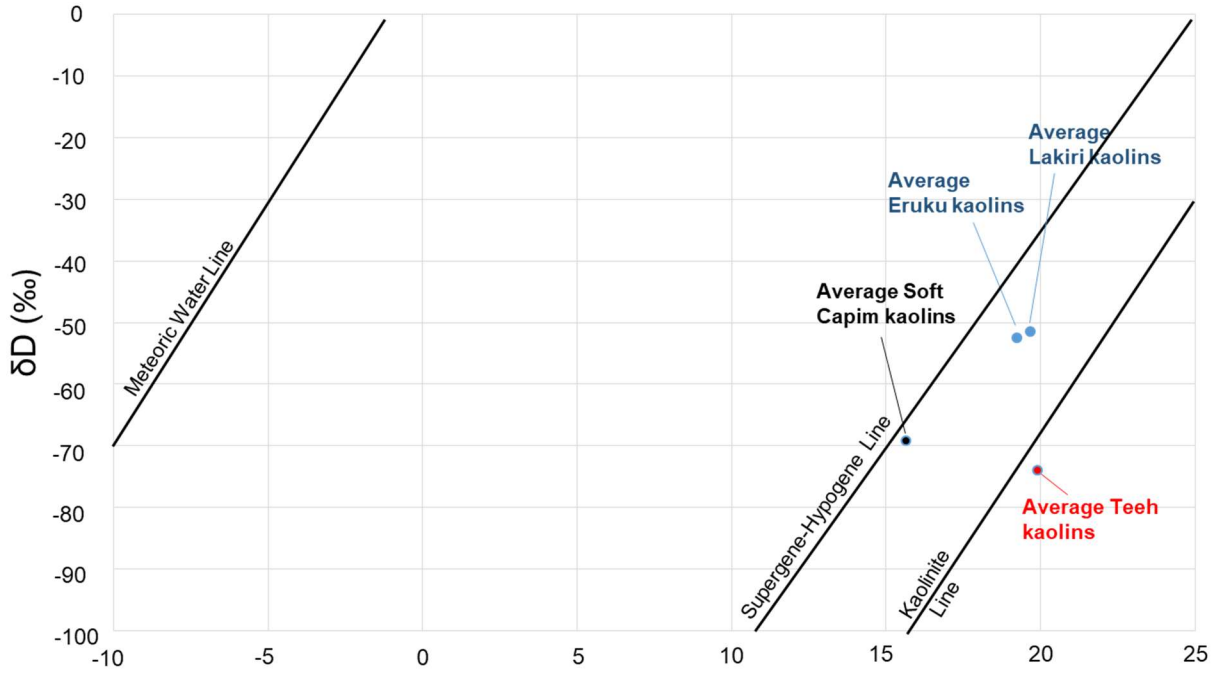

Figure 8.8: Average δD versus $\delta^{18}O$ isotopic compositions diagram of the selected Cretaceous kaolins.

The calculated average temperatures of kaolinisation (T_c) for the selected Cretaceous kaolins using the Clauer *et al*. (2015) and Galan *et al*. (2016) equation are given in Table 8.4. The average T_c for the Nigerian Eruku and Lakiri kaolins (31.2 and 29.9 ˚C) were lower than 38.4 ˚C obtained for the Brazilian soft Capim River kaolins. However, these average T_c values obtained for both the Nigerian and Brazilian kaolins suggest that the kaolins were formed under warm conditions, whereas the Egyptian Teeh kaolin deposit with an average T_c of 16.8 ˚C suggests formation under cooler conditions.

The low T_c for the Egyptian Teeh kaolins could be attributed to the post-formational modifications of the isotopic compositions of the kaolinite due to their interaction with meteoric water depleted in $\delta^{18}O$ and δD, and temperature are generally low (Mizota and Longstaffe, 1996; Baioumy, 2013). Noteworthy is that the T_c values below 50 ˚C do not relate kaolinisation with low-temperature hydrothermal event (Clauer *et al*., 2015). The average paleotemperatures obtained for the Nigerian and Brazilian kaolins are characteristic of paleoweathering formation under tropical climate. This confirms previous work by Scotese (2001) (Fig. 8.9) that concluded that the two locations have identical tropical climate during the Late Cretaceous.

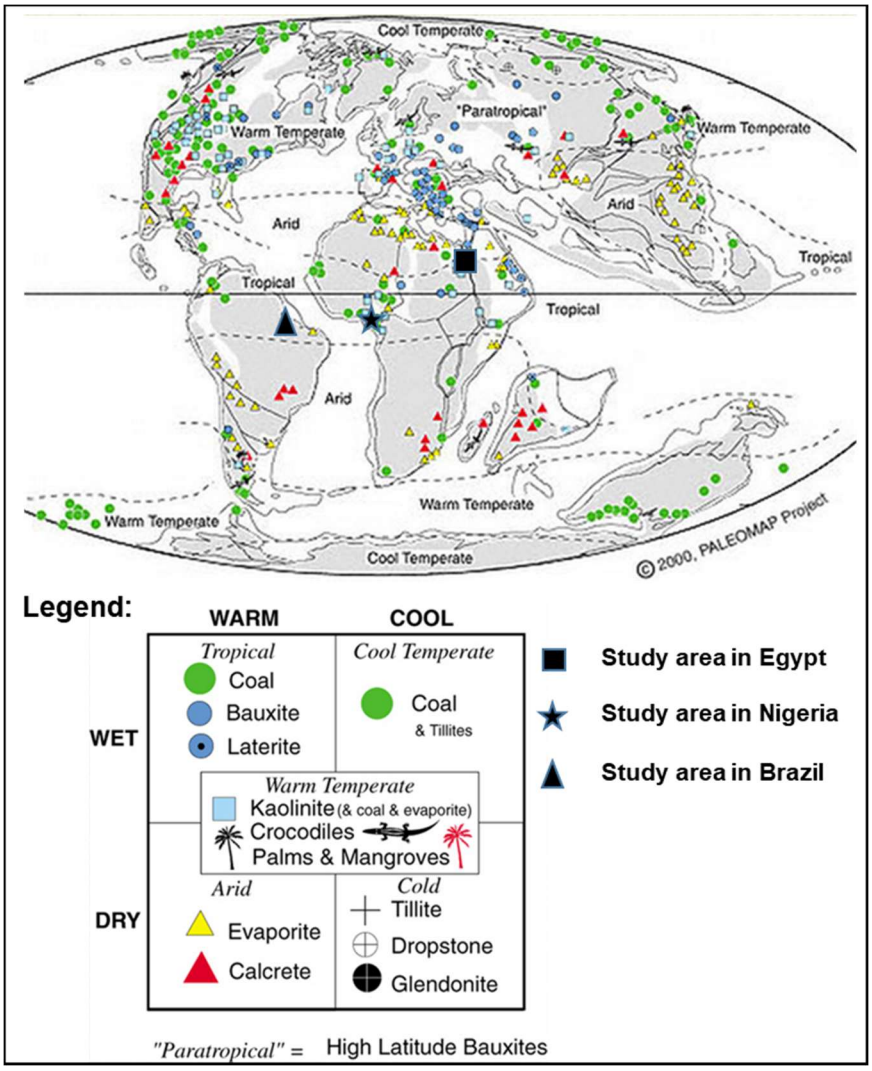

Figure 8.9: Paleoclimate map showing the locations of the selected Cretaceous kaolin deposits during the Cretaceous Period (Modified after Scotese, 2001).

8.5 Detrital Zircon Geochronological Considerations

The correlation of the detrital zircon geochronology of the Egyptian Teeh kaolin deposit is not possible due to lack of data.

Statistical analysis of thirty zircon grains from the soft Capim River kaolins indicated that the age 2.146±0.023 Ga is the most representative with the highest number zircons followed by 1.881±0.08 Ga (Sousa *et al*., 2007a). Percentage contributions of the various detrital zircons from known orogenic events (Table 8.5) show that the source sediments for the selected Cretaceous kaolins were mostly from areas related to the Transamazonian orogenic event in Brazil which corresponds to the Eburnean orogenic event in Nigeria except for the Nigerian Eruku kaolins with more contributions from areas related with the Pan African orogenic event. In addition, the Nigerian Lakiri kaolin deposit also had sediment contributions from areas related with the Pan African orogenic event in Nigeria which corresponds to the Braziliano orogenic event in Brazil. The Brazilian soft Capim River kaolin deposit had considerable contributions from rocks with ages between 2000 – 1100 Ma which corresponds to the Kibaran orogenic event in Africa. Despite the similar time equivalence with respect to source rock ages and terranes, the available data is not sufficient enough to establish possible input of detritus from the West African Craton to South American Craton or vice versa. In addition, the current available geological evidences from the surrounding rocks and paleocurrent data have demonstrated that the source sediments came from basement rocks around the various deposits on their respective continents.

Table 8.5: Percentages of Ages of Detrital Zircons within the selected Cretaceous Kaolins.

Orogeny*	**Ages (Ma)***	**Nigeria**		**Brazil**
		Lakiri (n=68)	**Eruku (n=89)**	**Soft Capim River (n=30)**
Liberian (Archean)	2700 - 2500	2%	-	10%
Eburnean (Mid - Late Paleopro)	2500 - 2000	67%	34%	50%
Kibaran (Early Mesopro - Mid Paleopro)	2000 - 1100	3%	6%	37%
Pan African	750 - 450	28%	60%	3%

*Oyinloye, 2011.

8.6 Conclusions

Based on the mineralogical, geochemical, stable isotopic, and geochronological considerations, the following deductions have been made:

a) The Nigerian Lakiri and Brazilian soft Capim River kaolins have similar mineralogical characteristics and were classified as pure kaolins. The Nigerian Eruku and Egyptian Teeh kaolins were classified as sandy kaolins. The kaolinite crystal morphology of the Nigerian Lakiri and Eruku kaolins were comparable to that of the Brazilian soft Capim River kaolins. They occur as thin platy particles and pseudohexagonal plates.
b) The kaolins were formed under intense chemical weathering in a restricted oxygen-poor (anoxic) depositional environment. This is consistent with the structural framework of the basins in which the kaolins occur.
c) The calculated average paleotemperatures obtained for the Nigerian Lakiri, Eruku, and Brazilian soft Capim River kaolins suggest that they were formed under warm conditions. In paleoclimatic interpretation, the temperatures were characteristic of paleoweathering formation under tropical climate.
d) Detrital zircon geochronological data indicated that the source sediments for the Nigerian (except for Eruku kaolins with more input from areas related to the Pan African orogenic event) and Brazilian kaolins were predominantly from areas related to the Transamazonian orogenic event in Brazil which corresponds to the Eburnean orogenic event in Nigeria with contributions from Pan African (Brasiliano) and Kibaran orogenic rocks, respectively.

Chapter Nine

Possible Industrial Applications of the Cretaceous-Tertiary kaolins within the Eastern Dahomey and Niger Delta Basins in Nigeria

This chapter aimed to appraise the possible industrial applications of the Cretaceous – Tertiary kaolins within the Eastern Dahomey and Niger Delta Basins in Nigeria (Specific Objective 5) based on Hypothesis 5. The physico-chemical, mineralogical, and geochemical compositions of the studied kaolins were used to achieve specific objective 5.

9.1 Physico-chemical Considerations

9.1.1 Colour

Raw kaolin colour and fired products have aesthetic importance in its application particularly in ceramics (Bloodworth *et al*., 1993; Murray, 1979; Ekosse *et al*., 2007). Colours are imparted by colour causing elements retained either in the structure of the kaolin mineral or as associated oxides occurring with the kaolin mineral (Ekosse *et al*., 2007). Fellman (1996) reported that clay minerals such as kaolin with Fe and Mg in its octahedral sites contain less structural water, hence less energy will be required for dihydroxylation and less temperature for vitrification than usual. The lesser temperature is possible because Fe, Mg, Ca, Na, and K oxides can act as fluxing agents (Kuscu and Yildiz, 2016).

The percentage colour distribution of the studied kaolins (Fig. 4.1) shows that pale red (39 %) is the most dominant colour followed by pinkish and light grey (35 %) as well as reddish yellow, light pink, light brown, reddish brown, and pinkish white. The various shades of red due to their iron contents particularly in the Tertiary kaolins will have implications in the energy consumption especially in bricks production (Emofurieta *et al*., 1992).

9.1.2 Hydrogen Ion Concentration (pH) and Electrical Conductivity (EC)

The pH values of the studied kaolins were generally acidic with values < 7 (4.27 – 5.29) (Fig. 4.3). The EC estimates the amounts of soluble salts (such as chlorides, phosphates, sulphates, carbonates, and nitrates), which could cause severe problems in many applications (Murray, 1986). In drying and firing of ceramic clay bodies, visible surface-scum due to the migration of soluble salts have been observed on the surface of vessels coupled with exfoliation and peeling of the surface under extensive crystallisation condition (Ekosse *et al*., 2007). The measured EC values for the Cretaceous-Tertiary kaolins ranged between 0.2 and 5.0 µS/cm (except for EP2 0m, LP1 2m, LP2 0m, AL1 1m, and UL2 2m with EC values >8.0 µS/cm) (Fig. 4.2). The relatively low EC values suggest little or no dissolved salts. Hence, these kaolins are considered to contain little or no soluble salts in them (Murray, 1986). Chemically inert (pH range of 4 – 9) and low conductivity kaolins will be useful in the production of excellent fillers and extenders (Murray, 2007). Considering the clayey nature of the samples in addition to the relatively low conductivity, production waste resulting from cracking due to shrinkage when fired would be low for ceramic applications (Ekosse *et al*., 2007).

9.1.3 Particle Size Distribution

The analysed samples showed wide variations in the particle size (Fig. 4.4a) with clay fraction (<2 µm) ranging from 55 to 90 % and 43 to 61 %, silt fraction fraction from 3 to 14 % and 1 to 11 %, and sand fraction from 4 to 39 % and 32 to 48 % for the Cretaceous and Tertiary kaolins, respectively. The control of the sand, silt, and clay fractions over porosity and permeability plotted based the ternary diagram of McManus (1988) (Figs. 9.1 a and b) show that the Lakiri kaolins plotted predominantly within the high porosity and very low permeability region (except for LP1 0m), whereas the Eruku (except EP1 4m and EP2 4m), Awo-Omama, and Ubulu-Uku kaolins all plotted in the low porosity and low permeability region. Based on the Strazzera *et al.* (1997) and Murray (2007) criteria, the more fine-grained Cretaceous kaolins with higher porosity will be suitable for the production of porous ceramic wares.

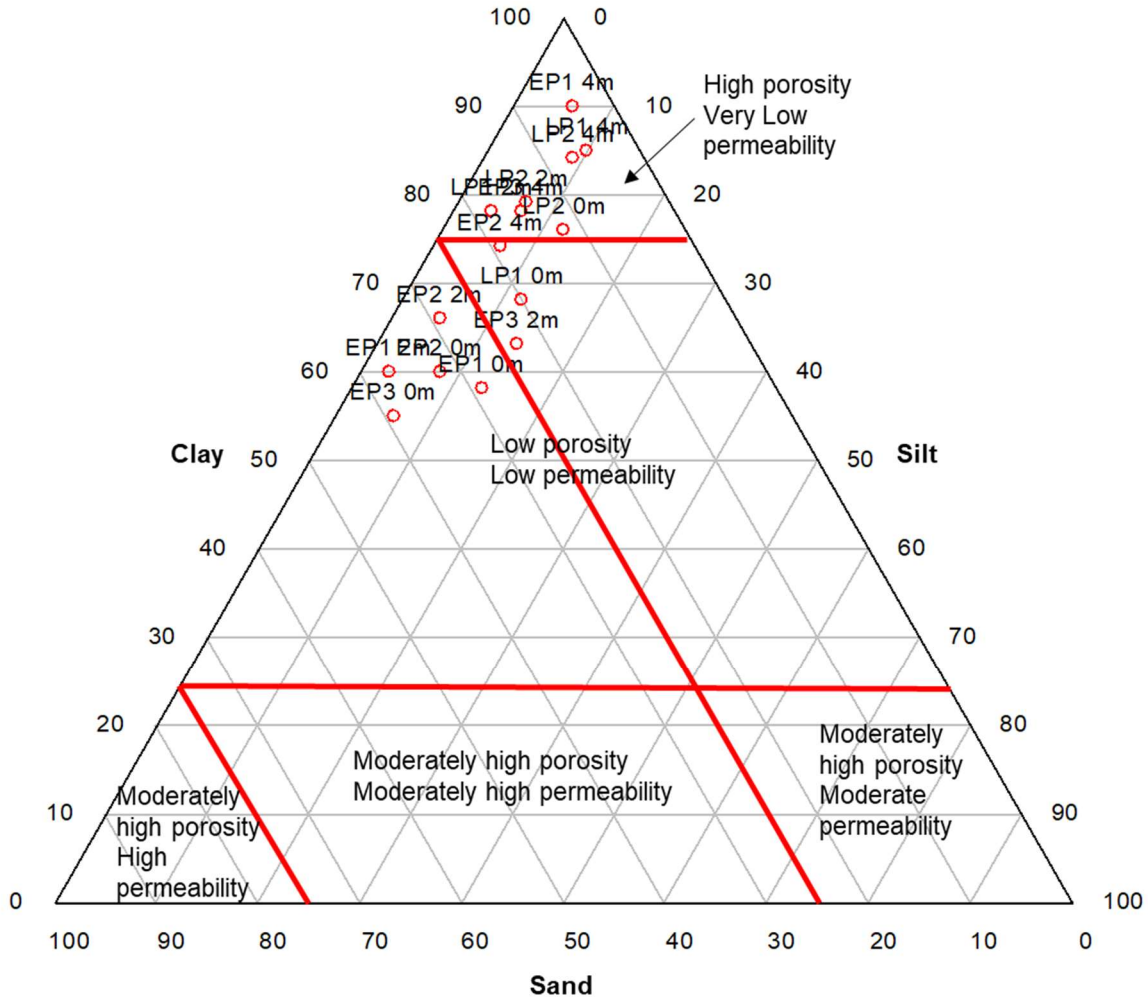

Figure 9.1a: Ternary diagram of studied Cretaceous kaolins following the relation between sand, silt, clay fractions and their controls over porosity and permeability (Fields after McManus, 1998).

The low - very low permeability is indicative of low cohesion and difficulty to extrude because moderate permeability will facilitate penetration of water into the kaolin, rendering its adsorption faster and more important. In addition, the water in the ceramic paste must provide enough cohesion to the ceramic body to equilibrate extrusion (El Ouahabi *et al*., 2014).

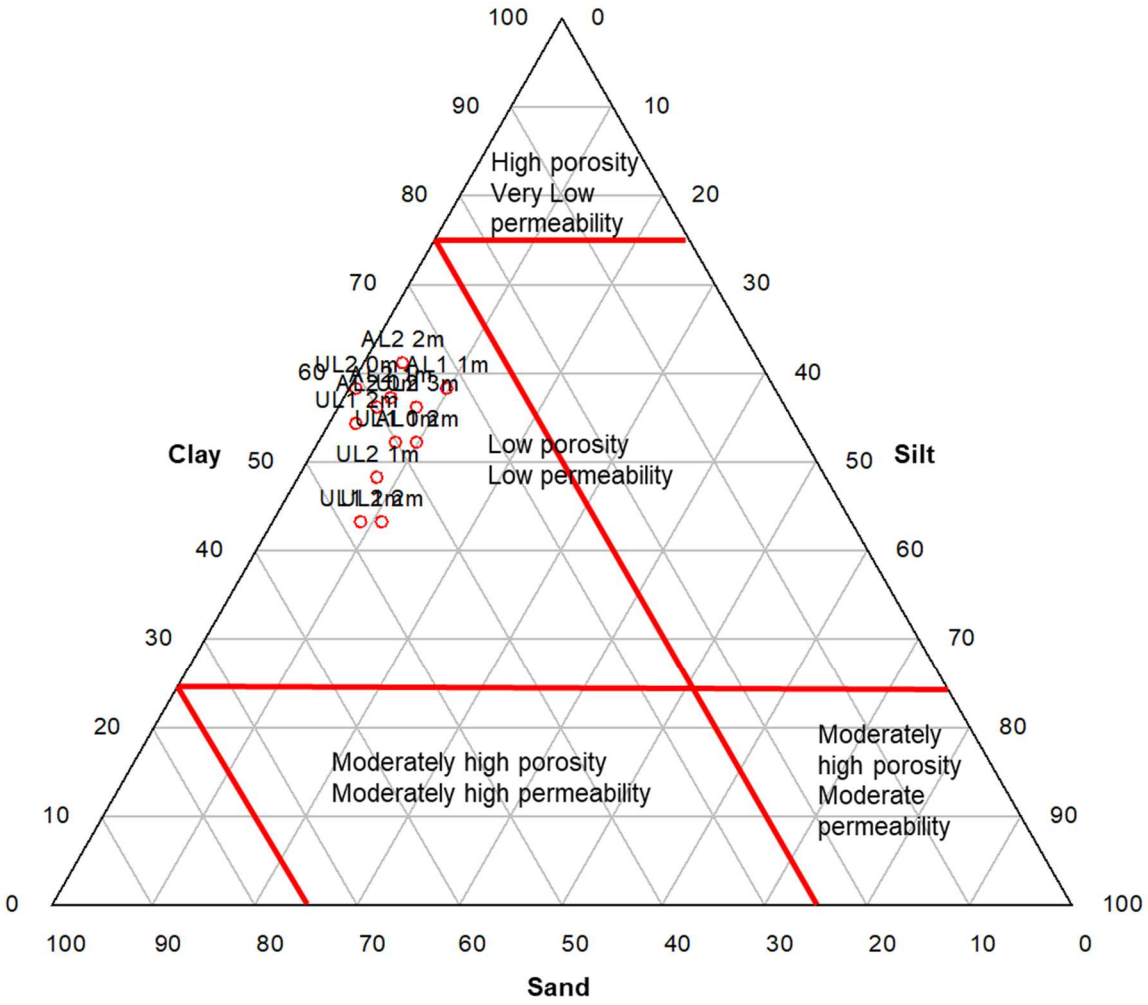

Figure 9.1b: Ternary diagram of studied Tertiary kaolins following the relation between sand, silt, clay fractions and their controls over porosity and permeability (Fields after McManus, 1998).

9.1.4 Plasticity

One of the most important factors in the industrial applications of kaolin is the plasticity. It is controlled by several factors, such as the particle size distribution, mineral composition, and the presence of organic matter (Lahcen *et al*., 2014). The plastic index (PI) and plastic limit (PL) values for the Cretaceous – Tertiary kaolins are plotted on the Holtz and Kovacs diagram (Holtz and Kovacs, 1981) (Fig. 9.2). The diagram shows that all the Cretaceous – Tertiary kaolins were plotted in the medium plastic region except for two Tertiary samples which are in the low (UL1) and high (AL2) regions.

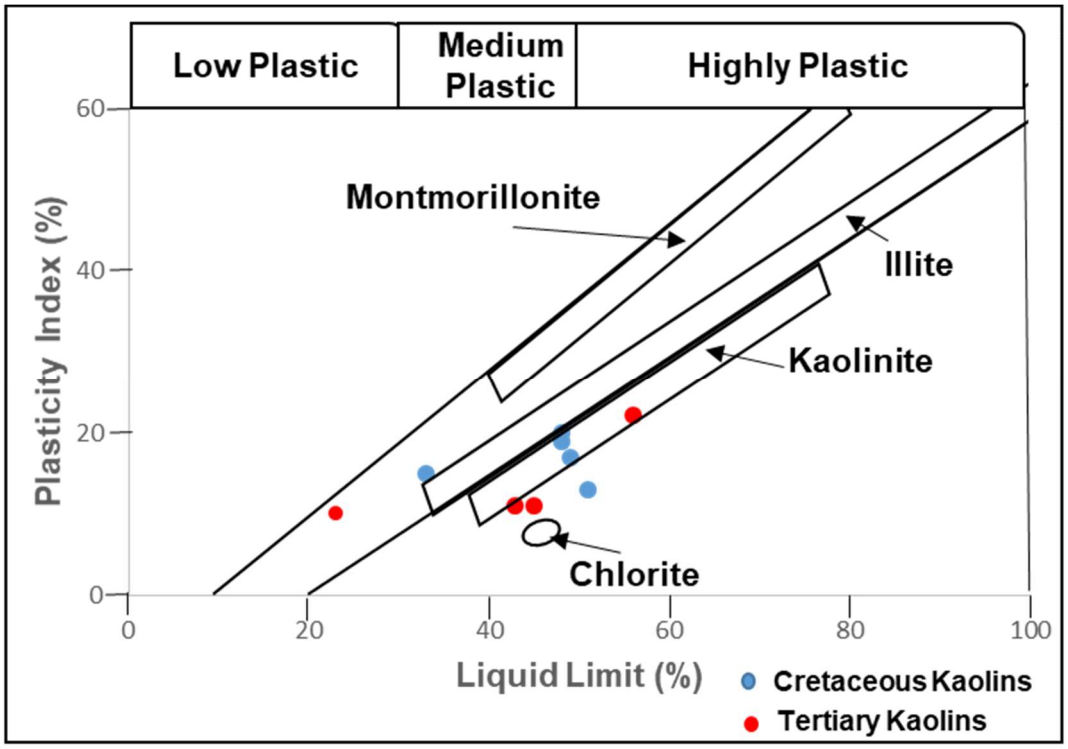

Figure 9.2: Position of the studied Cretaceous – Tertiary kaolins on the Holtz and Kovacs (1981) diagram.

The slight differences in the plasticity of the studied kaolins are related to the differences in the abundance of silt and clay fractions. Higher clay and silt fractions give rise to relatively higher plasticity (Lahcen *et al*., 2014). In addition, a moderate PI indicates moderate potential for swelling. However, excessive shrinkage is not expected since the PI values obtained were < 35 (Daniel, 1991).

Kaolins with PI < 10 % are not appropriate for building-related ceramic production due to the risk of problems related to the visible variation in the amount of extrusion water (Abajo, 2000; Vieira *et al*., 2008). These problems include inappropriate dimensional characteristics and even cracks during extrusion process (Abajo, 2000). Clays with low PI (7<PI<10) require the addition of polymers to obtain an adequate plastic behaviour and prevent cracking during extrusion (Bain, 1971; Dondi *et al*., 1998). Most of the studied kaolin have PI≥ 10 %. Hence, the Cretaceous – Tertiary kaolins might possibly be used in there raw state to produce structural clay products by extrusion.

Furthermore, the Casangrande chart (Fig. 9.3) reveals that the PL and PI of the studied kaolins fall in the category of kaolinitic clays that are suitable more for brick making and possibly pottery wares. They were predominantly located inside the region of acceptable properties except for sample LP1 within the optimum properties region and samples EP2 and UL1 located outside both the acceptable and optimum property regions.

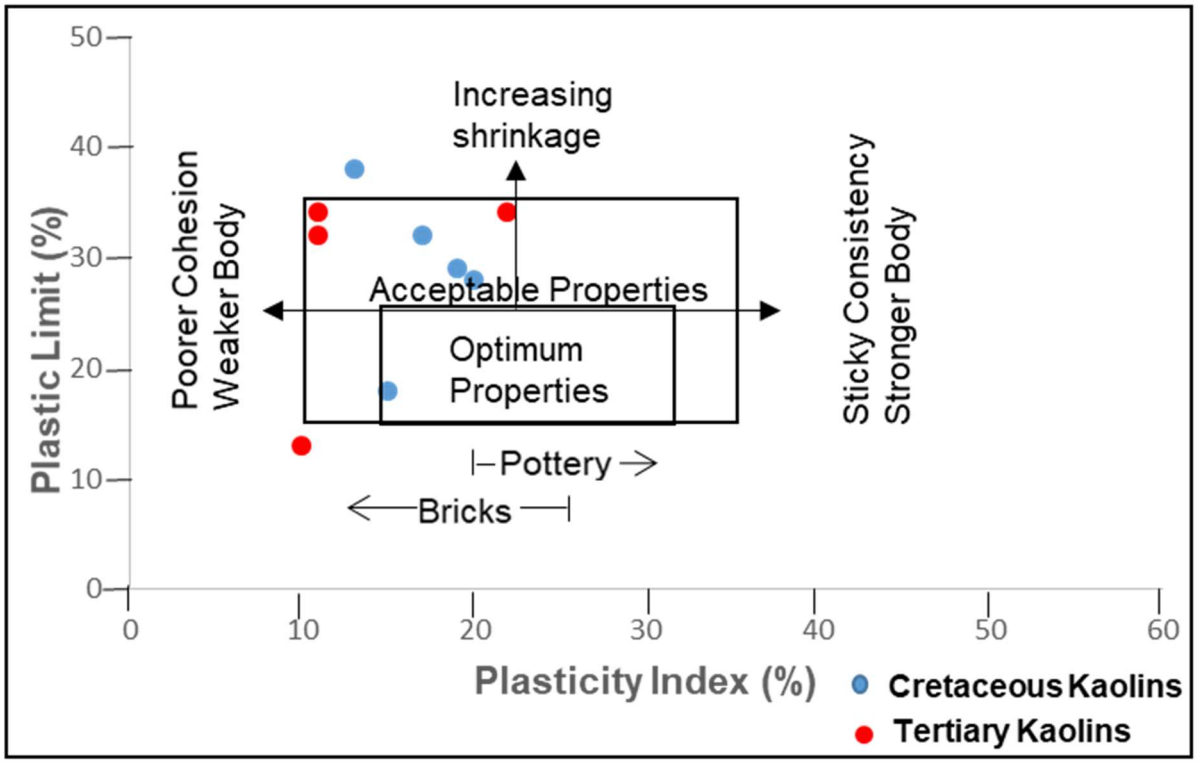

Figure 9.3: Position of the studied Cretaceous – Tertiary kaolins on the clay workability chart (After Casangrande, 1948).

9.2 Mineralogical Considerations

9.2.1 Mineral Compositions

In the bulk Cretaceous kaolins, kaolinite was indicated as the predominant kaolin mineral, followed by quartz, muscovite, anatase, goethite, and hematite, whereas in the Tertiary kaolins, kaolinite was also predominant followed by quartz, anatase, and goethite (Table 9.1).

A plot of the average bulk percentages of minerals present in each of the deposits on the ternary diagram for general mineralogical classification of economic kaolin deposits categorized the deposits into kaolin types (Fig. 9.4). The Lakiri deposit plotted in the region of pure kaolin, whereas the Eruku, Awo-Omama, and Ubulu-Uku deposits plotted in the region of sandy kaolins. This is indicative of the relatively higher percentages of quartz in the sandy kaolins.

Iron-bearing minerals such as hematite, goethite, and Ti-bearing mineral such as anatase are the discolouring minerals in the studied kaolins with abundances ranging from 1 to 2 wt% (Table 9.1). Keller (1968) described clays containing 3 wt% iron oxides with 1 to 3 wt% titania are useless to the ceramist. However, Pruett and Alves (2013) reported that the beneficiation of a kaolin to nearly white is probable for kaolins containing a total of <6 wt% iron oxides and hydroxides, and titania.

Based on the bulk mineralogical composition, the pure kaolin type Lakiri deposit will possibly be useful as raw materials for fiberglass (though ceramic raw materials can be nearly pure kaolin yet additional properties such as plasticity, colour, particle size, and melting point are important), whereas the sandy kaolin type Eruku, Awo-Omama, and Ubulu-Uku deposits will possibly be useful as pigments and additives (For example, paper coating) (Fig. 9.5) because of the higher amounts of non-clay minerals such as quartz which are easy to separate (Pruett, 2016).

Known world sedimentary economic kaolin deposits such as Georgia kaolins, Capim River kaolins, and Maoming kaolins in USA, Brazil, and China respectively are currently mined for various industrial applications. The average kaolinite abundances obtained for the Cretaceous and Tertiary kaolins (83 and 62 wt %, respectively) were lower when compared with the 98 wt % for the soft Late Cretaceous/Early Tertiary Capim kaolin in Brazil and 95.43 wt % for the soft Cretaceous Georgia kaolin in USA (Pruett, 2016) but higher than the 20 – 25 wt % for the Late Tertiary Maoming kaolins in China (Murray, 2007).

Table 9.1: Mineralogy of the bulk and <2 µm fractions of studied Cretaceous - Tertiary kaolins.

Age		Kaolinite		Quartz		Anatase		Hematite		Muscovite		Goethite	
		Bulk	Clay	Bulk	Clay	Bulk	Clay	Bulk	Clay	Bulk	Clay	Bulk	Clay
Cretaceous	Average	83	98	21	2	1	1	-	1	5	-	1	1
(n=15)	Max	99	99	57	6	2	1	-	1	9	-	1	1
	Min	49	93	1	1	1	1	tr	1	1	-	1	1
Tertiary	Average	62	82	37	18	1	1	-	1	-	-	1	1
(n=13)	Max	93	91	74	28	1	2	-	1	-	-	1	2
	Min	25	69	6	7	1	1	-	1	-	-	1	1

(tr) Trace, (-) Not detected

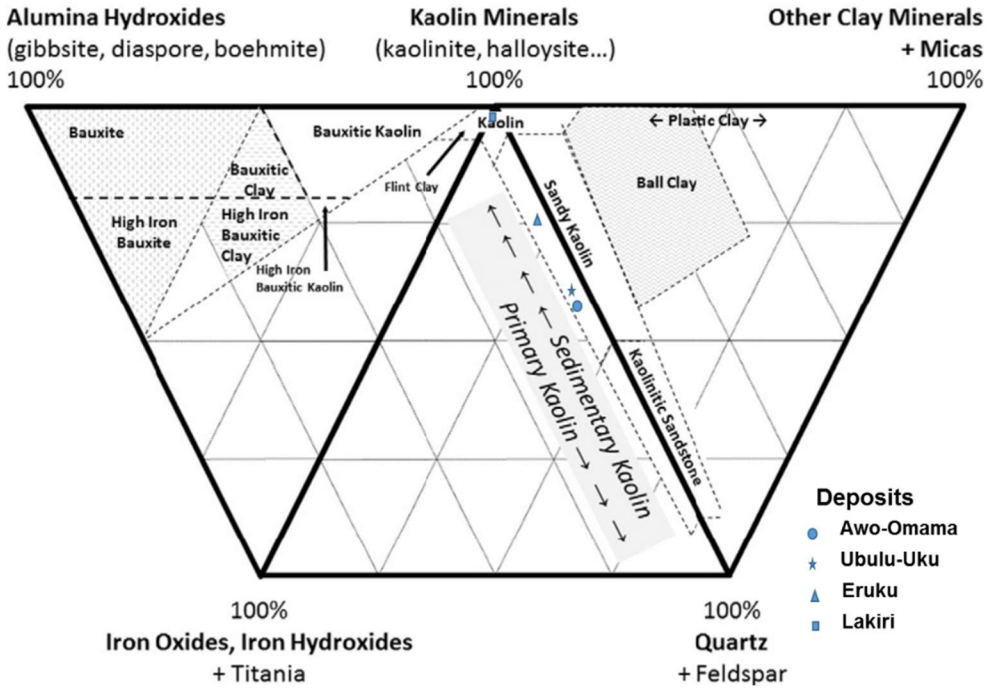

Figure 9.4: Bulk kaolin type mineralogical classification for the studied Cretaceous – Tertiary kaolins (Fields after Pruett, 2016).

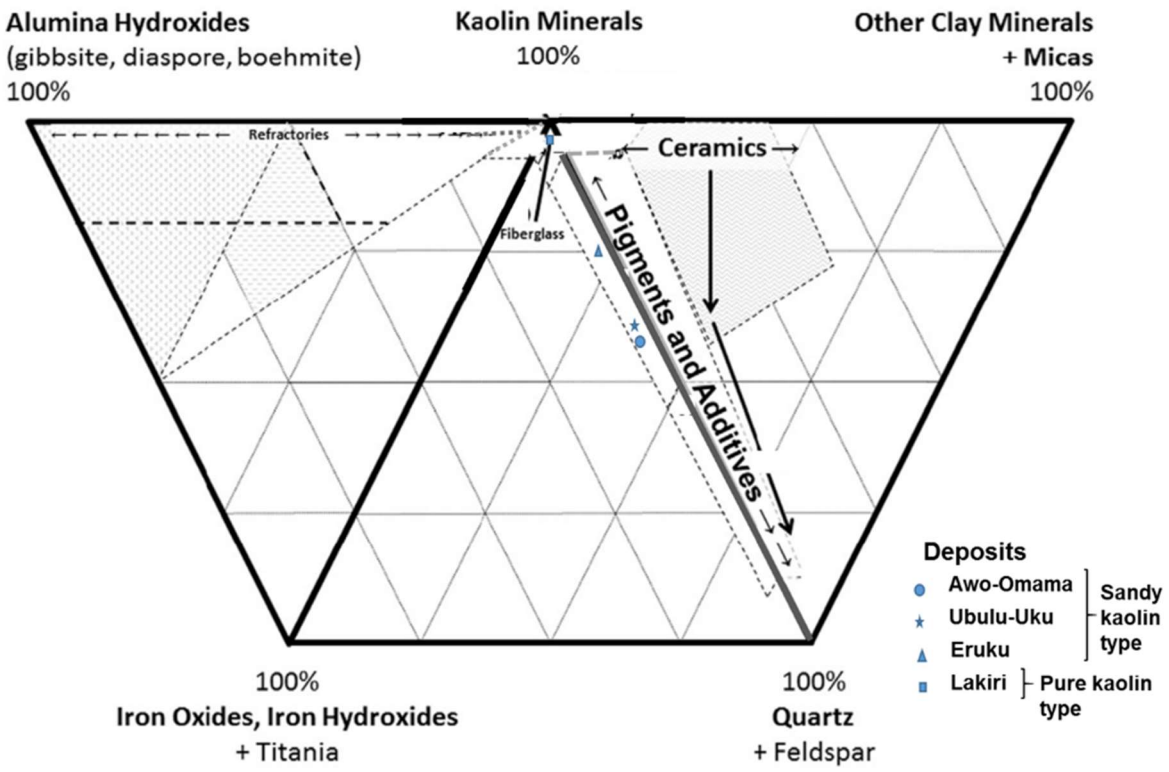

Figure 9.5: Possible industrial applications of the kaolin based on their mineralogical classification (Pruett, 2016) described in Fig. 9.4.

Physical size reduction to the clay fraction of the Cretaceous – Tertiary kaolins led to increase in the kaolinite contents as well as decrease in the quartz contents (Table 9.1). This allowed the Eruku kaolin to plot within the pure kaolin with Lakiri kaolin, whereas the Tertiary kaolins remained within the sandy kaolin region (Fig. 9.6) which will definitely allow the Eruku kaolins to be possibly used for fiberglass (Fig. 9.7).

9.2.2 Kaolinite Crystallinity

The physical and chemical properties of kaolinite is strongly influenced by its structural order (Vaculikova *et al*., 2011). Structural defects in the kaolinite crystal structure have been attributed to large number of stacking faults that may appear during its formation and growth.

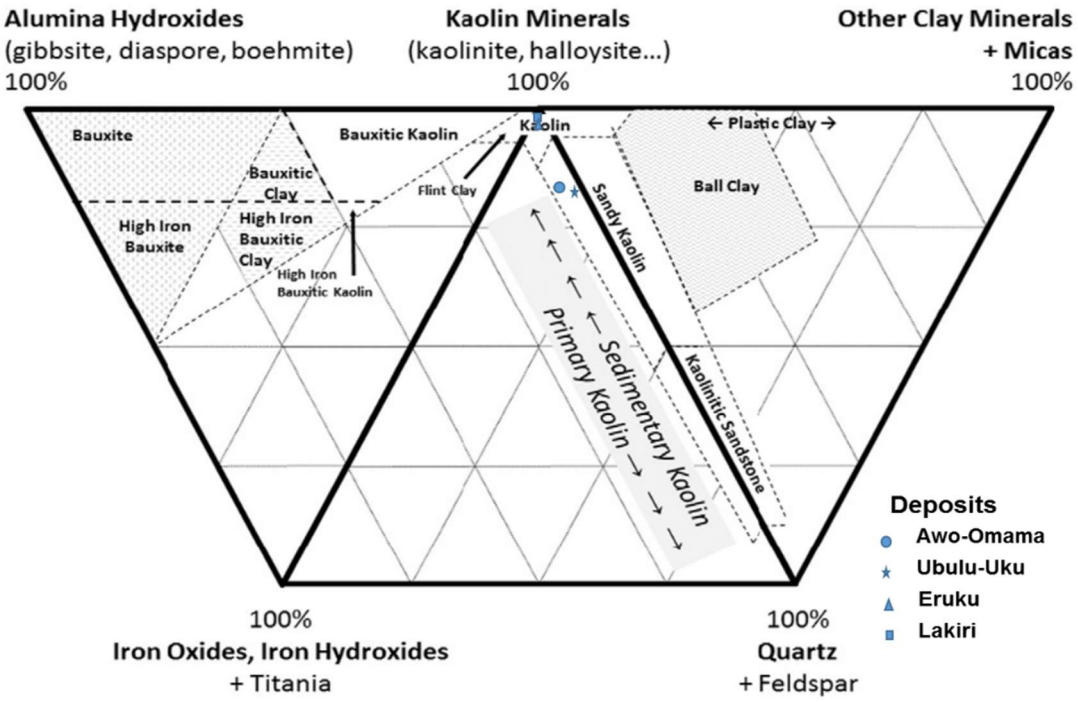

Fig. 9.6: Kaolin type mineralogical classification for the Clay fraction of the studied Cretaceous – Tertiary kaolins (Fields after Pruett, 2016).

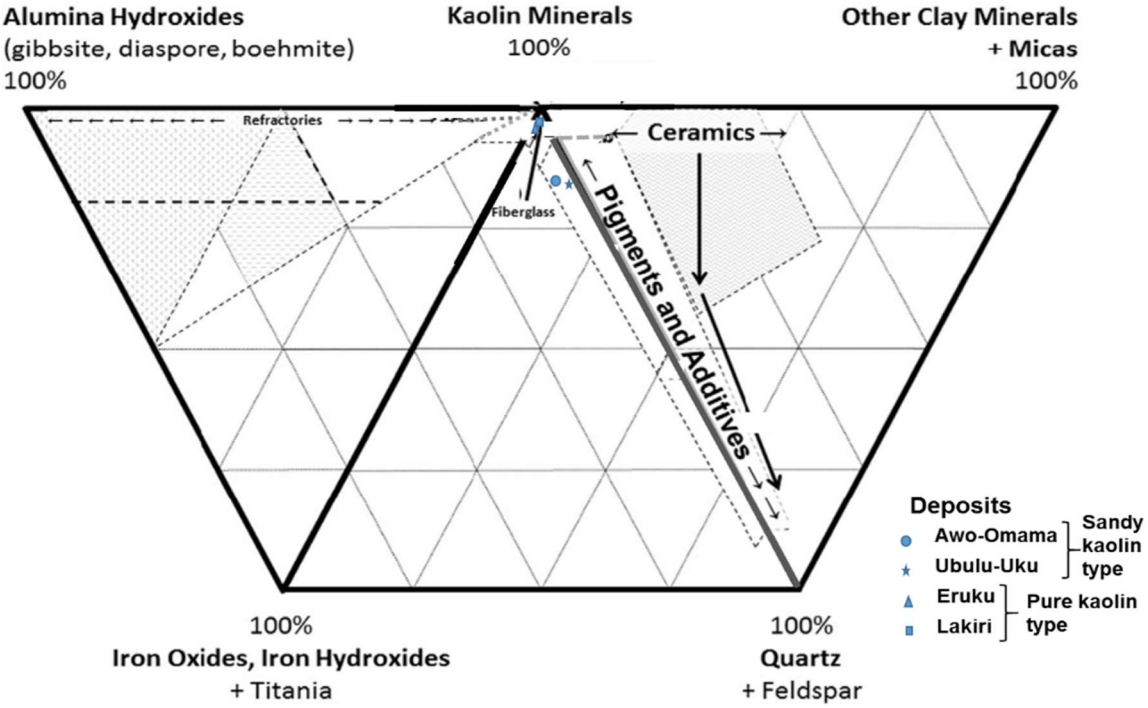

Figure 9.7: Possible industrial applications of the kaolin based on their mineralogical classification (Pruett, 2016) described in Fig. 9.6.

The knowledge of variations in the kaolinite structure is important in assessing its correlation with plasticity, brightness, and viscosity (Aparicio and Galan, 1999). In addition, the degree of defects in kaolinites for use in manufacturing of ceramics is linked to the mineralogical assemblage, structural order, and thermal stability of the material (Diko *et al*., 2016). Murray (1987) indicated that the kaolinite crystallinity can affect its paper coating properties and hence, good crystallinity is generally required for a kaolin to be used for paper coating.

The results of kaolinite HI obtained for the clay fractions are presented in Table 9.2. The Eruku kaolins have HI values between 0.8 (CF EP2 0m) and 1.38 (CF EP2 4m) with a mean value of 0.98, whereas HI for Lakiri kaolins were between 0.75 (CF LP1 0m) and 1.09 (CF LP1 2m) with a mean value of 0.99. These values correspond to moderate to high kaolinite structural order. For Awo-Omama kaolins, HI ranged from 0.27 (CFAL2 2m) to 0.41 (CF AL1 2m) with an average of 0.31 which corresponds to low kaolinite structural order, whereas HI of Ubulu-Uku kaolins between 0.58 (CF UL1 0m) and 1.36 (CF UL2 2m) with average of 0.97 corresponds to moderate to high kaolinite structural order. However, the increasing kaolinite structural order is Awo-Omama (with least orderliness) < Ubulu-Uku < Eruku < Lakiri (with best orderliness). This implies that the Cretaceous kaolinites are more ordered than the Tertiary kaolinites. The HI >1<1.5 values obtained for Cretaceous Lakiri kaolin deposit corresponding to partially ordered kaolinite structure is comparable to those reported for Maoming kaolins (1.05) in China (Liu *et al.,* 2001), Georgia kaolins (1.12) in the USA (Vaculikova *et al.*, 2011), and Capim River kaolins (1.06 – 1.16) in Brazil (Santos *et al.,* 2012).

The kaolinite degree of structural order was evaluated from IR spectra using IR-empirical (IR-E) and IR- numerical (IR-N) approaches (Vaculikova *et al*., 2011). According to the IR-E classification, kaolinite structure is considered ordered, if the four OH stretching and bending bands (3691/3689, 3669, 3651/3650, and 3619) were clearly resolved; partially ordered, if the individual OH bands at 3669, 3651/3650 and 937/935 cm^{-1} could be identified but intensities were low; and poorly ordered, if only one band near 3660 cm^{-1} or inflexions near 3669 cm^{-1}, 3651/3650 cm^{-1} and 937/935 cm^{-1} were observed in the spectra (Madejova *et al*., 1997; Vaculikova *et al*., 2011).

Table 9.2: Hinckley Indices of Clay fractions of the studied Cretaceous-Tertiary Kaolins.

Age	Deposit	Sample ID	HI	Degree of Crystallinity
Cretaceous	Eruku	CF EP1 0m	0.94	MH
		CF EP1 2m	0.86	MH
		CF EP1 4m	1	MH
		CF EP2 0m	0.8	MH
		CF EP2 2m	1.07	MH
		CF EP2 4m	1.38	MH
		CF EP3 0m	0.95	MH
		CF EP3 2m	0.86	MH
		CF EP3 4m	1	MH
	Lakiri	CF LP1 0m	0.75	M
		CF LP1 2m	1.09	MH
		CF LP1 4m	1	MH
		CF LP2 0m	1.03	MH
		CF LP2 2m	1	MH
		CF LP2 4m	1.05	MH
		Min	0.75	
		Max	1.38	
		Average	0.98	MH
Tertiary	Awo-Omama	CF AL1 0m	0.28	L
		CF AL1 1m	0.3	L
		CF AL1 2m	0.41	L
		CF AL2 0m	0.29	L
		CF AL2 1m	0.28	L
		CF AL2 2m	0.27	L
	Ubulu-Uku	CF UL1 0m	0.58	LM
		CF UL1 1m	1	MH
		CF UL1 2m	1.05	MH
		CF UL2 0m	0.68	LM
		CF UL2 1m	0.92	MH
		CF UL2 2m	1.36	MH
		CF UL2 3m	1.17	MH
		Min	0.27	
		Max	1.36	
		Average	0.61	LM

(L): Low (HI <0.5), (LM): Low to Moderate (HI >0.5<0.7), (M): Moderate (HI = 0.7), (MH): Moderate to High (HI >0.7<1.4)

From the IR spectra obtained for the samples, the four bands in the OH stretching region were observed with the 3669 band showing weak inflexions which is more pronounced particularly for the Awo-Omama kaolin clay fraction (Figure 9.8). This corresponds to partially ordered kaolinite structure for the samples. Based on the IR spectrum for the deposits, the order of increasing structural order is Awo-Omama, Ubulu-Uku, Eruku, and Lakiri deposits, respectively.

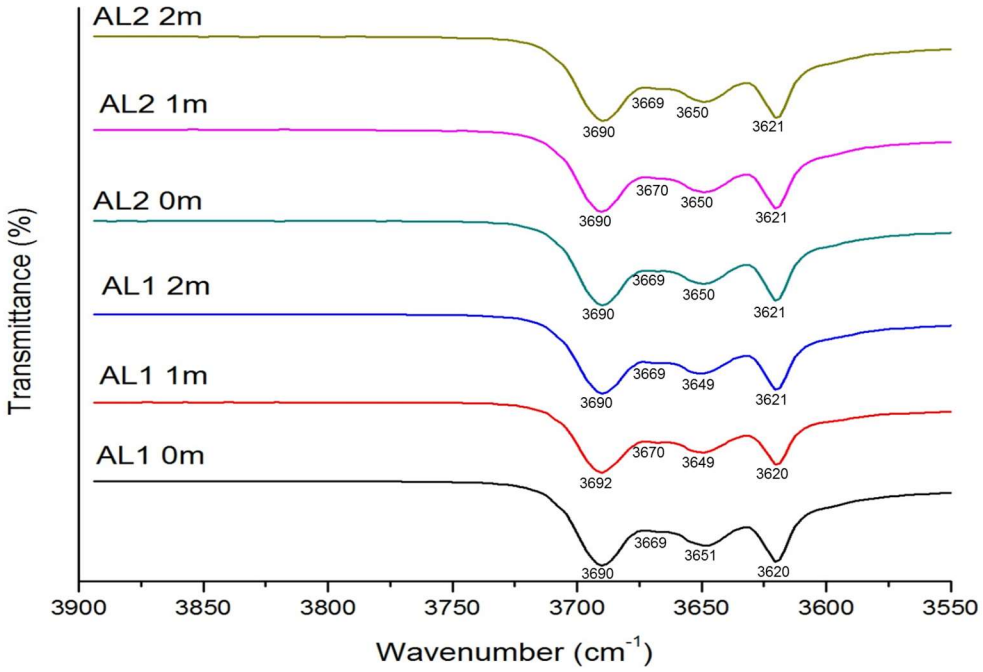

Figure 9.8: The IR spectra of Awo-Omama Kaolin Clay fraction between 3900 to 3550 cm^{-1}.

The IR-N approach is based on crystallinity indices CI_1 and CI_2 defined as $CI_1 = I(v_1)/I(v_3)$ and $CI_2 = I(v_4)/I(v_1)$ where $I(v_1)$ and $I(v_4)$ are intensities of OH stretching bands at 3691/3689 cm^{-1} and 3619 cm^{-1}, respectively, and $I(v_3)$ is the intensity of OH bending band at 912 cm^{-1}. The kaolinite structures are classified as poorly ordered, if $CI_1<0.7$ and $CI_2>1.2$; partially ordered; if $0.7<CI_1<0.8$ and $0.9<CI_2<1.2$; and ordered, if $CI_1>0.8$ and $CI_2<0.9$ (Russell and Fraser, 1994; Madejova and Komadel, 2001). The calculated CI_1

and CI_2 values obtained for the kaolinites correspond to partially ordered structures based on the IR-N classification (Table 9.3).

Table 9.3: Kaolinite Structural Order of Clay fractions of the studied Cretaceous-Tertiary Kaolins using IR-N classification.

Age	Deposit	Sample ID	V1	V3	V4	CI_1	CI_2	Degree of Crystallinity
Cretaceous	Eruku	CF EP1 0m	0.66	0.22	0.67	3.05	1.02	pa-o
		CF EP1 2m	0.64	0.2	0.65	3.12	1.02	pa-o
		CF EP1 4m	0.63	0.22	0.64	2.92	1.01	pa-o
		CF EP2 0m	0.65	0.21	0.68	3.03	1.05	pa-o
		CF EP2 2m	0.64	0.22	0.66	2.97	1.02	pa-o
		CF EP2 4m	0.66	0.23	0.69	2.83	1.05	pa-o
		CF EP3 0m	0.65	0.22	0.69	2.98	1.06	pa-o
		CF EP3 2m	0.65	0.21	0.65	3.02	1	pa-o
		CF EP3 4m	0.64	0.21	0.66	2.98	1.04	pa-o
	Lakiri	CF LP1 0m	0.65	0.22	0.64	3.05	0.99	pa-o
		CF LP1 2m	0.65	0.22	0.69	2.95	1.07	pa-o
		CF LP1 4m	0.64	0.2	0.65	3.24	1.03	pa-o
		CF LP2 0m	0.65	0.22	0.67	2.96	1.04	pa-o
		CF LP2 2m	0.64	0.2	0.66	3.16	1.02	pa-o
		CF LP2 4m	0.64	0.2	0.65	3.27	1.02	pa-o
		Min	0.63	0.2	0.64	2.83	0.99	
		Max	0.66	0.23	0.69	3.27	1.07	
		Average	0.65	0.21	0.66	3.04	1.03	pa-o
Tertiary	Awo-Omama	CF AL1 0m	0.66	0.2	0.68	3.38	1.02	pa-o
		CF AL1 1m	0.71	0.23	0.73	3.03	1.04	pa-o
		CF AL1 2m	0.67	0.2	0.69	3.32	1.02	pa-o
		CF AL2 0m	0.65	0.19	0.67	3.67	1.03	pa-o
		CF AL2 1m	0.67	0.2	0.69	3.33	1.02	pa-o
		CF AL2 2m	0.66	0.19	0.67	3.41	1.02	pa-o
	Ubulu-Uku	CF UL1 0m	0.72	0.23	0.74	3.11	1.03	pa-o
		CF UL1 1m	0.74	0.24	0.76	3.1	1.03	pa-o
		CF UL1 2m	0.66	0.22	0.71	3.04	1.06	pa-o
		CF UL2 0m	0.72	0.23	0.74	3.16	1.03	pa-o
		CF UL2 1m	0.73	0.24	0.76	3.07	1.03	pa-o
		CF UL2 2m	0.64	0.19	0.7	3.32	1.09	pa-o
		CF UL2 3m	0.69	0.23	0.73	3.06	1.06	pa-o
		Min	0.64	0.19	0.67	3.03	1.02	
		Max	0.74	0.24	0.76	3.67	1.09	
		Average	0.69	0.22	0.71	3.23	1.04	pa-o

(pa-o): Partially ordered.

There is an agreement between the IR-E and IR-N classifications in that the kaolinite structures were classified as partially ordered. This agreement is due to the absence of clay minerals like illite or smectite which could affect the IR pattern in OH stretching and bending region (Vaculikova *et al*., 2011). The IR and HI classifications agree with each other for the Ubulu-Uku, Eruku, and Lakiri deposits except for Awo-Omama deposit. This accordance further confirm that FTIR is a sensitive tool in the estimation of kaolinite crystallinity.

- **Kaolinite Dehydroxylation Temperature (T_d) Approach**

Decomposition peak temperatures in kaolinite sample obtained from DTA curves can be used to measure the degree of disorder. Well-ordered kaolin samples have T_d between 561 and 570 ˚C, poorly ordered samples have T_d between 546 and 560 ˚C, and disordered samples have T_d < 545 ˚C (Vaculikova *et al*., 2011). T_d values obtained for the studied Cretaceous – Tertiary kaolins were < 545 ˚C which corresponds to extremely disordered samples. Nevertheless, the determination of kaolinite structural order by thermal analysis cannot be applied in all circumstances unless the analysis was carried out under these conditions: heating rate 10 ˚C/min, sample fraction under 5 µm, and sample mass about 50 mg. This is crucial because the T_d values can vary under different conditions, so that the T_d interval of disorder can differ too (Guggenheim and van Gross, 2001; Vaculikova *et al*., 2011). Hence, the T_d kaolinite structural order classification will not be considered.

9.2.3 Kaolinite Morphology

The SEM images display the various morphologies and textures of the studied Cretaceous – Tertiary kaolins. Morphologically, the occurrence of the kaolins as pseudohexagonal stacks to books and thin platy particles is suggestive of kaolin emplacement through weathering processes. Texturally, kaolinite euhedral – subhedral – anhedral external forms and the irregular edges are characteristic of actively growing crystals (Keller, 1989). The presence of non-uniform crystal sizes is typical of sedimentary

kaolins. The absence of smaller and thinner packets or sheaves crystals typical of hydrothermally altered kaolins further affirms the formation of these kaolins from weathering processes (Keller, 1978).

The Tertiary kaolins were characterised by pseudohexagonal stacks to books with thin platy particles (Figs. 9.9a and e). This is comparable to the soft Cretaceous Georgia kaolin with large coarse stacks interspersed in a matrix of finer platy particles as well as the soft Late Cretaceous/Early Tertiary Capim kaolin with fairly larger stacks (Figs. 9.9b and c). However, the Cretaceous kaolins were comprised of thin platy kaolinite particles and they rarely contained stacks (Fig. 9.9d). It is comparable to the hard Tertiary Georgia kaolins with thin platy particles with no large books or stacks (Fig. 9.9f).

Particle morphology of kaolins directly translates to the brightness, glossiness, and printability of a coated paper (Pruett, 2016). The relatively finer particle sizes coupled with the platy kaolinite shapes observed within the Cretaceous kaolins are ideal for imparting a smooth, dense surface that is uniformly porous which will further give the paper a more uniform ink receptivity (Murray, 2007).

9.3 Geochemical Considerations

The average bulk geochemical compositions of the Cretaceous – Tertiary kaolins are presented in Table 9.4.

The most abundant oxides were SiO_2, Al_2O_3, Fe_2O_3, and TiO_2, whereas MgO, CaO, Na_2O, and K_2O were present in small quantities. The predominance of SiO_2 and Al_2O_3 were mainly associated with quartz and kaolinite minerals. Fe_2O_3 and TiO_2 are the main discolouring component. The presence of Fe_2O_3 and TiO_2 can associated hematite, goethite, and anatase minerals. Iron have been reported to be associated with rutile and anatase in some kaolins from Georgia, USA (Luz and Middea, 2004) and Egypt (Baioumy, 2014). The possible precursor for the occurrence of anatase in sedimentary kaolin deposits have been suggested to be ilmenite and biotite minerals (Schroeder *et al*., 2004).

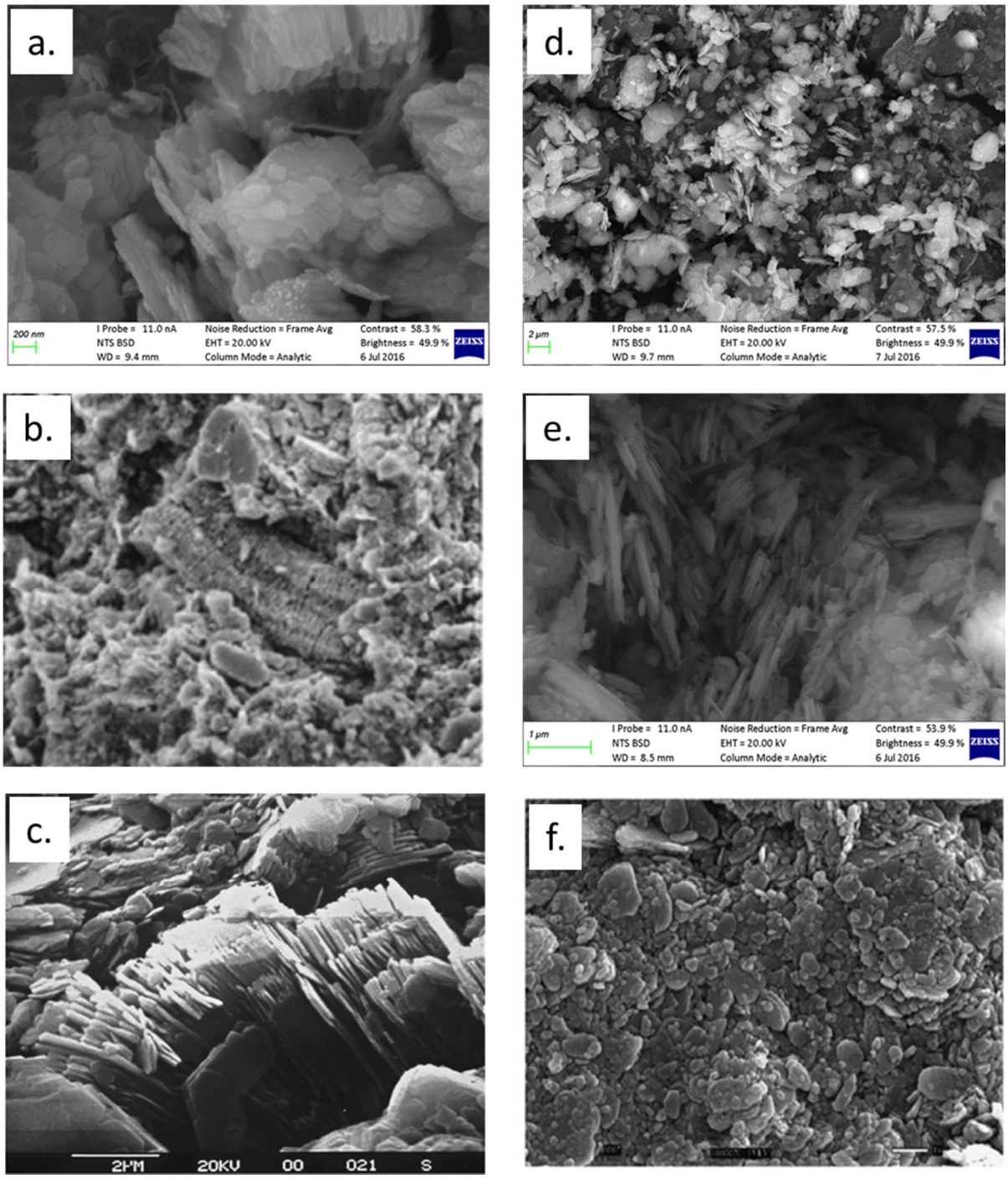

Figure 9.9: SEM micrographs of: (a) Awo-Omama Tertiary kaolin from this study, (b) Soft Cretaceous Georgia kaolin, (c) Soft Late Cretaceous/Early Tertiary Capim kaolin, (d) Lakiri Cretaceous kaolin from this study, (e) Awo-Omama Tertiary kaolin from this study, and (f) Hard Tertiary Georgia kaolin. Micrographs a – c shows pseudohexagonal stacks and books, whereas d – f shows thin platy particles. Micrographs b, c, and f are after Murray (2007).

Table 9.4: Average Bulk Geochemical Compositions of the studied Cretaceous – Tertiary kaolins compared with the World Sedimentary kaolin deposits.

	World Sedimentary kaolin deposits*			**Nigeria (This Study)**			
	USA		**Brazil**	**Cretaceous**		**Tertiary**	
	Soft Cretaceous Georgia kaolin	Hard Tertiary Georgia kaolin	Soft Late Cretaceous/Early Tertiary Capim kaolin	Eruku	Lakiri	Awo-Omama	Ubulu-Uku
SiO_2	45.3	44	46.56	56.06	49.64	71.04	59.95
TiO_2	1.44	2.43	0.78	2.11	1.60	1.35	2.03
Al_2O_3	38.38	39.5	38.03	28.85	35.55	18.02	22.65
Fe_2O_3	0.30	1.13	0.59	2.54	1.09	2.42	6.34
MgO	0.25	0.03	0.01	0.01	bdl	0.04	0.06
CaO	0.05	0.03	0.01	0.02	0.02	0.03	0.02
Na_2O	0.27	0.08	0.03	0.02	0.01	bdl	0.01
K_2O	0.04	0.06	0.02	0.40	0.20	0.16	0.46
LOI	13.97	13.9	13.8	10.22	12.57	6.87	8.71

(bdl) : below detection limit; (*): Murray, 2007.

Semi-quantitative analyses (SEM/EDS) conducted on the kaolinites indicated the possibility of the presence of lattice Fe (Table 9.5). Iron could be associated with kaolinite mineral by Fe substituting for Al in the octahedral sheet of the kaolinite and hence present in the kaolinite structure (Wilson, 2013; Gilkes and Prakongkep, 2016). The LOI average values for Tertiary kaolins were relatively lower when compared to that obtained for the Cretaceous kaolins. This is understandable since LOI is related to the dehydroxylation of clay minerals, organic matter oxidation, and decomposition of carbonates and hydroxides (Semiz, 2017).

The SiO_2/Al_2O_3 ratios were 1.94 and 1.39 for Cretaceous Eruku and Lakiri kaolins and 3.94 and 2.65 for Tertiary Awo-Omama and Ubulu-Uku kaolins. These SiO_2/Al_2O_3 ratios were higher when compared to the ideal kaolinite (1.18) (Ekosse, 2001) and some commercially marketed sedimentary kaolins (Table 9.4) due to higher SiO_2 concentrations in the Cretaceous – Tertiary kaolins. The average bulk TiO_2, MgO, CaO, Na_2O, and K_2O concentrations of the studied kaolins were comparable to the commercially marketed sedimentary kaolins, whereas the Fe_2O_3 concentrations were quite higher. However, the

average LOI values from 6.87 – 12.57 wt % were lower than compared to ideal kaolinite (13.9) and the commercially marketed sedimentary kaolins (Table 9.4).

Table 9.5: Percentage of different elements present in the studied Cretaceous – Tertiary kaolins obtained by SEM/EDS.

Age	Deposit	Sample ID	Na	Mg	Al	Si	K	Ca	Ti	Fe	Total
Cretaceous	Eruku	CF EP1 0m	0	0	42.64	54.2	0	0	0	3.16	100
		CF EP1 2m	0	0	44.31	53.71	0	0	0.96	1.03	100
		CF EP1 4m	0	0	42.31	56.67	0	0	0	1.03	100
		CF EP2 0m	0	0	41.86	57.07	0	0	0	1.07	100
		CF EP2 2m	0	0	42.51	56.49	0	0	0.42	0.58	100
		CF EP2 4m	0	0	43.01	55.95	0	0	0	1.04	100
		CF EP3 0m	0	0	44.55	55.45	0	0	0	0	100
		CF EP3 2m	0	0	42.19	56.84	0	0	0	0.97	100
		CF EP3 4m	0	0	38.05	58.96	0	0	0	3	100
	Lakiri	CF LP1 0m	0	0	39.63	58.96	0	0	0	1.4	100
		CF LP1 2m	0	0	36.75	59.65	0	0	0.53	3.06	100
		CF LP1 4m	0	0	38.55	57.64	0.93	0	0.5	2.39	100
		CF LP2 0m	0	0	40.72	56.25	0	0	1.11	1.92	100
		CF LP2 2m	0	0	39.18	57.57	0	0	0	3.25	100
		CF LP2 4m	0	0	37.35	58.11	0.46	0	0	4.07	100
		Min	0	0	36.75	53.71	0	0	0	0	100
		Max	0	0	44.55	59.65	0.93	0	1.11	4.07	100
		Average	0	0	40.84	56.59	0.09	0	0.24	2.24	100
Tertiary	Awo-Omama	CF AL1 0m	0	0	41.71	54.3	0	0	0.68	3.32	100
		CF AL1 1m	0	0	35.58	63.46	0	0	0.96	0	100
		CF AL1 2m	0	0	43.44	52.59	0.11	0	1.53	2.33	100
		CF AL2 0m	0	0	43.49	52.3	0.41	0	1.08	2.73	100
		CF AL2 1m	0	0	44.1	54.47	0	0	0	1.43	100
		CF AL2 2m	0	0	39.46	57.63	0	0	0.46	2.46	100
	Ubulu-Uku	CF UL1 0m	0	0	42.38	56.84	0.78	0	0	0	100
		CF UL1 1m	0	0	41.66	56.7	0	0	0.84	0.8	100
		CF UL1 2m	0	0	43.68	54.79	0.11	0	0.48	0.94	100
		CF UL2 0m	0	0	42.86	55.97	0	0	0	1.16	100
		CF UL2 1m	0	0	42.77	56.73	0.51	0	0	0	100
		CF UL2 2m	0	0	41.72	54.21	0	0	0.89	3.18	100
		CF UL2 3m	0	0	41.3	58.11	0	0	0.59	0	100
		Min	0	0	35.58	51.4	0	0	0	0	100
		Max	0	0	44.1	63.46	0.78	0	1.53	3.32	100
		Average	0	0	41.7	55.94	0.15	0	0.8	1.41	100

Specifications related to geochemical data are very important for industrial applications of the kaolins. In Tables 9.6 – 9.9, the average bulk geochemical compositions of the studied kaolins were compared with specifications of different industries (Siddiqui *et al.* (2005) and Lopez-Galindo *et al.* (2007)) and the most suited applications were also indicated for each of the deposits.

The average bulk geochemical compositions for the Cretaceous Eruku kaolins showed that it cannot be used in the paper coating, paper filler, ceramics, pharmaceutical, and cosmetics industries (Table 9.6a). However, physical size reduction to the clay fraction of the Eruku kaolins showed that it could be used in the pharmaceutical, cosmetics, and paper coating industries though additional modifications are required (Table 9.6b).

The average bulk geochemical compositions for the Cretaceous Lakiri kaolins showed that it could be used in the paper coating and ceramics industries with some improvements (Table 9.7a). However, physical size reduction to the clay fraction of the Lakiri kaolins showed that it could be used in the pharmaceutical, cosmetics, and paper coating industries though additional modifications are required (Table 9.7b).

The average bulk geochemical compositions for the Tertiary Awo-Omama kaolins showed that it cannot be used in the paper coating, paper filler, ceramics, pharmaceutical, and cosmetics industries without much improvements (Table 9.8a). However, physical size reduction to the clay fraction of the Eruku kaolins showed that it could be used in the paper coating, pharmaceutical, and cosmetics industries though additional modifications are required (Table 9.8b).

The average bulk geochemical compositions for the Tertiary Ubulu-Uku kaolins showed that it cannot be used in the paper coating, paper filler, ceramics, pharmaceutical, and cosmetics industries (Table 9.9a). In addition, physical size reduction to the clay fraction of the Eruku kaolins did not really improve its geochemical composition except for SiO_2 which is suggestive of the need for detailed industrial refinement for it to be used (Table 9.9b).

Table 9.6a: Average Bulk Geochemical Compositions of the studied Cretaceous Eruku kaolins compared with the Specifications of some industries.

	Eruku Bulk	Paper Coating	Status	Paper Filler	Status	Ceramics	Status	Pharmaceuticals and cosmetics	Status
SiO_2	56.06	45-49	x	46-48	x	48-50	x	44.6-46.4	x
TiO_2	2.11	0.5-1.3	x	0.5-1.5	x	0.02-0.1	x	0-1.4	x
Al_2O_3	28.85	36-38	x	37-38	x	36-38	x	38.1-39.5	x
Fe_2O_3	2.54	0.5-1.0	x	0.5-1.0	x	0.6-1	x	0.1-0.2	x
MgO	0.01	-		-		-		0.1-0.2	x
CaO	0.02	-		-		-		0.1-0.2	x
Na_2O	0.02	-		-		-		0-0.1	•
K_2O	0.40	0.5-1.5	x	0.5-1.5	x	1.2-2.7	x	0-0.2	x
LOI	10.22	-		-		11.2-12.5	x	13.8-13.9	x

• : Suited chemical compositions and x : Improvement is required

Table 9.6b: Average Geochemical Compositions for the <2 μm fraction of the studied Cretaceous Eruku kaolins compared with the Specifications of some industries.

	Eruku (<2 μm)	Paper Coating	Status	Paper Filler	Status	Ceramics	Status	Pharmaceuticals and cosmetics	Status
SiO_2	44.73	45-49	•	46-48	x	48-50	x	44.6-46.4	•
TiO_2	1.69	0.5-1.3	x	0.5-1.5	x	0.02-0.1	x	0-1.4	x
Al_2O_3	37.19	36-38	•	37-38	•	36-38	•	38.1-39.5	x
Fe_2O_3	2.98	0.5-1.0	x	0.5-1.0	x	0.6-1	x	0.1-0.2	x
MgO	bdl	-		-		-		0.1-0.2	x
CaO	0.02	-		-		-		0.1-0.2	x
Na_2O	0.21	-		-		-		0-0.1	•
K_2O	0.25	0.5-1.5	x	0.5-1.5	x	1.2-2.7	x	0-0.2	•
LOI	13.54	-		-		11.2-12.5	x	13.8-13.9	•

• : Suited chemical compositions and x : Improvement is required

Table 9.7a: Average Bulk Geochemical Compositions of the studied Cretaceous Lakiri kaolins compared with the Specifications of some industries.

	Lakiri Bulk	Paper Coating	Status	Paper Filler	Status	Ceramics	Status	Pharmaceuticals and cosmetics	Status
SiO_2	49.64	45-49	•	46-48	x	48-50	•	44.6-46.4	x
TiO_2	1.60	0.5-1.3	x	0.5-1.5	x	0.02-0.1	x	0-1.4	x
Al_2O_3	35.55	36-38	•	37-38	x	36-38	•	38.1-39.5	x
Fe_2O_3	1.09	0.5-1.0	•	0.5-1.0	•	0.6-1	•	0.1-0.2	x
MgO	bdl	-		-		-		0.1-0.2	x
CaO	0.02	-		-		-		0.1-0.2	x
Na_2O	0.01	-		-		-		0-0.1	•
K_2O	0.20	0.5-1.5	x	0.5-1.5	x	1.2-2.7	x	0-0.2	•
LOI	12.57	-		-		11.2-12.5	•	13.8-13.9	x

• : Suited chemical compositions and x : Improvement is required

Table 9.7b: Average Geochemical Compositions for the <2 μm fraction of the studied Cretaceous Lakiri kaolins compared with the Specifications of some industries.

	Lakiri (<2 μm)	Paper Coating	Status	Paper Filler	Status	Ceramics	Status	Pharmaceuticals and cosmetics	Status
SiO_2	44.55	45-49	•	46-48	x	48-50	x	44.6-46.4	•
TiO_2	1.41	0.5-1.3	•	0.5-1.5	•	0.02-0.1	x	0-1.4	•
Al_2O_3	39.19	36-38	x	37-38	x	36-38	x	38.1-39.5	•
Fe_2O_3	1.02	0.5-1.0	•	0.5-1.0	•	0.6-1	•	0.1-0.2	x
MgO	bdl	-		-		-		0.1-0.2	x
CaO	0.02	-		-		-		0.1-0.2	x
Na_2O	0.20	-		-		-		0-0.1	•
K_2O	0.18	0.5-1.5	x	0.5-1.5	x	1.2-2.7	x	0-0.2	•
LOI	13.51	-		-		11.2-12.5	x	13.8-13.9	•

• : Suited chemical compositions and x : Improvement is required

Table 9.8a: Average Bulk Geochemical Compositions of the studied Tertiary Awo-Omama kaolins compared with the Specifications of some industries.

	Awo-Omama Bulk	**Paper Coating**	**Status**	**Paper Filler**	**Status**	**Ceramics**	**Status**	**Pharmaceuticals and cosmetics**	**Status**
SiO_2	71.04	45-49	x	46-48	x	48-50	x	44.6-46.4	x
TiO_2	1.35	0.5-1.3	•	0.5-1.5	•	0.02-0.1	x	0-1.4	•
Al_2O_3	18.02	36-38	x	37-38	x	36-38	x	38.1-39.5	x
Fe_2O_3	2.42	0.5-1.0	x	0.5-1.0	x	0.6-1	x	0.1-0.2	x
MgO	0.04	-		-		-		0.1-0.2	x
CaO	0.03	-		-		-		0.1-0.2	x
Na_2O	bdl	-		-		-		0-0.1	•
K_2O	0.16	0.5-1.5	x	0.5-1.5	x	1.2-2.7	x	0-0.2	•
LOI	6.87	-		-		11.2-12.5	x	13.8-13.9	x

• : Suited chemical compositions and x : Improvement is required

Table 9.8b: Average Geochemical Compositions for the <2 μm fraction of the studied Tertiary Awo-Omama kaolins compared with the Specifications of some industries.

	Awo-Omama (<2 μm)	**Paper Coating**	**Status**	**Paper Filler**	**Status**	**Ceramics**	**Status**	**Pharmaceuticals and cosmetics**	**Status**
SiO_2	46.13	45-49	•	46-48	•	48-50	x	44.6-46.4	•
TiO_2	2.34	0.5-1.3	x	0.5-1.5	x	0.02-0.1	x	0-1.4	x
Al_2O_3	34.75	36-38	•	37-38	x	36-38	•	38.1-39.5	x
Fe_2O_3	3.80	0.5-1.0	x	0.5-1.0	x	0.6-1	x	0.1-0.2	x
MgO	bdl	-		-		-		0.1-0.2	x
CaO	0.02	-		-		-		0.1-0.2	x
Na_2O	0.25	-		-		-		0-0.1	•
K_2O	0.31	0.5-1.5	x	0.5-1.5	x	1.2-2.7	x	0-0.2	•
LOI	12.69	-		-		11.2-12.5	•	13.8-13.9	x

• : Suited chemical compositions and x : Improvement is required

Table 9.9a: Average Bulk Geochemical Compositions of the studied Tertiary Ubulu-Uku kaolins compared with the Specifications of some industries.

	Ubulu-Uku Bulk	**Paper Coating**	**Status**	**Paper Filler**	**Status**	**Ceramics**	**Status**	**Pharmaceuticals and cosmetics**	**Status**
SiO_2	59.95	45-49	x	46-48	x	48-50	x	44.6-46.4	x
TiO_2	2.03	0.5-1.3	x	0.5-1.5	x	0.02-0.1	x	0-1.4	x
Al_2O_3	22.65	36-38	x	37-38	x	36-38	x	38.1-39.5	x
Fe_2O_3	6.34	0.5-1.0	x	0.5-1.0	x	0.6-1	x	0.1-0.2	x
MgO	0.06	-		-		-		0.1-0.2	•
CaO	0.02	-		-		-		0.1-0.2	x
Na_2O	0.01	-		-		-		0-0.1	•
K_2O	0.46	0.5-1.5	•	0.5-1.5	•	1.2-2.7	x	0-0.2	x
LOI	8.71	-		-		11.2-12.5	x	13.8-13.9	x

• : Suited chemical compositions and x : Improvement is required

Table 9.9b: Average Geochemical Compositions for the <2 µm fraction of the studied Tertiary Ubulu-Uku kaolins compared with the Specifications of some industries.

	Ubulu-Uku (<2 µm)	**Paper Coating**	**Status**	**Paper Filler**	**Status**	**Ceramics**	**Status**	**Pharmaceuticals and cosmetics**	**Status**
SiO_2	49.69	45-49	•	46-48	x	48-50	•	44.6-46.4	x
TiO_2	2.05	0.5-1.3	x	0.5-1.5	x	0.02-0.1	x	0-1.4	x
Al_2O_3	30.65	36-38	x	37-38	x	36-38	x	38.1-39.5	x
Fe_2O_3	5.97	0.5-1.0	x	0.5-1.0	x	0.6-1	x	0.1-0.2	x
MgO	bdl	-		-		-		0.1-0.2	x
CaO	0.02	-		-		-		0.1-0.2	x
Na_2O	0.27	-		-		-		0-0.1	•
K_2O	0.51	0.5-1.5	•	0.5-1.5	•	1.2-2.7	x	0-0.2	x
LOI	11.10	-		-		11.2-12.5	•	13.8-13.9	x

• : Suited chemical compositions and x : Improvement is required

9.4 Conclusions

Based on the physico-chemical, mineralogical, and geochemical compositions of the studied kaolins, the following deductions have been made:

a. Based on the EC, the kaolins were considered to contain little or no soluble salts which can cause exfoliation and peeling of the surfaces of ceramic clay bodies.
b. According to the particle size distribution, the Lakiri kaolins were found to be highly porous with very low permeability, whereas the Eruku, Awo-Omama, and Ubulu-Uku kaolins have low porosity and permeability. This has implications on the cohesion and extrusion of the kaolins when used in the ceramic industry.
c. The PI $\geq 10\ \%$ values are appropriate for building related ceramic productions particularly in brick making. In addition, PI < 35 % suggest that excessive shrinkage is not expected.
d. The bulk mineralogical composition shows that the deposits can be classified into pure kaolins (Lakiri) and sandy kaolins (Eruku, Awo-Omama, and Ubulu-Uku) which is indicative of the increased abundance of quartz in the sandy kaolins.
e. The kaolinite structural order from the XRD based HI method and the FTIR based IR-E and IR-N methods in increasing orderliness is Awo-Omama (with least structural orderliness) < Ubulu-Uku < Eruku < Lakiri (with best structural orderliness). This could as well be taken as the order of their applications as pigments in paper coating which is consistent with the kaolinite morphology since the Cretaceous kaolins (Eruku and Lakiri) have finer particle sizes and platy shapes which is ideal for imparting better paper quality.
f. Considering both mineralogical, and geochemical specifications, the raw kaolins were almost not applicable except for Lakiri kaolins in the paper coating and ceramic industries though improvement is required. However, by physical process of particle size reduction, the Cretaceous – Tertiary kaolins could be used in the paper coating, ceramics, pharmaceutical, and cosmetics industries though improvement will be required. Hence, this implies that detailed industrial refinement of the studied kaolin deposits could give wider applications in many industries as well as improved quality.

Chapter Ten
Conclusions and Recommendations

10.1 Conclusions

This study examined the provenance and tectonic settings (Chapter five), paleoenvironmental conditions (Chapter six), detrital zircon geochronology (Chapter seven), comparative analysis between selected Cretaceous African and South American kaolins (Chapter eight), and industrial applications (Chapter nine) of the Cretaceous-Tertiary kaolins within the Eastern Dahomey and Niger Delta Basins in Nigeria. To achieve these objectives, the physico-chemical, mineralogical, geochemical, isotopic and geochronological characteristics of the kaolins were determined using latest available techniques. The results were interpreted to come up with the following important conclusions:

1. The studied Cretaceous-Tertiary kaolins were formed under intense chemical paleoweathering of rocks predominantly derived from felsic rocks in addition to contributions from intermediate and mafic rocks. Sediment recycling was proven due to the enrichment of Zr with more influence in the Tertiary kaolins. Anoxic conditions during the deposition were detectable in the redox-proxy signals which is consistent with the horst and graben structural geotectonic settings of the Eastern Dahomey and Niger Delta Basins. The provenance characteristics suggest that the kaolins were deposited in passive margin settings.

2. The supergene type of kaolin deposits were confirmed for studied Cretaceous - Tertiary kaolins from the δD and $\delta^{18}O$ values. Depleted (lighter) meteoric water during the formation of the Tertiary kaolins relative to the Cretaceous kaolins and enriched (heavier) meteoric water during the Recent were evident from the $\delta^{18}O$ and δD values for the paleometeoric water from Cretaceous and Tertiary kaolins and the present day meteoric water. The tropical climatic conditions during the formation of the kaolins were inferred from the paleotemperatures which indicated a warmer period of formation for the Cretaceous kaolins (32.5 ˚C) relative to the

Tertiary kaolins (21.5 ˚C), whereas the period of formation for the Tertiary kaolins was cooler relative to the Recent (26.1 ˚C).

3. The sediment sources for studied Cretaceous – Tertiary kaolins were predominantly from rocks of Eburnean and Pan African ages located in the West African Massif for the Cretaceous kaolins, whereas for the Tertiary kaolins were from both the West African and Northern Nigerian Massifs with little contributions from rocks of Liberian and Kibaran ages. The maximum depositional age estimates for the Cretaceous - Tertiary kaolins in the Eastern Dahomey and Niger Delta Basins in Nigeria corresponds to the Ediacaran Period (645 – 541 Ma) of the Neoproterozoic Era (1000 – 541 Ma). Due to lack of consistency with previous studies, this estimated age is taken as part of the provenance ages of rocks from which the sediments were derived. The most probable timing of kaolinisation for the kaolins occurred between the Ediacaran (645 – 541 Ma) and Early Cretaceous Periods for the Cretaceous kaolins and between the Ediacaran Period (645 – 541 Ma) and Oligo – Miocene age for the Tertiary kaolins.

4. The Nigerian Lakiri and Brazilian soft Capim River kaolins have similar mineralogical characteristics and were classified as pure kaolins, whereas the Nigerian Eruku and Egyptian Teeh kaolins were classified as sandy kaolins. The kaolinite crystal morphology of the Nigerian Lakiri and Eruku kaolins were comparable to that of the Brazilian soft Capim River kaolins with moderate structural order. The kaolins were formed under intense chemical weathering in a restricted oxygen-poor depositional environment. The Nigerian Lakiri, Eruku, and Brazilian soft Capim River kaolins were formed under warm conditions with temperatures characteristic of paleoweathering formation under tropical climate. The source sediments for the Nigerian (except for Eruku kaolins with more input from areas related to the Pan African orogenic event) and Brazilian kaolins were predominantly from areas related to the Transamazonian orogenic event in Brazil which corresponds to the Eburnean orogenic event in Nigeria with contributions

from Pan African (Brasiliano) and Kibaran orogenic rocks, respectively. The presence of detrital zircons with similar ages further corroborated the globally synchronous orogenic events across the African and South American continents.

5. The bulk mineralogical composition shows that the deposits can be classified into pure kaolins (Lakiri) and sandy kaolins (Eruku, Awo-Omama, and Ubulu-Uku) which is indicative of the increased abundance of quartz in the sandy kaolins. The kaolins were characterised by pseudohexagonal stacks to books and thin platy kaolinite particles with moderate structural order in increasing orderliness from Awo-Omama (with least structural orderliness) followed by Ubulu-Uku, Eruku, and Lakiri (with best structural orderliness), respectively. Comparison with various industry specifications revealed that the raw kaolins were almost not applicable except for Lakiri kaolins in the paper coating and ceramic industries though improvement is required. Simple particle size reduction to <2 μm fraction showed that the Cretaceous – Tertiary kaolins could be used in the paper coating, ceramics, pharmaceutical, and cosmetics industries though improvement will be required.

The study has contributed to the body of knowledge in Applied Clay mineralogy in the following ways:

1. Kaolins and Gondwana

- Better understanding of past environmental conditions in the African continent where few of such studies have been carried out.
- The probable timing of kaolinisation for the Cretaceous and Tertiary kaolins were better constrained.
- African and South American paleoclimates have been synchronised.

2. Kaolins and Geotectonics

- Valid geochemical data have contributed to the novel understanding of the geotectonic settings within the Eastern Dahomey and Niger Delta Basins.

3. Kaolin Provenance and African Orogeny

- Based on the geochronological data, rocks of Eburnean and Pan African ages were the predominant sediment sources for the Cretaceous – Tertiary kaolins.

4. Kaolin Applications

- Through a combination of various analytical techniques, appropriate applications for the use of kaolins is advanced.

10.2 Recommendations

Proposal for further investigations include:

a. Establishment of a stable isotopic geochronological system for West Africa through geologic time scale is needed for a better understanding of the evolution of paleoclimates in the region. This will also allow better constraint of the timing of kaolinisation.

b. To establish possible input of detritus from the West African Craton to South American Craton or vice versa, detrital zircon inclusion analysis, trace element composition, and isotopic signatures are needed. This will allow the determination of clear relationships between the detrital zircons and their potential source areas.

c. Considering the large kaolin reserves, beneficiation of the kaolins should be carried to strengthen large scale industrial applications listed in this work.

REFERENCES

Abajo, M. (2000). Manual sobre Fabricacio´n de Baldosas, Tejas y Ladrillos (S.A. Beralmar, editor), Barcelona, 125 pp.

Abu-Zied, R.H. (2008). Lithostratigraphy and biostratigraphy of some Lower Cretaceous outcrops from Northern Sinai, Egypt. *Cretaceous Res*. **29**, 603–624.

Adegoke, O.S. (1969). Eocene stratigraphy of Southern Nigeria. *Bur. Rech. Geol. Min. Mem*., **69,** 23-48.

Adegoke, O.S., Adeleye, D.R., Odebode, M.O., Petters, S.W., and Ejeagba, D.M. (1980). Geological guide to some Nigerian Cretaceous to Recent localities. In Adegoke, O.S. (Ed), NMGS 16th Annual Conference, Special publ., **2**, 1-26.

Ajayi, J.O. and Agagu, O.K. (1981). Mineralogy of primary clay deposits in the basement complex of Nigeria. *J. Min. Geol.,* **18**(1): 27-30.

Ajayi, T.R., Oyawale, A.A., Islander, F.Y., Asubiojo, O.I., Klein, D.E. and Adediran, A.I. (2006). Trace and Rare Earth Elements Geochemistry of Oshosun Sediments of Dahomey Basin, Southwestern Nigeria. Journal of Applied Science, **6 (9)**, 2067-2076.

Ajayi, O.A. and Adefila, S.S. (2012). Comparative study of chemical and biological methods of beneficiation of Kankara kaolin. *International Journal of Scientific and Technology research*, **1 (8)**, 13-18.

Ajibade, A.C. (1980). Mylonic and the cataclastic rocks from the Zungeru area, Nigeria. 10coll.Geol. Africaine, Montpellier Resumes; pp 25.

Akinlua, A., Adekola, S.A., Swakamisa, O., Fadipe, O.A., Akinyemi, S.A. (2010). Trace element characterisation of Cretaceous Orange Basin hydrocarbon Source rocks. *Applied Geochemistry*, **25:**1587–1595.

Allard, G.O. and Hurst, V.J. (1969). Brazil-Gabon geologic link supports continental drift, *Science*, **163**, 528-532.

Almeida, F.F.M. (1968). Precambrian geology of Northeastern Brazil and Western Africa and the theory of continental drift. *Nat. Resour. Res.,* **4**, 151-162 (Proceed. Symp. on the Granites of West Africa, UNESCO).

Almeida,F.M., Amaral, G., Cordani, U.G., and Kawashita, K. (1973). The Precambrian evolution of the South America cratonic margin south of the Amazon River, In

A.E.M. Nairn and F.G. Stehli (Editors), The Ocean Basins and Margins, 1. The Sout Atlantic. Plenum Press, New York. pp. 411-446.

Alvarez, L.W., Alvarez, W., Asaro, F., and Michel, H.V. (1980). Extraterrestrial cause for the Cretaceous–Tertiary extinction. *Science* **208**, 1095–1108.

Alverson, K., Oldfield, F., and Bradley, R. (2000). Past Global Changes and Their Significance for the Future. *Quaternary Science Reviews* **19**:479 pp.

Andrade, F.A., Al-Qureshi, H.A., and Hotza, D. (2011). Measuring the plasticity of clays: a review. *Appl. Clay Sci.* **51**, 1–7.

Ansdell, K.M, Kyser, T.K., and O'Hanley, D.S. (1991). Comparison between the single-zircon Pb-evaporation technique and high-precision U-Pb geochronology: Relevance of $^{207}Pb/^{206}Pb$ ages. Geological Society of America Abstracts with Programs 23, A149-A150.

Aparicio, P. and Galán, E. (1999). Mineralogical interference on kaolinite crystallinity index measurements. *Clays and Clay Miner.*, **47**, 12–27.

Aparicio, P., Galan, E., and Ferrell, R.E. (2006). A new kaolinite order index based on XRD profile fitting. *Clay Minerals,* **41,** 811–817.

Avbovbo, A.A. (1978). Tertiary lithostratigraphy of Niger Delta. *AAPG Bull.*, **62**, 295-306.

Badmus, B.S. and Olatinsu, O.B. (2009). Geophysical evaluation and chemical analysis of kaolin clay deposit of Lakiri village, southwestern Nigeria. *International Journal of Physical Sciences*, **4 (10)**, 592-606.

Bain, J.A. (1971). A plasticity chart as an aid to the identification and assessment of industrial clays. *Clay Minerals*, **9,** 1-17.

Baioumy, H., Gilg, H.A., and Taubald, H. (2012). Mineralogy and geochemistry of the sedimentary kaolin deposits from Sinai, Egypt: implications for source rock control. *Clays and Clay Miner*. **60**, 633–654.

Baioumy, H. (2013). Hydrogen and oxygen isotopic compositions of sedimentary kaolin deposits, Egypt: Paleoclimatic implications. *Applied Geochemistry*, **29**, 182-188.

Baioumy, H.M. (2014). Geochemistry and origin of the Cretaceous sedimentary kaolin deposits, Red Sea, Egypt. *Chemie der Erde* **74**, 195–203.

Bhatia, M.R. (1983). "Plate tectonics and geochemical composition of sandstones". *Journal of Geology*, **91,** pp. 611-627.

Bhatia, M.R. and Crook, K.A.W. (1986). Trace element characteristics of graywackes and tectonic setting discrimination of sedimentary basins. *Contrib. Mineral. Petrol.* **92**, 181–193.

Billman, A, (1976). Offshore stratigraphy and paleontology of the Dahomey Basin (Benin embayment), West Africa. Paper presented at the 7th African Micropaleontological coll., Ile-Ife.

Bird, M.I. and Chivas, A.R. (1988). Stable isotope evidence for low temperature kaolinite weathering and post-formational hydrogen isotope exchange in Permian kaolinite. *Chem. Geol.* **72,** 249–265.

Bird, M.I. and Chivas, A.R. (1989). Stable isotope geochronology of the Australian regolith.*Geochim. et Cosmochim. Acta,* **53***, 3239-3256.*

Bird, M.I. and Chivas, A.R. (1993). Geomorphic and paleoclimatic implications of an oxygen isotope geochronology for Australian deeply weathered profiles. *Australian Journal of Earth Sciences*, **40**, 345-358.

Bloodworth, A.J., Highley, D.E. and Mitchell, C.J. (1993). Industrial minerals laboratory manual - kaolin. Tech. Rep. Brit. Geol. Surv. WG/93/1. 76 pages.

Bock, B., McLennan, S.M., and Hanson, G.H. (1998). Geochemistry and provenance of the Middle Ordovician Austin Glen Member (Normanskill Formation) and the Taconian Orogeny in New England. *Sedimentology* **45**, 635– 655.

Borthwick, J. and Harnon, R.S. (1982). A note regarding ClF_3 as an alternative to BrF_5 for oxygen isotope analysis. *Geochimica et Cosmochimica Acta* **46(9):**1665-1668.

Brady, N.C. and Weil, R.R. (1999). The nature and properties of soils. 12th ed. Prentice Hall. Upper Saddle River, NJ.

Brenchley, P.J. and Harper, D.A.T. (1998). Paleoecology: Ecosystems, Environments and Evolution. Chapman and Hall, London. 402 pp.

Bullard, E., Everett, J.E., and Smith, A.G. (1965). The fit of continents around the Atlantic. *Philos. Trans. R. Soc*. London, **258,** 41-51.

Bundy, W.M. (1993). The diverse industrial applications of kaolin, *in* Murray, H.H., et al., eds., Kaolin Genesis and Utilization: The Clay Minerals Society, Special Publication No. 1, 43–73.

Burke, K., Dessauvagie, T.F.G., and Whiteman, A.J. (1972). The opening of the Gulf of Guinea and geological history of the Benue depression and Niger Delta. *Nature Phys. Sci*., **233,** 51-55.

Caby, R. (1989). Precambrian terranes of Benin-Nigeria and northeast Brazil and the late Proterozoic South Atlantic fit. Geol. SOCA. mer., Spl. Paper, **230**, pp. 145-158.

Campbell, F.A. and Williams, G.D. (1965). Chemical composition of shales of the Mannville Group, Lower Cretaceous of central Alberta, Canada. *Bull. Am. Assoc. Petrol. Geol*. **49**, 81–87.

Carey, S. W. (1958). *"The tectonic approach to continental drift". In Carey, S.W. Continental Drift—A symposium, held in March 1956. Hobart: Univ. of Tasmania. pp. 177–363.*

Carneiro, B.S., Ange´lica, R.S., Scheller, T., Neves, R.F., and Castro, E.A.S. (2002). Transformac¸o˜es te´rmicas do caulim duro da regia˜o do Rio Capim, Para´. CD-ROM in: XV Congresso Brasileiro de Engenharia e Cieˆncia dos Materiais, Natal, RN.

Casagrande, A. (1948). Plasticity chart for the classification of cohesive soils. *Trans. Am. Soc. Civ. Eng*. 113, 901.

Castaing, C., Feybesse, J.l., Thieblemont, D., Triboulet, C., and Chevremont, P. (1994). Palaeogeographical reconstructions of the Pan African/Brasiliano orogen: closure of an oceanic domain or intracontinental convergence between major blocks. *Precambrian Research,* **67**, 327–344.

Chamley, H. (1989). Clay Sedimentology. Springer-Verlag, Berlin, Heidelberg, New York. 623 pp.

Chivas, A.R. and Bird, M.I. (1995). Palaeoclimate from Gondwanaland clays. In: Churchman, G. J., Fitzpatrick, R.W., and Eggleton, R.A. (Eds.), Clays controlling the Environment: Proceedings of the 10th International Clay Conference, pp. 333–338.

Chaves. A.O. and Neves, J.M.C. (2005). Radiometric ages, aeromagnetic expression, and general geology of mafic dykes from southeastern Brazil and implications for

African-South American correlations. *Journal of South American Earth Science* **19**, 387–397.

Clauer, N. and Chaudhari, S. (1995). Clays in crustal environments. Isotope dating and tracing. *Springer, Berlin- Heidelberg.*

Clauer, N. (2013). The K-Ar and $^{40}Ar/^{39}Ar$ methods revisited for dating fine-grained K-bearing clay minerals. *Chemical Geology* **354**, 163–185.

Clauer, N., Fallick, A.E., Galán, E., Aparicio, P., Miras, A., Fernandez-Caliani, J.C., and Aubert, A. (2015). Stable isotope constraints on the origin of kaolin deposits from Variscan granitoids of Galicia (NW Spain). Chem. Geol. **417**, 90–101.

Cochrane, H. (1996). Adhesives and sealants. In: Ciullo, P.A. (Ed.), Industrial Minerals and their uses. A handbook and formulary. Noyes Publications, New Jersey, pp. 275–352.

Colbert, E.H. (1973). Continental drift and the distribution of fossil repltiles. In D.H. Tarling and S.K. Runcorn (Editors), Implications of Continental Drift to the Earth Sciences. Academic Press, London, pp. 395-412.

Coleman, M.L., Shepherd, T.J., Durham, J.J., Rouse, J.E. and Moore, G.R. (1982). Reduction of water with zinc for hydrogen isotope analysis. *Anal. Chem*., **54:** 993-995.

Condie, K.C., Boryta, M.D., Liu, J., Quian, X. (1992). The origin of Khondalites: geochemical evidence from the archean to Early Proterozoic granulitic belt in the North China craton: Precambrian Research, **59(3-4)**, 207-223.

Cordani, U.G., Fraga, L.M., Reis, N., Tassinari, C.C.G., and Brito-Neves, B.B. (2010). On the origin and tectonic significance of the intra-plate events of Grenvillian-type age in South America: A discussion. *Journal of South American Earth Sciences,* **29**, 143-159.

Corfu, F., Hanchar, J.M., Hoskin, P.W.O., Kinny, P. (2003). Atlas of zircon textures. *Reviews in Mineralogy and Geochemistry*, DOI: 10.2113/0530469.

Cox, R., Lowe, D.R., and Cullers, R.L., (1995). The influence of sediment recycling and basement composition on evolution of mudrock chemistry in the southwestern United States: *Geochimica et Cosmochimica Acta*, **59(14),** 2919-2940.

Craig, H., 1961. Isotopic variations in meteoric waters. *Science*, **133**, 1702–1708.

Cravero, F., Marfil, S. A., and Maiza, P. J. (2010). Statistical analysis of geochemical data: a tool for discriminating between kaolin deposits of hypogene and supergene origin, Patagonia, Argentina. *Clay Minerals,* ***45*****,** 183-196.

Cullers, R.L., Basu, A., and Suttner, L. (1988). Geochemical signature of provenance in sand-size material in soils and stream sediments near the Tobacco Root batholite, Montana, USA. *Chem. Geol.,* **70,** 335– 348.

Cullers, R.L. (1994). The controls on the major and trace element variation of shales, siltstone and sandstones of Pennsylvanian – Permian age from uplifted continental blocks in Colorado to platform sediment in Kansas, USA: *Geochimica et Cosmochimica Acta,* **58(22**), 4955-4972.

Cullers, R.L., Graf, J. (1983). Rare earth elements in igneous rocks of the continentalcrust: intermediate and silicic rocks, ore petrogenesis. In: Henderson, P. (Ed.), Rare Earth Geochemistry. Elsevier, Amsterdam, pp. 275–312.

Cullers, R.L. (2000). The geochemistry of shales, siltstones and sandstones of Pennsylvanian-Permian age, Colorado, U.S.A.: implications for provenance and metamorphic studies: *Lithos*, **51**, 305-327.

Cullers, R.L. and Podkovyrov, V.N. (2000). Geochemistry of the Mesoproterozoic Lakhanda shales in southeastern Yakutia, Russia: implications for mineralogical and provenance control, and recycling. *Precambrian Research*, **104 (1-2),** 77-93.

Dada, S.S. (2006). Proterozoic evolution of Nigeria. In: Oshi O (ed) The basement complex of Nigeria and its mineral resources (A Tribute to Prof. M. A. O. Rahaman). Akin Jinad & Co. Ibadan, pp 29–44.

Daniel, D.E. (1991). Seminar publication: Design and construction of RCRA/CERCLA final covers. Environmental Protection Agency, USA.

Davis, J.C. (2002). Statistics and Data Analysis in Geology, New York: John Wiley & Sons Inc., third edition, 638 pp.

Deepthy, R. (2008). Clay mineralogical and geochemical studies on the weathering profiles developed on either side of Western Ghats, Karnataka, India. Unpublished PhD Thesis, Pondicherry University, 165 pp.

Delgado, A. and Reyes, A. (1996). Oxygen and hydrogen isotope compositions in clay minerals: A potential single-mineral geothermometers. *Geochemica et Cosmochimica Acta*, **60 (21),** 4285-4289.

Diamond, R. E. and Harris, C. (1997). Oxygen and hydrogen isotope composition of Western Cape meteoric water, Research letter, *South African Journal of Science*, **93**, pp 371 – 374.

Dickson, W., Schiefelbein, C., Zumberge, J., and Odegard, M. (2005).Basin analysis in Brazilian and West African conjugates: Combining disciplines to deconstruct petroleum systems. GCSSEPM Foundation 25th Annual Bob F. Perkins Research Conference, Houston TX, December 4-7, 2005.

Dickinson, W.R. and Gehrels, G.E. (2009). Use of U–Pb ages of detrital zircons to infer maximum depositional ages of strata: a test against a Colorado Plateau Mesozoic database Earth Planet. *Sci. Lett.*, **288**, pp. 115-125

Diko, M. L. and Ekosse, G. E. (2013). Characterisation of two kaolin facies from Ediki, Southwest Cameroon. Academic Journal, **8(18),** 698-704.

Diko M., Ekosse G. and Ogola J. (2016). Fourier transform infrared spectroscopy and thermal analyses of kaolinitic clays from South Africa and Cameroon. *Acta Geodyn. Geomater.*, **13 (2),** xx1–x10, DOI: 10.13168/AGG.2015.0052

Dill, H.G., Bosse, H.R., Henning, K.H., and Fricke, A. (1997). Mineralogical and chemical variations in hypogene and supergene kaolin deposits in a mobile fold belt the Central Andes of Northwestern Peru. *Mineralium Deposita* **32**, 149–163.

Dingle, R.V. and Lavelle, M. (1998). Late Cretaceous–Cenozoic climatic variations of the Northern Antarctic Peninsula: new geochemical evidence and review. *Palaeogeography, Palaeoclimatology, Palaeoecology* **141**, 215–232.

Dobrzinski, N., Bahlburg, H., and Strauss, H. (2004). Geochemical Climate Proxies Applied to the Neoproterozoic Glacial Succession on the Yangtze Platform, South China. American Geophysical Union 10.1029/Series.

Dombrowski T., (1982). Abundance, distribution and origin of thorium in the Georgia kaolins [unpublished M.S. thesis]: Indiana University, South Bend, Indiana, 85 p.

Dombrowski T., and Murray H.H., (1984). Thorium - a key element in differentiating Cretaceous and Tertiary kaolins in Georgia and South Carolina: Proceedings of the 27th International Geological Congress, **15**, p. 305–317.

Dondi, M., Marsigli, M. and Venturi, I. (1998). Technological requirements of raw materials for heavy clay products. Pp. 204-207 in: Proceedings of the 2nd Mediterranean Clay Meeting, Aveiro, Portugal, 2.

dos Santos Jr., A.E.A., Rosetti, D.F. and Murray, H.H. (2007). Origins of the Rio Capim kaolinites (northern Brazil) revealed by $\delta^{18}O$ and δD analyses. *Applied Clay Science*, **37**, 281-294.

dos Santos, E., Scorzelli, R.B., Bertolino, L.C., Alves, O.C., and Munayco, P. (2012). Characterization of kaolin from the Capim River region — Brazil. *Applied Clay Science*, **55**, 164-167.

Durugbo, E.U. and Aroyewun, F.R., 2011. Palynology and paleaeoenvironments of Late Cretaceous Araromi Formation, Dahomey Basin, Nigeria. *Asian Journal of Earth Sciences* **5**(2), 50–62.

Durugbo, E.U. and Olayiwola, M.A., 2017. Palynological dating and palaeoenvironments of the M1 well, Middle Miocene, Niger Delta, Nigeria. *Palaeontologia Africana 52, 46-57.*

DuToit A.L. (1921). Land connections between the other continents and South Africa. *South African Journal of Science*, **18**, 120-140.

DuToit A.L. (1937). Our wandering continents. An hypothesis of continental drifting, Oliver and Boyd, Edinburgh, 366 pp.

Dypvik, H., Brunfelt, A.O. (1976). Rare earth elements in lower Paleozoic epicontinental and eugeosynclinal sediments from the Oslo and Trondheim regions. *Sedimentary*, **23**:363-378.

Ekosse, G. (1990). Physico-chemical studies of some clay deposits in Anambra State, Nigeria. Unpublished PGD thesis, Anambra State University of Science and Technology, Nigeria, 112 pp.

Ekosse, G. (2001). Provenance of the Kgwakgwe kaolin deposit, southeastern Botswana and its possible utilization. *Applied Clay Science* **20**, 137–152.

Ekosse, G. (2007). Thermoanalytical characterisation, stable isotope and paleoenvironmental considerations of kaolinite from two genetic sources. *Fresenius Environmental Bulletin*, **16 (12),** 1-15.

Ekosse, G. (2010). Kaolin deposits and Occurrences in Africa: Geology, Mineralogy and Utilization. *Applied Clay Science* **50**, 212-236.

Ekosse, G., Mulaba-Bafubiandi, A., and Nkoma, J.S. (2007). Physico-Chemistry of Continental Bentonites and Kaolin for Ceramic Applications. *African Journal of Science and Technology (AJST) Science and Engineering Series* ***8 (1),*** *pp. 107 – 115.*

El Ouahabi, M., Daoudi, l. and Fagel, N. (2014). Mineralogical and geotechnical characterization of clays from northern Morocco for their potential use in the ceramic industry. *Clay Minerals*, **49**, 35–51

Elueze, A.A. (1989). Geological distribution, applications and occupational potentials of non- metallic mineral resources in Nigeria. Proc. 25th Annual Conf. Nigeria, Min. Geosc. Soc., Ibadan, pp 10.

Elueze, A.A. and Bolarinwa, A.T. (1995). Assessment of Functional Applications of Lateritic clay bodies in Ekiti environ, Southwestern Nigeria. *J. Min. Geol.,* **31**, 79-87.

Emofurieta, W.O., Kayode, A.A., and Coker, S.A. (1992). Mineralogy, Geochemistry and Economic Evaluation of the Kaolin Deposits near Ubulu-Uku, Awo-Omama and Buan in Southern Nigeria. *Journal of Mining and Geology*, **28 (2**), 211- 220.

Ernst, R.E., Bleeker, W., Söderlund, U., and Kerr, A.C. (2013). Large Igneous Provinces and supercontinents: Toward completing the plate tectonic revolution. *Lithos*, **174**, 1-14.

Fagel, N., 2007. Clay minerals, deep circulation and climate. *Dev. Mar. Geol*., **1**, 139-176.

Falconer, J.D. (1911). The Geology and Geography of Northern Nigeria. McMillan; London. P. 295.

Fedo, *C.M.,* Nesbitt, H.W., and Young, G.M. (1995). Unravelling the effects of potassium metasomatism in sedimentary rocks and paleosols, with implications for paleoweathering conditions and provenance. *Geology*, **23**, 921-924.

Fedo, C.M., Sircombe, K.N., and Rainbird, R.H. (2003). Detrital zircon analysis of the sedimentary record. In: Hanchar, J.M., Hoskin, P.O. (eds) Zircon, Rev Mineral Geochem, **53**, pp 277–303.

Fellman, C. (1996). Clays and pottery. http://www.acad.carleton.edu. 4pp.

Floyd, P.A., Winchester, J.A., Park, R.G. (1989). Geochemistry and tectonic setting of Lewisian clastic metasediments from the Early Proterozoic Loch Maree Group of Gairloch, NW Scotland. *Precambrian Res*. **45**, 203–214.

Frei, D. and Gerdes, A. (2009). Precise and accurate in situ U-Pb dating of zircon with high sample throughput by automated LA-SF-ICPMS. *Chemical Geology*, **261,** 261–270, doi:10.1016/j.chemgeo.2008.07.025.

Fuerstenau, D. W. (1986). Mineral Processing In Bever, M. B. (ed.), *Encyclopedia of Materials Science and Engineering*, vol.4 Oxford: Pergamon Press/The MIT Press. pp. 3062-3070.

Gálan, E., Aparicio, P., Fernández-Caliani, J.C., Miras, A., Márquez, M.G., Fallick, A.E. and Clauer, N. (2016). New insights on mineralogy and genesis of kaolin deposits: The Burela kaolin deposit (Northwestern Spain). *Applied Clay Science*, **131**, 14-26.

Gao, Y., Masuda, Y., Peng, Z., Yonezawa, T., and Koumoto. K. (2003). Room temperature deposition of a TiO_2 thin film from aqueous peroxotitanate solution. *J. Mater. Chem*., **13,** 608–613.

Gaspe, A., Messer, P., and Young, P. (1994). Selection and preparation of claybodies for stove manufacture. Clay testing. A manual on clay/non-clay ratio measurement technique. 10 pp.

Gentry, R.V., Sworski, T.J., McKown, H.S., Smith, D.H., Eby, R.E., and Christie, W.H. (1982). Differential lead retention in zircons: implications for nuclear waste containment. *Science* **216**:296-297.

Gerdes, A. and Zeh A., (2006). Combined U–Pb and Hf isotope LA-(MC) ICP-MS analyses of detrital zircons: comparison with SHRIMP and new constraints for the provenance and age of an Armorican metasediment in Central Germany. *Earth Planet. Sci. Lett*., **249**, 47–61.

Gilg, H.A. (2000). D–H evidence for the timing of kaolinization in Northeast Bavaria, Germany. *Chem. Geol.* **170**, 5–18.

Gilg, H.A. (2003). Isotopic tool of dating paleoweathering in Europe. *Géologie de la France*, **1**, 49-51.

Gilg, H. A., Weber, B., Kasbohm, J., and Frei, R. (2003). Isotope geochemistry and origin of illite-smectite and kaolinite from the Seilitz and Kemmlitz kaolin deposits, Saxony, Germany. *Clay Minerals* **38**, 95–112.

Gilg, H.A. and Sheppard, S.M.F. (1996). Hydrogen isotope fractionation between kaolinite and water revisited. *Geochim. Cosmochim. Acta* **4**, 89–103.

Gilg, H.A. and Frei, R. (1997). Isotope dating of residual kaolin deposits in Europe Tirschenreuth, Germany and St. Yrieix, France). *Energy and Mineral Resources for the 21st Century, Geology of Mineral Deposits, Mineral Economics* (P. Rongfu, editor). Proceedings of the 30th International Geological Congress, Beijing, Vol. 9, VSP International Science Publisher, Zeist. pp. 123 – 132.

Gilg, H.A., Hülmeyer, S., Miller, H., and Sheppard. S.M.F. (1999). Supergene origin of the Lastarria kaolin deposit, South-Central Chile, and paleoclimatic implications. *Clays and Clay Minerals,* 47 (2), 201 –211.

Gilg, H.A., Hall, A.M., Ebert, K., and Fallick, A.E. (2013). Cool kaolins in Finland. *Palaeogeography, Palaeoclimatology, Palaeoecology* **392**, 454-462.

Gilkes, R.J., Prakongkep, N. (2016). How the unique properties of soil kaolin affect the fertility of tropical soils, *Appl. Clay Sci*., **131**, 100-106.

Girard, J. P., Freyssinet, P., and Chazot, G. (2000). Unraveling climatic changes from intraprofile variation in oxygen and hydrogen isotopic composition of goethite and kaolinite in laterites: an integrated study from Yaou, French Guiana. *Geochim. Cosmochim. Acta* **64**, 409–426.

Giral-Kacmarcik, S., Savin, M.S., Nahon, D.B., Girard, J.P., Lucas, Y., and Abel, L.J. (1998). Oxygen isotope geochemistry of kaolinite in laterite-forming processes, Manaus, Amazonas, Brazil. *Geochim. Cosmochim. Acta* **62**, 1865–1879.

Grant, N.K. (1978). Orogeny and reactivation to the west and southwest of the West African Craton - in: The ocean basins and margins. (ed. A.E.M. NAIRN & EG. STEHLI), Plenum Press, New York: **1**, pp. 447-492.

Grim, R.E. (1962). Applied Clay Mineralogy. McGraw-Hill, London, 422 pp.

Gromet, L.P., Dymek, R.F., Haskin, L.A., and Korotev, R.L. (1984). The North American Shale composite: its compilation, major and trace element characteristics. *Geochimica et Cosmochimica Acta*, 48, 2469-2482.

Gross, M.G. (1964). Heavy-metal concentrations of diatomaceous sediments in a stagnant Fjord. *Geol. Soc. Am.*, 76:69.

Guadagnin, F., Chemale, F., Magalhães, A.J.C., Santana, I.D., and Takehara, L. (2013). Age constraints on crystal-tuff from the Espinhaço Supergroup - Insight into the Paleoproterozoic to Mesoproterozoic intracratonic basin cycles of the Congo–São Francisco Craton. *Gondwana Res.,* http://dx.doi.org/10.1016/j.gr.2013.10.009.

Guggenheim, S. and van Groos, A.F.K. (2001). Baseline studies of the Clay Minerals Society Source Clays: Thermal analysis. *Clays and Clay Minerals*, **49 (5),** 433-443.

Günther, D. and Hattendorf, B. (2005). Solid sample analysis using laser ablation inductively coupled plasma mass spectrometry, Trends in Analytical Chemistry, **24(3),** 255-265.

Guo, M.R., Lin, Y.M., Xu, X.P., and Chen, Z.L. (2010). Bioleaching of iron from kaolin using Fe (III)-reducing bacteria with various carbon nitrogen sources. *Appl. Clay Sci*. **48**, 379–383.

Gyollai, I., Mader, D., Polgári, M., Popp, F., and Koeberl, C. (2014). Lack of evidence for impact signatures in Neoproterozoic postglacial deposits from NW-Namibia. *Austrian Journal of Earth Sciences*, **107 (2),** 100-111.

Harnois, L. (1988). The CIW index: A new chemical index of weathering. *Sedimentary Geology,* **55**, 319–322.

Harris, C., Compton, J.S. and Bevington, S.A. (1999). Oxygen and hydrogen isotope composition of kaolinite deposits, Cape Peninsula, South Africa: Low-temperature, meteoric origin. *Economic Geology*, **94**, 1353-1366.

Haskin, L.A., Helmke, P.A., Paster, T.P., Allen, R.O (1971). 'Rare earths in Meteoric, terrestrial, and lunar matter', In Activation Analysis in Geochemistry and Cosmochemistry.

Hassanipak, A.A. and Elsinger, E. (1985). Mineralogy, crystallinity, O^{18}/O^{16}, and D/H of Georgia kaolins. *Clays and Clay Minerals*, **33 (2),** 99-106.

Herbillon, A. J., Mestdagh, M. M., Vielvoye, L. and Derouane. E. (1976). Iron in kaolinite with special reference to kaolinite from tropical soils. *Clay Minerals* 11: 201-220.

Hinckley, D.N. (1963). Variability in “crystallinity” values among the kaolin deposits of the coastal plain of Georgia and South Carolina. Clays and Clay Minerals, II, 229–235.

Hofer, G., Wagreich, M., Neuhuber, S. (2013). Geochemistry of fine-grained sediments of the upper Cretaceous to Paleogene Gosau Group (Austria, Slovakia): Implications for paleoenvironmental and provenance studies *Geoscience Frontiers* **4**, 449-468.

Hofmann, P., Ricken, W., Schwark, L., and Leythaeuser, D. (2001). Geochemical signature and related climatic-oceanographic processes for early Albian black shales: site 417D, North Atlantic Ocean. *Cretaceous Research* **22**, 243-257.

Holtz, R.D. and Kovacs, W.D. (1981). An Introduction to Geotechnical Engineering. Prentice-Hall, Inc., New Jersey.

Hosseini, M.R., Ahmadi, A. (2015). Biological beneficiation of kaolin: A review on iron removal *Applied Clay Science* **107**, 238–245.

Hurley, F.M., Almeida, F.M., Melcher, G.C., Cordani, U.G., Rand, J.R.,Kawashita, K., Vandoros, P., Pinson, W.H., and Fairbairn, H.W. (1967). Test of continental drift by comparison of radiometric ages. *Science*, **157,** 495-500.

IAEA/WMO (2017). Global Network of Isotopes in Precipitation. The GNIP Database. Accessible at: http://www.iaea.org/water

Ilić, B.R., Mitrović and Miličić, L.R. (2010). Thermal treatment of kaolin clay to obtain metakaolin. *Hem. Ind*., 64 (4), 351-356.

International Centre for Diffraction Data (2002). Mineral Powder diffraction file data book. 941p.

Iloeje, N.P. (1981). A New Geography of Nigeria. Longman Publishers; Ibadan, Nigeria. pp. 203.

Ishiga, H., Dozen, K., and Sampei, Y. (1999). Geochemical constraints on marine invasion and provenance change related to the opening of the Japan Sea: an example from the Lower Miocene shales in the Hoda section, Shimane Peninsula, SW Japan. *Journal of Asian Earth Sciences,* **17**, 443-457.

Jackson, M.L. (1979). Soil chemical analysis- Advanced course, 2nd edition, 11th printing, published by the author, Madison, WI, USA, 895 pp.

Jackson, S.E., Pearson., N.J., Griffin, W.L. and Belousova, E.A. (2004). The application of laser ablation-inductively coupled plasma-mass spectrometry to in situ U-Pb zircon geochronology. *Chemical Geology*, **211**, 47-69, doi:10.1016/j.chemgeo.2004.06.017

Jan du Chene R.E., De Klasz, I., and Archibong, E.E. (1979). Biostratigraphic study of the borehole Ojo- 1, SW Nigeria, with special emphasis on the Cretaceous microflora. Revue de Micropalaeontologie **21**:123–139.

Jones, B. and Manning, D.C., (1994), Comparison of geochemical indices used for the interpretation of paleo-redox conditions in Ancient mudstones: *Chemical Geology*, **111(1-4),** 111-129.

Kearey, P., and Vine, F. J. (1990). Global tectonics: Oxford, Blackwell Scientific Publications, 302 p.

Keller, W.D. (1968). Flint clay and flint-clay facies. *Clay Clay Miner*. **16,** 113–128.

Keller, W.D. (1976a). Scan electron micrographs of kaolins collected from diverse environments of origin--I. *Clays and Clay Minerals,* **24**, 107-113.

Keller, W.D. (1976b). Scan electron micrographs of kaolins collected from diverse environments of origin--II. *Clays and Clay Minerals,* **24**, 114-117.

Keller, W.D. (1978). Classification of kaolins exemplified by their textures in scan electron micrographs. *Clays and Clay Minerals*, **26 (1),** 1-20.

Kirschvink, J. L. (1992). Late Proterozoic low-latitude global glaciation: the Snowball Earth. In: J.W. Schopf and C. Klein (eds.), The Proterozoic Biosphere: a multidisciplinary study. Cambridge University Press, pp. 51-52.

Kissinger, H.M. (1956). Variation of peak temperature with heating rate in differential thermal analysis. *Journal of Research of the National Bureau of Standards*, **57 (4),** 217-221.

Kober, B. (1986). Whole-grain evaporation for $^{207}Pb/^{206}Pb$ age investigations on single zircons using a double-filament thermal ion source. Contributions to Mineralogy and Petrology, **93**,482-490.

Kober, B. (1987). Single-grain evaporation combined with Pb* emitter bedding for $^{207}Pb/^{206}Pb$ age investigations using thermal ion mass spectrometry, and implications for zirconology. Contributions to Mineralogy and Petrology, **96**, 63-71.

Kosztolanyi, C. (1965). Nouvelle methode d'analyse isotopique des zircons a l'etat naturel apres attaque directe sur le filament. *C R Acad Sci* **261**: 5849-5851.

Kotschoubey, B., Truckenbrodt, W. and Hieronymus, B. (1996). Depo´sitos de caulim e argila semi-flint no nordeste do Estado do Para´. Revista Brasileira de Geocieˆncias, **26**, 71-80.

Kuscu, M. and Yildiz, A. (2016). The mineralogy, geochemistry, and suitability for ceramic applications of Akharm (Afyonkarahisar, W Turkey) kaolinitic clay. *Arab J. Geosci*, **9**, 510.

Lacoviello, F., Giorgetti, G., Nieto, F., Memmi, I. (2012). Evolution with depth from detrital to authigenic smectites in sediments from AND-2A drill core (McMurdo Sound, Antarctica). *Clay Minerals* **47**, 481-498.

Lahcen, D., Hicham, E., Latifa, S., Abderrahmane, A., Jamal, B., Mohamed, W., Meriam, E., and Nathalie, F. (2014). Characteristics and ceramic properties of clayey materials from Amezmiz region (Western High Atlas, Morocco). *Applied Clay Science* **102**, 139–147.

Landergreen, S. and Manhem, P. (1963). Geochemical Facies Analysis Methods in Geochemistry and Geophysics II. Elsevier Publ. Co., pp 101.

Lawrence, J.R. and Taylor, H.P. Jr (1972). Hydrogen and oxygen isotope systematics in weathering profiles. Geochim. Cosmochim. Acta, **36**, 1377-1393.

Lawrence, J.R. and Rashkes Meaux, J., 1993. The stable isotope composition of ancient kaolinite of North America. In *Stable Isotope Geochemistry: A tribute to Samuel Epstein* (eds. H. P. Taylor, J. R. O'Neil, and I. R. Kaplan), The Geochemical Society, Special Publication No. 3, pp. 249–261.

Leonard, D. N., Chandler, G. W. and Seraphin, S. (2012). Scanning Electron Microscopy. *Characterization of Materials*. 1–16.

Li, Y.H. (2000). A Compendium of Geochemistry. Princeton University Press, Princeton. 475 pp.

Loehnert, E.P. (1988). Major chemical and isotope variation in surface and subsurface waters of West Africa. *J. Afr. Earth Sci*., **7(3),** 588-589.

Longstaffe, F.J. and Ayalon, A. (1990). Hydrogen–isotope geochemistry of diagenetic clay minerals from Cretaceous sandstone. Alberta. Canada: evidence for exchange. *Appl. Geochem.* **5,** 657–668.

Lopez, J.M.G., Bauluz, B., Fernández-Nieto, C., Oliete, C.Y. (2005). Factors controlling the trace-element distribution in fine-grained rocks: the Albian kaolinite rich deposits of the Oliete Basin (NE Spain). *Chem. Geol.* **214,** 1–19.

Lopez-Galindo, A., Viseras, C. and Cerezo, P. (2007). Compositional, technical and safety specifications of clays to be used as pharmaceutical and cosmetic products. *Applied Clay Science*, **36**:51–63 pp.

Ludwig, K.R. (2003). Isoplot/EX version 3.0, A geochronological toolkit for Microsoft Excel, Berkeley Geochronology Center Special Publication.

Luz, A.B. and Middea, A. (2004). Purification of kaolin by selective flocculation. Paper presented at the 43rd Annual conference of Metallurgist of CIM, Ontario, Canada.

Madejová, J. and Komadel, P. (2001). Baseline studies of the clay minerals source society: infrared methods. *Clays and Clay Miner*., **49,** 410–432.

Madejová, J., Kraus, I., Tunega, D. and Šamajová, E. (1997). Fourier transform infrared spectroscopic characterization of kaolin group minerals from the main Slovak deposits. Geologica Carphatica – Series Clays, **6(1)**, 3–10.

Maksaev, V., Arancibia, J., Munizaga, F. and Tassinari, C. (2015). Detrital-zircon U-Pb geochronology of the Quebrada del Carrizo Metamorphic Complex and El Jardín Schists and spatially-related granitoids of the Sierra Castillo Batholith. *Andean Geology*, **42 (3):** 285-312.

Marumo, K.., Matsuhisa, Y., and Nagasawa, K. (1982). Hydrogen and oxygen isotopic composition of kaolin minerals in Japan. International Clay Conference 1981 (eds Olphen, H.V. and Veniale, F.), Elsevier, Amsterdam, Dev. Sediment, **35**, 315-320.

McCurry, P. (1976). The geology of the Precambrian to Lower Paleozoic rocks of Northern Nigeria. In: Kogbe, C.A. (ed.) Geology of Nigeria. Elizabethan Publishing Company, Lagos, pp. 67-99.

McLennan, S.M. (1989). Rare earth elements in sedimentary rocks: influence of provenance and sedimentary processes. In Lipin, B.R., and McKay, G.A., eds., Geochemistry and Mineralogy of Rare Earth Elements: Mineralogical Society of America Reviews in Mineralogy, **21**, 169–200.

McLennan, S., Taylor, S., McCulloch, M., Maynard, J. (1990). Geochemical and Nd-Sr isotopic composition of deep-sea turbidites: crustal evolution and plate tectonic associations. *Geochimica et Cosmochimica Acta* **54,** 2015–2050.

McLennan, S.M., Hemming, S., McDaniel, D.K., and Hanson, G.N. (1993). Geochemical approaches to sedimentation, provenance, and tectonics. In Johnsson, M.J., and Basu, A., eds., Processes Controlling the Composition of Clastic Sediments: Geological Society of America, Special Paper **284**, 21–40.

McLennan, S. M. (2001). Relationships between the trace element composition of sedimentary rocks and upper continental crust, *Geochem. Geophys. Geosyst.*, **2**, 1021.

McManus, J. (1988). Grain size distribution and interpretation. Pp. 63-85 in: Techniques in Sedimentology (M.E. Tucker, editor). Blackwell Scientific Publications, Oxford.

Meinhold, G., Kostopoulos, D., Frei, D., Himmerkus, F., and Reischmann, T. (2010). U–Pb LA-SF-ICP-MS zircon geochronology of the Serbo-Macedonian Massif, Greece: palaeotectonic constraints for Gondwana-derived terranes in the Eastern Mediterranean. *Int J Earth Sci* (Geol Rundsch), **99**:813–832.

Millot, G. (1970). Geology of Clays. Springer Verlag, Berlin. 499 pp.

Minapuye, I.O. (1981). Appraisal of clay deposits at Ifon and its environs. Unpublished M.Sc. thesis, University of Ibadan, Nigeria, 200 pp.

Mishra, M. and Sen, S. (2012). Provenance, tectonic setting and source-area weathering of Mesoproterozoic Kaimur Group, Vindhyan Supergroup, Central India. *Geol Acta* **10**:283–293.

Mizota, C., and Longstaffe, F.J. (1996). Origin of Cretaceous and Oligocene kaolinites from the Iwaizumi clay deposit, Iwate, Northeastern Japan. *Clays and Clay Miner*. 44, 408–416.

Murray, H.H. (1980). Diagnostic tests for evaluation of Kaolin physical properties. *Acta Mineralogica Petrographica* **24**, 1-24.

Murray, H. H. (1986). Clays. In: Ullman's encyclopedia of industrial chemistry. 5th Edition. Pp 109-136.

Murray, H.H. (1998). Kaolin Minerals: their genesis and occurrences. In: Bailey, S.W. (Ed.), Hydrous phyllosilicates (exclusive of Micas). ; Reviews in Mineralogy, 19, Mineralogical Society of America, Washington D.C., pp 67-89.

Murray, H.H. (2007). Applied Clay Mineralogy. Ocurrences, Processing and Application of Kaolins, Bentonites, Palygorskite–Sepiolite, and Common Clays, 1st ed. Elsevier, Oxford. 189 pp.

Murray, H.H., Janssen, J. (1984). Oxygen isotopes-indicators of kaolinite genesis. In: Proc. 27th Internat. Geological Congress, Non Metallic ores, vol. 15. VNU Science Press, pp. 287–303.

Murray, H.H. and Keller, W.D. (1993). Kaolins, Kaolins and Kaolins. In: Murray, H., Bundy, W.,Harvey, C. (Eds.), Kaolin Genesis and Utilization, vol. 1. Clay Mineral Society Special Publication, pp. 1–24.

Murray, H.H. and Kogel, J.E. (2005). Engineered clay products for the paper industry. *Applied Clay Science*, **19 (3-4),** 199-206.

Nakamura, N. (1974). Determination of REE, Ba, Fe, Mg, Na, and K in carbonaceous and ordinary chondrites: *Geochimica et Cosmochimica Acta,* **38**, 757–775.

Nasdala, L., Corfu, F., Valley, J.W., Spicuzza, M.J., Wu, F-Y., Li, Q-L., Yang, Y-H., Fisher, C., Münker, C., Kennedy, A.K., Reiners, P.W., Kronz, A., Weidenbeck, M., Wirth, R., Chanmuang, C., Zeug, M., Vácsi, T., Norberg, N., Häger, T., Kröner, A., and Hofmeister, W. (2016). *Zircon M127—a homogeneous reference material for SIMS U-Pb geochronology combined with hafnium, oxygen and, potentially, lithium isotope analysis*. *Geostand. Geoanal. Res.,* **40**, 457–475.

Nesbitt, H.W. and Young, G.M. (1982). Early Proterozoic climates and plate motions inferred from major elemental chemistry of lutites. *Nature*, **299**, 715-717.

Nesbitt, H.W. and Young, G.M. (1984). Prediction of some weathering trends of plutonic and volcanic rocks based on thermodynamic and kinetic considerations. *Geochim. Cosmochim. Acta* **48,** 1523- 1534.

Nesbitt, H. W. and Young, G. M. (1989). Formation and Diagenesis of weathering profiles. *Journal of Geology*, 97(2), pp. 129-147.

Neves, S.P. (2003). Proterozoic history of the Borborema province (NE Brazil): Correlations with neighboring cratons and Pan-African belts and implications for the evolution of western Gondwana. *Tectonics*, **22 (4),** 1-14.

Nwajide, C.S. (2013). Geology of Nigeria's Sedimentary Basins. CSS Press, Nigeria. 565 pp.

Obaje, N.G. (2009). Geology and Mineral Resources of Nigeria. Lecture Notes in Earth Sciences. *Springerverlag*, Berlin, Heildeberg, **120,** 57-68.

Oboh-Ikuenobe, F.E., Obi, C.G., and Jaramillo, C.A. (2005). Lithofacies, palynofacies, and sequence stratigraphy of Palaeogene strata in southern Nigeria. *J. Afr. Earth Sci.*, **41**: 79-101.

Obradovich, J.D. (1965). Problems in the use of glauconite and related minerals for radioactive dating. Unpublished PhD. Thesis, Univ. of California, Berkeley.

Ogezi, A.E.O. (1977). Geochemistry and geochronology of basement rocks from north-western Nigeria. Unpublished PhD. Thesis, Univ. of Leeds. England, pp. 295.

Ogunseiju, P. (1989). Characterization of Ilafon-Isan Ekiti clay deposits in Ondo State. Unpublished M.Sc thesis, Department of Geology, Obafemi Awolowo University, Ile-Ife. pp 124.

Ohta, T. and Arai, H. (2007). Statistical empirical index of chemical weathering in igneous rocks: a new tool for evaluating the degree of weathering. *Chem. Geol*. **240**, 280–297.

Okezie, C.N. and Onuogu, S.A. (1985). The lignites of Southeastern Nigeria. Geological Survey of Nigeria Occasional paper, **10**, 28 pp.

Okunlola, O.A. and Idowu, O. (2012). The geochemistry of claystone-shale deposits from the Maastritchian Patti formation, Southern Bida basin, Nigeria. *Earth sci. res. j.*, **16 (2),** 1-19.

Olarewaju, V.O. (2006). The Charnockitic Intrusives of Nigeria. In: Oshi O (ed) The basement complex of Nigeria and its mineral resources (A Tribute to Prof. M. A. O. Rahaman). Akin Jinad & Co. Ibadan, pp 45–70.

Omatsola, M.E. and Adegoke, O.S. (1981). Tectonic evolution and cretaceous stratigraphy of Dahomey Basin. *J. Mining and Geol.,* **18**, 130-137.

Omran, A. and El Sharawy, S. (2014). Tectonic evolution of the Southern Gulf of Suez, Egypt: a comparison between depocenter and near peripheral basins. *Arab J Geosci* **7**:87–107.

O'Neil, J.R., Kharaka, Y.K. (1976). Hydrogen and oxygen isotope exchange reactions between clay minerals and water. *Geochim. Cosmochim. Acta* **40**, 241–246.

Oni, S. O., Olatunji, A. S., Ehinola, O. A. (2014). "Determination of Provenance and Tectonic Settings of Niger Delta Clastic Facies Using Well-Y, Onshore Delta State, Nigeria," *Journal of Geochemistry*, Article ID 960139, 13 pages.

Onuoha, K.M. (1999). Structural features of Nigeria's coastal margin: an assessment based on age data from wells. *Journal of African Earth Sciences*, **29 (3),** 485 - 499.

Onyemaobi, O. O. (2002). Mineral Resources Exploitation, Processing and Utilization – A Sine Qua Non for Nigeria's Metallurgical Industrial Development Inaugural Lecture Series 5 of FUTO, Owerri: FUTO Press. 48 pp.

Oyawoye, M.O. (1964): The geology of the Nigeria basement Complex. *Journal of Nigeria Mining, Geological and Metallurgical Society*, **1**, 87-102.

Oyebanjo, O.M., Ajayi, T.R., Tchokossa, P. (2014). Geochemistry of Kolmani-1 Well Sediments from the Upper Benue Trough, Gongola Basin, Northeastern Nigeria. *British Journal of Applied Science & Technology **4(20)**: 2931-2945.*

Oyinloye, A.O. (2011). Geology and Geotectonic Setting of the Basement Complex Rocks in South Western Nigeria: Implications on Provenance and Evolution, Earth and Environmental Sciences, Dr. Imran Ahmad Dar (Ed.), ISBN: 978-953-307-468-9, InTech.

Paikaray, S., Banerjee, S., Mukherji, S. (2008). Geochemistry of shales from the Paleoproterozoic to Neoproterozoic Vindhyan Supergroup: implications on provenance, tectonics and paleoweathering. *Journal of Asian Earth Sciences*, **32** (1), 34–48.

Pankhurst, R. J., Trouw, R. A. J., Brito Neves, B. B. & de Wit, M. J. (eds) (2008). West Gondwana: Pre-Cenozoic Correlations across the South Atlantic Region. Geological Society, London, Special Publications, 294.

Parrish, J., Ziegler, A., and Scotese, C. (1982) Rainfall patterns and the distribution of coals and evaporites in the Mesozoic and Cenozoic. *Paleogeography Paleoclimatology and Paleoecology,* **40**, 67-101.

Paton, C., Hellstrom, J., Paul, B., Woodhead, J., Hergt, J. (2011). Iolite: freeware for the visualisation and processing of mass spectrometric data. *J. Anal. At. Spectrom*., **26**, 2508–2518.

Pe-Piper, G., Triantafyllidis, S., Piper, D.J.W. (2008). Geochemical identification of clastic sediment provenance from known sources of similar geology: the Cretaceous Scotian Basin, Canada. *J. Sediment. Res.* **78**, 595–607.

Petrus, J.A. and Kamber, B.S. (2012). VizualAge: A Novel Approach to Laser Ablation ICP-MS U-Pb Geochronology Data Reduction: *Geostandards and Geoanalytical Research*, **36**, 247-270.

Petschick, R., Kuhn, G., and Gingele, F. (1996). Clay Mineral Distribution in Surface Sediments of the South Atlantic: Sources, Transport, and Relation to Oceanography. *Marine Geology*, **130**, 203-229.

Pickering, S.M. and Murray, H.H. (1995). Clays. Industrial minerals and rocks. Society of Mining Engineers.

Poorni, S. and Natarajan, K.A. (2013). Microbially induced selective flocculation of hematite from kaolinite*. Int. J. Miner. Process*. **125**, 92–100.

Potter, P.E., Maynard, J.B., and Depetris, P.J. (2005). "Mud and Mudstone: Introduction and overview," Springer-Verlag Berlin Heidelberg.

Price, J.R. and Velbel, M.A. (2003). Chemical weathering indices applied to weathering profiles developed on heterogeneous felsic metamorphic parent rocks. *Chemical Geology* **202**, 397– 416.

Prudêncio, M. I., Figueiredo, M. O., and Cabral, J. M. P. (1989). Rare earth distribution and its correlation with clay mineralogy in the clay-sized fraction of Cretaceous and Pliocene sediments (Central Portugal). *Clay Minerals* **24**, 67-74.

Pruett, R.J. and Alves, P.A. (2013). Compositions comprising fine sedimentary kaolin and methods for preparing same. U.S. Patent 8,465,583.

Pruett, R.J. (2016). Kaolin deposits and their uses: Northern Brazil and Georgia, USA. *Applied Clay Science*, **131**, 3-13.

Rahaman, M.A. (1976). Review of the Basement Geology of Southwestern Nigeria. Geology of Nigeria Text (edited by Kogbe, C.A.). pp 39-56.

Rahaman, M.A. and Ocan, O. (1978). On relationships in the Precambrian Migmatite-gneisses of Nigeria. *Niger J Min Geol*. **15**:23–32.

Rahaman, M.A. (1988). Recent advances in the study of the basement complex of Nigeria. In: Oluyide et. al (eds) Precambrian Geology of Nigeria. Publ Geological Survey of Nigeria, Kaduna, pp. 11-43.

Raw Materials Research and Development Council (RMRDC) Multidisciplinary Committee Techno-Economic Survey (MCTS) Report (2003). Chemicals and Pharmaceutical Sector. 4th Update. pp 16-69, 102.

Rogers, J.J.W. and Santosh, M. (2004). Continents and supercontinents. Oxford Univ. Press, Oxford. 289 pp.

Roser, B.P. and Korsch, R.J. (1986). Determination of tectonic setting of sandstone–mudstone suites using SiO_2 content and K_2O/Na_2O ratio. *J. Geol*. **94,** 635–650.

Roser, B.P. and Korsch, R.J. (1988). Provenance signatures of sandstone-mudstone suites determined using discriminant function analysis of major-element data. *Chemical Geology* **67**, 119-139.

Roser, B.P., Cooper, R.A., Nathan, S., and Tulloch, A.J. (1996). Reconnaissance sandstone geochemistry, provenance, and tectonic setting of the lower Paleozoic terraines of the West Coast and Nelson, New Zealand. *New Zealand J. Geol. Geophys*, **39**, 1-16.

Roskill Information Services Ltd. (1979). The economics of kaolin, second edition, London, 148pp.

Rozanski, K., Araguas-Araguas, L., and Gonfiantini, R. (1993). Isotopic patterns in modem global precipitation, in: Climate Change in Continental Isotopic Records – Geophysical Monograph 78, edited by: Swart, P. K., Lohman, K. C., McKenzie, J., and Savin, S., American Geophysical Union, Washington, DC, 1–36.

Ruck, L. and Brown, C.T. (2015). Quantitative analysis of Munsell color data from archeological ceramics *Journal of Archaeological Science*: Reports **3**, 549-557.

Russel, O. (1988). Minerals in pharmaceuticals, the key is quality assurance. Ind. Miner. August, 32–43.

Russell, J.D. and Fraser, A.R. (1994). in: M.J. Wilson (Ed.), Clay Mineralogy: Spectroscopic and Chemical Determinative Methods, Chapman & Hall, London, UK, p. 11.

Santos Jr., A.E.A. and Rossetti, D.F. (2003). Paleoambiente e estratigrafia da Formação Ipixuna, Área do Rio Capim, Leste da bacia de Cametá. Rev. Bras. *Geocienc*. **33**, 313–324.

Santos Jr., A.E.A., Rossetti, D.F. (2006). Depositional model of the Ipixuna Formation (late cretaceous? early tertiary), Rio Capim area, northern Brazil. *Latin American Journal of Sedimentology and Basin Analysis* **13**, 65–87.

Savin, S.M. and Epstein, S. (1970). The oxygen and hydrogen isotope geochemistry of clay minerals.*Geochim.Cosmochim.Acta* **34**, 25–42.

Savin, S. M. (1977). The History of the Earth's Surface Temperature during the Past 100 Million Years. *Annual Review of Earth and Planetary Sciences*, **5(1),** 319-355.

Savin, S.M. and Lee, M., (1988). Isotopic studies of phyllosilicates. In: Bailey, S.W. (Ed.), Hydrous Phyllosilicates (exclusive of micas). *Rev. Mineral*., **19,** pp. 189–219.

Savin S.M. and Hsieh J. C. C., 1998. The hydrogen and oxygen isotope geochemistry of pedogenic clay minerals: principles and theoritical background. *Geoderma* **82,** 227–254.

Schiefelbein, C.F., Zumberge, J.E., Cameron, N.C., and Brown, S.W. (2000). Geochemical comparison of crude oil, South Atlantic Margins, *in* M.R. Mello, and B.J. Katz, eds., Petroleum Systems of the South Atlantic Margin: *AAPG Memoir* **73,** 15-26.

Schiefelbein, C.F., Dickson, W.G., Odegard, M.E., and Brooks, J. (2003). South Atlantic Margin Basin Analysis using a G3 Approach (Geophysical, Geological and Geochemical):8th International Congress of the Brazilian Geophysical Society and 5th Latin American Geophysical Conference, (Abstract).

Schroeder, P.A., Pruett, R.J., and Melear, N.D. (2004). Crystal-chemical changes in an oxidative weathering front in a Georgia kaolin deposit. *Clays Clay Miner*. **52**, 211–220.

Scotese, C.R., Gahagan, L.M., and Larson, R.L. (1988). Plate tectonic reconstructions of the Cretaceous and Cenozoic ocean basins. *Tectonophysics* **155**:27-48.

Scotese, C. R., (2001). *Atlas of Earth History*, Volume 1, Paleogeography, PALEOMAP Project, Arlington, Texas, 52 pages

Selvaraj, K. and Chen, C.T.A. (2006). Moderate chemical weathering of subtropical Taiwan: constraints from solid-phase geochemistry of sediments and sedimentary rocks. *Jour. Geol.* **114**, 101–116.

Semiz, B. (2017). Characteristics of clay-rich raw materials for ceramic applications in Denizli region (Western Anatolia). *Applied Clay Science*, **137,** 83-93.

Sheppard, S.M.F. and Gilg, H.A. (1996). Stable isotope geochemistry of clay minerals. *Clay minerals*, **31,** 1-24.

Sheppard, S.M.F., Nielsen, R.L., and Taylor, H.P. (1969). Oxygen and hydrogen isotope ratios of clay minerals from porphyry copper deposits. *Econ. Geol.* **64,** 755-777.

Siddiqui, M.A., Ahmed, Z. and Saleemi, A.A. (2005). Evaluation of Swat kaolin deposits of Pakistan for industrial uses. *Applied Clay Science*, **29**, 55-72.

Singer, A. (1980). The paleoclimatic interpretation of clay minerals in soils and weathering profiles - A review. *Earth-Sci. Rev.* **21**, 251–293.

Singer, A. (1984). The paleoclimatic interpretation of clay minerals in sediments. *Earth-Sci. Rev.* **15**, 303–326.

Sláma, J., Košler, J., Condon, D.J., Crowley, J.L., Gerdes, A., Hanchar, J.M., Horstwood, M.S.A., Morris, G.A., Nasdala, L., Norberg, N., Schaltegger, U., Schoene, B., Tubrett, M.N., Whitehouse, M.J. (2008). Plešovice zircon – a new natural reference material for U-Pb and Hf isotopic microanalysis. *Chemical Geology*, **241**, 1–35,

Soil Survey Staff (2014). Soil Survey Field and Laboratory Methods Manual. Soil Survey Investigations Report No. 51, Version 2.0. R. Burt and Soil Survey Staff (ed.). U.S. Department of Agriculture, Natural Resources Conservation Service. 487 pp.

Sousa, D.J.L., Varajão, A.F.D.C., Yvon, J., Scheller, T., and Moura, C.A.V. (2007a). Ages and possible provenance of the sediments of the Capim River kaolin, northern Brazil. *Journal of South American Earth Sciences* **24**, 25–33.

Sousa, D.J., Varajao, A.F., Yvon, J. and Da Costa, G.M (2007b). Mineralogical, micromorphological and geochemical evolution of the kaolin facies deposit from the Capim region (northern Brazil). *Clay Minerals*, **42**, 69–87.

Stoneley, R. (1966). The Niger Delta region in the light of the theory of continental drift. *Geol. Mag.*, **103**, 385-396.

Stern, L.A., Chamberlain, C.P., Reynolds, R.C. and Johnson, G.D. (1997). Oxygen isotope evidence of climate change from pedogenic clay minerals in the Himalayan molasse *Geochimica et Cosmochimica Acta*, **61 (4),** 731-744.

Strazzera, B., Dondi, M. and Marsigli, M. (1997). Composition and ceramic properties of tertiary clays from southern Sardinia (Italy). *Applied Clay Science*, **12**, 247-266.

Tabor, N.J., Montanez, I.P., and Southard, R.J. (2002). Paleoenvironmental reconstruction from chemical and isotopic compositions of Permo-Pennsylvanian pedogenic minerals. *Geochimica et Cosmochimica Acta*, **66 (17),** 3093–3107.

Tabor, N.J. and Montanez, I.P. (2005). Oxygen and hydrogen isotope compositions of Permian pedogenic phyllosilicates: Development of modern surface domain arrays and implications for paleotemperature reconstruction. *Palaeogeography, Palaeoclimatology, Palaeoecology*, **223**, 127-146.

Talabi, A. O. and Tijani, M. N. (2013). Hydrochemical and stable isotopic characterization of shallow groundwater system in the crystalline basement terrain of Ekiti area, southwestern Nigeria. *Appl Water Sci*, **3,** 229–245.

Tan, K.H. (1996). Soil sampling preparation and analysis. Marcel Dekker Inc. New York, 392 pp.

Tan, K. H. (1998). Principles of soil chemistry. Mariel Dekker Inc. USA. 521 pp.

Tao, H.F., Wang, Q.C., Yang, X., Lin, J., (2013). Provenance and tectonic setting of Late Carboniferous clastic rocks in West Junggar Xinjiang, China: a case from the Hala'alat Mountains. *Journal of Asian Earth Sciences*, **64**, 210-222.

Tardy, Y., Kobilsek, B., and Paquet, H. (1991). Mineralogical composition and geographical distribution of African and Brazilian periatlantic laterites. The influence of continental driftand tropical paleoclimates during the past 150 million years and implications for India and Australia. *Journal of African Earth Sciences* **12 (1/2),** 283-295.

Taupin, J.D., Coudrain-Ribstein, A., Gallaire, R., Zuppi, G.M., Filly, A. (2000). Rainfall characteristics ($\delta^{18}O$, δD, ΔH, and ΔHr) in Western Africa: regional scale and

influence of irrigated areas. Journal of Geophysical Research-Atmospheres **105,** 11911–11924.

Taylor, S.R. and McLennan, S.M. (1985). The Continental Crust: Its Composition and Evolution. Blackwell Scientific Publications, Oxford, 312 pp.

Taylor, J., Zeh, A., and Gerdes, A. (2016). U–Pb–Hf isotope systematics of detrital zircons in high-grade paragneisses of the Ancient Gneiss Complex, Swaziland: Evidence for two periods of juvenile crust formation, Paleo- and Mesoarchaean sediment deposition, and 3.23 Ga terrane accretion. *Precambrian Research*, **280**, 205–220.

Teklay, A., Yin, C., Rosendahl, L. and Bøjer, M. (2014). Calcination of kaolinite clay particles for cement production: a modeling study. *Cem. Concr. Res*., **61–62**, pp. 11-19.

Thiry, M. (2000). Palaeoclimatic interpretation of clay minerals in marine deposits: an outlook from the continental origin. *Earth-Science Reviews* **49**, 201–221.

Thompson, G.R. and Hower, J. (1973). An explanation for low radiometric ages from glauconite. *Geochimica et Cosmochimica Acta* **37**, 1473–1491.

Torquato, J.R. and Cordani, U.C. (1981). Brazil-Africa geological links. *Earth-Science Reviews*, **17,** 155-176.

Torquato, J.R. (1975). Geotectonic correlation between SE Brazil and SW Africa. An Acad. Brazil, Ciênc., 48 (Supl.), 353-363.

Trompette, R. (1997). Neoproterozoic (~ 600 Ma) aggregation of Western Gondwana: a tentative scenario. *Precambrian Res*. **82**, 101-112

Trivedi, N.C. and Hagemeyer, R.W. (1995). Fillers and coatings. Industrial Minerals and Rocks. Society of Mining Engineers.

Tubosun, I.A., Lancelot J.R., Rahaman M.A. and Ocan O. (1984): U-Pb Pan-African ages of two charnockites-granites associations from Southwestern Nigeria. *Contrib Mineral Petrol*, **88**, 188-195.

Tucker, R.T., Roberts, E.M., Hu, Y., Kemp, A.I.S., and Salisbury, S.W. (2013). Detrital zircon age constraints for the Winton formation, Queensland: contextualizing Australia's Late Cretaceous dinosaur faunas. *Gondwana Research***, 24,** 767-779.

Tugarinov, A.I. (1967). Geochronology of West Africa and Northeast Brazil. *Geokhimiya*, **11**, 1336-1349.

Turner, D.C. (1983). Upper Proterozoic schist belts in the Nigerian sector of the Pan-African Province of West Africa. *Precambrian Res* **21**:55–79.

Vaculíková, L., Plevová, E., Vallová, S., and Koutník, I. (2011). Characterization and differentiation of kaolinites from selected Czech deposits using infrared spectroscopy and differential thermal analysis. *Acta Geodyn. Geomater*., **8 (1)** (161), 59–67.

Valiani, Z. and Rezaee, P. (2014). Chemical Characteristics, Provenance Determination and Genesis Conditions of Clay Deposits of Kahrizak Formation (Early-Late Pleistocene), East of Tehran, Iran. *GSTF International Journal of Geological Sciences* **1 (2),** 15 – 22.

van Hinsbergen, D.J.J., de Groot, L.V., van Schaik, S.J., Spakman, W., Bijl, P.K., Sluijs, A., Langereis, C.G. and Brinkhuis, H. (2015). A Paleolatitude Calculator for Paleoclimate Studies (model version 2.0), *PLOS ONE*, **10(6):** e0126946. doi:10.1371/journal.pone.0126946

Van Reeuwijk, L.P. (2002). Procedures for soil analysis. International Soil Reference and Information Centre, Wageningen, The Netherlands, Tech. Paper 9, 100 pp.

Verma, S.P. and Armstrong-Altrin, J.S. (2013). New multi-dimensional diagrams for tectonic discrimination of siliciclastic sediments and their application to Precambrian basins. *Chemical Geology,* **355**, 117–133.

Verma, S. P. and Armstrong-Altrin, J. S. (2016). Geochemical discrimination of siliciclastic sediments from active and passive margin settings. *Sedimentary Geology*, **332**, 1-12.

Vieira, C.M., Sa'nchez, R. and Monteiro, S.N. (2008). Characteristics of clays and properties of building ceramics in the state of Rio de Janeiro, Brazil. *Construction and Building Materials*, **22**, 781-787.

Virta, R.L. (2004). Kaolin Industrial Mineral. *Rev. Min. Eng*., **56,** 28–29.

Wanniarachchi, D.U., Akasaka, M., Hayasaka, Y., and Perera, L.R. (2016). Internal textures and U–Pb geochronology of zircons in metamorphic rocks from the Southwestern Highland Complex, Sri Lanka. *Journal of Miner. and Petro. Sci.,* **111**, 373-384.

Weischet, W. (1970). *Chile, Seine Landeskundliche Individulita't und Struktur.* Wissenschaftliche Buchgesellschaft, Darmstadt, 268-365.

Whiteman, A. (1982). Nigeria: Its Petroleum Geology, Resources and Potential. Graham and Trotman, London, 381pp.

Wilson, S.A. (1997). The collection, preparation, and testing of USGS reference material BCR-2, Columbia River, Basalt: U.S. Geological Survey Open-File Report 98-xxx.

Wilson, M.J. (2013). Rock-Forming Minerals, Vol. 3c, Sheet Silicates–Clay Minerals, 2nd edition. The Geological Society, London, 724 pp.

Xu, Y. J., Cawood, P. A., Du, Y. S., Hu, L. S., Yu, W. C., Zhu, Y. H. and Li, W. C. (2013). Linking South China to northern Australia and India on the margin of Gondwana: Constraints from detrital zircon U-Pb and Hf isotopes in Cambrian strata, *Tectonics*, **32**, 1547–1558.

Zawada, P.K., (1988). Trace elements as possible paleosalinity indicators for the Ecca and Beaufort Group mudrocks in the southwestern Orange Free State. *S. Afr. J. Geol*. **91**, 18–26.

Zhou, L., Liang, Y., Gong, Y., and Yan, C. (2014). Modes of occurrence of Fe in kaolin from Yunnan China. *Ceramics International* **40(9):**14579–14587.